

Some pages of this thesis may have been removed for copyright restrictions.

If you have discovered material in AURA which is unlawful e.g. breaches copyright, (either yours or that of a third party) or any other law, including but not limited to those relating to patent, trademark, confidentiality, data protection, obscenity, defamation, libel, then please read our [Takedown Policy](#) and [contact the service](#) immediately

**DIELECTRIC AND ELECTRO-OPTICAL PROPERTIES OF SOME
CYANOBIPHENYL LIQUID-CRYSTALS**

ALI GHANADZADEH GILANI BSc MSc

A thesis submitted for the degree of

Doctor of Philosophy

The University of Aston in Birmingham

May 1995

This copy of the thesis has been supplied on condition that anyone who consults it is understood to recognise that its copyright rests with its author and that no quotation from the thesis and no information derived from it may be published without proper acknowledgement.

The University of Aston in Birmingham

**DIELECTRIC AND ELECTRO-OPTICAL PROPERTIES OF SOME
CYANOBIIPHENYL LIQUID CRYSTALS**

A thesis submitted for the degree of Doctor of philosophy

by

ALI GHANADZADEH GILANI

May 1995

Summary

A variety of methods have been reviewed for obtaining parallel or perpendicular alignment in liquid-crystal cells. Some of these methods have been selected and developed and were used in polarised spectroscopy, dielectric and electro-optic studies. Also, novel dielectric and electro-optic cells were constructed for use over a range of temperature.

Dielectric response of thin layers of E7 and E8 (eutectic mixture liquid-crystals) have been measured in the frequency range (12 Hz-100 kHz) and over a range of temperature (183-337K). Dielectric spectra were also obtained for supercooled E7 and E8 in the Hz and kHz range. When the measuring electric field was parallel to the nematic director, one loss peak (low-frequency relaxation process) was observed for E7 and for E8, that exhibits a Debye-type behaviour in the supercooled systems. When the measuring electric field was perpendicular to the nematic director, two resolved dielectric processes have been observed.

The phase transitions, effective molecular polarisabilities, anisotropy of polarisabilities and order parameters of three liquid crystal homologs (5CB, 6CB, and 7CB), 6OCB and three eutectic nematic mixtures E7, E8, and E₆₀₇ were calculated using optical and density data measured at several temperatures. The order parameters calculated using the different methods of Vuks, Neugebauer, Saupe-Maier, and Palffy-Muhoray are nearly the same for the liquid crystals considered in the present study. Also, the interrelationship between density and refractive index and the molecular structure of these liquid crystals were established.

Accurate dielectric and dipole results of a range of liquid-crystal forming molecules at several temperatures have reported. The role of the cyano-end group, biphenyl core, and flexible tail in molecular association, were investigated using the dielectric method for some molecules which have a structural relationship to the nematogens. Analysis of the dielectric data for solution of the liquid-crystals indicated a high molecular association, comparable to that observed in the nematic or isotropic phases.

Electro-optic Kerr effect were investigated for some alkyl cyanobiphenyls, their nematic mixtures and the eutectic mixture liquid-crystals E7 and E8 in the isotropic phase and solution. The Kerr constant of these liquid crystals found to be very high at the nematic-isotropic transition temperatures as the molecules are expected to be highly ordered close to phase transition temperatures. Dynamic Kerr effect behaviour and transient molecular reorientation were also observed in thin layers of some alkyl cyanobiphenyls.

Dichroic ratio *R* and order parameters of solutions containing some azo and anthraquinone dyes in the nematic solvent (E7 and E8), were investigated by the measurement of the intensity of the absorption bands in the visible region of parallel aligned samples. The effective factors on the dichroic ratio of the dyes dissolved in the nematic solvents were determined and discussed.

Keywords: Liquid crystals, Alkyl (alkoxy) cyanobiphenyls, Dielectric permittivity, Dielectric relaxation, Electro-optical birefringence.

Dedicated to my parents

Acknowledgements

I would like to express my thanks and gratitude to my supervisor, Dr Martin. S. Beevers for his valuable advice, help and support during this project.

I also extend my thanks to the academic and the technical staff of the department, in particular to Dr M. Yasin, Dr J. Robson, Dr D. Walton and Mr P. Tack for their valuable advice concerning certain experimental aspects of the work.

Thanks to my fellow postgraduate friends of the department who all proved to be friendly and helpful.

I am indebted to Dr Jenkins who kindly gave permission to use a PAAR DMA Density Meter and a GPR Refractometer.

Special thanks are due to my wife and my parents for their moral support and encouragement.

Thanks also due to my brother Dr Hossein Ghanadzadeh Gilani for his encouragement and valuable advice during my academic life

I highly acknowledge the financial support by the Ministry of Culture and Higher Education, Islamic Republic of Iran and thank Gilan University who gave me the opportunity to study for a Higher Degree.

I also thank BDH Company for support in the form of a generous gift of liquid-crystal samples.

ABBREVIATIONS

\AA	Ångstrom
A	Absorption
a	Internal field parameter (Saupe-Maier model)
a	Dimensions of long axis of the molecular ellipsoid
α	Polarisability
$\overline{\alpha}$	Mean polarisability
α_{el}	Electronic polarisability
α_{at}	Atomic polarisability
α_{or}	Orientation polarisability
β	Volume expansion coefficient
D	Electric displacement
d	Density
Δ	Depolarisation ratio
δ	optical phase difference
E	External electric field (applied field)
E_{eff}	Effective field
E_i	Internal field
E_L	Lorentz field
ϵ	Dielectric permittivity (static dielectric constant)
ϵ_{∞}	High frequency dielectric constant
ϵ_0	Dielectric constant of the free space ($8.854 \times 10^{-12} \text{ Fm}^{-1}$)
f	Frequency
γ_i	Internal field constant (Neugebauer method)
Hz	Hertz
η_{ii}	Internal field constant (Palffy-Muhoray method)
K	Kelvin
kV	Kilovolts

k	Boltzmann constant
κ	Length-to-breadth ratio
L	Nematic director
LC	Liquid crystal
λ	Wavelength
M	Molecular weight
ml	Millilitres
μ	Dipole moment
μm	Micrometres
N	Number of molecules per unit volume (cm^3)
N_A	Number of molecules per mole (Avogadro number, $6.02 \times 10^{23} \text{ mol}^{-1}$)
nm	Nanometres
n_{iso}	Isotropic refractive index
n_e	Extraordinary refractive index
n_o	Ordinary refractive index
P	Total polarisation
P_D	Dispersion polarisation
P_e	Electronic polarisation
P_a	Atomic polarisation
P_0	Orientation polarisation
R	Molar refraction
S	Order parameter
T_{NI}	Nematic-isotropic transition temperature, (clearing temperature, T_c)
τ	Relaxation time
V	Molar volume
V_n	Molar volume in the nematic phase
w/v	Weight per volume (g/100ml)
Ω	Shape factor

LIST OF CONTENTS

Title Page	1
Summary	2
Dedication	3
Acknowledgements	4
Abbreviations	5
List of contents	7
List of figures	16
List of tables	28

CHAPTER 1 INTRODUCTION

1.1	Introduction	34
1.2	Historical review	34
1.3	Types of liquid crystals	36
1.3.1	Nematic liquid crystals	37
1.3.2	Cholesteric liquid crystals	37
1.3.3	Smectic liquid crystals	38
1.4	Molecular structure and nematogen stability	39
1.5	The lateral and terminal attractions	40
1.6	Molecular theory (the mean field approximation)	41
1.7	Chemical classes	42
1.7.1	Benzyldeneanilines ($X = -CH=N-$)	43
1.7.2	Esters and diesters ($X = -CO.O-$)	44
1.7.3	Cyanobiphenyls ($X = \text{simple bond}$)	44
1.8	Physical properties of nematic liquid crystals	46
1.8.1	Dielectric properties	46
1.8.2	Optical anisotropy	47

1.8.3	Order parameters	48
1.9	Nematic liquid crystals in a uniform electric field	49
1.10	Nematic mixtures	51
1.11	Applications of liquid crystals	51
1.12	Scope of this work	53

CHAPTER 2 SURFACE TREATMENT FOR LIQUID CRYSTAL ALIGNMENT

2.1	Introduction	56
2.2	Parallel alignment of liquid crystals	57
2.3	Perpendicular alignment of liquid crystals	59
2.4	The effect of surface energy on surface alignment	61
2.5	The preparation of a liquid crystal cell	61
2.5.1	Liquid crystal cell with parallel alignment	63
2.5.1.1	Rubbing of the glass plates	63
2.5.1.2	Polyvinyl alcohol as a coating agent	63
2.5.1.3	Cellulose acetate butyrate as a coating agent	64
2.5.2	Liquid crystal cell with perpendicular alignment	65
2.5.2.1	Cleaning method	65
2.5.2.2	Lecithin as a surface active agent	65
2.5.2.3	HTAB as a surface active agent	66
2.6	Discussion of surface alignment	67
2.7	Stability of CAB as coating agent	68
2.8	Summary	69

CHAPTER 3 THE MICROSCOPIC STUDIES OF LIQUID CRYSTALS

3.1	Introduction	70
3.2	Electro-optic phenomena	70
	3.2.1 Dynamic scattering	70
3.3	Experimental	71
	3.3.1 The polarising microscope	71
	3.3.2 Materials	72
3.4	The microscopic observations	75
	3.4.1 The microscopic observation of E7	75
	3.4.2 The microscopic observation of alkyl cyanobiphenyls	78
	3.4.3 The microscopic observation of alkoxy cyanobiphenyls	78
	3.4.4 The microscopic and electro-optic studies of MBBA	82

CHAPTER 4 THE PHASE TRANSITION AND ORDER PARAMETER OF LIQUID CRYSTALS

4.1	Introduction	89
4.2	Theory	90
	4.2.1 Polarisation and polarisability	90
	4.2.2 The internal field E_i , (local field)	91
	4.2.3 Optical polarisability	93
	4.2.4 Polarisabilities in anisotropic medium	94
	4.2.4.1 The Vuks's Method	97
	4.2.4.2 The Neugebauer method	98
	4.2.4.3 The Saupe and Maier method	100
	4.2.4.4 The Palffy-Muhoray method	101
4.3	Experimental	104
	4.3.1 Refractive index measurements	104

4.3.2	Density measurements	105
4.3.2.1	Measuring method	105
4.3.2.2	Calibration of the density meter	106
4.4	Results	110
4.4.1	Densities	110
4.4.1.1	Change in molar volumes at T_{NI}	115
4.4.1.2	Volume expansion coefficients	118
4.4.2	Refractive indices	119
4.4.3	Determination of the order parameter	125
6.4.4	The internal field factor	131

CHAPTER 5 DIELECTRIC RESPONSE OF E7 AND E8 NEMATIC MIXTURE LIQUID CRYSTALS

5.1	Introduction	138
5.2	Theory	140
5.2.1	Dielectrics in static electric field	140
5.2.2	The relationship between dielectric constant and polarisation	140
5.2.3	Dielectrics in alternating fields	142
5.2.4	Dipole polarisation	142
5.2.5	Dielectric relaxation	143
5.2.6	Debye relaxation	145
5.2.7	Cole-Cole Plot	147
5.2.8	The Cole-Davidson arc	148
5.2.9	The activation energy	149
5.3	Experimental	150
5.3.1	Dielectric apparatus	150
5.3.2	Dielectric cell	150
5.3.3	Temperature control	151

5.3.4	Material	151
5.3.5	Measurements	151
5.4	Results of the measurement	152
5.4.1	Dielectric results for the electric field parallel to the director	152
5.4.2	Dielectric results for the electric field perpendicular to the director	158
5.5	Discussion	162
5.5.1	Temperature dependence of the static dielectric constant and dielectric loss	162
5.5.2	Dipole moments and relaxation mechanisms	165
5.5.2.1	The reorientation of μ_1 for ($E = E_{\parallel D}$)	167
5.5.2.2	The reorientation of $\mu_{2\perp}$ for ($E = E_{\perp D}$)	168
5.5.3	Activation energies	170
5.5.3.1	The activation energy for the low-frequency relaxation of μ_1 \parallel	170
5.5.3.2	The activation energy for the high-frequency relaxation ($\mu_{2\perp}$)	170

CHAPTER 6 DIPOLE MOMENT AND MOLECULAR ASSOCIATION

6.1	Introduction	173
6.2	Dielectric permittivity and dipole moment	175
6.2.1	The Debye theory	175
6.2.2	The Guggenheim method	177
6.2.3	The Onsager theory	177
6.2.4	The Kirkwood-Frohlich theory	178
6.2.5	Molecular association in solutions:	179

6.2.6	Anisotropy of the dielectric permittivity	181
6.3	Experimental	185
6.3.1	Materials	185
6.3.2	Dielectric apparatus	186
6.3.3	Dielectric cell	186
6.3.3.1	The cylindrical gold-plated dielectric cell	186
6.3.3.2	Small sample volume dielectric cell	188
6.3.4	Refractive index measurements	190
6.3.5	Density measurements	190
6.3.6	The measurement of the dielectric permittivity of solutions	190
6.4	Dielectric results for dilute solutions	193
6.5	Dielectric results for concentrated solutions	198
6.5.1	Intermolecular association of cyano compounds	204
6.6	Dielectric results for the pure phases of liquid crystals	208
6.6.1	Alkyl cyanobiphenyls in the isotropic phase	208
6.6.2	Alkoxy cyanobiphenyls	211
6.6.2.1	Dielectric results	211
6.6.2.2	The correlation factors in the nematic and isotropic phase	215
6.7	Types of associated pairs	221

CHAPTER 7 DYNAMIC LIGHT SCATTERING IN LIQUID CRYSTAL SOLUTIONS

7.1	Introduction	224
7.2	Theory	225
7.2.1	Light scattering	225
7.2.2	Depolarisation ratio	225
7.3	Measurement of I_v and I_h	228

7.4	Results and Discussion	228
-----	------------------------	-----

CHAPTER 8 THE ELECTRO-OPTIC KERR EFFECT OF CYANOBIPHENYL LIQUID CRYSTALS

8.1	Introduction	233
8.2	Theory	236
8.2.1	Optical anisotropy	236
8.2.2	The Kerr effect	237
8.2.3	Kerr effect theory	238
8.2.4	The electro-optic effect in the liquid crystals	239
8.3	Experimental	242
8.3.1	Kerr effect apparatus	242
8.3.1.1	Light source	244
8.3.1.2	Polariser/Analyser	244
8.3.1.3	Quarter-wave plate retarder	244
8.3.1.4	Photomultiplier	245
8.3.1.5	Signal display and recording	245
8.3.1.6	The high voltage power supply	246
8.3.2	The Kerr cell.	246
8.3.2.1	The spectrophotometer cuvette-type cell	247
8.3.2.3	The long-path length Kerr cell	249
8.3.4	The nulled-pulse technique	251
8.4	Results and Discussion	255
8.4.1	Kerr effect measurements in dilute solution	255
8.4.2.1	Calculation of molar Kerr constant	258
8.4.2	Kerr Effect measurements of the isotropic phase	261

CHAPTER 9 THE DYNAMIC ELECTRIC BIREFRINGENCE OF LIQUID-CRYSTALS

9.1	Introduction	268
9.2	Theory	269
9.2.1	The optical transients	269
9.2.2	Dynamic behaviour and rotational diffusion	270
9.3	Experimental	272
9.3.1	The electro-optical cell	272
9.3.2	Measuring apparatus	274
9.3.3	Analysis of time dependent optical transients	274
9.4	Results and Discussion	277
9.4.1	Electric field dependence of relaxation times	278
9.4.1	Temperature dependence of relaxation times	280
9.5	Dynamic Kerr studies-using MathCad 4.0	284

CHAPTER 10 GUEST-HOST INTERACTIONS IN NEMATIC LIQUID-CRYSTALS

10.1	Introduction	290
10.2	Theory	292
10.2.1	Absorption anisotropy	292
10.2.2	Order parameter of a dichroic dye	293
10.2.3	Infrared-dichroism in nematic liquid crystals	296
10.2.4	IR-dichroism in nematics without using polarised light	297
10.2.5	The interpretation of band intensity changes	298
10.2.6	Electronic color-switching interaction	299
10.2.7	The solute-solvent intermolecular interaction	300
10.3	Experimental	303

10.3.1	Materials	303
10.3.2	Preparation of samples	303
10.3.3	Measurements	304
10.4	Results and Discussion	306
10.4.1	Visible spectroscopy	306
10.4.1.1	The direction of polarised light relative to the director	313
10.4.1.2	The effect of substitution on the dichroic ratio	314
10.4.1.3	The effect of temperature on the dichroic ratio	316
10.4.1.4	The effect of cell gap on the dichroic ratio	318
10.4.1.5	The effect of dye concentration on the dichroic ratio	320
10.4.2	Effect of electric field strength on the degree of color switching	320
10.4.3	Infrared spectroscopy	324
 CHAPTER 11 CONCLUSIONS AND FUTURE WORK		
11.1	Conclusions	328
11.2	Future work	337
 REFERENCES		339
 APPENDIX A		358
APPENDIX B		362
APPENDIX C		367
APPENDIX D		371
APPENDIX E		374

LIST OF FIGURES

Figure		Page
Figure 1.1	Molecular order in the nematic phase.	37
Figure 1.2	Molecular order in the cholesteric phase.	38
Figure 1.3	Molecular order in the nematic phase.	39
Figure 1.4	N-methoxybenzylidene-4-n-butylaniline (MBBA).	43
Figure 1.5	4-n-alkyl- and 4-n-alkoxy-4'-cyanobiphenyls.	45
Figure 1.6	The directions of the maximum polarisability and dipole moment of the nematic molecule.	47
Figure 1.7	The orientation of long molecular axis of a nematic molecule and the optic axis (director).	48
Figure 1.8	Schematic representation of the orientations before and after the application of an electric field.	50
Figure 1.9	Schematic representation of the various techniques used in the present studies.	55
Figure 2.1	Bell-Jar arrangement of angular deposition. The control substrate is placed in the centre of the area.	58
Figure 2.2	Chemical formula for silane coupling agent and its geometric relationship to a substrate.	59
Figure 2.3	Homeotropic alignment by the alkoxy silane.	60
Figure 2.4	Cross-section of the experimental liquid-crystal cell. The inner surface of the cell were covered by In/Sn oxide.	62
Figure 2.5	Side-view of the parallel alignment.	64

Figure 2.6	Cross-sectional of the experimental cell with homeotropic alignment.	66
Figure 2.7	Dipolar interactions between polar groups of the surface agent polar groups of liquid-crystals and silanol groups of glass surfaces.	67
Figure 2.8	Homeotropic alignment by van der Waal's interactions between nonpolar alkyl groups of the liquid-crystal molecules and aligned nonpolar alkyl groups of lecithin as a surface agent.	68
Figure 3.1	The polarising microscope.	71
Figure 3.2	Schematic of a nematic liquid-crystal cell with parallel wall alignment when the direction of grooves are, a) parallel, b) perpendicular, c) at 45° to the direction of the polarised light.	76
Figure 3.3	Parallel aligned film of nematic mixture (E7) between glass plates which is coated by rubbed CAB at 22 °C.	77
Figure 3.4	Parallel aligned film of E7 at 22 °C; film between rubbed glass slides; thickness 12.5 µm; crossed polarisers.	77
Figure 3.5	Smectic A focal-conic texture of 8CB; film between glass slides at 22 °C; thickness 12.5 µm; crossed polarisers.	79
Figure 3.6	Smectic A focal-conic texture of 8CB; film between glass slides at 22 °C ; thickness 12.5 µm; crossed polarisers.	79
Figure 3.7	The nematic-isotropic transition, T_{NI} , and melting point, T_m , as a function of the number of carbon atoms, n , in the alkoxy chain of 4- n -alkoxy-4-cyanobiphenyls.	80
Figure 3.8	Phase diagram of nematic mixtures of 6OCB/7OC; eutectic mixture (41.5% 6OCB+ 58.5% 7OCB).	80
Figure 3.9	Crystalline phase of 6OCB/7OCB at 23 °C; film between glass slides; thickness 12.5 µm; crossed polarisers.	81

Figure 3.10	Nematic phase of 6OCB/7OCB at 74.8 °C; film between glass slides; thickness 12.5 µm; crossed polarisers.	81
Figure 3.11	Optical texture of MBBA at a field strength of 12 V and a frequency about 100 Hz at 22 °C; thickness 12.5 µm; crossed polarisers.	84
Figure 3.12	William domains in a 12.5 µm thick sample of MBBA at 22 °C and 15V(100 Hz); crossed polarisers.	84
Figure 3.13	Dynamic scattering in a 12.5 µm thick sample of MBBA at 22 °C and 25V(100 Hz); crossed polarisers.	85
Figure 3.14	Charge segregation and the resulting transverse field F_x in an applied field F_z if the conductivity along the nematic axis is larger than the perpendicular to it.	85
Figure 3.15	Cross section through the flow and orientation patterns of Williams domains, indicated by velocity vectors and rod-like molecules.	86
Figure 3.16	Frequency dependence of threshold voltage for dynamic scattering in MBBA; sample thickness, 12 µm.	86
Figure 3.17	Schlieren texture in a 12.5 µm thick sample of MBBA showing "nucleated domains". The brushes (4) can clearly be seen; film between glass slides at 22 °C; crossed polarisers.	88
Figure 4.1	The internal field, $E_i = E_{\text{eff}} = E + E_p$.	92
Figure 4.2	Ellipsoid of indices.	95
Figure 4.3	A beam of light with two orthogonal field components can be split into two beams by a doubly refracting crystal.	96
Figure 4.4	Density for cyclohexane plotted as a function of temperature.	109
Figure 4.5	Molar volume of pentyl cyanobiphenyl, 5CB, as a function of temperature.	111

Figure 4.6	Molar volume of heptyl cyanobiphenyl, 7CB, as a function of temperature.	112
Figure 4.7	Molar volume of hexyl cyanobiphenyl, 6CB, as a function of temperature.	112
Figure 4.8	Molar volume of hexoxy cyanobiphenyl, 6OCB, as a function of temperature.	113
Figure 4.9.	Molar volume of E7 as a function of temperature.	113
Figure 4.10	Molar volume of E8 as a function of temperature.	114
Figure 4.11	Molar volume of eutectic mixture, E ₆₀₇ , (6OCB/7OCB) as a function of temperature.	114
Figure 4.12	Molar volume of hexyl and heptyl cyanobiphenyl as a function of temperature.	115
Figure 4.13	The nematic-isotropic transition, T_c , (dashed lines) and molar volume increment at the transition temperature (full lines) as a function of the number of carbon atoms, n , in the alkyl chain of 4- n -alkyl-4- cyanobiphenyls.	116
Figure 4.14	Variation of molar volumes of the three liquid crystal homologs (5CB, 6CB, and 7CB) as function of reduced temperature.	117
Figure 4.15	Molar structures of 7CB and 6OCB.	117
Figure 4.16	Molar volume of E7 and E8 nematic mixtures liquid crystals as a function of temperature.	118
Figure 4.17	Refractive indices of the nematic phase (n_o , n_e) and of the isotropic phase (n_{iso}) at different temperatures for eutectic nematic mixtures E ₆₀₇ , E7, and E8.	120
Figure 4.18	Refractive indices of the nematic phase (n_o , n_e) and of the isotropic phase (n_{iso}) at different temperatures for 6OCB, 7OCB, and 8OCB.	121

Figure 4.19	Refractive indices of the nematic phase (n_o , n_e) and of the isotropic phase (n_{iso}) at different temperatures for 5CB, 6CB, and 7CB.	121
Figure 4.20	The calculated order parameter S by different methods versus temperature for E7 and E8 nematic mixture liquid crystals.	130
Figure 4.21	The calculated order parameter S versus temperature for E _{6O7} and 6OCB.	130
Figure 4.22	The Saupe-Maier internal field factor “ a ” as function of temperature for 5CB, 6CB, 7CB, E7, and E8.	134
Figure 4.23	The anisotropy of internal field factor ($\Delta\gamma = \gamma_o - \gamma_e$) as a function of temperature for 5CB, 6CB, 7CB, E7, and E8.	135
Figure 4.24	The plots of $(1 - d_i/d_n)/(T_{NI} - T)$ vs $S^2/(T_{NI} - T)$ for three homologous cyanobiphenyl liquid crystals.	137
Figure 5.1	The polarisation of the dielectric molecules due to displacement of charges.	141
Figure 5.2	Current-voltage diagram of a dielectric with loss.	145
Figure 5.3	Cole-Cole plot, (a) Arc plot for a Debye dielectric; (b) Arc plot for a dielectric with a Cole-Cole distribution characterised by the parameter α .	148
Figure 5.4	The dielectric loss of E7 as function of frequency and temperature. The measuring electric field is parallel to the director ($E = E_{\parallel D}$).	154
Figure 5.5	The effect of temperature and frequency on dielectric constant of E7 ($E = E_{\parallel D}$).	154
Figure 5.6	The dielectric loss of E8 as function of frequency and temperature. The measuring electric field is parallel to the director ($E = E_{\parallel D}$).	155

Figure 5.7	The effect of temperature and frequency on dielectric constant of E8 ($E = E_{\parallel D}$).	155
Figure 5.8	Cole-Cole plot for E7 at several temperatures, in which measuring electric field is parallel to the director ($E = E_{\parallel D}$).	156
Figure 5.9	Cole-Cole plot for E8 at several temperatures, in which measuring electric field is parallel to the director ($E = E_{\parallel D}$).	157
Figure 5.10	The dielectric loss of E7 as function of frequency and temperature. The measuring electric field is perpendicular to the director.	159
Figure 5.11	The effect of temperature and frequency on dielectric constant of E7 ($E = E_{\perp D}$).	159
Figure 5.12	Cole-Cole plot for E7 at several temperatures ($E = E_{\perp D}$).	160
Figure 5.13	The dielectric loss of E8 as function of frequency and temperature. The measuring electric field is perpendicular to the director.	161
Figure 5.14	Temperature dependence of the dielectric constants measured at 1kHz for nematic mixture of E7.	162
Figure 5.15	The dielectric loss at 1kHz of E8 plotted against temperature in the supercooled and glassy states with electric field parallel to the nematic director.	163
Figure 5.16	The temperature dependence of the dielectric loss of E8 at 1kHz for the electric field perpendicular to the nematic director.	163
Figure 5.17	Phase transitions for E7.	164
Figure 5.18	Nematic mixture of E7. Direction of main dipole moments are indicated by \Rightarrow .	165
Figure 5.19	Nematic mixture of E8.	165
Figure 5.20	Schematic representation of dipole components in an aligned nematogen.	166

Figure 5.21	The Activation diagram, $\log f(\text{Hz})$ vs. $1/T$ for E8 in the supercooled nematic state.	172
Figure 5.22	The Activation diagram, $\log f(\text{Hz})$ vs. $1/T$ for E8 in the supercooled nematic state.	172
Figure 6.1	Simple forms of association, due to dipole-dipole interaction, in which two molecules may associate to give a dimer.	180
Figure 6.2	Dielectric cell A used for measurements on dilute solutions, A) screw-top lid, B) outer cylinder, C) inner cylindrical lid, D) perforated lid, E) stopper.	187
Figure 6.3	Dielectric cell B. (a) Cross-sectional view, (b) Top-view.	189
Figure 6.4	The static dielectric permittivity of cyclohexane and 1,4-dioxane as a function of temperature.	192
Figure 6.5	Dielectric increments, Δ , of solutions of cyanobiphenyl, CB, in 1,4-dioxane at 25.0 °C versus concentration, c .	194
Figure 6.6	Dielectric permittivity of solutions of E7 in cyclohexane plotted as a function of temperature.	197
Figure 6.7	The temperature dependence of the dipole moment of E7 in cyclohexane.	197
Figure 6.8	The dielectric permittivity of solutions of hexyl and heptyl cyanobiphenyl liquid crystals in cyclohexane and cyanobiphenyl in 1,4-dioxane as a function of mole fraction of solute at 25 °C.	199
Figure 6.9	The dielectric permittivity of solutions of pentoxy and octoxy cyanobiphenyl liquid crystals and octoxy cyanophenyl, in 1,4-dioxane as a function of the mole fraction of solute.	199
Figure 6.10	The density, d_{12} , of solutions of 5OCB, 8OCB and 8OCP (not-mesogenic), in 1,4-dioxane as a function of the mole fraction of solute, f_2 , at 25 °C.	200

Figure 6.11	The refractive index, n_{12}^2 , of solutions of 5OCB, 8OCB and 8OCP in 1,4-dioxane as a function of the mole fraction of solute, f_2 , at 25 °C.	200
Figure 6.12	The dipole moment of solutions of 6CB in cyclohexane as a function of the mole fraction of solute, f_2 , at 25 °C.	205
Figure 6.13	The dipole correlation factor, g , of solutions of hexyl, heptyl cyanobiphenyls 6CB, 7CB and cyanobiphenyl, CB, in cyclohexane as a function of the mole fraction of solute, f_2 , at 25 °C.	207
Figure 6.14	The correlation factor, g , of solutions of pentoxy, octoxy cyanobiphenyls and octoxy cyanophenyl, in 1,4-dioxane as a function of the mole fraction of solute, f_2 , at 25 °C.	207
Figure 6.15	The effective dipole moment (m_{eff}) of pentyl, hexyl, and heptyl cyanobiphenyls (5CB, 6CB, and 7CB) in the isotropic phase and in the nematic phase close to the clearing temperatures, T_C .	210
Figure 6.16	Temperature variation of the permittivity of 6OCB, 7OCB, and a eutectic mixture of hexoxy and heptoxy cyanobiphenyls E6O7 (41.5 : 58.5).	212
Figure 6.17	Isotropic dielectric permittivity of n-alkoxy cyanobiphenyls at several temperatures.	212
Figure 6.18	Temperature variation of the permittivity of 8OCB and permittivity of 8OCB in surface treated by lecithin.	213
Figure 6.19	Adsorption of an 8OCB molecule on a stainless-steel surface.	214
Figure 6.20	Temperature variation of the perpendicular components dielectric permittivity, ϵ_{\perp} of 7OCB.	215
Figure 6.21	The effective dipole moment (μ_{eff}) of alkoxy cyanobiphenyls in the isotropic phases as a function of reduced temperature.	217

Figure 6.22	Possible arrangement of molecules in the anti-parallel association of alkyl cyanobiphenyl liquid crystals.	222
Figure 6.23	The configuration of the neighbouring molecules in the 6OCB dimer. Close contact CN-CN is shown by broken lines with distance in Å.	222
Figure 7.1	Depolarisation of scattered light.	226
Figure 7.2	Depolarisation ratio, Δ_{12} , for hexyl cyanobiphenyl, 6CB, in cyclohexane plotted as a function of solute mole fraction, f_2 .	231
Figure 7.3	Depolarisation ratio for dilute solutions of pentyl, hexyl and octyl cyanobiphenyls in cyclohexane plotted as a function of solute mole fraction, f_2 .	231
Figure 8.1	Diagrammatic representation of anisotropic molecules in: a) the absence of an electric field, b) in an electric field.	236
Figure 8.2	The Schematic diagram of the Kerr effect equipment	243
Figure 8.3	The Kerr effect apparatus, the optical bench is enclosed in a totally black-painted cabinet.	243
Figure 8.4	Construction of Kerr cell A	247
Figure 8.5	The calibration plot obtained for correction of the Kerr cell temperatures.	248
Figure 8.6	The long-path-length Kerr cell B	250
Figure 8.7	Relative orientational setting of, a) the optical components, b) electric vectors components of light.	252
Figure 8.8	Schematic diagram of typical optical pulse recording during the pulse nulling procedure.	254

Figure 8.9	The measured phase-difference, δ , against the square of applied voltage for the different weight fractions, w_2 , of the solutions of 5CB in cyclohexane.	256
Figure 8.10	Kerr constants B_{12} , of solutions of alkyl cyanobiphenyls in cyclohexane at 25 °C.	258
Figure 8.11	Induced birefringence, Δn , as a function of applied field, E , for pentyl and heptyl cyanobiphenyls mixtures F1 (71: 29), at the several temperatures.	262
Figure 8.12	Temperature dependence of B for 5CB, F1 and F2 using the pulsed d.c. field method.	266
Figure 8.13	Temperature dependence of B^{-1} for 5CB, F1 and F2 using the pulsed d.c. field method.	266
Figure 8.14	Temperature dependence of B^{-1} for E7 using the pulsed d.c. field method.	267
Figure 8.15	Temperature dependence of B^{-1} for E8 using the pulsed d.c. field method.	267
Figure 9.1	The optical response (lower trace) to a pulse applied field shown as a function of time.	269
Figure 9.2	Construction of the Kerr cell for nematic phase.	273
Figure 9.3	Side view of the experimental cell with homeotropic alignment.	273
Figure 9.4	Optical arrangement for the measurement of the dynamic behaviour of a thin liquid crystal cell.	274
Figure 9.5	Analysis of time dependent optical transient.	275
Figure 9.6	Determination of I_0	276
Figure 9.7	Recorder plot showing the optical response for pentyl cyanobiphenyl, 5CB, as a function of time.	277

Figure 9.8	Rise of normalised birefringence at various applied voltage for 5CB.	279
Figure 9.9	Decay of normalised birefringence at various applied voltage for 6CB.	279
Figure 9.10	Rise curve of normalised birefringence of 5CB obtained at various temperatures using a fixed voltage of 180 V.	280
Figure 9.11	Analysis of the birefringence-decay curve for 6CB at 20.4°C.	281
Figure 9.12	The activation diagram, $\ln\tau$ vs. $1/T$ for 6CB in the nematic state.	282
Figure 9.13	The variation of the electrically-induced phase retardation with time for 6CB in 28.2 °C.	286
Figure 9.14	The intensity of light transmitted by the Kerr cell for 6CB.	286
Figure 9.15	The intensity of light transmitted by the Kerr cell for 6CB.	287
Figure 9.16	The intensity of light transmitted by the Kerr cell for 6CB.	288
Figure 10.1	Deviation of dichroic dye geometric axis, M, and oscillator transition, T, from liquid crystal director, L.	296
Figure 10.2	The Intensity differences due to the molecular orientation change.	298
Figure 10.3	Guest-host interaction in a nematic liquid crystal.	299
Figure 10.4	Polarised absorption spectra of 1% Sudan black B in nematic solvent (E7).	309
Figure 10.5	Polarised absorption spectra of 1% Sudan III in the oriented nematic phase of E7. The electric vector of light is polarised parallel and perpendicular to the nematic director.	309
Figure 10.6	Polarised absorption spectra of 1% nematic solution of Oil red.	310

Figure 10.7	Polarised absorption spectra of 1% Indophenol blue in the nematic solvent of E7.	310
Figure 10.8	Molecular structure of anthraquinone dyes with a symmetry of C_2 .	311
Figure 10.9	Polarised absorption spectra of 1% Solvent green 3 in the oriented nematic phase of E8 at 22°C.	312
Figure 10.10	Transmittance of Sudan black B as a function of the angle between direction of polarised light and nematic director.	313
Figure 10.11	Polarised absorption spectra of 1% nematic solution of Sudan-black B at different angle (ϕ) between polarised light and the nematic director.	314
Figure 10.12	The molecular structures of sudan III and Oil red.	315
Figure 10.13	Temperature dependence of the order parameter of Sudan black B in E7 liquid crystal.	318
Figure 10.14	The order parameter of the nematic solution of Sudan black B as a function of the cell gap.	319
Figure 10.15	Molecular orientation in the planar cell for field-off and field-on condition.	322
Figure 10.16	The voltage dependence of transmittances of $(P_{\parallel})_{620\text{nm}}$ and $(P_{\parallel})_{420\text{nm}}$ in the planar alignment (sudan black B-E7) cell.	323
Figure 10.17	The voltage dependence of transmittances of polarised light with the wavelength of 585 nm for 1% indophenol blue dissolved in E7.	323
Figure 10.18	The FT infrared spectra of E7 in the nematic state (N), and in the isotropic phase (I).	326
Figure 10.19	The FT infrared spectra of octyl cyanobiphenyl, 8CB, in the nematic state (n), and in the isotropic phase (I).	327

LIST OF TABLES

Table		page
Table 1.1	Summary of some important nematic devices.	52
Table 2.1	Liquid crystal (E7) alignment on four kinds of CAB films.	69
Table 3.1	The effect of electric field on molecular alignment of MBBA.	83
Table 4.1	Temperature dependence of the density for air and H ₂ O.	108
Table 4.2	Period reading (T) for Air and H ₂ O.	108
Table 4.3	Period reading and temperature dependence of the density for cyclohexane.	109
Table 4.4	Transition temperatures of the nematic liquid crystals.	110
Table 4.5	The molar volume, molecular volume, percent transition volume change and the mean expansion coefficients in the nematic and isotropic phases.	119
Table 4.6	The effective polarisabilities α_o and α_e at several temperatures for 5CB calculated using different theoretical models.	122
Table 4.7	The effective polarisabilities α_o and α_e at several temperatures for 6CB calculated using different theoretical models.	122
Table 4.8	The effective polarisabilities α_o and α_e at several temperatures for 7CB calculated using different theoretical models.	123
Table 4.9	The effective polarisabilities α_o and α_e at several temperatures for 6OCB calculated using different theoretical models.	123
Table 4.10	The effective polarisabilities α_o and α_e at several temperatures for E ₆₀₇ calculated using different theoretical models.	124

Table 4.11	The effective polarisabilities α_o and α_e at several temperatures for E7 calculated using different theoretical models.	124
Table 4.12	The effective polarisabilities α_o and α_e at several temperatures for E8 calculated using different theoretical models.	125
Table 4.13	Values of the mean polarisabilities, $\bar{\alpha}$, and the anisotropies of polarisability calculated by different methods.	127
Table 4.14	Values of the order parameter S at several temperatures for 5CB calculated by different methods.	128
Table 4.15	Values of the order parameter S at several temperatures for 6CB calculated by different methods.	128
Table 4.16	Values of the order parameter S at several temperatures for 7CB calculated by different methods.	128
Table 4.17	Values of the order parameter S at several temperatures for 6OCB calculated by different methods.	128
Table 4.18	Values of the order parameter S at several temperatures for E ₆₀₇ calculated by different methods.	129
Table 4.19	Values of the order parameter S at several temperatures for E7 calculated by different methods.	129
Table 4.20	Values of the order parameter S at several temperatures for E8 calculated by different methods.	129
Table 4.21	The temperature dependence of the internal field constants for 5CB.	131
Table 4.22	The temperature dependence of the internal field constants for 6CB.	132
Table 4.23	The temperature dependence of the internal field constants for 7CB.	132

Table 4.24	The temperature dependence of the internal field constants for 6OCB.	132
Table 4.25	The temperature dependence of the internal field constants for E _{6O7} .	132
Table 4.26	The temperature dependence of the internal field constants for E7	133
Table 4.27	The temperature dependence of the internal field constants for E8.	133
Table 4.28	Values of the length-to-breadth ratio κ for the various nematic liquid-crystals calculated using Palffy-Muhoray <i>et al.</i> method.	136
Table 5.1	Dielectric absorption of supercooled E7 for parallel relaxation.	153
Table 5.2	Dielectric absorption of supercooled E8 for parallel relaxation.	153
Table 5.3	Dielectric absorption of supercooled E7 for ($E_{\perp D}$).	160
Table 5.4	Dielectric absorption of supercooled E7 for ($E_{\perp D}$).	160
Table 5.5	The frequency of maximum loss (f_m) for E7 and E8 for the relaxation of $\mu_{2\perp}$	171
Table 6.1	Compounds chosen for study.	185
Table 6.2	Dielectric permittivities, ϵ , for pure standard liquid cyclohexane and 1,4-dioxane.	192
Table 6.3	Physical properties of cyclohexane and 1,4-dioxane.	193
Table 6.4	The molecular dipole moment of the cyano biphenyl and its derivatives obtained in non-polar solvent at 25.0 °C.	196
Table 6.5	The effective dipole moment of cyanobiphenyl in 1,4-dioxane as a function of the solute mole fraction at 25.0 °C.	201

Table 6.6	The effective dipole moment of octyloxycyanophenyl in 1,4 dioxane as a function of the solute mole fraction at 25 °C.	201
Table 6.7	The effective dipole moment of hepty cyanobiphenyl in cyclohexane as a function of the solute mole fraction at 25.0 °C.	202
Table 6.8	The effective dipole moment of hexyl cyanobiphenyl in cyclohexane as a function of the solute mole fraction at 25.0 °C.	202
Table 6.9	The effective dipole moment of octyloxy cyanobiphenyl in 1,4-dioxane as a function of the solute mole fraction at 25.0 °C.	203
Table 6.10	The effective dipole moment of pentyloxy cyano biphenyl in cyclohexane as a function of the solute mole fraction at 25.0 °C.	203
Table 6.11	The dielectric permittivities, effective dipole moment and Kirkwood factor, g, of n-pentyl cyanobiphenyl, 5CB, in the isotropic phase.	209
Table 6.12	The dielectric permittivities, effective dipole moment and Kirkwood factor, g, of n-hexyl cyanobiphenyl, 6CB, in the isotropic phase.	209
Table 6.13	The dielectric permittivities, effective dipole moment and Kirkwood factor, g, of n-pentyl cyanobiphenyl, 5CB, in the isotropic phase	210
Table 6.14	The dielectric permittivity and effective dipole moment of n-hexoxy cyanobiphenyl, 6OCB, in the isotropic phase.	216
Table 6.15	The dielectric permittivity and effective dipole moment, of n-heptoxy cyanobiphenyl, 7OCB, in the isotropic phase.	216
Table 6.16	The dielectric permittivity and effective dipole moment of mixture E ₆₀₇ composed of hexoxy and heptoxy cyanobiphenyl in the isotropic phase.	216
Table 6.17	The dielectric permittivity and effective dipole moment of n-octyloxy-cyanobiphenyl, 8OCB, in the isotropic phase.	217
Table 6.18	The molecular parameters of hexoxy, heptoxy and octoxy cyano-	

	biphenyls (6OCB, 7OCB and 8OCB).	219
Table 6.19	Dipole correlation factors for hexoxy cyanobiphenyl, 6OCB, in the nematic phase.	220
Table 6.20	Dipole correlation factors for heptoxy cyanobiphenyl, 7OCB, in the nematic phase.	220
Table 7.1	Depolarisation ratio and anisotropy parameter for pure cyclohexane.	229
Table 7.2	Rayleigh depolarisation ratios Δ_{12} , of solutions of pentyl, hexyl and octyl cyanobiphenyls in cyclohexane at 25.0 °C.	229
Table 7.3	Anisotropy parameter for alkyl cyanobiphenyls solutions at 25.0°C.	232
Table 8.1	The measured phase-difference, δ , induced at several voltage for toluene and cyclohexane at 25°C.	255
Table 8.2	Experimental Kerr constants B_{12} , of solutions of pentyl, hexyl and octyl cyanobiphenyls in cyclohexane at 25 °C.	257
Table 8.3	Kerr constant, B_1 , dielectric permittivity, ϵ_1 , refractive index, n_1 , and density, d_1 , of cyclohexane obtained at 25.0 °C.	259
Table 8.4	Molar Kerr constant, $_mK_{12}$, Kerr constant, B_{12} , dielectric permittivity, ϵ_{12} , refractive index, n_{12} , and density, d_{12} , of solutions of 5CB in cyclohexane obtained at 25.0 °C.	260
Table 8.5	Molar Kerr constant, $_mK_{12}$, Kerr constant, B_{12} , dielectric permittivity, ϵ_{12} , refractive index, n_{12} , and density, d_{12} , of solutions of 6CB in cyclohexane obtained at 25.0 °C.	260
Table 8.6	Kerr constants, B , of 5CB for $\lambda = 632.8$ nm.	262
Table 8.7	Kerr constants, B , of F1 and F2 for $\lambda = 632.8$ nm.	263
Table 8.8	Kerr constants, B , of E7 and E8 for $\lambda = 632.8$ nm.	263

Table 9.1	The rise and decay times for 5CB.	278
Table 9.2	The decay times for pentyl cyanobiphenyl in the nematic phase.	282
Table 9.3	The decay times for hexyl cyanobiphenyl in the nematic phase.	282
Table 9.4	The decay times for octyl cyanobiphenyl in the nematic phase.	282
Table 9.5	The Kerr constant (B) for pentyl cyanobiphenyl (5CB) in the nematic phase ($\delta_{\max} = 180^\circ$).	289
Table 9.6	The Kerr constant (B) for hexylcyanobiphenyl (6CB) in the nematic phase ($\delta_{\max} = 180^\circ$).	289
Table 10.1	Liquid crystals used in the experiments.	303
Table 10.2	Dichroic ratios (R) and order parameters (S) measured for dyes used in the guset-host experiments.	306
Table 10.3	Order paramets of anthraquinone dyes and Sudan black B.	312
Table 10.4	Transmission (T) of Sudan black B at different angles (ϕ).	313
Table 10.5	Temperature dependence of the order parameter of Sudan black B.	317
Table 10.6	The dichroic ratio and order parameter (Sudan black B in E7) dependence on thickness of spacer.	319
Table 10.7	The salient features of the visible spectrum of a 1% solution of Sudan black B in the oriented nematic E7.	321
Table 10.8	Polarised spectra data of a 1% solution of Indophenol blue in the oriented nematic E7.	322
Table 10.10	Vibrational assignments and dichroic data for E7.	325
Table 10.11	Vibrational assignments and dichroic data for 8CB.	325

CHAPTER 1

INTRODUCTION

1.1 Introduction

A crystalline phase (anisotropic) is characterised by precise, long-range, positional and orientational order. A typical (isotropic) liquid phase is characterised by random long-range molecular position and orientation. In a liquid, the orientation of a molecule does not provide information about other molecules in the liquid. There is an intermediate phase or mesophase that lies between a liquid and a solid. A crystal can lose positional order, while still retaining its orientational order. In this case the mesophase can flow freely, even if only along certain selected directions, while it retains the anisotropy of almost all its physical properties. Such a mesophase is called a liquid-crystal and is generally characteristic of materials with molecules which are highly anisotropic in shape. It is then usually the case that their optical, electric and elastic properties are anisotropic. Subsequent heating of the mesophase will result in the break-up of its residual ordering (orientational ordering) and the material converts to an isotropic liquid.

1.2 Historical review

The existence of a liquid-crystalline phase was first shown by an Austrian botanist Friedrich Reinitzer¹ (1888), who was measuring the melting point of cholesteryl benzoate. He found that the compound exhibited two apparent melting points. It first melted to a cloudy liquid at 145 °C and then became a clear liquid at a higher temperature at 179 °C. Then Otto Lehmann² found that the mesophase had an unusual effect on the polarised light. When he looked at it through cross polarisers, the mesophase appeared brightly coloured, unlike a normal liquid which would appear dark. Finally, in 1890 Lehmann accepted that it was a very soft liquid, and he named it Liquid-crystal. These

new states of matter were soon observed in other organic compounds. The first completely synthetic organic compound found to exhibit such characteristics was p-azoxyanisole³.

It became clear that the liquid-crystalline behaviour tended to occur in systems in which the molecules (a) are rod-like and anisotropic, (b) are rigid along the long axis, with double bonds, and (c) have strong dipoles along the molecular axis. Therefore, aromatics are useful for making liquid-crystalline phases, due to their rigidity, planarity and polarisability of the aromatic nuclei⁴.

In terms of their potential applications, liquid-crystals remained like Sleeping Beauty for almost 80 years, until the mid-60s, when an American James L. Ferguson⁵ perceived that certain liquid-crystals (cholesteric) could be used as temperature indicators. Also, George Heilmeyer⁶, discovered the so-called "dynamic scattering" of light through liquid-crystals in an electric field. His publication of this discovery in 1968 was the starting signal for a headlong process of technical development, based on the principle of permitting or preventing the transmission of light in predetermined patterns through a liquid-crystal phase.

Liquid-crystal technology is determined by the same rules of chemistry that apply to molecules and their structure. The correct choice of molecule is crucial in order to ensure liquid-crystal properties and a potential for technical applications. Therefore, considerable basic research has been directed towards the synthesis of new compounds with the desirable liquid-crystalline range, optical and electrical properties. The major revolution in the use of liquid-crystals came in 1973 with the discovery at Hull University by Gray, Harrison and Nash of the cyanobiphenyls⁷ and the evaluation of their properties at the Royal Signals and Radar Establishment (R.S.R.E). These compounds were relatively stable chemically and photochemically and produced reliable liquid-crystal displays (LCDs), such as fast switching times. These compounds are still key materials in an

industry which has made such rapid progress in the last few years that the LCD is now as familiar as the cathode ray tube (CRT).

1.3 Types of liquid-crystal

Liquid-crystals existing at temperatures between the isotropic liquid and crystalline phases are called thermotropic liquid-crystals. They can be divided into three groups⁸;

a) *The nematic mesophase* - a turbid but mobile state. On surfaces such as glass, this mesophase frequently adopts a characteristic "threaded" texture, clearly visible between crossed polaroids. The word nematic is in fact derived from the Greek nematos thread-like.

b) *The smectic mesophase* - a turbid, viscous state, with certain properties reminiscent of soaps. The term smectic again stems from the Greek smectos -i.e. soap-like.

c) *The cholesteric mesophase* - a turbid and mobile mesophase exhibiting some unique optical characteristics, quite different from those of the smectic and nematic mesophases. The majority of compounds exhibiting this type of behaviour are derived from cholesterol or other sterol systems.

If a liquid-crystalline phase is produced by the action of the solvent, then the phenomenon is referred to as *lyotropic mesomorphism*⁹ (solvent induced). Lyotropic liquid-crystals are formed by mixing amphiphilic compounds with other liquids. Amphiphilic molecules have both hydrophilic (polar) parts and hydrophobic parts which interact with the solvent to form multi-molecular ordered units termed micelles. Detergents in water are an example of lyotropic liquid-crystals, and exist within definite concentration ranges of the bi-component system.

1.3.1 Nematic liquid-crystals

Nematic liquid-crystals¹⁰ are characterised by random molecular position as in the ordinary liquid phase, and differ from the liquids by a long-range orientational order. The nematic phase consists of rod-like molecules aligned parallel to each other, as shown in Figure 1.1. Therefore, their long molecular axes are parallel to a common direction D (the director). In practice, thermal motions of individual molecules cause deviation from the ideal case of parallel alignment, but the average bulk director is invariant^{9,10}. The molecules can rotate (freely or hindered) around both their short and long axes. Due to the orientational order, nematic liquid-crystals are uniaxial with respect to all physical properties.

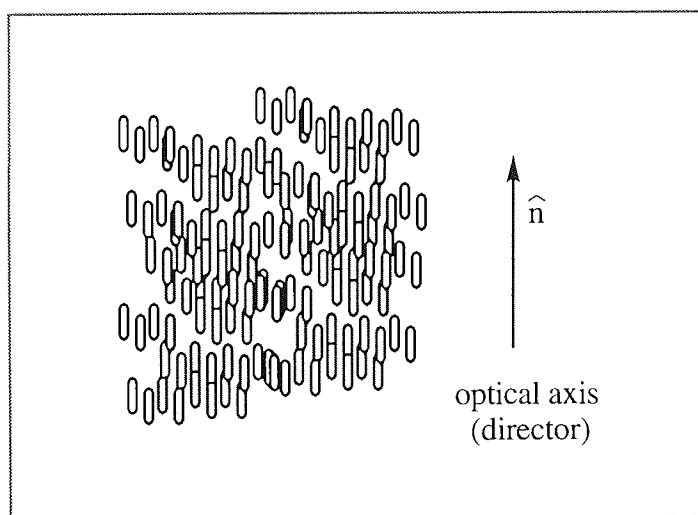


Figure 1.1 Molecular order in the nematic phase

1.3.2 Cholesteric liquid-crystals

Cholesterics¹⁰ are similar to nematics and are in fact a chiral nematic phase. Like the nematic phase, the cholesteric phase is characterised by random molecular position and parallel alignment of directors within layers parallel to the director. Cholesterics are formed by optically active molecules which consist of sheets combined to produce a helix (Figure 1.2). Cholesterics structures may be formed by adding optically active

compounds to nematics in which case the pitch can be controlled by the amount of additive (the distance for a 360° turn is the pitch).

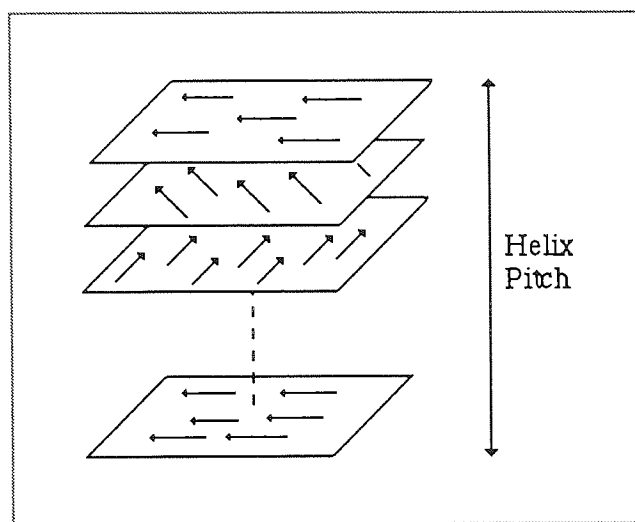


Figure 1.2 Cholesteric structure

1.3.3 *Smectic liquid-crystals*

The structure of smectic liquid-crystals^{9,10} can be regarded as the result of imposing a higher degree of order on the nematic structure. Thus, not only are the long-axes of the molecules parallel to one another, but the molecules are also arranged within stacked layers. Therefore, smectic liquid-crystals are characterised by ordering in layers. The arrangement and orientation of molecules in these layers serves to differentiate a number of different types of smectic liquid-crystal, denominated by A, B, C, etc. All smectic liquids crystals have a layered structure.

Smectic A - like the nematic phase, the smectic A phase is characterised by parallel alignment of the molecular director. However, there is also positional order such that the molecules form layers with the molecular director parallel to the layer normal (Figure 1.3).

Smectic C - the smectic C phases have a similar layered structure to the S_A phase, except that the molecular directors are tilted at a constant angle (the tilt angle) to the layers normal direction.

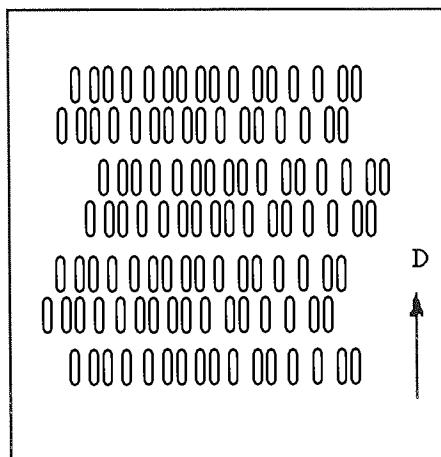


Figure 1.3 Molecular order in the Smectic A phase

1.4 Molecular structure and nematogen stability

Early studies⁴ suggested that, liquid-crystalline behaviour tended to occur in systems in which the molecules consist of rigid aromatic or aliphatic rings with flexible alkyl or alkoxy chains attached to one or both ends. It was suggested that strong permanent dipole moments present in the structure of molecule promote liquid-crystal formation. It was also suggested that, for the liquid-crystal molecules, the cohesive forces between the elongated molecules must be anisotropic and also of a certain magnitude. If the intermolecular forces are very strong then the melting point of the material will be very high and thermal agitation after melting will not permit the existence of order in the liquid phase. If intermolecular forces are very weak then liquid-crystalline order will be insufficiently stabilised and only isotropic liquids will be observed. It has been generally assumed that the stability of nematic liquid-crystals depends primarily on the anisotropy of intermolecular forces⁴. The forces responsible for the nematic stability are dipole-dipole (both permanent and induced) and dispersion forces.

It is clear that those factors which determine the formation and stability of liquid-crystals such as anisotropic intermolecular forces depend in part on the structures of the individual molecules. Many investigations^{11,12,13,14} have been carried out to improve mesomorphic behaviour of liquid-crystals, according to favourable characteristics such as higher dielectric anisotropy, lower viscosity, greater nematic-isotropic transition temperature (nematic range). It is clear that the improvements of physical properties of these systems require a full understanding of the anisotropic nature of these systems and of the forces leading to the formation of orientational order in liquid-crystals.

1.5 The lateral and terminal attractions

The way in which the molecules pack together in the crystal is of importance in determining the mesophase type exhibited. Thus, an imbricated arrangement of the parallel molecules may give a nematic mesophase if the melting point of the compound is not very high, but cannot give a smectic phase, whilst a layer arrangement in the solid may reveal either a smectic or nematic mesophase depending on the melting point of the compound. The relative strengths of the lateral and cohesive forces are of greater importance. A layered crystal structure, in which strong lateral and weak terminal intermolecular cohesions operate, will probably give rise to a smectic mesophase which, if the lateral cohesions are high enough, may persist on heating until the isotropic liquid is formed. Weaker lateral attractions will probably lead to the production of a nematic mesophase, before the isotropic liquid is formed. For systems comprised of rod-like molecules between which there is a more equal balance between the lateral and terminal attractions, the nematic mesophase will most probably be formed from the crystalline solid when the compound melts.

The distribution and strength of dipole moments in the molecule may also determine whether the system exhibits smectic or nematic properties, e.g. if the dipoles are situated near the ends of the molecules, they may enhance the terminal intermolecular attractions

and so favour nematic behaviour. For this reason, long alkyl (alkoxy) chains in the terminal group favour the occurrence of smectic properties, because the dipolar centres of the molecules which are arranged end-to-end must lie far apart, and the terminal interactions will be weak. Conversely, short alkyl (alkoxy) chains exhibit nematic properties because of the lower ratio of lateral to terminal interactions.

1.6 Molecular theory (the mean field approximation)

The stability of the nematic liquid-crystal phase arises from the existence of strong interactions between pairs of the constituent molecules⁸. In the case of rod-like nematic molecules, these interactions are highly anisotropic, i.e., the forces acting on such molecules depend not only on their separation but also, on their relative orientations. However, a molecular theory of a fluid system based on a pair wise interaction potential is complicated.

Maier and Saupe¹⁵ developed a statistical theory to describe the liquid-crystalline state and the molecular ordering for the nematic phase. This theory described the intermolecular orientation forces by a mean-field method. According to this theory, it is possible to derive a single molecule potential that serves to orient the molecule along the symmetry axis (the director) of the nematic phase. The single-molecule potential represents (approximately) the mean-field of intermolecular forces acting on a given molecule. According to this theory, each individual molecule feels a “nematic potential” $W = f(\theta, S, V)$ which depends on the instantaneous angle θ between its long axis and the optic axis, the order parameter S and the molar volume V . The effective anisotropic potential of a molecule l in the anisotropic dispersion field generated by its oriented neighbours s is calculated by averaging the pair potential between two molecules l and s and over all distances between l and s . For rod-like molecules the anisotropic contribution to this average potential is given by

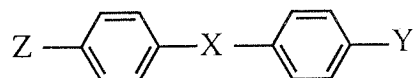
$$W = - AS (3\cos^2\theta - 1) / 2V^2 \quad (1.8)$$

where A is a constant which depends on the nature of the liquid-crystal, V is the molar volume of the liquid-crystal and S is the order parameter of the nematic phase. θ is the angle between the long axis of the molecule **l** and the nematic director (optic axis of the liquid-crystal). The potential of dispersion forces is volume dependent, and is expected to depend on the intermolecular separation as r^{-6} . Maier and Saupe^{15,8} then attempted to elucidate the nature of the intermolecular forces in nematic phase. They concluded that induced dipole-induced dipole interaction play a major role in determining the stability of the nematic phase.

In conclusion, the Maier and Saupe theory is based on the assumption that the intermolecular interaction potential in nematic liquid-crystals is determined primarily by London dispersion forces (induced dipole-induced dipole). In this theory only attractive intermolecular forces are considered, and the nematic to isotropic transition temperature T_{NI} is predicted to vary as $I(\Delta\alpha)^2/V^2$, where I is the ionisation potential, $\Delta\alpha$ is the polarisability anisotropy and V is the molecular volume.

1.7 Chemical classes

The most common structure exhibiting liquid-crystal properties is^{4,8}:



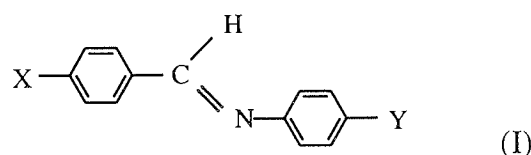
where, X is a simple bond or a group such as - N=N -, - CH=N -, - CH=CH -, - CO.O - and Y, Z are alkyl, alkoxy, cyano or nitro groups.

The nature of the central linkage has a very important effect on the stability of nematic liquid-crystals in addition to the terminal groups. Dewar *et al*^{11,16}. have reported the

specific role of the central group on the stability of nematic liquid-crystals. They have concluded that rigidity is more important than the presence of π -electrons in the central group of the nematic molecules. Dewar *et al.* have also concluded that the predominant factor that influences nematic stability is molecular geometry, while unsaturation and polarity (in the central group) play relatively unimportant roles. It is possible to classify the nematic liquid-crystals in terms of the structure of central linking group.

1.7.1 Benzylideneanilines ($X = -CH=N-$)

A large family of liquid-crystals which are classified as Schiffs bases and represented by the general formula¹⁰ (I):



The benzylideneanilines, although readily synthesised from the substituted benzaldehyde and aniline derivatives, have chemical instability. They readily hydrolyse in the presence of trace acid and moisture.

In 1969 the first room-temperature Schiffs base compound was prepared by Kelker and Scheurle¹⁷. The compound N-methoxybenzylidene-4-butylaniline (MBBA) exhibited nematic liquid-crystalline behaviour between 22°C and 47°C. MBBA (Figure 1.4) was the first synthesised liquid-crystal that displayed nematic behaviour at room temperature.

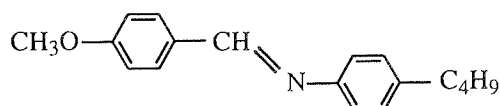
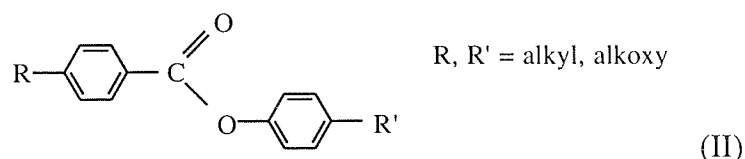


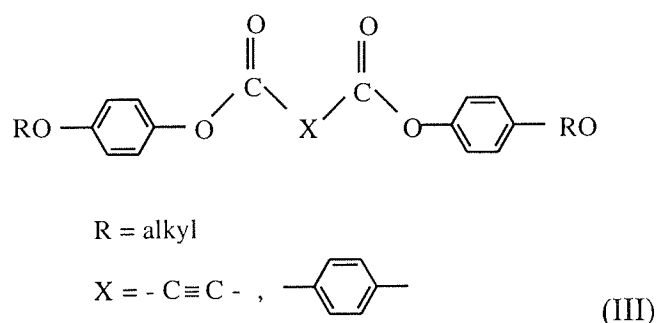
Figure 1.4 N-methoxybenzylidene-4-n-butylaniline (MBBA)

1.7.2 Esters and diesters (X = -CO.O-)

Nematic liquid-crystals of the ester and diester type^{11,16} (II, III) offer increased chemical stability over the benzylideneaniline compounds. Esters are easily prepared, thermally stable, fairly planar systems and quite strongly nematogenic.



In 1972, Verbit and Tuggey¹⁸ reported the synthesis of a series of ester derivatives with the general structure in an attempt to interrelate changes in molecular structure and mesophase behaviour. The mesomorphic behaviour of this series of compounds indicates that π -electron density in the central group is not a necessary condition for mesophase formation. This series of liquid-crystals are represented by the general formula:



1.7.3 Cyanobiphenyls (X = simple bond)

This class of liquid-crystalline compounds are derivatives of cyanobiphenyls (Figure 1.5), and have been reported by Gray^{7,14}. The compounds are colourless and relatively stable chemically and photochemically, and eutectic mixtures give wide temperature-range nematics covering room temperature. Due to their high dielectric and optical anisotropy, they are very useful materials for room temperature electro-optic display devices. By simply observing the structure of these liquid-crystals (Figure 1.5), it can

clearly be seen that the molecules are geometrically anisotropic. This is a necessary requirement since it allows large aggregates of molecules to be arranged parallel to one another in an anisotropic melt. Secondly, the rigidity along the long-axis of the molecule arising from the biphenyl core assists in maintaining molecular order.

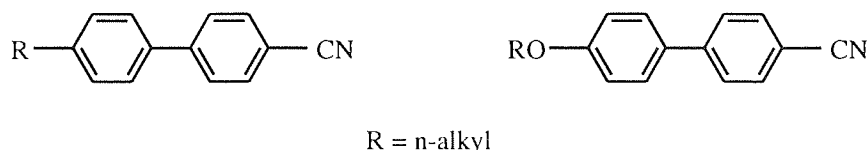


Figure 1.5 4-n-alkyl- and 4-n-alkoxy-4'-cyanobiphenyls

As well as the purely geometric aspects of the molecule, the strength of intermolecular interactions must also be considered⁴. The attractive forces operating between the molecules should be sufficiently strong to maintain a parallel arrangement of molecules to constitute a potentially mesomorphic system. The rod-like molecules must therefore contain groups of atoms with which are associated permanent dipole moments and the molecule itself must be highly polarisable. The high polarizability of alkyl (alkoxy) cyanobiphenyls is mainly due to the aromatic rings and the CN group.

1.8 Physical properties of nematic liquid-crystals

The combination of molecular order and fluidity in a nematic phase results in several remarkable properties unique to liquid-crystals. Due to anisotropic shape of nematic molecules, all the molecular response functions, such as the electric polarisability, are anisotropic. Also, due to long-range orientational order, all the macroscopic response functions of the bulk material, such as the dielectric constant, are anisotropic as well. Since nematic liquid-crystals behave like optically uniaxial crystals, therefore, many of their physical properties, such as the dielectric constant, are described by a tensor.

1.8.1 Dielectric properties

In the optically uniaxial nematic phase (choosing the z-axis parallel to the nematic director), the dielectric tensor, $\epsilon_{\alpha\beta}$ is described by⁸

$$\epsilon_{\alpha\beta} = \begin{pmatrix} \epsilon_{\perp} & 0 & 0 \\ 0 & \epsilon_{\perp} & 0 \\ 0 & 0 & \epsilon_{\parallel} \end{pmatrix} \quad (1.2)$$

were, ϵ_{\parallel} , ϵ_{\perp} are dielectric constants of the liquid-crystal measured with the electric field parallel and perpendicular to the long molecular axis, respectively. Therefore, the dielectric behaviour of a nematic liquid-crystal is described by two dielectric constants, ϵ_{\parallel} and ϵ_{\perp} . The dielectric anisotropy is defined as

$$\Delta\epsilon = \epsilon_{\parallel} - \epsilon_{\perp} \quad (1.3)$$

The dielectric anisotropy plays an important role in all electro-optical applications of liquid-crystals. The sign of the dielectric anisotropy depends on the molecular polarisability and the direction of the permanent dipole moment with respect to long molecular axis. Positive values of $\Delta\epsilon$ are characteristic of the nematics in which the

molecular dipole moment lies along or forms a small angle to the long molecular axis, while negative values of $\Delta\epsilon$ result when the molecular dipole moment is perpendicular (or nearly perpendicular) to the axis of maximum electronic polarisability. For example, MBBA and PAA (p-azoxyanisole) have negative anisotropy¹⁰, while compounds with a *p*-cyano group¹⁴ ($-\text{C}\equiv\text{N}$) in the terminal position normally exhibit $\Delta\epsilon > 0$.

1.8.2 Optical anisotropy

Because of orientational order, nematics are optically uniaxial. Therefore, nematics are highly birefringent materials, i.e. $n_{\parallel} \neq n_{\perp}$, where n is the refractive index of light polarised parallel or perpendicular to an orienting field. The refractive index n_{\parallel} (parallel to the field) can be greater or less than the refractive index n_{\perp} (perpendicular to the field). It depends on the angle between the molecular dipole and the long molecular axis (the axis of maximum electronic polarisability).

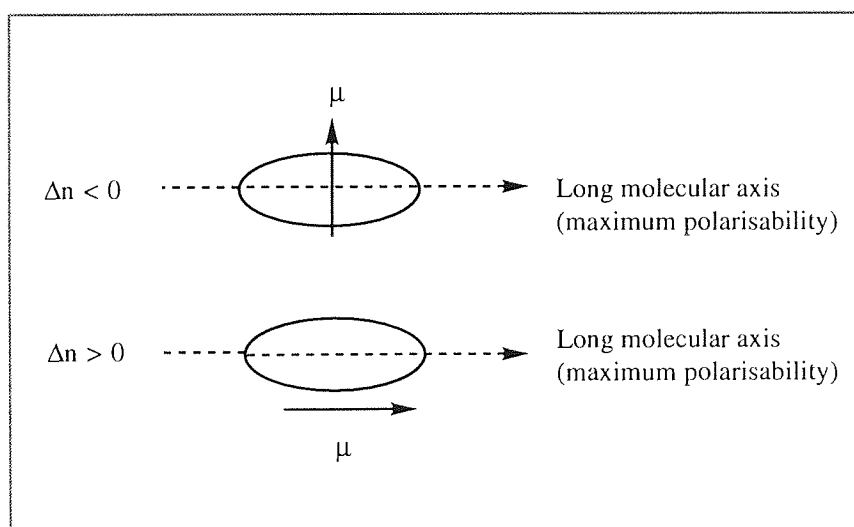


Figure 1.6 The directions of the maximum polarisability and dipole moment of the nematic molecule

The optical anisotropy (birefringence) is defined as $\Delta n = n_{\parallel} - n_{\perp}$. Positive values of Δn are characteristic of the nematics in which the molecular dipole moment lies along or forms a small angle to the long molecular axis, while negative values of Δn result when

the molecular dipole moment is perpendicular (or nearly perpendicular) to the axis of maximum electronic polarisability as shown in Figure 1.6.

1.8.3 Order parameters

The orientational order parameter, S , of liquid-crystals is an essential parameter for scientific and technological purposes. In an ordered nematic liquid-crystal sample, the long molecular axes are, on average, parallel to a preferred direction (director). However, the direction of each liquid-crystal molecule deviates from the direction of the director, due to thermal motions (Figure 1.7). The average molecular orientation in the liquid-crystals can be described by a single order parameter $S^{8,19}$,

$$S = 1/2 \langle 3 \cos^2\theta - 1 \rangle, \quad (1.4)$$

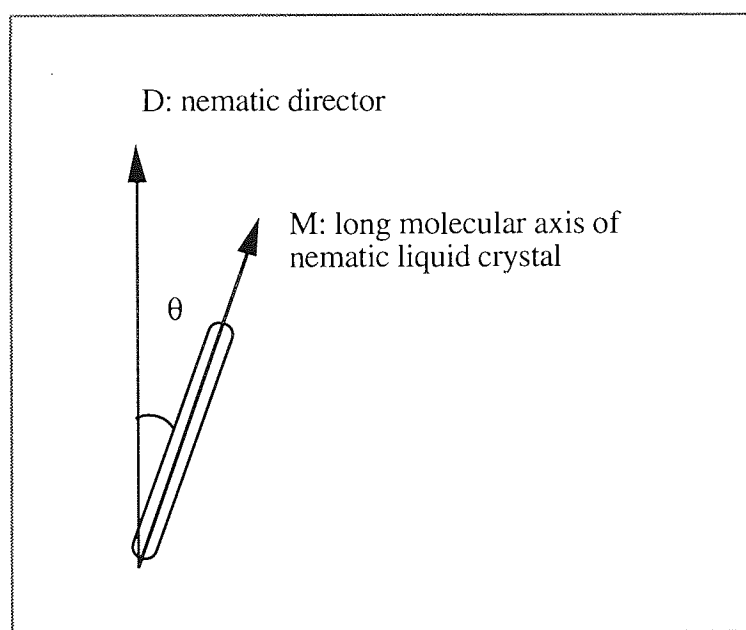


Figure 1.7 The orientation of long molecular axis of a nematic molecule and the optic axis (director).

where θ is the angle between the axis of an individual molecule and the director, and the brackets mean the time or space average. In a perfect crystal, $\theta = 0$, or $S = 1$, whereas in

the isotropic phase $S = 0$. Nematic liquid-crystals exhibit order parameters between about 0.4 to 0.7, depending on temperature¹⁹.

Various methods are used to measure the order parameter and include dielectric relaxation, UV and IR dichroism, nmr, and the analysis of optical and density data. A critical comparison of the various methods was given by Saupe and Maier²⁰.

1.9 Nematic liquid-crystals in a uniform electric field

The response of the nematics to electric fields involves a process of orientation of the rod-like molecules. The response of a nematic liquid-crystal to an external electric field depends on both the sign and magnitude of $\Delta\epsilon$. Nematic liquid-crystals with positive dielectric anisotropy, tend to align with the long molecular axis parallel to an applied field^{8,9}. While, negative nematics tend to align perpendicular to the field. Electric effects in liquid-crystals generally are studied in cells with a sandwich structure, as shown in Figure 1.8.

For nematic liquid-crystals with positive dielectric anisotropy originally in the parallel alignment, (the long molecular axes are parallel to the electrodes), application of an electric field gives the perpendicular alignment, as is shown in Figure 1.8 (a). In negative dielectric anisotropic nematics, which are originally in the perpendicular alignment, application of an electric field gives parallel alignment, as is shown in Figure 1.8 (b). For liquid-crystals with negative dielectric anisotropy, originally with parallel alignment (Figure 1.8(c)), application of an electric field can not change the molecular orientation, (the dipoles need only rotate about the molecular axis). However, above a threshold voltage a uniform cigar shaped domain can result^{21,22} (see Chapter 3).

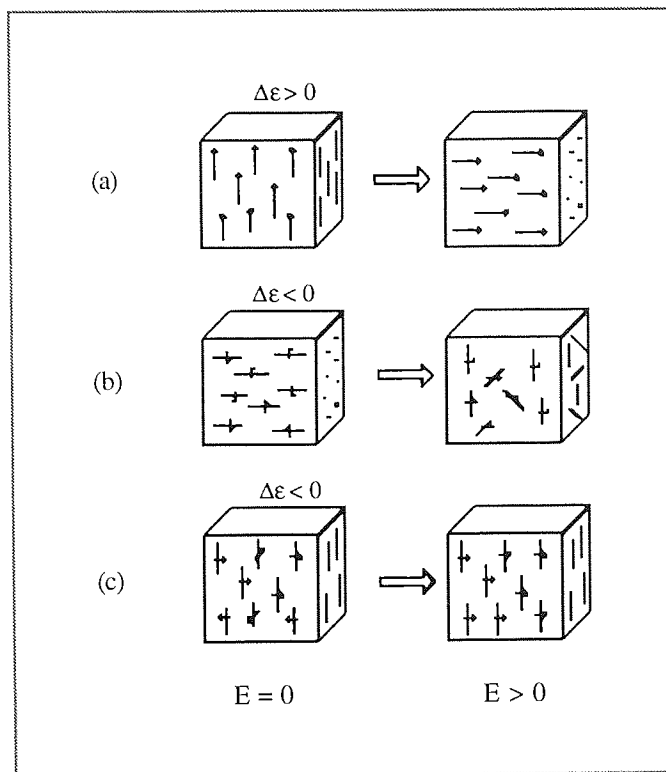


Figure 1.8 Schematic representation of the orientations before and after the application of an electric field. The lines represent the alignment of individual molecules, with arrows (\rightarrow) representing the dipole moments.

Due to the fluid nature of the nematic phase, the field strength necessary to cause such realignment of the nematic axis is not very large. This ability to control the orientation of the nematic axis by means of weak external field is the basis for several applications of nematic liquid-crystals in optical display devices.

1.10 Eutectic mixtures

The application of liquid-crystal displays is limited by the physical and chemical properties of the liquid-crystal material. Since it is often the case that no single component has the required nematic range, mixtures of mesomorphic compounds are used for this purpose. In recent years, the physical properties of nematic mixture liquid-crystals have received much attention^{23,24,25}. This interest is due to their desirable liquid-crystalline range, optical, and electrical properties. Eutectic mixtures are necessary in order to avoid segregation of the components and due to their broad nematic temperature range. The physical properties of a eutectic mixture depend on those of the components used and on their relative concentrations.

To be able to predict and/or rationalise the properties of a mixture it is necessary to know the properties of the components as well as their molecular behaviour in dilute solution. Osman *et al.*^{24,25} concluded that some physical properties of nematic mixtures (homologs) such as the nematic isotropic transition and the dielectric constant are approximately additive in terms of component properties. However, mixtures of nematogens of different chemical structures possess different packing arrangements of the molecules and show deviations from single additivity rules. The nematic-isotropic transition temperature is more sensitive to small changes in the packing of the molecules than the dielectric or diamagnetic properties.

1.11 Applications of liquid-crystals

Today, liquid-crystals are used in the electric displays of digital watches, clocks, and calculators. The most important applications of liquid-crystals are for flat optical display devices (LCDs). There are several types of displays such as twist nematic devices²⁶ (TND), and guest-host devices²⁷ (Table 1.1). The first generation of liquid-crystal displays were based on the principle of “dynamic scattering”, after the discovery of

dynamic scattering at RCA laboratories during the mid-sixties. The second generation was based on the principle of the “twisted nematic cell”, discovered at the beginning of the 70’s by M. Schadt and W. Helfrich²⁶.

Liquid-crystals also have many medical applications. The sharp changes in the colour of cholesteric liquid-crystals with small changes in temperature have resulted in a number of unique temperature-sensing applications. Breast tumours have been detected by this technique.

In addition, liquid-crystals are very useful laboratory tools as anisotropic solvents for polarised spectroscopy¹⁹. The use of nematic liquid-crystals in this manner provides a quick and simple method for spectroscopic studies of the anisotropy of physical molecular properties²⁸ (guest-host interaction).

Table 1.1 Summary of some important nematic devices

Device type	Phenomenon	original alignment	Field off → on	Materials property
Dynamic scattering	hydrodynamic turbulence	perpendicular or parallel	clear → scattering	negative $\Delta\epsilon$ + conductivity
Twisted nematic	Reorientation	parallel	change in polarisation	positive $\Delta\epsilon$
Guest-host	Reorientation	parallel	colour → colourless	positive $\Delta\epsilon$ + dichroic dye
Deformation of aligned phases	Reorientation	perpendicular	change in polarisation	negative $\Delta\epsilon$

1.12 Scope of this work

The most significant part of the work reported here involves the measurement and interpretation of a number of important physical properties of various liquid-crystal materials in different physical states, e.g. dielectric response, density, refractive index, electric birefringence, electric dichroism and IR spectroscopy (see Figure 1.9). The accurate dielectric, electro-optical and density data obtained at several temperatures, constitutes an very important for both scientific and technological purposes. Some of these data have either not been previously reported or are more accurately measured than in earlier studies.

One of the aims of this of project was to try and understand the role of various factors, such as intermolecular forces and molecular association, that determine the stability and properties of liquid-crystals (mainly 4,4'-alkyl (alkoxy) cyanobiphenyls). This requires an understanding of how these factors depend on the structures and composition of the individual molecules. Hopefully, such studies should help to elucidate and rationalise statements such as liquid-crystal molecules should have certain structural requirements, that are widespread in literature concerned with liquid-crystalline materials.

The work reported here was also intended to provide information about molecular association the and specific role of the dipole interactions and to show how such factors influence the physical properties of liquid-crystals. It was, therefore, desirable to study the relationship between measurable liquid-crystal properties and molecular parameters by using as many different techniques as possible. A number of anisotropic physical properties have been measured in order to correlate the physical behaviour of the liquid-crystal with their molecular structures, for the nematic and isotropic phase as well as in solution. The experiments described have provided valuable information on molecular association, the nature of the intermolecular interactions and the degree of orientational

order in nematic liquid-crystal forming materials possessing structures based on the biphenyl moiety.

This work reports a series of measurements of the dielectric, electro-optical, density and spectroscopy properties of 4,4'-alkyl (alkoxy)-cyanobiphenyls. The physical properties of some nematic mixtures of cyanobiphenyl liquid-crystals are also reported and interpreted in terms of specific intermolecular dipole interactions.

In order to make dielectric and electro-optic measurements on small volumes of liquid crystals over a range temperature, it was necessary to design, construct novel dielectric and electro-optic cells.

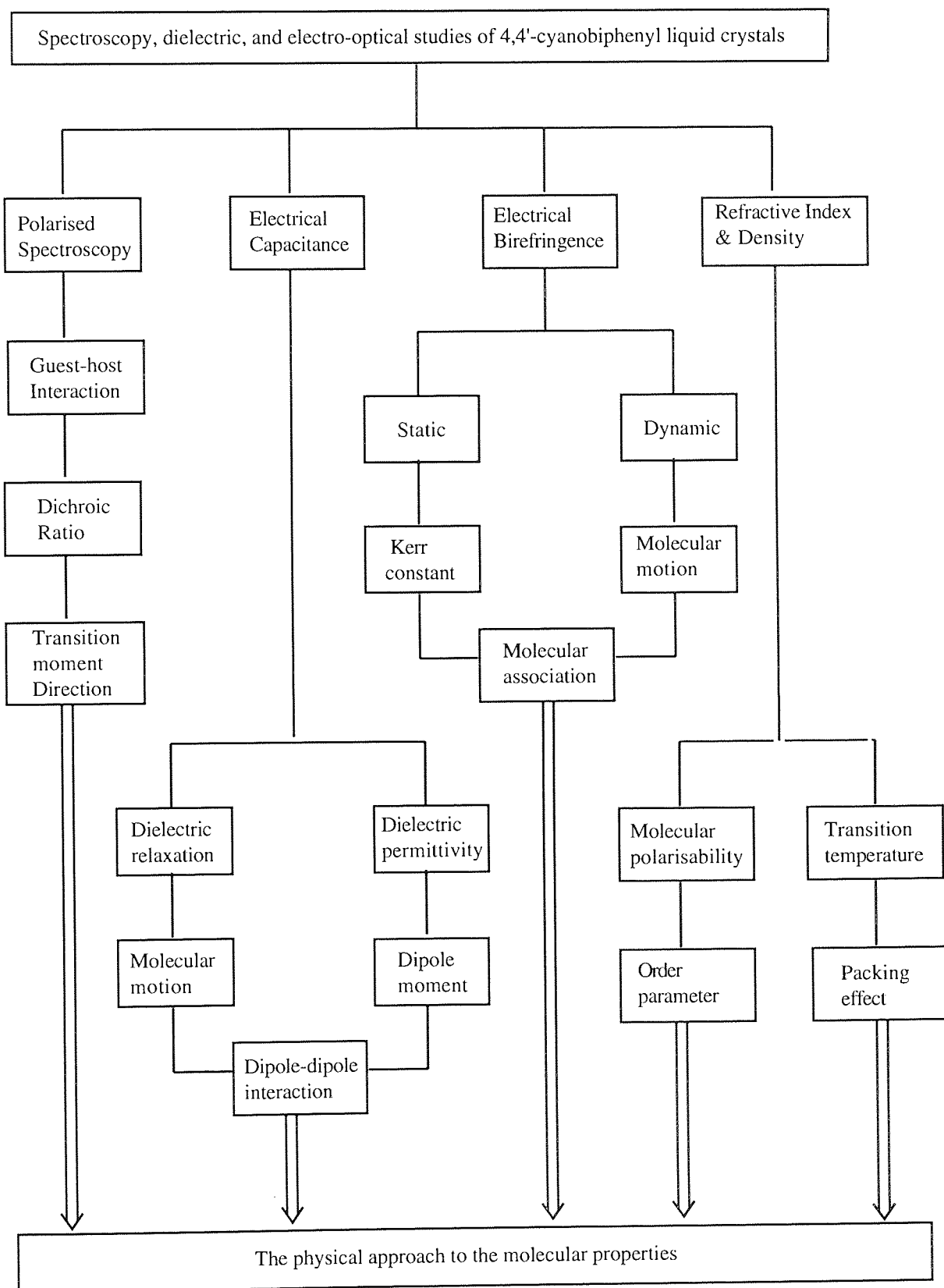


Figure 1.9 Schematic representation of the various techniques used in the present studies.

CHAPTER 2

SURFACE TREATMENT FOR LIQUID CRYSTAL ALIGNMENT

2.1 Introduction

Liquid crystal alignment is very important in liquid crystal (LC) display technology. Uniformly oriented thin layers of liquid-crystals are required for most liquid-crystal device applications. According to the nature of the liquid-crystal and the electro-optical effect required, the axes of the molecules must be either perpendicular (homeotropic) or parallel (homogeneous) to the substrates (electrodes). A number of investigators have described different methods for obtaining perpendicular and parallel alignments. In the following section the most important techniques of the liquid-crystal alignment are summarised.

The sandwich type liquid-crystal cells are widely applicable in the LC display technology and they are also very useful for spectroscopic and electro-optical studies.

The aims of this part of the project are as follows;

1. To review and develop the surface treatments necessary to obtain parallel and perpendicular alignment and compare with results in the literature,
2. To make and modify liquid-crystal cells, and
3. To use cellulose acetate butyrate (CAB) polymer as a new coating agent to obtain good parallel alignment and check the degree of alignment with nematic liquid-crystals (E7 and MBBA) using crossed polarisers.

2.2 Parallel alignment of liquid-crystals

Parallel alignment of nematic phase can be obtained by rubbing the glass surface with paper, cotton, cloth and diamond paste⁸. The rubbing of glass plates in one direction before introduction of the sample was first demonstrated by Chatelain¹⁰. The rubbing process produces micro grooves in the glass surface, and the molecules of the liquid-crystals tend to align parallel to the direction of the grooves. Berreman²⁹ introduced a simple explanation (elastic-energy mechanism) for the tendency of the nematic liquid-crystals to lie parallel to the direction of rubbing. He showed that the elastic strain energy may account for the orientation parallel to the rubbing direction on a solid surface that has been slightly deformed by rubbing.

Parallel alignment can also result from the application of a thin layer of rubbed polymeric material³⁰. When the inside surface of the glass plates are covered with polymeric material such as polyimide (PI) or polyvinyl alcohol (PVA) this results in parallel alignment. This process will make the rubbing of the surface easier, because the polymer is softer than glass.

Janning³¹ has reported that good parallel alignment of nematic liquid-crystals can be achieved by the vacuum evaporation of silicon monoxide or gold onto a substrate. The orientation process involved depositing a thin film of the material onto selected clean glass plates at an angle ϕ , as shown in Figure 2.1. The angular deposit causes the film to grow in a preferred direction. When liquid-crystals are applied, the liquid-crystal molecules become aligned to the direction of film growth. The thickness of the angular deposition, T_a , is calculated from the thickness of control-plate film thickness, T_{co} .

$$T_a = \cos \phi T_{co}$$

Janning³¹ indicated that various materials have been deposited with differing results. For example, a copper film will give excellent homeotropic alignment, while aluminium, platinum, gold, and silicon monoxide aligned along the directions parallel to the deposition direction.

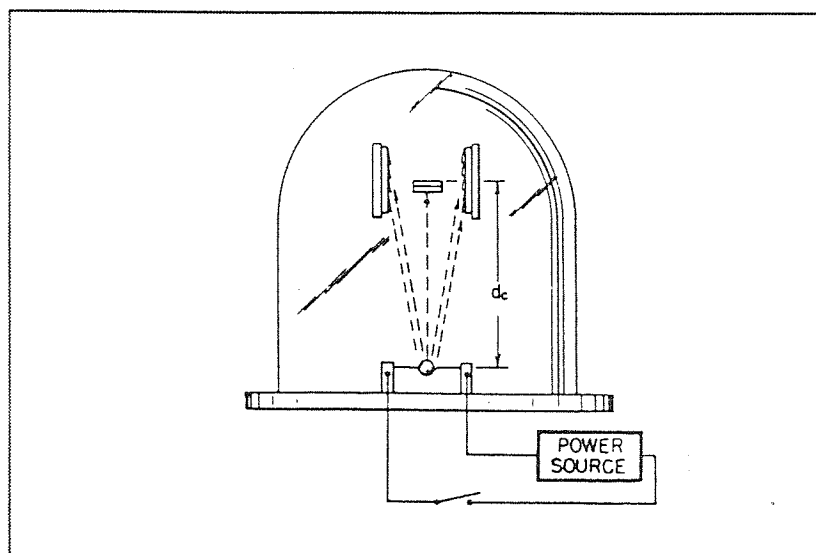


Figure 2.1 Bell-Jar arrangement of angular deposition. The control substrate is placed in the centre of the area.

Dixon *et al.*³² have used the oblique evaporation of silicon monoxide, SiO_x , to find the alignment mechanism. They have examined the surface deposits by electron microscopy which indicated that alignment occurred due to the presence of islands and holes in the silicon monoxide modified surface.

Kahn³³ has reported that parallel alignment can be obtained by treating a glass surface with the silane coupling agent (N-methyl-3-aminopropyl trimethoxy silane) MAP. This agent is chemically bonded to the surface, as shown in Figure 2.2. Using MAP, he could create surfaces which consist mainly propyl hydrocarbon chains lying parallel to the substrate. The propyl chains are randomly aligned and do not have any axis of symmetry in the substrate plane. Therefore, liquid-crystal molecules will tend align with their long axes parallel to the plane but with random azimuth. Kahn³³ pointed out that both the

amino and silane sites of the surface agent molecules are believed to adsorb or bond to the substrate.

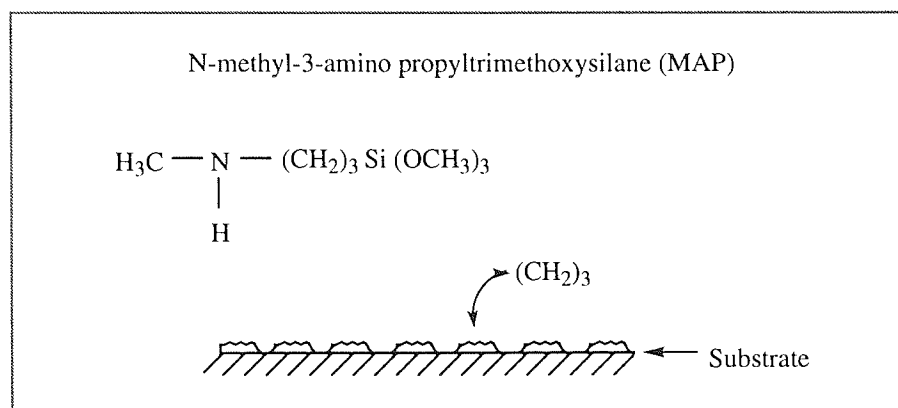


Figure 2.2 Chemical formula for silane coupling agent and its geometric relationship to a substrate.

Recently, Ichinose *et al.*³⁴ have used phthalocyanine, Pc, derivatives as an alignment layer. They obtained parallel alignment by deposition of a Pc layer on glass plates of a liquid-crystal cell, and showed that liquid-crystal alignment is determined by the Pc aggregate orientation and the side-chain length. The parallel (homogeneous) alignment force is originated from orientation of the rod-like aggregates of the Pc derivatives. On the other hand, the liquid-crystal alignment changes from homogeneous alignment to homeotropic alignment with the increase in the number of alkyl side chain carbon atoms of the Pc derivative.

2.3 Perpendicular alignment of liquid-crystals

Kelker *et al.*³⁵ have prepared homeotropic alignment by cleaning the glass surface with inorganic acids. The mechanism of attachment is due to the dipolar interaction between polar groups of liquid-crystals and the silanol group of the glass surface⁸ (Figure 2.3).

A homeotropic alignment can result from the coating of glass with a thin layer of egg-lecithin¹⁹. For this purpose the two substrates were repeatedly dipped into an ether solution of lecithin.

Kahan³³ has prepared homeotropic alignment by coating of silane coupling agent, N,N-dimethyl-octadecyl-3-aminopropyltrimethoxysilyl chloride (DMOAP) that was chemically bonded to the glass surface. As shown in Figure 2.3, the octadecyl ($C_{18}H_{37}$) chains are lying perpendicular to the substrate. Therefore, liquid-crystal molecules will tend align with their long axes perpendicular to DMOAP-coated substrates.

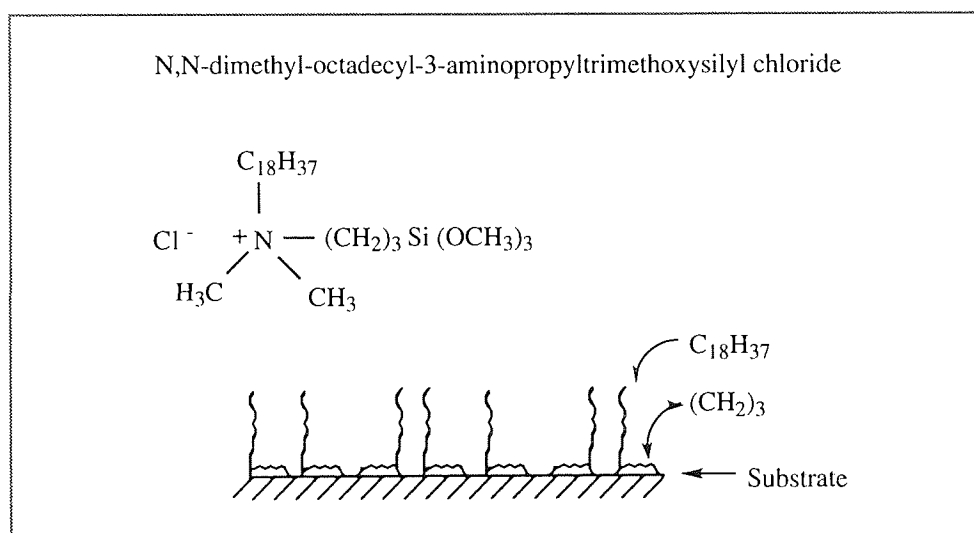


Figure 2.3 Homeotropic alignment by the alkoxy silane

Prout *et al.*³⁶ have obtained perpendicular alignment by depositing a thin layer of hexadecyl trimethyl ammonium bromide (HTAB) onto glass plates before insertion of the liquid-crystal between the plates.

Grabmaier¹⁹ explained that homeotropic alignment by surface active agents such as lecithin, HTAB, and DMOAP is due to van der Waal's interactions between nonpolar alkyl-groups of the liquid-crystal molecules and the aligned non polar alkyl-groups of surface active agents.

Dubois *et al.*³⁷ indicated that plasma-polymerised films as orienting layers gave a homeotropic alignment. They described a method to deposit a film giving a perpendicular orientation to the liquid-crystal layer. The investigated monomer was hexamethyl disiloxane.

2.4 The effect of surface energy on surface alignment

Greagh and Kmetz³⁸ have shown that the liquid-crystal wets the solid surface, when

$$\gamma_L < \gamma_C$$

where γ_L is the surface tension of the liquid-crystal, and γ_C is the critical surface tension of the substrate. In this case the liquid-crystal molecules align parallel to the surface. The liquid-crystal does not wet the surface, when

$$\gamma_L > \gamma_C$$

In this case, the liquid-crystal exists as a sessile drop on the surface, and molecules align perpendicular to surface. They observed that when the solid surface tension is low, the intermolecular forces within the liquid-crystal are stronger than the forces across the interface. Therefore, the liquid-crystal does not wet the solid and the molecules align perpendicular to the surface. However, if the surface energy of the substrate is high, the molecules align parallel to the surface.

Kahn *et al.*³⁹ noted that high γ_C of a solid surface can be reduced by the presence of a layer of liquid molecules that has been absorbed at the solid-liquid interface.

2.5 The preparation of a liquid-crystal cell

A large number of liquid-crystal cells were used in the experiments. They were all parallel flat glass plates (2cm x 2cm), coated with indium/tin oxide (ITO). In order to produce transparent, electrically conductive electrodes, a very thin layer of a mixture of SnO_2 and In_2O_3 have been deposited on the glass plates, by a spraying method conducted at high temperatures⁸. The conductivity of the plates were checked by an ohm-meter.

The surface treated glass plates were cleaned by first soaking in a concentrated detergent (Teepol™) over night and finally cleaned by spraying either acetone or chloroform.

The liquid-crystal samples were sandwiched between two plates of each cell by the following methods. In all cases, the introduction of the samples was achieved by capillary action or by using a micro-pipette. The spacing between the electrodes surfaces was $12.5\text{ }\mu\text{m}$ and was set by use of a Mylar (Polyester Conveters LTD). The plates were sealed together by a suitable sealing material (epoxy resin glue). Copper wires were connected to the glass plates using two-part silver-loaded epoxy (RS components 567-604) and electrically conductive paint (RS components 555-156).

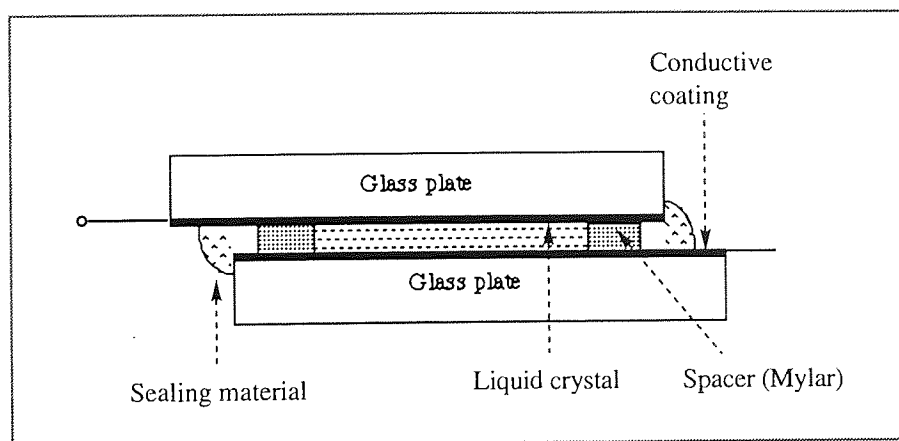


Figure 2.4 Cross-section of the experimental liquid-crystal cell. The inner surface of the cell were covered by In/Sn oxide.

The commercial material E7 (BDH mixture of cyanobiphenyl and terphenyl) and MBBA are used in these investigations as liquid-crystal samples (Figure 2.4). The MBBA was made in this laboratory by a condensation method using distilled n-butylaniline and methoxybenzaldehyde.

2.5.1 LC cell with parallel alignment

2.5.1.1 Rubbing of the glass plates

One side of each glass plates was rubbed approximately 100 times in one direction with a fine paper. The plates were placed in an oven at $\sim 110^{\circ}\text{C}$ (Absorbed moisture can cause a significant reduction in critical surface tension). The liquid-crystal cell was sandwiched between glass plates, with a gap of $12.5\text{ }\mu\text{m}$ maintained by Mylar spacers. The liquid-crystal cell was placed on an optical microscope, and the molecular alignment checked using crossed polarisers. Although, parallel alignment could be achieved by the simple rubbing method, the experiments did not show a uniform parallel alignment. The liquid-crystal appeared patchy (some dark, some bright area) when viewed between crossed polarisers, due to the formation of random areas of parallel alignment.

2.5.1.2 polyvinyl alcohol (PVA) as a coating agent

Parallel alignment of liquid-crystal molecules was obtained by surface treatment of a cast film of polyvinyl alcohol (Sigma) followed by the rubbing process. For this purpose the plates were dipped into an aqueous solution of about 5% of the material. The plates were placed in an oven at $\sim 110^{\circ}\text{C}$ for 24 hours. The surfaces were rubbed approximately 5 to 10 times with a soft paper. The liquid-crystal was sandwiched between two rubbed glass plates, using Mylar sheets as spacers. The liquid-crystal cell was checked under a crossed polarisers, and was used in subsequent dichroism studies.

2.5.1.3 Cellulose acetate butyrate (CAB) as a coating agent

Good parallel alignment was achieved on the substrates by coating glass plates with cellulose acetate butyrate (CAB-381-20 Eastman Kodak) and rubbing the cast film. The coating process was done by dipping the plates into a CAB solution for a few seconds. The solutions were in concentration range 1 to 10% in chloroform. The coated plates were then placed in an oven at $\sim 90^\circ\text{C}$ for about 5 hours. One side of each of two plates was then rubbed approximately between 2 to 10 times in one direction with a fine paper. Mylar film ($12.5\ \mu\text{m}$) was used as the spacer material. The spacers were placed on one of the plates on the side that had been rubbed, along the short edges. A few micro-drops of the liquid-crystal material (E7 or MBBA) were pipetted on the glass plate that was fitted with the spacers. The other plate was fixed in place (rubbing directions of the two plates parallel to each other). The plates were then fixed together by a suitable adhesive (epoxy resin).

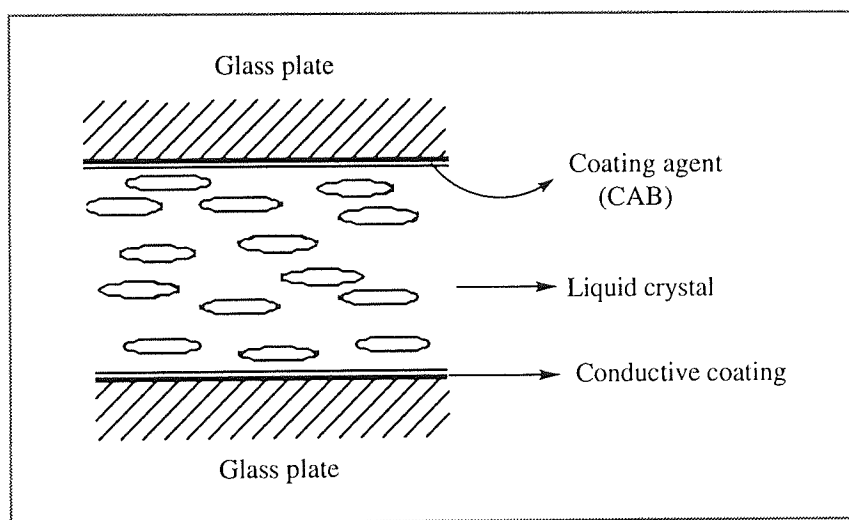


Figure 2.5 Side-view of the parallel alignment

The liquid-crystal cell was placed between crossed polarisers, and was observed through the microscope. The mesophase appeared bright, when the direction of the grooves were at 45° to the direction of the plane polarised light, and appeared dark when the direction of grooves were parallel or perpendicular to the electric field vector of plane polarised

light. The liquid-crystal cell construction is shown in Figure 2.5. A number of test cells were made by this method and they were used in spectroscopic and electro-optical studies.

2.5.2 *LC with perpendicular alignment*

2.5.2.1 *Cleaning method for preparation of glass plates*

A number of (2cm x 2cm) glass plates were used for obtaining homeotropic alignment following appropriate chemical treatment. The plates were cleaned by soaking in a sulphuric acid solution over night. They were then placed into a concentrated detergent for about 24 hours, rinsing in distilled water, and finally washing in chloroform. The liquid-crystal cell was obtained by fastening together two plates with using a suitable glue. The cell was filled with the chosen nematic liquid-crystal by capillary action. Microscopic studies did not show a good perpendicular alignment, and the mesophase was not sufficiently dark between crossed polarisers. Therefore, this treatment was not used in the following work.

2.5.2.2 *Lecithin as a surface active agent*

A homeotropic alignment was most easily obtained by depositing a thin layer of egg-lecithin on very clean glass surface. For this purpose, the glass plates were dipped into a dilute ethereal solution of lecithin (Sigma). The lecithin solution (0.01% w/v) was made by dissolving appropriate amount of the material in the diethy ether. The material was quite soluble and dissolved rapidly at room temperature. The glass plates were soaked in this solution for about 10 minutes, removed and air dried. Introduction of the liquid-crystal was done in the manner previously described. The orientation of the liquid-crystals inside the cells was observed with a microscope using a crossed polariser and analyser. Excellent homeotropic alignment was observed, as depicted in Figure 2.6.

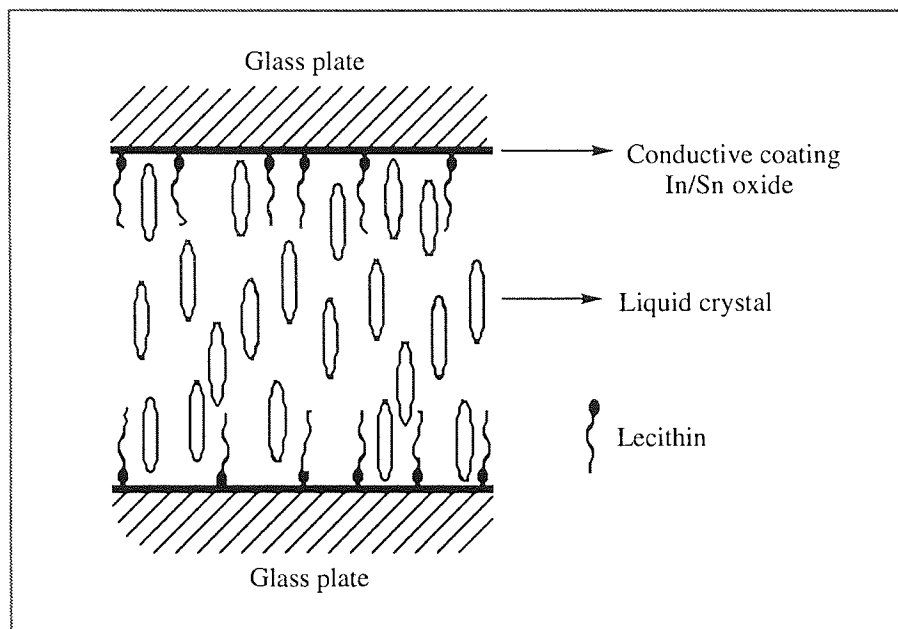


Figure 2.6 Cross-sectional of the experimental cell with homeotropic alignment.

2.5.2.3 *Hexadecyltrimethylammoniumbromide (HTAB) as a surface active agent*

The second treatment for obtaining homeotropic alignment was done by the deposition of hexadecyltrimethylammoniumbromide (HTAB, Aldrich) on glass plates. The HTAB solution was made by dissolving a small amount of the material in water by the aid of heat. As it was necessary to have a high concentration of HTAB for perpendicular alignment, it is important to make a concentrated solution of HTAB. The glass plates were then dipped for about 20 minutes into an aqueous solution of the material and dried in an oven for ~1 hour before the insertion of the liquid-crystal between the plates. Monolayer or multilayer films of HTAB were then examined in 12.5 μm thick cells containing the liquid-crystal E7 or MBBA. The liquid-crystal cells when viewed between crossed polarisers appeared dark. Therefore, it was concluded that using HTAB as a surface active agent is a very effective and simple method to obtain perpendicular alignment. The best alignments were obtained when the surface active agent was densely packed on the surface. This is in agreement with the results reported by Proust *et al.*³⁶.

2.6 Discussion of surface alignment

The surface energy of glass plates can be varied by surface treatment to obtain parallel or perpendicular alignment. It can be achieved by using various surface active agents. For alignment of liquid-crystal molecules, surface agents must have two different kind of groups. One of the groups must interact with glass surface and another acts as the orienting group by interacting with the liquid-crystal molecules.

For example, lecithin is a surface coupling agent that possesses polar and nonpolar groups. The polar groups of the surface agent adsorb on the glass surface and react (chemically or physically) with the glass surface to form a bond. The formation of the bond is due to the dipolar interaction between polar groups of the surface agent and the silanol group of the glass surface⁴⁰ (Figure 2.7). Therefore, nonpolar alkyl groups (orientating groups) of lecithin lie perpendicular to the surface and they are free to interact with the nonpolar groups of liquid-crystal to form perpendicular alignment, as shown in Figure 2.8. In this particular case of alignment there is interaction between the alkyl groups of lecithin and the alkyl groups of the liquid-crystal molecules.

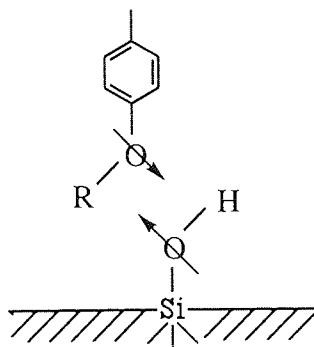


Figure 2.7 Dipolar interactions between polar groups of the surface agent polar groups of liquid-crystals and silanol groups of glass surfaces.

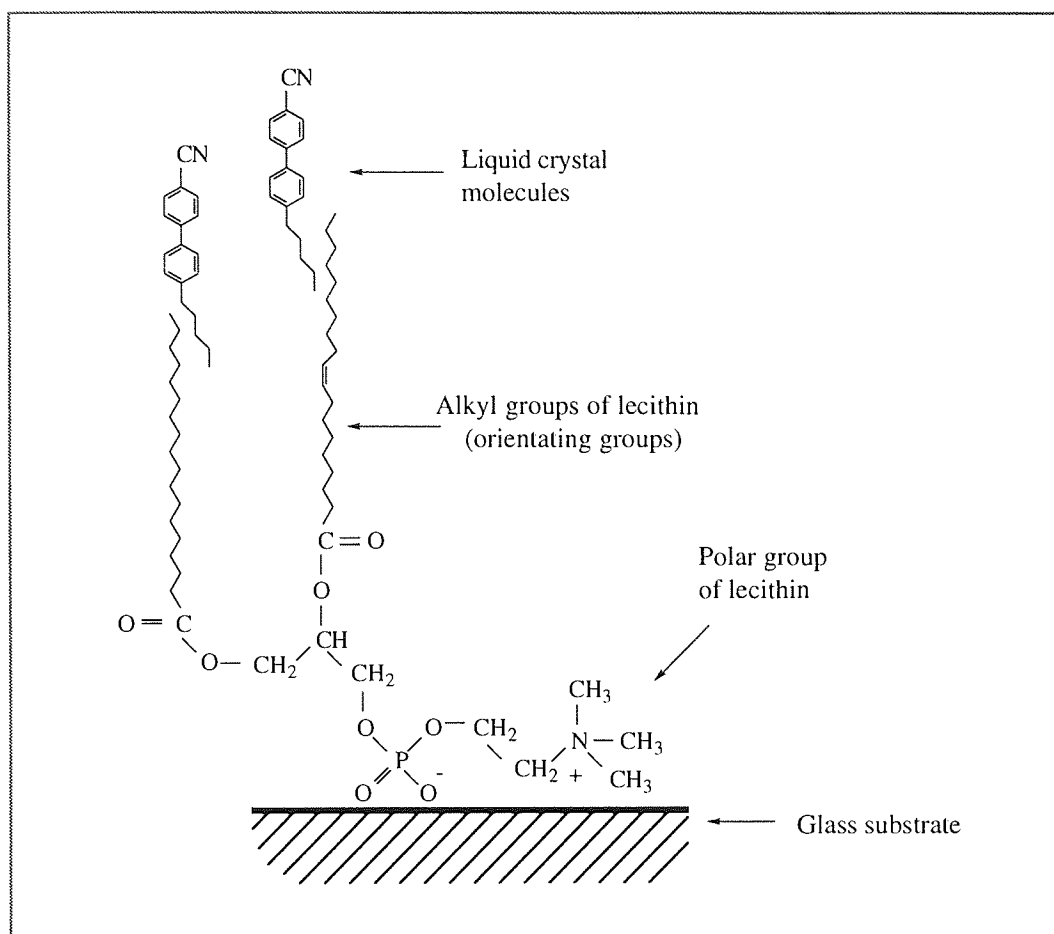


Figure 2.8 Homeotropic alignment by van der Waal's interactions between nonpolar alkyl groups of the liquid-crystal molecules and aligned nonpolar alkyl groups of lecithin as a surface agent.

2.7 Stability of CAB as coating agent

The stability of alignment of a liquid-crystal using CAB (CAB -381 - 20) was examined over a period of 3 months using microscopy and by the measurement of dichroic ratio $R=A_{\parallel}/A_{\perp}$ (in which A_{\parallel} and A_{\perp} are absorbances parallel and perpendicular to the direction of the molecular alignment, respectively). A guest-host LC system (E7 + Sudan Black B) was used for this purpose. The investigations showed that alignment of the system judged by a constant dichroic ratio was stable within this period of time. There was an initial increase in the dichroic ratio that then became independent of time. It seems that this improvement in the dichroic ratio was due to parallel absorption of the LC molecules

adjacent to the CAB surface during the first few days, which induces molecules in the bulk to lie parallel to the more ordered adsorbed molecules of the liquid-crystal.

Alignment of E7 was examined using four kinds of CAB films, that each exhibited parallel alignment (Table 2.1). Microscopic studies showed that alignment is affected by molecular weight, M_n , of CABs. Good parallel alignment was achieved using cellulose acetate butyrate with an average molecular weight of 7000 (CAB-381-20).

Table 2.1 Liquid-crystal (E7) alignment on four kinds of CAB films

cellulose acetate butyrate	%acetyl	%butyryl	Mn	LC alignment
CAB -381 - 2	13.5	38	40000	parallel
CAB -381 -20	13.5	38	70000	parallel
CAB -500 - 5	4.0	51	57000	parallel
CAB -531 - 1	3.0	50	40000	parallel

2.8 Summary

A variety of methods have been reviewed for obtaining parallel or perpendicular alignment in liquid-crystal cells. These are based on the generation of substrate interfaces which have an orienting action on the LC molecules. These orienting surfaces can be created by a number of different surface treatments, including chemical cleaning of the surface, physical adsorption, rubbing of the solid substrate and by deposition of organic or inorganic thin films. The most important factor concerned with production of parallel or perpendicular alignment is chemisorption at the liquid-crystal-solid interface.

CHAPTER 3

THE MICROSCOPIC STUDIES OF LIQUID-CRYSTALS

3.1 Introduction

The first systematic study of mesophases by microscopical techniques was made by Lehmann (Chapter-1). Major contributions to the understanding of mesomorphism were later made by Friedel¹⁹. The optical properties of nematics have been studied mostly by the combined techniques of hot-stage and polarised microscopy. These enable one to determine the transition points between phases. On the other hand, by using polarising microscopy it is possible to determine the orientation of nematic molecules in parallel cell (Chapter-2). Finally, this method is very useful in electro-optic effect studies²¹.

3.2 Electro-optic phenomena

Liquid-crystal electro-optic phenomena can be divided into two categories. Those caused only by dielectric forces or field effects such as guest-host interaction, the twisted nematic effect, and those induced by the combination of dielectric and conduction forces such as dynamic scattering.

3.2.1 *Dynamic scattering*

Dynamic scattering can easily be observed in a transparent sandwich cell with parallel molecular alignment (with respect to the cell walls), for nematic liquid-crystals that possess negative dielectric anisotropy. Above a threshold voltage, an ordered pattern of cigar shaped domains (a striped pattern) appears, known as William domains^{21,22}. At higher voltages, the regularly shaped pattern is destroyed and is replaced by a turbulent state which strongly scatters light (dynamic scattering).

3.3 Experimental

3.3.1 *The polarising microscope*

Optical microscopy of the liquid-crystals was carried out using a Reichert polarising microscope equipped with a hot stage and d.c. supply with a heating rates in the range 0.1 to $10\text{ }^{\circ}\text{C min}^{-1}$.

The basic components of the polarising microscope are indicated in Figure 3.1. The source may give either white or monochromatic light. The light passes through a polariser and only that component whose vibration direction is parallel to that of the polariser is permitted to pass through. The plane polarised light passes through lenses, apertures and accessories and on to the sample which is mounted on the microscope stage. Light transmitted by the sample is picked up by the objective lens.

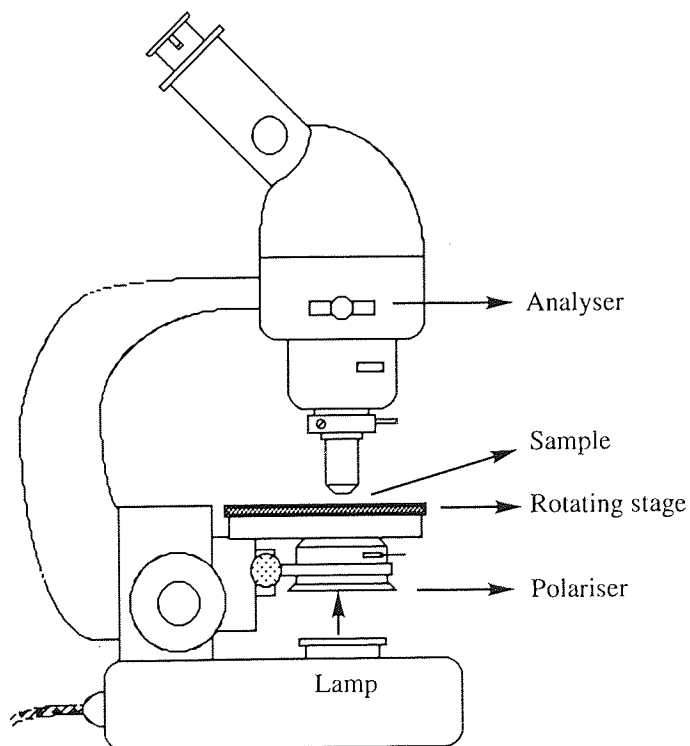


Figure 3.1 The polarising microscope

The analyser may be placed in or out of the path of light. It is similar to the polariser but is oriented so that its vibration direction is perpendicular to that of the polariser. With the analyser 'in', the sample is viewed between crossed polarisers, and one can immediately tell whether the sample is isotropic or anisotropic. Isotropic substances appear 'dark' between crossed polarisers since plane polarised light is transmitted without modification.

Anisotropic substances cause a partial rotation of the plane of polarisation of light as it passes through them. The emergent beam has a component that is vibrating parallel to the transmission plane of the analyser and hence anisotropic substances appear 'light'. On rotating the sample on the microscope stage, the sample may become dark in certain positions. This is known as extinction. On rotating the sample, extinction occurs every 90°; at the 45° positions, the sample exhibits maximum brightness.

3.3.2 Materials

The following liquid-crystal materials were kindly supplied by BDH Chemicals Ltd. as a gift, and were used without further purification. The formulae and transition temperatures are listed in Table 3.1 to Table 3.4. The measured transition temperatures (using the hot-stage polarising microscopy) agreed with the literature values.

Table 3.1 Formulae and transition temperatures of 4,4'- alkyl cyanobiphenyls

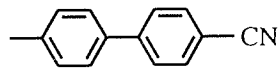
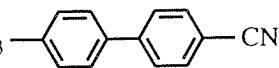
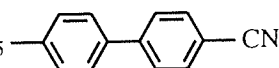
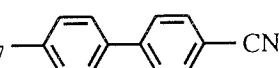
Structure	Abbreviation	K-A	A-N	N-I
C_5H_{11}  CN	5CB	22.5	--	35.0
C_6H_{13}  CN	6CB	14.3	--	28.8
C_7H_{15}  CN	7CB	28.5	--	41.9
C_8H_{17}  CN	8CB	20.9	33.5	40.5

Table 3.2 Formulae and transition temperatures of 4,4'- alkoxy cyanobiphenyls

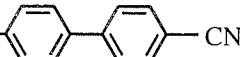
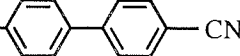
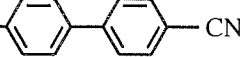
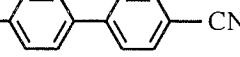
Structure	Abbreviation	K-A	A-N	N-I
$C_5H_{11}O$ -  -CN	50CB	47.5	--	67.5
$C_6H_{13}O$ -  -CN	60CB	57.0	--	75.5
$C_7H_{15}O$ -  -CN	70CB	53.5	--	74.0
$C_8H_{17}O$ -  -CN	80CB	54.5	65.5	79.0

Table 3.3 Composition of the nematic mixture E7: ($T_{NI} = 59.8^\circ\text{C}$)

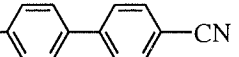
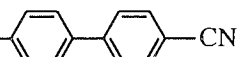
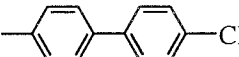
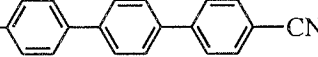
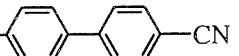
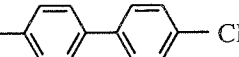
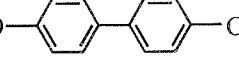
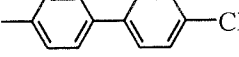
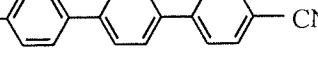
C_5H_{11} -  -CN	5CB	(51.0%)
C_7H_{15} -  -CN	7CB	(25.0%)
$C_8H_{17}O$ -  -CN	80CB	(16.0%)
C_5H_{11} -  -CN	5CT	(8.0%)

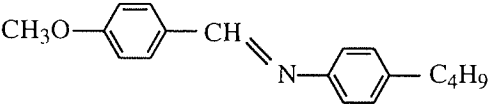
Table 3.4 Composition of the nematic mixture E8: ($T_{NI} = 70.5^\circ\text{C} - 72.0^\circ\text{C}$)

C_5H_{11} -  -CN	5CB	(45.0%)
C_3H_7O -  -CN	3OCB	(16.0%)
$C_5H_{11}O$ -  -CN	5OCB	(12.0%)
$C_8H_{17}O$ -  -CN	8OCB	(16.0%)
C_5H_{11} -  -CN	5CT	(11.0%)

K = Crystal; A = Smectic A; N = Nematic; I = Isotropic

The nematic liquid-crystal 4-methoxybenzylidene-4-n-butyraniline (MBBA) has been made in our laboratory by a condensation method using distilled n-butyraniline and methoxybenzaldehyde¹⁷ (Table 3.5).

Table 3.5 Formula and transition temperatures of MBBA

Structure	K-N/°C	N-I/°C
$\text{CH}_3\text{O}-\text{C}_6\text{H}_4-\text{CH}=\text{N}-\text{C}_6\text{H}_4-\text{C}_4\text{H}_9$ 	21.5	48.0

3.4 The microscopic observations

3.4.1 *The microscopic observation of E7*

The parallel-wall-alignment of E7 (a nematic mixture of four compounds) was achieved by surface treatment of cellulose acetate butyrate (CAB) and rubbing process (Chapter 2). Mylar (12.5 μm) was used as the spacer material. The nematic liquid-crystal cell was placed between crossed polarisers, and was observed through the microscope. The mesophase appeared bright, when the direction of the grooves were at 45° to the plane polarised light (Figure 3.2.c), and dark when the direction of grooves were parallel or perpendicular to the electric field vector of polarised light (Figure 3.2.a,b)

Figures 3.3 and 3.4 show the nematic film of E7 with uniform molecular alignment. The optic axis (nematic director) is parallel to the direction of rubbing, and the direction of grooves are at 45° to the direction of the electric field of the polarised light. At the 45° position the sample exhibits maximum brightness. These observations are explained as follows:

The electric vector of a plane polarised light (E) can be considered as being composed of two equiphase and equiamplitude components at right angles (E_x and E_y). Because of orientational order, nematics are optical anisotropic in nature (birefringence). Therefore, when the electric vector passes through the short axis of the molecules it will be retarded less compared to its passage parallel to the long molecular axis. Thus, after passage of the polarised light through the nematic sample, the light is elliptically polarised. The elliptically polarised emergent light falls on the analyser. It means that the emergent beam have a component that is vibrating parallel to the vibration direction of the analyser and hence a bright image can be observed.

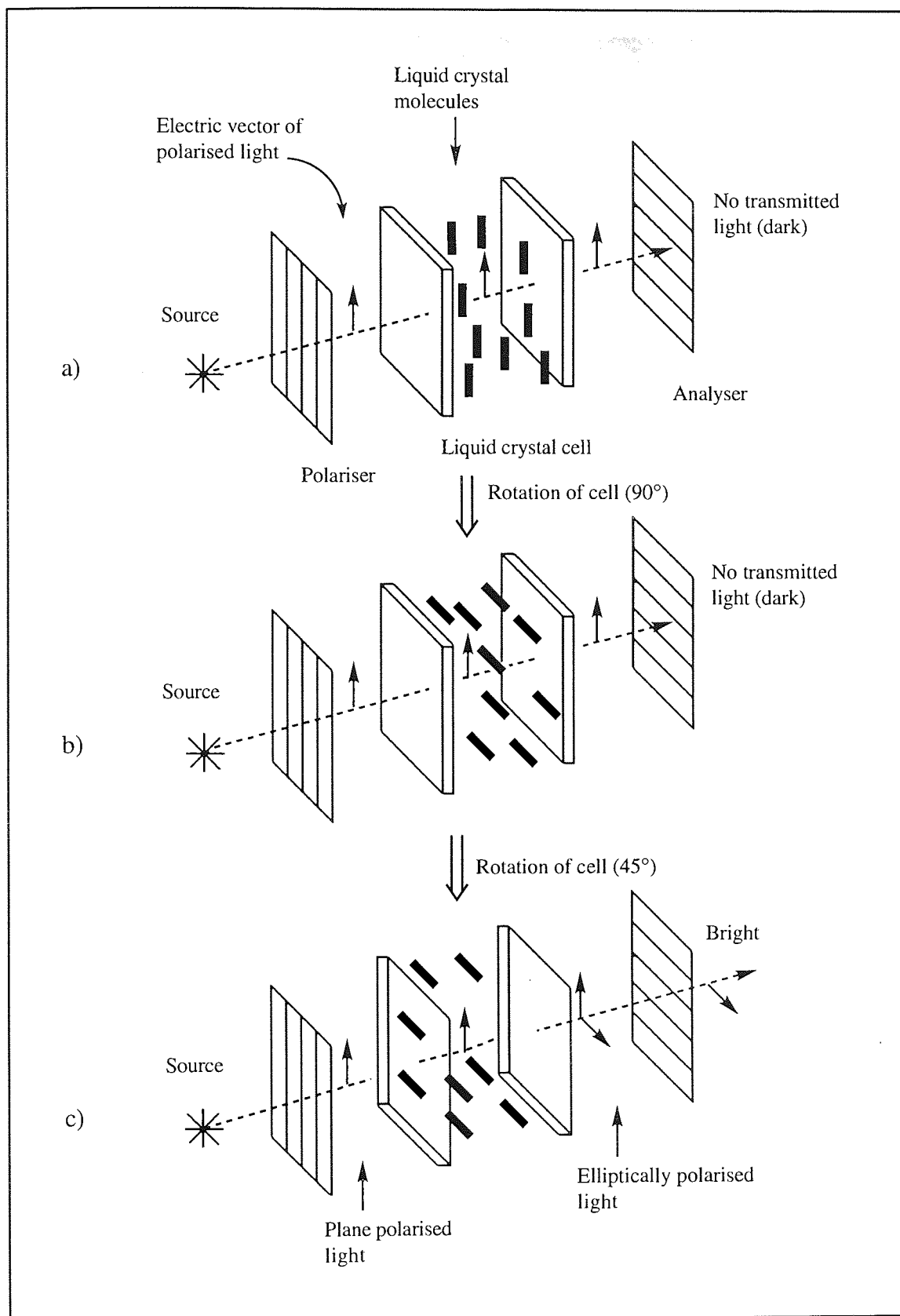


Figure 3.2 Schematic of a nematic liquid-crystal cell with parallel wall alignment when the direction of grooves are, a) parallel, b) perpendicular, c) at 45° to the direction of the polarised light.

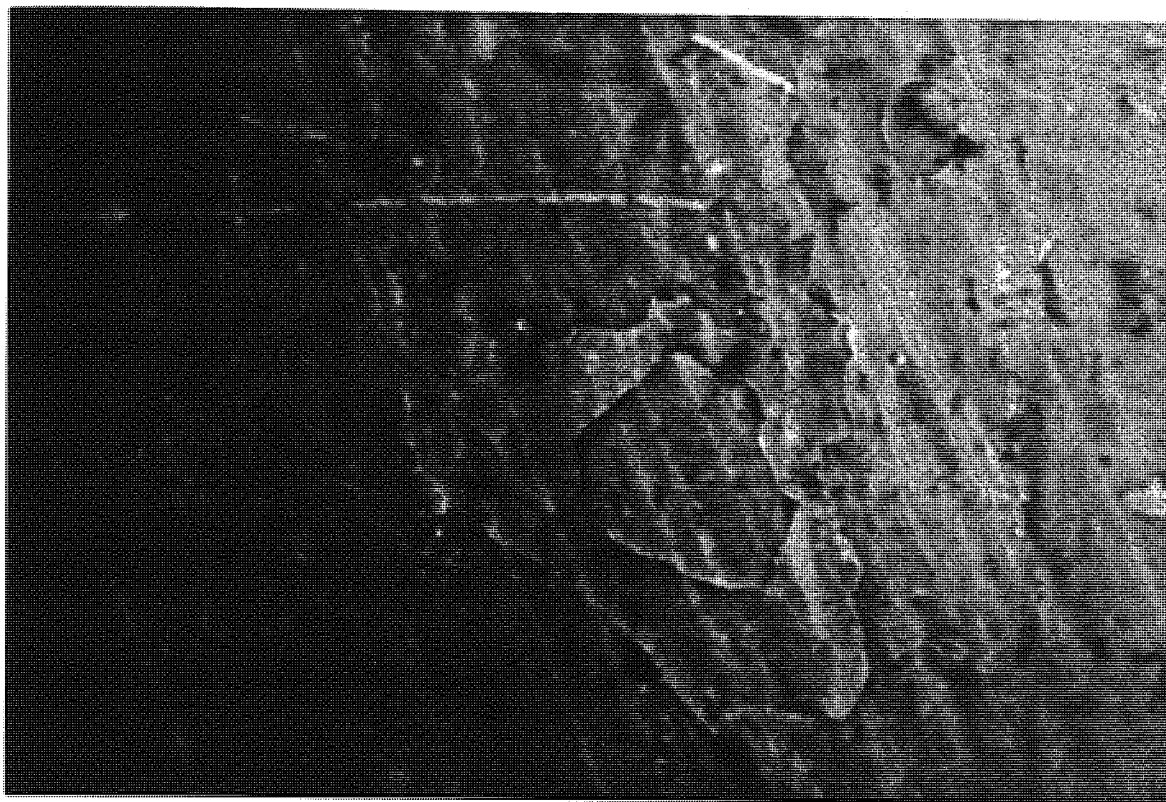


Figure 3.3 Parallel aligned film of nematic mixture (E7) between glass plates which is coated by rubbed CAB at 22 °C; thickness 12.5 μm ; crossed polarisers; magnification x200.

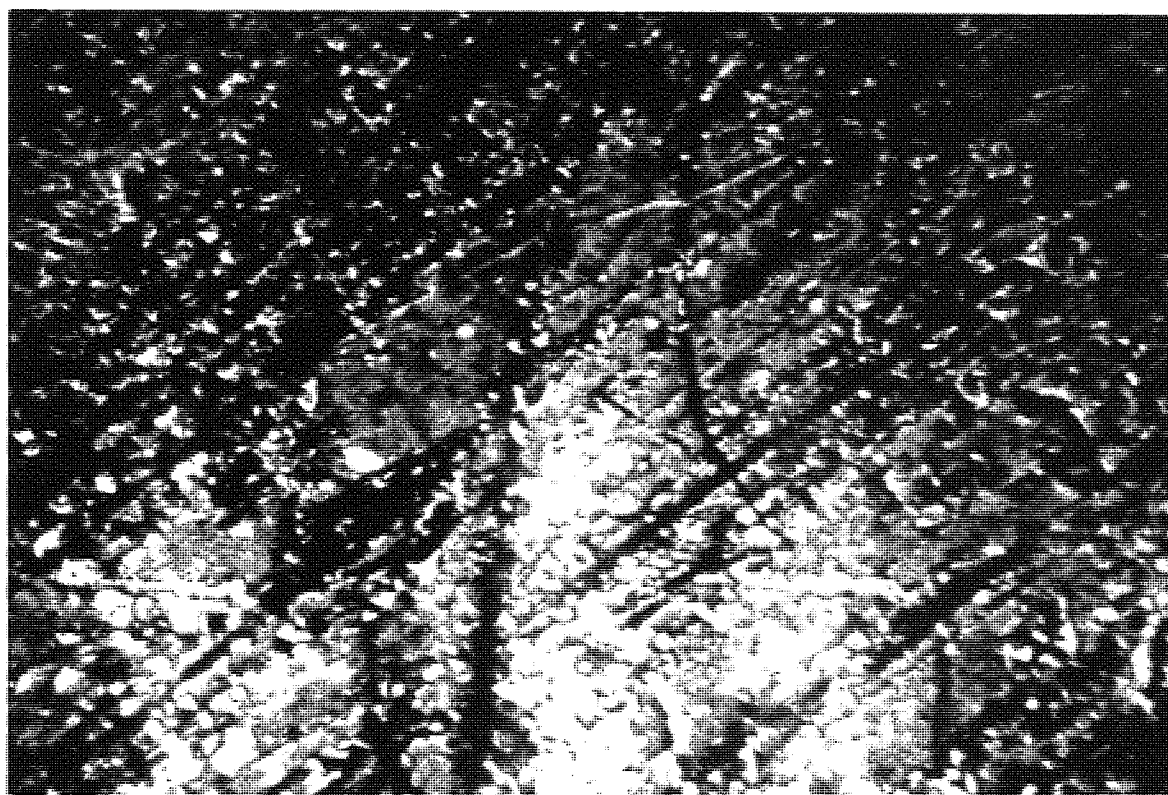


Figure 3.4 Parallel aligned film of E7 at 22 °C; film between rubbed glass slides; thickness 12.5 μm ; crossed polarisers; magnification x200

3.4.2 *The microscopic observation of alkyl cyanobiphenyls*

The transition temperatures of the alkyl cyanobiphenyl compounds (5CB to 8CB) were measured using a polarising microscope with a hot-stage arrangement and are listed in Table 3.1. In the homologous series of alkyl cyanobiphenyls only the lower homologues are purely nematic (5CB to 7B). In this family, 4,4'-octyl cyanobiphenyl (8CB) is the first of the cyanobiphenyls to exhibit a smectic phase at lower temperatures. This liquid-crystal usually undergoes several structural transitions following the melting process. As can be seen from Table 3.1 the transitions of 8CB are crystalline state to smectic phase (20.9°C), smectic phase to nematic phase (33.5°C), and nematic phase to isotropic liquid (40.5°C). Figures 3.5 and 3.6 show the texture of a smectic film of 8CB observed between crossed polarisers prepared using an untreated liquid-crystal cell. This is a smectic A phase which often display a focal conic texture, as shown in Figures 3.5 and 3.6.

3.4.3 *The microscopic observation of alkoxy cyanobiphenyls*

The transition temperatures of the alkoxy cyanobiphenyl liquid-crystals (5OCB to 8OCB) were obtained by hot-stage polarised microscopy. Liquid-crystal cells of conventional sandwich type, with a gap of 12.5 μm determined by Mylar spacers, were used for this purpose. Figure 3.7 shows the well known even-odd alternation¹⁴ associated with crystal-mesophase and nematic-isotropic transitions. This effect is due to the alternation of the alkyl chain ordering which is responsible for other even-odd behaviour of macroscopic properties of liquid-crystals⁴¹. Therefore, it is clear that molecular end chains have important effects on the properties of liquid-crystals.

Figures 3.9 and 3.10 show the optical texture of eutectic mixture of 6OCB/7OCB. The optical texture was observed between crossed polarisers using an untreated liquid-crystal cell.

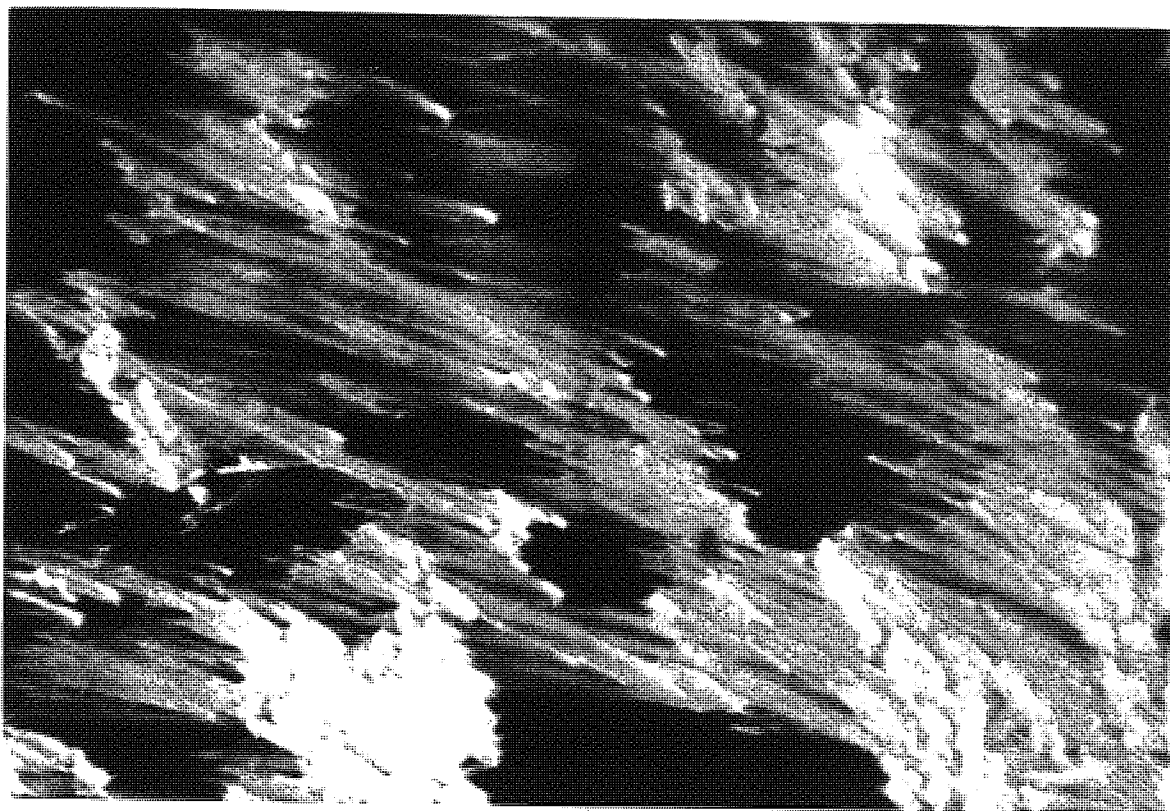


Figure 3.5 Smectic A focal-conic texture of 8CB; film between glass slides at 22 °C; thickness 12.5 μm ; crossed polarisers; magnification x200.

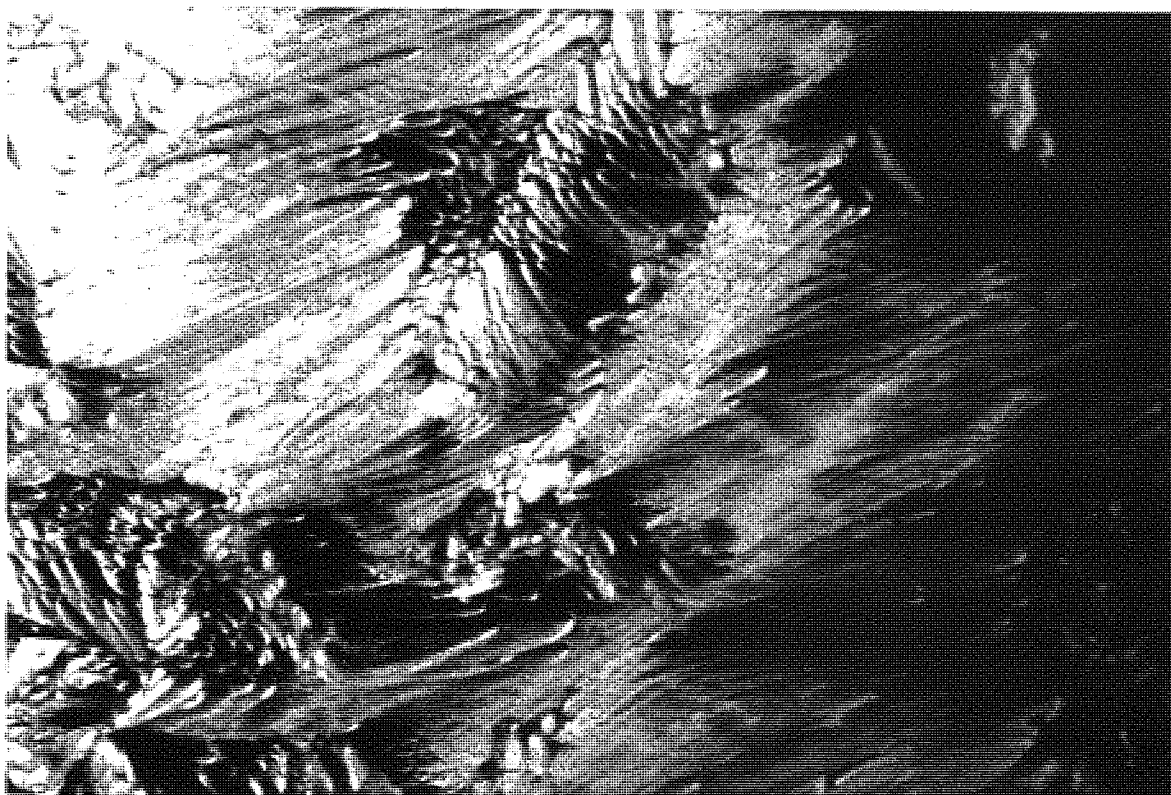


Figure 3.6 Smectic A focal-conic texture of 8CB; film between glass slides at 22 °C ; thickness 12.5 μm ; crossed polarisers; magnification x200.

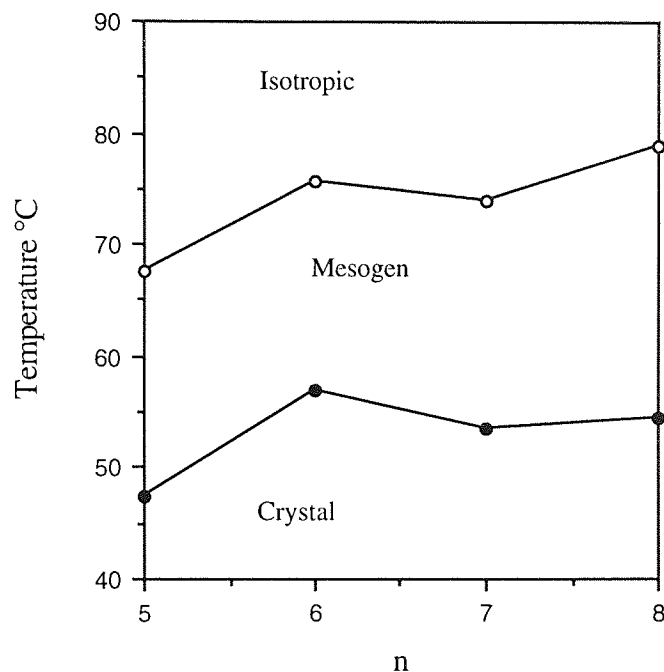


Figure 3.7 The nematic-isotropic transition, T_{NI} , and melting point, T_m , as function of the number of carbon atoms, n , in the alkoxy chain of 4-n-alkoxy-4-cyanobiphenyls.

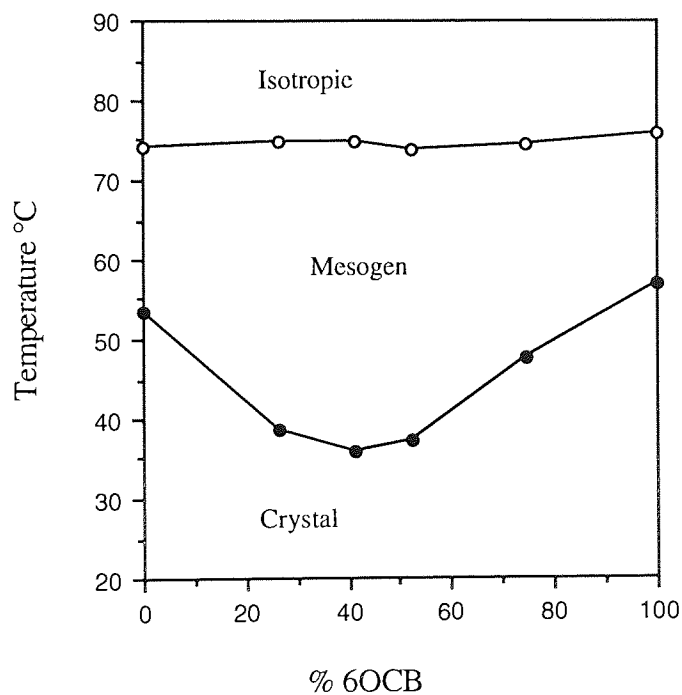


Figure 3.8 Phase diagram of nematic mixtures of 6OCB/7OC; eutectic mixture (41.5% 6OCB+ 58.5% 7OCB).



Figure 3.9 Crystalline phase of 6OCB/7OCB at 23 °C; film between glass slides; thickness 12.5 μm ; crossed polarisers; magnification x200.

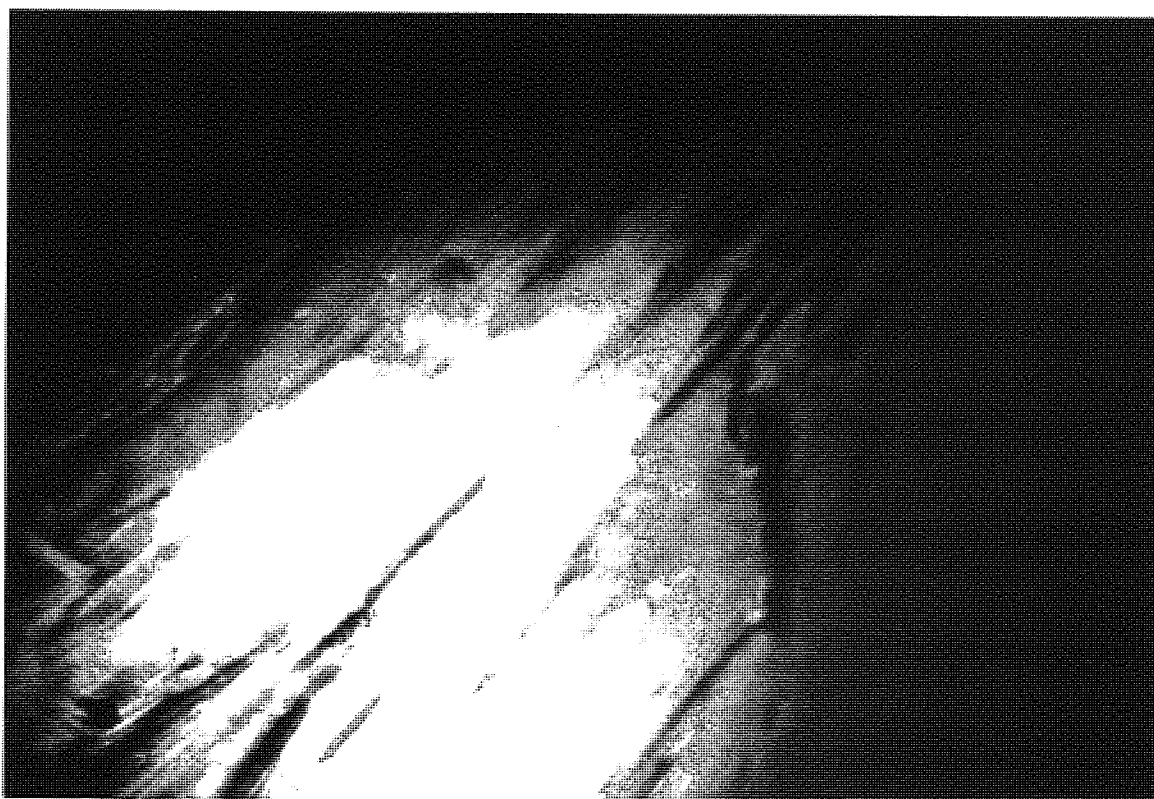


Figure 3.10 Nematic phase of 6OCB/7OCB at 74.8 °C; film between glass slides; thickness 12.5 μm ; crossed polarisers; magnification x200.

3.5 The microscopic and electro-optic studies of MBBA

In all of the experiments described in the following section, a cell of conventional sandwich type was used. The cell had a gap of $12.5\ \mu\text{m}$ maintained by Mylar spacers. The inner surface of the glass substrates were covered by indium/tin oxide (ITO). Coating a very thin layer of hexadecyl trimethyl ammonium bromide (HTAB) from aqueous solution on the plates induced the homeotropic molecular alignment of the sample (Chapter-2). A trial liquid-crystal (MBBA) was used in these experiments. This material has a negative dielectric anisotropy. The liquid-crystal was confined by capillary action alone.

The nematic liquid-crystal cell was placed between crossed polarisers, and observed through the microscope. The mesophase appeared dark as expected for a uniform homeotropic phase. The investigations on the liquid-crystal alignment and electro-optic characteristics were carried out at room temperature. When the electric field was applied, a transition from homeotropic to planar alignment took place, and the mesophase then appeared bright. Figure 3.11 shows the optical texture of MBBA at a electric field strength of $10^6\ \text{mV}^{-1}$ and a low frequency (100 Hz). As can be seen in Figure 3.11, there is a characteristic threaded texture, typical of nematic liquid-crystals. The transition from homeotropic molecular alignment to planar depends on the voltage and frequency. At low frequencies the reorientation needs a lower voltage, whereas at high frequencies (5 - 50 kHz) this reorientation was not observed.

When an increasing voltage was applied, a striped pattern appeared (Figure 3.12), known as Williams domains^{21,22}. The onset of this domain structure occurred at a threshold (minimum voltage at which this phenomenon is observed) electric field of $1.2 \times 10^6\ \text{mV}^{-1}$ and a low frequency of 100 Hz. At higher voltages (above the threshold) the Williams domains became more complicated and a turbulent instability (worm-like motion) giving

rise to dynamic scattering resulted (Figure 3.13). The results are summarised in Table 3.1.

Table 3.1 The effect of electric field on molecular alignment of MBBA

Electric field (E) $\times 10^{-6}/\text{mv}^{-1}$	Alignment	Microscopy observations
0	homeotropic	dark
1.0	planar	bright
1.2	electrohydrodynamic	William domains
2.0	electrohydrodynamic	dynamic scattering

The interpretation of the formation of William domains has been given by Carr and Helfrich²¹. According to this model, the anisotropies of the dielectric constant and of the electric conductivity play an important role. The appearance of William domains is due to electrohydrodynamic effect which depends on the electrical current and mechanical fluid flow. The presence of space charge is necessary for electrohydrodynamic interaction. The space charge may, in principal, be injected from the electrodes. However, the space charge can also be formed by ion segregation in the liquid-crystal itself provided that the material is conductive.

Charge segregation in an electric field can arise from the conductivity anisotropy which in the case of nematic is mostly positive ($\sigma_{\parallel} > \sigma_{\perp}$). In addition, it is a function of dielectric anisotropy. How charges form is indicated in the wavy orientation pattern of Figure 3.14. The interaction of the applied field with the space charges will lead to material flow in alternating directions. Therefore, in the sandwich cell with parallel alignment and the field across the nematic film, electrohydrodynamic alignment reveals itself by the appearance of Williams domains. The underlying orientation and flow patterns are sketched in Figure 3.15. The applied electric field exerts forces on the charge volume elements which try to increase the deformation. At higher voltages the patterns tend to become unstable and a turbulent intensity of light results (dynamic scattering).



Figure 3.11 Optical texture of MBBA at a field strength of 12 V and a frequency about 100 Hz at 22 °C; thickness 12.5 μm ; crossed polarisers; magnification x200.

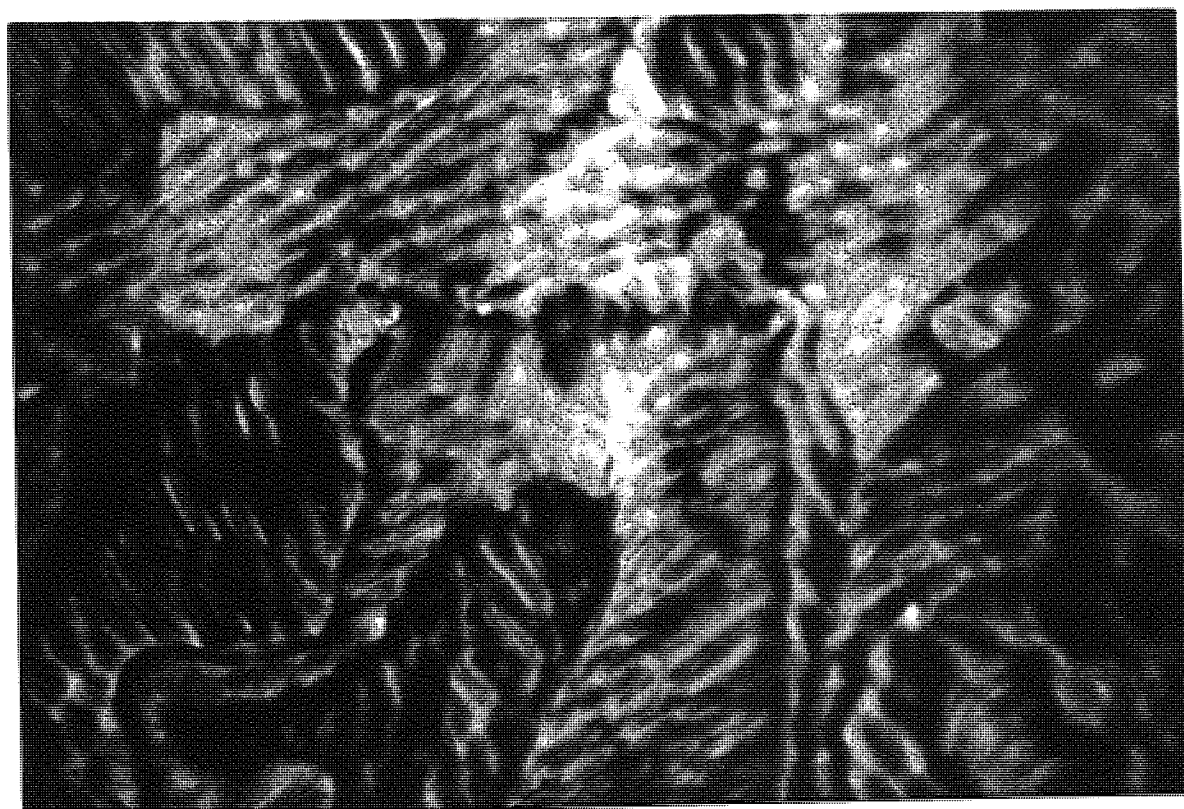


Figure 3.12 William domains in a 12.5 μm thick sample of MBBA at 22 °C and 15V (100 Hz); crossed polarisers; magnification x200

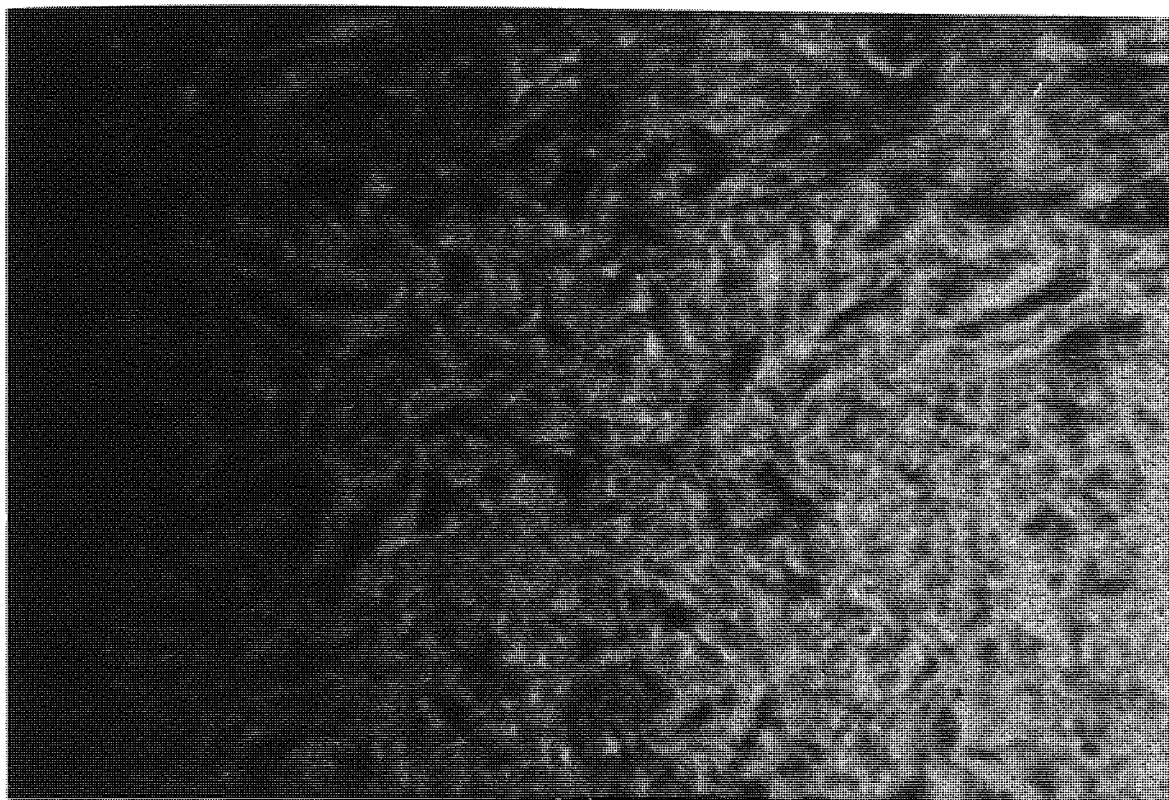


Figure 3.13 Dynamic scattering in a 12.5 μm thick sample of MBBA at 22 $^{\circ}\text{C}$ and 25V (100 Hz); crossed polarisers; magnification x200.

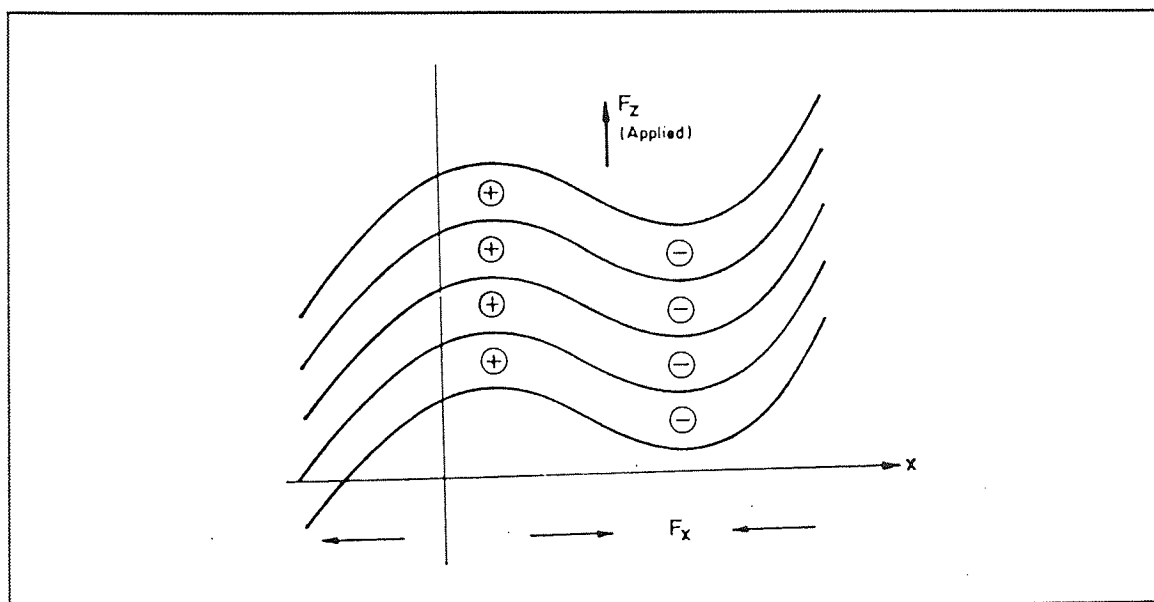


Figure 3.14 Charge segregation and the resulting transverse field F_x in an applied field F_z if the conductivity along the nematic axis is larger than the perpendicular to it.

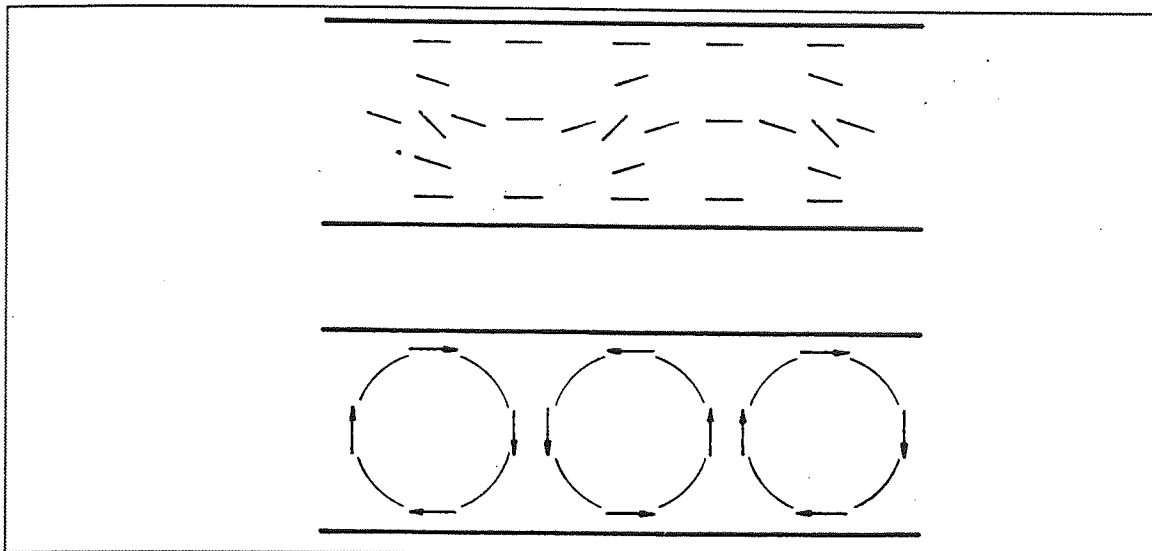


Figure 3.15 Cross section through the flow and orientation patterns of Williams domains, indicated by velocity vectors and rod-like molecules.

It should be noted that threshold voltage for the dynamic scattering to exist depends on frequency of the electric field. It was found that dynamic scattering occurs only below a certain frequency (critical frequency). In fact, the existence of dynamic scattering becomes more difficult as the frequency of the ac field increases. From the experimental data, dynamic scattering was not observed at high frequencies. The results have been plotted as threshold voltage versus frequency on graph 3.16.

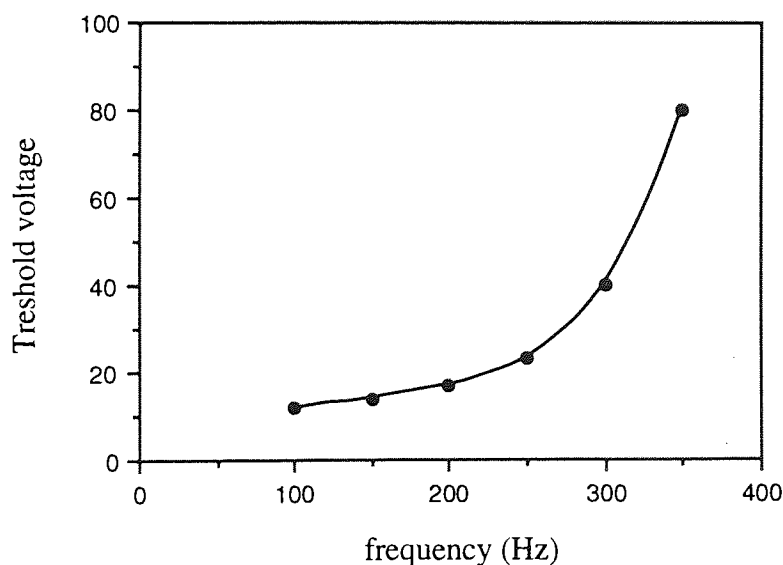
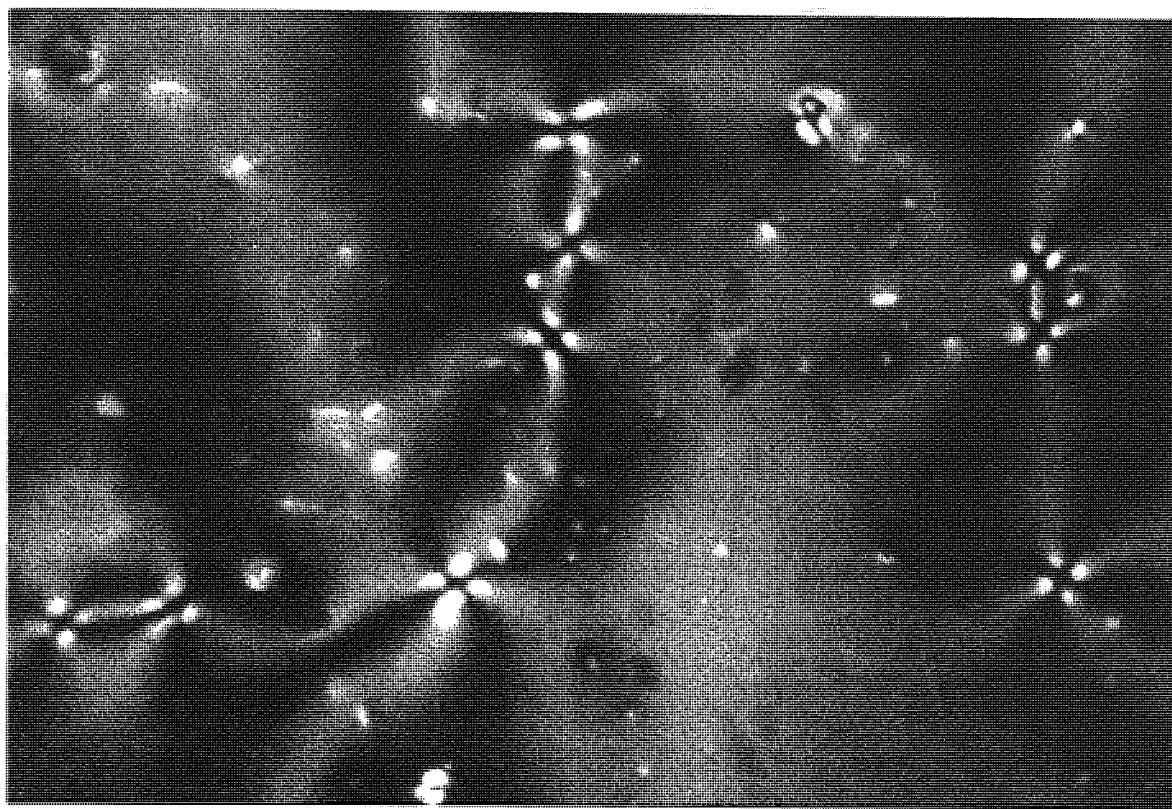


Figure 3.16 Frequency dependence of threshold voltage for dynamic scattering in MBBA; sample thickness, 12 μm .

Figures 3.17(a) and 3.17(b) show the Schlieren texture (nucleated domains) with disclination points of MBBA. The optical texture was observed between crossed polarisers using an untreated liquid-crystal cell. The Schlieren texture observed between crossed polarisers is characterised by dark brushes which start from points (a number of scattered points or nuclei) that pass continuously from one nucleus to another. Usually, points with two or four dark brushes can be observed.



(a)

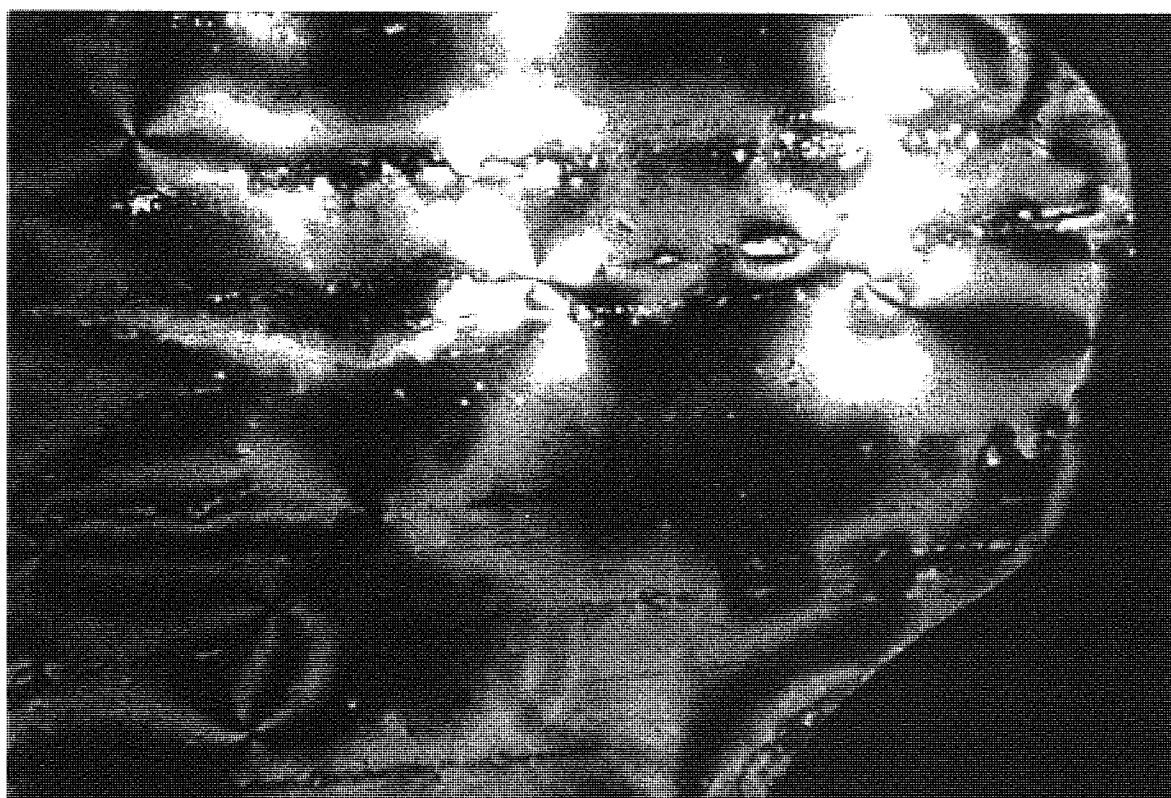


Figure 3.17 Schlieren texture in a 12.5 μm thick sample of MBBA showing "nucleated domains". The brushes (4) can clearly be seen; film between glass slides at 22 $^{\circ}\text{C}$; crossed polarisers; magnification x200.

CHAPTER 4

THE PHASE TRANSITION AND ORDER PARAMETER OF CYANO-BIPHENYL LIQUID CRYSTALS

4.1 Introduction

The phase transition investigations on liquid crystals are very important as they exhibit intermediate phases between isotropic liquid and crystalline phases. Differential Scanning Calorimetry (DSC)⁴², Hot stage polarised microscopy⁹ and density measurements⁴³ are the main techniques for the detection of phase transitions. On the other hand, the orientational order parameter, S , of liquid crystals is an essential parameter for scientific and technological purposes. Various methods are used to measure the order parameter. These are based mainly, dielectric relaxation⁴⁴, UV and IR dichroism^{45,46}, nmr^{47,48}, and from refractive index and density data^{49,50}.

The purpose of this chapter is to establish the relationship between density and refractive index (the bulk properties) and various molecular parameters. The densities of liquid crystals provided information regarding the nature of the phase transition, such as order of the transition, and molecular packing in various phases^{51,52,53}.

In addition, the availability of optical and density data at several temperatures makes it possible to calculate the effective molecular polarisabilities and anisotropy of polarisabilities in nematic liquid crystals. Temperature dependent density and refractive index measurements are usually interpreted using anisotropic and or isotropic internal field models, which relate the macroscopic properties to the molecular polarisability. The polarisabilities can be calculated by using the methods of Neugebaure⁵⁴, Saup-Maier⁵⁵, and Palffy-Muhoray et al^{56,57}, and Vuks⁵⁸.

4.2 Theory

4.2.1 Polarisation and polarisability

In the case of a capacitor with a dielectric material, the presence of the electric field E on the plates polarises the dielectric molecules (see section 5.2.2). Non-polar molecules may acquire a temporary or induced dipole moment when they are exposed to an external electric field E . Under the influence of this field the positive and negative charges in the molecule are moved apart (i.e. the molecule is polarised). The magnitude of this induced dipole moment, μ_{ind} , is proportional to the effective field E_{eff} in which the molecule finds itself. Using a proportionality constant, α , then

$$\mu_{\text{ind}} = \alpha E_{\text{eff}} \quad (4.1)$$

This proportionality constant (i.e. $\alpha = \alpha_{\text{orientation}} + \alpha_{\text{atomic}} + \alpha_{\text{electronic}}$) is called the polarisability of the molecule²⁰. From the dimensions of the dipole moment $[e] [l]$, and the field intensity, $[e] [l]^{-2}$, (e and l denoting charge and length respectively), α is seen to have the dimensions of volume $[l]^3$. If the molecule is assumed to be isotropic (i.e. same properties in all directions), then α may be regarded as a scalar quantity. In general however, the molecule is elliptical in shape and anisotropic and the polarisability α is then a second rank tensor (see section 4.2.4). If there are N molecule per unit volume (cm^3) in the medium, each with effective dipole moment, μ , then the total electric moment per unit volume (polarisation) is given by

$$P = N\mu_{\text{ind}} = N \alpha E_{\text{eff}} \quad (4.2)$$

here $P = (P_{\text{orientation}} + P_{\text{atomic}} + P_{\text{electronic}})$. From the definitions of the electric displacement D (see section 5.2.5):

$$D = \epsilon E \quad (4.3)$$

$$D = E + 4\pi P \quad (4.4)$$

Elimination of D by combining these two equations gives the well-known expression for the polarisation for an isotropic material^{59,60}

$$P = \frac{(\epsilon - 1)}{4\pi} E \quad (4.5)$$

4.2.2 The internal field E_i , (local field)

When a dielectric material is placed into external electric field, every particle of the material is exposed to an internal field E_i . E_i is defined as the total electric field at the position of the molecule (particle) minus the field due to the molecule itself⁶⁰. Lorentz calculated the internal field in homogeneously polarised matter as the field in a virtual spherical cavity of macroscopic diameter (Lorentz field). Lorentz showed for a cubical arrangement of identical particles, the internal field is the sum of two parts ($E + E_p$). Here, E is an external field which acts on the medium, and is due to the net charges per unit area at the capacitor plates, and E_p is a field due to the polarisation of material outside the sphere, i.e. the field arises from the charges on the surface of the spherical cavity that surrounds a central molecule (Figure 4.1).

The effective field can be divided into three parts; $E_{\text{eff}} = E + E_p + E_m$, where, E_m is the molecular field due to the other molecules within the sphere E_m , i.e. the field arising from the orientation and polarity of the molecules near the center of the sphere. Due to the Lorentz assumption^{60,61}, for a cubic arrangement, and for molecules with completely random orientation E_m is zero, and then E_{eff} may be regarded as arising from two components ($E + E_p$). Therefore, the internal field E_i introduced by the Lorentz is equivalent to E_{eff} .

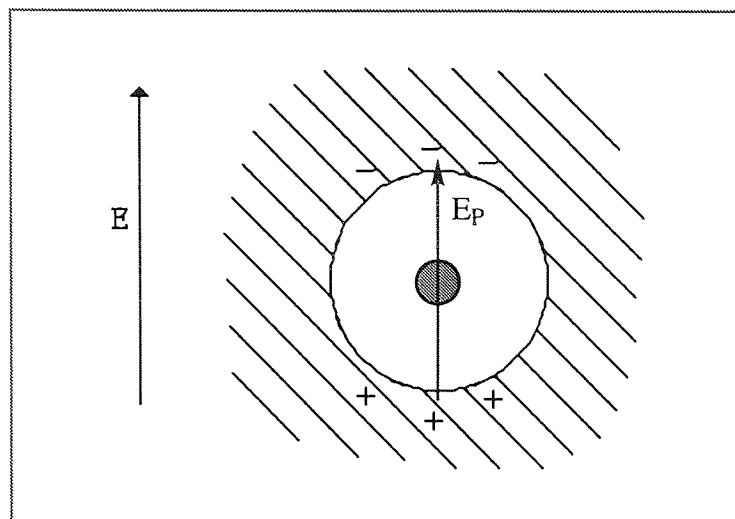


Figure 4.1 The internal field, $E_i = E_{\text{eff}} = E + E_p$

The effective field experienced by a molecule at the center of a spherical cavity within a continuous dielectric in an external electric field E (Figure 4.1) is given by

$$E_{\text{eff}} = E + \frac{4\pi}{3} P \quad (4.6)$$

The relationship between the effective field acting on a molecule and the external field, E , was given by Mossotti (1850), and independently deduced by Clausius (1879)⁵⁹;

$$E_{\text{eff}} = \frac{(\epsilon + 2)}{3} E \quad (4.7)$$

Elimination of P from equations 4.2 and 4.5, together with equation 4.7, gives a relationship between the static dielectric constant, ϵ , for non-polar molecules, and the polarisability α , namely

$$\left(\frac{\epsilon - 1}{\epsilon + 2} \right) = \frac{4\pi}{3} N \alpha \quad (4.8)$$

where $N = N_A (d/M)$ is the number of molecules per cm^3 , M is the molar mass, $N_A = 6.02 \times 10^{23}$ is Avogadro's number, and d is the density. Equation 4.8 is generally called

the Clausius-Mossotti equation^{59,60,61}. The Clausius-Mossotti equation can also be used to describe the dielectric response of polar systems in high-frequency alternating fields:

$$\left(\frac{\epsilon_{\infty} - 1}{\epsilon_{\infty} + 2} \right) = \frac{4\pi}{3} N \alpha \quad (4.9)$$

in which ϵ_{∞} may be regarded as the dielectric constant at frequencies where the permanent dipole moments can no longer follow the changes of the field. Under these circumstances, the orientation polarisation does not make any contribution in the total molecular polarisation, and the dielectric constant is a function of the induced polarisation ($P_a + P_e$), where P_a is the atomic polarisation and P_e is the electronic polarisation.

4.2.3 Optical polarisability

At very high frequencies (i.e. optical frequencies, $\sim 10^{15}$ Hz), only the electrons are able to respond to the rapidly changing direction of the applied field and the molecular polarisation is due to the electronic polarisability only. Using the Maxwell relation at optical frequencies⁶¹,

$$\epsilon_{\infty} = n^2 \quad (4.10)$$

and equation (4.9) then becomes

$$\left(\frac{n^2 - 1}{n^2 + 2} \right) = \frac{4\pi}{3} N \alpha_{\text{electronic}} \quad (4.11)$$

Equation 4.11 is called the Lorenz-Lorentz equation⁶⁰ and is applicable to both polar and nonpolar systems. Therefore, for normal gases and liquids the refractive index at optical frequencies correlates with the mean molecular polarisability via equation 4.11. The

Lorentz-Lorentz equation is often expressed as molar refraction, R , defined analogously to the molar polarisability at optical frequencies⁶⁰:

$$R = \left(\frac{n^2 - 1}{n^2 + 2} \right) \frac{M}{d} = \frac{4\pi}{3} N_A \alpha \quad (4.12)$$

In the above expression $\alpha = \alpha_{\text{electronic}}$. From the definition of R in equation 4.12 its units are seen to be cm^3 . The molar refraction is essentially the total polarisability of a mole of the substance. Equation 4.12 implies that R will be a constant for any chemical compound, i.e. provided that the structure of the molecules are unchanged, i.e., α , and hence R , will be independent of the state (gas, liquid, solid) or of temperature. To determine R experimentally it is necessary to measure the refractive index, n , and the density, d , at the same temperature.

4.2.4 Polarisabilities in anisotropic medium

Due to orientational order, nematic liquid crystals are anisotropic and birefringent materials. The Clausius-Mossotti and the Lorentz-Lorentz equations 4.8 and 4.11 are applicable only to isotropic materials, and therefore they cannot be used, without modification to calculate the polarisability of crystals and nematic liquid crystals. Thus, it is necessary to consider a more detailed picture of the polarisability of anisotropic material.

In an anisotropic system the electrons are bound in the molecules with force constants differing in various directions, therefore, the polarisabilities of the molecule will have different values in three space directions, $\alpha_x, \alpha_y, \alpha_z$. These polarisabilities will be specified by an ellipsoid giving their values in any direction; each polarisability has a corresponding refractive index n (n_x, n_y, n_z). In the most general case this ellipsoid has three different main axes (Figure 4.2) which are said to be optically biaxial⁶², i.e. $n_x \neq n_y \neq n_z$. If the axes of a Cartesian co-ordinate system (x, y, z) is in the direction of

the principal axes of the ellipse of polarisability, then α can be described by a second rank tensor^{62,63} in diagonalised form.

For uni-axial media the ellipsoid has an axis of symmetry o_z (optical axis) and $n_x = n_y \neq n_z$. Therefore, the ellipsoid has two axes of equal length and one unequal (a spheroid, i.e. an ellipsoid of revolution). Materials having this property are said to be doubly refracting, and exhibit birefringence. In other words, their optical properties are not the same in all direction, and they have two different values for refractive index. This will be true for ordered nematic liquid crystals, since nematics behave like optically uniaxial crystals.

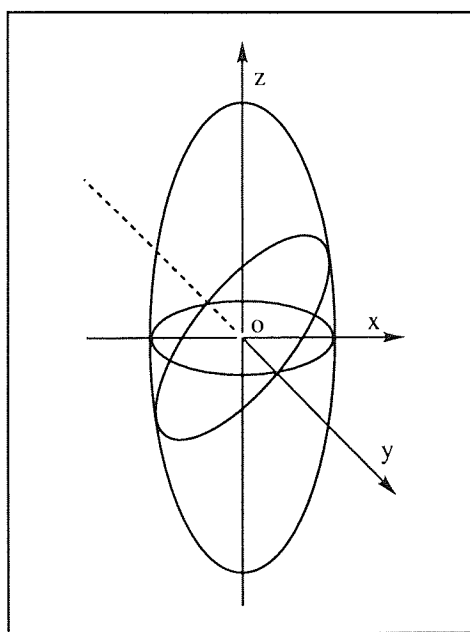


Figure 4.2 Ellipsoid of indices

A ray of light incident normally on the doubly refracting crystal is broken up into two rays as it traverses the crystal. The ray corresponding to wave front tangent to the spherical wavelets is undeviated and is called the ordinary ray. A ray corresponding to a wave front tangent to the ellipsoidal wavelets is deviated and is called the extraordinary ray. Figure 4.3 shows an initially unpolarised beam traversing a principal section of a doubly refracting crystal. The filled-in circles and/or arrows drawn along each ray

indicate that the ordinary ray has its electric field vector normal to the principal section, while the field of the extraordinary ray is parallel to the principal section. The index of refraction of a material is defined as the ratio of the velocity of light in empty space to the velocity in the material. Evidently a doubly refracting material has one index for the ordinary and another for the extraordinary ray.

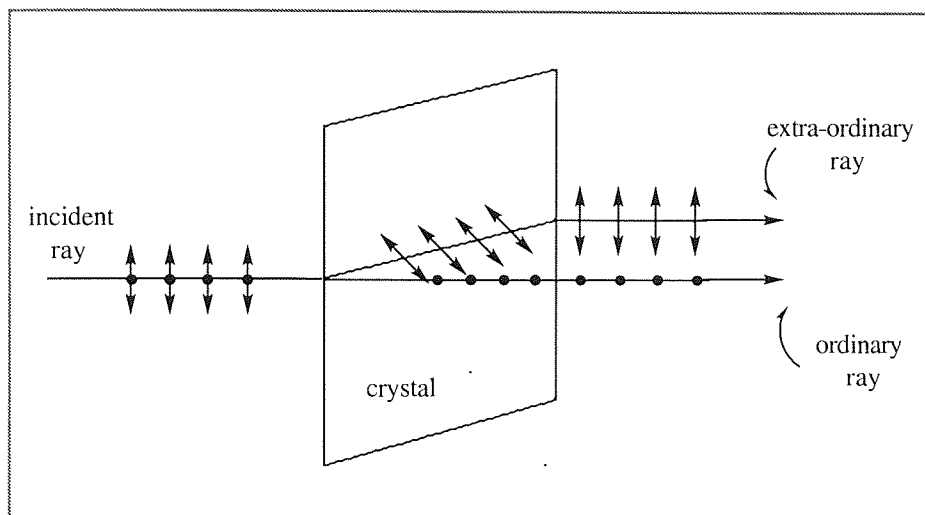


Figure 4.3 A beam of light with two orthogonal field components can be split into two beams by a doubly refracting crystal.

For an optically uni-axial system, with the optic axis in the z direction, the components of polarisability along the co-ordinate axes ox , oy , oz are as follows:

$$\alpha = \begin{bmatrix} \alpha_{\perp} & 0 & 0 \\ 0 & \alpha_{\perp} & 0 \\ 0 & 0 & \alpha_{\parallel} \end{bmatrix} \quad (4.13)$$

Therefore, α has the form of a diagonal matrix, for all the off-diagonal elements are zero⁶⁴. The polarisabilities along the long axis (molecular axis) and perpendicular to it and are described as $\alpha_{\parallel} = \alpha_{zz}$, and $\alpha_{\perp} = \alpha_{xx} = \alpha_{yy}$, respectively. In general, the polarisability ellipsoid is spheroid for any molecule that possesses a single three-fold (or higher) symmetry axis⁶⁴. When a molecule has more than one three-fold symmetry axis, the polarisability ellipsoid is a sphere.

In order to calculate the polarisability α in the nematic phase, specific models taking account of the polarisation in an anisotropic medium need to be considered. These models all involve making assumptions about the internal field (responsible for polarising the molecules) acting on the molecule.

The relationship between the dielectric permittivity and the molecular polarisability of liquid crystals is described by the Maier-Meier equations⁶⁵ for low frequencies. The relationship between the refractive index (the macroscopic observable) and the molecular polarisability (microscopic property) is described by several methods. These are described in the following sections.

4.2.4.1 *The Vuks's method*

Vuks⁵⁸ assumed the internal field to be isotropic and his equation relates the refractive indices of liquid crystal molecules to the molecular polarisability by the modified Lorentz-Lorenz equation for optical frequencies. Vuks showed, experimentally, that the Lorentz-Lorenz formula also gives very good results for anisotropic materials (crystals). If n^2 is taken to be $n^2 = (n_1^2 + n_2^2 + n_3^2)/3$ and α is assumed to be the mean polarisability $\alpha = (\alpha_1 + \alpha_2 + \alpha_3)/3$ where n_i 's are the principal refractive indices and α_i 's are the principal polarisabilities of the molecules and the subscripts 1, 2, 3 denote the principal axes of the two tensors n^2 and α . According to this approach, for crystals, the Lorentz-Lorenz equation 4.11 may be written as

$$\frac{n_1^2 - 1}{n^2 + 2} + \frac{n_2^2 - 1}{n^2 + 2} + \frac{n_3^2 - 1}{n^2 + 2} = \frac{4\pi}{3} N (\alpha_1 + \alpha_2 + \alpha_3) \quad (4.14)$$

In order to determine the anisotropic polarisability α_1 , α_2 , and α_3 of the molecules it is necessary to find the relationship between the individual components of the two tensors n_i^2 and α_i .

$$\frac{n_i^2 - 1}{n^2 + 2} = \frac{4\pi}{3} N \alpha_i, \quad i = 1, 2, 3 \quad (4.15)$$

A doubly refracting material such as liquid crystal has one index for the ordinary (n_o) and another for the extraordinary ray (n_e). Therefore, using the generality of Vuks approach, the expressions for the extraordinary and ordinary indices of the nematic phase, are

$$\frac{(n_e^2 - 1)}{(n^2 + 2)} = \frac{4\pi}{3} N \alpha_e \quad (4.16)$$

and

$$\frac{(n_o^2 - 1)}{(n^2 + 2)} = \frac{4\pi}{3} N \alpha_o \quad (4.17)$$

where N is the number of molecules per unit volume, cm^3 , n_e and n_o are the extraordinary and ordinary refractive indices. The relationship between n_o , n_e , n can be shown to be isobestic, via.

$$n^2 = \frac{1}{3} (2n_o^2 + n_e^2) \quad (4.18)$$

where n is the average value of the refractive indices in the nematic phase. The assumption of isotropic internal field in a liquid crystalline phase (anisotropic medium) has no theoretical basis. However, the Vuks relation gives good results when used to derive the polarisabilities from the refractive indices and densities, and several authors have supported the validity of the Vuks method^{66,67}.

4.2.4.2. *The Neugebauer method*

The Neugebauer method^{54,68} for calculating the anisotropy of polarisability of the crystalline phase is based on the following equations

$$n_i^2 - 1 = 4\pi N_c \alpha_i (1 - N_c \alpha_i \gamma_i)^{-1} \quad (4.19)$$

and

$$\gamma_1 + \gamma_2 + \gamma_3 = 4\pi \quad (4.20)$$

where the n_i 's (n_1, n_2, n_3) are the principal refractive indices and the α_i 's ($\alpha_1, \alpha_2, \alpha_3$) are the principal polarisabilities of the molecules, and the γ_i 's are internal field constants. N_c is the number of molecules per cm^3 in the crystalline phase. If the polarisabilities along the long and short axes of the polarisability ellipsoid are described as α_{\parallel} , and α_{\perp} , respectively, the above relation reduces to

$$\frac{1}{\alpha_{\parallel}} + \frac{2}{\alpha_{\perp}} = \frac{4\pi N_c}{3} \left[\frac{n_1^2 + 2}{n_1^2 - 1} + \frac{n_2^2 + 2}{n_2^2 - 1} + \frac{n_3^2 + 2}{n_3^2 - 1} \right] \quad (4.21)$$

The Neugebauer method assumes an anisotropic internal field and introduces γ_e and γ_o as the internal field constants parallel and perpendicular to long molecular axis, respectively. Due to the assumption of an anisotropic internal field in an anisotropic molecular distribution, this model has the advantage of theoretical basis. The expressions for the extraordinary and ordinary indices of the nematic phase, are

$$(n_e^2 - 1) = 4\pi N \alpha_e (1 - N \alpha_e \gamma_e)^{-1} \quad (4.22)$$

and

$$(n_o^2 - 1) = 4\pi N \alpha_o (1 - N \alpha_o \gamma_o)^{-1} \quad (4.23)$$

Here, N is the number of molecules per cm^3 , γ_e and γ_o are similar to the case for a crystal, and they satisfy the relation $\gamma_e + 2\gamma_o = 4\pi$. The relevant equations for calculating the polarisabilities α_e and α_o obtained from equations 4.24 and 4.25 are

$$\frac{1}{\alpha_e} + \frac{2}{\alpha_o} = \frac{4\pi N}{3} \left[\frac{n_e^2 + 2}{n_e^2 - 1} + \frac{2(n_o^2 + 2)}{n_o^2 - 1} \right] \quad (4.24)$$

and

$$\alpha_e + 2\alpha_o = \alpha_{||} + 2\alpha_{\perp} = \frac{9}{4\pi N} \left[\frac{n^2 - 1}{n^2 + 2} \right] \quad (4.25)$$

Equation 4.25 is the Lorentz-Lorenz relation (molar refraction) for the liquid phase, and is independent of temperature and of the state of matter.

4.2.4.3. The Saupe and Maier method

The Saupe-Maier model⁵⁵ assumes an anisotropic internal field and incorporates a internal field correction though the use of a quantity “a” expressed as a function of the coordinates of the molecules within the Lorentz sphere. The equations relating refractive index and polarisabilities are then

$$\frac{n_e^2 - 1}{n_e^2 + 2 - 2a(n_e^2 - 1)} = \frac{4\pi}{3} N \alpha_e \quad (4.26)$$

and

$$\frac{n_o^2 - 1}{n_o^2 + 2 + a(n_o^2 - 1)} = \frac{4\pi}{3} N \alpha_o \quad (4.27)$$

The effective polarisabilities α_e and α_o of the liquid crystal molecules can be obtained from equations 4.26 and 4.27, and the internal field parameter “a” can be calculated using equations 4.28 and or 4.29 as follows:

$$\frac{n^2 - 1}{n^2 + 2} V_{iso} = \frac{1}{3} \left[\frac{n_e^2 - 1}{n_e^2 + 2 - 2a(n_e^2 - 1)} + \frac{2(n_o^2 - 1)}{n_o^2 + 2 + a(n_o^2 - 1)} \right] V_n \quad (4.28)$$

where, V_n and V_{iso} are molar volumes, M/d, in the nematic and isotropic phases, respectively, and

$$\frac{a}{V_n} = \frac{-2 R_e R_i + R_o R_i + R_e R_o \pm \sqrt{(2R_e R_i - R_o R_i - R_e R_o)^2 - \frac{8R_e R_o R_i (R_e + 2R_o - 3R_i)}{3}}}{4 R_i R_e R_o} \quad (4.29)$$

Where, $R_{e,o} = V_n (n_{e,o}^2 - 1) / (n_{e,o}^2 + 2)$, and R_i is the molar refraction in the isotropic phase. According to the Saupe-Maier approach, the internal field parameter is assigned the same value for directions parallel and perpendicular to the molecular axis. However, the correction parameter “a” is a function of temperature and should decrease monotonically with increasing temperature.

4.2.4.4. The Palffy-Muhoray method

Palffy-Muhoray *et al*^{56,57} introduced a model that shows that the internal field, local field, anisotropy is proportional to the orientational order parameters, and that the proportionality constant is simply related to the length-to-breadth ratio of the molecular hard core. According to the model of Palffy-Muhoray *et al.*, in an anisotropic fluid, the internal field, E_i , is given by

$$E_i = \left[\frac{1}{3} (\epsilon_{ii} + 2) + \eta_{ii} (\epsilon_{ii} - 1) \right] E \quad (4.30)$$

where E is the external field. Consequently, the relation between refractive indices, density and effective molecular polarisability α_{ii} is given by

$$\frac{n_{ii}^2 - 1}{n_{ii}^2 + 2} = \frac{4\pi}{3} N \alpha_{ii} (1 - 4\pi N \eta_{ii} \alpha_{ii})^{-1} \quad (4.31)$$

where $i = x, y, z$ refers to directions in a laboratory fixed co-ordinate system and η_{ii} is the local field anisotropy tensor. The anisotropy tensor and the polarisability tensor are all

diagonal in the same laboratory fixed co-ordinate system x, y, z. The average polarisability can be obtained from the Lorentz-Lorenz equation in the isotropic phase

$$\bar{\alpha} = \frac{1}{3}(\alpha_{\parallel} + 2\alpha_{\perp}) = \frac{3}{4\pi N} \left[\frac{n^2 - 1}{n^2 + 2} \right] \quad (4.32)$$

Letting

$$\delta = \frac{(\alpha_{\parallel} - \alpha_{\perp})}{3\bar{\alpha}} \quad (4.33)$$

and eliminating η_{ij} from equation 4.31 gives

$$4\delta S = 1 - 3A + \sqrt{9A^2 - 30A + 9} \quad (4.34)$$

where

$$\frac{1}{A} = \frac{4\pi}{3} N\bar{\alpha} \left(\frac{n_e^2 + 2}{n_e^2 - 1} + \frac{2(n_o^2 + 2)}{n_o^2 - 1} \right) \quad (4.35)$$

To determine δ , Haller's method⁶⁶ can be used by extrapolating the straight line sections of the plot of $\ln(\delta S)$ vs $\ln(1-T/T_N)$ to zero temperature. When the order parameter is unity ($S = 1$), should give an intercept δ . This may then be used to calculate the polarisability $\Delta\alpha$. The order parameter S can then be determined using equation 4.34. The internal field factor η_{zz} can be obtained from equation 4.36,

$$\eta_{zz} = \frac{1}{4\pi N \bar{\alpha} (1 + 2\delta S)} - \frac{(n_e^2 + 2)}{3(n_e^2 - 1)} \quad (4.36)$$

According to the Palffy-Muhoray assumption⁶⁹, for molecules with axial ratio $\kappa \leq 2$, where κ is the length-to-breadth ratio (L/B), the internal field factor, to a good approximation, is given by,

$$\eta_{zz} = -\frac{4}{5} \left(\frac{\kappa - 1}{\kappa + 2} \right) S \quad (4.37)$$

Therefore, η_{zz} is nearly proportional to order parameter, and the length-to-breadth ratio κ can be determined from the slope of a plot of η_{zz} vs. S .

4.3 Experimental

4.3.1 *Refractive index measurements*

The refractive indices in the nematic phase and isotropic phase at different temperatures were measured using a polariser at the ocular of an Abbe refractometer. The functioning of this instrument is based on internal reflection of light at the interface between the liquid and the surface of an optically dense glass prism⁷⁰. Therefore the maximum measurable refractive index is that of the glass. The refractive index of the extraordinary ray, n_e , in nematics can be larger than that of the glass in the refractometer.

The values of the ordinary (perpendicular) and extraordinary (parallel) refractive indices in the nematic phases were obtained by surface treatment of the prism of the refractometer⁷¹. The glass prisms of the refractometer were rubbed with a lens paper along the length of the prisms several times. A few drops of the nematic compound on the interest are then spread with a Teflon spatula along the length of the lower prism. The alignment was complete when the upper prism was clamped in place. A polaroid sheet placed over the eyepiece allowed a distinct separation of the dark and bright space in the eyepiece. A second polaroid was placed between the light source and the illuminating prism in order to improve the contrast between the dark and bright space⁷¹.

The value for the extraordinary ray, n_e , in the nematic phase lay outside the range of the Abbe refractometer and was calculated using the isobestic relationship (equation 4.18). The temperature of the refractometer was measured with a copper-constantin thermocouple located near the sample. The temperature was estimated to be accurate to within ± 0.1 °C and was maintained by circulation of water.

4.3.2 Density measurements

The density of the liquid crystals in the nematic and isotropic phases were measured using PAAR DMA 60 Digital Density Meter, in combination with a DMA 602 remote U-shape cell. The measuring cell was initially calibrated and used to perform density measurements. A 2cm³ Teflon syringe was used to fill the cell slowly via a length of Teflon tubing, so that no air bubbles were entrapped. The temperature of the densitometer was controlled by circulation of water and was measured with a copper-constantin thermocouple. The estimated accuracies in the measurement of density and temperature are $\pm 1 \times 10^{-4}$ g cm⁻³ and $\pm 0.1^\circ\text{C}$, respectively.

4.3.2.1 Measuring method

The measuring principle of the instrument is based on the change of the natural frequency of a hollow oscillator when filled with different liquids. The mass, and thus the density, of the liquid changes this natural frequency due to a gross mass change of the oscillator caused by the introduction of the liquid. The frequency of the oscillator is only influenced by that fraction of the volume of liquid which is actually in the vibrating part of the sample tube. It is essential to ensure that the oscillator (sample tube) is completely filled. For the calculation of density, the system is considered to be represented by a hollow body of mass M suspended on a spring with an elasticity constant c , its volume V filled with a sample of density d .

The natural frequency of this system will be

$$f = \frac{1}{2\pi} \sqrt{\frac{c}{M + dV}} \quad (4.32)$$

and, the period of the oscillation is therefore

$$T = 2\pi \sqrt{\frac{M + dV}{c}} \quad (4.33)$$

Taking the square of this expression and inserting

$$A = \frac{4\pi^2 V}{c} \quad , \quad B = \frac{4\pi^2 M}{c} \quad (4.34)$$

gives

$$d = \frac{1}{A} (T^2 - B) \quad (4.35)$$

The difference in the densities of two samples is then

$$d_1 - d_2 = \frac{1}{A} (T_1^2 - T_2^2) \quad (4.36)$$

Since the constants A and B contain the same volume, spring constant and mass, they may be regarded as apparatus constants and may be determined from two calibration measurements of samples of known density.

4.3.2.2 Calibration of the density meter

The calibration constant, $k = 1/A$, was determined for the DMA 602 U-shape cell over the temperature range 20 - 75 °C. The samples used were distilled HPLC grade H₂O and air. The instrument constant was calculated from the following formula:

$$d_{H_2O} - d_{Air} = k (T_{H_2O}^2 - T_{Air}^2) \quad (4.37)$$

The density of water and air at various temperature were obtained from Ref. 72, and listed in Table 4.1. Measurements of the period of oscillation of the cell were taken with

the "period select" switch set to 2k. the period readings for air and distilled water, and the instrument constant, k , over the above temperature range can be seen in Table 4.2. The density of an unknown sample, d_x with a period value of T can now be determined from

$$d_x = k (T_X^2 - T_{H_2O}^2) + d_{H_2O} \quad (4.38)$$

Density measurements were made on pure cyclohexane at different temperatures, and the results are given in Table 4.3.

Table 4.1 Temperature dependence of the density for air and H₂O

Temperature °C	Density of Air g cm ⁻³	Density of H ₂ O g cm ⁻³
20.0	0.001205	0.99820
25.0	0.001169	0.99704
30.0	0.001150	0.99565
35.0	0.001131	0.99403
40.0	0.001113	0.99221
45.0	0.001095	0.99025
50.0	0.001078	0.98807
55.0	0.001062	0.98573
60.0	0.001046	0.98324
65.0	0.001030	0.98059
70.0	0.001029	0.97781
75.0	0.001015	0.97483

Table 4.2 Period reading (T) for Air and H₂O

Temperature °C	Period (T) of Air	Period (T) of H ₂ O	Constant (k) g cm ⁻³
20.0	0.55235 (7)	0.76995 (9)	3.464 (89)
25.0	0.55222 (9)	0.76955 (5)	3.466 (80)
30.0	0.55200 (5)	0.76896 (6)	3.469 (89)
35.0	0.55193 (8)	0.76854 (0)	3.471 (22)
40.0	0.55175 (1)	0.76796 (6)	3.473 (32)
45.0	0.55156 (6)	0.76735 (1)	3.475 (41)
50.0	0.55138 (8)	0.76671 (0)	3.477 (53)
55.0	0.55121 (6)	0.76604 (8)	3.479 (64)
60.0	0.55104 (8)	0.76536 (1)	3.481 (38)
65.0	0.55088 (5)	0.76465 (3)	3.483 (20)
70.0	0.55072 (8)	0.76392 (1)	3.485 (14)
75.0	0.55057 (1)	0.76316 (5)	3.486 (71)

Table 4.3 Period reading and temperature dependence of the density for cyclohexane

Temperature °C	Period (T) of C ₆ H ₁₂	Density of C ₆ H ₁₂ (g cm ⁻³)
25.0	0.7264 8 (0)	0.773 (64)
30.0	0.72530 (1)	0.769 (24)
35.0	0.72412 (6)	0.763 (85)
40.0	0.72292 (0)	0.758 (95)
45.0	0.72173 (9)	0.754 (17)
50.0	0.72056 (3)	0.749 (40)
55.0	0.71938 (2)	0.744 (52)
60.0	0.71822 (0)	0.739 (76)
65.0	0.71704 (1)	0.734 (86)
70.0	0.71585 (9)	0.729 (94)

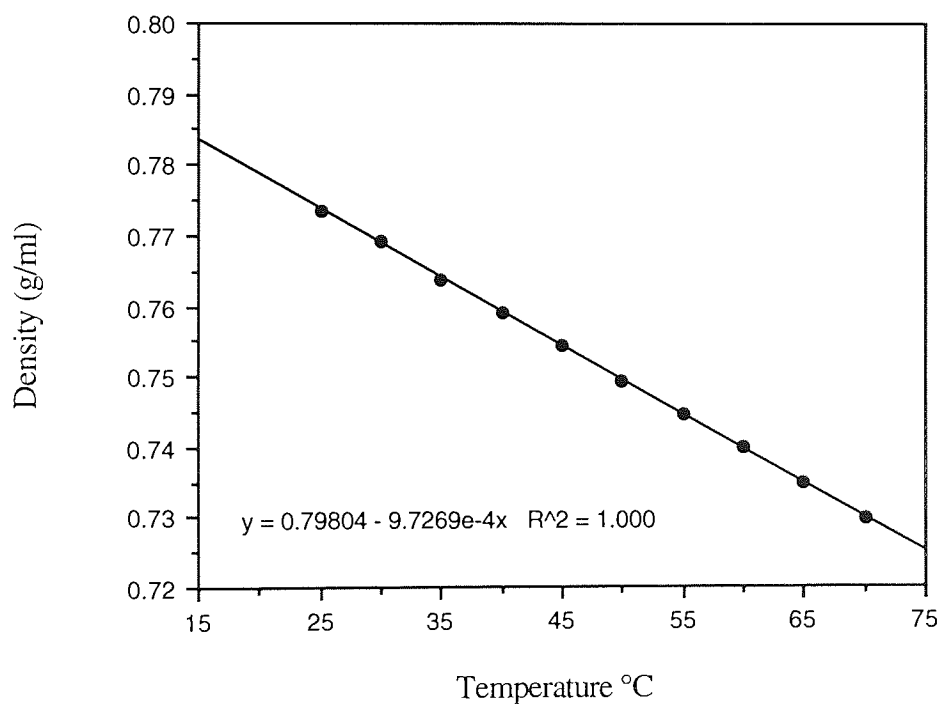


Figure 4.4 Density for cyclohexane plotted as a function of temperature

4.4 Results

The densities and the refractive indices of three liquid crystal homologs (5CB, 6CB, and 7CB), 6OCB and three eutectic nematic mixtures E7, E8, and E₆₀₇ (6OCB/7OCB) in the nematic phase and in the isotropic phase at different temperatures are given in Appendix A. The molecular structures of these liquid crystal materials are shown in Chapter 3 (section 3.3.2). The transition temperatures of the compounds are listed in Table 4.4. The melting temperatures T_{KI} and the clearing temperatures T_{NI} were obtained using a polarising microscope (Reichert) with a hot-stage arrangement. The transition temperatures measured in the present studies are in the agreement with the literature values^{49,67,73}.

Table 4.4 Transition temperatures of the nematic liquid crystals

Transition temperature	mesogen						
	5CB	6CB	7CB	6OCB	E ₆₀₇	E7	E8
T_{KI} (°C)	22.4	14.3	28.5	57.0	35.9	—	—
T_{NI} (°C)	35.0	28.8	41.9	75.8	74.8	59.9	70.5

4.4.1 Density results

The molar volumes (V = molecular weight/density) of the liquid crystals as a function of temperature are shown in Figure 4.5 to 4.11. In the all cases the molar volume increases linearly with the increase of temperature, for both the isotropic and nematic phases, except in the vicinity of the isotropic-nematic transition. A sudden increase in the molar volume at the phase transition is related to a sudden structural change that arises from the ordered nematic state to the disordered isotropic phase. Below the nematic-isotropic transition temperature there are the pronounced pretransition effects, in contrast to the post-transition effects in the isotropic phase that are not so pronounced. However, the pretransition effects are observed only on the lower side of the transition temperature (i.e.

nematic side). Similar trends were reported by earlier investigators over a number nematic liquid crystals^{74,75}.

For the alkyl cyanobiphenyl liquid crystals (5CB to 7CB), 6OCB, and E₆₀₇ deviations from linearity become noticeable in the nematic phase at temperatures less than 4° below the transition temperature, but for the eutectic nematic mixtures E7 and E8, a deviation is noticeable at temperatures as low as 10 °C below the transition.

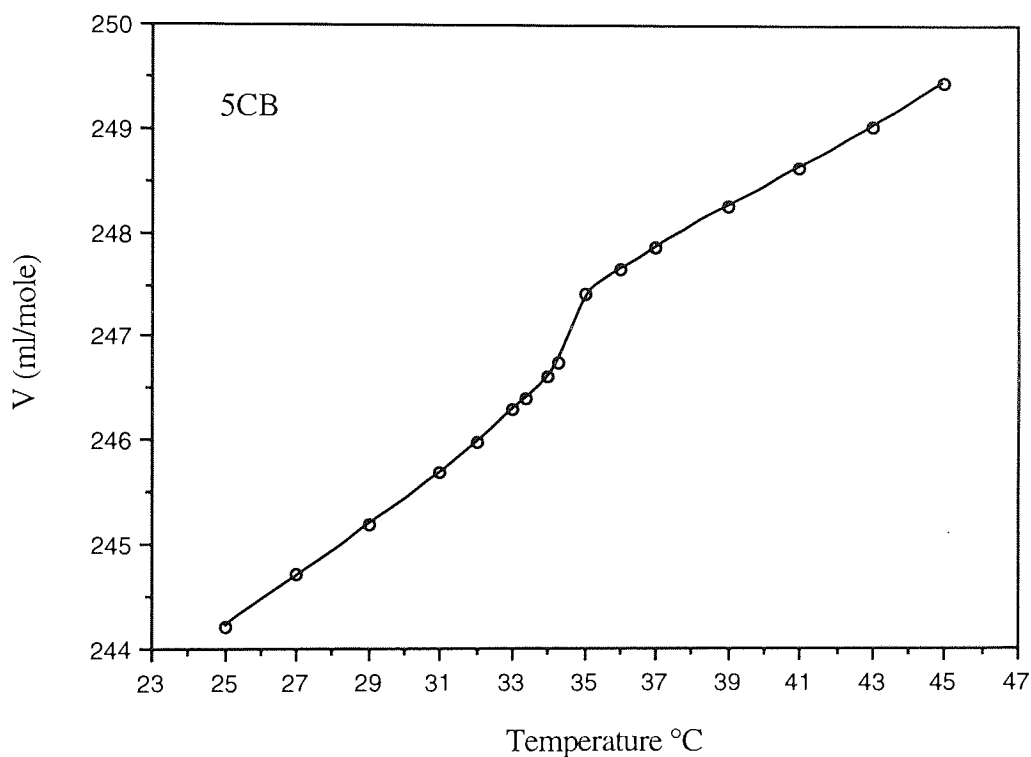


Figure 4.5 Molar volume of pentyl cyanobiphenyl, 5CB, as a function of temperature

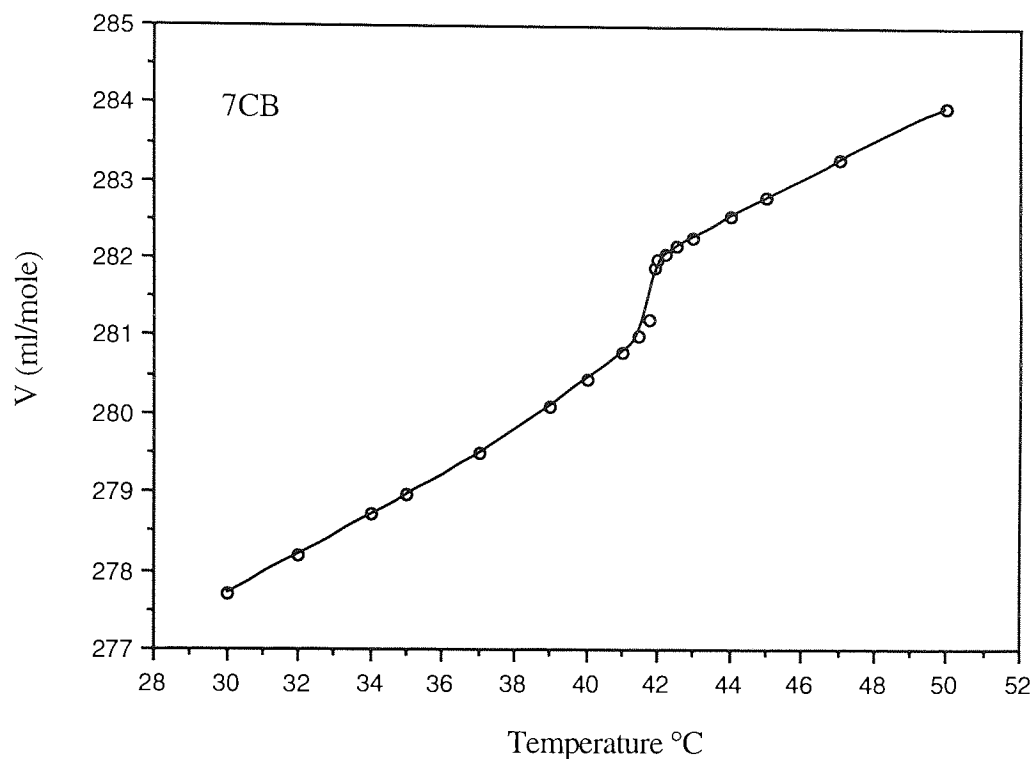


Figure 4.6 Molar volume of heptyl cyanobiphenyl, 7CB, as a function of temperature

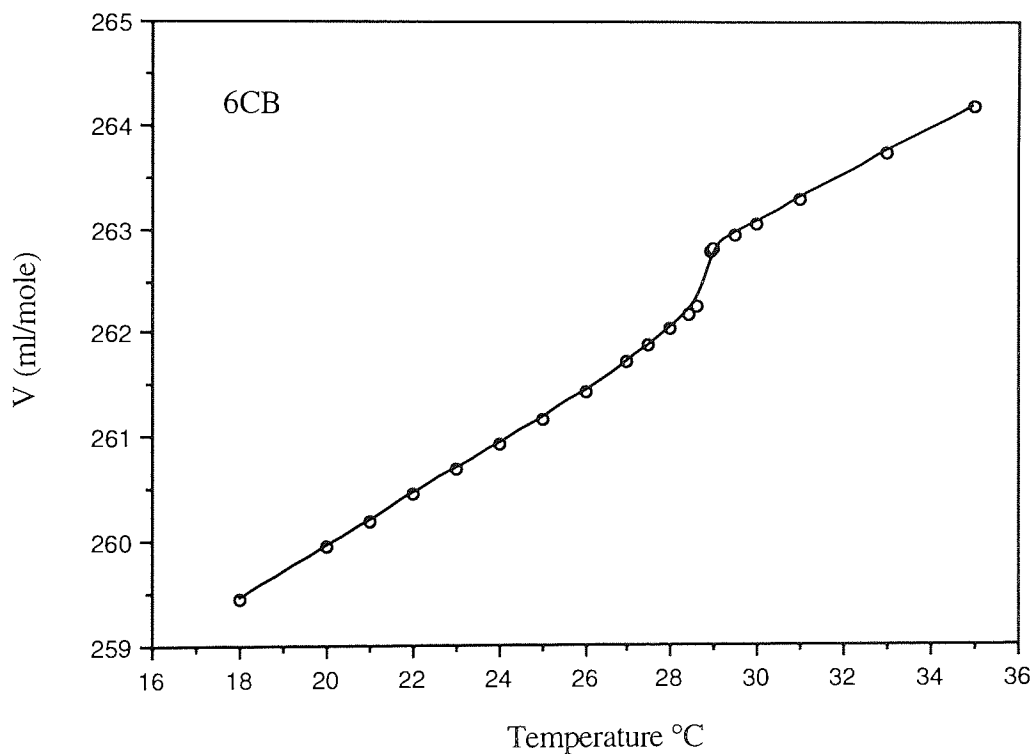


Figure 4.7 Molar volume of hexyl cyanobiphenyl, 6CB, as a function of temperature

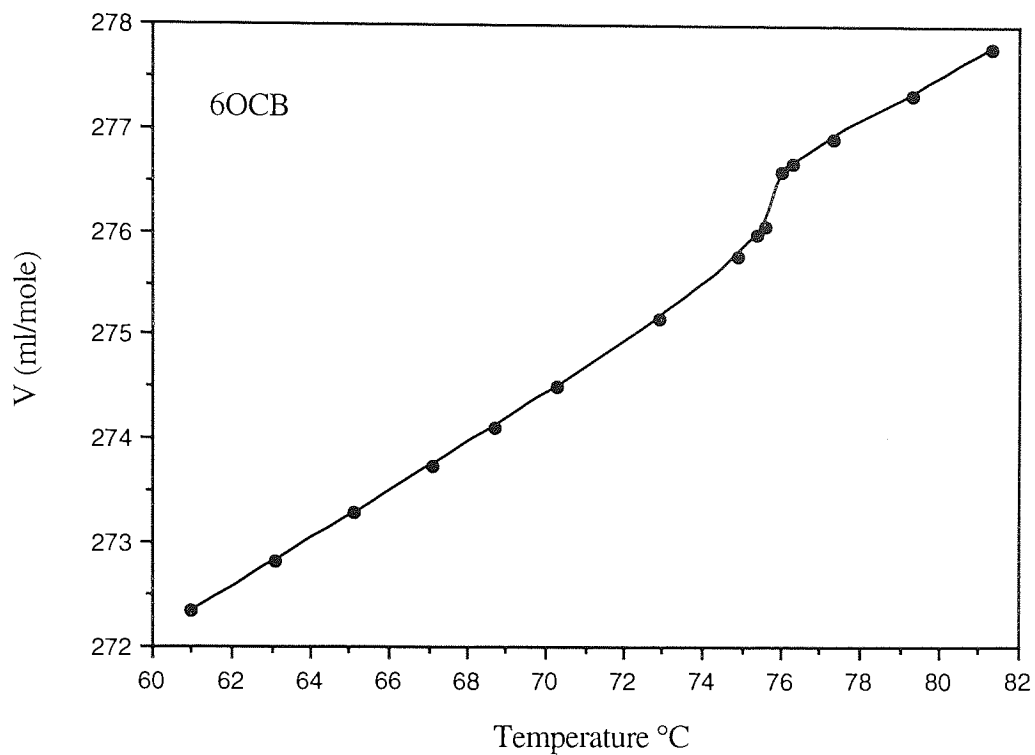


Figure 4.8 Molar volume of hexoxy cyanobiphenyl, 6OCB, as a function of temperature

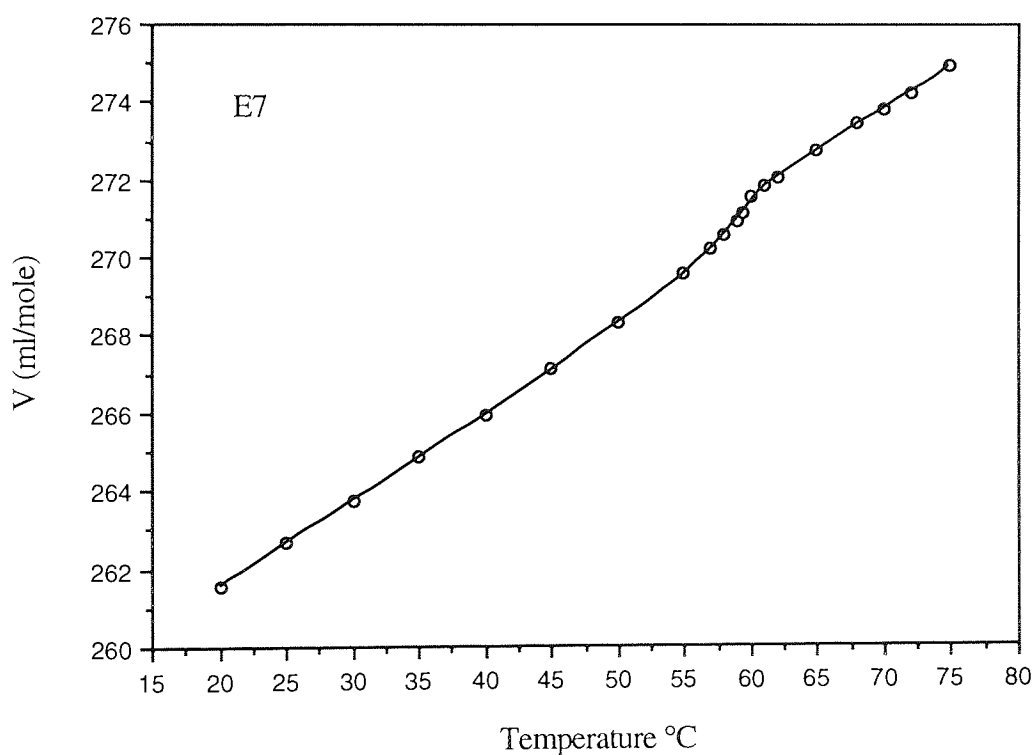


Figure 4.9. Molar volume of E7 as a function of temperature

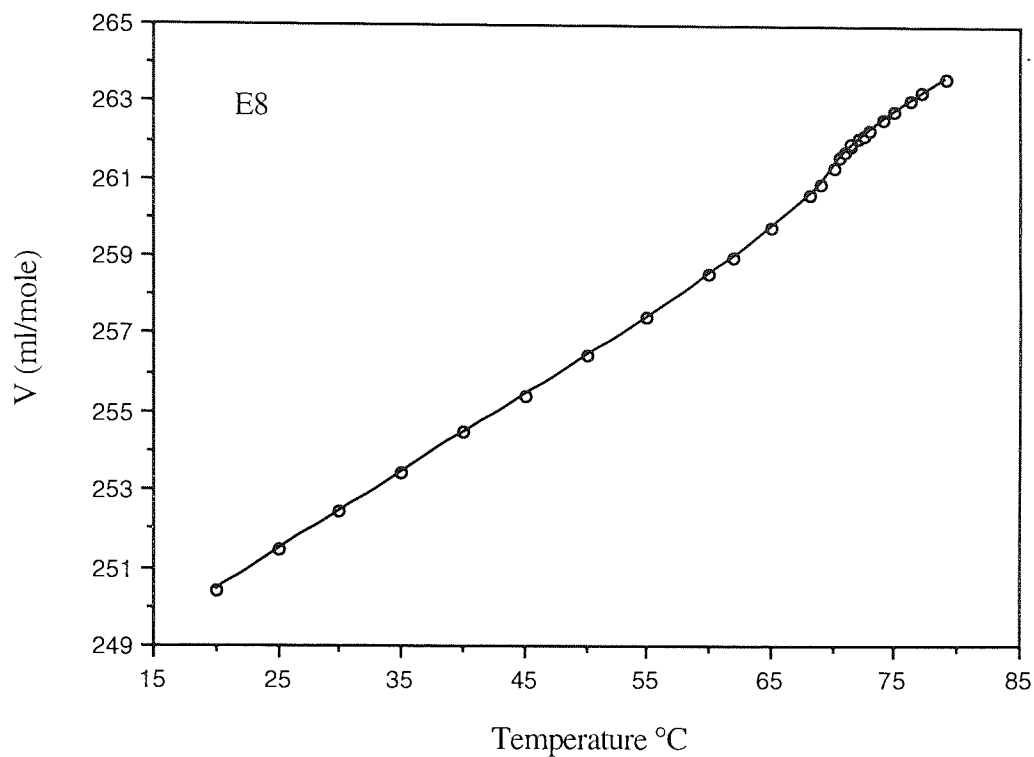


Figure 4.10 Molar volume of E8 as a function of temperature

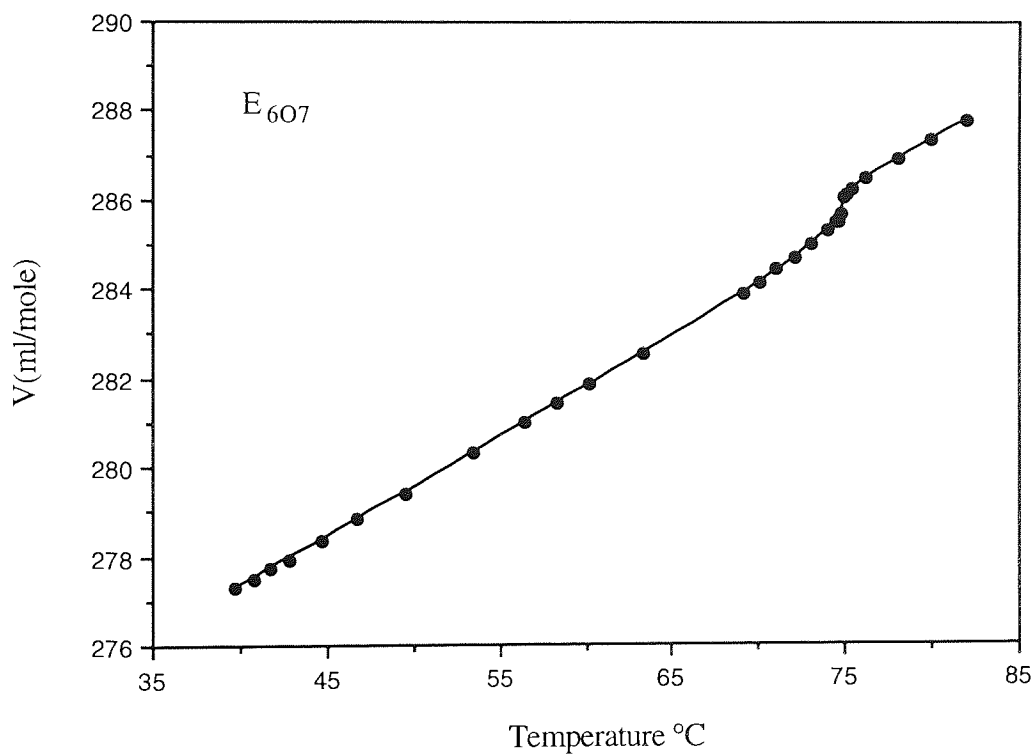


Figure 4.11 Molar volume of eutectic mixture, E_{607} , (6OCB/7OCB) as a function of temperature

4.4.1.1 Change in molar volumes at the T_{NI} transition

The molar volume increment ($\Delta V/V\%$) at the transition temperature of the liquid crystals is measured from an extrapolation of the data in the nematic and isotropic phases. The extrapolated line in the nematic phase includes all points to 4°C below the transition temperature.

The high molar volume increment at the transition temperature T_{NI} for alkyl cyano biphenyls indicates a first-order transition. However, as Figure 4.12 shows that the increment for the odd members of this series is higher than a neighbouring member. This behaviour probably reflects being dependent on an odd-even alternation for the orientational order parameter as well as other physical properties such as transition temperature, T_{NI} (Figure 4.13).

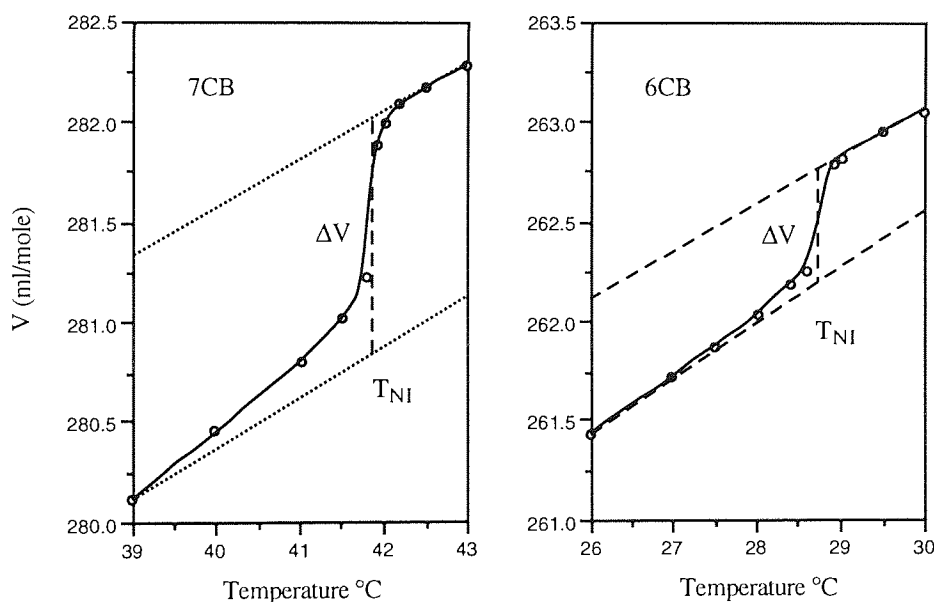


Figure 4.12 Molar volume of hexyl and heptyl cyanobiphenyl as a function of temperature.

If additivity of molar volume is assumed, the increment per methylene group may be estimated from the difference in the molar volumes of the 5CB and 7CB, i.e. $V_{CH_2} = (V_{7CB} + V_{5CB})/2$. The contribution of a methylene group is calculated to be $16.4 \text{ cm}^3/\text{mol}$ at 30°C in the nematic phase and is close to the contribution of a methylene group reported

in alkylbiphenyls⁷⁶ ($17.1 \text{ cm}^3/\text{mol}$) in the isotropic phase, but it is higher than that for n-alkanes in the solid state⁶⁶ ($14.5 \text{ cm}^3/\text{mol}$). This shows that in the nematic phase the packing of alkyl chain is closer to the isotropic than to the solid phase. As it can be seen in Figure 4.14, the increment in molar volume is smaller on going from the odd member such as 5CB to 6CB, ($\Delta V=15.5 \text{ cm}^3/\text{mol}$), compared to the change from 6CB to 7CB ($\Delta V = 18.5 \text{ cm}^3/\text{mol}$), probably as a consequence of the alternation in T_{NI} .

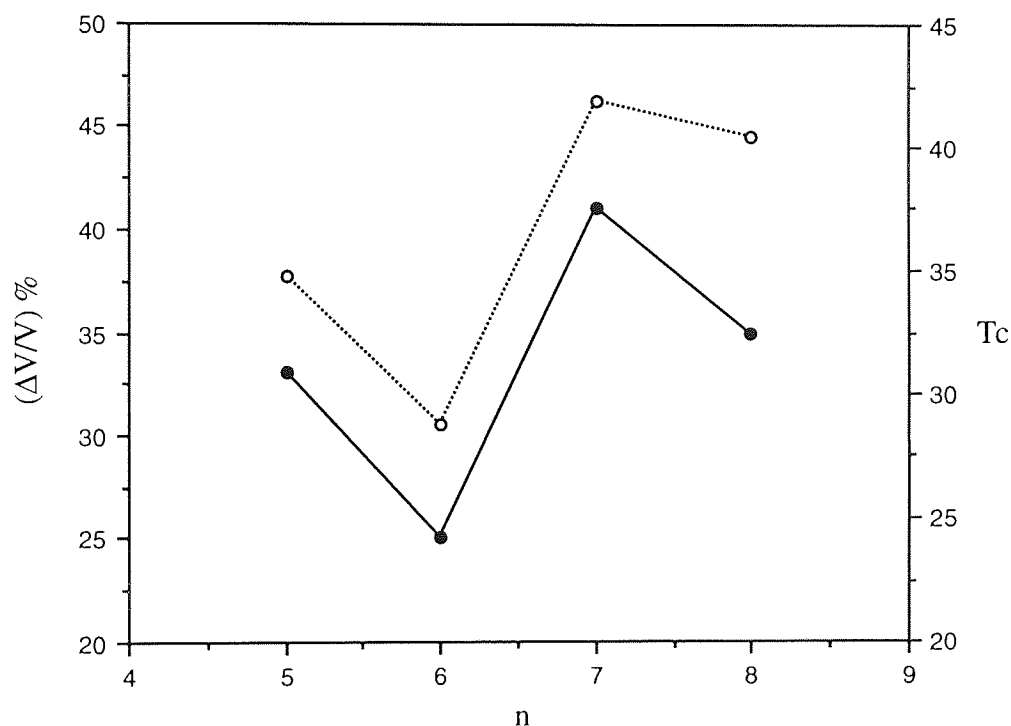


Figure 4.13 The nematic-isotropic transition, T_{NI} , (dashed lines) and molar volume increment at the transition temperature (full lines) as a function of the number of carbon atoms, n , in the alkyl chain of 4- n -alkyl-4-cyanobiphenyls.

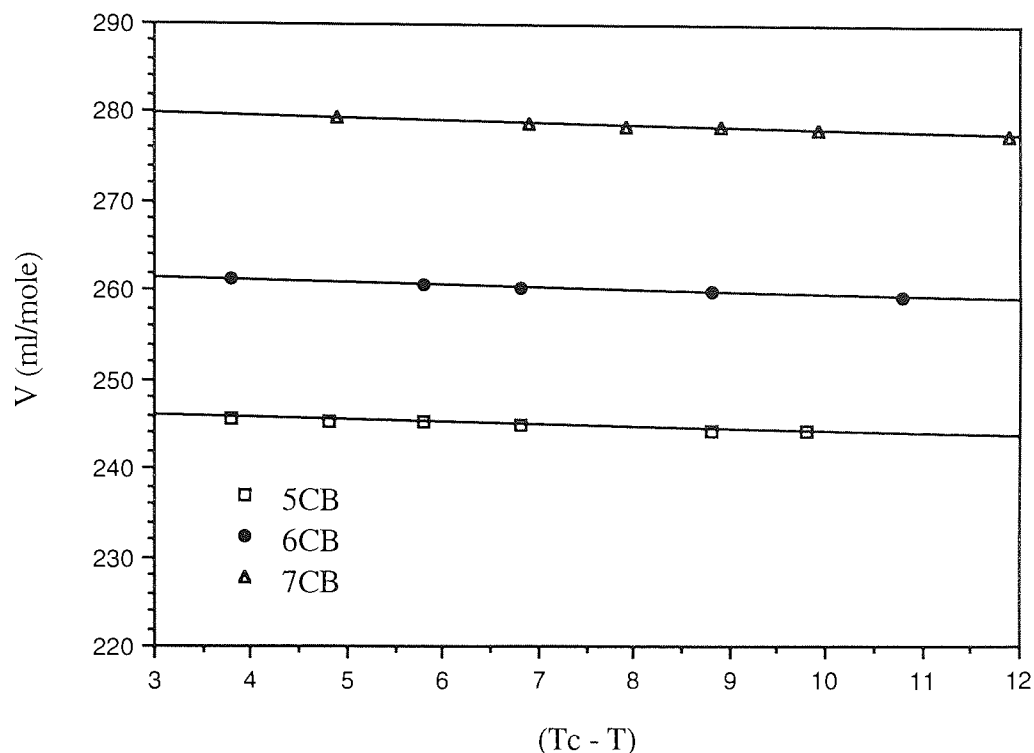


Figure 4.14 Variation of molar volumes of the three liquid crystal homologs (5CB, 6CB and 7CB) as function of reduced temperature, $T_c = T_{NI}$.

The molecular volumes, V_M , of 7CB and 6OCB are close 464 \AA^3 and 456 \AA^3 , respectively (Table 4.5). This shows that packing of molecules in the both liquid crystals are similar. The molecular structures of 7CB and 6OCB are shown in Figure 4.15. The flexible parts of the molecular end group are identical for both 6OCB and 7CB, i.e. $-\text{C}_6\text{H}_{15}$. This is because in 7CB the first methylene group which is linked to the phenyl ring is essentially immobile. Therefore, 7CB could be regarded as equivalent to 6OCB with regard to the extent of the flexible part of the molecules.

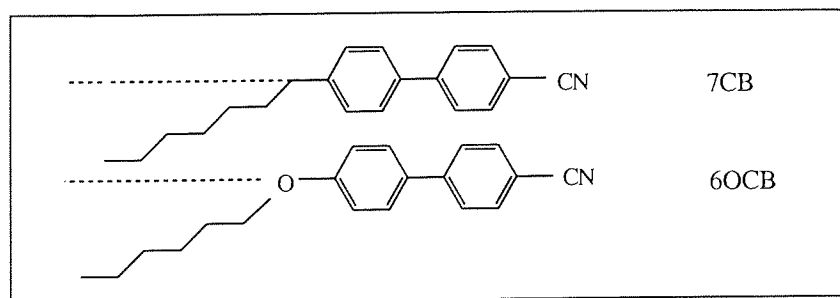


Figure 4.15 Molar structures of 7CB and 6OCB

The biphasic range (Figure 4.16) indicates where nematic and isotropic phases were visually observed to coexist. The coexistence of the two phases or the existence of an “intermediate phase” was readily observed in E8 (70.2 - 72.4 °C). For the odd members of the alkyl cyanobiphenyl series (5CB and 7CB) biphasic region has not been observed, but was observed for the even member, 6CB (28.8 - 28.9 °C).

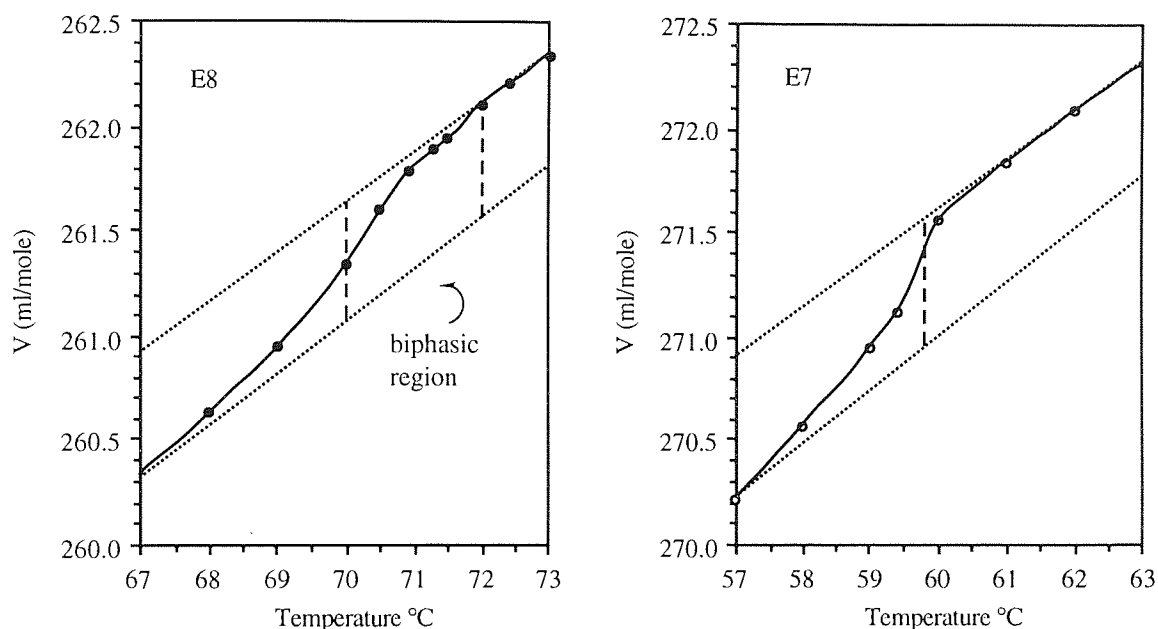


Figure 4.16 Molar volume of E7 and E8 nematic mixtures liquid crystals as a function of temperature.

4.4.1.2 Volume expansion coefficient

The volume expansion coefficient⁵⁰, β , is normally defined as

$$\beta \equiv \frac{1}{V} \left(\frac{\partial V}{\partial T} \right)_P \quad (4.39)$$

(i.e., the rate of change of volume with temperature, per unit volume). The subscript P is a reminder that pressure is constant (isobaric). The mean expansion coefficients were obtained from least-squares fit of $\ln V$ versus temperature of all points with $T < T_{NI} - 5$ in the nematic phase of alkyl cyanobiphenyls, 6OCB, and E₆₀₇. While for E7 and E8, all points with $T < T_{NI} - 10$ were considered. The mean expansion coefficients were obtained

from least-squares fit of all points in the isotropic phase (for E8 all points with $T > T_{NI} - 4$). The volume expansion coefficients are presented in Table 4.5.

Apart from E8 and E_{6O7}, the expansion coefficient for a liquid crystal in the nematic phase is greater than that for the isotropic phase. For E8 and E_{6O7} the mean expansion coefficients for the nematic and isotropic phases are almost equal, i.e. $8.0 \times 10^{-4} \text{ } ^\circ\text{C}$. In the nematic mixture E8 the molar volume (or density) curve for the isotropic phase deviates from linearity up to $4 \text{ } ^\circ\text{C}$ above the transition temperature. In addition, E8 was found to exhibit a broad biphasic region that overlaps or add to the pretransitional behaviour. However, for the pure alkyl (alkoxy) cyanobiphenyl liquid crystals the temperature dependence in the isotropic phase is more linear.

Table 4.5 The molar volume, V , molecular volume, V_M ,* at $T_{NI} - T = 5$, percent transition volume change and the mean expansion coefficients in the nematic, N, and isotropic, I, phases.

compound	V (cm^3/mol)	V_M (\AA^3)	β_N / 10^{-4}	β_I / 10^{-4}	$\frac{\Delta V_{NI}}{V} \%$	biphasic range / $^\circ\text{C}$
5CB	245.4	407.5	9.1	8.0	0.33	---
6CB	260.9	433.2	9.5	8.6	0.25	0.1
7CB	279.5	464.1	9.1	8.5	0.41	---
6OCB	274.5	455.8	8.5	7.8	0.29	---
E _{6O7}	284.1	471.8	8.0	8.0	0.31	---
E7	249.9	415.0	8.4	8.0	0.26	0.2
E8	259.8	431.4	8.0	8.0	0.23	2.2

* Molecular volume ($V_M = \text{molar volume}/\text{Avogadro's number}$)

4.4.2 Refractive indices results

The refractive indices of the liquid crystals in the nematic phase, n_e , n_o and in the isotropic phase n_{iso} at different temperatures are listed in Appendix A. The refractive index anisotropies for the liquid crystals are shown in Figure 4.17 to 4.19. The value for

the extraordinary ray, n_e , in the nematic phase was calculated using the isobestic relationship

$$n^2 = \frac{1}{3}(2n_o^2 + n_e^2) \quad (4.40)$$

where n is the mean (bulk) isotropic refractive index, often derived by extrapolating to an appropriate temperature. The effective polarisabilities α_e and α_o of the liquid crystals were calculated by different methods of Vuks⁵⁸, Neugebauer⁵⁴, Saupe-Maier⁵⁵, and Palffy-Muhoray⁵⁶ (see Section 4.2.4). The polarisabilities obtained from these models are given in Tables 4-6 to 4-12. The principal polarisabilities $\alpha_{||}$ and α_{\perp} , parallel and perpendicular to the long molecular axis were obtained from a graph⁴⁹ of $\log(\alpha_e/\alpha_o)$ and/or $\log(T_{NI} - T)$ vs. $\log(T_{NI} - T)$, where T_{NI} is the nematic-isotropic temperature.

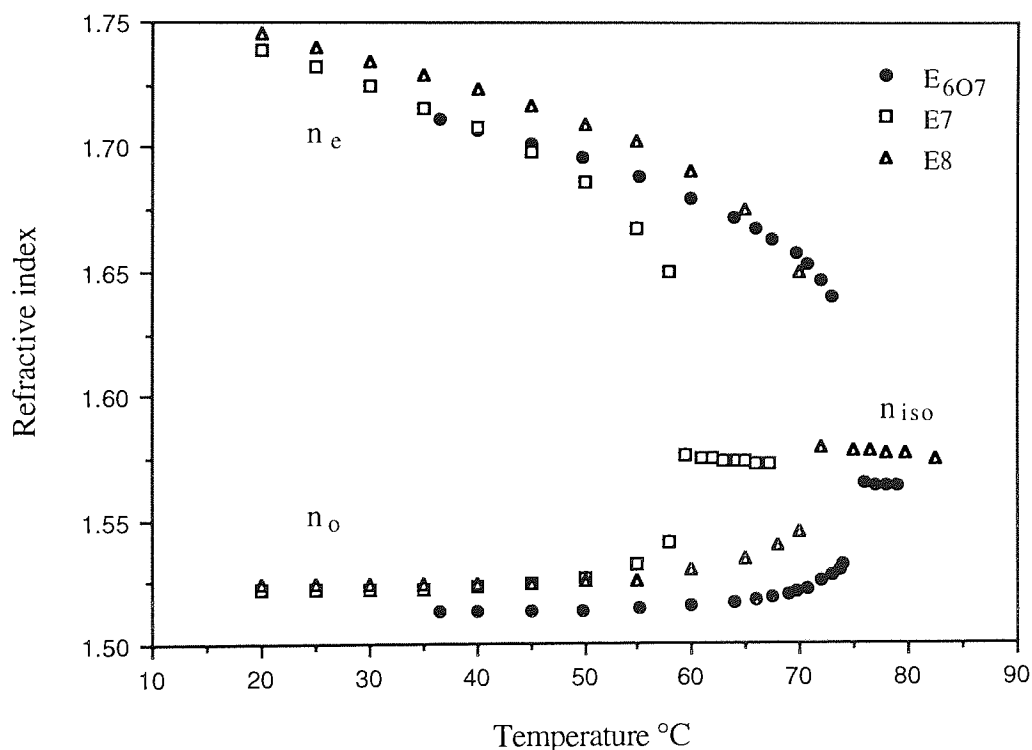


Figure 4.17 Refractive indices of the nematic phase (n_o , n_e) and of the isotropic phase (n_{iso}) at different temperatures for eutectic nematic mixtures E_{6O7}, E7, and E8.

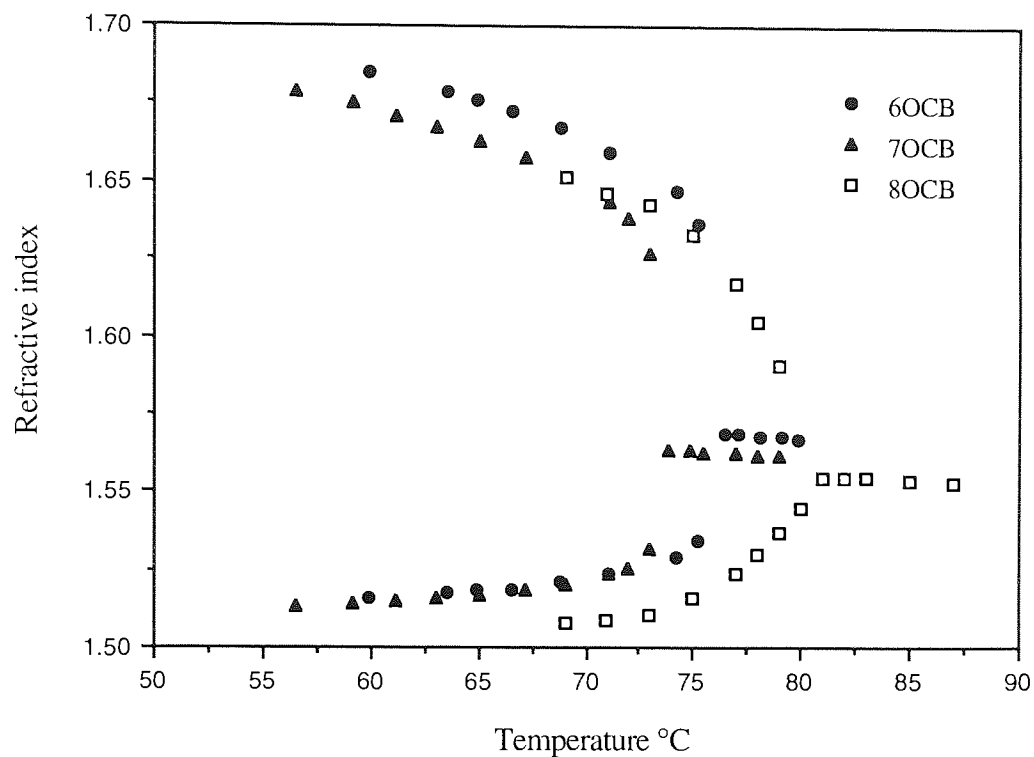


Figure 4.18 Refractive indices of the nematic phase (n_o , n_e) and of the isotropic phase (n_{iso}) at different temperatures for 6OCB, 7OCB, and 8OCB.

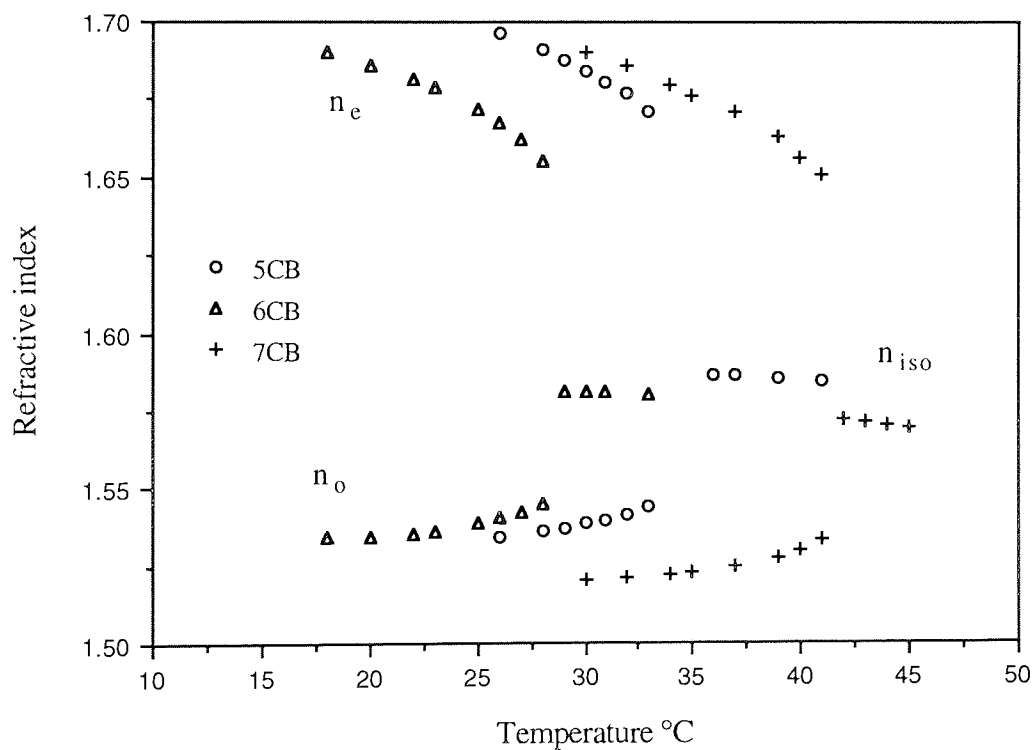


Figure 4.19 Refractive indices of the nematic phase (n_o , n_e) and of the isotropic phase (n_{iso}) at different temperatures for 5CB, 6CB, and 7CB.

Table 4.6 The effective polarisabilities α_o and α_e at several temperatures for $\lambda = 589.3$ nm of 5CB calculated using different theoretical models.

Temp. °C	Vuks		Neugebauer		Saupe-Maier		Palffy-Muhoray	
	α_e	α_o	α_e	α_o	α_e	α_o	α_e	α_o
25.0	40.25	28.93	38.81	29.65	40.71	29.13	39.60	29.43
28.0	39.90	29.18	38.54	29.86	40.20	29.39	39.03	29.72
29.0	39.75	29.29	38.42	29.95	39.98	29.50	38.77	29.84
30.0	39.54	29.41	38.25	30.05	39.76	29.61	38.52	29.97
31.0	39.33	29.54	38.09	30.16	39.50	29.74	38.21	30.12
32.0	39.15	29.67	37.95	30.27	39.23	29.87	37.90	30.28
33.0	38.74	29.90	37.63	30.46	38.80	30.09	37.38	30.54

Polarisabilities in units of $10^{-24} \text{ cm}^3 (\text{\AA}^3)$

Table 4.7 The effective polarisabilities α_o and α_e at several temperatures for $\lambda=589.3$ nm of 6CB calculated using different theoretical models.

Temp. °C	Vuks		Neugebauer		Saupe-Maier		Palffy-Muhoray	
	α_e	α_o	α_e	α_o	α_e	α_o	α_e	α_o
18.0	42.28	30.81	41.89	31.23	41.81	31.25	41.87	31.24
20.0	42.07	30.92	41.71	31.32	41.63	31.34	41.69	31.33
22.0	41.83	31.06	41.43	31.46	41.36	31.48	41.41	31.46
23.0	41.65	31.16	41.31	31.52	41.23	31.54	41.27	31.53
25.0	41.24	31.41	40.79	31.78	40.71	31.81	40.77	31.79
26.0	40.96	31.56	40.54	31.90	40.46	31.93	40.52	31.91
27.0	40.61	31.74	40.26	32.05	40.16	32.08	40.22	32.06
28.0	40.16	32.01	39.67	32.34	39.57	32.38	39.64	32.35

Polarisabilities in units of $10^{-24} \text{ cm}^3 (\text{\AA}^3)$

Table 4.8 The effective polarisabilities α_o and α_e at several temperatures for $\lambda = 589.3$ nm of 7CB calculated using different theoretical models.

Temp. °C	Vuks		Neugebauer		Saupe-Maier		Palffy-Muhoray	
	α_e	α_o	α_e	α_o	α_e	α_o	α_e	α_o
30.0	45.51	32.16	43.84	32.99	45.12	32.65	45.10	32.65
32.0	45.26	32.29	43.63	33.10	44.92	32.74	44.90	32.75
33.0	45.06	32.37	43.48	33.17	44.84	32.79	44.82	32.79
34.0	44.90	32.46	43.35	33.24	44.70	32.86	44.67	32.86
35.0	44.65	32.58	43.15	33.33	44.56	32.92	44.54	32.93
37.0	44.33	32.77	42.89	33.48	44.22	33.10	44.19	33.10
39.0	43.79	33.06	42.48	33.72	43.72	33.34	43.70	33.35
40.0	43.32	33.31	42.08	33.93	43.33	33.54	43.31	33.55
41.0	42.90	33.63	41.75	34.20	42.49	33.96	42.46	33.97

Polarisabilities in units of $10^{-24} \text{ cm}^3 (\text{\AA}^3)$

Table 4.9 The effective polarisabilities α_o and α_e at several temperatures for $\lambda = 589.3$ nm of 6OCB calculated using different theoretical models.

Temp. °C	Vuks		Neugebauer		Saupe-Maier		Palffy-Muhoray	
	α_e	α_o	α_e	α_o	α_e	α_o	α_e	α_o
60.0	44.31	31.32	42.70	32.12	44.73	31.58	44.71	31.59
63.6	43.96	31.54	42.42	32.31	44.31	31.79	44.29	31.80
65.0	43.86	31.63	42.34	32.39	44.10	31.90	44.08	31.90
66.6	43.67	31.73	42.20	32.47	43.94	31.98	43.92	31.98
68.8	43.28	31.99	41.88	32.69	43.41	32.24	43.39	32.25
70.3	43.08	32.15	41.73	32.82	43.01	32.44	42.99	32.45
74.9	41.49	33.04	40.46	33.56	41.43	33.23	41.41	33.24
75.4	41.13	33.24	40.17	33.72	41.06	33.42	41.04	33.42

Polarisabilities in units of $10^{-24} \text{ cm}^3 (\text{\AA}^3)$

Table 4.10 The effective polarisabilities α_o and α_e at several temperatures for $\lambda = 589.3$ nm of E₆₀₇ calculated using different theoretical models.

Temp. °C	Vuks		Neugebauer		Saupe-Maier		Palfly-Muhoray	
	α_e	α_o	α_e	α_o	α_e	α_o	α_e	α_o
38.0	46.92	31.46	44.98	32.43	47.26	31.88	47.26	31.88
40.0	46.82	31.53	44.91	32.49	47.13	31.94	47.13	31.94
45.0	46.58	31.70	44.72	32.63	46.79	32.11	46.79	32.11
50.0	46.30	31.89	44.50	32.79	46.42	32.30	46.42	32.29
55.0	45.93	32.12	44.22	32.98	46.00	32.51	46.00	32.51
60.0	45.48	32.40	43.86	33.21	45.49	32.77	45.49	32.77
70.0	44.01	33.24	42.69	33.90	44.04	33.49	44.04	33.49
74.0	42.25	34.22	41.27	34.71	42.31	34.35	42.31	34.35

Polarisabilities in units of $10^{-24} \text{ cm}^3 (\text{\AA}^3)$

Table 4.11 The effective polarisabilities α_o and α_e at several temperatures for $\lambda = 589.3$ nm of E7 calculated using different theoretical models.

Temp. °C	Vuks		Neugebauer		Saupe-Maier		Palfly-Muhoray	
	α_e	α_o	α_e	α_o	α_e	α_o	α_e	α_o
20.0	46.18	30.02	44.07	31.03	45.71	30.68	45.53	30.72
30.0	45.61	30.34	43.62	31.32	45.07	31.00	44.89	31.04
35.0	45.22	30.55	43.31	31.49	44.72	31.18	44.53	31.22
40.0	44.78	30.78	42.97	31.68	44.35	31.36	44.15	31.41
45.0	44.28	31.06	42.57	31.91	43.83	31.62	43.63	31.68
50.0	43.58	31.46	42.03	32.22	43.19	31.94	42.97	32.00
55.0	42.46	31.98	41.12	32.73	42.27	32.40	41.91	32.54
58.0	41.22	32.67	40.13	33.39	41.21	33.43	39.89	33.54

Polarisabilities in units of $10^{-24} \text{ cm}^3 (\text{\AA}^3)$

Table 4.12 The effective polarisabilities α_o and α_e at several temperatures for $\lambda = 589.3$ nm of E8 calculated using different theoretical models.

Temp. °C	Vuks		Neugebauer		Saupe-Maier		Palffy-Muhoray	
	α_e	α_o	α_e	α_o	α_e	α_o	α_e	α_o
20.0	44.57	28.78	42.53	29.80	45.69	29.10	45.55	29.13
30.0	44.18	29.10	42.24	30.07	45.06	29.40	44.91	29.44
40.0	43.81	29.42	41.97	30.34	44.38	29.75	44.23	29.76
45.0	43.54	29.59	41.76	30.48	44.08	29.90	43.92	29.94
50.0	43.24	29.79	41.53	30.64	43.71	30.09	43.55	30.13
55.0	42.93	30.01	41.30	30.83	43.26	30.31	43.08	30.36
60.0	42.23	30.43	40.74	31.17	42.53	30.68	42.35	30.73
65.0	41.34	30.97	40.04	31.62	41.55	31.17	41.35	31.23
70.0	39.95	31.81	38.70	32.45	39.62	32.13	39.36	32.22

Polarisabilities in units of $10^{-24} \text{ cm}^3 (\text{\AA}^3)$

4.4.3 Determination of the order parameter, S

The average molecular orientation in the liquid crystals is characterised by an order matrix, S . Since nematic liquid crystals behave like optically uniaxial crystals, the traceless tensor order parameter S_{ij} has the form of the diagonal matrix, and all the off-diagonal elements must be zero.

$$S_{ij} = \begin{bmatrix} S_{xx} & 0 & 0 \\ 0 & S_{yy} & 0 \\ 0 & 0 & S_{zz} \end{bmatrix}$$

The order parameter S associated with direction parallel and perpendicular to the long axis of the molecule are defined to be $S_{||} = S_{zz}$ and $S_{\perp} = S_{xx} = S_{yy}$, respectively. However, the orientation of the molecules in nematic liquid crystals can be described by a single order parameter $S = S_{||} = -2S_{\perp}$. Nematic liquid crystals exhibit typical order parameter S

of about 0.4 to 0.7, depending on temperature. Here, the author used optical and density data to calculate the order parameters of a number of liquid crystal systems.

In the nematic phase, the effective polarisabilities of the molecules α_e and α_o , corresponding to the extraordinary and ordinary optic axes, respectively, are given by ⁶⁶

$$\alpha_e = \bar{\alpha} + \frac{2}{3}(\alpha_{\parallel} - \alpha_{\perp}) S \quad , \quad \alpha_o = \bar{\alpha} - \frac{1}{3}(\alpha_{\parallel} - \alpha_{\perp}) S \quad (4.41)$$

here, $\alpha = (1/3)(\alpha_{\parallel} + 2\alpha_{\perp})$, $\Delta\alpha = (\alpha_{\parallel} - \alpha_{\perp})$, and α_{\parallel} and α_{\perp} , are the principal polarisabilities parallel and perpendicular to the long molecular axis. The order parameter S may be expressed as

$$S = \frac{(\alpha_e - \alpha_o)}{(\alpha_{\parallel} - \alpha_{\perp})} \quad (4.42)$$

Therefore, it is obvious that in order to derive S it is necessary to know the anisotropy of the polarisability $\Delta\alpha$. The latter can be obtained from either bond polarisability calculations or from a combination of refractive index and density data obtained for the crystalline phase and isotropic phase. However, in this work $\Delta\alpha$ was determined using Haller's method^{49,66} by extrapolating the straight line sections of plots of $\log(\alpha_e/\alpha_o)$ vs. $\log(T_{NI} - T)$ to zero temperature (0°K). The intercept on the $\log(\alpha_e/\alpha_o)$ axis was assumed to correspond to $\log(\alpha_{\parallel}/\alpha_{\perp})$ for the perfectly ordered crystalline state, where the order parameter is unity. From equation 4.25 the values of α_{\parallel} and α_{\perp} were determined. In the case of 6CB the extrapolating the straight line sections of the plot of $\log(\alpha_e - \alpha_o)$ vs $\log(T_{NI} - T)$ to zero temperature was used. The mean polarisabilities and the anisotropies of polarisability, calculated using the methods of Neugebaure⁵⁴, Saup-Maier⁵⁵, Palffy-Muhoray *et al.*^{56,57}, and Vuks⁵⁸ are given in Table 4.13.

The addition of a methylene group increases the overall polarisability of the molecule, consequently, the mean polarisability, $\bar{\alpha}$, is expected to increase as the chain length

grows as it can be seen from Table 4.13. According to the vuks method, the values of mean polarisability $\bar{\alpha}$ for alkyl cyanobiphenyls (5CB to 8CB) are 32.7, 34.6, 36.6, and 38.6. The $\bar{\alpha}$ -value for 8CB is estimated by adding to $\bar{\alpha}_{7CB}$ the polarisability of a CH_2 group, which is equal to $(\bar{\alpha}_{7CB} - \bar{\alpha}_{5CB})/2$.

Table 4.13 Values of the mean polarisabilities, $\bar{\alpha}$, and the anisotropies of polarisability calculated by different methods.

liquid crystal	Neugebauer		Vuks		Saupe-Maier		Palffy-Muhoray	
	$\Delta\alpha$	$\bar{\alpha}$	$\Delta\alpha$	$\bar{\alpha}$	$\Delta\alpha$	$\bar{\alpha}$	$\Delta\alpha$	$\bar{\alpha}$
5CB	14.22	32.7	17.49	32.7	18.66	33.0	18.69	33.0
6CB	15.06	34.6	18.75	34.8	16.91	34.8	17.13	34.8
7CB	17.22	36.6	21.23	36.6	19.03	36.8	19.21	36.8
6OCB	16.07	35.7	19.73	35.7	20.66	36.0	20.62	36.0
E _{6O7}	17.69	36.7	21.86	36.6	22.04	37.0	22.03	37.0
E7	18.66	35.4	23.38	35.4	21.07	35.7	20.99	35.7
E8	17.40	34.2	21.17	34.2	21.89	34.6	21.76	34.6

It can be seen from Tables 4.14 to 4.20 that the order parameters S obtained from the different methods of Vuks⁵⁸, Neugebauer⁵⁴, Saupe-Maier⁵⁵, and Palffy-Muhoray⁵⁶ are nearly the same. This is illustrated for the nematic mixtures E7 and E8 (Figure 4.20). The order parameter S of the nematic mixtures E7 and E8 are larger than those of each of their two main components, pentyl and heptyl cyanobiphenyl. (Tables 4.14 to 4.20). Also, the order parameter for hexoxy cyanobiphenyl, 6OCB, measured at the lowest temperature in the nematic phase is about 0.65, but the order parameter of the eutectic mixture E_{6O7}, composed of hexoxy and heptoxy cyanobiphenyls (41.5 : 58.5), is about 0.70 at 38 °C, which is larger than the S -value of 6OCB (Figure 4.21). The same trend has been reported for a nematic mixture E₁ composed of pentyl and heptyl cyanobiphenyl (59 : 41)⁴⁹. The order parameter of E₁ is about 0.70 at 28 °C and is higher than the S -value of each of the pure components. However, in the present studies E8 has the highest order parameter.

Table 4.14 Values of the order parameter S at several temperatures for 5CB calculated by different methods.

Temp. °C	order parameter S			
	V	N	S-M	P-M
25	0.64	0.64	0.62	0.62
28	0.61	0.61	0.58	0.58
30	0.58	0.58	0.54	0.54
32	0.54	0.54	0.50	0.50
33	0.50	0.50	0.45	0.46

Table 4.15 Values of the order parameter S at several temperatures for 6CB calculated by different methods.

Temp. °C	order parameter S			
	V	N	S-M	P-M
18	0.61	0.62	0.62	0.62
20	0.60	0.60	0.61	0.61
25	0.53	0.53	0.53	0.53
27	0.47	0.48	0.48	0.48
28	0.45	0.44	0.43	0.43

Table 4.16 Values of the order parameter S at several temperatures for 7CB calculated by different methods.

Temp. °C	order parameter S			
	V	N	S-M	P-M
30	0.63	0.63	0.66	0.66
32	0.61	0.61	0.65	0.64
35	0.57	0.57	0.62	0.61
37	0.55	0.55	0.59	0.59
40	0.49	0.49	0.52	0.52

Table 4.17 Values of the order parameter S at several temperatures for 6OCB calculated by different methods.

Temp. °C	order parameter S			
	V	N	S-M	P-M
60	0.66	0.66	0.64	0.64
64	0.63	0.63	0.61	0.61
65	0.62	0.62	0.59	0.59
69	0.57	0.57	0.54	0.54
75	0.43	0.43	0.40	0.40

Table 4.18 Values of the order parameter S at several temperatures for E_{6O7} calculated by different methods.

Temp. °C	order parameter S			
	V	N	S-M	P-M
40	0.70	0.70	0.69	0.69
45	0.68	0.68	0.67	0.67
50	0.66	0.66	0.64	0.64
55	0.63	0.64	0.61	0.61
60	0.60	0.60	0.58	0.58
66	0.54	0.54	0.52	0.52
70	0.49	0.50	0.48	0.48
74	0.37	0.37	0.36	0.36

Table 4.19 Values of the order parameter S at several temperatures for E7 calculated by different methods.

Temp. °C	order parameter S			
	V	N	S-M	P-M
20	0.69	0.70	0.71	0.71
30	0.65	0.66	0.67	0.66
40	0.60	0.61	0.62	0.61
45	0.56	0.57	0.58	0.57
50	0.51	0.53	0.53	0.52
55	0.44	0.45	0.47	0.45
58	0.36	0.36	0.32	0.30

Table 4.20 Values of the order parameter S at several temperatures for E8 calculated by different methods.

Temp. °C	order parameter S			
	V	N	S-M	P-M
20	0.73	0.73	0.74	0.73
30	0.71	0.70	0.71	0.70
40	0.68	0.67	0.69	0.66
50	0.64	0.63	0.62	0.62
60	0.56	0.55	0.54	0.53
65	0.49	0.48	0.47	0.47
68	0.42	0.42	0.42	0.41
70	0.39	0.36	0.34	0.33

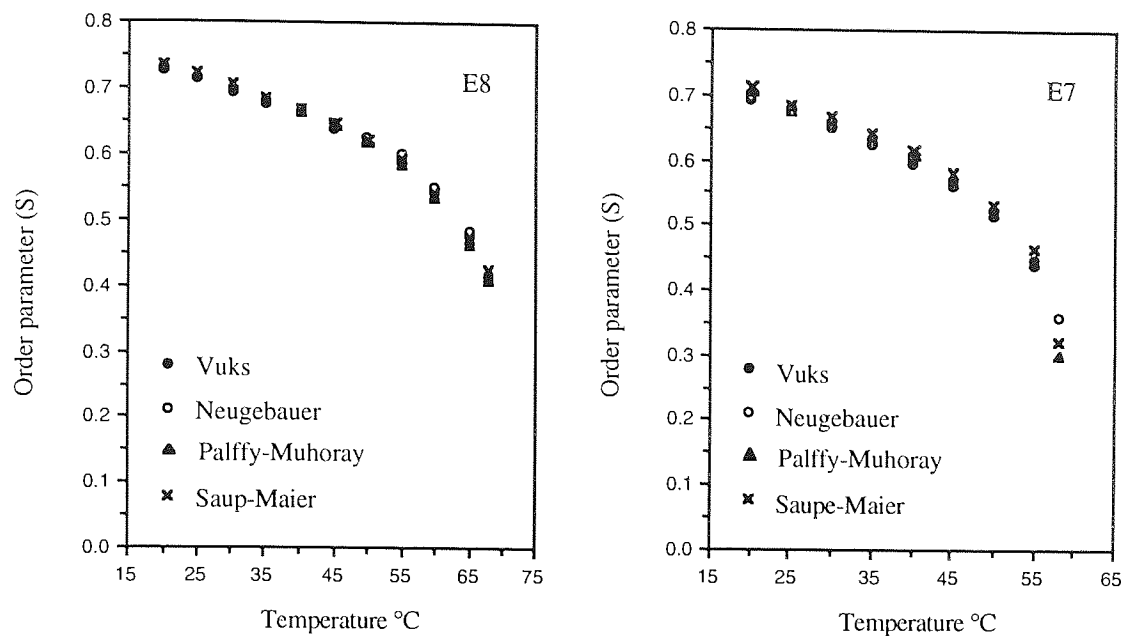


Figure 4.20 The calculated order parameter S by different methods versus temperature for E7 and E8 nematic mixture liquid crystals.

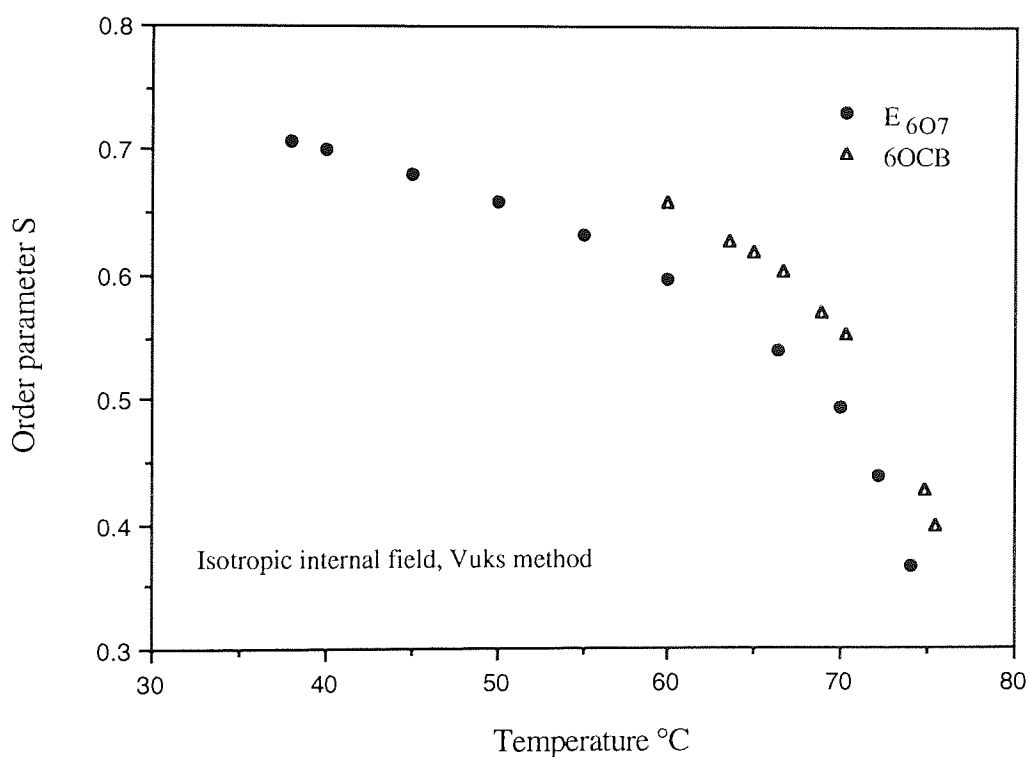


Figure 4.21 The calculated order parameter S versus temperature for E₆O₇ and 6OCB.

6.4.4 The internal field factor

In the calculate of the polarisability and its anisotropy in the nematic phase, different methods have been used to account the internal fields. The internal field, E_i , is defined as the total electric field that acts on a molecule, taken to be equal to the external field plus the average field due to other molecules (surrounding molecules). The internal field responsible for polarising the molecules depends on the molecular properties and the orientation of the molecules for which the internal field is being considered⁶⁹. However, the major contribution to the internal field around a molecule arises from near neighbour molecules.

Vuks assumed the internal field in anisotropic material to be the same in all directions (isotropic), and therefore, this method does not provide any internal field factor. The assumption of isotropic internal field in a medium that possesses an anisotropic molecular distribution, such that of liquid crystalline phase appear to be illogical and lacks theoretical bases. However, the Vuks relation gives good results for the polarisabilities derived from the refractive indices and densities, when compared to values calculated using more elaborate theories.

The internal field factors calculated by using Neugebaure, Saup-Maier, and Palffy-Muhoray methods given in Tables 4-21 to 4-22.

Table 4.21 The temperature dependence of the internal field constants for 5CB

Temp. (°C)	γ_e	γ_o	a	$-\eta$ $\times 10^2$
25	3.776	4.392	0.107	0.492
28	3.797	4.381	0.099	0.415
30	3.818	4.371	0.092	0.353
31	3.830	4.365	0.088	0.312
32	3.841	4.360	0.084	0.265
33	3.863	4.348	0.078	0.201

Table 4.22 The temperature dependence of the internal field constants for 6CB

Temp. (°C)	γ_e	γ_o	a	$-\eta$ $\times 10^2$
18	3.792	4.384	0.077	0.523
20	3.803	4.378	0.076	0.514
22	3.815	4.372	0.072	0.488
25	3.846	4.357	0.063	0.432
27	3.879	4.341	0.059	0.404
28	3.903	4.328	—	0.338

Table 4.23 The temperature dependence of the internal field constants for 7CB

Temp. (°C)	γ_e	γ_o	a	$-\eta$ $\times 10^2$
30	3.754	4.404	0.087	0.579
32	3.766	4.397	0.086	0.572
35	3.793	4.383	0.088	0.581
37	3.809	4.375	0.084	0.554
39	3.835	4.363	0.079	0.524
40	3.847	4.356	0.077	0.510

Table 4.24 The temperature dependence of the internal field constants for 6OCB

Temp. (°C)	γ_e	γ_o	a	$-\eta$ $\times 10^2$
60	3.754	4.403	0.109	0.724
64	3.772	4.394	0.104	0.689
65	3.779	4.391	0.100	0.661
69	3.809	4.375	0.091	0.602
70	3.821	4.370	0.083	0.546
75	3.901	4.329	0.066	0.435

Table 4.25 The temperature dependence of the internal field constants for E₆₀₇

Temp. (°C)	γ_e	γ_o	a	$-\eta$ $\times 10^2$
40	3.695	4.432	0.117	0.777
50	3.722	4.419	0.107	0.713
60	3.763	4.398	0.096	0.641
66	3.803	4.379	0.088	0.589
70	3.835	4.362	0.083	0.550
74	3.922	4.319	0.065	0.437

Table 4.26 The temperature dependence of the internal field constants for E7

Temp. (°C)	γ_e	γ_o	a	$-\eta$ $\times 10^2$
20	3.653	4.453	0.105	0.669
30	3.683	4.439	0.098	0.620
40	3.723	4.419	0.092	0.581
50	3.782	4.389	0.081	0.501
55	3.838	4.361	0.076	0.430
58	3.906	4.327	0.035	0.159

Table 4.27 The temperature dependence of the internal field constants for E8

Temp. (°C)	γ_e	γ_o	a	$-\eta$ $\times 10^2$
30	3.670	4.445	0.131	0.850
40	3.692	4.434	0.124	0.802
50	3.724	4.418	0.116	0.747
60	3.778	4.391	0.102	0.643
65	3.826	4.367	0.090	0.559
68	3.875	4.343	0.086	0.527
70	3.917	4.321	0.063	0.365

For the Saupe-Maier method it is assumed that there is an anisotropic internal field which is quantified by means of a single internal field factor “ a ”, expressed as a function of the co-ordinates of the molecules within the Lorentz sphere. Saupe-Maier’s results showed that a is independent of wavelength “ λ ”, but weakly dependent on temperature⁵⁵. The use of only a single internal field factor means that the internal field factors along and perpendicular to long molecular axis have the same value. This can be regarded as a disadvantage for this theory since the internal field factors along and perpendicular to long molecular axis are expected to be different.

The experimental results presented in Tables 4.21 to 4.27 indicate that the internal field factor is nearly proportional to the order parameter S . Figure 4.22 also shows a sudden decrease in the Saupe-Maier internal field factor in the vicinity of the nematic-isotropic transition (similar trend also observed for the order parameter), which is more clear in the case of nematic mixtures of E7 and E8. However, it seems that the internal field factor

“ a ” decreases as the anisotropy of the internal field decreases with increase of temperature up to nematic-isotropic transition temperature, i.e. as a becomes smaller the internal field gets closer to the Lorentz field. Therefore, the internal field E_i responsible for polarising the molecules, depends on internal field factor “ a ”.

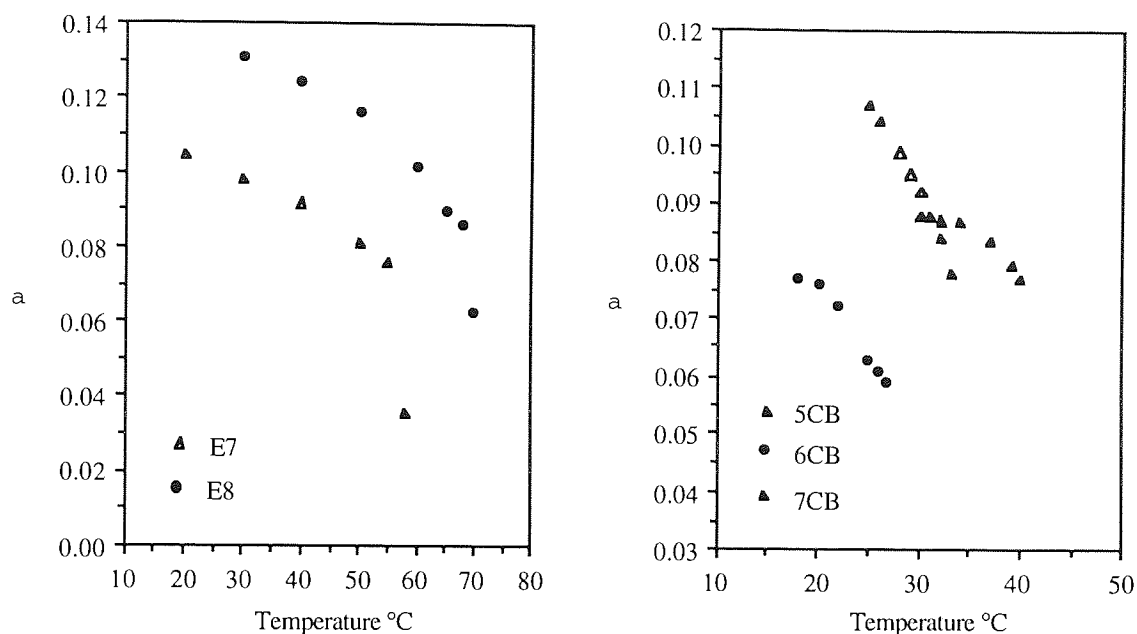


Figure 4.22 The Saupe-Maier internal field factor “ a ” as function of temperature for 5CB, 6CB, 7CB, E7, and E8.

The Neugebauer method assumed an anisotropic internal field in which the polarisabilities of molecules depend on the direction of the field. Neugebauer introduced γ_e and γ_o as the internal field factors along and perpendicular to long molecular axis and such that $\gamma_e + 2\gamma_o = 4\pi$. The assumptions of anisotropic internal field in an anisotropic molecular distribution is logical, and due to its firmer theoretical basis, Neugebauer's method is preferable. Additionally, it has been shown by several authors^{49,68} that the anisotropy of polarisabilities obtained by Neugebauer method are in a good agreement with the values calculated using bond polarisability data.

The internal field factors γ_e and γ_o along and perpendicular to long molecular axis have different values. Tables 4.21 to 4.27 show that γ_e is always less than γ_o , and γ_e increases monotonically with increase of temperature up to the transition temperature. Figure 4.23

shows the anisotropy of internal field factor ($\Delta\gamma = \gamma_o - \gamma_e$) as a function of temperature (similar trend also observed for the order parameter) for the liquid crystals.

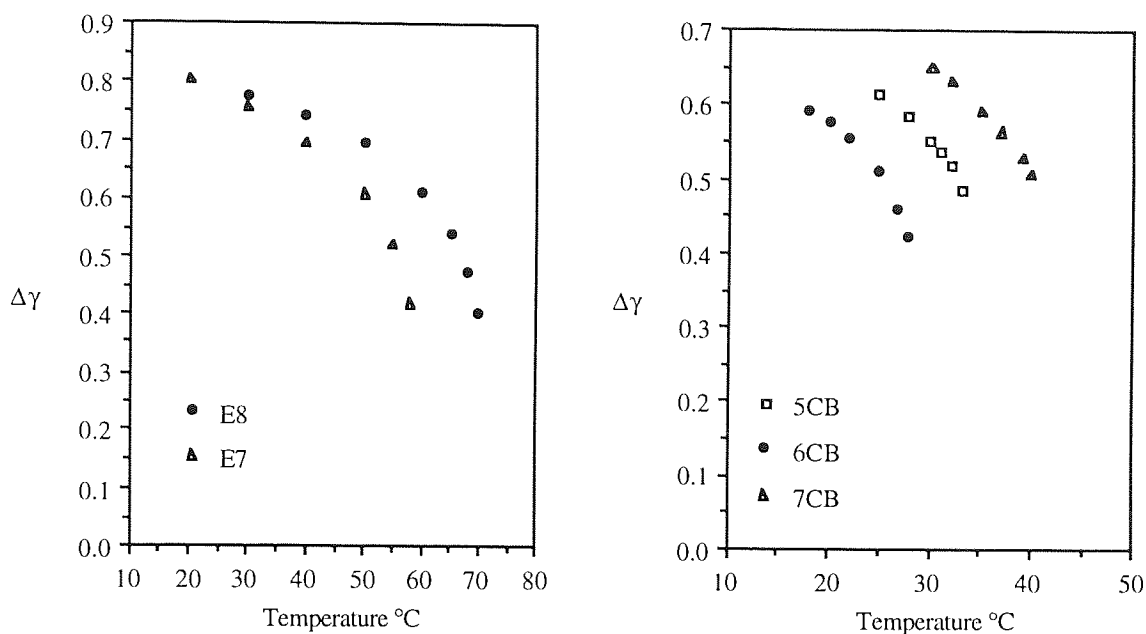


Figure 4.23 The anisotropy of internal field factor ($\Delta\gamma = \gamma_o - \gamma_e$) as a function of temperature for 5CB, 6CB, 7CB, E7, and E8.

Palfy-Muhoray *et al.*⁶⁹ introduced a model that indicates that the internal field anisotropy is proportional to the orientational order parameters. According to the Palfy-Muhoray method, the internal field E_i responsible for polarising the molecules in an anisotropic fluid, depends on an internal field tensor (η_{ij}). The internal field factors along the long molecular axis and perpendicular to it are described as $\eta_{||} = \eta_{zz}$, and $\eta_{\perp} = \eta_{xx} = \eta_{yy}$, respectively, such that $\eta_{||} = -2\eta_{\perp}$. This method not only can be used to calculate effective polarisabilities, order parameter, and internal field factor but can also be used to determine the length-to-breadth ratio κ . On the basis of this model, it is possible to estimate the dependence of the density on the order parameters⁶⁹, using

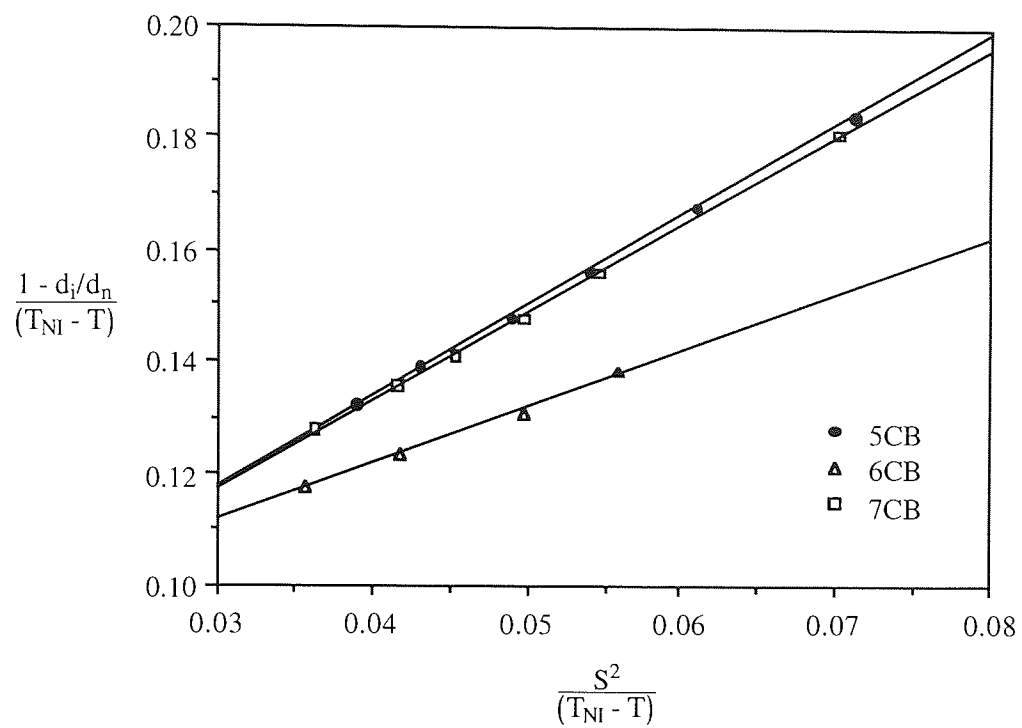
$$\frac{d_i}{d_n} = 1 - 3 \left(\frac{\kappa - 1}{\kappa + 2} \right)^2 \times \left(S^2 + \frac{P^2}{3} \right) + \beta (T_{NI} - T) \quad (4.43)$$

here, d_i is the density of the isotropic phase at the nematic-isotropic transition temperature, T_{NI} . The parameter d_n is the density of the nematic phase, β is the coefficient of thermal expansion of volume of the isotropic phase. S and P are the order parameters, for which $P = 0$ for a uni-axial nematic molecule. Equation 4.43 gives the density variation due to changes in the order parameter and normal thermal expansion. Therefore, an estimate of κ can be obtained from density and order parameter data which results are given in Table 4.28. The length-to-breadth ratio can then be determined from the slope of $(1 - d_i/d_n)/(T_{NI} - T)$ vs. $S^2/(T_{NI} - T)$. Figure 4.24 shows plots for three homologous cyanobiphenyl liquid crystals are linear with a slope of $3[(\kappa-1)/(\kappa+2)]^2$.

The length-to-breadth ratio κ calculated from the density data shows the same trend as $\Delta\alpha/\alpha$ (Table 4.28). On the other hand, the local field factor $\eta_{||}$ and the order parameter S shows the same dependence on temperature.

Table 4.28 Values of the length-to-breadth ratio κ for the various nematic liquid crystals calculated using Palffy-Muhoray *et al.* method.

Compound	Gradient $\times 10^2$	Gradient Error $\times 10^2$	$\kappa = \frac{L}{B}$	$\frac{\Delta\alpha}{\alpha}$
5CB	1.619	0.021	1.238 ± 0.002	0.566
6CB	1.008	0.043	1.185 ± 0.004	0.492
7CB	1.576	0.029	1.234 ± 0.003	0.522
E7	1.975	0.026	1.265 ± 0.002	0.588
E8	2.631	0.034	1.310 ± 0.002	0.629



4.24 The plots of $(1 - d_i/d_n)/(T_{NI} - T)$ vs $S^2/(T_{NI} - T)$ for three homologous cyano-biphenyl liquid crystals.

CHAPTER 5

DIELECTRIC RESPONSE OF E7 AND E8 NEMATIC MIXTURE LIQUID-CRYSTALS

5.1 Introduction

One of the earliest studies of dielectric relaxation of liquid-crystals was that by Maier and Meier⁷⁷ in 1961. They discovered a low-frequency relaxation in the nematic phase of p-azoxyanisole (PAA). They also found that the critical frequency (the frequency of maximum loss) depends strongly on temperature. In 1962, Carr⁷⁸ measured, for the first time, dielectric relaxation in liquid-crystals in the microwave region. He found a high frequency relaxation in the isotropic and nematic phases of PAA.

To date a number of low molecular weight liquid-crystals have been studied by dielectric relaxation methods. Most of them have been made at micro-wave frequencies, and a magnetic or electric field has been used to align the liquid-crystal molecules.

Molecular reorientation processes can be observed directly by the dielectric relaxation method. Measurements of the temperature and frequency dependence of the dielectric relaxation, especially on oriented samples, gives information about the dynamics of polar groups and about molecular motion^{79,80,81}. On the other hand, dielectric spectroscopy is a very good method for characterising the solid, liquid-crystalline, and isotropic phases^{82,83}. Also, through the measurement of the intensity of the dielectric absorption the order parameter S can be calculated⁸⁴.

For low molecular weight liquid-crystals two principal types of motions are known^{84,85,86}. These correspond to rotations around the short axis of the molecule, and at higher frequencies, fast rotations about the long axis. For example, in 4-pentyl-4-

ciano-biphenyl there is a low-frequency dielectric relaxation correspond to about 6.5 MHz at room temperature^{88,89}.

The effect of viscosity on the motions of dipoles of a system has also been studied by the dielectric method^{90,91,92}. In a very viscous medium or in the supercooled liquid state, the re-orientational motions of small molecules is a slow process, and may be conveniently studied by low-frequency dielectric relaxation methods^{93,94}. The dielectric study of liquid-crystals in a variable viscosity medium is also very interesting. The viscosity can be varied, of course, by changing the temperature. Molecular motions are possible in the supercooled system, and even below the glass transition temperature, T_g , due to the retainment of free volume in the system^{95,96}.

In recent years, dielectric studies of mixture of nematic liquid-crystals have received much attention^{97,98,99,100}. This interest is due to their broad nematic temperature range, ease of supercooling, and the presence of low frequency relaxation processes. Finally, nematic mixtures have become increase important as anisotropic solvents for use in dielectric studies of a variety of solute molecules^{101,102,103}.

One of the aims of this part of the project is to present some dielectric data obtained for thin layers of an eutectic mixture liquid-crystals E7 and E8. The elute mixture exhibits strong positive dielectric anisotropy in the nematic, supercooled nematic, and glass nematic phases. The dielectric results obtained for these systems at several temperatures represent an important addition to the database of dielectric properties of liquid-crystals for scientific and technological purposes. As far as the author is aware these measurements have not been previously reported.

5.2 Theory

5.2.1 Dielectrics in Static Electric Fields

First consider a capacitor consisted of two parallel plates with the area A , separated by a distance d in a vacuum (Figure 5.1.a). If a potential difference V is applied across two electrodes it produces an electric field $E = V/d$ perpendicular to the plates. The electric field produces charges $+Q$ and $-Q$ per unit area on the electrodes, which are proportional to the magnitude of the field, i.e.

$$Q = \epsilon_0 E \quad (5.1)$$

Where ϵ_0 is dielectric constant (permittivity) of the free space, and it is $8.854 \times 10^{-12} \text{ Fm}^{-1}$ in M.K.S. system¹⁰⁴. The capacitance of the capacitor in the absence of a dielectric is

$$C_0 = Q/V \quad (5.2)$$

Where C_0 is a constant determined by the geometry of the capacitor $C_0 = \epsilon_0 A/d$. On the other hand, the capacitor with a material between the plates, has capacitance $C = \epsilon C_0$ or

$$\epsilon = C/C_0 \quad (5.3)$$

In which ϵ is a ratio of capacitance with and without the dielectric, and is often simply called the dielectric constant of material^{104,105}.

5.2.2 The Relationship Between Dielectric Constant and Polarisation

In the case of a capacitor with a dielectric, the presence of electric field on the plates will polarise the molecules. Therefore, the positive charges will be attracted by the negative

electrode and vice versa. This effect is polarisation of the material, P . The displacement of the charges within the dielectric, produce charges $+PA$ on one surface of the dielectric and $-PA$ on the other surface. Therefore an electric moment $P(Ad)$ or PV is produced. The polarisation P is thus the average dipole moment per unit volume (Figure 5.1.b).

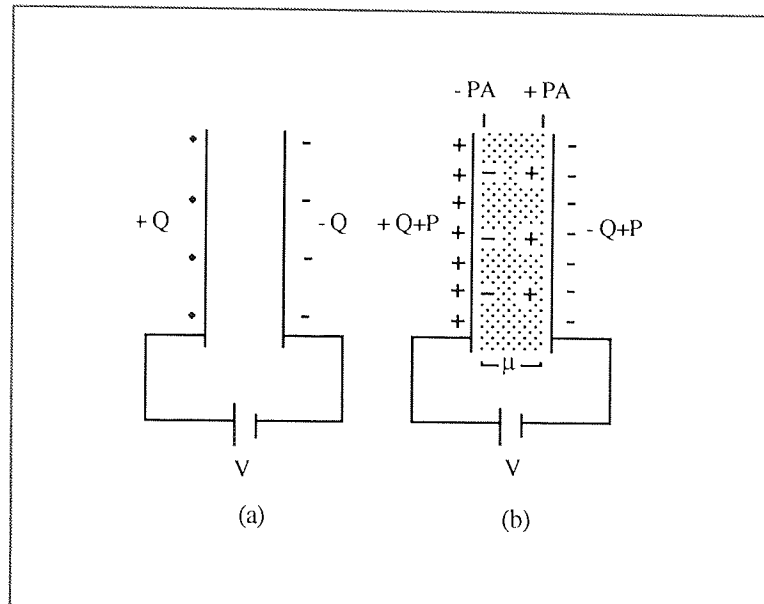


Figure 5.1 The polarisation of the dielectric molecules due to displacement of charges.

The presence of the charges on the surface of the dielectric, causes more charges to be stored on the electrodes, and capacitance of the system is increased to

$$C = (Q + P)/V. \quad (5.4)$$

The dielectric constant (ϵ) of the material is defined as

$$\epsilon = C/C_0 = (Q + P)/Q \quad (5.5)$$

Eliminating Q from equations (5.1) and (5.5) gives

$$\epsilon = (\epsilon_0 E + P)/\epsilon_0 E$$

or

$$P = (\epsilon - 1) \epsilon_0 E \quad (5.6)$$

where $\epsilon_0 \epsilon E$ is the dielectric displacement D in the material. Equation (5.6) demonstrates the relationship between dielectric constant and polarisation of the materials^{106,107}.

5.2.3 *Dielectrics in Alternating Fields*

When a dielectric material is placed to an alternating field, the orientation of the dipoles tend to reverse with changes in the electric field. This phenomenon can be observed only when there is a sufficient time for the polarisation of material. If this is the case, then the dielectric is in equilibrium with the applied field. Therefore, maximum polarisation occurs and the dielectric constant has the highest possible value. This dielectric constant is the static, low-frequency, dielectric constant ϵ_s . On the other hand, for very high frequencies there is not time enough for the dipole orientation. Therefore, the dielectric constant has a low value (due to distortion polarisation only) equal to the limiting high frequency dielectric constant, ϵ_∞ . Between frequencies corresponding to low and high dielectric constant there must be at least one dispersion process¹⁰⁴.

5.2.4 *Dipole polarisation*

Orientation or dipole polarisation is a relatively slow process corresponding to electronic polarisation or molecular vibrations. The time required for the electronic and vibration displacements process are normally below 10^{-12} sec., but the time required for the orientation polarisation depends on the viscosity of the dielectric. For small molecules in liquids of low viscosity this time is about 10^{-11} to 10^{-10} sec., and frequencies are in the microwave region. For viscous molecules the time required is about 10^{-6} sec., i.e. radio frequencies. For very viscous liquids, the time required for the polarisation process may be seconds or even longer⁹⁰.

5.2.5 Dielectric Relaxation

Dielectric relaxation is the lag in dipole orientation behind an alternating electric field. When the polar molecules are very large, or the viscosity of the dielectric is high, or at high frequencies, the molecules are not able to rotate sufficiently rapidly for the attainment of equilibrium with the field as a consequence of this behaviour, energy is absorbed and the dielectric constant decreases¹⁰⁴.

If an alternating electric field E is applied across a dielectric material, then

$$E = E_0 \cos \omega t \quad (5.7)$$

Where E_0 is amplitude, and ω is the angular frequency. Instead of equation 5.7, we can write

$$E = E_0 e^{i\omega t} \quad (5.8)$$

This will produce an alternating polarisation in the field direction with time. At low frequencies of the electric field, the dipoles can follow the reversing field. Under these conditions, the charging or capacitive current is 90° out of phase with the alternating potential, therefore, there is no phase difference between the dielectric displacement D vector and alternating field E vector, and consequently, the relation between D and E at low frequency is

$$D(t) = \epsilon' E(t) \quad (5.9)$$

in which ϵ' is the real value of the dielectric constant. At high enough frequencies, the dipoles are not able to follow immediately the reversing field and there is a phase angle

difference δ between the D and E vectors (Figure 5.2). The dielectric displacement is also periodic in the time

$$D = D_0 \cos(\omega t - \delta) \quad (5.10)$$

this may be written as

$$D = D_1 \cos \omega t + D_2 \sin \omega t \quad (5.11)$$

where

$$D_1 = D_0 \cos \delta \quad \text{and} \quad D_2 = D_0 \sin \delta \quad (5.12)$$

Two different dielectric constant may be defined as

$$\epsilon' = D_1/\epsilon_0 E_0 \quad \text{and} \quad \epsilon'' = D_2/\epsilon_0 E_0 \quad (5.13)$$

It follows then from 5.12 and 5.13 that

$$\epsilon''/\epsilon' = \tan \delta \quad (5.14)$$

where ϵ'' is the imaginary part of the dielectric constant and is called the dielectric loss factor. A complex dielectric constant may be defined as

$$\epsilon^* = \epsilon' - i\epsilon'' \quad (5.15)$$

where $i = (-1)^{1/2}$.

As shown in Figure 5.2, in the presence of a loss mechanism, the current also has a component $V\omega\epsilon''C_0$ in phase with the potential and possessing a magnitude is determined

by Ohm's law. This ohmic or loss current, is due to dissipation of part of the electric field as heat. In vector notation, the total current is the sum of charging current and the loss current¹⁰⁴. Therefore, the physical meaning of the quantity $\tan\delta$ is

$$\tan\delta = \epsilon''/\epsilon' = \text{loss current /charging current} \quad (5.16)$$

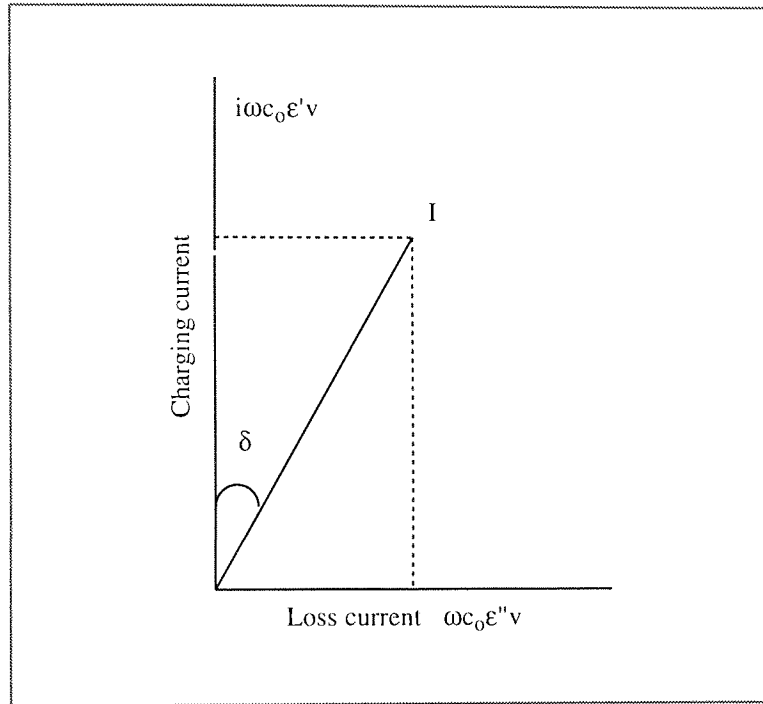


Figure 5.2 Current-voltage diagram of a dielectric with loss

5.2.6 Debye Relaxation; Single Relaxation Behaviour

The frequency dependence of ϵ'' and ϵ' are given by the equations of Debye (1929)¹⁰⁴.

$$\epsilon' = \epsilon_{\infty} + \frac{(\epsilon_s - \epsilon_{\infty})}{(1 + \omega^2\tau^2)} \quad (5.17)$$

and

$$\epsilon'' = \frac{(\epsilon_s - \epsilon_{\infty})\omega\tau}{(1 + \omega^2\tau^2)} \quad (5.18)$$

Equations 5.17 and 5.18 were derived by separation of real and imaginary parts in the equation

$$\epsilon^* = \epsilon_\infty + \frac{(\epsilon_s - \epsilon_\infty)}{(1 + i\omega\tau)} \quad (5.19)$$

where ϵ_s is the static (low frequency) dielectric constant; ϵ_∞ is the high frequency dielectric constant, ω is the angular frequency, $2\pi f$, and τ is the relaxation time. Equation 5.18 shows that ϵ'' approaches zero both for small and for large values of $\omega\tau$, and ϵ'' reaches a maximum value at $\omega = 1/\tau$ or

$$\omega\tau = 1 \quad (5.20)$$

For $\omega\tau = 1$ equation 5.17 and 5.18 reduce to

$$\epsilon''_m = (\epsilon_s - \epsilon_\infty) / 2 \quad (5.21)$$

and

$$\epsilon'_m = (\epsilon_s + \epsilon_\infty) / 2 \quad (5.22)$$

respectively. At very high frequencies (a rapidly reversing electric field) the dipoles of dielectric will not absorb energy from the ac field. As the frequency decreases, the dipoles will move to a limited extent, and energy is absorbed. The absorption peak is caused by dipole orientation at the frequency that dielectric constant is changing rapidly. The loss will increase as the frequency decreases. For the lowest frequencies, the dipoles attain equilibrium with the applied field and the dielectric constant will reach the highest value ϵ_s ¹⁰¹.

5.2.7 Cole-Cole Arc Plot

For a dielectric with a single relaxation time, Cole and Cole (1941)¹⁰⁴ combined equations 5.17 and 5.18 to obtain

$$\left[\epsilon' - \frac{(\epsilon_s + \epsilon_\infty)}{2} \right]^2 + \epsilon''^2 = \left[\frac{(\epsilon_s - \epsilon_\infty)}{2} \right]^2 \quad (5.23)$$

This equation represents a circle [centre $(\epsilon_s + \epsilon_\infty)/2$, 0, radius $(\epsilon_s - \epsilon_\infty)/2$]. Only the semi-circle over which ϵ'' is positive has physical significance, so that a plot of ϵ'' against ϵ' gives a semi-circle, as shown in Figure 5.3(a). For a dielectric with a single relaxation time, the Cole-Cole plot is a semi-circle. Experimental results for many simple liquids give excellent agreement with this theoretical curve.

In order to adequately describe the dielectric response of systems possessing multiple relaxation processes Cole and Cole modified equation (5.19) by the introduction of an empirical constant α to give

$$\epsilon^* = \epsilon_\infty + \frac{(\epsilon_s - \epsilon_\infty)}{[1 + (i\omega\tau)^{1-\alpha}]} \quad (5.24)$$

where α is an empirical constant with values between 0 and 1, and is a measure of the broadness of the distribution. The centre of the semi-circle is below the dielectric constant axis, and the diameter drawn through the centre from the ϵ_∞ point makes an angle $\alpha\pi/2$ with the ϵ' axis, as shown in Figure 5.4(b).

The relaxation time may be calculated from the relation

$$u/v = (\omega\tau_0)^{1-\alpha} \quad (5.25)$$

Where v is the distance on the Cole-Cole plot between ϵ_s and the experimental point, and u is the distance between the point and ϵ_∞ . If α was zero, u/v would equal $\omega\tau_0$, which is true for the Debye equations.

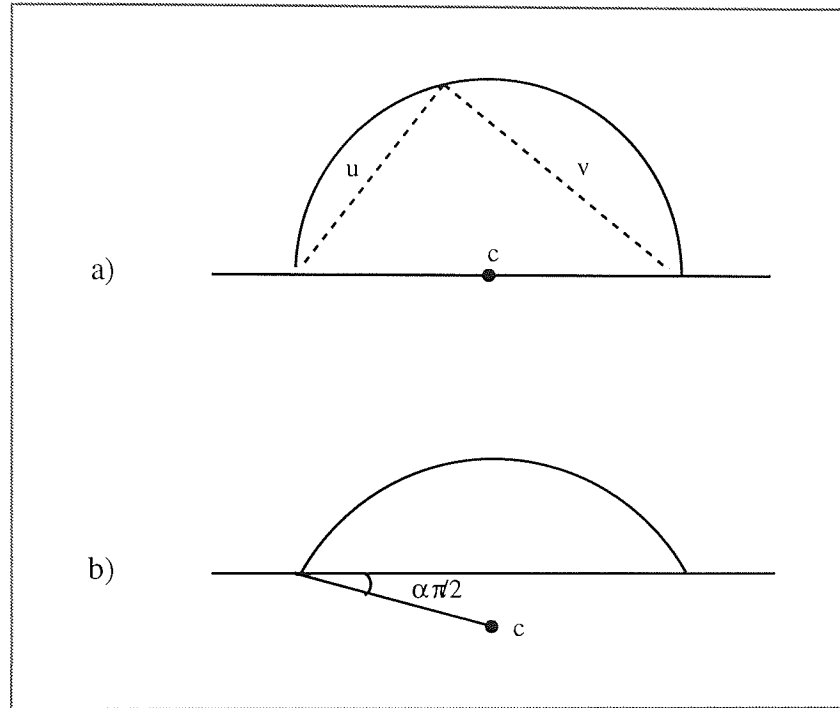


Figure 5.3 Cole-Cole plot, (a) Arc plot for a Debye dielectric; (b) Arc plot for a dielectric with a Cole-Cole distribution characterised by the parameter α .

5.2.8 The Cole-Davidson Arc

Instead of the usual symmetrical arc plot, a skewed-arc plot is sometimes obtained. Cole and Davidson (1950)¹⁰⁴ found that experimental results for certain materials, for example glycerol, the $(\epsilon'' - \epsilon')$ plot was a skewed arc. They represented this behaviour by the equation.

$$\epsilon^* = \epsilon_\infty + \frac{(\epsilon_s - \epsilon_\infty)}{(1 + i\omega\tau)^\beta} \quad (5.26)$$

In which β is an empirical constant with a value between 0 and 1. When $\beta = 0$ in equation 5.26, it becomes identical with equation 5.19, which represents Debye behaviour.

In which β is an empirical constant with a value between 0 and 1. When $\beta = 0$ in equation 5.26, it becomes identical with equation 5.19, which represents Debye behaviour.

The Cole-Cole arc would arise from a symmetrical distribution of relaxation times, while the Cole-Davidson arc would be obtained from a series of relaxation mechanisms of decreasing importance extending to the high-frequency side of the main dispersion.

5.2.9 The Activation Energy

Because of hindered rotational motion of the rod-like nematic molecules around the short and long molecular axis, activation barriers arise. From the dielectric measurements at different temperatures and with aid of the Arrhenius law (equation 5.27) these activation energies E_A can be calculated. In practice, the activation energy can be calculated if the frequency of maximum absorption (f_m) is plotted logarithmically against reciprocal temperature ($1/T$). This will usually result in a straight line with a gradient of $-E_A/R$.

$$\ln f_m = \ln f_0 - E_A/RT \quad (5.27)$$

Due to the increasing cooperativity of the reorientational processes with decreasing temperature T , (free volume decreasing), the Arrhenius plot one is curved and can observe continuously increasing activation energies, as T approaches T_g . Therefore a Vogel-Fulcher-Tammann-equation^{95,109} including T_g would be more appropriate to represent the frequency of maximum loss, f_m .

$$f_m = A \cdot \exp\left(-\frac{B}{T - T_0}\right) \quad (5.28)$$

in which A , B and T_0 are empirical constants for a particular chemical system. At $T = T_0$ the relaxation frequency is zero⁹⁶.

5.3 Experimental

5.3.1 Dielectric Apparatus

The capacitance and the dielectric loss tangent (dissipation factor) were measured in the range 12 Hz to 100 kHz using a GenRad 1689 Digibridge. Electrical connections were made using stiff copper wires between the Digibridge and the dielectric cell. The Digibridge had an accuracy of 0.01% in capacitance and 0.1% in dissipation factor.

5.3.2 Dielectric Cell

A variety of liquid-crystal cells were used in the experiments. They were all constructed using parallel glass plate capacitors ($\sim 2\text{cm} \times \sim 1.2\text{cm}$). The liquid-crystal cells were made by using indium/tin oxide (ITO) coated glass plates, and sandwiching the liquid-crystal between the two plates (see Chapter 2). A 12.5 micron thick Mylar film was used as the spacer material. The spacers were placed along the short edge of one of the plates. The other plate was then carefully fixed in place after insertion of a few micro-drops of the liquid-crystal. The two glass plates were then sealed together with epoxy adhesive. The cell volumes were estimated to be between 1.2 μl and 1.8 μl .

Liquid crystal cells with homeotropic alignment (long axis of molecules perpendicular to the cell walls) were used for measuring ϵ_{\parallel} . Planar (long molecular axes parallel to surface) alignment was used to obtain ϵ_{\perp} . Here, ϵ_{\parallel} , ϵ_{\perp} are respectively the dielectric constant of the liquid-crystal with electric field parallel ($E_{\parallel D}$) and perpendicular ($E_{\perp D}$) to the director. Two surface active agents were used for obtaining parallel and homeotropic alignments of the liquid-crystal. The planar alignment was achieved by rubbing the surface a thin coating of cellulose acetate butyrate (CAB), while the homeotropic alignment was obtained by coating a thin layer of lecithin from its dilute solution in diethyl ether (Chapter 2).

5.3.3 *Temperature Control*

Temperatures were measured with a copper-constant thermocouple which was placed on the outside of the glass and glued in position with epoxy adhesive. Measurements of temperature were estimated to be accurate to within ± 0.1 K. The liquid-crystal cells were placed inside a glass tube, and were immersed in an acetone/solid carbon dioxide thermostat bath (Townson & Mercer) for 213 K-298 K, and in a liquid nitrogen bath for temperatures below 213 K. For the later method the temperature of the sample was controlled by passing an electric current through a matrix of resistors wrapped around the sample tube.

5.3.4 *Materials*

An eutectic nematic mixtures of E7 and E8 (see Chapter 3) was used in this part of project. The clearing point or nematic isotropic transition temperature for E7 and E8 were 332.8 K and 343.5 K, respectively . The melting point of E7 and E8 are about 263 K and 261 K, respectively, with their exact determinations made difficult because the nematic phase readily supercooled to temperatures below their melting point temperatures.

5.3.5 *Measurements*

Dielectric measurements in the frequency range from 12 Hz to 100 kHz at different temperatures (343 -183 K), have been carried out. The supercooled or glassy state of the nematic mixtures could be obtained by heating the mixture into the isotropic phase and cooling down with a cooling rate $> 2\text{K min}^{-1}$. The heating process was achieved using the same rate. A check was made for any dielectric loss due to the Mylar spacer and CAB coating agent in the cells by measuring the dielectric loss of the empty cell. No detectable loss was found from 183 K to 343 K in the frequency range 12 Hz to 100 kHz.

5.4 Results of the Measurement

5.4.1 Dielectric results for the electric field parallel to the nematic director ($E = E_{\parallel D}$)

Dielectric spectra were obtained for supercooled E7 and E8 in the Hz and kHz range, from 223 to 263K. Figures 5.4 to 5.7 show the frequency dependence of the dielectric loss (ϵ''_{\parallel}) and dielectric constant (ϵ'_{\parallel}) measured for the nematic mixtures with electric field parallel to the long molecular axis. The bulk of the dielectric data obtained for the E7 and E8 for the condition denoted by $E = E_{\parallel D}$, are listed in Appendix B.

Figures 5.8 and 5.9 show the Cole-Cole plots of the nematic eutectic mixture of E7 and E8 at different temperatures. From the experimental data, and Cole-Cole plots (nearly a semi-circle), indicate that only one loss process is present. This is low-frequency relaxation process of Debye-type behaviour in the supercooled state, which we assign to hindered rotational motion of the rod-like molecules around their short molecular axes. Characteristic data are listed in Tables 5.1 and 5.2.

The dielectric increment values, ($\Delta_{\parallel} = \epsilon_{\parallel 01} - \epsilon_{\parallel \infty}$), of the respective relaxation process, associated with the reorientation of the dipole moment around the short molecular axis, are also listed in Tables 5.1 and 5.2.

Table 5.1 Dielectric absorption of supercooled E7 for parallel relaxation ($E_{\parallel D}$)

Temp. °K	$\epsilon_{\parallel 01}$	$\tau_{\parallel}/\mu\text{s}$	α_{\parallel}	$\epsilon_{\parallel\infty}$	log (f_m/Hz)	Δ_{\parallel}
289	16.2	6	~ 0	3.7	4.4	12.5
252	16.2	16	~ 0	3.7	4.0	12.5
248	16.2	32	~ 0	3.7	3.7	12.5
243	16.2	80	~ 0	3.6	3.3	12.4
238	16.2	230	~ 0	3.6	2.8	12.4
231	15.0	1600	~ 0	3.6	2.0	11.4
226	13.5	8000	~ 0	3.6	1.3	9.9

α : Cole-Cole distribution parameter

Table 5.2 Dielectric absorption of supercooled E8 for parallel relaxation ($E_{\parallel D}$)

Temp. °K	$\epsilon_{\parallel 01}$	$\tau_{\parallel}/\mu\text{s}$	α_{\parallel}	$\epsilon_{\parallel\infty}$	log (f_m/Hz)	Δ_{\parallel}
263.5	18.6	7	~ 0	4.5	4.3	14.1
258.0	18.6	13	~ 0	4.5	4.1	14.1
251.7	18.5	25	~ 0	4.5	3.7	14.0
247.5	18.5	63	~ 0	4.5	3.4	14.0
242.5	18.4	159	~ 0	4.5	3.0	13.9
237.3	18.0	504	~ 0	4.5	2.6	13.5
230.9	15.4	5040	~ 0	4.5	1.7	10.9
225.8	14.5	12650	~ 0	4.5	1.1	10.0

The equations, $\epsilon_{\parallel 01}$ and $\epsilon_{\parallel\infty}$, listed in these tables represent the limiting dielectric constant (dielectric permittivity) on the low-frequency and on the high frequency side of the first absorption, respectively. $\epsilon_{\perp\infty}$ is the limiting dielectric constant on the high frequency side of the second absorption for the condition $E = E_{\parallel D}$.

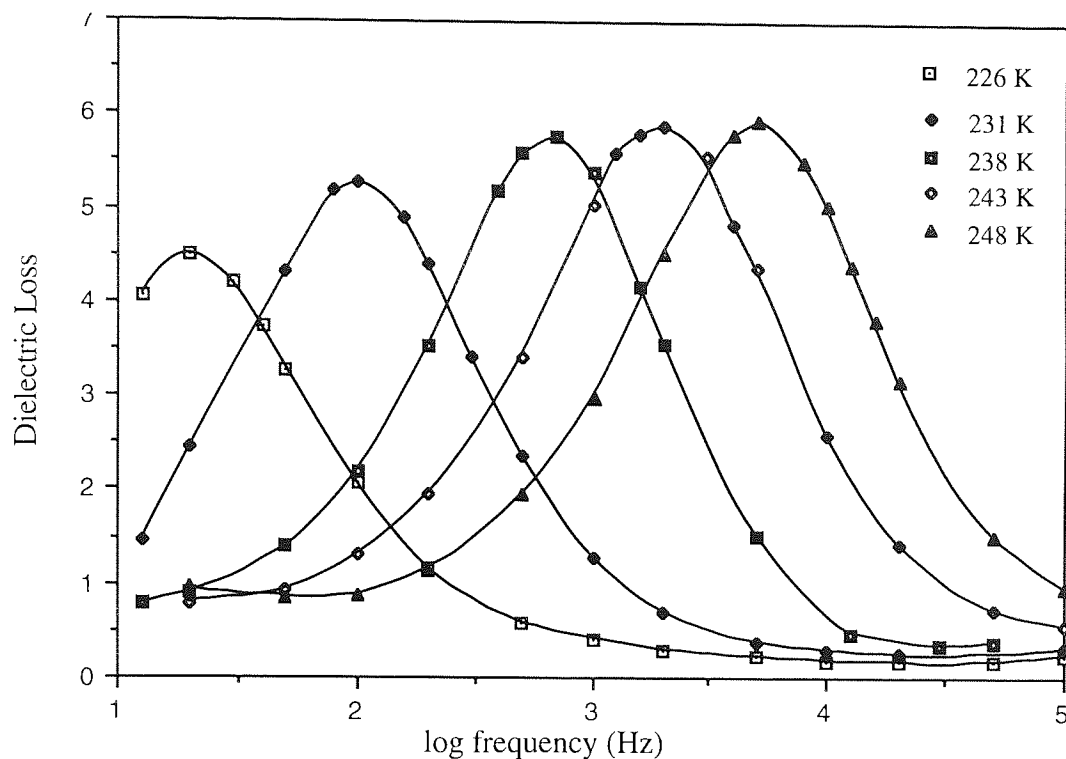


Figure 5.4 The dielectric loss of E7 as function of frequency and temperature. The measuring electric field is parallel to the director ($E_{\parallel D}$).

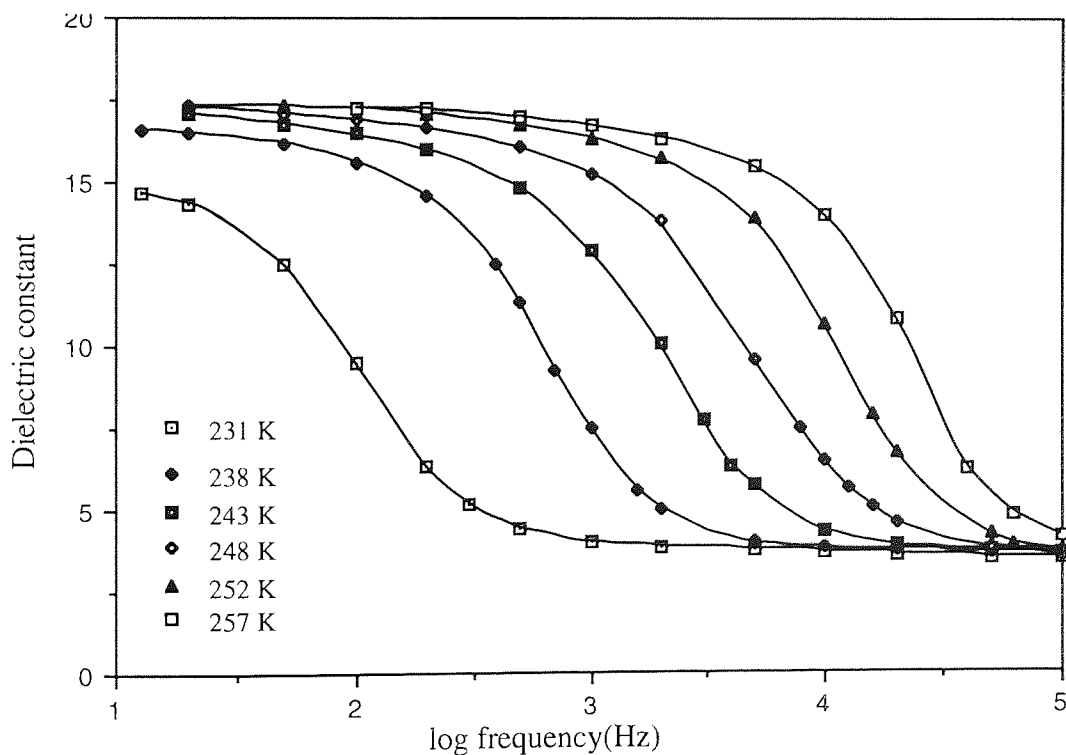


Figure 5.5 The effect of temperature and frequency on dielectric constant of E7 ($E_{\parallel D}$).

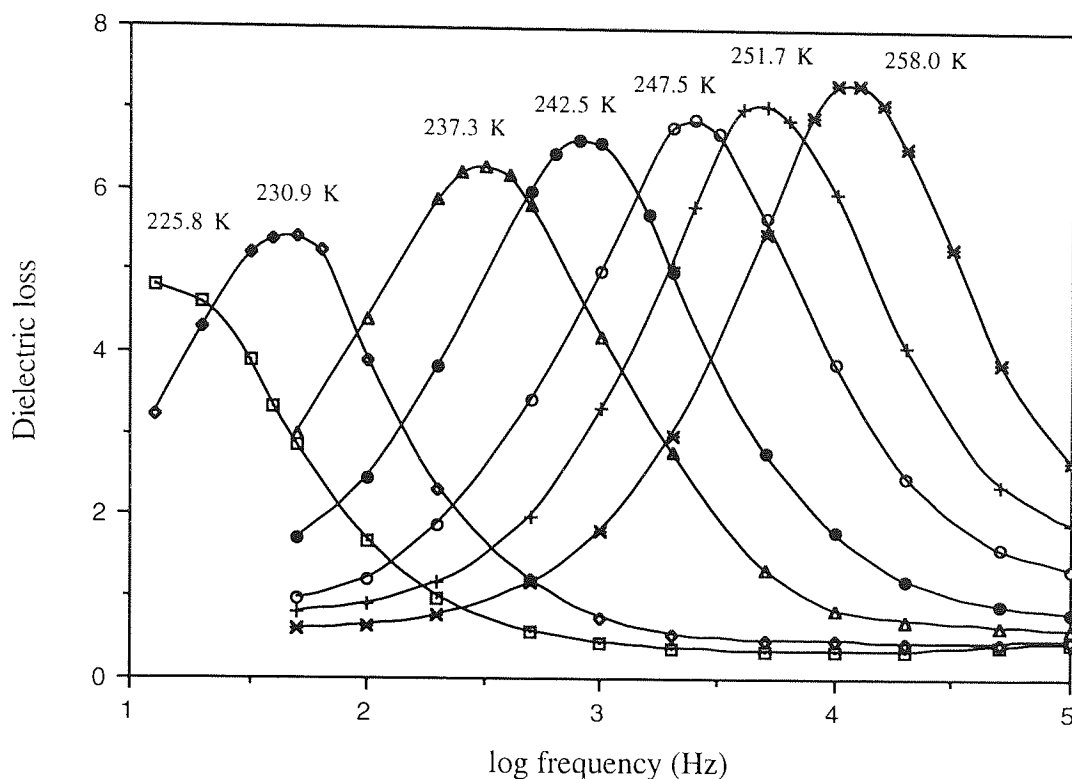


Figure 5.6 The dielectric loss of E8 as function of frequency and temperature. The measuring electric field is parallel to the director ($E_{\parallel D}$).

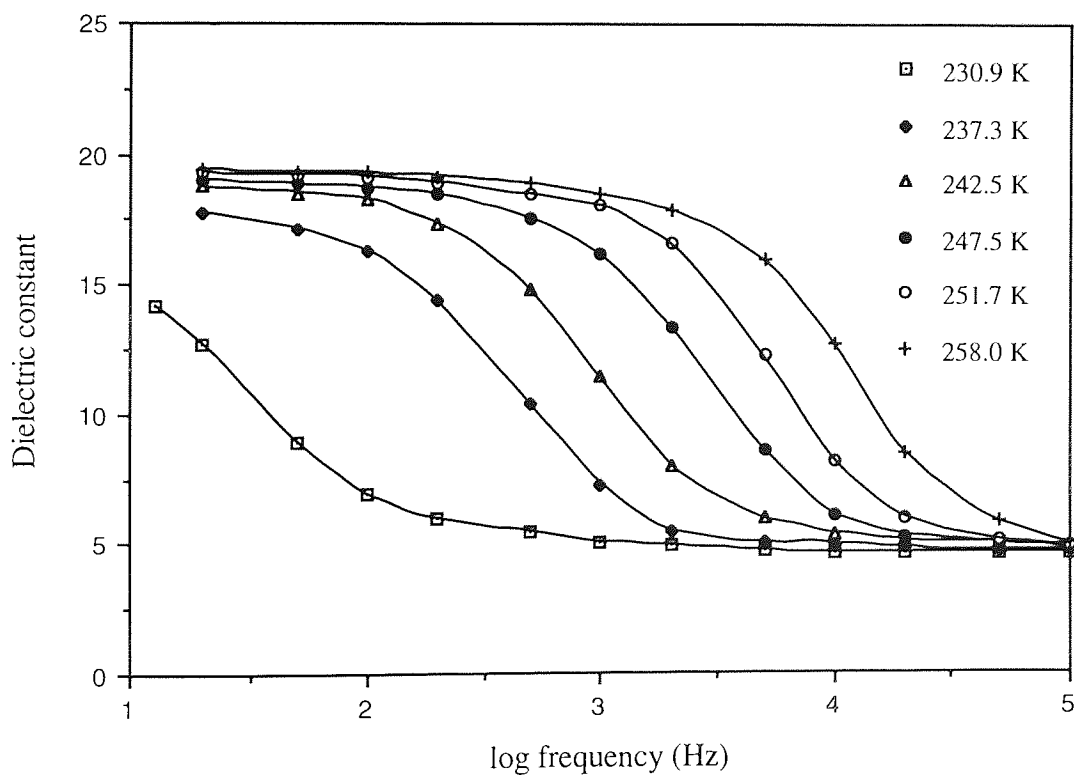


Figure 5.7 The effect of temperature and frequency on dielectric constant of E8 ($E_{\parallel D}$).

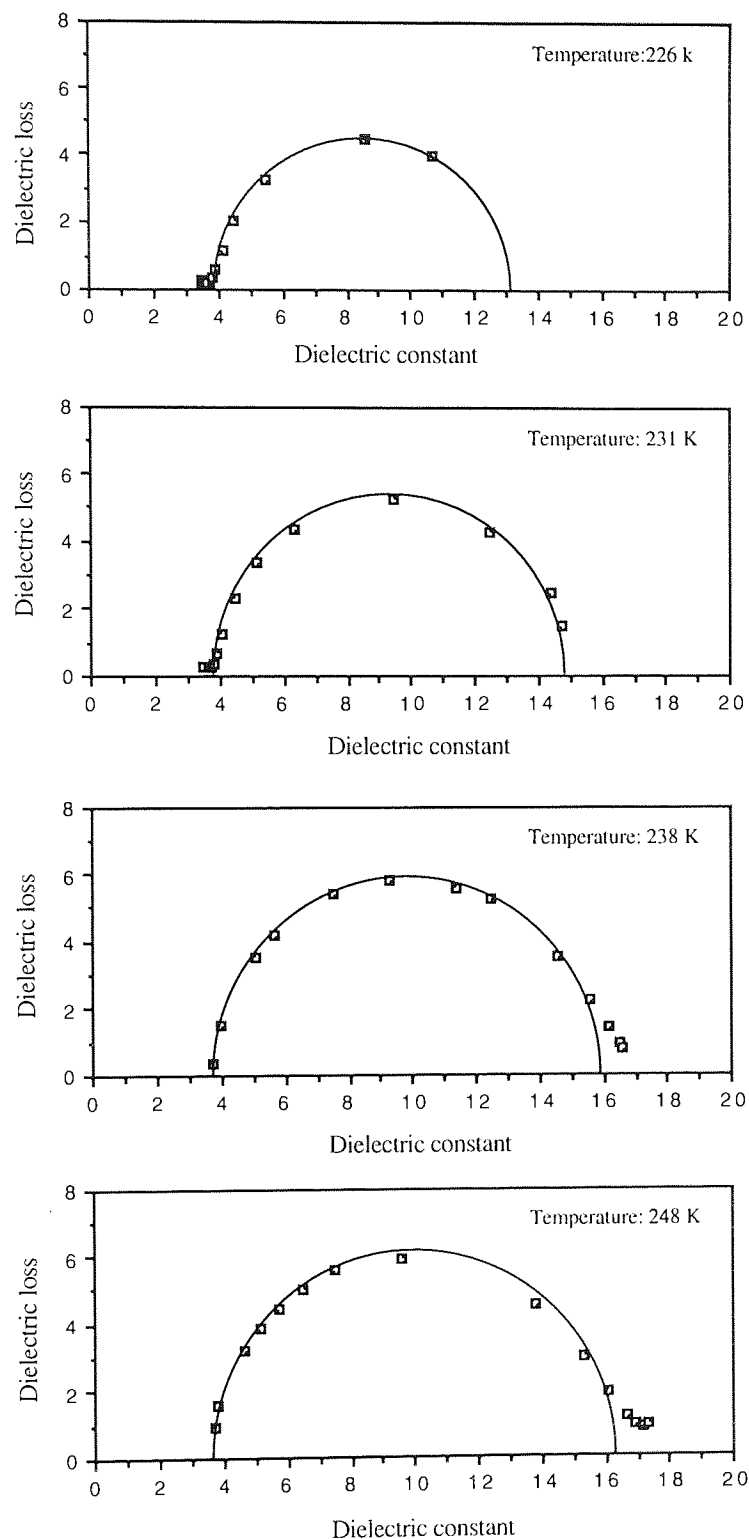


Figure 5.8 Cole-Cole plot for E7 at several temperatures, in which measuring electric field is parallel to the director ($E_{\parallel D}$)

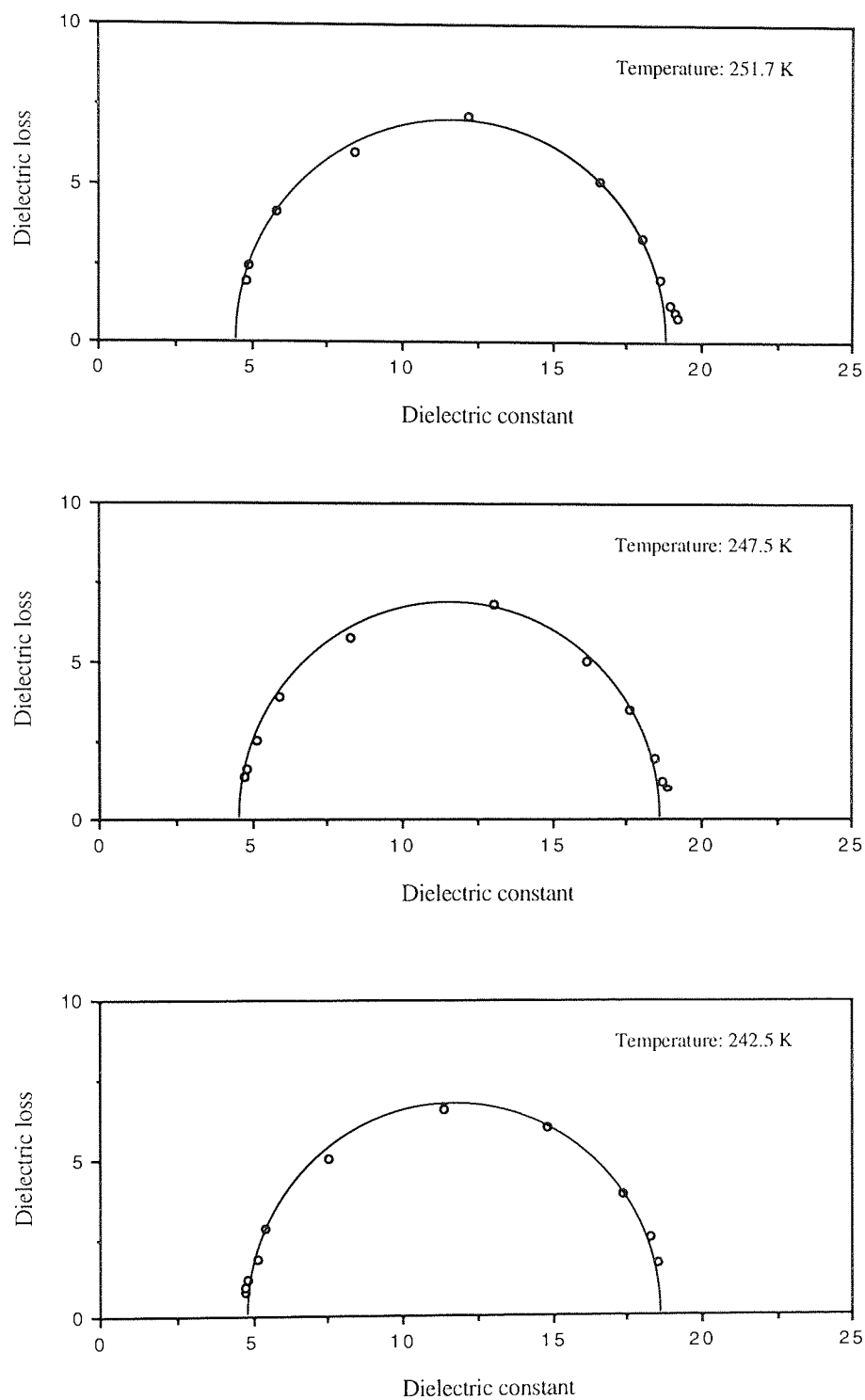


Figure 5.9 Cole-Cole plot for E8 at several temperatures, in which measuring electric field is parallel to the director ($E_{\parallel D}$)

5.4.2 Dielectric results for the electric field perpendicular to the nematic director ($E = E_{\perp D}$)

In the planar alignment of E7 and E8 (long axes of molecules parallel to the cell walls), in which the measuring electric field was perpendicular to the long molecular axis (director), two distinct loss processes have been observed. Curves of the dielectric loss ϵ''_{\perp} and dielectric constant ϵ'_{\perp} plotted against logarithm of frequency, f , at several temperatures are shown in Figures 5.10 and 5.11. The bulk of the dielectric loss and constant data obtained for E7 and E8 for $E = E_{\perp D}$ are listed in Appendix B.

Figure 5.12 shows the Cole-Cole plots of E7 at several temperatures resolved into a Debye mechanism at lower and a Cole-Cole mechanism at the higher frequencies. Characteristic data are listed in Tables 5.3 and 5.4. The dielectric increments, $\Delta_{\perp 1}$ and $\Delta_{\perp 2}$ for the relaxation processes associated with the reorientation of the dipole moment around the short and long molecular axis, respectively, are given in Tables 5.3 and 5.4.

Figure 5.12 shows the dielectric loss ϵ''_{\perp} of E8 for the condition $E = E_{\perp D}$ plotted against $\log f$ of at several temperatures.

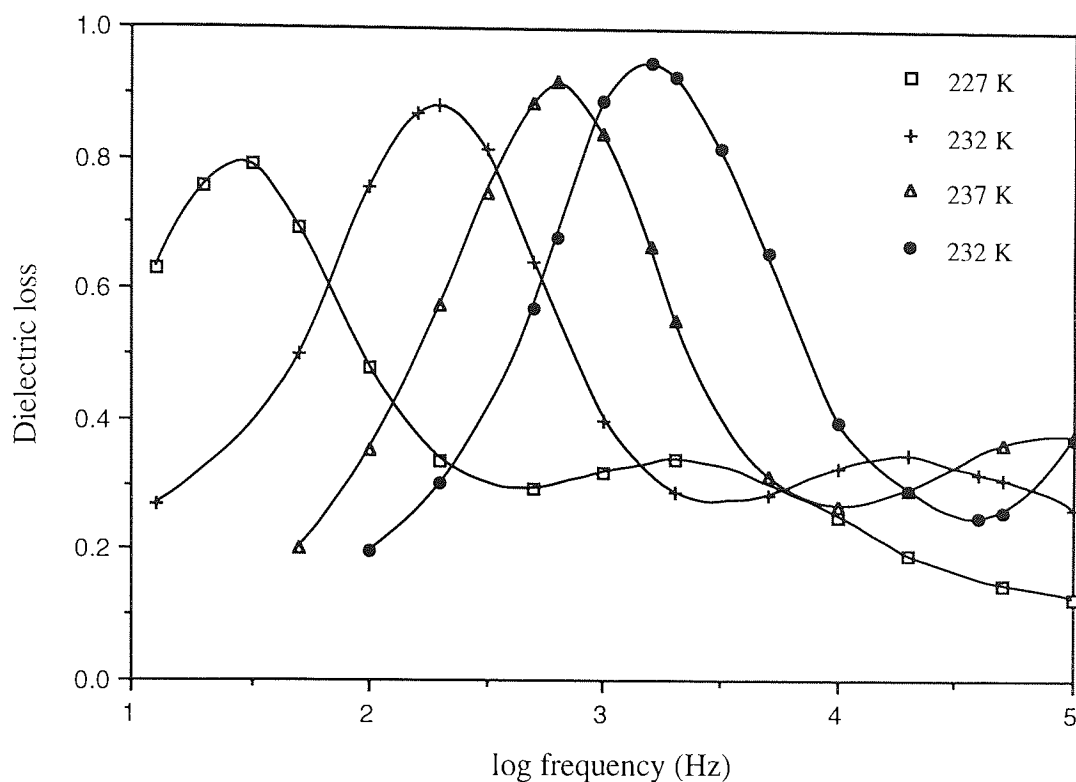


Figure 5.10 The dielectric loss of E7 as function of frequency and temperature. The measuring electric field is perpendicular to the director.

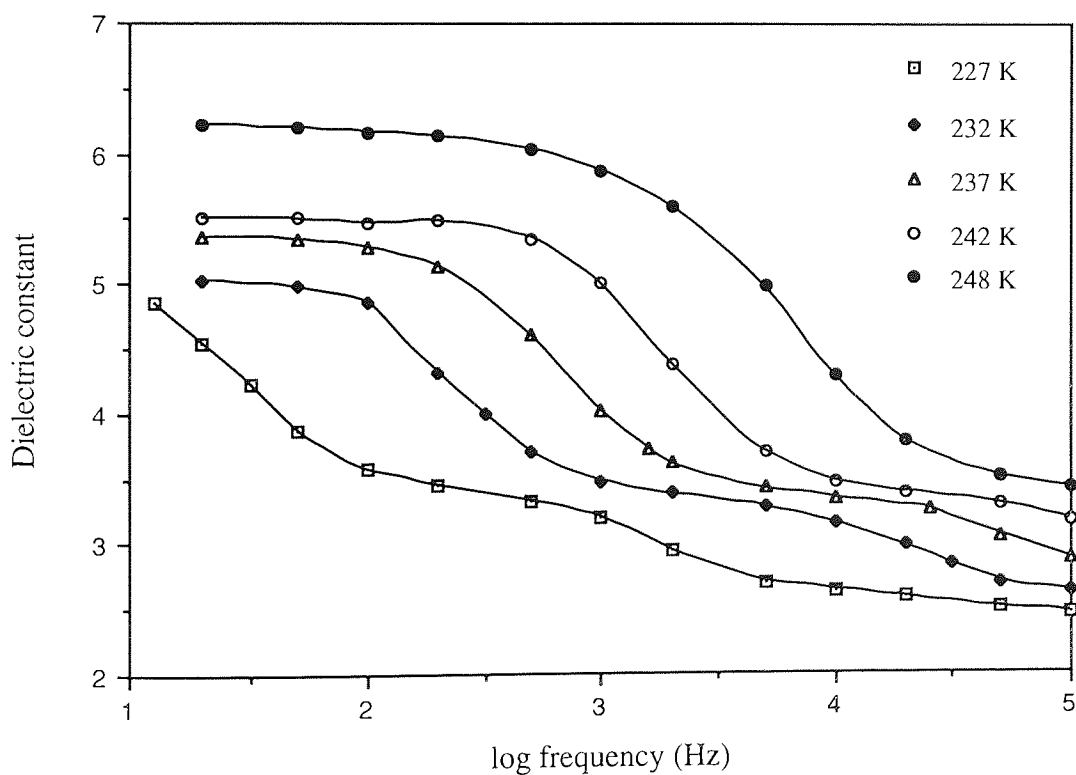


Figure 5.11 The effect of temperature and frequency on dielectric constant of E7 ($E = E_{\perp D}$)

Table 5.3 Dielectric absorption of supercooled E7 for ($E_{\perp D}$) (Debye mechanism)

Temp. °K	$\epsilon_{\perp 01}$	$\epsilon_{\perp 02}$	$\tau_{\perp 1}/\mu s$	$\alpha_{\perp 1}$	$\Delta_{\perp 1}$
242	5.50	3.40	100	~ 0	2.10
237	5.35	3.50	252	~ 0	1.95
232	5.32	3.39	796	~ 0	1.93
227	5.15	3.41	5039	~ 0	1.70

$$\Delta_{\perp 1} = (\epsilon_{\perp 01} - \epsilon_{\perp 02})$$

Table 5.4 Dielectric absorption of supercooled E7 for ($E_{\perp D}$) (Cole-Cole mechanism)

Temp. °K	$\epsilon_{\perp \infty}$	$\tau_{\perp 2}/\mu s$	$\alpha_{\perp 2}$	$f_{\perp 2} \text{ (max)}$ /kHz	$\Delta_{\perp 2}$
237	2.47	1.59	0.12	100	2.88
232	2.47	7.96	0.12	20	2.85
227	2.44	79.6	0.15	2	2.71

Where $\Delta_{\perp 2} = (\epsilon_{\perp 02} - \epsilon_{\perp \infty})$. $\epsilon_{\perp 01}$ and $\epsilon_{\perp 02}$ represent the limiting dielectric constant on the low-frequency and on the high frequency side of the first absorption. $\epsilon_{\perp \infty}$ is the limiting dielectric constant on the high frequency side of the second absorption for ($E_{\parallel D}$).

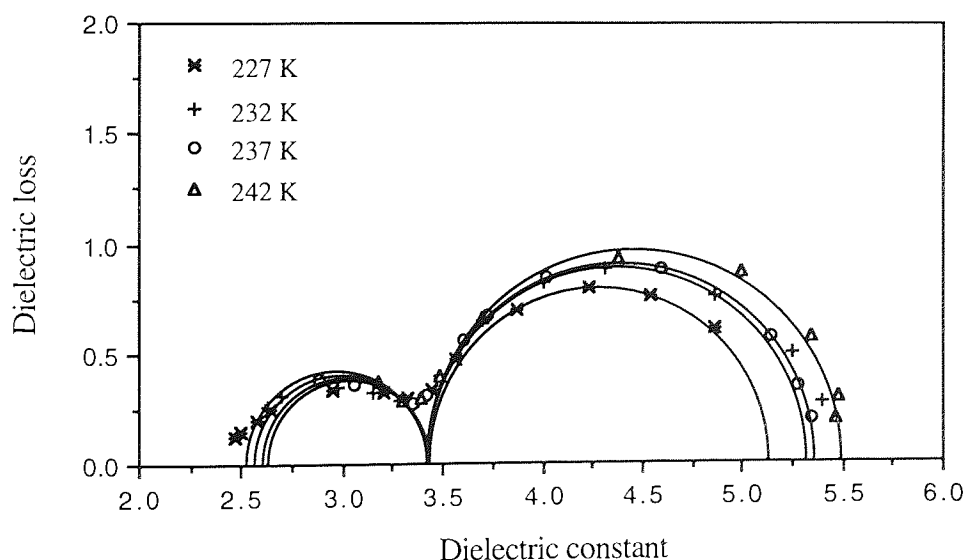


Figure 5.12 Cole-Cole plot for E7 at several temperatures ($E_{\perp D}$).

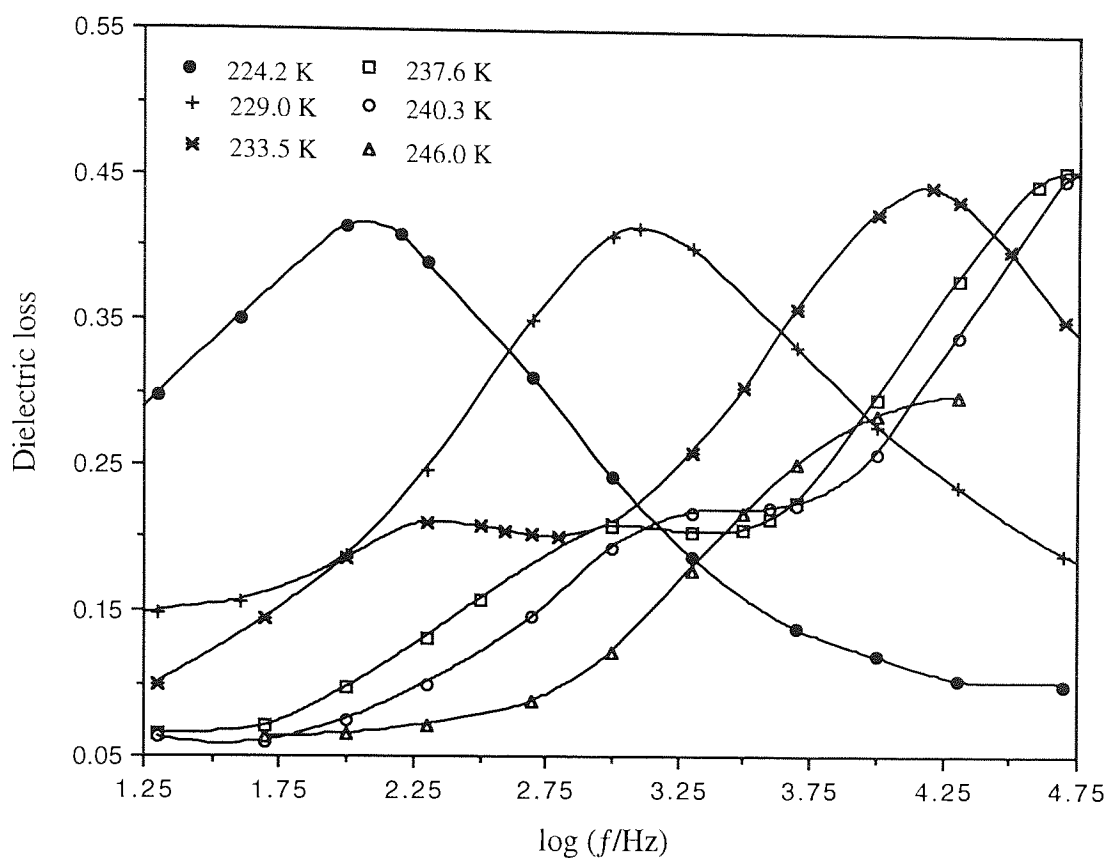


Figure 5.13 The dielectric loss of E8 as function of frequency and temperature. The measuring electric field is perpendicular to the director.

5.5 Discussion

5.5.1 Temperature Dependence of the Static Dielectric Constant and Dielectric Loss

The temperature dependence of the static dielectric constants ϵ_{\parallel} and ϵ_{\perp} of E7, measured at 1kHz, for the electrical field parallel and perpendicular to the long molecular axis, respectively are shown in Figure 5.14. At the nematic-isotropic transition temperature ($T_{NI} = 333$ K) from the nematic to the isotropic state, the dielectric anisotropy vanished discontinuously in accordance with a first-order phase transition. The dielectric losses at 1kHz for the oriented of supercooled nematic mixture E8 are plotted against temperature from 183 to 253 K (Figure 5.15 to 5.16). It was found that the dielectric anisotropy is positive (for E7 and E8) over this range of temperature, as a consequence of the strong permanent dipole moment of the cyano-group parallel to the long molecular axis.

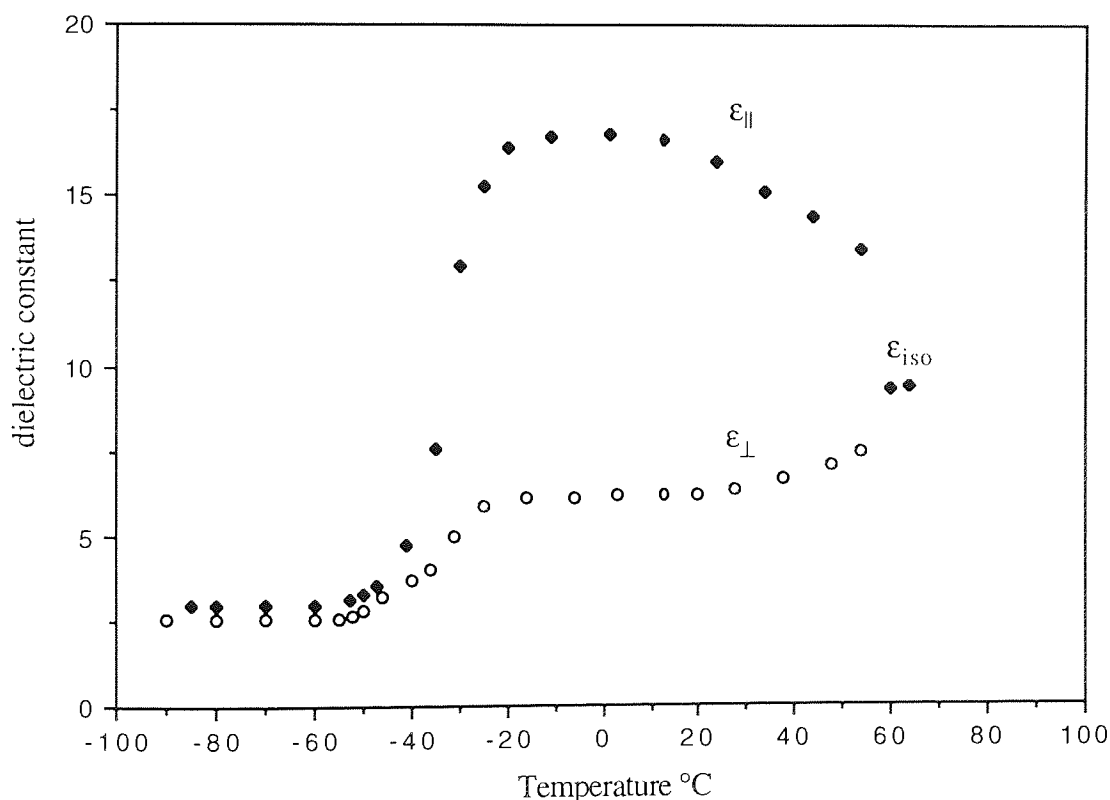


Figure 5.14 Temperature dependence of the dielectric constants measured at 1kHz for nematic mixture of E7.

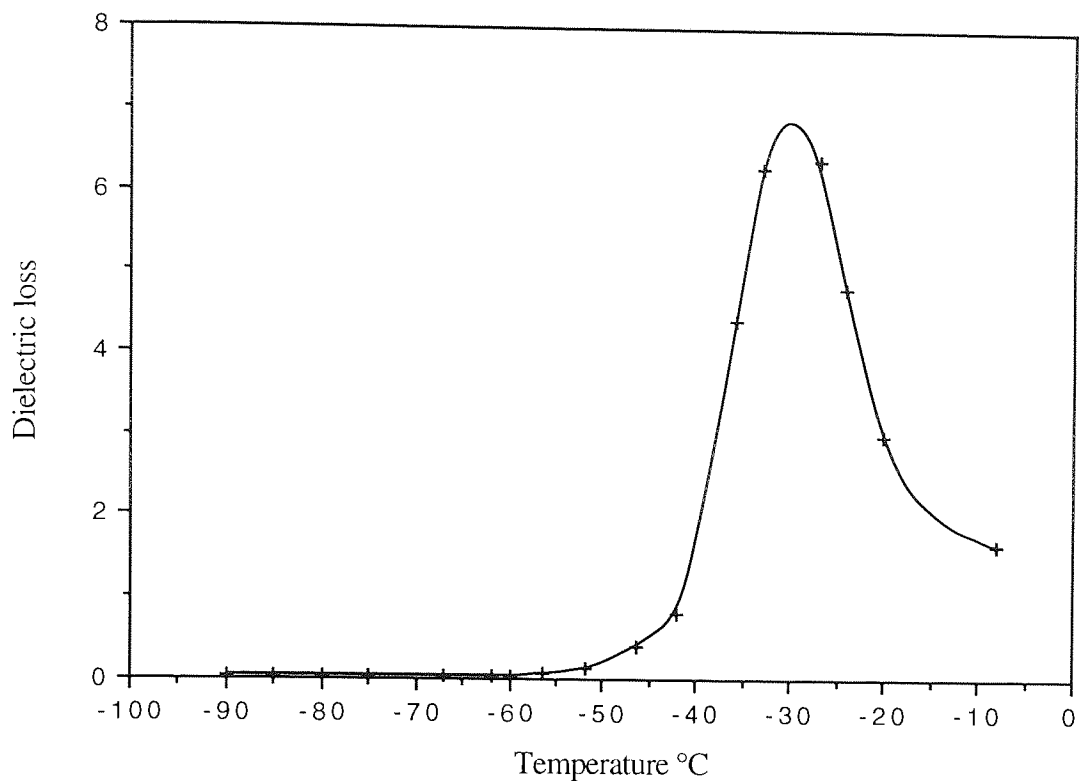


Figure 5.15 The dielectric loss at 1kHz of E8 plotted against temperature in the supercooled and glassy states with electric field parallel to the nematic director ($E_{\parallel D}$).

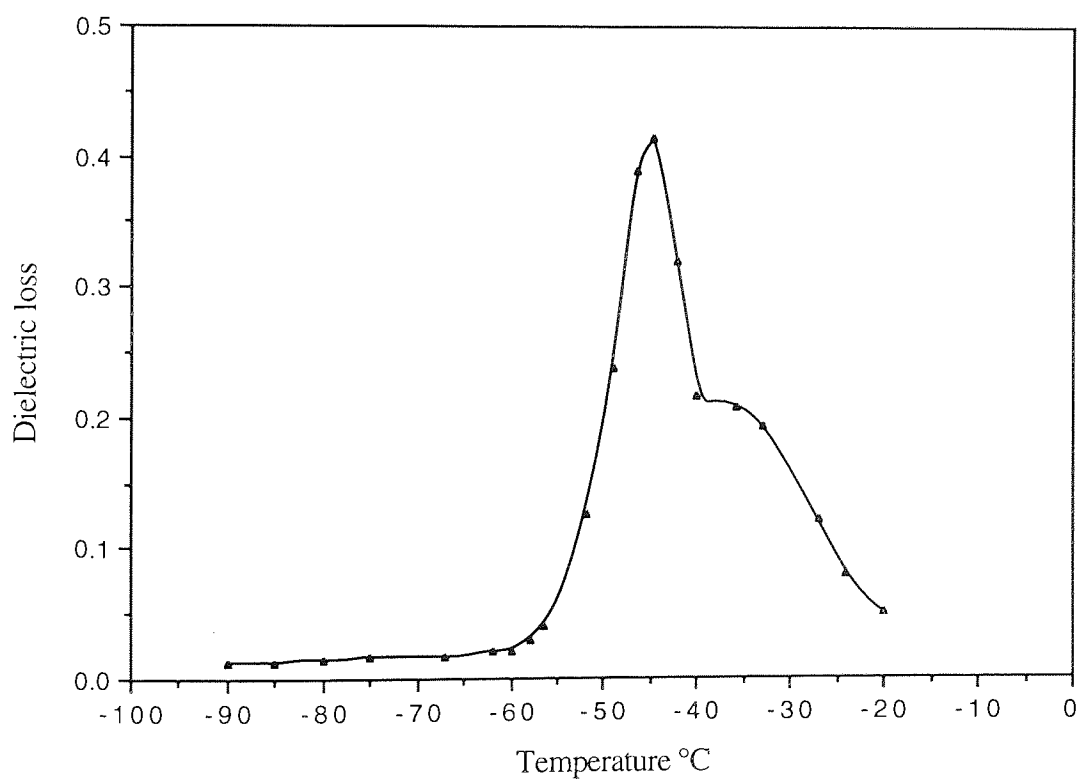


Figure 5.16 The temperature dependence of the dielectric loss of E8 at 1kHz for the electric field perpendicular to the nematic director ($E_{\perp D}$).

It can be seen from Figure 5.14, that as the temperature decreases, ϵ'_{\parallel} increases until the structure changes to the pseudo-order of the glassy state (see also Figure 5.17). At the higher temperatures (near to T_{NI}) thermal motion can cause a significant reduction in the order parameter of E7 (or E8), since the electric field has relatively less effect on the molecular dipoles. At lower temperatures thermal motion has less effect and order parameter has a relatively high value. As seen in Figure 5.14, at temperatures below about 253 K, both ϵ'_{\parallel} and ϵ'_{\perp} decrease rapidly because the rate of locking of dipoles with the decrease in temperature is very high. However, in the supercooled state the unlocked dipoles are more easily influenced by the electric field. In the supercooled state, although the reorientation motions of molecules is a slow process they still can contribute to the dielectric adsorption^{93,96}. On the other hand, the oriented liquid-crystal molecules tend to form interacting pairs (anti-parallel pairs), thereby tending to cancel each others moments^{100,110,111} (see Chapter 6). The large reduction of the relaxation intensity in the mixture is partly caused by this effect.

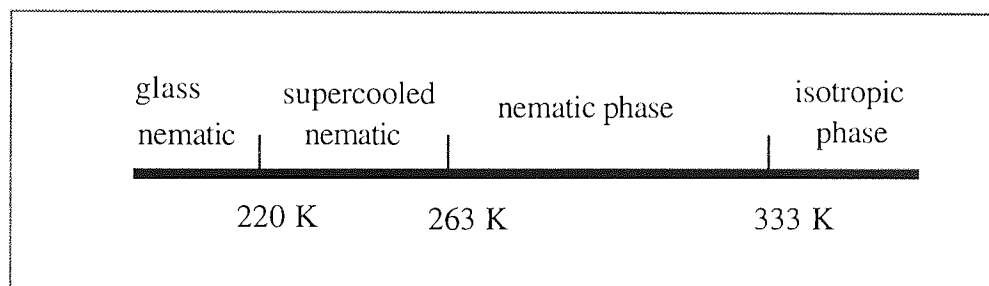


Figure 5.17 Phase transitions for E7

5.5.2 Dipole Moments and Relaxation Mechanisms

The Nematic mixture E7 consist of four components, as listed in Figure 5.18

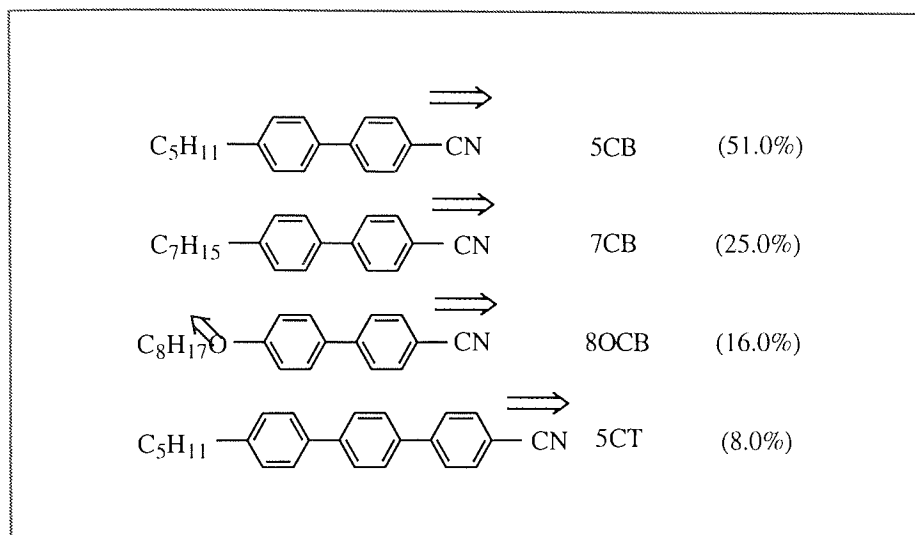


Figure 5.18 Nematic mixture of E7. Direction of main dipole moments are indicated by \Rightarrow

The nematic mixture E8 consist of five components, as listed in Table 5.19.

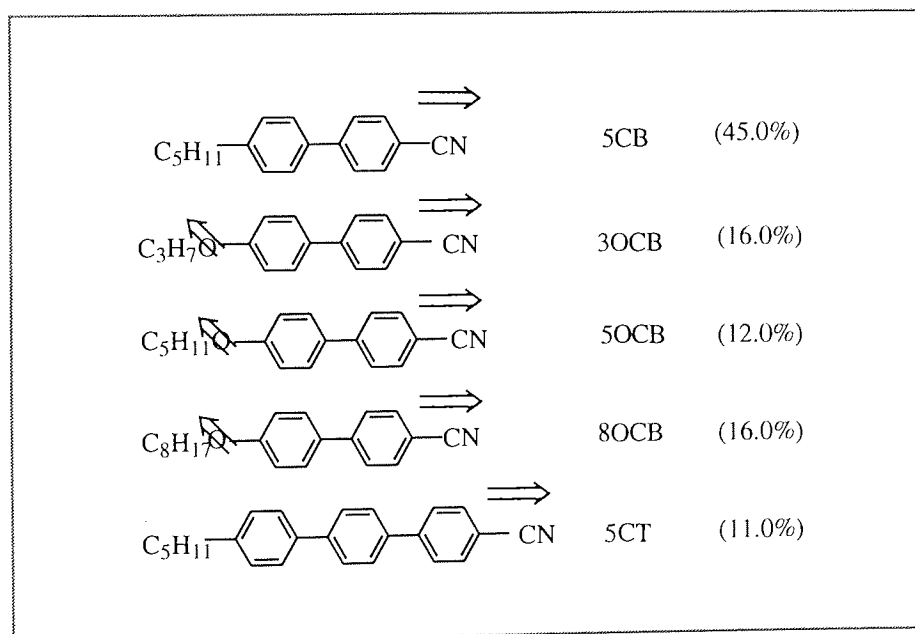


Figure 5.19 Nematic mixture of E8.

For the molecular components in E7/E8, it is reasonable to assume that there are two group dipole moments, associated with the two polar groups $-\text{CN}$ and $-\text{OC}_n\text{C}_{n+1}$. In vector notation, the dipole moments give components parallel (longitudinal dipole component) and perpendicular (transverse dipole component) to the molecular axes, denoted by μ_1 and μ_2 , respectively (Figure 5.20). According to the Nordio *et al.*⁸⁷ who discussed the theory of dielectric relaxation in aligned nematics, four different relaxation processes are possible^{85,112}. Two relaxation processes are found when the measuring electric field is parallel to the director, and these are attributed to dipole reorientation about the short and long molecular axes, $(\mu_{1\parallel})$ and $(\mu_{2\parallel})$, respectively. The two absorptions expected when the measuring electric field is perpendicular to the director ($E_{\perp D}$), are a consequence of reorientation around the short and long molecular axis $(\mu_{1\perp})$ and $(\mu_{2\perp})$, respectively. The dipole reorientation about the short molecular axis is responsible for the low-frequency absorption, while the reorientation around the long molecular axis is responsible for the high frequency absorption. In practice, the resolution of the two absorption peaks, due to reorientation of $\mu_{1\perp}$ and $\mu_{2\perp}$ is difficult and a broad absorption is often detected¹¹².

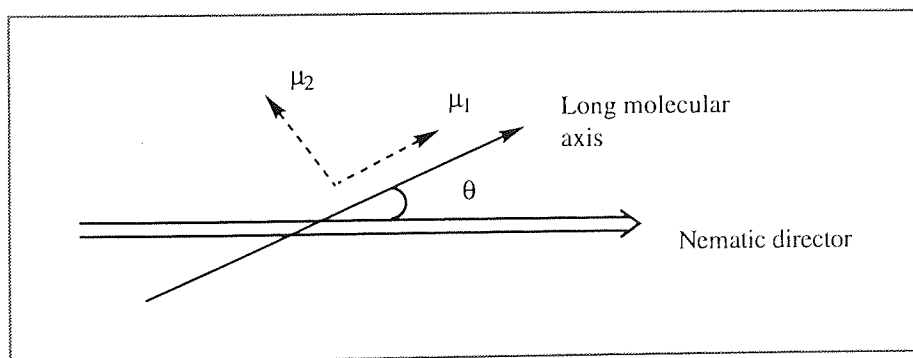


Figure 5.20 Schematic representation of dipole components in an aligned nematogen

The dipole part of the dielectric constant can be characterised by the Maier and Meier equations¹¹². These equations relate the dielectric constant (dielectric permittivity) components to the molecular dipole moment components and may be stated as

$$\varepsilon_{\parallel}(\mu) = 1 + NhF^2/3kT [\mu_1^2(1 + 2S) + \mu_2^2(1-S)] \quad (5.29)$$

$$\varepsilon_{\perp}(\mu) = 1 + NhF^2/3kT [\mu_1^2(1 - S) + \mu_2^2(1+S/2)] \quad (5.30)$$

where F and h are constants (see Section 6.2.6), k is the Boltzmann constant, S is the order parameter, and μ_1 and μ_2 are the components of the dipole vector along directions parallel and perpendicular to long molecular axes, respectively. The overall dipole moments for the electric field parallel and perpendicular to the long molecular axis (director) are given by

$$\mu_{1\parallel}^2 = \mu_1^2(1 + 2S) \quad , \quad \mu_{2\parallel}^2 = \mu_2^2(1 - S) \quad (5.31)$$

$$\mu_{1\perp}^2 = \mu_1^2(1 - S) \quad , \quad \mu_{2\perp}^2 = \mu_2^2\left(1 + \frac{S}{2}\right) \quad (5.32)$$

The intensity of the dielectric absorption depends on the square of the dipole moment component vector reorientation in the direction of the applied field vector. The intensity of the low-frequency absorption for the parallel alignment (with respect to electric field) is dependent on $\mu_1^2(1 + 2S)$, whereas the high frequency absorption associated with the parallel alignment is dependent on $\mu_2^2(1 - S)$. For the electric field perpendicular to the nematic director, the intensities of the two possible relaxation peaks are dependent on either $\mu_1^2(1 - S)$ or $\mu_2^2(1 + S/2)$.

5.5.2.1 The reorientation of μ_1 for ($E = E_{\parallel D}$)

For E7, the dipolar reorientation responsible for the low-frequency absorption observed for $E = E_{\parallel D}$, is shown in Figure 5.4. Although, in principle, two polar groups -CN and -OC₈H₁₇ can contribute to the dielectric absorption, the dipole moment is dominated by the large dipole moment of the cyano group, which lies parallel to the long molecular

axis. Similarly, Figure 5.5 shows the strong dispersion which occurred at low frequencies due to the hindered rotation of the dipole component around the short molecular axis ($\mu_{1\parallel}$). For the parallel relaxation process ($\mu_{1\parallel}$) the Cole-Cole plot gives nearly a semi-circle, as shown in Figure 5.8. Therefore, the parallel relaxation mechanism can be characterised by a single, Debye type, relaxation process. A similar explanation can be used to describe the dielectric relaxation processes for the nematic mixture E8.

Although, it is often the case for nematic mixtures that different molecules relax with slightly different relaxation times, the low-frequency relaxation did not show significant deviation from a Debye process, i.e. Cole-Cole plots were semi-circles (Figures 5.8 and 5.9).

5.5.2.2 *The reorientation of $\mu_{2\perp}$ for ($E = E_{\perp D}$)*

Figures 5.10 and 5.11 show the frequency dependence of the dielectric loss ϵ''_{\perp} and dielectric constant ϵ'_{\perp} of E7 measured at various temperatures, with the electric field perpendicular to long molecular axis ($E = E_{\perp D}$). Figure 5.12, which shows Cole-Cole plots of this mixture, reveals two distinct relaxation mechanisms. The low-frequency absorption can be described by the Cole-Cole equation with a distribution parameter of $\alpha=0$. It may be concluded that there is a single relaxation process (Debye mechanism) associated with 180°-jumps of the dipole component around the short molecular axis. This low-frequency relaxation can be due to the contribution of some misaligned molecules in the parallel low-frequency relaxation.

The second relaxation, which occurred at higher frequencies (Cole-Cole mechanism), is ascribed to the rotation of the dipole component around the long molecular axis (the rotation of $\mu_{2\perp}$).

More detailed information about the nature of the different relaxations can be obtained using the Cole-Cole modification of the Debye-equation.

$$\epsilon^* = \epsilon_\infty + (\epsilon_s - \epsilon_\infty) / [1 + (i\omega\tau)^{1-\alpha_\perp}] \quad (5.29)$$

Where the parameter α_\perp is commonly interpreted as a measure of the breadth of a symmetric distribution relaxation process centred at $\tau = \tau_\perp$.

The high-frequency spectrum is mainly due to relaxation of the dipole moment of the $-\text{OC}_8\text{H}_{17}$ group. In this case the dipole component μ_2 is dominated by the dipole moment of the octoxy group.

As it can be seen from Figure 5.13 for E8, the intensity of the high-frequency spectrum is higher than that observed for E7 (Figure 5.10), due to the higher proportion of alkoxy groups ($-\text{OC}_8\text{H}_{17}$, $-\text{OC}_5\text{H}_{11}$ and $-\text{OC}_3\text{H}_7$) and the consequential effect on the perpendicular dipole moment component, μ_2 .

From the experimental data for E7 shown in Figures 5.10 to 5.12 and listed in Table 5.4 for $E = E_{\perp D}$, the α_\perp parameter is significantly greater than zero, which means that there is a distribution of relaxation times. This distribution is partly caused by the conformational dynamics of the flexible alkyl/alkoxy chains. Although, the effects of conformational changes usually can only be seen in the microwave region^{80,113,114}, in the supercooled state their life-time is comparable with the relaxation time for reorientation around the long molecular axis. Also, a spread of relaxation times may be due to the complex environment of 8OCB molecules (in E7). On the other hand, the low-frequency absorption did not exhibit any distribution of the relaxation times, because the conformational change are so fast that an average conformation is seen at radio-frequencies.

The dielectric constant of E7 measured at temperatures below the glass transition temperature is very close to the square of the refractive index (n^2). It is also noted that ϵ'_{\parallel} is closer to n^2 than ϵ'_{\perp} . It seems that the effect of the alkoxy chain on the dielectric constant and loss is more significant for the processes involving reorientation of dipoles around the long molecular axis of the alkoxy component of E7.

5.5.3 Activation energies

5.5.3.1 The activation energy for the low-frequency relaxation of μ_{\parallel}

From dielectric measurements made at different temperatures, the activation energy can be calculated. A plot of frequency of maximum loss, f_m , vs. $1/T$ does not give a straight line for the low-frequency relaxation (Figures 5.21 and 5.22). These activation energy can be associated with the end-over-end motion of the rod-like molecules around their short molecular axis. This reorientation process become more restricted at the lower temperatures and the relaxation frequency decreases more rapidly (or activation energy is higher) at lower temperatures. The activation energies for rotation around the short molecular axis ($E=E_{\parallel D}$) of E8 are 84 kJ/mol (i.e., in a temperature range of 258K-242K) and 127 kJ/mol at lower temperatures (237K-225K). The activation energies for E7 are 97 kJ/mol in a temperature range of 263K-238K, and 134 kJ/mol at lower temperatures.

5.5.3.2 The activation energy for the higher frequency relaxation of μ_{\perp}

Figures 5.21 and 5.22 show also the plot of the $\log f_m$ vs. $1/T$ for E7 and E8 for the electric field parallel or perpendicular to the nematic director ($E=E_{\parallel D}$ or $E=E_{\perp D}$). Since the plot of $\log(f/\text{Hz})$ vs. $1/T$ for the relaxation process around the long molecular axis ($E=E_{\perp D}$) is linear, therefore, the dielectric relaxation process may be analysed using an Arrhenius plot. The activation energies for rotation around the long molecular axis ($E=E_{\perp D}$) of E7 and E8 were found to be about 173 kJ/mol and 218 kJ/mol, respectively.

It is surprising that the activation energy for rotation around the long molecular axis ($E=E_{\perp D}$) is higher than for the first one in the supercooled state of E7 and E8. This is probably due to the type of molecular packing in the supercooled state. On the other hand, It is claimed¹⁰⁵ that the interaction between 8OCB and other molecules in a mixture leads to the formation of an induced smectic A and that, as a consequence, lateral intermolecular interactions are strong at lower temperatures and the activation energy has a higher than expected value. The frequencies of maximum loss (f_m) for E7 and E8, corresponding to the relaxation of $\mu_{2\perp}$ are given in Table 5.5.

Table 5.5 The frequency of maximum loss (f_m) for E7 and E8 for the relaxation of $\mu_{2\perp}$

E7 (E = $E_{\perp D}$)		E8 (E = $E_{\perp D}$)	
T/°K	log(f /Hz)	T/°K	log(f /Hz)
237	5.0	223.2	1.7
232	4.3	225.0	2.2
227	3.3	227.1	2.7
—	—	228.8	3.00
—	—	233.7	4.00
—	—	237.6	4.70
—	—	240.3	4.85

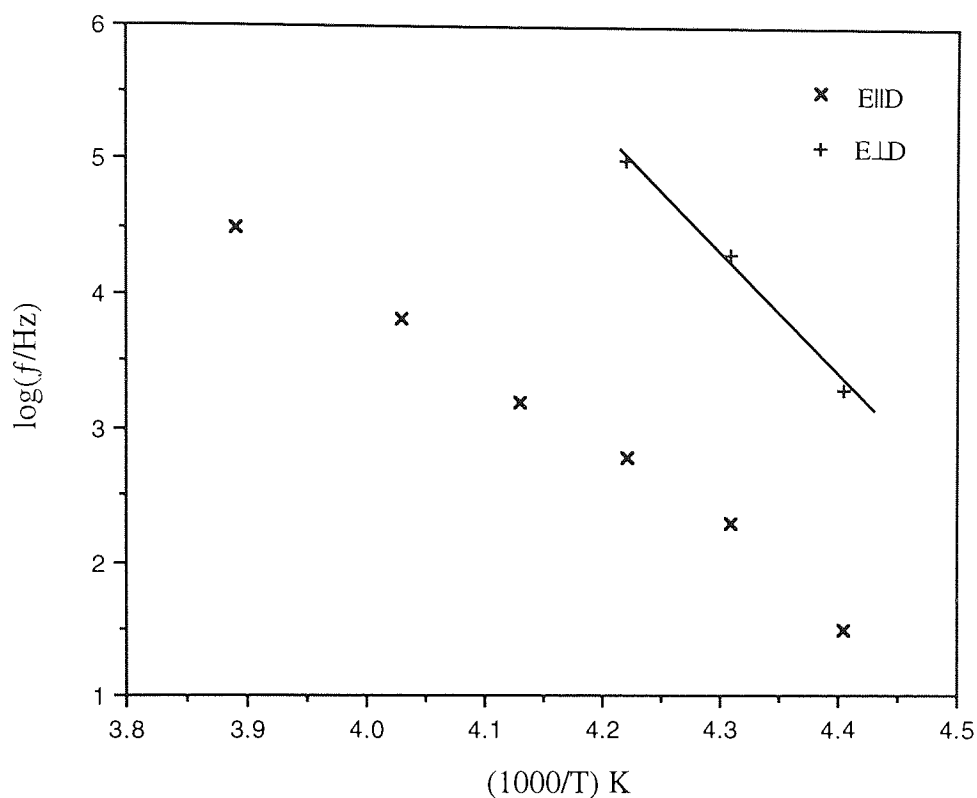


Figure 5.21 The activation diagram, $\log f$ vs. $1/T$ for E7 in the supercooled nematic state. Rotation around the short molecular axis ($E=E_{\parallel D}$), x, Rotation around the long molecular axis ($E=E_{\perp D}$), +.

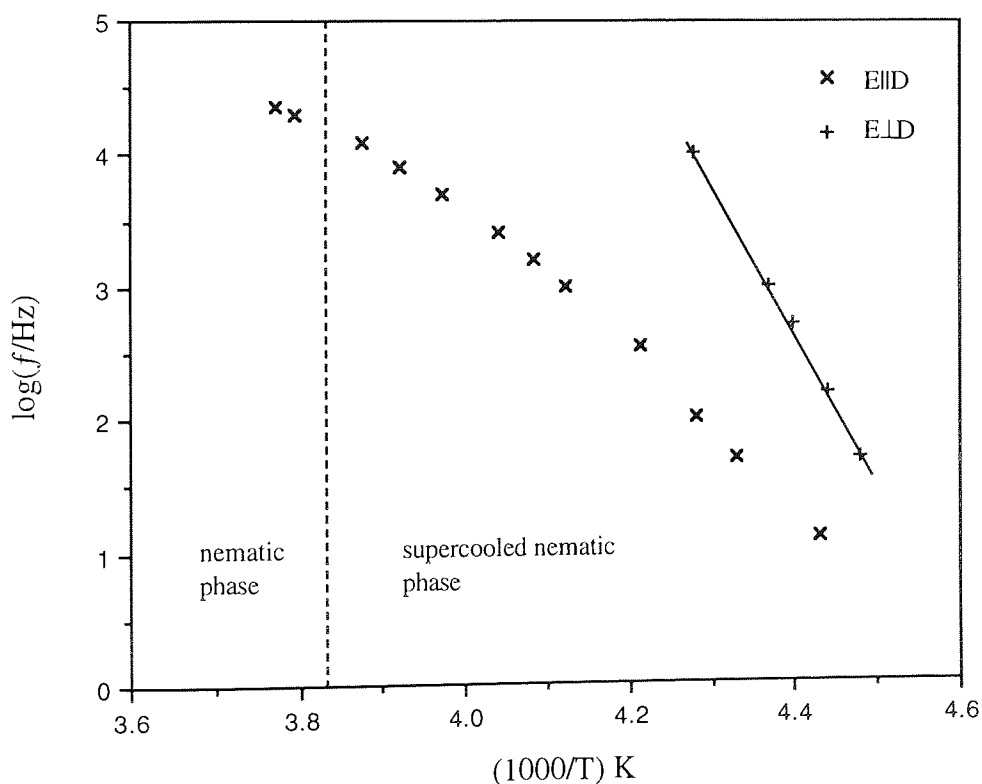


Figure 5.22 The activation diagram, $\log f$ vs. $1/T$ for E8 in the supercooled nematic state. Rotation around the short molecular axis ($E=E_{\parallel D}$), x, Rotation around the long molecular axis ($E=E_{\perp D}$), +.

CHAPTER 6

DIPOLE MOMENT AND MOLECULAR ASSOCIATION

6.1 Introduction

The relationship between dielectric permittivity (dielectric constant) and molecular properties has long been an objective of dielectric studies^{116,117}. With regard to electric permittivity, density and refractive index measurements, it is possible to obtain the electric dipole moment with the aim of giving valuable information about the geometrical structure of molecules. Another important application involving dipole moment is in the study of the molecular association and dipole-dipole interactions^{61,118}.

Dipole moments can be measured in several ways. The most accurate method for the determination permanent dipole moments is based on measurements made on dilute gases, using rotational spectroscopy (Stark effect)⁶⁴ or dielectric measurements^{60,61,119}. When the molecule cannot be examined in gas phase, then the possible method for determination of the dipole moment is from dielectric measurements on the dilute solution. In this case the best method is that involving the measurement of the static dielectric permittivity (ϵ) of a dilute solution of the polar compound in a non-polar solvent¹¹⁶.

The aim of the this part of project is to present accurate dielectric and dipole results of a range of liquid-crystal forming molecules at several temperatures. The dielectric data at several temperatures reported here add to an important data base for scientific and technological purposes. Some of these data have either not been previously reported and/or represent more accurate data. It is necessary to understand fully the role of molecular factors that determine the stability and properties of liquid-crystals such as intermolecular forces and molecular association. This requires a detailed knowledge of

the structures of the individual molecules, and an appreciation of why liquid-crystal molecules should have certain structural requirements⁴. However, much useful progress may be made by establishing correlations between macroscopic liquid-crystal properties, e.g. the dielectric permittivity and molecular properties such as dipole moment, with the object of understanding the properties of liquid-crystals.

Since the calculation of the molecular dipole moment from the measured dielectric permittivity of the bulk materials depends on the molecular interactions^{120,121,122}, it is possible, therefore, to obtain important information about dipole-dipole interactions and molecular association in liquid-crystals. With regard to dielectric studies made on nematic or isotropic phases of liquid-crystals over a range of temperature or dielectric studies of molecular association in solutions in liquid-crystals over a range of concentrations, it is possible to obtain valuable information on the progressive association of molecules and its effect on the formation of orientational order of nematic liquid-crystals.

In order to investigate the role of the cyano-end group, biphenyl core, and flexible tail in molecular association, dielectric studies have been carried out for some molecules which have a structural relationship to the nematogens. Various alkyl (alkoxy) cyanobiphenyls have been studied in solution in cyclohexane and/or 1,4-dioxane at 298K. Cyano biphenyl, CB, without a flexible tail, pentyl biphenyl, 5B, without a cyano-end group, and alkyl (alkoxy) cyanobiphenyl liquid-crystal molecules, 5CB (5OCB) to 8CB (8OCB), have all been investigated.

A three-terminal dielectric cell was designed and used for dielectric permittivity measurements on small volume of solutions over a range of temperature. Due to the high stability and reproducibility of the electrical capacity of the cell, it was possible to obtain accurate dielectric results for solutions of liquid-crystals over a wide range of solute concentrations.

6.2 Dielectric permittivity and dipole moment: Theoretical background

In the past a variety of equations have been used to calculate electric dipole moments from static dielectric permittivity data, but the most popular methods are based on relationships deduced by Debye¹²³ or Onsager¹²⁴.

6.2.1 The Debye theory

Debye (1929) showed that for a molecule in the gaseous phase (near ideal behaviour) the dipole moment, μ , can be derived from the following equation⁵⁹.

$$\left(\frac{\epsilon - 1}{\epsilon + 2}\right) \frac{M}{d} = \frac{4\pi N_A}{3} \left(\alpha_o + \frac{\mu^2}{3kT} \right) \quad (6.1)$$

where ϵ is the static dielectric constant (dielectric permittivity), N_A is the Avogadro constant, k is the Boltzmann constant and, α_o is the molecular polarisability, that is, the dipole moment induced in the molecule by unit electric field. In fact, α_o is the sum of electronic polarisability (major component) and atomic polarisability, i.e. $\alpha_o = \alpha_{\text{electronic}} + \alpha_{\text{atomic}}$.

The molar polarisation defined by Mosotti and Clausius⁵⁹, is defined by

$$[P] = \left(\frac{\epsilon - 1}{\epsilon + 2}\right) \frac{M}{d} \quad (6.2)$$

where M and d are the molecular weight and density, respectively, of the material. For non-polar molecules the molar polarisation does not vary with temperature, but for polar molecules it decreases as the temperature is raised¹²⁵.

Using the molar polarisation $[P]$, defined by 6.2, the Debye equation can be written as

$$[P] = \frac{4\pi N_A}{3} \left(\alpha_o + \frac{\mu^2}{3kT} \right) \quad (6.3)$$

The molar polarisation [P] can be written as the sum of three terms⁶¹,

$$[P] = P_e + P_a + P_o \quad (6.4)$$

where P_o is the dipole orientation polarisation, P_e the electronic polarisation, and P_a the atomic polarisation. It follows from equations 6.3 and 6.4 that

$$P_o = 4\pi N \mu^2 / 9kT \quad (6.5)$$

and

$$P_e + P_a = 4\pi N \alpha_o / 3 \quad (6.6)$$

Together, $P_e + P_a$ are often referred to as the distortion polarisation, P_D , which arises through the displacement of the electrons and nuclei with respect to one another in an applied field. The Debye equation has been used successfully for gases and very dilute solutions of a polar solutes in non-polar solvents. By measuring dielectric permittivity at different temperatures, it is possible to determine both α_o and μ . However, this equation cannot normally be used to calculate dipole moment of a pure polar liquid. Dipole moment calculated from measurements made concentrated solutions and on pure polar liquids do not generally agree with the gas value. The deviations are often attributed to association. The Debye equation neglects the local field (internal field) due to neighbouring molecules and also neglects the local directional forces on the molecules due to their nearest neighbours¹¹⁸.

For dilute solutions the Debye equation gives the dipole moment of dipolar molecules separated from one another by non-polar solvent molecules. It is clear that the value of dipole moment will depend on the nature of non-polar solvent. This dipole moment

often deviates from the moment of the isolated molecule in the dilute gas. This effect (the solvent effect) is usually due to specific interactions between the solute molecule and the solvent molecules¹¹⁸.

6.2.2 The Guggenheim method

The dipole moment of a solute molecule in dilute solution in a non-polar solvent can be calculated using the Guggenheim equation¹²⁶

$$\mu^2 = \frac{27kT\epsilon_0}{N_A(\epsilon_1+2)(n_1^2+2)} \left(\frac{\Delta}{C} \right)_{C \rightarrow 0} \quad (6.7)$$

where ϵ_1 is the static dielectric permittivity and n_1 is the refractive index of the non-polar solvent. The quantity ϵ_0 is the permittivity of free space ($8.854 \times 10^{-12} \text{ Fm}^{-1}$). The concentration of the solute, C , is expressed in units of mol/cm^3 and Δ is given by

$$\Delta = (\epsilon_{12} - n_{12}^2) - (\epsilon_1 - n_1^2) \quad (6.8)$$

where the double subscript denotes a property of the solution. The slope $(\Delta/C)_0$ of the curve at $C = 0$ is then used to calculate the dipole moment. On the other hand, a plot of $\epsilon_{12} - n_{12}^2$ against C gives a intercept of $\epsilon_1 - n_1^2$. The Guggenheim equation leads to a value of the dipole moment, μ , expressed in Cm. The Guggenheim method needs accurate measurement of the refractive index of solutions but the accurate measurement of density is not necessary.

6.2.3 The Onsager theory

In 1936, Onsager¹²⁴ gave the first relation between static dielectric permittivity and molecular dipole moment for a pure polar liquid and concentrated solutions. The Onsager Theory takes account of the local field due to molecules and introduced an

important factor known as the Reaction Field. The latter is due to the polarisation of the medium surrounding a molecule by the molecule itself, and this additional polarisation reacts back on the molecule. The Onsager Theory applies only to systems where there is no orientation correlation between the individual molecules. The following relation was obtained,

$$\mu^2 = \frac{9kT\epsilon_0}{N} \frac{(\epsilon - n^2)(2\epsilon + n^2)}{\epsilon(n^2 + 2)^2} \quad (6.9)$$

where ϵ and n are the mean permittivity and refractive index of liquid, $N = N_A d/M$ is the number of molecules per cm^3 , M is the molar mass, and d is the density.

6.2.4 The Kirkwood-Fröhlich theory

Kirkwood¹²⁷ (1939) obtained a more general equation which takes into account the short-range interactions between molecules in the liquid state. Fröhlich¹²⁸ (1949) developed a theory which included the short-range correlations considered by Kirkwood, and also included the deformation polarisability of the molecules. The following relation was obtained by Kirkwood-Fröhlich.

$$g\mu^2 = \frac{9kT\epsilon_0}{N} \frac{(\epsilon - \epsilon_\infty)(2\epsilon + \epsilon_\infty)}{\epsilon(\epsilon_\infty + 2)^2} \quad (6.10)$$

If the high frequency dielectric constant, ϵ_∞ , is taken to be given by the Maxwell relation

$$\epsilon_\infty = n^2 \quad (6.11)$$

then the Kirkwood-Fröhlich equation may be written as

$$g \mu^2 = \frac{9 k T \epsilon_0 (\epsilon - n^2)(2\epsilon + n^2)}{N \epsilon (n^2 + 2)^2} \quad (6.12)$$

in which μ is the moment of the molecule in the liquid state, g is the Kirkwood correlation parameter; a measure of the molecular association between a reference molecule and its nearest neighbours. The departure of g from unity is indicative of molecular association. Positive deviations of g from unity, i.e. $g > 1$, result from parallel orientation of the dipoles of neighbouring molecules, while negative deviations, $g < 1$, result from antiparallel orientation. For no association between molecules, $g = 1$, and the Kirkwood-Fröhlich equation reduces to the Onsager equation.

6.2.5 Molecular association in solutions: dipole-dipole interactions

In dipolar liquids and in solutions of dipolar molecules in non-polar solvents, particularly, in concentrated solutions, dipoles may line up head-to-tail, pointing in the same direction (parallel orientation), and the moment of the aggregate will be double that of a single molecule. Such association will be favoured by molecules in which the dipoles are perpendicular to the long molecular axis (Figure 6.1.b). On the other hand, in anti-parallel orientation the dipoles are parallel to each others but in opposite direction and cancel each other moments¹¹⁸. Such association is likely to occur between molecules that can be regarded as ellipsoidal in shape and where the dipoles are parallel to the longest axis of the ellipsoid (Figure 6.1.a). Thus, it can be seen that the resultant dipole moment may be either decreased or increased by association.

For a solution of polar molecules in a non-polar solvent the effective dipole moment, $g\mu^2$, is given by^{60,122}

$$g\mu^2 = \frac{9kT\epsilon_0(2\epsilon+n^2)^2}{N_A x_2 (n^2+2)^2(2\epsilon+1)} \left\{ \frac{\epsilon-1}{\epsilon} \left[\frac{x_1 M_1 + x_2 M_2}{d} \right] - \frac{3x_1 M_1 (\epsilon_1-1)}{d_1 (2\epsilon+\epsilon_1)} - \frac{3x_2 M_2 (n^2-1)}{d_2 (2\epsilon+n^2)} \right\} \quad (6.13)$$

where, ϵ , d and n are the permittivity, density and refractive index of the solution respectively, x_2 , d_2 and M_2 are the total mole fraction, density, and molecular weight of solute molecules, M_1 , ϵ_1 , d_1 and x_1 are the molecular weight permittivity, density, and mole fraction of the pure solvent, respectively. The Kirkwood factor $g = \mu_{\text{eff}}^2/\mu^2$, where μ is the molecular dipole moment, measured for dilute solution and μ_{eff} is the effective dipole moment as calculated from the dielectric data using the equation 6.13.

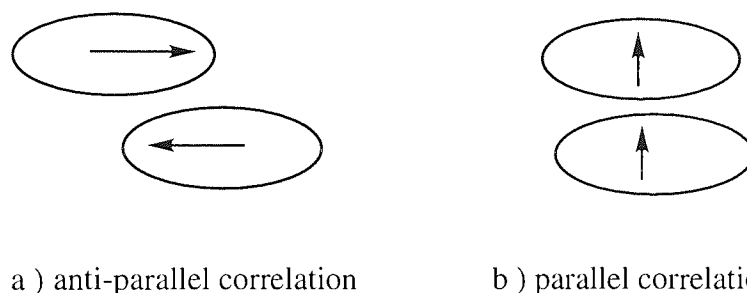


Figure 6.1 Simple forms of association, due to dipole-dipole interaction, in which two molecules may associate to give a dimer.

For a pure undiluted polar liquid, $x_1 = 0$ and $x_2 = 1$, and equation 6.13 reduces to the Kirkwood-Frohlich equation 6.12.

A simple model for dipole association of a cyano compound has been presented in ref. 117. This model is based on the assumption that a polar compound is considered as a mixture of "free" molecules (monomers) and associated molecular pairs (dimers). A dynamic equilibrium between the single molecules and the associated pairs exists, represented as



The equilibrium constant (in mole fraction units) is then given by

$$K = \frac{x(M_2)}{(x(M_1))^2} = \frac{n_2 n}{n_1^2} = \left(\frac{n}{n_1}\right) \left(\frac{n}{n_1} - 1\right) \quad (6.15)$$

where n_1 is the number of moles of monomer, n_2 is the number of moles of dimer, and $n = n_1 + n_2$. Assuming that the dimers have vanishing dipole moments (anti-parallel alignment), the g values give directly the proportion of free molecules. Therefore, the correlation factor, g_1 , is unity for monomer, and the average correlation factor per molecule in the dimer, g_2 , is zero. It is then possible to define an experimental correlation factor, g_{exp} .

$$g_{\text{exp}} = x_1 g_1 + 2x_2 g_2 = x_1 = n_1/n \quad (6.16)$$

The equilibrium constant, K , may then be written as

$$K = \frac{1}{g} \times \left(\frac{1}{g} - 1 \right) \quad (6.17)$$

The equilibrium constant is temperature dependent and is responsible for the temperature dependence of g .

6.2.6 Anisotropy of the dielectric permittivity

Due to long-range orientational order, many of the macroscopic response functions of the bulk material, such as the dielectric permittivity, are anisotropic (see Chapter 5). The dielectric behaviour of a nematic liquid-crystal is described by two dielectric constants, ϵ_{\parallel} and ϵ_{\perp} , and the dielectric anisotropy is defined as

$$\Delta\epsilon = \epsilon_{\parallel} - \epsilon_{\perp} \quad (6.18)$$

Maier and Meier¹²⁹ extended the Onsager theory of isotropic dielectric to the nematic phase, and for molecules assumed to have axial symmetry. This theory relates the dielectric permittivity components ϵ_{\parallel} and ϵ_{\perp} to the molecular dipole moment μ , mean

polarisability $\bar{\alpha}$, and polarisability anisotropy, $\Delta\alpha$, of a nematogen. The Maier and Meier equations are

$$\epsilon_{\parallel} = 1 + \left(\frac{NhF}{\epsilon_0} \right) \left\{ \bar{\alpha} + \frac{2\Delta\alpha S}{3} + \frac{F\mu^2}{3kT} [1 - (1 - 3 \cos^2 \beta) S] \right\} \quad (6.19)$$

$$\epsilon_{\perp} = 1 + \left(\frac{NhF}{\epsilon_0} \right) \left\{ \bar{\alpha} - \frac{\Delta\alpha S}{3} + \frac{F\mu^2}{3kT} \left[1 + \frac{1}{2} (1 - 3 \cos^2 \beta) S \right] \right\} \quad (6.20)$$

where β is the angle between the dipole moment of the isolated molecule and its long axis, $h = 3\epsilon/(2\epsilon + 1)$ is the cavity field factor, $F = 1/(1 - \bar{\alpha}f)$ is the reaction field factor with $f = (2\epsilon - 2)/4\pi\epsilon_0 a^3(2\epsilon + 2)$, k is Boltzmann constant, S is the order parameter and a is the molecular radius. The factors h and F were introduced by Onsager¹²⁴ to account for the cavity field and reaction field in an isotropic dielectric. In Maier and Meier's extension of Onsager's theory to anisotropic media it was assumed that these factors remain equal to the isotropic values.

The Maier and Meier theory is not capable of taking short-range correlation into account. The Kirkwood-Frohlich theory does take into account the short-range interactions between molecules in the isotropic liquid state. However, for the nematic phase, in which anisotropy of the dielectric permittivity occurs, two correlation factors are involved to describe the ordering with respect to the long and short axes of the liquid-crystal molecule. Bordewijk and De Jue¹³⁰, have extended the Kirkwood's theory to account for observed aggregation in liquid-crystals and their analysis yielded the correlation factors g_{\parallel} , g_{\perp} for the anisotropy of permittivity in the mesophase, as defined in

$$\frac{(\epsilon_{\parallel} - \epsilon_{\infty\parallel}) \left[\epsilon_{\parallel} + (\epsilon_{\infty\parallel} - \epsilon_{\parallel}) \Omega_{\parallel} \right]}{\epsilon_{\parallel}} = \frac{N}{kT\epsilon_0} g_{\parallel} \langle \mu_d^2 \rangle_{\parallel} \quad (6.21)$$

and

$$\frac{(\epsilon_{\perp} - \epsilon_{\infty\perp}) [\epsilon_{\perp} + (\epsilon_{\infty\perp} - \epsilon_{\perp}) \Omega_{\perp}]}{\epsilon_{\perp}} = \frac{N}{kT\epsilon_0} g_{\perp} \langle \mu_d^2 \rangle_{\perp} \quad (6.22)$$

where the dipole components¹³⁷ of μ_d^2 , along and perpendicular to the director are

$$\langle \mu_d^2 \rangle_{\parallel} = \frac{\mu_l^2(1 + 2S)}{3 \left(1 - \frac{N \alpha_l \Omega_l}{\epsilon_0} \right)^2} + \frac{\mu_t^2(1 - S)}{3 \left(1 - \frac{N \alpha_t \Omega_t}{\epsilon_0} \right)^2} \quad (6.23)$$

and

$$\langle \mu_d^2 \rangle_{\perp} = \frac{\mu_l^2(1 - S)}{3 \left(1 - \frac{N \alpha_l \Omega_l}{\epsilon_0} \right)^2} + \frac{\mu_t^2 \left(1 + \frac{1}{2} S \right)}{3 \left(1 - \frac{N \alpha_t \Omega_t}{\epsilon_0} \right)^2} \quad (6.24)$$

where $\Omega_{\parallel}, \Omega_{\perp}$, are numerical (geometrical) factors^{130,131} which depend on the anisotropy of the permittivity of the system. For positive dielectric anisotropy, $\epsilon_{\parallel} > \epsilon_{\perp}$, and these factors become:

$$\Omega_{\parallel} = \frac{\epsilon_{\parallel}}{\epsilon_{\parallel} - \epsilon_{\perp}} - \frac{\epsilon_{\parallel} \epsilon_{\perp}^{1/2}}{(\epsilon_{\parallel} - \epsilon_{\perp})^{3/2}} \operatorname{arctg} \left(\frac{\epsilon_{\parallel} - \epsilon_{\perp}}{\epsilon_{\perp}} \right)^{1/2} \quad (6.25)$$

and

$$\Omega_{\perp} = \frac{\epsilon_{\parallel} \epsilon_{\perp}^{1/2}}{2 (\epsilon_{\parallel} - \epsilon_{\perp})^{3/2}} \operatorname{arctg} \left(\frac{\epsilon_{\parallel} - \epsilon_{\perp}}{\epsilon_{\perp}} \right)^{1/2} - \frac{\epsilon_{\perp}}{2 (\epsilon_{\parallel} - \epsilon_{\perp})} \quad (6.26)$$

For a prolate spheroid the shape parameters Ω_l and Ω_t are as follows

$$\Omega_l = 1 - w^2 + \frac{1}{2} w(w^2 - 1) \ln \frac{w+1}{w-1} \quad (6.27)$$

$$\Omega_t = \frac{1}{2} (1 - \Omega_l)$$

with

$$w^2 = \frac{a^2}{a^2 - b^2} \quad (6.28)$$

in which a , b are the dimensions of the long and short axes of the molecular ellipsoid.

A simplification of these equations occurs if the dipole moment lies along the long axis of the molecule, as is the case for the 4,4-alkyl cyanobiphenyls¹³². Then the correlation factors of the components of the isolated molecules, along directions parallel and perpendicular to the director, and are given by:

$$\mu^2 g_{\parallel} = \frac{3kT \left(1 - \frac{N}{\epsilon_0} \alpha_l \Omega_l\right)^2 (\epsilon_{\parallel} - \epsilon_{\infty\parallel}) [\epsilon_{\parallel} - (\epsilon_{\infty\parallel} - \epsilon_{\parallel}) \Omega_{\parallel}]}{\frac{N}{\epsilon_0} (1 + 2S) \epsilon_{\parallel}} \quad (6.29)$$

and

$$\mu^2 g_{\perp} = \frac{3kT \left(1 - \frac{N}{\epsilon_0} \alpha_l \Omega_l\right)^2 (\epsilon_{\perp} - \epsilon_{\infty\perp}) [\epsilon_{\perp} - (\epsilon_{\infty\perp} - \epsilon_{\perp}) \Omega_{\perp}]}{\frac{N}{\epsilon_0} (1 - S) \epsilon_{\perp}} \quad (6.30)$$

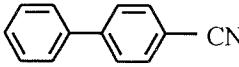
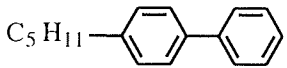
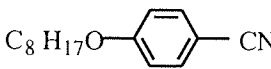
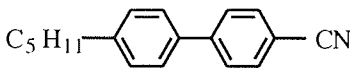
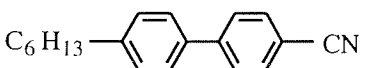
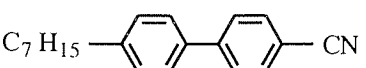
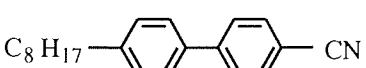
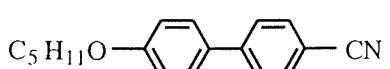
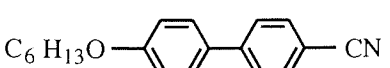
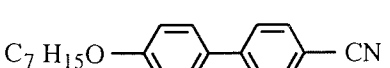
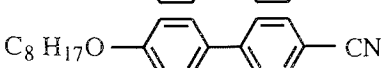
respectively.

6.3 Experimental

6.3.1 Materials

The compounds studied in this investigation are listed in Table 6.1. Solutions of these material were prepared by accurately weighing appropriate amounts of solute in 10 cm³ volumetric flasks (50 cm³ is required for the cylindrical gold-plated dielectric cell) and, then, adding sufficient amount of cyclohexane and or 1,4-dioxane to give a total volume of 50 cm³.

Table 6.1 Compounds chosen for study

Compound	System	Abbreviation
	cyanobiphenyl	CB*
	pentyl biphenyl	5B*
	octoxy cyanophenyl	8OCP*
	pentyl cyanobiphenyl	5CB
	hexyl cyanobiphenyl	6CB
	heptyl cyanobiphenyl	7CB
	octyl cyanobiphenyl	8CB
	pentoxy cyanobiphenyl	5OCB
	hexoxy cyanobiphenyl	6OCB
	heptoxyl cyanobiphenyl	7OCB
	octoxy cyanobiphenyl	8OCB
* not a mesogen		

6.3.2 *Dielectric apparatus*

The electrical capacitance of the dielectric cell was measured using a GenRad GR 1689 Digibridge. Measurements of the capacitance required for calculating the static dielectric permittivity were performed at a frequency of 1kHz (for this frequency the accuracy of the digibridge was highest). The Digibridge had an accuracy of 0.02% in capacitance measuring mode. Electrical connections were made using copper wires between the Digibridge and the dielectric cell. The temperature was controlled by using a thermostat water bath.

6.3.3 *Dielectric cell*

Two different types of dielectric cell have been used for the measurement of dielectric permittivity. Both cells were three-terminal type capacitors. The first cell (cell A) was convenient for measurements on large amounts of solution (approximately 25 cm³), and it was used only for measurements on dilute solutions. The second dielectric cell (cell B) was suitable for measurements on small volume of samples (about 3.5 cm³), but could be used for undiluted samples of liquid-crystals.

6.3.3.1 *The cylindrical gold-plated dielectric cell (cell A)*

Dielectric cell A (manufacturer unknown) was used to measure the static dielectric permittivity on dilute solution in this part of project and was constructed of two cylindrical plates of brass (Figure 6.2). The internal surfaces (C) in contact with the sample were gold plated. The outer cylinder (B) was hollow to allow passage of a cooling or heating liquid.

The height and diameter of the inner electrode were 35mm and 33mm, respectively. The gap between the inner and the outer electrodes was about 1.5 mm. The cell was

filled through an external screw-top lid (A). An internal perforated lid (D) ensured that the effective sample volume was constant and independent of total sample volume. The sample volume of the cell was about 25 cm³. The temperature of the cell was measured using a thermocouple and a digital thermometer accurate to $\pm 0.1\text{K}$.

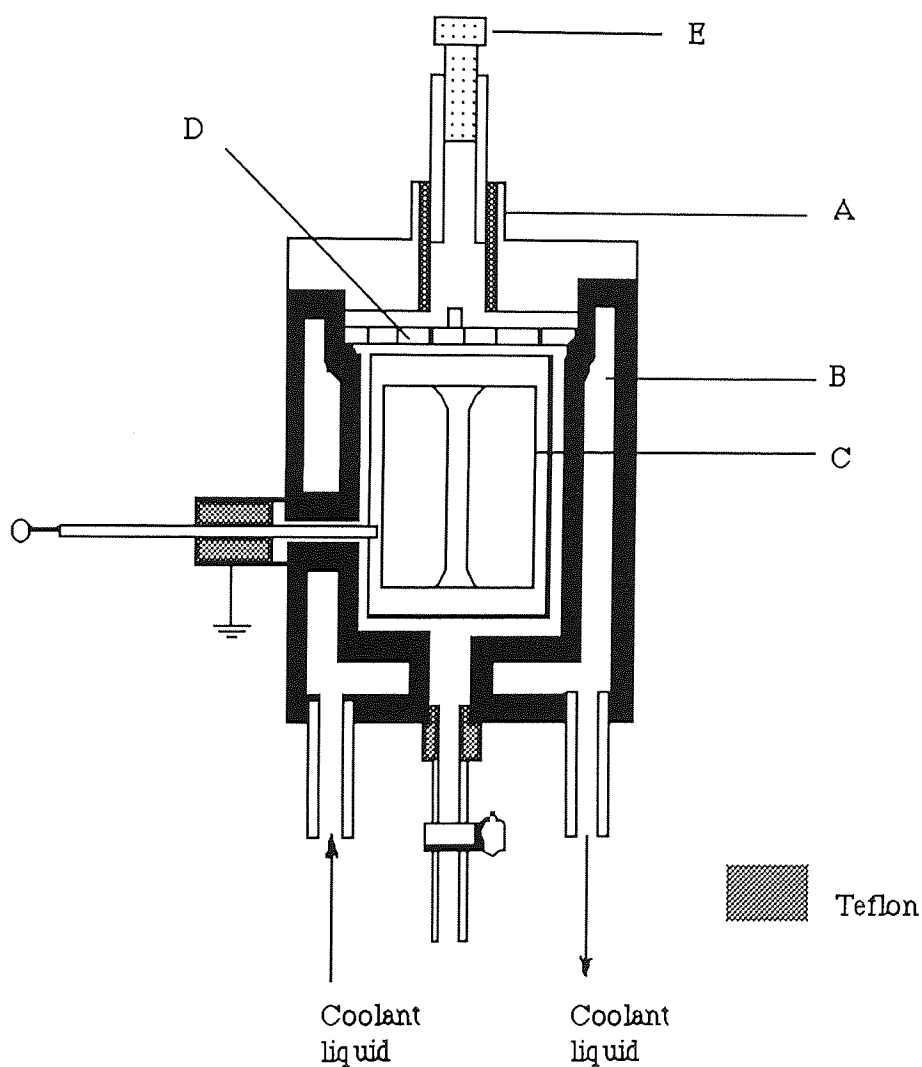


Figure 6.2 Dielectric cell A used for measurements on dilute solutions, A) screw-top lid, B) outer cylinder, C) inner cylindrical lid, D) perforated lid, E) stopper.

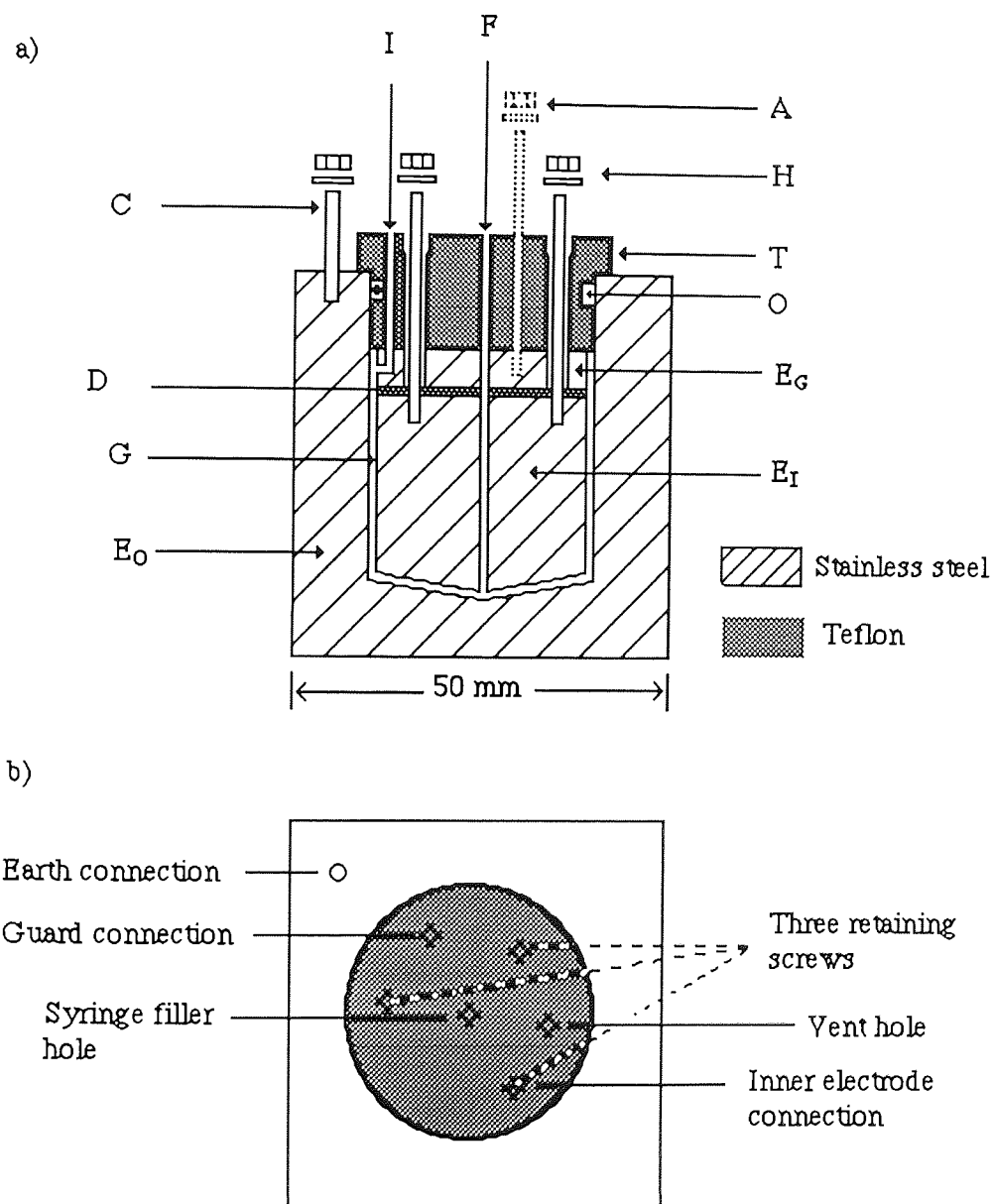
6.3.3.2 *Small sample volume dielectric cell (stainless-steel) - cell B*

Dielectric cell B (cylindrical capacitor) was constructed for measurements on small volumes of solutions (approximately 3.5 cm^3). It was also suitable for the measurements on the pure phase of the liquid-crystals. A cross-sectional diagram and top view of the cell are shown in Figure 6.3. The outer, inner and guard electrodes of the cell were made from stainless-steel. The inner cylinder (E_I) forms the high-voltage electrode and the outer body forms the earth electrode (E_O). The gap (G) between the inner and the outer electrodes was about 1mm. The cell is also fitted with a guard electrode which renders the capacitance independent of sample volume, provided that the cell is completely filled.

A 2mm diameter Teflon disk (D) for electrical isolation was placed between the guard electrode and the inner electrode. The outer electrode and inner electrode were electrically insulated from each other by a Teflon lid (T). The lid was fixed to the inner electrode, guard electrode and Teflon insulator disk by three retaining screws. The electrical capacitance of the empty cell was about 30 pF. The capacitance of this dielectric cell was stable and reproducible. The reproducibility of the air capacity after repeated heating and cooling was better than 0.02%..

The possibility of trapping air bubbles during the filling the cell was reduced by a 2mm diameter vent hole (I) and the bottom surfaces of the inner and outer cylindrical electrodes were sloped. In addition, a Teflon syringe was used to fill the cell slowly via a 2mm diameter hole (F) located at the center of the inner cylinder, so that no air bubbles were entrapped. The cleaning, filling and emptying of the cell was easy and practical. Following removal of a solution the cell was washed with a solvent such as cyclohexane and then dried. The temperature of the solutions were measured by inserting a thermocouple into the filler hole of the cell.

Using cell B it was found that, the dielectric results obtained for dilute solutions were in a very good agreement with those measured using the large sample volume (cell A). In addition, the high stability and reproducibility of the capacity indicates that this small volume dielectric cell gave very reliable and accurate results.



- | | | |
|--------------------------------|-------------------------|-------------------------|
| E_O - Outer electrode | E_I - Inner electrode | E_G - Guard electrode |
| D - Teflon disk (2mm) | C - Earth connection | A - Guard connection |
| H - Inner electrode connection | G - Electrode gap (1mm) | T - Teflon lid |
| O - O-ring | F - Syringe filler hole | I - Vent hole |

Figure 6.3 Dielectric cell B. (a) Cross-sectional view, (b) Top-view.

6.3.4 *Refractive index measurements*

The refractive indices of the solutions were determined at a wavelength of 589 nm using a Automatic Digital GPR Model 11-37-X Refractometer (with a display of RI 1.xxxxx @ xx.x °C and with an accuracy of ± 0.00005). The refractometer was initially calibrated by automatic zeroing function and then used to perform refractive indices measurements at 25.0 °C. To check the instrument's zero, a water sample (HPLC grade H₂O, $n = 1.3325$) was used. The temperature of the refractometer was controlled by circulation of water through an internal prism jacket which allowed water to impinge directly on the walls and base of a sapphire prism. A thermocouple was mounted between the prism and its temperature control jacket in order to give an accurate as possible value of the prism temperature.

6.3.5 *Density measurements*

The densities of the solutions were measured at 25.0°C using DMA 60 digital density meter, in combination with a DMA 602 remote measuring cell. The measuring cell was initially calibrated before being used to perform density measurements. A Teflon syringe was used to fill the cell slowly via a length of Teflon tubing, so that no air bubbles were entrapped, and the solutions were filtered through a 0.22 μm Millipore filter before use. The temperature of the density meter was controlled by circulation of water through a jacket surrounding the cell and was measured to an accuracy of $\pm 0.1^\circ\text{C}$. The background theory involved in density measurements described in Chapter 4.

6.3.6 *The measurement of the dielectric permittivity of solutions*

Electrical capacitance data were used to calculate the static dielectric permittivities (dielectric constants) of a solution with the object of determining the solute's molecular dipole moment. The capacitance of the dielectric cell was measured when empty (C_{air}),

when filled with the standard liquid (C_1), and when filled with solution of the interest (C_{12}). Assuming that the stray capacitance remained constant then⁴

$$\epsilon_{12} = 1 + \frac{(C_{12} - C_{\text{air}})}{(C_1 - C_{\text{air}})} (\epsilon_1 - 1) \quad (6.31)$$

where, ϵ_1 and ϵ_{12} are the dielectric permittivities of standard liquid and solution, respectively. ϵ_0 is the permittivity of free space ($8.854 \times 10^{-12} \text{ Fm}^{-1}$). The measured capacities are

$$C_{\text{air}} = (\epsilon_0 A/d) + \Delta C, \quad (6.32)$$

$$C_1 = (\epsilon_0 \epsilon_1 A/d) + \Delta C, \quad (6.33)$$

$$C_{12} = (\epsilon_0 \epsilon_{12} A/d) + \Delta C. \quad (6.34)$$

The static dielectric permittivities of the standard liquids (HPLC grade cyclohexane and 1,4-dioxane) used to calibrate the dielectric cell are listed in Table 6.2. Figure 6.4 shows plots of the dielectric permittivity results as a function of temperature. For non-polar molecules the molar polarisation does not vary with temperature¹²⁵. This enables the Mosotti and Clausius equation (Equation 6.2) to be used to calculate the dielectric permittivities of cyclohexane, using the experimental density data (Chapter 4) obtained at several temperatures. The dielectric permittivities of 1,4-dioxane at several temperatures measured in this laboratory are listed in Table 6.2.

Table 6.2 Dielectric permittivities, ϵ , for liquid cyclohexane and 1,4-dioxane

Temperature /°C	ϵ	
	cyclohexane	1,4-dioxane
25.0	2.02 (1)	2.22 (7)
30.0	2.01 (2)	2.21 (7)
35.0	2.00 (3)	2.20 (6)
40.0	1.99 (4)	2.19 (5)
45.0	1.98 (6)	2.18 (4)
50.0	1.97 (8)	2.17 (3)
55.0	1.96 (9)	2.16 (2)
60.0	1.96 (1)	2.15 (1)
65.0	1.95 (3)	2.13 (9)
70.0	----	2.12 (8)

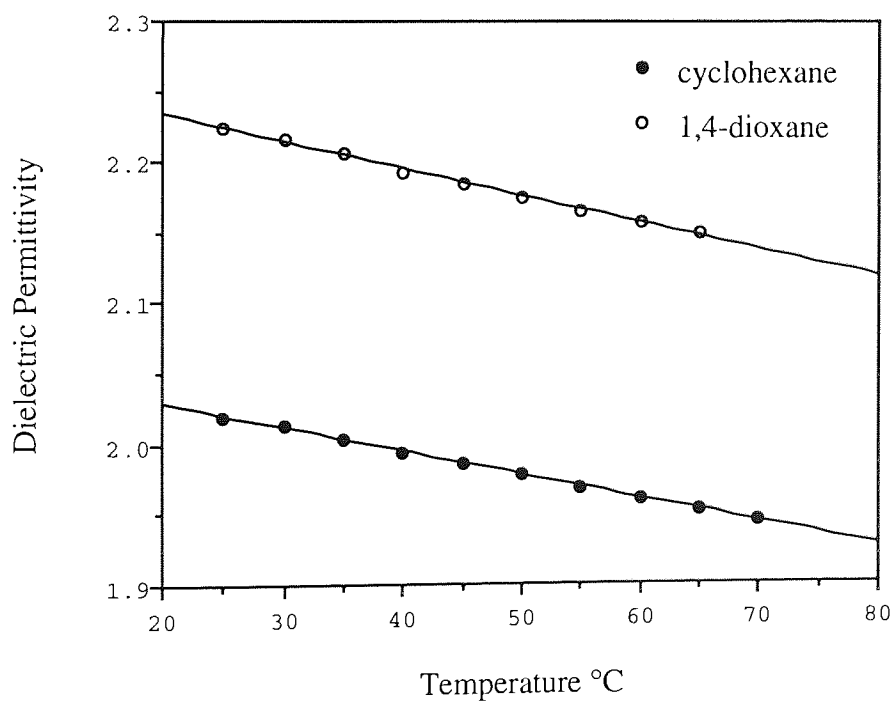


Figure 6.4 The static dielectric permittivity of cyclohexane and 1,4-dioxane as a function of temperature.

6.4 Dielectric results for dilute solutions: dipole moment measurements

The dipole moment of cyanobiphenyl and its derivatives in dilute solution in a non-polar solvent can be calculated using the Guggenheim equation (Equation 6.7).

$$\mu^2 = \frac{27kT\epsilon_0}{N_A(\epsilon_1+2)(n_1^2+2)} \left(\frac{\Delta}{C} \right)_{c \rightarrow 0}$$

The dielectric permittivity, ϵ_1 , refractive index, n_1 , and density, d_1 , of solvents, as used for the calculation of dipole moment of the compounds, are listed in Table 6.3. The dielectric increments, $\Delta = (\epsilon_{12} - n_{12}^2) - (\epsilon_1 - n_1^2)$, obtained for solutions of the cyanobiphenyl and its derivatives in a non-polar solvent at 25 °C, are listed in Appendix C. The errors in the dielectric permittivity and refractive index results are less than 1% and 0.1%, respectively. All experimental data were obtained at a temperature of 25.0 °C ($\pm 0.1^\circ\text{C}$). According to Guggenheim equation a graph of dielectric increment plotted against concentration gives a limiting gradient at zero concentration that can be used to calculate the dipole moment, μ . Dipole moments obtained in this manner are shown in Table 6.4 and are compared with the literature values wherever possible.

Table 6.3 Physical properties of cyclohexane and 1,4-dioxane obtained at 25.0 °C

Solvent	ϵ_1	n_1	d_1
Cyclohexane	2.02 (1)	1.423 (5)	0.7736 (2)
1,4-Dioxane	2.22 (7)	1.420 (1)	1.0276 (7)

Figure 6.5 shows a typical graph of dielectric increments for solution of cyanobiphenyl (CB). From the gradient of the graph the dipole moment was found to be 4.41D (14.71×10^{-30} Cm) for CB at 25.0 °C. This is higher than the literature value⁶¹ (4.33D), and significantly greater than 4.22D calculated using group moments⁶¹.

The molecular dipole moments for all compounds in this part of the project were obtained in the same manner. The dipole moment data (dipole moment of the free molecule) measured for solutes in dilute solutions will be compared to the effective dipole moment (μ_{eff}) calculated using dielectric data obtained for high concentration solutions or the undiluted liquid-crystalline state, with aim of deducing information about molecular association.

It is noted that for the most of the compounds dipole moment values are in good agreement with the previously published values, but there are some important differences between literature values and those reported here. These disagreements may possible involve several factors, such as the use of a different theory or the employment of an approximation in the calculation dipole moments from the dielectric data. Due to specific interactions between the solute and the solvent molecules, the calculated dipole moment value can depend on the nature of the solvent.

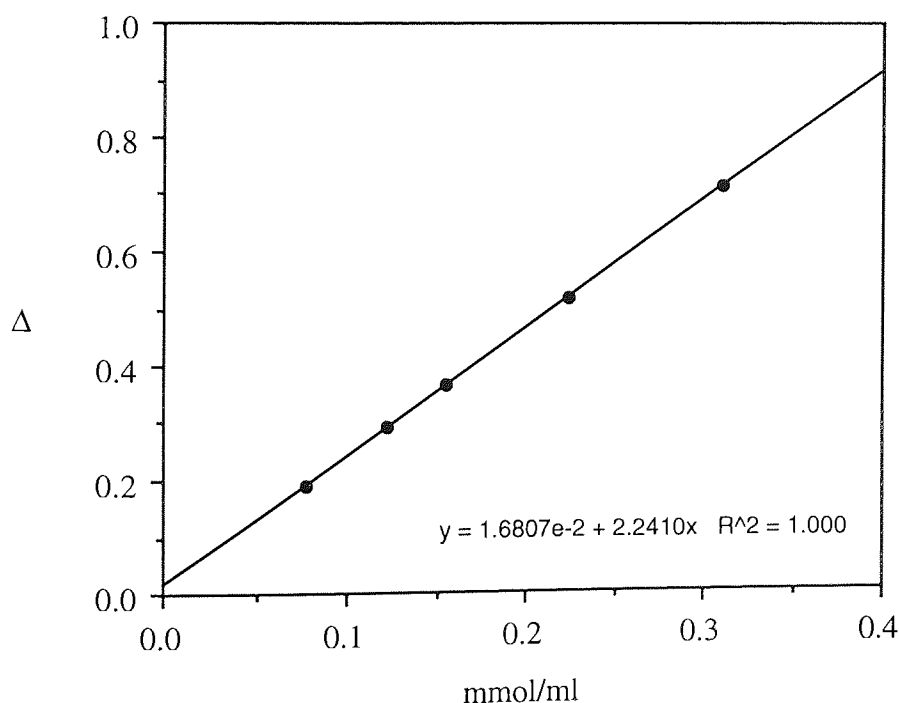


Figure 6.5 Dielectric increments, Δ , of solutions of cyanobiphenyl, CB, in 1,4-dioxane at 25.0 °C versus concentration.

The dipole moment obtained for 5CB (15.85 ± 0.09) $\times 10^{-30}$ Cm, is in very good agreement with the value reported by Dunmur⁷³ (15.9 ± 0.2) $\times 10^{-30}$ Cm, and with the value of 16.1×10^{-30} Cm, calculated using group moments. The dipole moment of 7CB was found to be (15.89 ± 0.08) $\times 10^{-30}$ Cm, and may be compared to previously reported values of 14.5×10^{-30} Cm (Ref. 132), 15.68×10^{-30} Cm (Ref. 133), 16.4×10^{-30} Cm (Ref. 73).

In order to quantify the effect of temperature on measured dipole moments, the electrical capacitance of solution of E7 in cyclohexane was measured at several temperatures. The dielectric permittivity of dilute solutions of E7 in cyclohexane were observed to decrease as the temperature increased (Figure 6.6) as a consequence of $\epsilon \approx \mu^2/kT$. The dielectric data are listed in Appendix C.

From an inspection of Figure 6.7, it can be seen that the molecular dipole moment of E7, calculated using the Guggenheim equation, increases slightly with increasing temperature. This effect is due to the existence of short-range dipole interactions, even in low concentration solutions. At a temperature of 50°C, the molecular dipole moment of E7 is 16.67×10^{-30} Cm and significantly higher than the value of 16.55×10^{-30} Cm found at 20°C.

Table 6.4 The molecular dipole moment (μ) of cyano biphenyl and its derivatives obtained in non-polar solvent at 25.0 °C.

Compound	Solvent	$10^{30} \mu / \text{Cm}$ (± 0.08)	$10^{30} \mu / \text{Cm}$ (literature)
CB	1,4-dioxane	14.71	14.42 (Ref. 61)
5B	cyclohexane	2.01
5CB	cyclohexane	15.85	15.9 (Ref. 73)
6CB	cyclohexane	15.95
7CB	cyclohexane	15.89	14.5 (Ref. 132)
8CB	cyclohexane	16.11	16.2 (Ref. 134)
5OCB	1,4-dioxane	17.45
7OCB	1,4-dioxane	17.40	17.0 (Ref. 135)
8OCB	1,4-dioxane	17.61
8OCP	1,4-dioxane	16.98
E7	cyclohexane	16.57

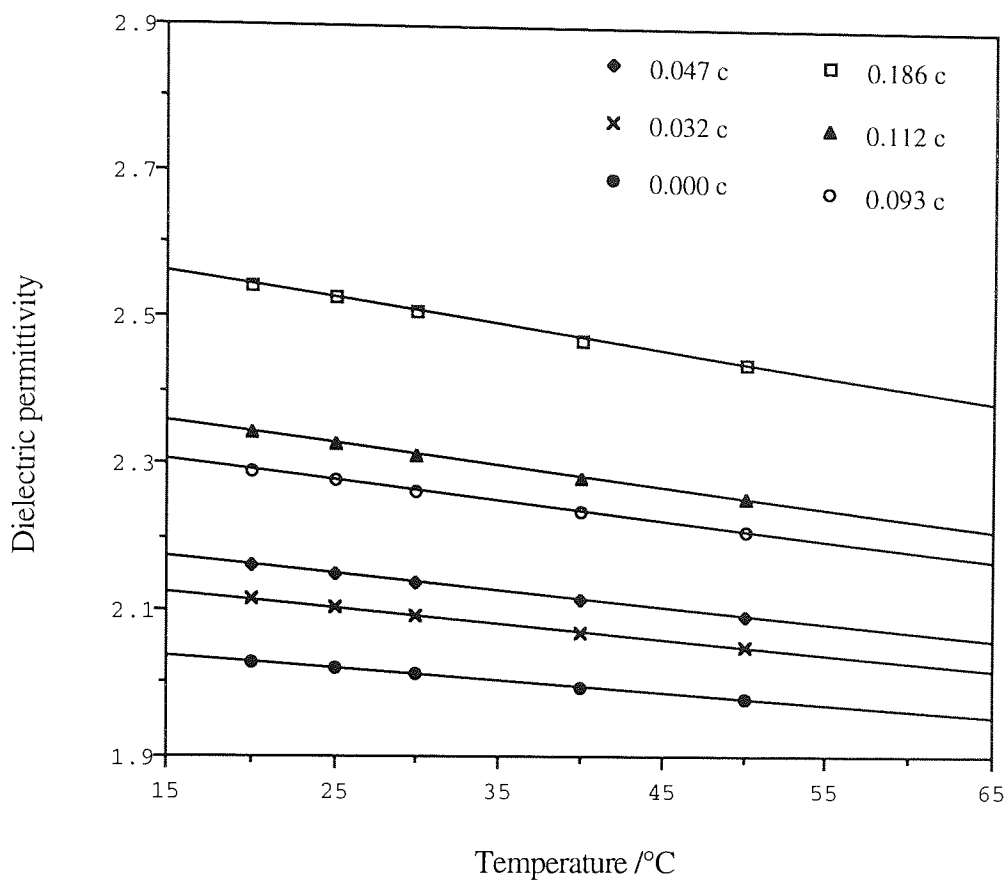


Figure 6.6 Dielectric permittivity of solutions of E7 in cyclohexane plotted as a function of temperature. Concentration is in terms of $c = \text{mol/dm}^3$.

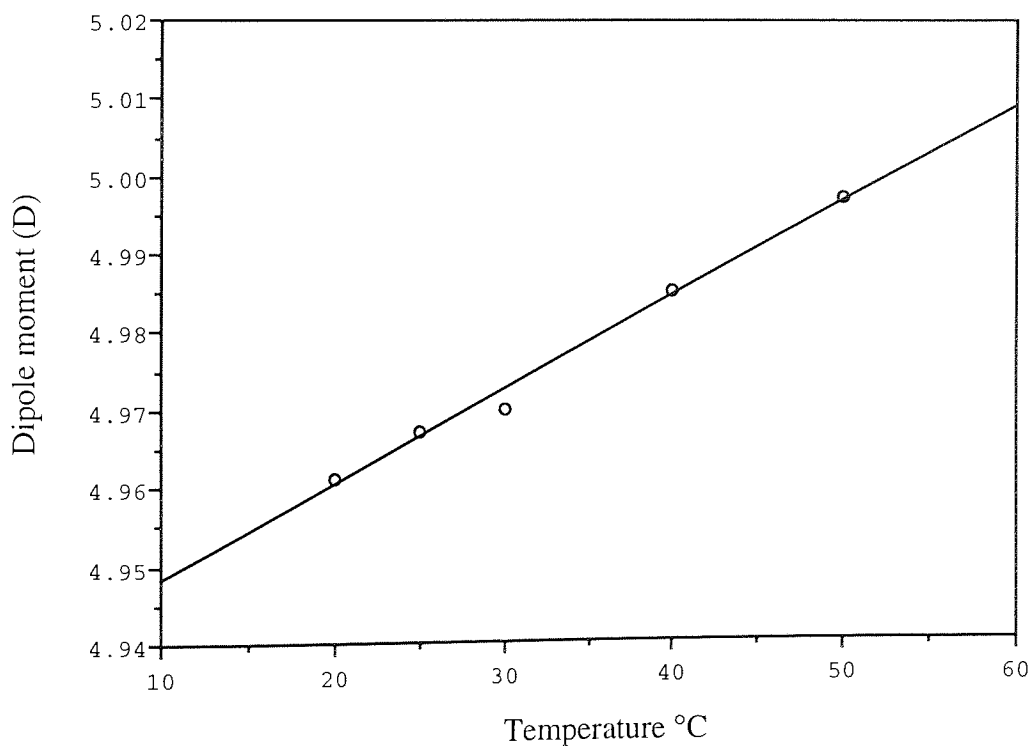


Figure 6.7 The temperature dependence of the dipole moment of E7 in cyclohexane.

6.5 *Dielectric results for concentrated solutions*

The dielectric permittivities of cyanobiphenyl (CB) and some closely related structures of its derivatives are shown in Figures 6.8 and 6.9 as a function of concentration. For 6CB and 7CB the transition from the solution to the nematic phase appears to be accompanied by a smooth change in the dielectric permittivity (Figure 6.8). Figures 6.9 to 6.11 show the dielectric permittivity, ϵ_{12} , density, d_{12} , and refractive index, n_{12} , of solutions of the alkoxy cyanobiphenyl liquid-crystals (5OCB and 8OCB) and octyloxy cyanophenyl 8OCP (non-mesogen) in 1,4-dioxane as a function of mole fraction of solute.

Because of solubility problems, cyanobiphenyl (CB) was studied in solution 1,4-dioxane up to a maximum concentration of 35% w/v, whereas 7CB and 6CB were investigated in solution of cyclohexane over the concentrations range 1-60% (w/v).

The dielectric data obtained for these solutions show high degree of molecular association. Values of the correlation factors "g" at different concentrations for these materials are less than 1 (see Tables 6.5 to 6.10). This suggests increasing anti-parallel molecular dipole association as the concentration of solute is increased, thereby reducing the effective dipole moment of the solute molecules.

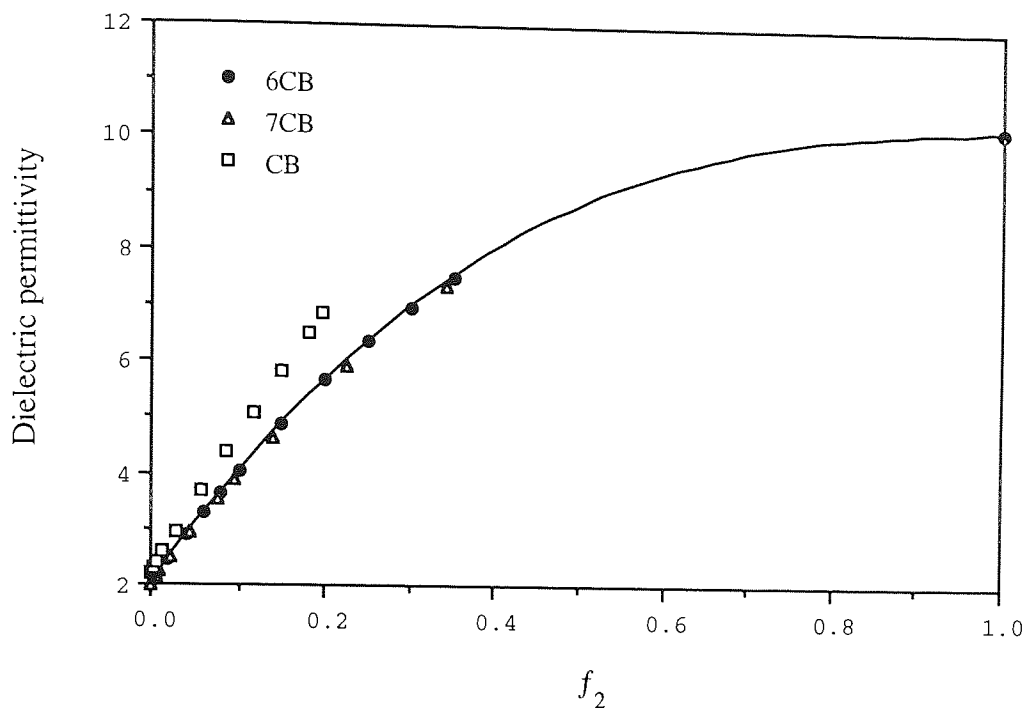


Figure 6.8 The dielectric permittivity (ϵ_{12}) of solutions of hexyl and heptyl cyanobiphenyl liquid-crystals (6CB and 7CB) in cyclohexane and cyanobiphenyl (CB) in 1,4-dioxane as a function of mole fraction, f_2 , of solute, f_2 , at 25 °C.

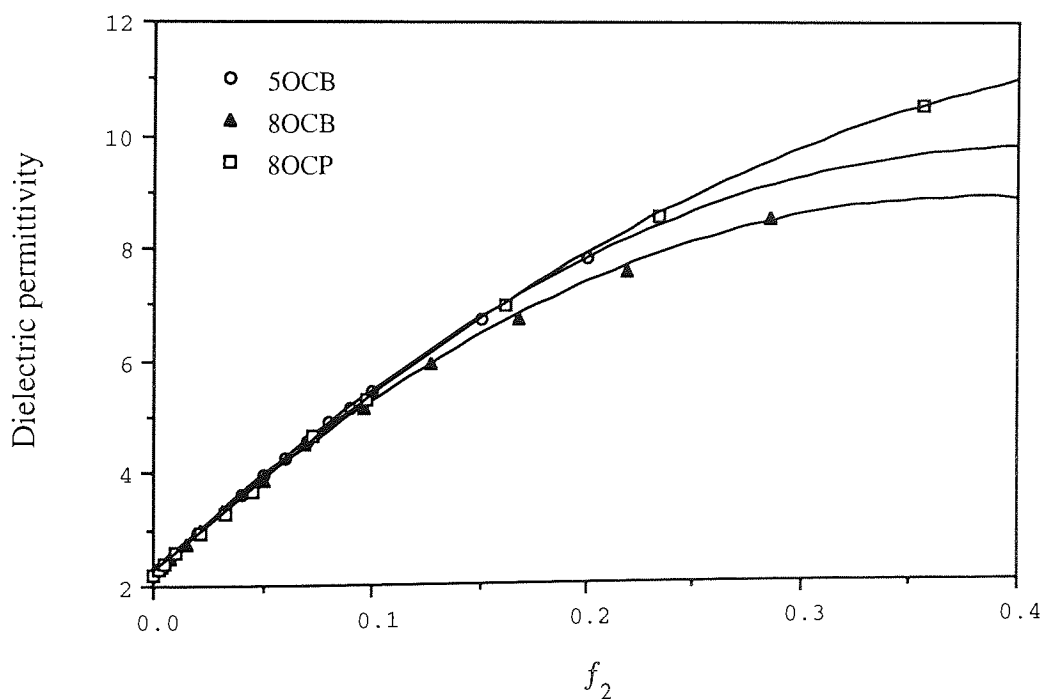


Figure 6.9 The dielectric permittivity, ϵ_{12} , of solutions of pentoxy and octoxycyanobiphenyl liquid-crystals and octoxy cyanophenyl, 8OCP in 1,4-dioxane as a function of the mole fraction of solute, f_2 , at 25 °C.

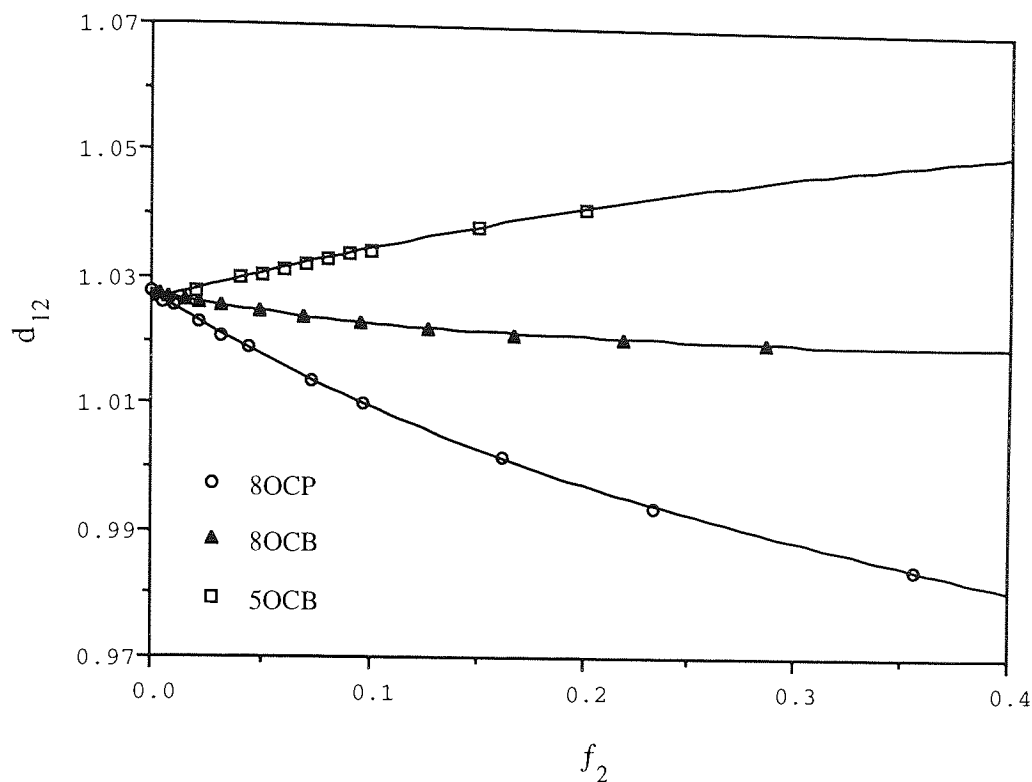


Figure 6.10 The density, d_{12} , of solutions of 5OCB, 8OCB and 8OCP (non-mesogenic), in 1,4-dioxane as a function of the mole fraction of solute, f_2 , at 25 °C.

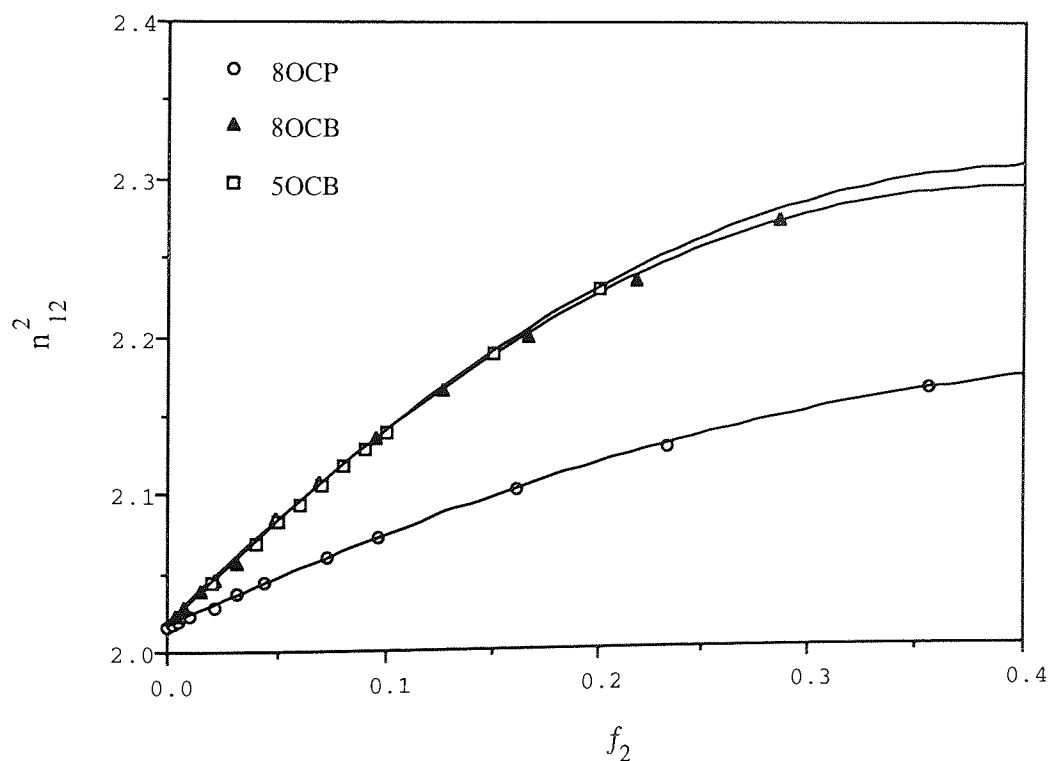


Figure 6.11 The refractive index, n_{12}^2 , of solutions of 5OCB, 8OCB and 8OCP in 1,4-dioxane as a function of the mole fraction of solute, f_2 , at 25 °C.

Table 6.5 The effective dipole moment of cyanobiphenyl, CB*, in 1,4-dioxane as a function of the solute mole fraction (f_2) at 25.0 °C.

f_2	ϵ_{12}	d_{12}	n_{12}^2	$\mu_{\text{eff}}/\text{Cm}$ $\times 10^{30}$	Kirkwood factor (g) [†]
0.197	6.8590	1.0508	2.2095	13.11	0.79
0.180	6.4885	1.0491	2.1958	13.16	0.80
0.160	6.0538	1.0472	2.1796	13.24	0.81
0.145	5.7380	1.0456	2.1670	13.33	0.82
0.112	4.9958	1.0421	2.1369	13.53	0.85
0.092	4.5297	1.0396	2.1177	13.69	0.87
0.074	4.1002	1.0375	2.0994	13.85	0.89
0.055	3.6363	1.0350	2.0795	14.06	0.91
0.041	3.2876	1.0332	2.0641	14.26	0.94
0.033	3.0852	1.0322	2.0552	14.40	0.96

[†] Calculated using the molecular dipole moment $\mu_{\text{CB}} = 14.71 \times 10^{-30}$ Cm.

Table 6.6 The effective dipole moment of octyloxycyanophenyl, 8OCP*, in 1,4-dioxane as a function of the solute mole (f_2) fraction at 25 °C.

f_2	ϵ_{12}	d_{12} (g cm ⁻³)	n_{12}^2	$\mu_{\text{eff}}/\text{Cm}$ $\times 10^{30}$	Kirkwood factor (g) [†]
0.350	10.436	0.9846	2.1632	15.15	0.80
0.300	9.7066	0.9876	2.1511	15.29	0.81
0.233	8.5401	0.9940	2.1290	15.45	0.83
0.197	7.8595	0.9968	2.1179	15.66	0.84
0.161	6.9802	1.0010	2.1014	15.69	0.85
0.096	5.274	1.0101	2.0722	15.95	0.88
0.080	4.8220	1.0129	2.0626	16.05	0.89
0.044	3.6970	1.0187	2.0432	16.32	0.92
0.032	2.3002	1.0208	2.0365	16.43	0.94
0.021	2.9388	1.0228	2.0289	16.68	0.97

[†] Calculated using the molecular dipole moment $\mu_{8\text{OCP}} = 16.98 \times 10^{-30}$ Cm.

*non-mesogen

Table 6.7

The effective dipole moment of hepty cyano biphenyl, 7CB, in cyclohexane as a function of the solute mole fraction at 25 °C.

f_2	ϵ_{12}	d_{12} (g cm ⁻³)	n_{12}^2	$\mu_{\text{eff}}/\text{Cm}$ $\times 10^{30}$	Kirkwood factor (g) [†]
0.342	7.2560	0.8951	2.2906	13.13	0.68
0.300	6.8502	0.8849	2.2668	13.31	0.70
0.250	6.2797	0.8713	2.2355	13.52	0.72
0.200	5.6071	0.8559	2.2010	13.72	0.74
0.150	4.8602	0.8336	2.1639	13.98	0.77
0.095	3.9130	0.8182	2.1173	14.31	0.81
0.080	3.6451	0.8096	2.1023	14.46	0.83
0.060	3.2649	0.8010	2.0842	14.65	0.85
0.044	2.9723	0.7921	2.0698	15.01	0.89
0.021	2.4994	0.7830	2.0446	15.57	0.96

[†] Calculated using the molecular dipole moment $\mu_{7\text{CB}} = 15.89 \times 10^{-30}$ Cm.

Table 6.8

The effective dipole moment of hexyl cyano biphenyl, 6CB, in cyclohexane as a function of the solute mole fraction at 25 °C.

f_2	ϵ_{12}	d_{12} (g cm ⁻³)	n_{12}^2	$\mu_{\text{eff}}/\text{Cm}$ $\times 10^{30}$	Kirkwood factor (g) [†]
0.384	7.8750	0.9081	2.3207	12.97	0.66
0.325	7.2490	0.8936	2.2848	13.15	0.68
0.250	6.3480	0.8727	2.2356	13.43	0.71
0.209	5.7545	0.8584	2.2041	13.58	0.72
0.174	5.2481	0.8466	2.1784	13.76	0.74
0.131	4.5431	0.8325	2.1468	13.94	0.76
0.080	3.6400	0.8096	2.1013	14.36	0.81
0.060	3.2631	0.8015	2.0837	14.57	0.83
0.043	2.9403	0.7935	2.0677	14.89	0.87
0.029	2.6741	0.7886	2.0563	15.32	0.92

[†] Calculated using the molecular dipole moment $\mu_{6\text{CB}} = 15.95 \times 10^{-30}$ Cm.

Table 6.9

The effective dipole moment of octyloxy cyano biphenyl (8OCB) in 1,4-dioxane as a function of the solute mole fraction at 25.0 °C.

f_2	ϵ_{12}	d_{12} (g cm ³)	n_{12}^2	$\mu_{\text{eff}}/\text{Cm}$ $\times 10^{30}$	Kirkwood factor (g) [†]
0.286	8.4895	1.0201	2.2728	14.79	0.71
0.250	8.0820	1.0204	2.2554	14.99	0.73
0.218	7.5830	1.0207	2.2345	15.12	0.74
0.167	6.7294	1.0213	2.1993	15.42	0.77
0.150	6.4361	1.0216	2.1867	15.59	0.78
0.096	5.1710	1.0228	2.1361	15.93	0.82
0.080	4.7502	1.0235	2.1175	16.08	0.83
0.060	4.1838	1.0243	2.0950	16.28	0.86
0.040	3.5812	1.0251	2.0709	16.58	0.89
0.021	2.9790	1.0260	2.0465	17.19	0.95

[†] Calculated using the molecular dipole moment $\mu_{8\text{OCB}} = 17.61 \times 10^{-30}$ Cm.

Table 6.10

The effective dipole moment of pentyloxy cyano biphenyl (5OCB) in cyclohexane as a function of the solute mole fraction at 25 °C.

f_2	ϵ_{12}	d_{12} (g cm ⁻³)	n_{12}^2	$\mu_{\text{eff}}/\text{Cm}$ $\times 10^{30}$	Kirkwood factor (g) [†]
0.20	7.7921	1.0413	2.2292	15.18	0.76
0.15	6.7370	1.0381	2.1886	15.52	0.79
0.10	5.4618	1.0345	2.1397	15.92	0.83
0.09	5.1770	1.0337	2.1289	16.01	0.84
0.08	4.8861	1.0329	2.1174	16.10	0.85
0.07	4.5862	1.0322	2.1059	16.22	0.86
0.05	3.9580	1.0305	2.0821	16.48	0.89
0.04	3.6339	1.0297	2.0696	16.67	0.91
0.02	2.9505	1.0279	2.0436	17.18	0.97

[†] Calculated using the molecular dipole moment $\mu_{5\text{OCB}} = 17.45 \times 10^{-30}$ Cm.

6.5.1 Intermolecular association of cyano compounds

The effective dipole moments (μ_{eff}) for polar compounds in concentrated solutions are evaluated using the Equation 6.13. The Kirkwood factor "g" can then be obtained using the simple relationship

$$\mu^2 = \mu_{\text{eff}}^2 \times g \quad (6.35)$$

where μ is the actual dipole moment (dipole moment of the single molecule in the gas phase), measured in dilute solution and μ_{eff} is the effective dipole moment as calculated from the dielectric data using equation 6.13. Three independent measurements, performed on the same samples and the same temperature, give the dielectric permittivity, ϵ_{12} , density, d_{12} , and refractive index, n_{12} . These data are presented in Tables 6.5-6.10. All the "g" values are less than 1, indicating anti-parallel association.

The effective dipole moments of 6CB in cyclohexane solution as a function of the solute mole fraction, are shown in Figure 6.12. It can be seen that the effective solution dipole moment decreases with increasing solute concentration, indicating a high degree of anti-parallel association.

It was found that pentyl biphenyl (5B) was not significantly associated in the range of concentration covered in this study ($f_2 < 0.6$). However, the dielectric data obtained for 5B in the pure phase, gave an effective dipole moment of 1.92×10^{-30} Cm, and the permittivity is proportional to μ^2/kT . Measurements made on dilute solutions of 5B in cyclohexane yield a dipole moment of 2.0×10^{-30} Cm, and correspond to a Kirkwood factor "g" of 0.92, indicating a low degree of anti-parallel dipole association. In contrast to 5B, the cyano containing molecule (CB) shows a high degree of anti-parallel molecular dipole association, even at low solute mole fractions $f_2 \geq 0.03$.

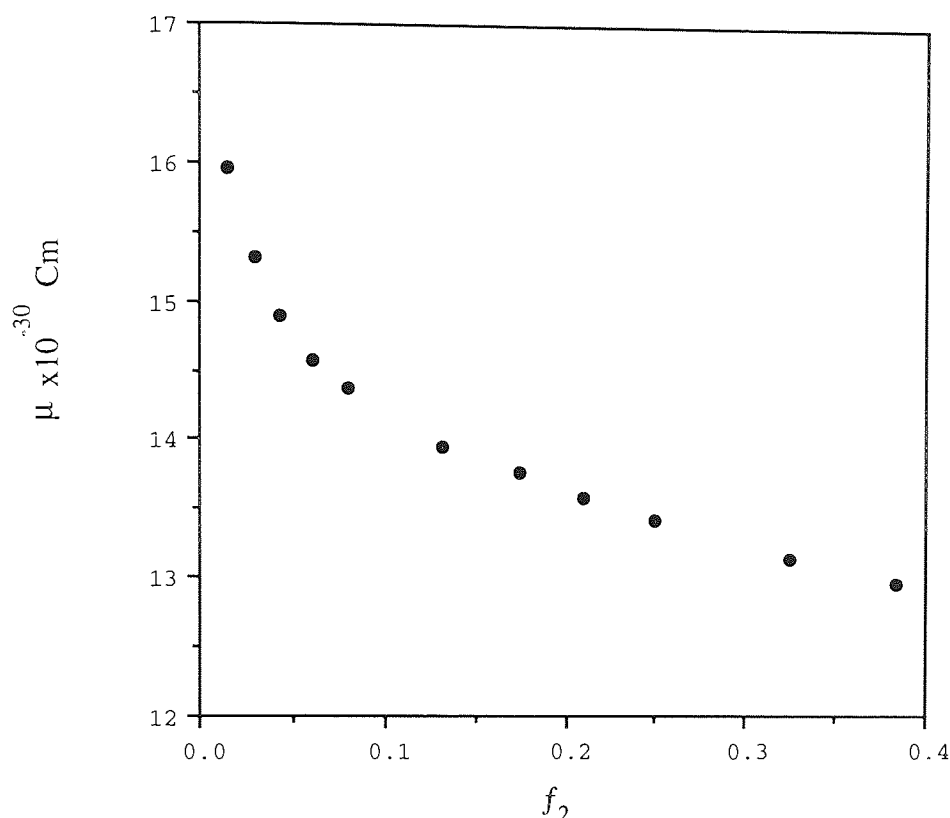


Figure 6.12 The dipole moment of solutions of 6CB in cyclohexane as a function of the mole fraction of solute, f_2 , at 25 °C.

The concentration dependence of dipole correlation factor, $g = (\mu_{\text{eff}}/\mu)^2$, for pentyl and heptyl cyanobiphenyls (6CB and 7CB) and 4-cyanobiphenyl, CB, (non-mesogen) is shown in Figure 6.13. Although, 4-cyanobiphenyl (CB) shows a significant degree of anti-parallel association, the liquid-crystal compounds (6CB and 7CB) show higher degree of association. This behaviour serves to indicate the important role played by alkyl chain in the molecular interactions.

The concentration dependence of dipole correlation factor, g , of solutions of pentoxy and octoxy cyanobiphenyl and of octoxy cyanophenyl, 8OCP in 1,4-dioxane, as a function of the mole fraction of solute at 25 °C is shown in Figure 6.14. The two alkoxy cyanobiphenyls, 5OCB and 8OCB show a high degree of anti-parallel molecular association at low concentrations, but for 8OCP (non-mesogen) the association develops more slowly as the concentration increases. This behaviour may be due to the higher polarisability of cyanobiphenyls molecules along the long molecular axis compared to

that for the cyanophenyl molecules. This demonstrate the importance of biphenyl core in determining molecular interactions and its role also in the formation of nematogenic materials.

It can be concluded that there is a complicated interplay between dipolar groups and polarisable groups. However, the contribution of high polar CN- end group in the aggregation is very significant.

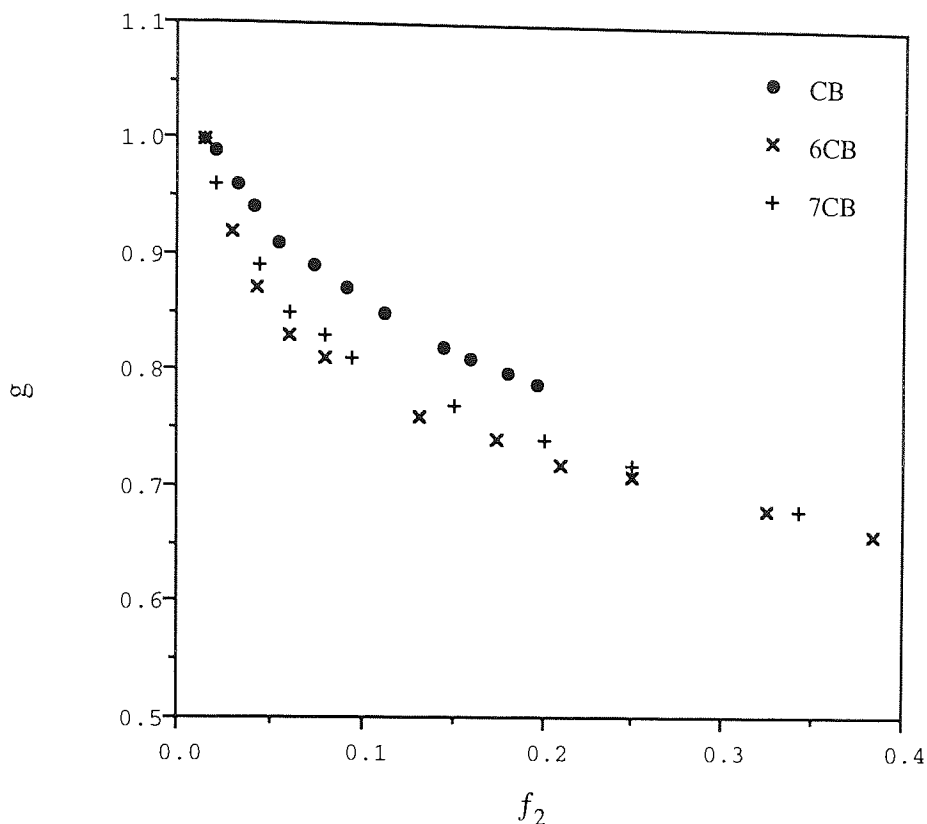


Figure 6.13 The dipole correlation factor, g , of solutions of hexyl, heptyl cyanobiphenyls (6CB, 7CB) and cyanobiphenyl, CB, in cyclohexane as a function of the mole fraction of solute, f_2 , at 25 °C.

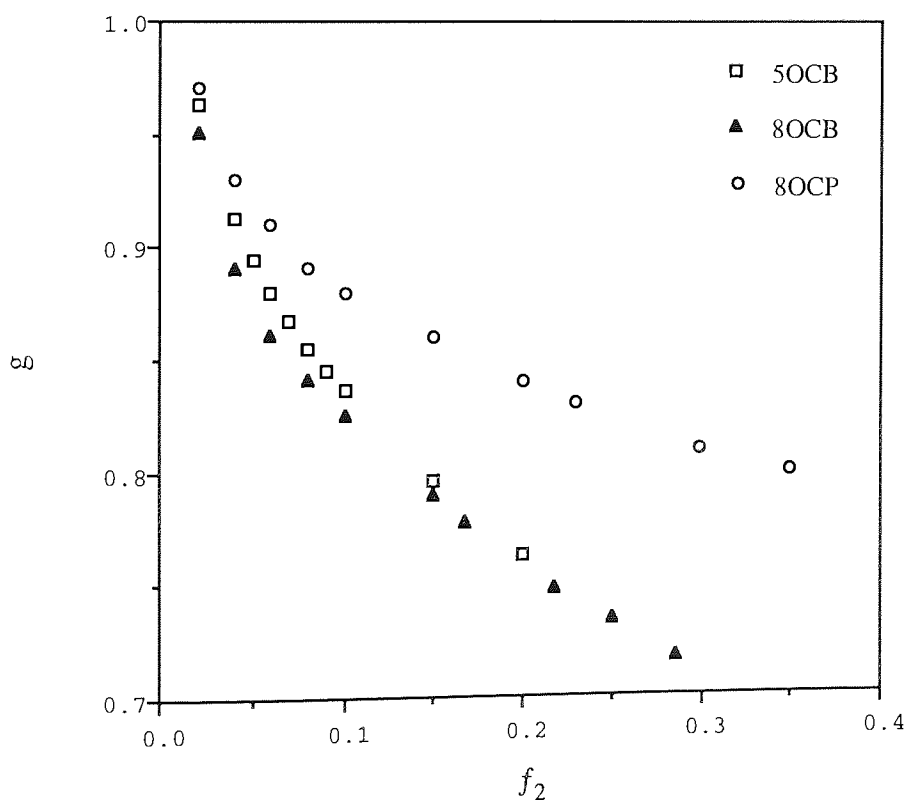


Figure 6.14 The correlation factor, g , of solutions of pentoxy, octoxy cyanobiphenyls, 5OCB, 8OCB and octoxy cyanophenyl, 8OCP, in 1,4-dioxane as a function of the mole fraction of solute, f_2 , at 25 °C.

6.6 Dielectric results for undilute liquid-crystals

6.6.1 Alkyl cyanobiphenyls in the isotropic phase

The dielectric permittivities of the isotropic phase of alkyl cyanobiphenyls indicate the presence of significant molecular association. The dielectric permittivity ϵ_{iso} decreases with decreasing temperature just above T_{NI} . This anomalous behaviour (pre-transition effect) of ϵ_{iso} for alkyl cyanobiphenyls has been reported by Bradshaw and Raynes¹³⁶. The dielectric data obtained for the liquid-crystals considered in the present study are in good agreement with the dielectric data reported by Bradshaw and Raynes¹³⁶.

The effective dipole moment ($\mu g^{1/2}$) of a pure liquid can be calculated using the Kirkwood-Frohlich equation (Equation 6.12):

$$g\mu^2 = \frac{9kT\epsilon_0}{N} \frac{(\epsilon - n^2)(2\epsilon + n^2)}{\epsilon(n^2 + 2)^2}$$

in which μ is the moment of the molecule in the liquid state, g is the Kirkwood correlation parameter and is a measure of the molecular association between a reference molecule and its nearest neighbours, and N is the number of molecules per cm^3 . According to the Kirkwood-Frohlich^{127,128} equation to calculate the effective dipole moment need to know the value of dielectric permittivity, density and refractive index. The density and refractive index data, obtained at several temperatures are given in Chapter 4 and in Appendix A. The dielectric permittivities (ϵ), effective dipole moments (μ_{eff}) and Kirkwood correlation factors (g) of three homologous cyanobiphenyl liquid-crystals (5CB, 6CB, and 7CB) are listed in Tables 6.11-6.13.

The effective dipole moments of 5CB to 7CB show an increase in μ_{eff} with increasing temperature (Figure 6.16). It can be attributed to a decrease in the anti-parallel molecular association at higher temperatures. A sudden increase in the effective dipole

moment at the phase transition is related to a sudden structural change that arises in going from the ordered nematic state to the disordered isotropic phase. At the nematic to isotropic phase transition the long range nematic ordering vanishes.

Table 6.11 The permittivities, ϵ_{iso} , effective dipole moment, μ_{eff} , and Kirkwood factor, g , of n-pentyl cyanobiphenyl, 5CB, in the isotropic phase

Temp. $\pm 0.1^\circ\text{C}$	Phase	ϵ_{iso}	$\mu_{\text{eff}}/\text{Cm}$ $\times 10^{30}$	g^\dagger
34.0	nematic	10.96	11.2 (7)	0.506
34.9	nematic	11.37	11.5 (5)	0.531
35.2	isotropic	11.62	11.7 (1)	0.546
37.0	isotropic	11.65	11.7 (4)	0.549
40.0	isotropic	11.61	11.8 (2)	0.556
45.0	isotropic	11.51	11.8 (9)	0.563
50.0	isotropic	11.44	11.9 (7)	0.570

† Calculated using the molecular dipole moment, $\mu_{5\text{CB}} = 15.85 \times 10^{-30} \text{ Cm}$

* $T_{\text{NI}} = 35.0^\circ\text{C}$

Table 6.12 The permittivities, ϵ_{iso} , effective dipole moment, μ_{eff} , and Kirkwood factor, g , of n-hexyl cyanobiphenyl, 6CB, in the isotropic phase.

Temp. $\pm 0.1^\circ\text{C}$	Phase	ϵ_{iso}	$\mu_{\text{eff}}/\text{Cm}$ $\times 10^{30}$	g^\dagger
27.5	nematic	9.93	10.87	0.464
28.4	nematic	9.98	10.94	0.470
29.0	isotropic	10.60	11.36	0.507
30.0	isotropic	10.72	11.41	0.511
32.0	isotropic	10.62	11.48	0.518
35.0	isotropic	10.63	11.54	0.523
40.0	isotropic	10.58	11.62	0.531
45.0	isotropic	10.52	11.69	0.537

† Calculated using the molecular dipole moment, $\mu_{6\text{CB}} = 15.95 \times 10^{-30} \text{ Cm}$

* $T_{\text{NI}} = 28.8^\circ\text{C}$

Table 6.13 The permittivities, ϵ_{iso} , effective dipole moment, μ_{eff} , and Kirkwood factor, g , of n-pentyl cyanobiphenyl, 5CB, in the isotropic phase

Temp. $\pm 0.1^\circ\text{C}$	Phase	ϵ_{iso}	$\mu_{\text{eff}}/\text{Cm}$ $\times 10^{30}$	g^\dagger
40.0	nematic	9.12	10.99	0.478
43.0	isotropic	9.78	11.59	0.532
45.0	isotropic	9.89	11.73	0.545
47.0	isotropic	9.98	11.86	0.557
50.0	isotropic	9.94	11.92	0.563

† calculated using the molecular dipole moment, $\mu_{5\text{CB}} = 15.89 \times 10^{-30} \text{ Cm}$

* $T_{\text{NI}} = 41.9^\circ\text{C}$

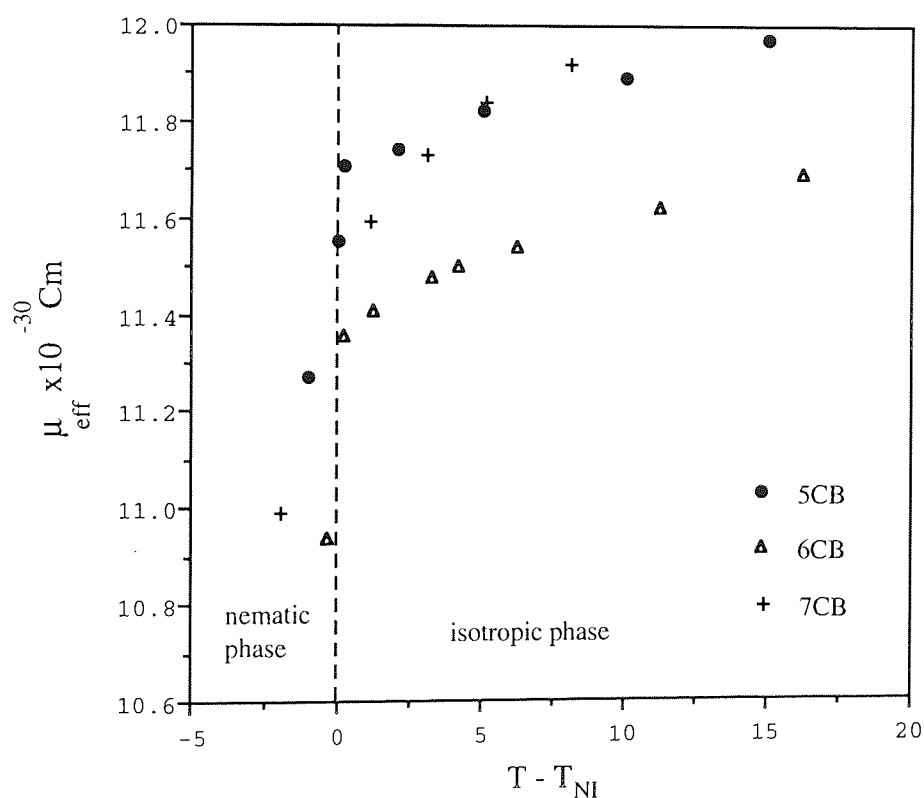


Figure 6.15 The effective dipole moment (μ_{eff}) of pentyl, hexyl, and heptyl cyanobiphenyls (5CB, 6CB, and 7CB) in the isotropic phase and in the nematic phase close to the clearing temperatures, T_c .

6.6.2 Alkoxy cyanobiphenyls

6.6.2.1 Dielectric results

The temperature dependence of the dielectric permittivity of alkoxy cyanobiphenyls in the nematic and isotropic phases is shown in Figure 6.16. The electrode surfaces of the dielectric cell produced a molecular alignment with the optic axis parallel to the electrodes for the alkoxy cyanobiphenyls. Thus the dielectric permittivities measured for the nematic phase are the perpendicular components, ϵ_{\perp} . The parallel components, ϵ_{\parallel} , were calculated from

$$\bar{\epsilon} = \frac{1}{3}(\epsilon_{\parallel} + 2\epsilon_{\perp}) \quad (6.36)$$

where $\bar{\epsilon}$ is the mean permittivity, where was obtained by extrapolation of isotropic dielectric permittivities, ϵ_{iso} , at the appropriate temperature.

The isotropic dielectric permittivity (dielectric constant) of the alkoxy cyanobiphenyls measured at 10kHz and several temperatures is in Figure 6.17. The dielectric permittivity (ϵ_{iso}) decreases with decreasing temperature just above T_{NI} . The same anomalous behaviour (pre-transition effect) of ϵ_{iso} for alkyl cyanobiphenyls has been reported by Bradshaw and Raynes¹³⁶. In the present study this behaviour was found here to extend over 10° above T_{NI} . It has been observed that anti-parallel ordering which produced the discontinuity in $\bar{\epsilon}$ at T_{NI} between highly polar materials also influenced the behaviour of the dielectric permittivity above the transition temperature in the isotropic phase¹³⁴. On approaching T_{NI} from the isotropic phase there is increasing anti-parallel correlation which reduces the effective dipole moment contribution to ϵ_{iso} .

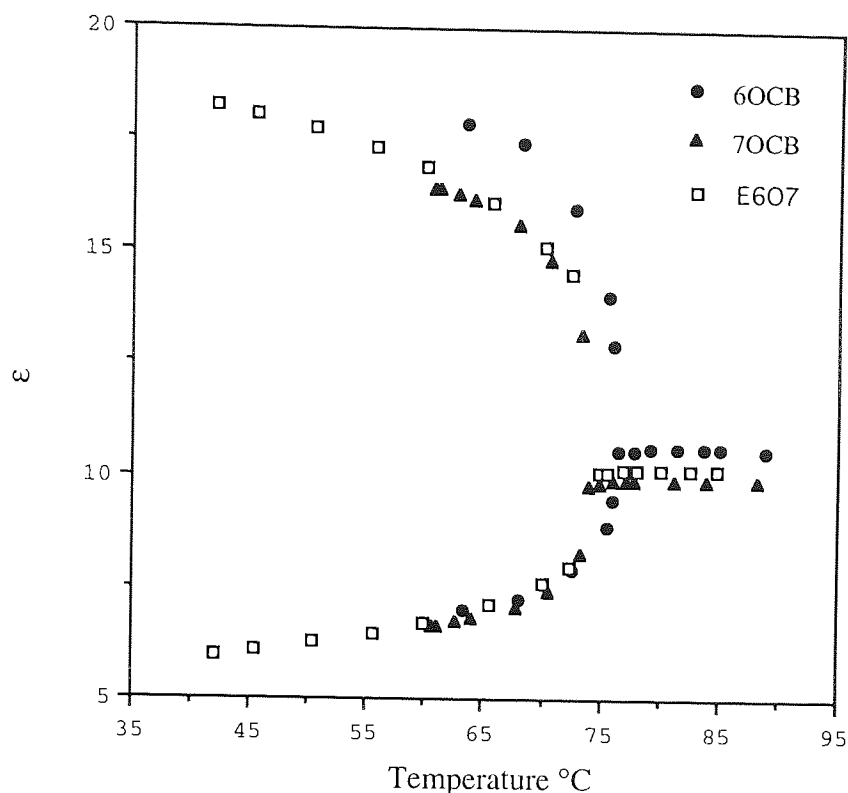


Figure 6.16 Temperature variation of the permittivity of 6OCB, 7OCB, and a eutectic mixture of hexoxy and heptoxy cyanobiphenyls E₆₀₇ (41.5:58.5).

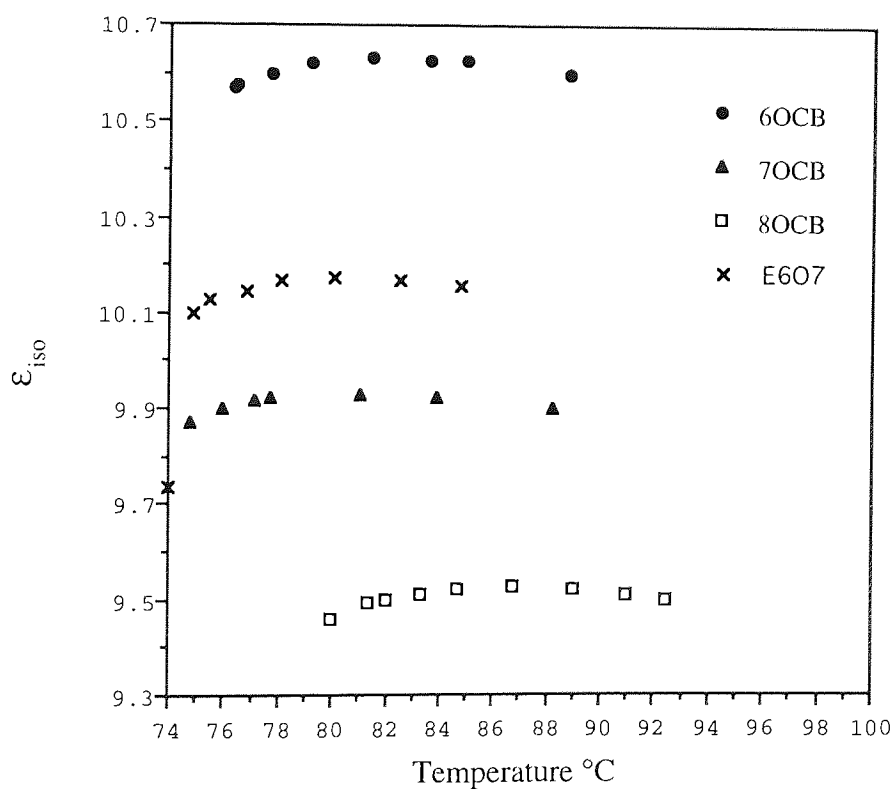


Figure 6.17 Isotropic dielectric permittivity of n-alkoxy cyanobiphenyls at several temperatures.

In order to adequately clarify the effect of stainless steel (type 304) (the surfaces of the dielectric cell) on molecular alignment, the surface of the steel electrodes were coated with lecithin, a surface active agent (see Chapter 2). Referring to Figure 6.18, it can be seen that the dielectric permittivities reported for 8OCB in the nematic and smectic phases are the close to the parallel component, ϵ_{\parallel} . Therefore, the liquid-crystal molecules are aligned with the optic axis perpendicular to the electrodes (i.e., parallel to the electric field direction). The permittivities in the smectic phase (55°C to 65°C) is almost independent of temperature and show the highest dielectric permittivities measured for 8OCB.

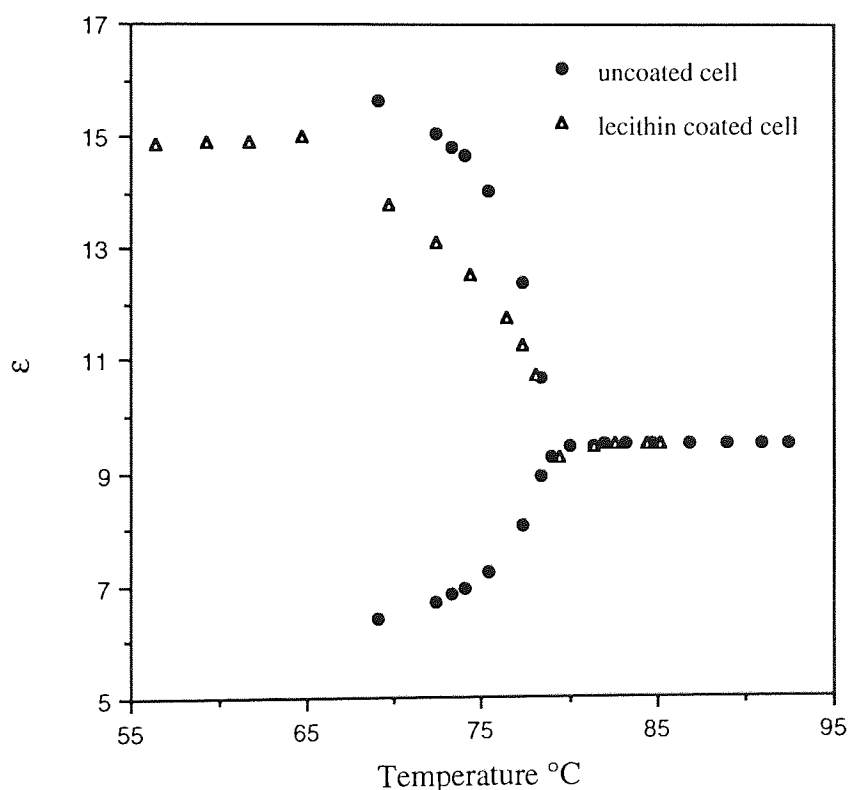


Figure 6.18 Temperature variation of the permittivity of 8OCB in an uncoated stainless steel cell and permittivity of 8OCB for lecithin coated stainless steel electrodes.

The temperature variation of the dielectric permittivity of octoxy cyanobiphenyl, 8OCB, in the nematic and isotropic phases is also shown in Figure 6.18. The permittivities reported for the nematic phase are the perpendicular components, ϵ_{\perp} . The parallel components were calculated from the isobestic equation 6.36. Without surface

treatment (i.e. absence of lecithin) the surface energy is high and the liquid crystals molecules are aligned with the optic axis parallel to the electrodes (Figure 6.19). Such molecular alignment has not been observed for alkyl cyanobiphenyl possibly because there is no oxygen atom in this molecular structure.

The permittivity values of alkyl cyanobiphenyl (5CB to 7CB) in the nematic phase indicate imperfect alignment of the liquid-crystal molecules. These observations demonstrate the sensitive relationship between molecular alignment, molecular structure and surface treatment.

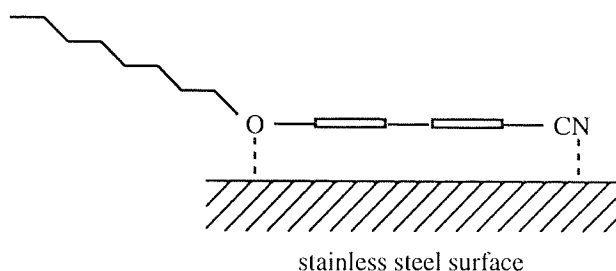


Figure 6.19 Adsorption of an 8OCB molecule on a stainless-steel surface.

It can be seen from Figure 6.20 that the static dielectric permittivities found in the present study are in a good agreement with the dielectric data reported by Buka, Owen, and Price¹³⁵. However, the dielectric data obtained in the present work cover a more extensive temperature range and therefore the presence of a pre-transition just above the nematic-isotropic transition can be shown. Buka et al.¹³⁵ used a solenoid wound around the coaxial cell to induce liquid-crystal alignment. In this study the surface effect was enough to obtain almost perfect perpendicular alignment of alkoxy cyanobiphenyl molecules with respect to electric field direction.

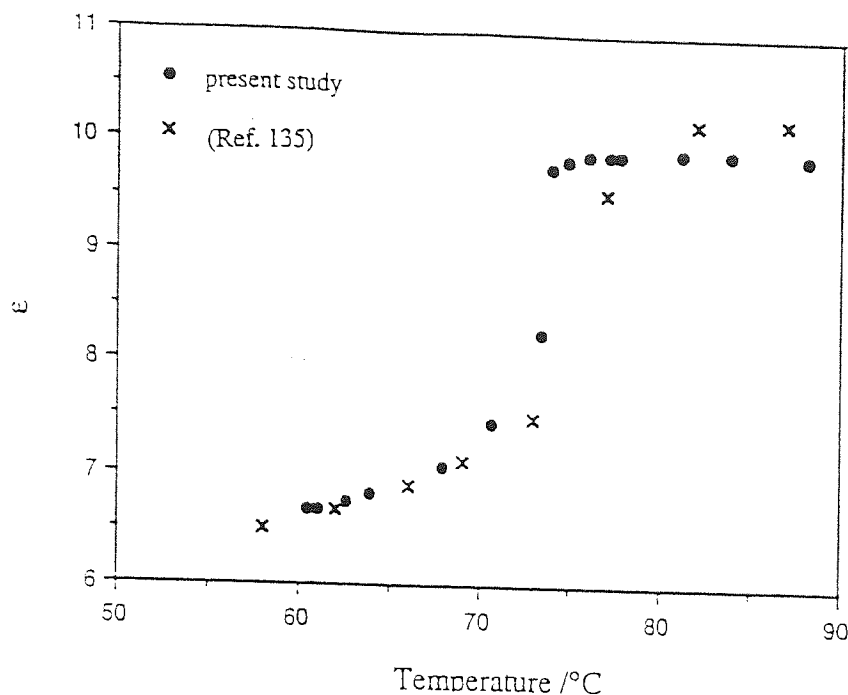


Figure 6.20 Temperature variation of the perpendicular components dielectric permittivity, ϵ_{\perp} of 7OCB.

6.6.2.2 The correlation factors in the nematic and isotropic phase of alkoxy cyanobiphenyls

A. Isotropic phase

The dielectric permittivities in the isotropic phase of alkoxy cyanobiphenyls show the presence of significant molecular association. This is confirmed by dipole moment measurements (see Tables 6.14-6.17). For example, a dipole moment of 13.13×10^{-30} Cm was calculated from the permittivity of 8OCB in the isotropic phase at 89.0°C (Figure 6.21). Measurements in cyclohexane solution gives a dipole moment of 17.61×10^{-30} Cm. These results correspond to a Kirkwood factor (g) of 0.56, and indicate a high degree of anti-parallel dipole association. Similarly a dipole moment of 12.9×10^{-30} Cm was calculated from the permittivity of 7OCB in the isotropic phase at 87°C with a g -factor of 0.55. This is in good agreement with the value of 12.6×10^{-30} Cm reported by Buka, Owen and Price¹³⁵ for 7OCB at 87°C .

Table 6.14 The dielectric permittivity, ϵ_{iso} , and effective dipole moment, μ_{eff} , of n-hexoxy cyanobiphenyl, 6OCB, in the isotropic phase ($T_{\text{NI}} = 75.8^\circ\text{C}$).

Temp. $^\circ\text{C}$	ϵ_{iso}	$\mu_{\text{eff}}/\text{Cm}$ $\times 10^{30}$	g^\dagger
88.8	10.60	13.04	0.55
85.0	10.63	12.96	0.54
81.5	10.63	12.86	0.53
79.2	10.62	12.79	0.53
77.7	10.60	12.74	0.52
76.4	10.57	12.68	0.52

\dagger Calculated using $\mu_{6\text{OCB}} = 17.50 \times 10^{-30} \text{ Cm}$

Table 6.15 The dielectric permittivity, ϵ_{iso} , and effective dipole moment, μ_{eff} , of n-heptoxy cyanobiphenyl, 7OCB, in the isotropic phase ($T_{\text{NI}} = 74.0^\circ\text{C}$).

Temp. $^\circ\text{C}$	ϵ_{iso}	$\mu_{\text{eff}}/\text{Cm}$ $\times 10^{30}$	g^\dagger
88.2	9.90	13.01	0.55
83.9	9.93	12.91	0.54
81.1	9.93	12.84	0.54
77.7	9.92	12.73	0.53
76.0	9.90	12.67	0.52
74.8	9.87	12.61	0.52

\dagger Calculated using $\mu_{7\text{OCB}} = 17.55 \times 10^{-30} \text{ Cm}$

Table 6.16 The dielectric permittivity and effective dipole moment, μ_{eff} , of mixture E₆₀₇ composed of hexoxy and heptoxy cyanobiphenyl (41.5 : 58.5) in the isotropic phase ($T_{\text{NI}} = 74.9^\circ\text{C}$).

Temp. $^\circ\text{C}$	ϵ_{iso}	$\mu_{\text{eff}}/\text{Cm}$ $\times 10^{30}$	g^\dagger
84.8	10.15	12.87	0.54
82.5	10.16	12.81	0.54
80.1	10.17	12.75	0.53
78.1	10.17	12.69	0.53
76.8	10.15	12.64	0.52
75.5	10.13	12.59	0.52

\dagger Calculated using $\mu = 17.5 \times 10^{-30} \text{ Cm}$

Table 6.17 The dielectric permittivity and effective dipole moment, μ_{eff} , of n-octyloxy-cyanobiphenyl, 8OCB, in the isotropic phase ($T_{\text{NI}} = 79.0^\circ\text{C}$).

Temp. $^\circ\text{C}$	ϵ_{is0}	$\mu_{\text{eff}}/\text{Cm}$ $\times 10^{30}$	g^\dagger
92.4	9.50	13.21	0.56
89.0	9.52	13.13	0.56
86.8	9.53	13.07	0.55
84.7	9.52	13.00	0.55
83.3	9.51	12.95	0.54
82.0	9.50	12.90	0.54
81.4	9.49	12.88	0.53

† Calculated using $\mu_{8\text{OCB}} = 17.61 \times 10^{-30} \text{ Cm}$

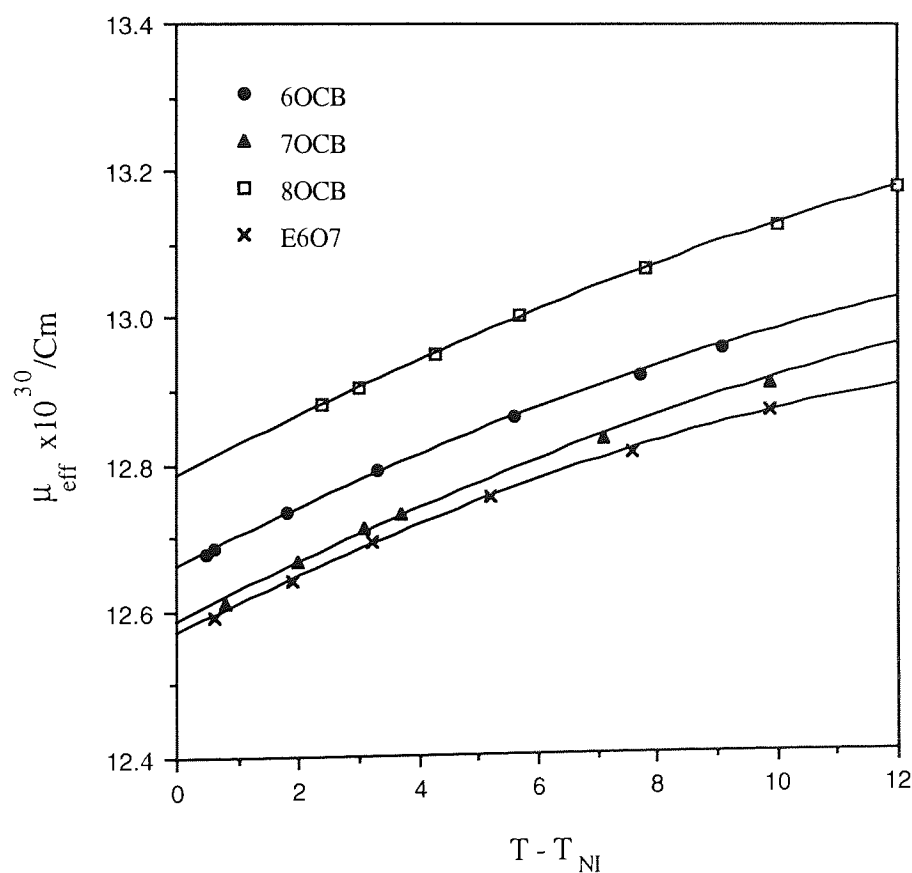


Figure 6.21 The effective dipole moment (μ_{eff}) of alkoxy cyanobiphenyls in the isotropic phases as a function of reduced temperature ($T - T_{\text{NI}}$).

B. Nematic phase

For the nematic phase, in which anisotropy of the dielectric permittivity occurs, two correlation factors are required in order to describe ordering with respect to the long and short axes of the liquid-crystal molecules. Bordewijk¹³⁷ has extended the Kirkwood-Frohlich theory¹²⁸ to uniaxial liquid-crystals and De Jue and Bordewijk¹³⁰ have calculated the dipole-dipole correlation between the molecules for nematic and smectic-A phases. Therefore, the dipole correlation factors g_{\parallel} and g_{\perp} for the nematic phase of the hexoxy, heptoxy, and octoxy cyanobiphenyls (6OCB to 8OCB), can be calculated, at several temperatures, using the De Jue and Bordewijk equations (Equations 6.21 and 6.22). In order to calculate the correlation factors g_{\parallel} and g_{\perp} in the nematic phase of the liquid-crystals, the following procedure was used:

The values for the long (a) and short (b) axes of the molecular ellipsoid have to be estimated: a is taken equal to the length of the fully extended molecule and calculated in terms of bond lengths and angles using Desktop Molecular Modeller (DMM). Using the literature values for the density taken from Ref. 49, and density data from Chapter 4, b is chosen such that the volume of the spheroid is equal to the volume available to a molecule in the nematic phase at T_{NI} .

$$V = \pi (b/2)^2 a \quad (6.37)$$

The value of molecular dipole moment, μ , was calculated using dielectric measurements in 1,4-dioxane and the Guggenheim's equation (see Section 6.4.1). Taking 14.7° as the angle between the dipole moment and long axis of the molecule (estimated from the molecular structure¹³¹), the dipole component parallel and transverse to the long molecular axis, μ_{\parallel} and μ_{\perp} , were calculated. Values of $\epsilon_{\infty\parallel}$ and $\epsilon_{\infty\perp}$ were obtained by multiplying the values of n_e^2 and n_o^2 by 1.05 to account for the atomic polarisation. The principal polarisabilities α_{\parallel} and α_{\perp} along and transverse to the long axis of the molecule

axis of the molecule were determined using refractive index and density data (see Chapter-4). The results for the liquid-crystal compounds are given in Table 6.18.

Table 6.18 The molecular parameters of hexoxy, heptoxy and octoxy cyanobiphenyls (6OCB, 7OCB and 8OCB). a and b , are the dimensions of long and short axis of the molecular ellipsoid, respectively.

liquid crystal	a Å	b Å	α_l $\times 10^{39}$	α_t $\times 10^{39}$	Ω_l	Ω_t	$\mu_{ }/\text{Cm}$ $\times 10^{30}$	μ_{\perp}/Cm $\times 10^{30}$
6OCB	20.94	5.28	5.46	3.27	0.078	0.462	16.8	4.42
7OCB	22.23	5.30	5.77	3.47	0.071	0.465	16.8	4.42
8OCB	23.31	5.33	6.33	3.49	0.067	0.467	17.0	4.47

For example, for hexoxy cyanobiphenyl (6OCB), a is taken to be equal to the length of the fully extended molecules, which was calculated from molecular models to be 20.94 Å. Using the density ($d = 1012 \text{ kg m}^{-3}$) and the molecular weight ($M = 0.279 \text{ kg.mol}^{-1}$), the molecular volume of 6OCB a single molecule (V) was found to be 458.5 Å^3 . By using equation 6.37, b was found to be 5.28 Å and $w^2 = 1.068$. From equation 6.27 (see Section 6.2.6), the shape factors, Ω_l and Ω_t were calculated to be 0.076 and 0.462. respectively. The dipole moment components parallel and transverse to the long molecular axes, are calculated to be $\mu_l = 16.9 \times 10^{-30}$ and $\mu_t = 4.42 \times 10^{-30}$. At $T = 341 \text{ K}$, $\epsilon_{||} = 17.43$, $\epsilon_{\perp} = 7.22$, $n_e = 1.670$, $n_o = 1.520$. An order parameter S of 0.57 was obtained from the degree of anisotropy of the polarisability (Section 4.4.3). Using this data correlation factors were calculated for the nematic phase and found to be

$$g_{||} = 0.66 \qquad g_{\perp} = 1.06$$

The dipole correlation factors for 6OCB in the nematic phase at several temperatures, are given in Table 6.19.

The experimental data (Tables 6.19-6.20) show that for the dipole components along the director, the tendency for anti-parallel alignment increases with increasing nematic order, whereas no such increase is found for the dipole components perpendicular to the director.

Table 6.19 Dipole correlation factors for hexoxy cyanobiphenyl, 6OCB, in the nematic phase.

Temp. °C	$\epsilon_{ }$	ϵ_{\perp}	$\Omega_{ }$	Ω_{\perp}	S	$g_{ }$	g_{\perp}
63.4	17.88	6.99	0.465	0.268	0.63	0.62	1.06
68.0	17.43	7.22	0.457	0.272	0.57	0.66	1.06
72.5	15.99	7.93	0.431	0.284	0.50	0.67	1.07
75.5	14.07	8.90	0.397	0.301	0.40	0.67	1.08

Table 6.20 Dipole correlation factors for heptoxy cyanobiphenyl, 7OCB, in the nematic phase.

Temp. °C	$\epsilon_{ }$	ϵ_{\perp}	$\Omega_{ }$	Ω_{\perp}	S	$g_{ }$	g_{\perp}
61.0	16.45	6.66	0.460	0.270	0.62	0.63	1.06
65.0	16.02	6.86	0.452	0.274	0.59	0.64	1.08
69.0	15.35	7.20	0.439	0.281	0.56	0.66	1.09
73.0	13.43	8.07	0.404	0.298	0.44	0.67	1.09

The calculated correlation factors (g) of the alkoxy cyanobiphenyl liquid-crystals in the isotropic phase are smaller than $g_{||}$ obtained for the nematic phase. This difference could be due, in part, to the use of different theories employed in the calculation for the g factors. The Kirkwood-Frohlich equation was used to calculate the g values in the isotropic phases, whereas the De Jue and Bordewijk equations were used to calculate the g factors for the nematic phases. These two theories have the different assumptions when allowing for the effects of the internal field¹³⁸ (see p. 444, 467). If the De Jue and Bordewijk equations are used for the isotropic phase ($S = 0$), the g -value in the isotropic phase obtained will be higher than the $g_{||}$ -value deduced for the nematic phase. These

values deviate remarkably from the values obtained using the Kirkwood-Frohlich equation. For example The Kirkwood-Frohlich equation gives a g -value 0.53 for 6OCB in the isotropic phase at 80°C, while the De Jue and Bordewijk equations give a g -value of 0.8 for this compound.

6.7 Types of associated pairs

Many authors have previously indicated that anisotropic molecules with strong dipole moments along their long molecular axes do associate, and that strong anti-parallel correlations are normally present in cyanobiphenyls^{117,122,131}. The simplest model for dipole association considers only pairs of associated molecules and the liquid phase of a cyano compound may be regarded as a binary mixture of dimer molecules and single molecules¹¹⁷. The dimer is assumed to have an anti-parallel dipole configuration.

This molecular pairing persists in the nematic and isotropic states and even in solutions of the cyanobiphenyls in non-polar solvents. The effective molecular length is therefore enhanced by this type molecular association and interpreted to be due to largely overlapped dimers formed by CN-phenyl contacts^{14,133,139}.

For the cyanobiphenyls each cyano group in a pair is located close to the opposite end of its neighbour and the cyano-group of one molecule overlaps with the phenyl ring of the adjacent molecule 6.22(II) or 6.22(III). In this way, the molecules pack with overlapping cores, as indicated in Figures 6.22(II) and 6.22(III).

Due to the out-of-plane twisting angle between the two phenyl rings^{140,141}, the conjugation between the two aromatic rings in alkyl or alkyloxy cyanobiphenyls is only partial. It is due to repulsion between the H atoms in the 2,6 and 2', 6' positions. The angle of twist between the ring planes ϕ (the dihedral angle) in pentyl cyanobiphenyl has been reported¹⁴⁰ to be $32 \pm 2^\circ$.

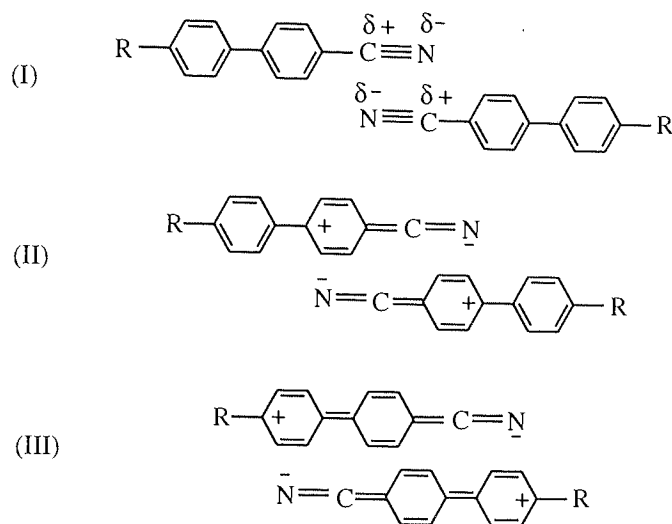


Figure 6.22 Possible arrangement of molecules in the anti-parallel association for the nCB series.

In the case of (6.22.I) although the effective length is longer than that in II and III, but due to the charge-transfer states in alkyl and alkyloxy cyanobiphenyls this type association seems unlikely. Recently, Hori et al.¹⁴² using X-ray studies, have shown that 6OCB and 7OCB dimers in the crystalline state are formed by close contacts of CN groups between neighboring molecules (Figure 6.23).

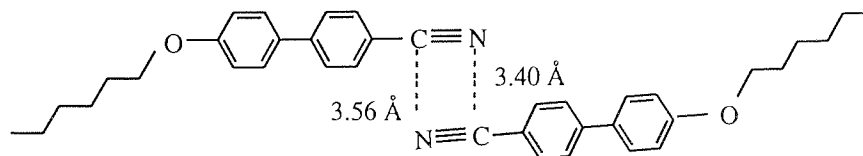


Figure 6.23 The configuration of the neighbouring molecules in the 6OCB dimer. Close contact CN-CN is shown by broken lines with distance in Å.

However, dielectric studies presented here, suggest that dimers formed by CN-phenyl contacts in which the cyano groups of the interacting molecules are the negative poles and the posit ends of the aromatic ring systems the positive ones (Figure 6.22.III). According to this model the alkyl chain lies outside of overlapping region in the dimer.

Another configuration of the neighbouring molecules in the alkyl (alkoxy) cyanobiphenyls is one that involves mainly dispersion forces between two polarisable phenyl cores. According to this model a biphenyl core of one molecule overlaps with the biphenyl core of another molecule. For this configuration of dimer, the intermolecular energy was calculated to be -34 kJ mol^{-1} by using Desktop Molecular Modeller (DMM).

CHAPTER 7

DYNAMIC LIGHT SCATTERING IN LIQUID-CRYSTAL SOLUTIONS

7.1 Introduction

In order to provide further information about molecular anisotropy and the influence of molecular association on the physical properties of the liquid-crystals, it was desirable to study the relationships between macroscopic liquid-crystal properties and molecular parameters by using as many different techniques as possible. In this chapter the Rayleigh depolarisation ratio has been measured to correlate physical behaviour of the liquid-crystals with their molecular parameters. From measurements of the intensity of depolarised light scattered by solutions of anisotropic molecules in an isotropic solvent, it is possible to obtain a correlation factor¹²² (see Chapter 6). However, the quantitative measurement of correlation factors is not the aim of this chapter.

The anisotropy parameter, δ^2 , of a molecule is an important molecular property and can be determined from the Rayleigh depolarisation ratio of scattered light^{143,144}. In addition, δ^2 is very important in all applications of the Kerr effect relating to the determination of molecular structure. The measurable property in the Kerr effect, the Kerr constant (B), is related to polarisability terms ($\theta_1 + \theta_2$) via the Langevin-Born equation, where θ_1 depends only on the electro-optical polarisabilities, b_1, b_2, b_3 , of the molecule¹⁴⁵. Since δ^2 is related to the induced term or anisotropy term, θ_1 (see Chapter 8) the importance of δ^2 becomes evidence.

7.2 Theory

7.2.1 Light-scattering

When light passes through a transparent medium, a small fraction of the light is scattered by the molecules present. The phenomenon is known generally as Rayleigh scattering⁶⁴. In the Rayleigh scattering, the light scattered and the incident radiation have the same frequency. The mechanism of light scattering is as follows. When an atom or molecule is placed in an electric field (the electric field of the incident light), the electrons interact with the field, and a electric dipole moment is induced in the molecule. This induced dipole oscillates at the same frequency as the incident radiation. The oscillating dipole in turn emits electromagnetic waves, and these comprise the scattered light. The magnitude of this induced dipole moment, μ_i , is proportional to the field strength, E , and thus

$$\mu_i = \alpha E \quad (7.1)$$

where the proportionality constant, α , is known as the polarisability (Section 4.2.1). In this case, the polarisability is due to the electron displacement only, and is related to the electronic polarisability, and for spherical molecules is the same in all directions.

7.2.2 Depolarisation ratio

In general, the molecule is elliptical and the polarisability is not the same in all directions. In this case, the polarisability α is then a second rank tensor⁶⁴. The intensity of the scattered light depends on the polarisability of the molecules, and therefore it is possible to measure the magnitude of the polarisability by determining the intensity of the scattering. The scattered light, which oscillates in the same plane as the induced dipole moment, is not in the case (anisotropic molecule) polarised in the same plane as the incident light⁶⁴.

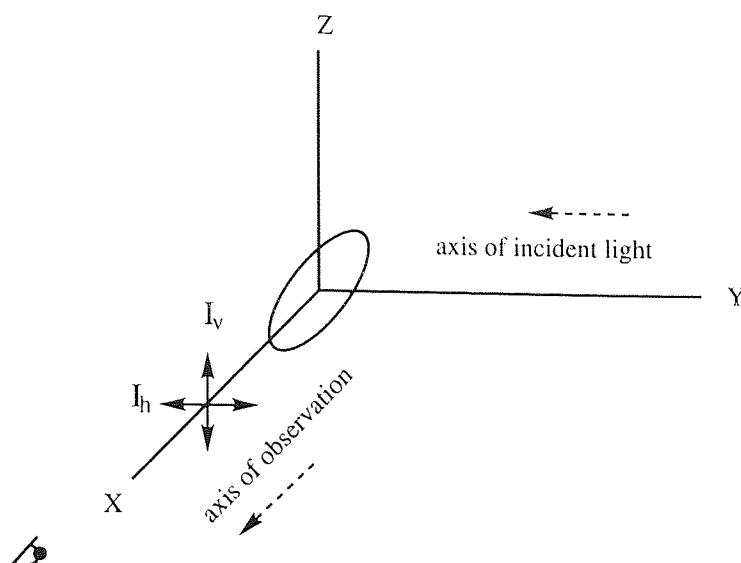


Figure 7.1 Depolarisation of scattered light

In Figure 7.1 the incident light travels along the y-axis, and that it is polarised in the yz-plane. The scattered light is observed in a direction perpendicular to y (in the direction of the x-axis). The scattered light will have components polarised in the xy and xz planes, as shown in Figure 7.1. The intensity of polarised light in the horizontal (xy) plane and vertical plane (xz) is denoted by I_h and I_v , respectively. A depolarisation ratio, Δ , may be then defined as¹⁴⁶

$$\Delta = \frac{I_h}{I_v} \quad (7.2)$$

For molecules whose polarisability is isotropic the depolarisation factor is zero (i.e. $I_h = 0$). High degrees of anisotropy are attained when the polarisability along one particular direction in a molecule is very great compared to the polarisabilities perpendicular to this direction.

The anisotropy parameter for a molecule for the case in which the incident light beam is vertically polarised can be calculated using¹⁴⁷:

$$\delta^2 = \frac{5\Delta}{(3 - 4\Delta)} \quad (7.3)$$

Equation 7.3 is only valid for light scattered by low density gases. For liquids the effect of fluctuations in the number of molecules in an element of volume V has to be considered¹⁴⁷. This is given by

$$(\overline{\Delta v})^2 = RT\beta v^2/NV \quad (7.4)$$

where $(\overline{\Delta v})^2$ is the mean-square deviation from the mean value v , β is the isothermal compressibility. The anisotropy parameter, δ^2 , for a liquids is given by¹⁴⁸

$$\delta^2 = \frac{5RT\beta v\Delta}{(3 - 4\Delta) N_A} \quad (7.5)$$

where v is the volume and $R = 8.314 \text{ JK}^{-1} \text{ mol}^{-1}$, N_A is Avogadro's number. Le Fevre and Rao¹⁴⁹ developed a procedure for determining the anisotropy parameter of a solution, such that equation 7.5 is rewritten for a solution containing a solute mole fraction f_2 of molecular weight M_2 in a solvent of molecular weight M_1 :

$$\delta_{12}^2 = \frac{5RTd_{12}\beta_{12}\Delta_{12}}{(3 - 4\Delta_{12}) M_{12}} \quad (7.6)$$

and

$$M_{12} = M_1 f_1 + M_2 f_2 \quad (7.7)$$

where Δ is the depolarisation ratio of solution, d_{12} is the density and T is the absolute temperature

7.3 Measurement of I_v and I_h

Measurements of the intensity of depolarised light scattered by solutions of the liquid-crystal were carried out using a Dynamic Light Scattering Spectrophotometer (Otsuka DLS-700). The incident light was a He/Ne laser emitting vertically polarised light at a wavelength of 632.8 nm with a power of 5mW.

As the existence of dust in solutions is a major problem in the performing of light scattering measurements, every sample was filtered using a Millipore Fluoropore 0.22mm filter. A 5cm³ glass syringe was used to slowly fill the spectrophotometer cell. The solutions were then checked for dust before depolarisation ratio measurements using the intensity monitor. All dynamic light scattering measurements were taken at a fixed temperature of 25.0°C. The temperature of the spectrophotometer was controlled by circulation of water.

7.4 Results and discussion

In order to minimize scattering from the solvent which could have a high contribution to the depolarisation for very dilute solutions, cyclohexane was chosen as solvent, since this has a very low depolarisation ratio. The depolarisation ratio (Δ_1) of pure cyclohexane measured obtained at 25.0 °C is listed in Table 7.1. The depolarisation ratio value is the average of three separate measurements and each of these was a set of ten measurements made over a short interval of time. The error in the depolarisation ratio is estimated to be better than $\pm 2\%$. The anisotropy factor (δ^2) of the solvent can be calculated using following equation:

$$\delta_1^2 = \frac{5RTd_1\beta_1\Delta_1}{(3 - 4\Delta_1)M_1} \quad (7.8)$$

where M_1 is the molecular weight and d_1 is the density.

Table 7.1 Depolarisation ratio and anisotropy factor for pure cyclohexane at 25 °C.

$\beta_1^*/10^{-10}$ m^2N^{-1}	d_1 kgm^{-3}	M_1 kg	Δ_1 ± 0.0005	δ^2 ± 0.0005
11.40	773.(6)	0.08416	0.024 (7)	0.011 (1)

* β_1 = isothermal compressibility

The values of depolarisation ratio (Δ_{12}) of the dilute solutions of pentyl, hexyl and octyl cyanobiphenyls (5CB, 6CB and 8CB) in cyclohexane were calculated using equation 7.2 at 25.0 °C ($\lambda = 632.8\text{nm}$) and are listed in Table 7.2. Figure 7.2 shows the variations of depolarisation ratio (Δ) of 6CB in cyclohexane for concentrations up to 27%. The concentration dependences of the depolarisation ratio of dilute solutions of the liquid-crystals in cyclohexane are shown in Figure 7.3.

Table 7.2 Rayleigh depolarisation ratios Δ_{12} of solutions of pentyl, hexyl and octyl cyanobiphenyls in cyclohexane at 25.0 °C ($\lambda = 632.8 \text{ nm}$).

5CB		6CB		8CB	
conc. mol/dm^3	Δ_{12}	conc. mol/dm^3	Δ_{12}	conc. mol/dm^3	Δ_{12}
0.2285	0.1019	1.0195	0.1441	0.1460	0.0907
0.1654	0.0920	0.5095	0.1151	0.1051	0.0735
0.1307	0.0871	0.2548	0.1072	0.0762	0.0667
0.1188	0.0849	0.1633	0.0919	0.0467	0.0593
0.0784	0.0690	0.1276	0.0869	0.0320	0.0525
0.0549	0.0577	0.0638	0.0656	0.0144	0.0398
0.0165	0.0401	0.0319	0.0474

It is well known that depolarisation Rayleigh scattering in dense fluids also includes contributions from orientational correlations between solute-solute and solute-solvent molecules¹⁵⁰ However, the solute-solute contributions can be eliminated using either

dilute solutions or by extrapolation to zero concentration when determining depolarisation ratios. The solute-solute contributions can be highly reduced by choosing a solvent such as cyclohexane which has a very low depolarisation ratio.

For dilute solutions of alkyl cyanobiphenyls (5CB, 6CB and 8CB), Δ_{12} increases non-linearly with solute mole fraction, f_2 (Figure 7.3). This effect is a part due to the existence of molecular association even in low concentration of the solutions. Dielectric study and Kerr effect confirm this highly molecular association (anti-parallel correlation) of alkyl cyanobiphenyls in dilute solutions (Chapters 6 and 8). This non-linearity is quite marked for highly concentrated solutions of the alkyl cyanobiphenyls (see Figure 7.2).

The anisotropy factor (δ^2) of a solution containing f_2 mole fraction of solute of molecular weight M_2 in a solvent of molecular weight M_1 can be calculated using

$$\delta_{12}^2 = \frac{5RTd_{12}\beta_{12}\Delta_{12}}{(3 - 4\Delta_{12})M_{12}} \quad (7.6)$$

where

$$M_{12} = M_1f_1 + M_2f_2$$

The isothermal compressibility, β_{12} , of the solutions was assumed to be approximately equal to the isothermal compressibility of the solvent, β_1 . The density data for the liquid-crystal solutions were taken from Chapter 4.

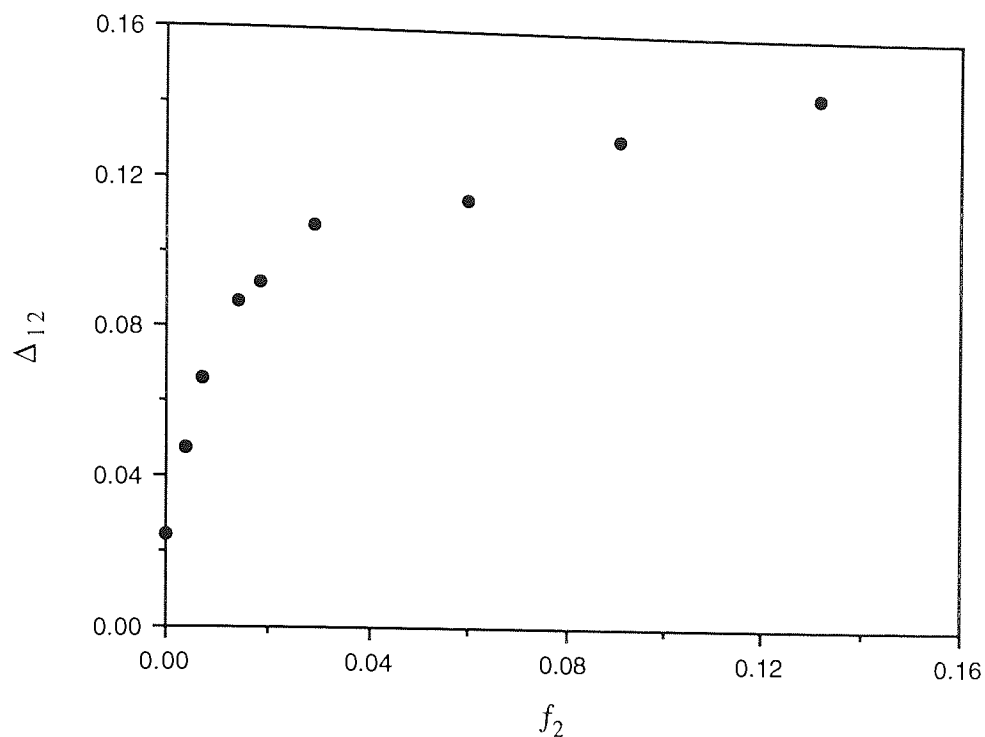


Figure 7.2 Depolarisation ratio, Δ_{12} , for hexyl cyanobiphenyl, 6CB, in cyclohexane plotted as a function of solute mole fraction, f_2 .

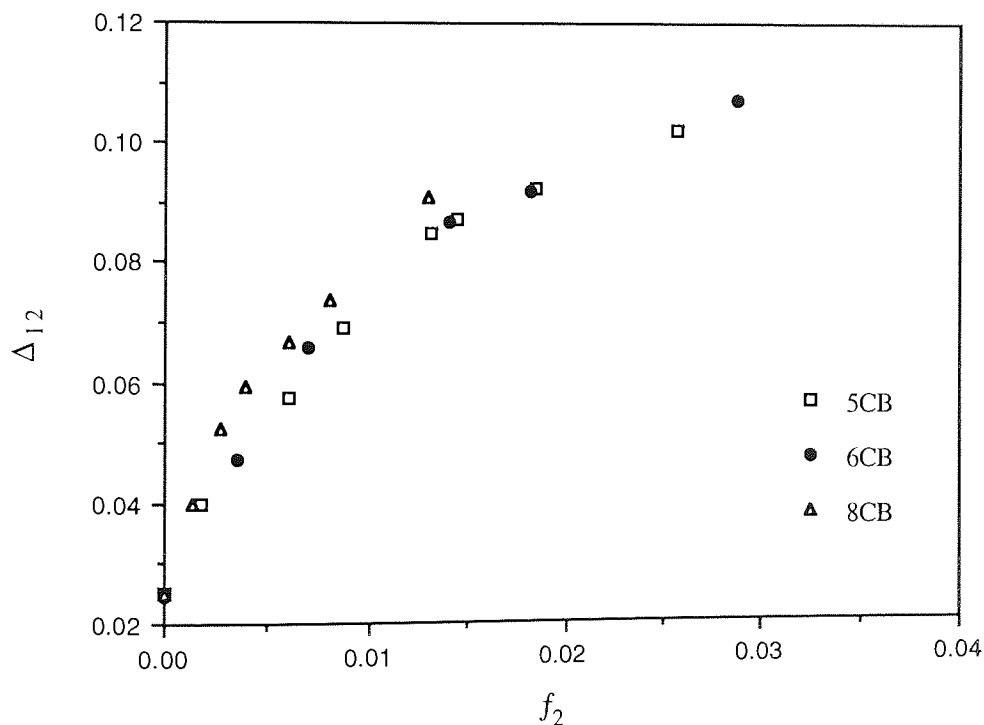


Figure 7.3 Depolarisation ratio for dilute solutions of pentyl, hexyl and octyl cyanobiphenyls in cyclohexane plotted as a function of solute mole fraction, f_2 .

Table 7.3 Anisotropy parameter for alkyl cyanobiphenyls solutions at 25.0°C

5CB		6CB		8CB	
conc. mol/dm ³	δ^2_{12}	conc. mol/dm ³	δ^2_{12}	conc. mol/dm ³	δ^2_{12}
0.2285	0.0494	1.0195	0.0649	0.1460	0.0437
0.1654	0.0443	0.5095	0.0541	0.1051	0.0348
0.1307	0.0415	0.2548	0.0520	0.0762	0.0314
0.1188	0.0407	0.1633	0.0442	0.0467	0.0277
0.0784	0.0325	0.1276	0.0417	0.0320	0.0243
0.0549	0.0288	0.0638	0.0308	0.0144	0.0182
0.0165	0.0178	0.0319	0.0218

CHAPTER 8

THE ELECTRO-OPTICAL KERR EFFECT OF CYANO-BIPHENYL LIQUID-CRYSTALS

8.1 Introduction

The Kerr effect is an electro-optical phenomenon involving the induction of optical birefringence in a fluid by application of an electric field. The electric birefringence of a compound is a property which can give valuable information about the geometrical structure molecules¹⁵¹, conformation analysis^{152,153} and the aggregation of molecules in solution^{154,155}. This applicability arises from the great sensitivity of the electric birefringence to the polarisability ellipsoid and electric dipole moment of the molecules. The magnitude of the Kerr effect is measured by the Kerr constant, B , or by the molar Kerr constant, ${}_mK$. The value of the molar Kerr constant is significant in relation to molecular structure. Le Fevre and Le Fevre^{145,156,157} have established extensive studies of the Kerr effect in solutions.

Electro-optic Kerr effect has been shown to be useful technique in characterising molecular anisotropy and intermolecular ordering in liquid-crystals^{158,159}. In general, the Kerr effect has been used as a means of (1) studying the electric dipole moment of liquids, liquid-crystals and molecules in solution^{63,160}, (2) estimating the chemical structure of such molecules using electrical and optical anisotropy¹⁴⁵, (3) analysing relaxation phenomena¹⁶¹.

In addition, the Kerr effect is particular sensitive to association effects in the liquid-crystal solutions as well as in pure, undiluted nematic and isotropic phases. Beevers and Williams¹⁵⁵ indicated that electro-optical Kerr effect is very sensitive to aggregation of molecules even in dilute solutions. They showed the existence of molecular association

for low concentration of MBBA in carbon tetrachloride using the electro-optical Kerr effect method. Coles¹⁵⁸ indicated extensive molecular association for MBBA in benzene at moderate concentration using the same method.

This electro-optical effect may be used to study pretransitional behaviour, related to order parameter fluctuations, in the isotropic phase of such systems^{162,163,164} by looking at the temperature dependence of their electrical birefringence. In the pre transition region (i.e. in the isotropic phase, but close to the isotropic to nematic transition temperature) the short range order leads to pseudo-nematic domains of highly correlated molecules in the isotropic phase.

Due to the strong permanent dipole moment and highly conjugated π -electron systems along their long molecular axis, alkyl (alkoxy) cyanobiphenyl molecules have extremely large and positive Kerr constant. Measurements of the temperature dependence of the static and dynamic electric Kerr effect in the isotropic phase of alkyl cyanobiphenyl liquid-crystals have been studied by a number of groups^{159,165,166}.

Coles has reported pretransitional behaviour in this group of liquid-crystals. They show deviation from mean-field behaviour close to isotropic nematic transition temperature (i.e. 5CB to 8CB). In later work a good agreement between experimental and mean-field theory for some eutectic mixtures was observed and discussed by Coles et al^{167,168}. Dunmur and Tomes¹⁶⁶ have reported the behaviour of the Kerr constant very close to isotropic nematic transition for pentyl cyanobiphenyl (5CB).

The main aim of this part of the project is to present and discuss electro-optic Kerr results obtained for some alkyl cyanobiphenyls, their nematic mixtures and the eutectic mixture liquid-crystals E7 and E8 in the isotropic phase and solution.

The Landau-de Gennes theory¹⁶⁹ was used to interpret the pre transitional behaviour in the isotropic phase of the liquid-crystals. As mention above, although the static Kerr effect in the isotropic phase of pure alkyl cyanobiphenyls have been studied by a number of researchers, there are still a lot of work to be carried out on mixtures of this family, in order to understand the temperature dependence of the Kerr effect.

The electric birefringence results reported here add to an expanding scientific and technological data base. As far as the author is aware some of these measurements have not been previously reported.

8.2 Theory

8.2.1 Optical anisotropy

The relationship between polarisability and refractive index, discussed in Chapter. 4 (see section 4.2), implies that an anisotropic molecule has a different refractive index along different directions in the molecule. This effect (double refraction) can be observed readily in the crystalline state where molecules are present in an ordered arrangement. Materials that show this effect are called optically anisotropic or birefringent.

Optical anisotropy may also be observed in the isotropic liquid and by molecules in solution through the application of an external electric field. The electric field produce some degree of order or an orientation of the particles in the solution, and the solution acquires the property of a uniaxial crystal with its axis in the direction of the applied field (Figure 8.1). Therefore, the solution becomes anisotropic and exhibit birefringence, i.e. has different refractive indices in different directions.

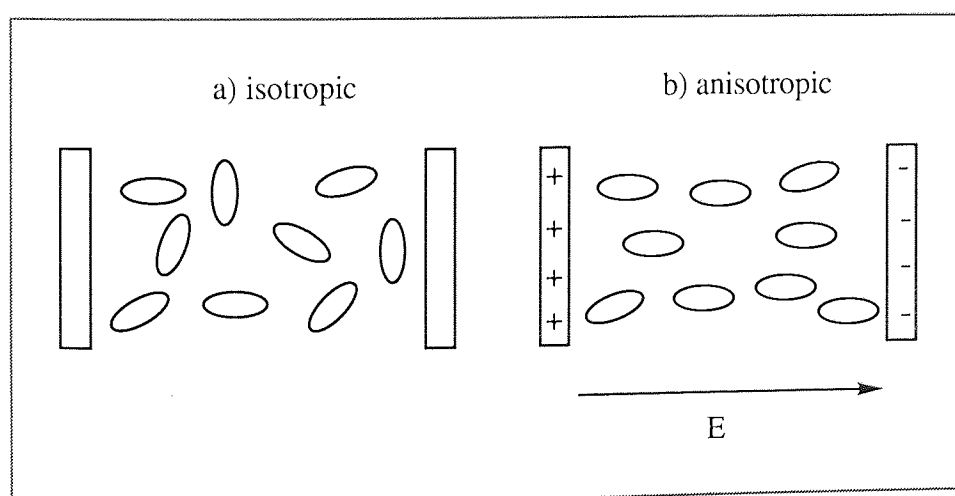


Figure 8.1 Diagrammatic representation of anisotropic molecules in: (a) the absence of an electric field, (b) in an electric field.

8.2.2 The Kerr Effect

The induction of double refraction or birefringence in a fluid by application of an external electric field is known as electro-optical Kerr effect¹⁷⁰. This effect is mainly due to the anisotropy of the polarisability, $\Delta\alpha$, of the molecules directed by the electric field. The electrically induced optical birefringence was first discovered in 1875 by John Kerr, who noticed that birefringence could be induced in glass by the application of a sufficiently intense electric field. Kerr established that the magnitude of this effect is proportional to the square of the applied field strength, E^2 , (Kerr law) and the length L of the optical path through the field. Therefore, the electric birefringence of the medium is defined as the difference between the refractive indices for light polarised parallel and perpendicular to the orienting field direction, and is related to optical retardation or optical phase difference, δ ,

$$\delta = 2\pi BLE^2 = \frac{2\pi L (n_{\parallel} - n_{\perp})}{\lambda} \quad (8.1)$$

where, n_{\parallel} and n_{\perp} are the refractive indices for a light having electric field vectors parallel and perpendicular to the electric field direction, respectively, λ is the wavelength of the incident light beam in vacuum. B is commonly called the "Kerr constant" of the substance, and is often used to denote the magnitude of the Kerr effect.

Another quantity used to express the magnitude of the Kerr effect is called the molar Kerr constant, ${}_mK$. This quantity was introduced by Otterbein¹⁷¹ in analogy with the molar polarisation, P , to express the electrically induced optical birefringence by an additive quantity which is independent of concentration for single compounds. The molar Kerr constant is defined by

$${}_mK = \frac{6\lambda nBM}{(n^2 + 2)^2 (\epsilon + 2)^2 d} = \frac{6nM}{(n^2 + 2)^2 (\epsilon + 2)^2 d} \cdot \frac{n_{\parallel} - n_{\perp}}{E^2} \quad (8.2)$$

where M is the molecular weight, n the refractive index, ϵ the dielectric constant, d the density of medium under examination, and λ is the wave-length of the light used to determine B .

8.2.3 *Kerr effect theory*

In 1910 Langevin¹⁷² assumed that the orientation of a molecule by the induced dipole of a molecule (when it is subjected to an electric field) resulted in an electrostatic and optical anisotropy in the molecule. Born¹⁷³ in 1918 extended this idea to include the effect of an electric field to molecules which possess a possible permanent electric doublet. Therefore for polar molecules both the Langevin and Born suggestions must be considered.

In the presence of an electric field even non-polar molecules will tend to align themselves with the axis of maximum polarisability along the electric field direction with lower polarisabilities perpendicular to the field. In the general case of compounds with permanent dipole moments, the Kerr constant is the resultant of two contributions, one arising from the dipole moment and its orientation with respect to the principal axes of polarisability, the second arising from the anisotropy of the polarisability. The latter is the only term present for non-polar molecules.

The Langevin-Born orientation theory expresses the Kerr constant, B , by the formula

$$B = \frac{\pi N}{27n\lambda} (n^2 + 2)^2 (\epsilon + 2)^2 (\theta_1 + \theta_2) \quad (8.3)$$

where N is the number of molecules cm^{-3} , ϵ the static dielectric constant, θ_1 is the so called anisotropy term, and θ_2 is the so called dipole term. The terms θ_1 , and θ_2 are expanded as

$$\theta_1 = [(a_1 - a_2)(b_1 - b_2) + (a_2 - a_3)(b_2 - b_3) + (a_3 - a_1)(b_3 - b_1)] \left(\frac{1}{45kT} \right) \quad (8.4)$$

$$\theta_2 = [(\mu_1^2 - \mu_2^2)(b_1 - b_2) + (\mu_2^2 - \mu_3^2)(b_2 - b_3) + (\mu_3^2 - \mu_1^2)(b_3 - b_1)] \left(\frac{1}{45k^2T^2} \right) \quad (8.5)$$

Equation 8.4 contain electrostatic polarisabilities (a_1 , a_2 and a_3) and electro-optical polarisabilities (b_1 , b_2 and b_3). Equation 8.5 contain also the dipole moment components (μ_1 , μ_2 and μ_3) along and the principal axes of the molecular polarisability ellipsoid. In 1921 Gans¹⁷⁴ suggested that the electrostatic and electro-optical polarisabilities are related by

$$\frac{a_1}{b_1} = \frac{a_2}{b_2} = \frac{a_3}{b_3} = \frac{(\epsilon - 1)}{(n^2 - 1)} \quad (8.6)$$

Le Fevre and Le Fevre¹⁴⁵ have achieved the same end by assuming

$$a_i/b_i = P_D/P_E \quad (8.8)$$

where P_D and P_E are the distortion and electronic polarisation respectively.

8.2.4 The electro-optic effect in the liquid-crystals

Nematic liquid-crystals behave optically like isotropic liquids at temperatures significantly above the nematic-isotropic transition temperature. The double refraction or birefringence can be induced in the isotropic phase by application of an external electric field. However, as the temperature decreases towards T_{NI} , the induced birefringence of the liquid-crystalline material (with $\Delta n > 0$) increases sharply. In liquid-crystalline materials the applied electric field induces order on the macroscopic rather than the microscopic level and therefore produces some degree of nematic-like ordering (nematic droplet) in the isotropic phase. As the temperature approaches T_{NI} the short-range order grows and

increasingly large droplets (or aggregates) contribute to the Kerr effect, thereby increasing birefringence.

The pretransitional Kerr effect is exhibited by liquid-crystal materials in the isotropic phase at a temperature which is close to the nematic-isotropic transition temperature, and the Theory of Landau-De Gennes¹⁶⁹ has been used to model this pre-transitional behaviour. Only a brief summary of the theory is only presented here. The Helmholtz free energy of a nematic liquid-crystal is given by the Landau expansion (in powers of the nematic order parameter, S):

$$f = f_i + \frac{1}{3} AS^2 - \frac{2}{27} BS^3 + \frac{1}{9} CS^4 \quad (8.9)$$

where f_i is the Helmholtz free energy of the isotropic phase, A , B , C are the Landau expansion terms and all are functions of pressure and temperature. The additional free energy density f_E provided by an electric field is:

$$f_E = -\frac{1}{3} \epsilon_0 \Delta\epsilon_0 S E^2 \quad (8.10)$$

where $\Delta\epsilon_0$ is the low frequency dielectric anisotropy in the completely ordered phase. For the isotropic phase in the presence of an applied electric field, $S \ll 1$ so the high order terms in S can be neglected and minimising f with respect to S gives

$$S = \frac{\epsilon_0 \Delta\epsilon_0 E^2}{2a(T - T^*)} \quad (8.11)$$

where $a = A/(T - T^*)$ is the temperature independent Landau coefficient, T^* is an extrapolated temperature just below the isotropic nematic phase transition. The induced birefringence Δn is given by

$$\Delta n = \frac{\Delta n_0 S}{2\sqrt{\epsilon}} \quad (8.12)$$

where $\bar{\epsilon}$ is the optical permittivity of the isotropic liquid-crystal and Δn_0 is the optical anisotropy in the perfectly aligned phase. Hence from equations 8.11 and 8.12

$$B = \frac{\Delta n}{\lambda E^2} = \frac{\epsilon_0 \Delta n_0 \Delta \epsilon_0}{4a \sqrt{\epsilon} \lambda (T - T^*)} \quad (8.13)$$

From this expression, it is clear that there is a reciprocal relationship between the Kerr constant, B , and temperature is linear, i.e.

$$B \propto (T - T^*)^{-1} \quad (7.14)$$

This relationship has been verified by a number of groups^{158,175,176}. However, close to the phase transition there is a critical region where this relationship (the mean-field approximation) fails^{166,177}.

8.3 Experimental

All measurements of the Kerr constant were made using the nulled intensity method¹⁷⁸, which involves the nulling of an optical response resulting from the application of a short duration rectangular shaped electric field across the Kerr cell.

8.3.1 *Kerr Effect Apparatus*

A diagram of the apparatus used to measure the electrically induced phase difference, δ , is shown in Figure 8.2. All the optical components were mounted on a 2m optical bench enclosed in a light-proof cabinet (Figure 8.3). A brief outline is given below, followed by a detailed description.

The thermostated sample cell was placed between crossed polariser and analyser. The polariser and the analyser were adjusted such that they crossed each other, and their transmission planes made an angle of 45° with respect to the electric field. Using this arrangement, a plain-polarised beam of monochromatic laser light was passed through the Kerr cell polarised at 45° to the direction of the applied pulse electric field, E . The light emerging from the Kerr cell was then passed through a quarter wave retarder, oriented with its principal optic axis at 45° to the direction of the applied field. The light then passed through a second polariser (analyser). The intensity of the light passing through the analyser was detected by a photomultiplier. The output of the photomultiplier was connected to a transient recorder which in turn was connected to an oscilloscope and an Apple II computer. In this way, the Kerr signal can be displayed on the oscilloscope and the computer. The high-voltage electric pulses that cause birefringence in the medium were monitored using a Tektronix high-voltage probe (model P6013A) which attenuated the voltage by a factor of approximation 10^3 . The voltage from the probe could then be measured using a Thurlby (1503-HA) digital multimeter.

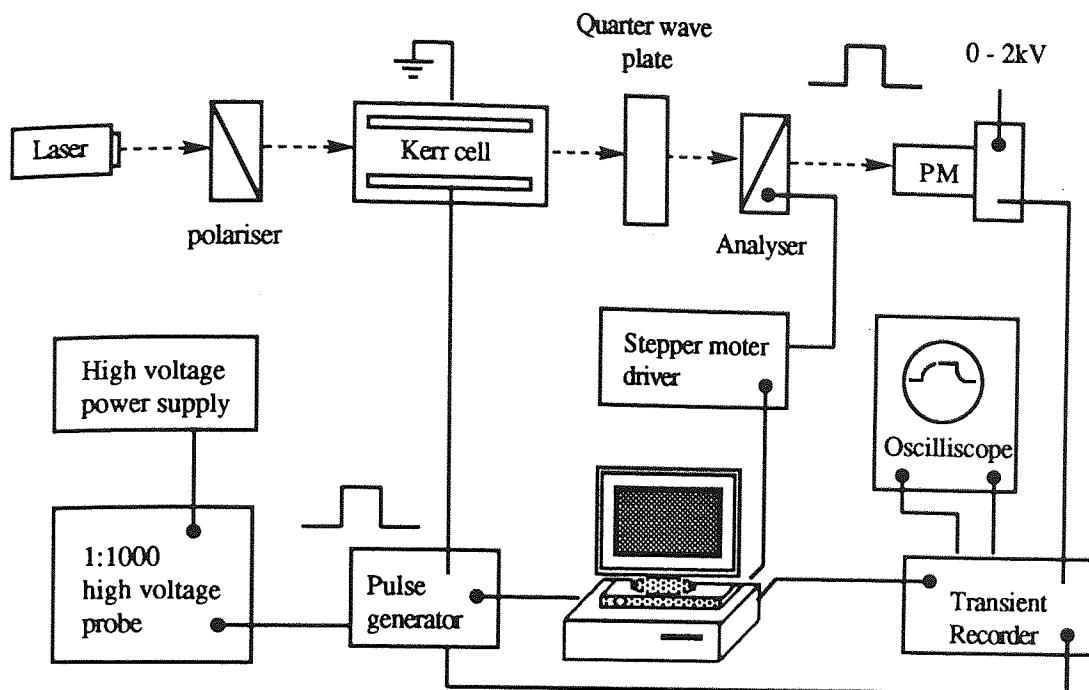


Figure 8.2 The Schematic diagram of the Kerr effect equipment

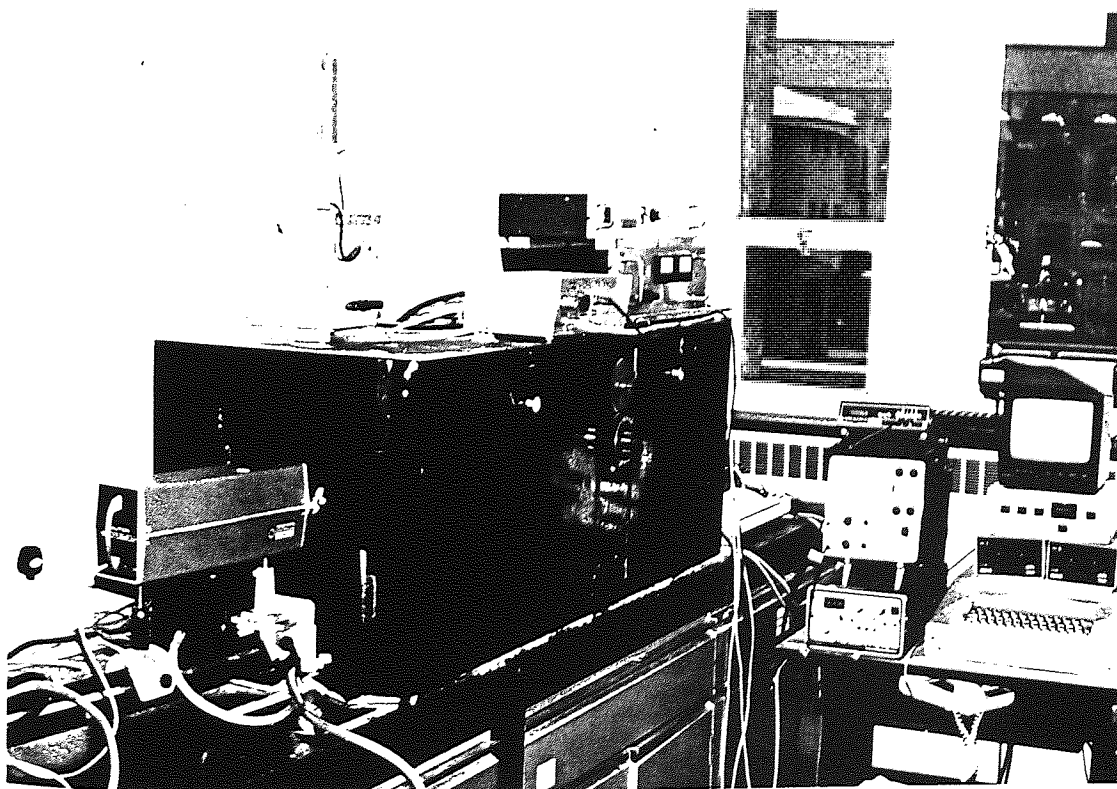


Figure 8.3 The Kerr effect apparatus, the optical bench is enclosed in a totally black-painted cabinet.

8.3.1.1 *Light source*

A Spectra physics He/Ne laser (Scientific and Cook, model SLH/2) emitting at a wavelength of 632.8 nm with a power of 5mW was used as a light source. The degree of polarisation of the light entering the Kerr cell was improved by passing the beam through a high quality polariser. The laser beam was plane polarised and had a diameter of approximately 1mm. The laser was mounted so that the beam of light was directed parallel to the optical bench.

8.3.1.2 *Polariser/Analyser*

The polariser and analyser were Glan-Thompson double refraction type prisms of commercial origin. Each of them was constructed from two calcite prisms glued together and mounted in a hollow brass cylinder. The brass tubes were held in a rotatable graduated circle, which enabled the angle of polarisation, with respect to a reference direction, to be estimated. The angle of polarisation of polariser could be stated with an accuracy of $\pm 0.25^\circ$. The rotatable graduated circle of analyser could be rotated via a set of gears, either manually or by a stepper motor. Each step of the stepper motor was equivalent to moving the analyser through 0.0045 degrees.

8.3.1.3 *Quarter-wave plate retarder*

The quarter wave plate is an optical component introduces a phase shift of 90° between the constituent orthogonal ordinary and extraordinary beam of light (see section 4.2.4). The plate consists of a section cut from a doubly-refracting material, and therefore, there exist two orthogonal direction of propagation that correspond to maximum and minimum refractive indices within the plate. These two directions correspond to slow and fast axes, respectively. The quarter wave plate can convert linear polarised light to elliptically polarised light and vice versa. The elliptically polarised light emerging from the Kerr cell,

therefore, can be converted into plane polarised light by using a quarter wave plate, oriented with its principal optic axis at 45° to the direction of the applied field. the advantages of using a quarter wave plate in the Kerr optical arrangement has been emphasised by several authors (O'Konski and Haltner 1956¹⁶¹, Houssier and Fredericq, 1966¹⁷⁹): It gives a greater sensitivity than without the plate, and it enables the sign of the birefringence to be determined from the sign of the change of light intensity. Also a allows higher accuracy in the measurement of the relaxation times¹⁸³.

The quarter wave plate used in these experiments was mica (F.Wiggins and Sons Ltd.) cut specifically for use at 632.8 nm and mounted between glass discs.

8.3.1.4 Photomultiplier

The detection of the Kerr signal was achieved using a photomultiplier tube, type E. M. I. 9816B. The photo multiplier was mounted in a brass tube that had a 20 mm aperture near the window of the photo multiplier. Interference from stray light was minimised by the addition of a collimating aluminium barrel, 80 mm long, with a 2mm diameter aperture place in front of aperture. The photomultiplier output could be adjusted by two rotary switches that vary the resistance and capacitance of the output circuit. A photomultiplier power supply 0-2kV (a Brandenburg model 472B generator) and a resistor chain were used to provide the required dipole voltages. Great care must be taken to avoid saturation of the photomultiplier tube during the measurement of the intensity of the light falling on the photo multiplier. A constant voltage of about 1kV was used to avoid saturation of the photomultiplier.

8.3.1.5 Signal display and recording

The optical signal from the photo multiplier was displayed using a Tektronix 465B oscilloscope and an Apple II computer. Since the maximum permitted voltage at the input

terminals of the oscilloscope was 10V, the high-voltage electric pulses were monitored using a Tektronix high-voltage probe (model P6013A) which attenuated the voltage by a factor of 10^3 .

Optical transients were recorder using a Datalab model DL905 transient recorder. The captured signal was displayed continuously on the oscilloscope which was set in the X,Y mode, the two channels acting as the X, Y inputs. a permanent copy of the optical signal was obtained using an Advance X,Y plotter model HR-96.

8.3.1.6 The high voltage power supply

The electric field is generated by means of a high-voltage power supply that was applied, as a short duration rectangular shaped pulse from a pulse generator, to the electrodes of the Kerr cell. A Wallis (Worthing) model S103/3 power pack was used as a high voltage power supply. The maximum d.c. voltage that the high-voltage was capable of producing was 10 kV. The voltage applied to Kerr cell was measured on a Thurlby digital multiplier (Model 1503-HA). The complete description of the circuit used to provide short duration electric field pulses can be found in references^{184,185}.

8.3.2 The Kerr cell

For the electro-optical studies of liquid-crystal compounds in the isotropic phase and solution, two different types of electro-optical Kerr cells have been used in the experiments. In order to perform accurate electro-optical measurements, the Kerr cell should possess good optical stability, good temperature stability, and should be easy to fill and empty. In addition, there should be little or no strain birefringence in the windows, the cell should have sufficiently long optical path length, and the sample volume should as small as possible. Two Kerr cells employed in these studies, Kerr cell A and Kerr cell B.

Kerr cell A (spectrophotometer cuvette-type cell) was suitable for measurements on small volume of bulk samples (about 1 cm³). This cell was used in the electro-optical investigation of the isotropic phase of liquid crystals. Kerr cell B (long optical path length, see below) was convenient for measurements on the large amount of solutions (approximately 25 cm³), and was used only for measurements on dilute solutions.

8.3.2.1 *The spectrophotometer cuvette-type cell*

For the electro-optical investigation in the isotropic phase, a sample holder similar to that described by O'Konski and Haltner¹⁶¹ was constructed (Figure 8.4). The sample holder was a quartz spectrophotometer cell with a path length of 10 mm. An optical-grade cell was chosen so that no strain birefringence in the windows observed. The stainless steel electrodes were inserted into the Kerr cell, leaving an active column of liquid 1.8 x 2 x 10 mm.

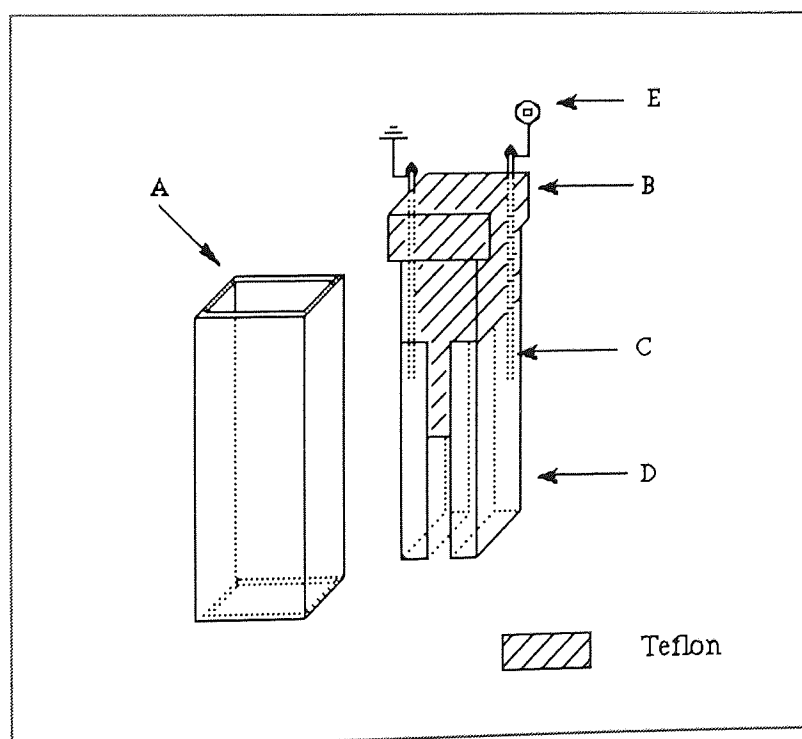


Figure 8.4 Construction of Kerr cell A, A) sample cell, B) the cell cap, C) metallic screw, D) the stainless-steel electrode, E) electrode connection

A Teflon spacer was used to provide insulation between the electrodes and to maintain an electrode gap of 1.8 mm. The Kerr cell was sealed by Teflon tape during the measurements in order to prevent evaporation. The cleaning, filling and emptying of the Kerr cell was very easy and prevented contamination of the liquid-crystals. The lower part of the Kerr cell fitted into a thermostated metal jacket, which was cut away to allow passage of the light beam.

The temperatures were determined with a copper-constantan thermocouple in contact with the glass cell. Temperature differences of the order 0.5-1.5°C were noted between the transition temperature as observed in the Kerr cell and when measured on a microscope hot stage. For this reason, the Kerr cell was calibrated to obtain a correction factor for the temperature. A plot of liquid temperatures against measured cell temperatures is shown in Figure 8.5.

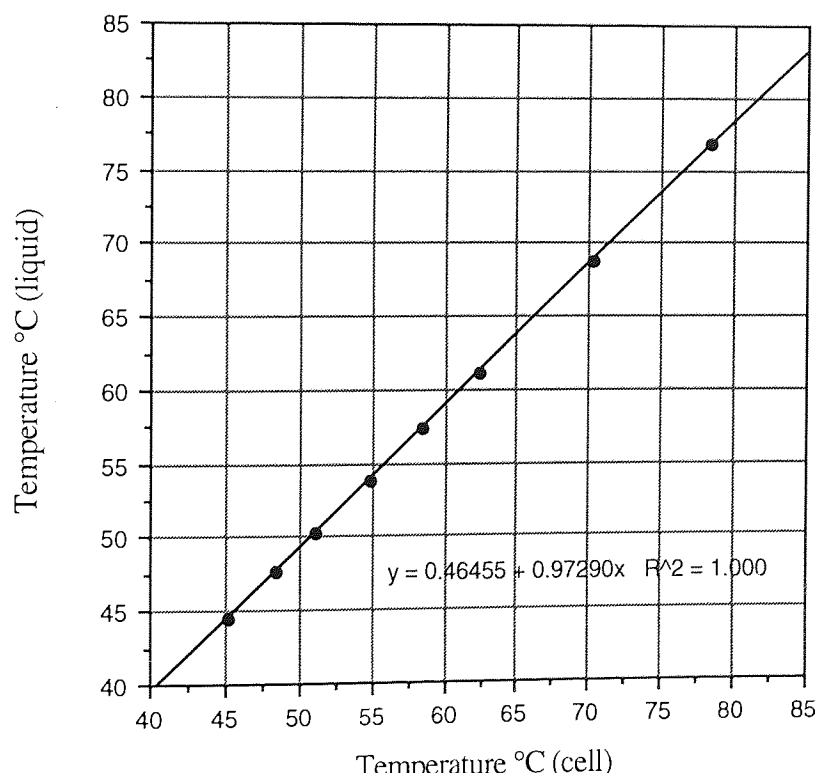
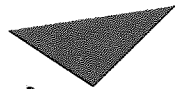


Figure 8.5 The calibration plot obtained for correction of the Kerr cell temperatures.

8.3.2.3 *The long-path-length Kerr cell B*

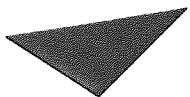
A detailed description of the long-path-length Kerr cell B (Figure 8.6) is given Ref. 148. The Kerr cell consists of two tubes (one of glass and the other Perspex). The glass tube is placed inside the Perspex tube. Two Teflon end caps hold the tubes in place. Each Teflon end cap has a hole drilled through its' center over which is placed a high quality optical quartz disk (window). A metal frame ensures a positive pressure between the glass tube and the Teflon by compressing the whole arrangement together. A silicon based sealant creates a seal between the Perspex tube and the Teflon end cap. The stainless-steel electrodes (highly polished) are placed into the inner chamber by four glass pegs and four spring loaded plungers. Two connections to the outer chamber make it possible to pass water from a water-bath through the outer chamber. A thermocouple allowed the temperature of the inner chamber to be measured to $\pm 0.1^{\circ}\text{C}$.



Aston University

Illustration has been removed for
copyright restrictions

Figure 8.6 Top-view diagram of Kerr cell



Aston University

**Illustration has been removed for copyright
restrictions**

8.3.4 The nulled-pulse technique

The electric birefringence of a sample can be measured using the nulled-pulse technique¹⁷⁸, which involves the “nulling” of an optical response resulting from the application of a short duration, rectangular-shaped electric pulse, to the sample. The pulse duration must be adjusted to be sufficiently long to obtain maximum orientation of the molecules at a given field strength but sufficiently short to prevent or minimise electrolysis or electrode polarisation. The higher the field, the shorter is the time required to reach the orientation equilibrium.

The pulse technique^{178,180} has the following advantages: (1) it is applicable to almost any type of solution or liquid, (2) The method is very fast, (3) it reduces the effect of conductivity, electrode polarisation and heating that accompany the application of continuous electric field and (4) it allows the study of relaxation phenomena. The practical optical arrangement for the nulled-pulse technique is as follows:

The axis of polarisation of polariser and the slow axis of the quarter-wave plate are set at 45° with respect to the direction of the applied electric field. The polariser and the analyser are initially adjusted while crossed (i.e. $\alpha = 0$), so as to make an angle 45° with respect to the Kerr cell electrode (Figure 8.7). In the absence of the electric field, $E = 0$, the light remains unaffected by the Kerr cell and the quarter-wave retarder. The light arriving on the analyser is still polarised at 45° to the Kerr cell electrode, and therefore no light emerges from the analyser to the photomultiplier detector.

When a potential difference is applied across the electrodes of the Kerr cell, the sample of the Kerr cell becomes anisotropic and birefringence results. A plane polarised light beam (polarised at 45° to the applied field) can be considered to be comprised of components, E_x and E_y , parallel and perpendicular to the applied electric field direction, respectively. Therefore, when the electric vector passes through the short axis of the molecules it will

be retarded less than when passing through the long molecular axis thereby resulting in a partial rotation of the plane of polarisation of the plane polarised light. Hence, a phase difference, δ , is introduced between the parallel and perpendicular vector components of the light beam. The phase retardation, δ , results in the light emerging from the cell being elliptically polarised.

The quarter-wave retarder converts this elliptically polarised light into plane polarised light that is rotated by an angle, α with respect to the incident light on the Kerr cell. The light emerging from the quarter-wave retarder can then be extinguished by rotating the analyser by an angle α from the crossed position. The quarter-wave plate between the Kerr cell and the analyser enables a distinction to be made between positive and negative birefringences.

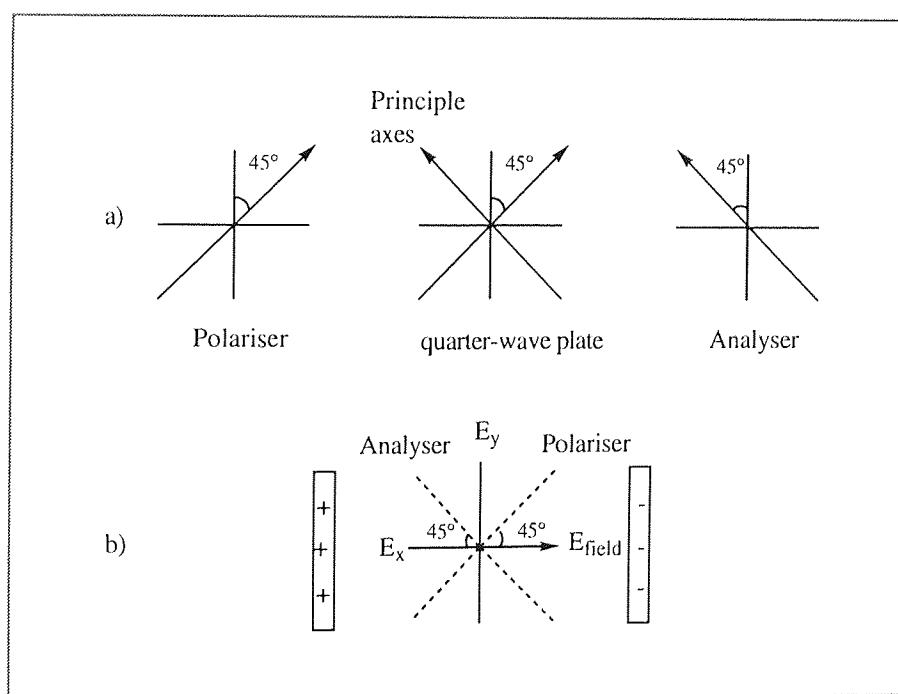


Figure 8.7 Relative orientational setting of, a) the optical components, b) electric vectors components of light, E_x and E_y , which are parallel and perpendicular to the applied electric field direction, respectively.

In the absence of the applied electric field, The intensity of the light detected by the photomultiplier is given by

$$I = I_0 \sin^2 \alpha \quad (8.15)$$

where α is the rotation of the analyser with respect to the nulled condition and I_0 is the maximum intensity of the probe beam when the polariser and analyser are completely uncrossed. On application of an electric field, the intensity of the light falling on the photomultiplier when the medium becomes birefringent, is given by

$$I = I_0 \sin^2 (\alpha + \delta/2) \quad (8.16)$$

A optical response resulting from the application a short duration rectangular electric field is shown in Figure 8.8.a. The analyser is then gradually rotated by an angle α from its normally crossed position to a final position or nulled point. The nulled point is achieved when the levels of light transmitted by the analyser are equal to each other, i.e. $I_{E=0} = I_{E>0}$ (Figure 8.8.d). For this condition the relationship between the angular rotation of the analyser required to null the optical signal, and the phase retardation, δ , may be shown to be

$$\alpha = \frac{\delta}{4} \quad (8.17)$$

The Kerr constant B can then be readily calculated from the phase difference δ , using

$$\delta = 2\pi L B E^2 \quad (8.18)$$

where L is the distance between electrodes and E the electric field strength. This method requires exact an accurate determination of the electrode length and voltage applied. Errors can also be introduced due to the field effects at the end of the electrodes.

Therefore, the Kerr cell was previously calibrated with a liquid of known Kerr constant, B_s to give a graph of α_1 vs. V^2 for the standard liquid and a gradient of m_s . The Kerr constant, B_x , of the unknown liquid is then found from

$$B_x = \frac{m_x}{m_s} B_s \quad (8.19)$$

where m_x is the gradient obtained from a graph of α vs. V^2 for the unknown liquid.

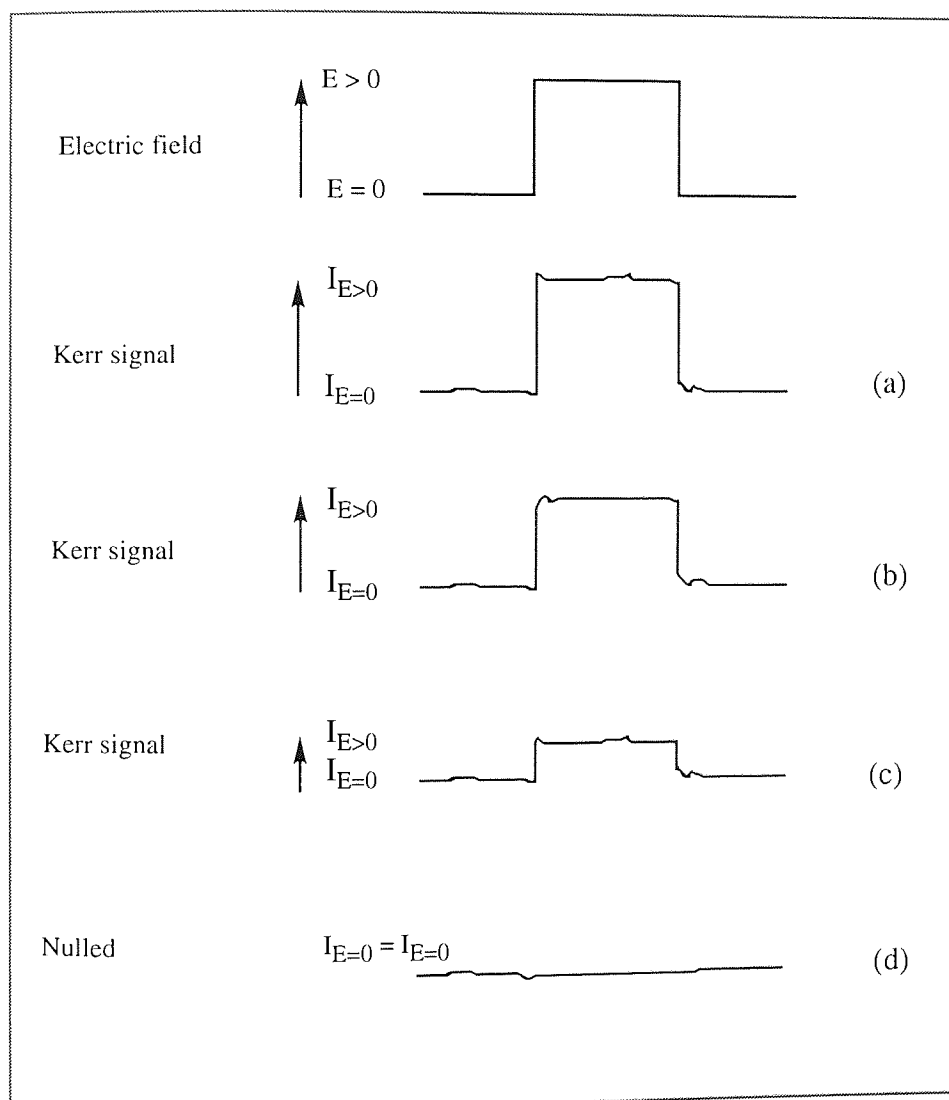


Figure 8.8 Schematic diagram of typical optical pulse recorded during the pulse nulling procedure.

8.4 Results

8.4.1 Kerr Effect Measurements on Dilute Solution

The large volume Kerr cell B was calibrated with a standard liquid of known Kerr constant, B_s , (HPLC grade toluene) at 25 °C and 632.8 nm. The graph of α (analyser rotation) vs. V^2 (the square of the applied voltage) for the standard liquid gave a gradient of 5.562×10^{-2} , as determined over a voltage range 2 - 4.5 kV ($\lambda = 632.8\text{nm}$) (see Table 8.1).

Table 8.1 The measured phase-difference, δ , induced at several voltages for toluene and cyclohexane at 25°C ($\pm 1^\circ\text{C}$).

Toluene (standard)		Cyclohexane (solvent)	
Voltage /kV	$\delta = 4\alpha$ /degree	Voltage /kV	$\delta = 4\alpha$ /degree
2.0	0.676	4.0	0.196
2.5	1.160	5.0	0.344
3.0	1.824	6.0	0.524
3.5	2.500	7.0	0.740
4.0	3.368	7.5	0.856
4.5	4.284	8.0	0.976

Taking the literature value for the Kerr constant of toluene¹⁸¹ at 25 °C to be 0.81×10^{-14} mV⁻², and the Kerr gradient to be m_x for the solutions, the Kerr constant of the solutions can be calculated using

$$B_x = \frac{0.81 \times 10^{-14}}{5.562 \times 10^{-2}} \times m_x \quad (8.20)$$

The gradient of the plot of α vs. V^2 for the solvent (HPLC grade cyclohexane, Aldrich) was determined to be 4.08×10^{-3} . A Kerr constant of 5.942×10^{-16} for cyclohexane was

resulted using equation 8.20. The gradients of pentyl, hexyl and octyl cyanobiphenyls (5CB, 6CB, and 8CB) in cyclohexane were also determined from the plots of α against the square of applied voltage for the different weight fractions of liquid crystals, w_2 . This is illustrated for the dilute solutions of 5CB in cyclohexane in Figure 8.9. All plots were found to be linear in the voltage-range 0-4 kV used here, and the same was found for 6CB and 8CB solutions. The Kerr constants, B_{12} , of the dilute solutions of the liquid-crystals were calculated using equation 8.20 at 25.0 °C ($\lambda = 632.8\text{nm}$) and are listed in Table 8.2. For all cases the sign of B_{12} is positive. The error in the Kerr constant measurements is approximately $\pm 1\%$. All solutions, solvent and standard liquid were filtered using a 0.22 μm Millipore Fluoropore filter. The temperature of the Kerr cell was controlled by circulation of water through a jacket surrounding the cell and was measured to an accuracy of $\pm 0.1^\circ\text{C}$.

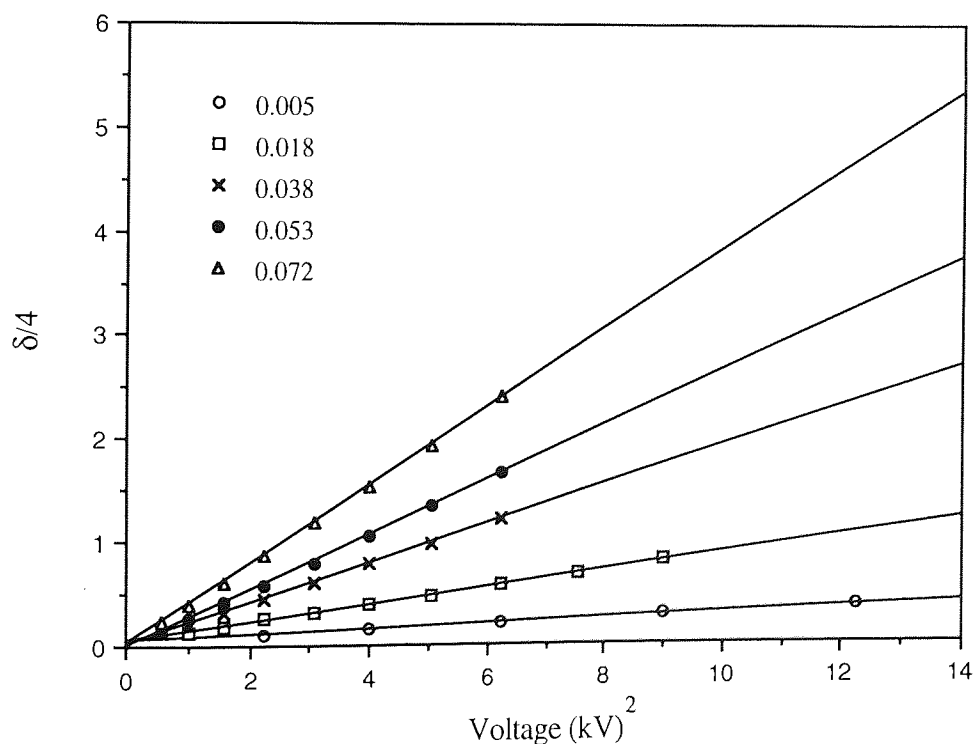


Figure 8.9 The measured phase-difference, δ , against the square of applied voltage for the different weight fractions, w_2 , of the solutions of 5CB in cyclohexane at 25°C.

Table 8.2 Experimental Kerr constants B_{12} , of solutions of pentyl, hexyl and octyl cyanobiphenyls in cyclohexane at 25 °C ($\lambda = 632.8$ nm).

5CB		6CB		8CB	
w_2	$10^{14}B_{12}$ /mV ⁻²	w_2	$10^{14}B_{12}$ /mV ⁻²	w_2	$10^{14}B_{12}$ /mV ⁻²
0.072	5.53	0.061	5.22	0.076	5.32
0.053	3.91	0.050	4.02	0.054	3.75
0.038	2.80	0.036	2.78	0.039	2.54
0.025	1.79	0.028	2.15	0.028	1.96
0.018	1.19	0.020	1.46	0.018	1.20
0.010	0.71	0.012	0.87	0.012	0.77
0.005	0.36	0.000	0.06	0.005	0.39

For dilute solutions of alkyl cyanobiphenyls (5CB, 6CB and 8CB), B_{12} increases non-linearly with solute weight fraction, w_2 (Figure 8.10). This effect is due to the existence of molecular association even at low concentration of solute. Dielectric studies confirm this high molecular association (anti-parallel correlation) of alkyl cyanobiphenyls in dilute solutions (see Chapter 6). The existence of molecular association in dilute solutions of a liquid-crystal such as MBBA had been reported by Beevers and Williams¹⁵⁵ using the electro-optical Kerr effect method. Also, Coles¹⁵⁸ showed extensive molecular association for MBBA at moderate concentrations using the same method.

The origin of such behaviour (association) in the alkyl cyanobiphenyls is due to the several factors (see Chapter 6), but is mainly due to the strong polar group, i.e. CN. However, van der Waal's interactions involving the flexible alkyl tail, the biphenyl core, and solvent molecules are also important.

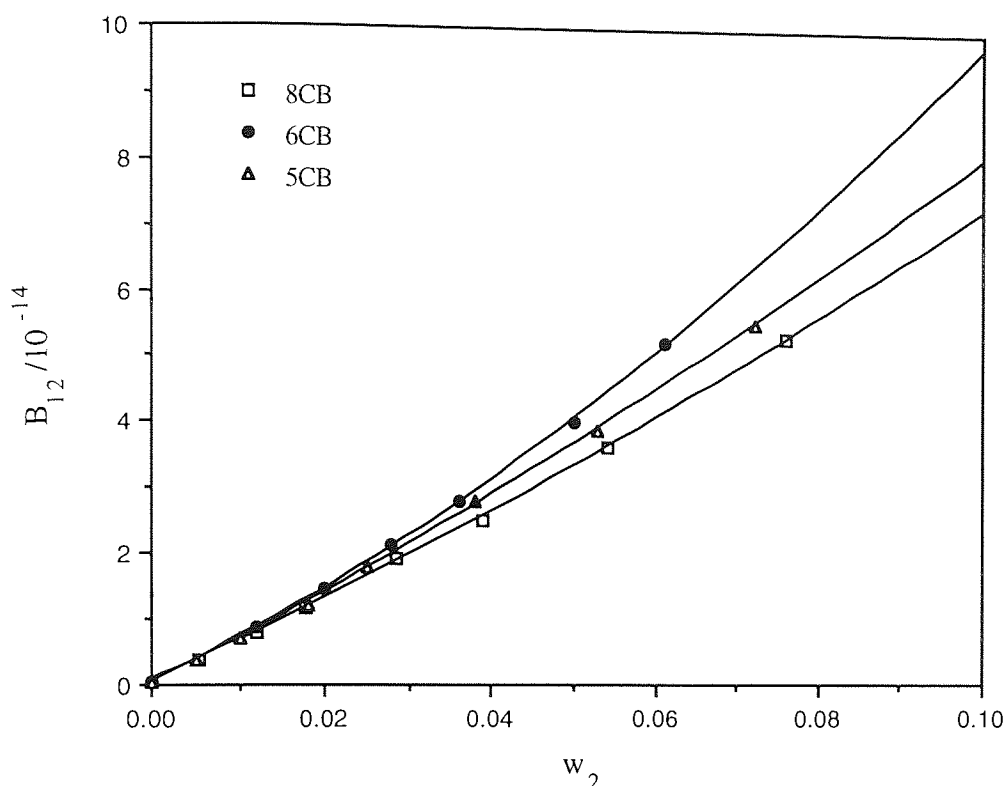


Figure 8.10 Kerr constants B_{12} , of solutions of alkyl cyanobiphenyls in cyclohexane at 25 °C ($\lambda = 632.8$ nm).

8.4.2.1 Calculation of molar Kerr constants

The molar Kerr constant, ${}_mK_{12}$, of the liquid-crystal solutions may be obtained from Kerr constants using the relationship

$${}_mK_{12} = \frac{6\lambda n_{12} B_{12} M_{12}}{(n_{12}^2 + 2)^2 (\epsilon_{12} + 2)^2 d_{12}} \quad (8.21)$$

where B_{12} , ϵ_{12} , n_{12} , M_{12} and d_{12} are the Kerr constant, dielectric permittivity, refractive index, molecular weight and density of the solution, respectively. The molar Kerr constant of the solvent is given by

$${}_mK_1 = \frac{6\lambda n_1 B_1 M_1}{(n_1^2 + 2)^2 (\epsilon_1 + 2)^2 d_1} \quad (7.22)$$

where B_1 , ϵ_1 , n_1 , M_1 and d_1 are the Kerr constant, dielectric permittivity, refractive index, molecular weight and density of the solvent, respectively. The molar Kerr constant of cyclohexane (solvent) and the other physical properties of cyclohexane obtained at 25°C that were used to calculate its molar Kerr constant are given in Table 8.3. The error in the molar Kerr constant is estimated to be less than $\pm 2\%$.

The molar Kerr constants of a solute, ${}_mK_2$, can be calculated using:

$${}_mK_{12} = {}_mK_1 f_1 + {}_mK_2 f_2 \quad (8.23)$$

where f_1 and f_2 are mole fractions of solvent and solute respectively. From equation 8.2 and 8.3 the molar Kerr constant follows as

$${}_mK_2 = \frac{2\pi N}{9} (\theta_1 + \theta_2) \quad (8.24)$$

Therefore, the molar Kerr constant of the solute in the dilute solution can be resolved into a term θ_2 (dipole term) involving the permanent dipole moment and an induced term θ_1 (anisotropy term) involving only induced dipole moments (see Section 8.2.3). For alkyl cyanobiphenyls for which there is usually a large permanent dipole moment $\theta_2 \geq \theta_1$

Table 8.3 Kerr constant, B_1 , dielectric permittivity, ϵ_1 , refractive index, n_1 , and density, d_1 , of cyclohexane obtained at 25.0 °C ($\pm 0.1^\circ\text{C}$).

Sample	ϵ_1	n_1	d_1 g cm^{-3}	$B_1 / 10^{-14}$ mV^{-2}	${}_mK_1 / 10^{-26}$ $(\text{m}^5 \text{V}^{-2} \text{mol}^{-1})$
cyclohexane	2.02 (0)	1.423 (5)	0.7736 (2)	0.06 (0)	0.13 (4)

Table 8.4 Molar Kerr constant, ${}_mK_{12}$, Kerr constant, B_{12} , dielectric permittivity, ϵ_{12} , refractive index, n_{12} , and density, d_{12} , of solutions of 5CB in cyclohexane obtained at 25.0 °C ($\pm 0.1^\circ\text{C}$).

w_2	ϵ_{12}	n_{12}	d_{12} g cm^{-3}	$B_{12} / 10^{-14}$ mV^{-2}	${}_mK_{12} / 10^{-26}$ $(\text{m}^5\text{V}^{-2}\text{mol}^{-1})$
0.072	2.584	1.4332	0.7865	5.53	9.79
0.053	2.431	1.4298	0.7820	3.91	7.35
0.038	2.318	1.4281	0.7796	2.80	5.46
0.025	2.196	1.4265	0.7773	1.79	3.72
0.018	2.151	1.4254	0.7760	1.19	2.53
0.010	2.091	1.4246	0.7748	0.71	1.54
0.005	2.050	1.4236	0.7742	0.36	0.80

Table 8.5 Molar Kerr constant, ${}_mK_{12}$, Kerr constant, B_{12} , dielectric permittivity, ϵ_{12} , refractive index, n_{12} , and density, d_{12} , of solutions of 6CB in cyclohexane obtained at 25.0 °C ($\pm 0.1^\circ\text{C}$).

w_2	ϵ_{12}	n_{12}	d_{12} g cm^{-3}	$B_{12} / 10^{-14}$ mV^{-2}	${}_mK_{12} / 10^{-26}$ $(\text{m}^5\text{V}^{-2}\text{mol}^{-1})$
0.085	2.674	1.4340	0.7886	7.59	14.48
0.061	2.490	1.4311	0.7846	5.22	9.61
0.050	2.405	1.4298	0.7828	4.02	7.65
0.036	2.301	1.4280	0.7804	2.78	5.53
0.028	2.237	1.4270	0.7788	2.15	4.39
0.020	2.176	1.4259	0.7774	1.46	3.06
0.012	2.112	1.4248	0.7759	0.87	1.87

8.4.2 Kerr Effect Measurements of the Isotropic Phase

The electrically induced birefringence, Δn , of pentyl cyanobiphenyls (5CB), two of pentyl and heptyl mixtures, (i.e. F1 [71% : 29%] and F2 [51% : 49%]), and two eutectic mixtures E7 and E8 in the isotropic phase was calculated using the equation 8.1.

$$\Delta n = \frac{\delta \lambda}{2\pi L}$$

where δ is the electrically induced phase difference between the components of plane polarised light possessing electric vectors parallel and perpendicular to the applied electric field, λ is the wavelength of the incident light beam in vacuo (632.8 nm), and L is the optical path length between the electrodes (1.8 mm). The bulk of the experimental results namely optical phase retardation, δ measured at different temperatures, are given in Appendix D. The electrically induced birefringence, Δn , is also related to the Kerr constant in the following way (Equation 8.1):

$$\Delta n = \lambda B E^2$$

According to the above equation, the Kerr constant, B , of a material, at a given temperature may be obtained from the gradient of a graph of induced birefringence, Δn , plotted against the square of applied electric field, E^2 . This is illustrated for the nematic mixture F1 comprised of pentyl and heptyl cyanobiphenyls (71% : 29%) in Figure 8.11. The Kerr constants of the samples measured at different temperatures are given in Tables 8.10-8.12. For each of the materials the electrically-induced birefringence was found to be a linear function of the square of the applied electric field, E^2 . For the voltage range, used in this study ($E = 0$ to $E = 1.7 \times 10^5 \text{ Vm}^{-1}$), no saturation of the photomultiplier were detected. In all cases the Kerr law was observed ($\Delta n \propto E^2$). The electro-optical data show that Kerr effect is positive in all cases ($\Delta n > 0$). The same trend has been reported by Coles¹⁵⁹ for the pure alkyl cyanobiphenyls (5CB, 6CB, 7CB and 8CB).

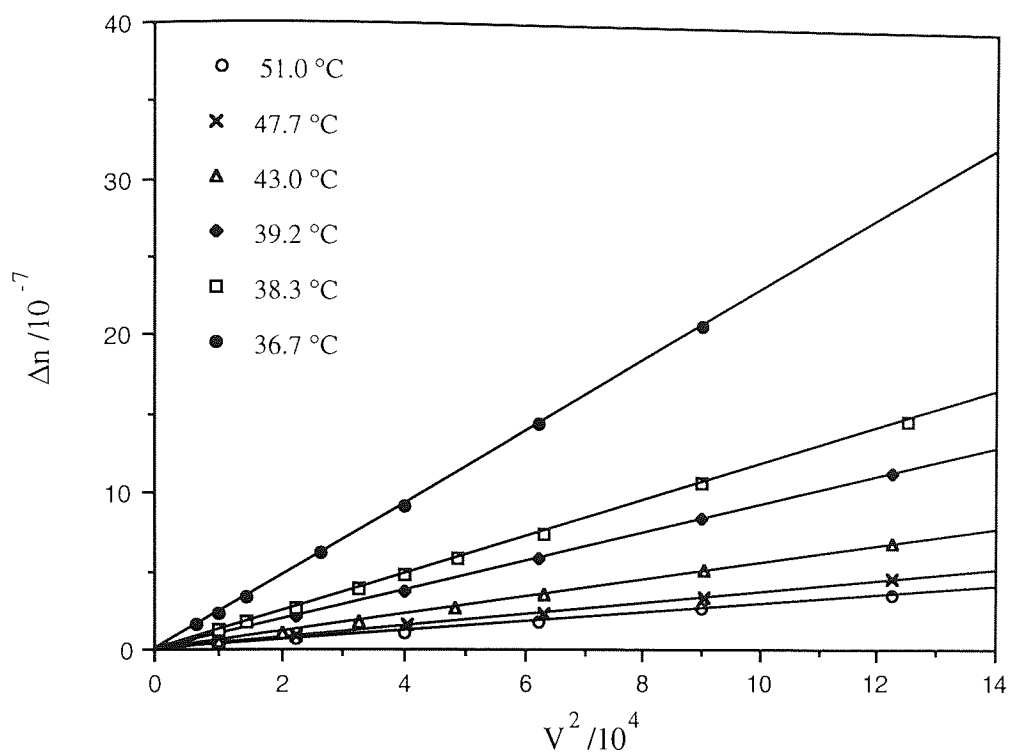


Figure 8.11 Induced birefringence, Δn , as a function of applied field, E , for pentyl and heptyl cyanobiphenyls mixtures F1 (71: 29), at the several temperatures.

Table 8.10 Kerr constants, B , of 5CB for $\lambda = 632.8$ nm

5CB	
Temperature °C	$10^{11}B$ /mV ⁻²
35.6	11.22
35.7	10.20
35.8	9.59
35.9	9.11
38.4	4.40
40.8	3.14
43.8	2.18
44.8	1.97
47.5	1.58

Table 8.11 Kerr constants, B, of F1 and F2 for $\lambda = 632.8$ nm

F1		F2	
Temperature °C	$10^{11}B$ /mV ⁻²	Temperature °C	$10^{11}B$ /mV ⁻²
36.5	11.86	38.2	15.40
36.8	10.47	38.4	12.40
38.1	6.08	38.6	10.99
39.0	4.78	38.7	6.75
40.8	3.58	39.6	5.50
42.5	2.86	42.2	3.56
44.2	2.28	42.6	3.31
46.5	1.86	44.1	2.59
48.0	1.61	45.1	2.26
59.5	1.46	46.9	1.98
---	---	47.6	1.79
---	---	48.9	1.59
---	---	49.9	1.47

Table 8.12 Kerr constants, B, of E7 and E8 for $\lambda = 632.8$ nm

E7		E8	
Temperature °C	$10^{11}B$ /mV ⁻²	Temperature °C	$10^{11}B$ /mV ⁻²
60.6	12.25	72.4	9.05
61.2	8.79	72.6	8.32
62.2	6.04	72.8	7.92
62.6	5.58	73.7	6.04
63.0	5.08	74.3	5.27
64.2	4.11	74.7	4.82
67.2	2.62	76.6	3.50
68.0	2.44	78.7	2.69

The dependence of the Kerr constant, B , on temperature for 5CB and for the mixtures F1 (71% 5CB, 29% 7CB) and F2 (51% 5CB, 49% 7CB) are shown in Figure 8.12. This data shows that, the birefringence depends strongly on temperature. The temperature dependence of the induced birefringence increases with decreasing temperature as the nematic transition temperature is approached. The Kerr constant, B , of these liquid-crystalline materials is found to be very high at the nematic-isotropic transition temperatures as the molecules are expected to be highly ordered close to phase transition temperatures. The Kerr constant tends to infinity as the hypothetical temperature or second-order isotropic-nematic transition temperature, T^* , is approached.

The pre-translational Kerr effect is exhibited by liquid-crystal materials that are in their isotropic phase at a temperature that is close to the nematic-isotropic transition temperature. The Theory of Landau-De Gennes¹⁶⁹ has often been used successfully to describe the pre-translational behaviour in the isotropic phase of liquid-crystals. This theory is essentially based on the assumption that short-range forces predominate in the region of the nematic-isotropic transition. According to the Landau-De Gennes model the birefringence (Δn) in the isotropic phase is

$$\Delta n \propto (T - T^*)^{-\gamma}$$

where T^* is the second-order pre-translational temperature, which is slightly less than T_{NI} (i.e. $T_{NI} - T^*$ is typically about 1°C), and γ is a numerical factor that equals unity in a mean-field theory such as the Maier-Saupe theory¹⁵. The linear dependence of $(T - T^*)^{-1}$ on the Kerr constant has been discussed in detail elsewhere. The temperature T^* can be obtained by a linear extrapolation of either the inverse of the birefringence (Δn^{-1}) or the inverse of the Kerr constant (B^{-1}) vs. temperature.

The variation of B^{-1} with temperature for nematic mixtures F1, F2, E7, E8 and 5CB is shown in Figures 8.13-8.15. For all of the samples studied the graphs of B^{-1} vs. T are

linear over the temperature range $T_{\text{NI}} + 2 < T < T_{\text{NI}} + 20^\circ\text{C}$. However, close to the transition temperature $T_{\text{NI}} < T < T_{\text{NI}} + 2^\circ\text{C}$, a systematic deviation from the mean-field theory is usually observed¹⁷⁷. The pretransitional behaviour and small deviations from mean-field theory, at temperatures close to T_{NI} , for alkyl cyanobiphenyls have been observed and discussed by Coles et al¹⁵⁹, and later by Dunmur and Tomes¹⁶⁶ for 5CB.

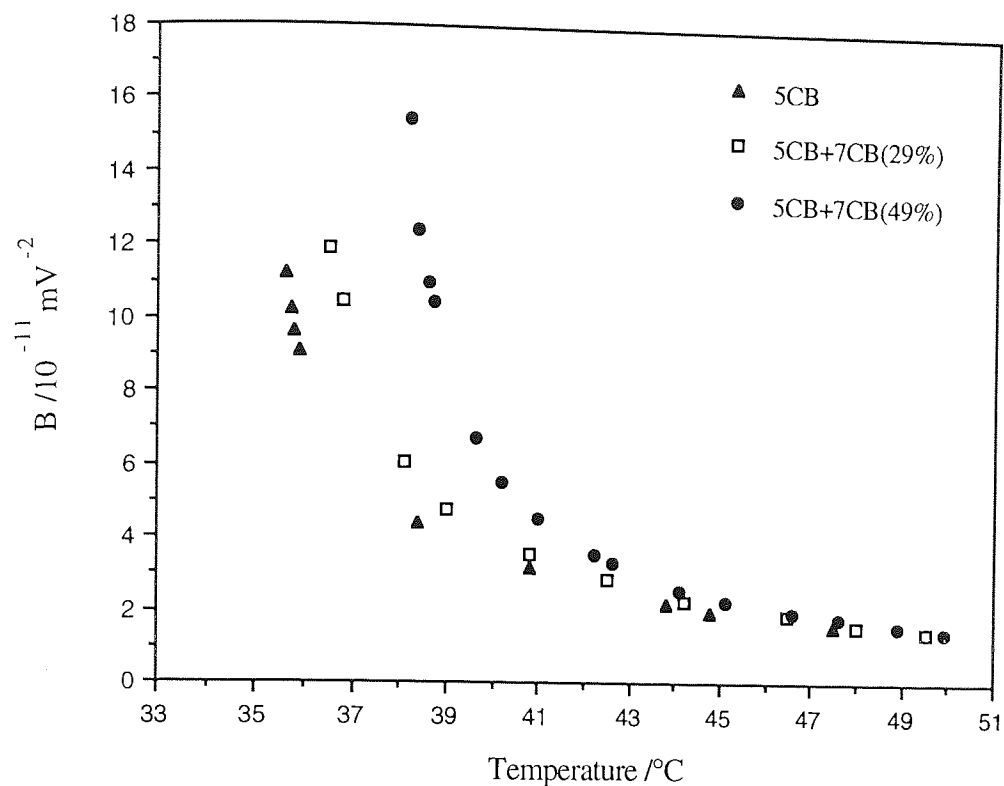


Figure 8.12 Temperature dependence of B for 5CB, F1 and F2 obtained using the pulsed d.c. field method.

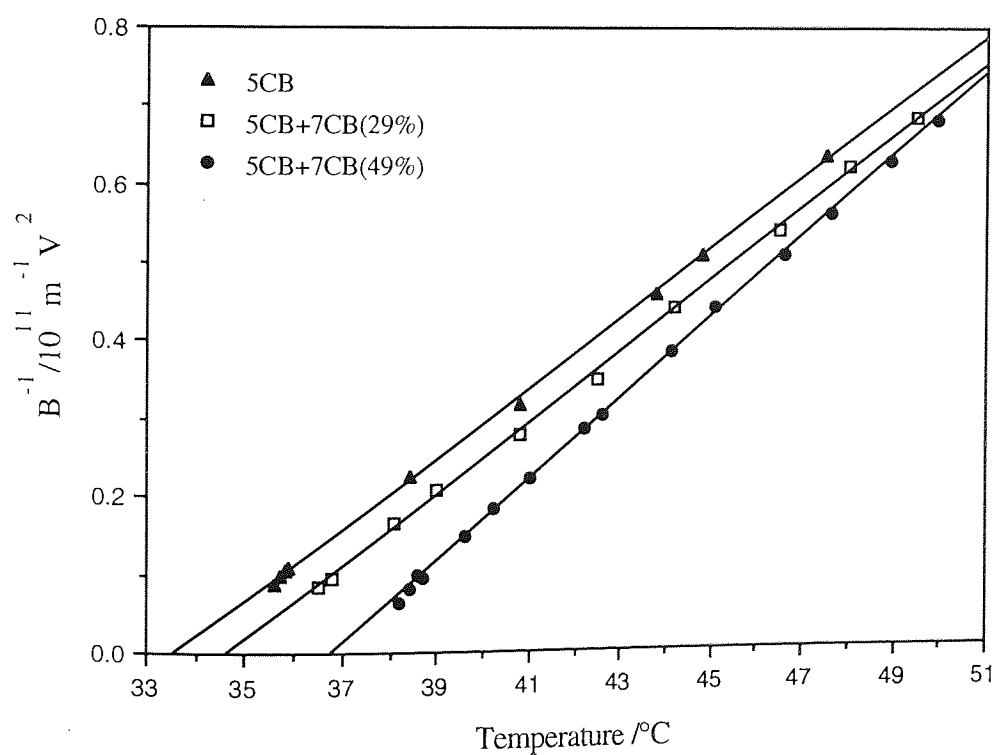


Figure 8.13 Temperature dependence of B^{-1} for 5CB, F1 and F2 obtained using the pulsed d.c. field method.

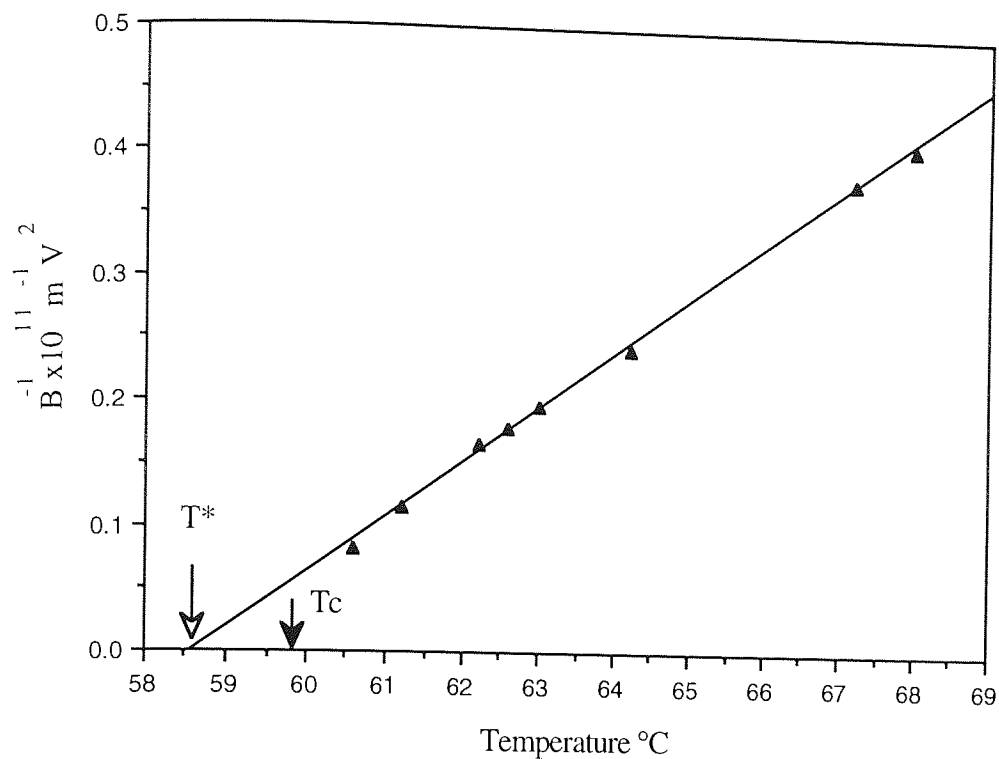


Figure 8.14 Temperature dependence of B^{-1} for E7 obtained using the pulsed d.c. field method.

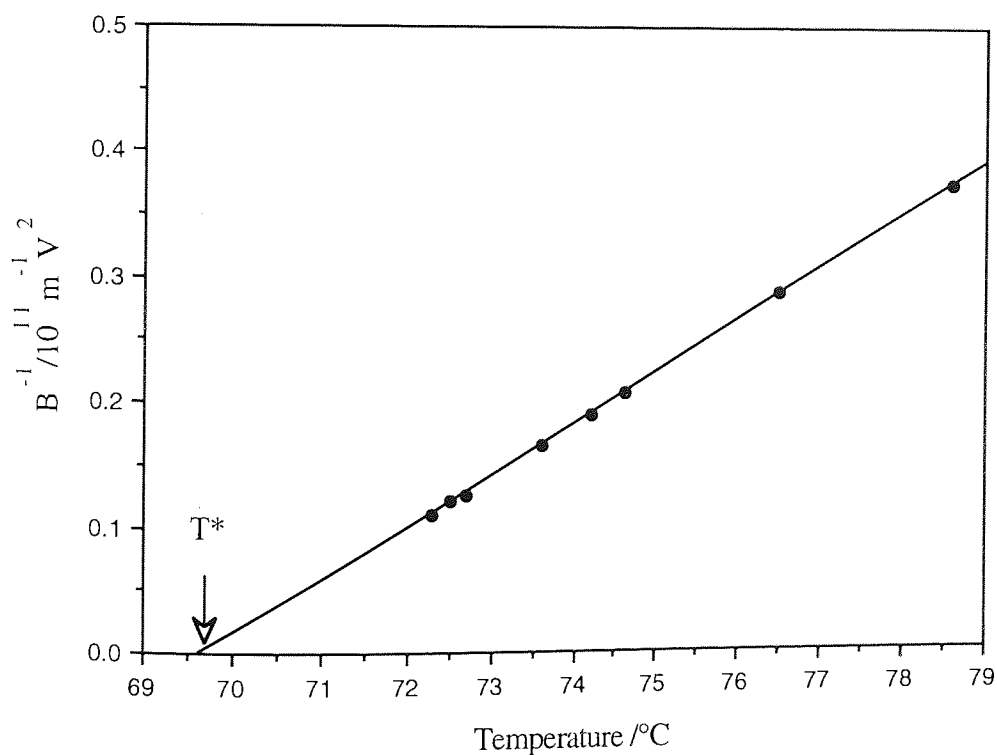


Figure 8.15 Temperature dependence of B^{-1} for E8 obtained using the pulsed d.c. field method.

CHAPTER 9

THE DYNAMIC ELECTRIC BIREFRINGENCE OF LIQUID-CRYSTALS

9.1 Introduction

Electro-optical properties of nematic liquid crystals are interesting from both a scientific and technological point of view. The dynamic electric birefringence technique may be used to study the rate of orientation, size, shape, and electrical properties of liquid and liquid crystal molecules^{182,183,184}. Although, the dynamic Kerr effect in the isotropic phase of liquid crystals has been studied in detail^{166,167} (see Chapter 8), relatively few investigations have involved measurements of the optical transients in the ordered nematic phase.

The purpose of this chapter is to present the main results of the dynamic Kerr effect behaviour and transient molecular reorientation observed in thin layers of some alkyl cyanobiphenyls (5CB, 6CB and 8CB). Dynamic induced birefringence experiments were performed on the nematic phases at several temperatures in order to determine the rise and decay times of the optical transient. A sandwich-type of electro-optical Kerr cell possessing homeotropic alignment, was used to determine the rise and decay times. In this arrangement the long molecular axes of the liquid crystal molecules are perpendicular to the windows of the cell, but parallel to the electrodes.

In the liquid-crystalline phase the applied electric field induces order on the macroscopic level rather than the microscopic level and therefore, the field strength necessary to reorientate the nematic axis is not very large. This ability to control the orientation of the nematic axis by means of weak external field is the basis for several applications of nematic liquid crystals in optical display devices.

9.2 Theory

9.2.1 The optical transients

When a short duration electric field is applied across the electrodes of the electro-optical cell, containing an isotropic liquid, the liquid sample becomes anisotropic and birefringence results⁶³. The pulse duration must be adjusted to be sufficiently long to obtain maximum orientation of the molecules for a given field strength. This situation is attained at a rate that depends on the size, shape, and electrical properties of the molecules and the viscosity, η , of the medium^{63,161}. When the electric field is suddenly removed, the aligned molecules return to their random orientation state and the birefringence returns to zero at a rate characterised by the rotary diffusion coefficient θ_r .

The optical response to a short duration applied field is transient in nature. Figure 9.1 shows a typical optical response due to the variation of the birefringence resulting from the application of a rectangular shaped electrical pulse.

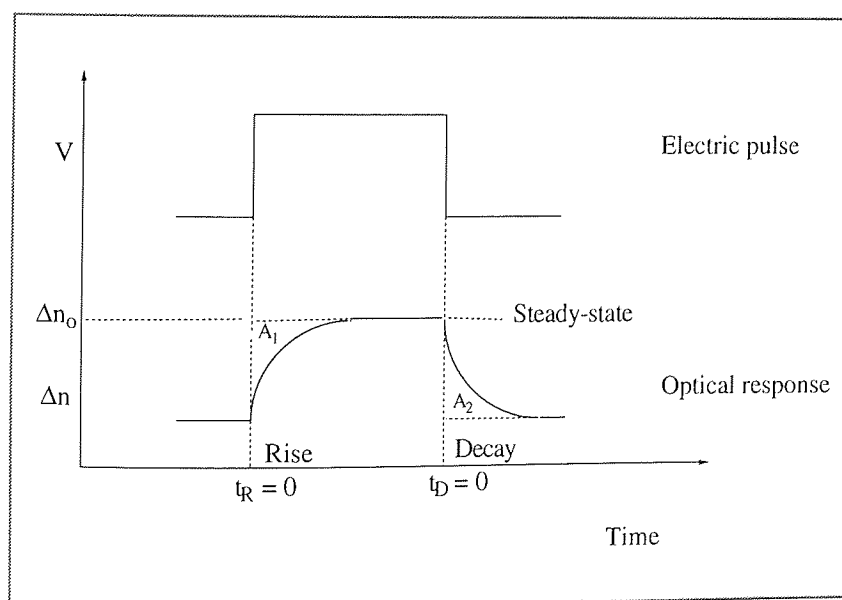


Figure 9.1 The optical response (lower trace) to a pulse applied field shown as a function of time.

Three distinct regions of optical response are observed, a "rise region" in which the birefringence is increasing and has a value $\Delta n_R(t)$ at time t following the application of the electric field, a "steady-state region" in which the birefringence remains constant ($\Delta n = \Delta n_0$) and a decay period during which the birefringence decreases to zero and has a value $\Delta n_D(t)$ at time t after the electric field has been removed. The rise and decay of the electro-optical parameters are characteristic of the particles and are usually referred to as relaxation curves or transient curves¹⁸³.

9.2.2 Dynamic behaviour and rotational diffusion

The rise and decay times of the transient Kerr effect are related to molecular length by a theory based on rotatory dispersion. Benoit^{185,186} has described the application of this theory to molecules having cylindrical symmetry. Benoit assumed that large rod-shape rigid molecules moving independently in a viscous medium. If a system of optically anisotropic particles are considered to be ellipsoids that they are able to rotate about their three principal axes, then their rotation may be characterised by three rotational diffusion coefficients¹⁸⁵. The combined coefficient of rotational diffusion, θ_r , may be regarded as a measure of the rate at which an ordered system of particles becomes random and is related to the dimensions of the particles. Powers and Peticolas¹⁸⁶ derived the following expression for the rotary diffusion coefficient θ_r , assuming the molecular shape to be approximated by an ellipsoid.

$$\theta_r = \frac{3kT}{8\pi\eta a^3} \left(\ln \left(\frac{2a}{b} \right) - 0.8 \right) \quad (9.1)$$

where η is the viscosity of the solvent, $2a$ is the length of the ellipsoid, and $2b$ is the diameter of the equivalent cylindrical rod. The dependence of θ_r on rod diameter b is a slowly varying logarithmic function¹⁸⁷, so that molecular length plays the dominant role in determining response time. The value of θ_r can be deduced by analysing the decay

curve of the birefringence. The decay time of birefringence, however, for a single relaxation process may be deduced by the simple formula

$$\Delta n_D(t) = \Delta n_0 \cdot e^{-t/\tau} \quad (9.2)$$

where τ is the relaxation time for the particles (molecules). The decay time of the induced birefringence is related to the rotational diffusion coefficient by the relationship

$$\tau_D = \frac{1}{6 \theta_r} \quad (9.3)$$

The rise time depends on both permanent and induced dipole moments, and has a complex dependence on electric field⁶³. For a single relaxation process the rise curve may be described by

$$\Delta n_R(t) = \Delta n_0 (1 - e^{-t/\tau_R}) \quad (9.4)$$

If equation 9.4 is compared with equation 9.2 then it is apparent that the rise curve is symmetrical to that of the decay in the case of orientation resulting from a purely induced dipolar mechanism. For a molecule which possesses a permanent dipole the relaxation time, τ_R , measured for the rise curve of birefringence is predicted to be greater than τ_D obtained for the decay curve of birefringence.

The ratio of the induced to the permanent dipolar contribution to the mechanism of orientation of a system of particles can be evaluated by comparing the areas under the rise (A_1) and decay (A_2) curves (Figure 9.1) The ratio $Q = A_1/A_2$ is unity for the case in which orientation is due solely to an induced dipolar mechanism. The ratio attains a maximum value of $Q = 4$ when the permanent dipolar orientation dominates⁶.

For liquid-crystal systems the interpretation of the optical transient is necessarily different from the approach used to analyse transients obtained for molecules in solutions or particles in suspension. For the latter systems the decay relaxation transient describe a transition from a partially ordered state to an essentially randomly ordered state. For liquid-crystal systems the decay transient serve to characterise the transition between two almost perfectly ordered states (e.g. homeotropic to planar or vice versa). Thus, for liquid-crystal systems the experimental derived time constant ($\tau_{K,D}$) of the decay curves are more appropriately regarded as a measure of the time taken for a cooperative re-orientations of the whole of the liquid crystal phase. The inverse of the magnitude of $\tau_{K,D}$ may then be interpreted as a measure of the elastic forces exerted on the liquid-crystal by the chemisorbed molecules on the internal surfaces of the cell, modulated by the visco-elastic properties of the liquid-crystal.

9.3 Experimental

Dynamic induced birefringence measurements were performed on the nematic phase at several temperatures in order to determine the rise and decay times. For this purpose the liquid-crystal samples were placed between two treated quartz plates. All the electro-optical measurements were made using homeotropically oriented samples (i.e., homeotropic with respect to windows of the cell).

9.3.1 *The electro-optical cell*

For the electro-optical studies of liquid-crystal compounds in the nematic phase, a sandwich type of electro-optical Kerr cell configured for homeotropic alignment (i.e., long axis of molecules perpendicular to the windows of the cell) was constructed (Figure 9.2). Good homeotropic alignment was obtained by using a thin layer of lecithin as a surface active agent (Chapter 2). The introduction of the sample was achieved by capillary action. The spacing between "top" and "bottom" quartz plates was 20 μm .

Aluminum electrodes (with a separation of 3 mm) were used as spacers. The plates were fixed together by an epoxy resin glue. Copper wires were connected to the aluminum electrodes.

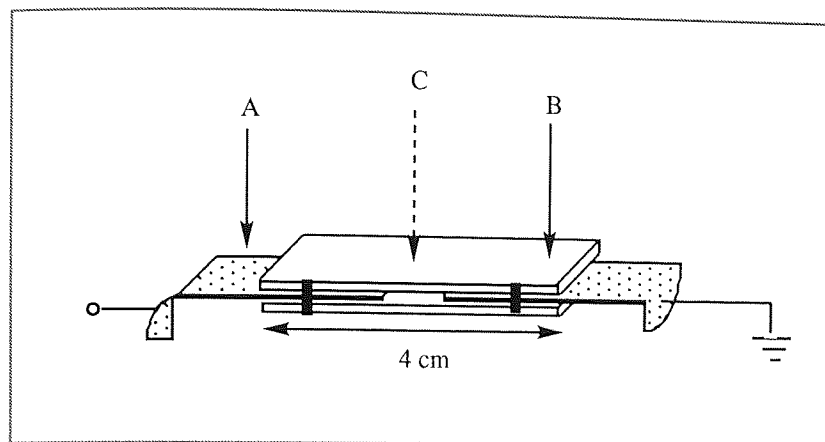


Figure 9.2 Construction of the Kerr cell for liquid-crystals, (A) 20 μm aluminum electrode, (B) 4 cm x 1 cm quartz slide with low strain birefringence, (C) light path.

The orientation of liquid-crystal inside the cells was checked using a polarising optical microscope (Chapter 3). The cell described was mounted in an oven which contained windows for the light beam. The temperature of the oven was measured using a copper-constantan thermocouple in contact with the glass cell.

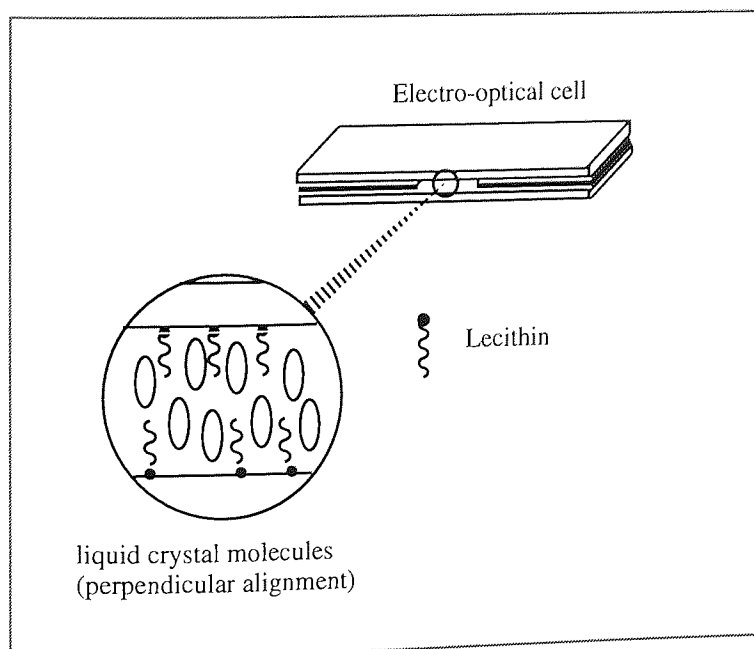


Figure 9.3 Side view of the experimental cell with homeotropic alignment

9.3.2 Measuring apparatus

The measurement of the dynamic behaviour and the determination of Kerr constants of a thin layer of ordered alkyl cyanobiphenyl liquid-crystals were performed with the Kerr effect apparatus depicted in Figure 9.4 (see also Figure 8.2, Chapter 8). The liquid-crystal cell was placed between the crossed polarisers and the beam of the laser light (632.8 nm) was extinguished by the second polariser (analyser). The zero electric field light level was recorded and displayed on the oscilloscope. A printed copy of the zero-level trace and was output to the X,Y plotter.

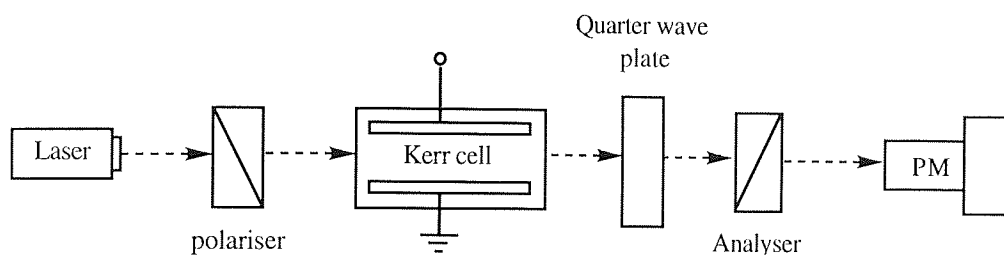


Figure 9.4 Optical arrangement for the measurement of Kerr constant and observation of the dynamic behaviour of a thin liquid crystal cell.

A pulse of voltage (660 ms) was applied to the cell, and corresponding optical signal was recorded by the transient recorder and displayed on the oscilloscope. The pulse duration was adjusted in order to obtain maximum orientation of the molecules at a given field strength. A printed copy of the optical transient was then over printed on the zero light-level trace.

9.3.3 Analysis of time dependent optical transients

A labelled schematic optical transient is shown in Figure 9.5. The optical transient curves were analysed using the following procedure: The zero time points ($t = 0$) were marked on the rise and decay curves. These corresponded to the times when the electric field was applied and removed. The height maximum ($I_0 = I_{\max}$) light level corresponding to the

light intensity which would reach the photomultiplier if the analyser was rotated to the completely uncrossed position (sample in the cell). The height, $I(t)$, of the curve from the zero intensity baseline ($I = 0$) was measured at different times along the transient (see Figure 9.5).

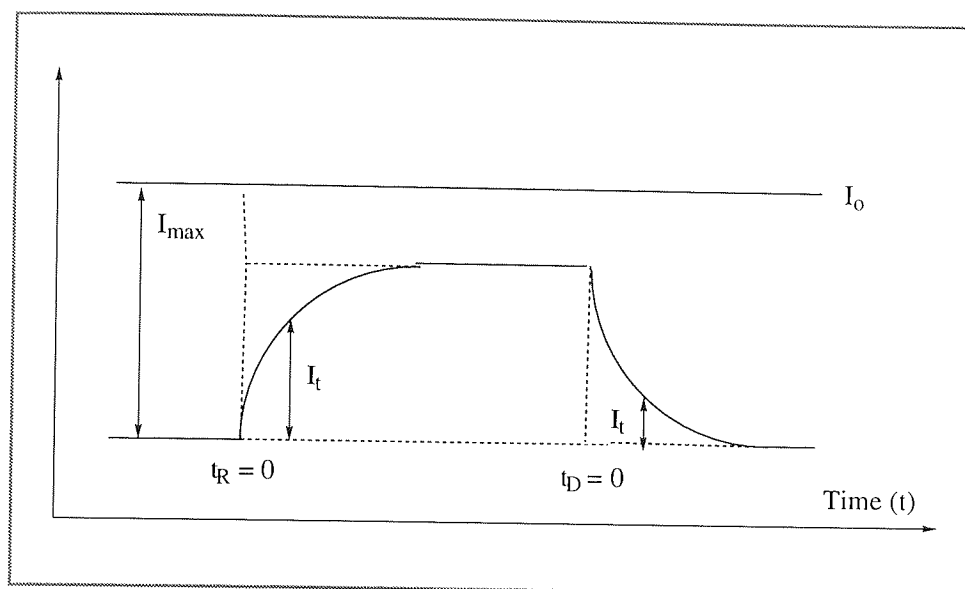


Figure 9.5 Analysis of time dependent optical transient

The determination of the I_0 (the maximum intensity of light) was carried out in the following way (Figure 9.6): After appropriately adjusting the optical elements, the analyser was rotated from the crossed position through an angle $\alpha = k$, e.g. $\alpha = 2^\circ$ and the corresponding signal was measured. In the absence of the applied electric field, the intensity of the light detected by the photomultiplier is given by

$$I = I_0 \sin^2 k \quad (9.5)$$

This permitted I_0 to be computed and expressed in terms of a height in millimeter.

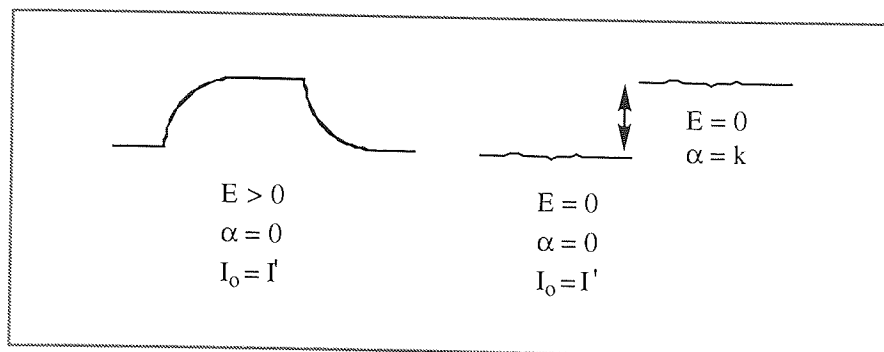


Figure 9.6 Determination of maximum light level, I_0

The optical transient recorded as changes in light intensity, i.e I_t (mm), and can be converted into a birefringence ($\delta(t)$) transient using the following equation

$$\delta(t) = 2 \sin^{-1} \left(\sqrt{\frac{I(t)}{I_0}} \right) \quad (9.6)$$

The relaxation time can be determined from the slope of a normalised graph of $\ln \delta/\delta_0$ (or $\ln \Delta n/\Delta n_0$) vs. time, where δ_0 is the equilibrium field-on birefringence. For the more accurate measurements of the birefringence $\delta(t)$, a decay (or rise) transient was recorded using an expanded time scale, set on the transient.

9.4 Results

The electrically induced birefringence $\delta(t)$ for the alkyl cyanobipenyls (5CB, 6CB and 8CB) for the transients are listed in Appendix E. A typical optical transient is shown in Figure 9.7 for 5CB. Approximation values of the relaxation times for the decay and rise can be calculated from the time at which the normalised birefringence attained the value $1/e$ and $(1 - 1/e)$, for the decay and rise, respectively. In practice, the relaxation-decay time (τ_D) were determined from plots of $\ln \delta/\delta_0$ versus time which for a single relaxation process, are straight lines with slope $= -1/\tau_D$.

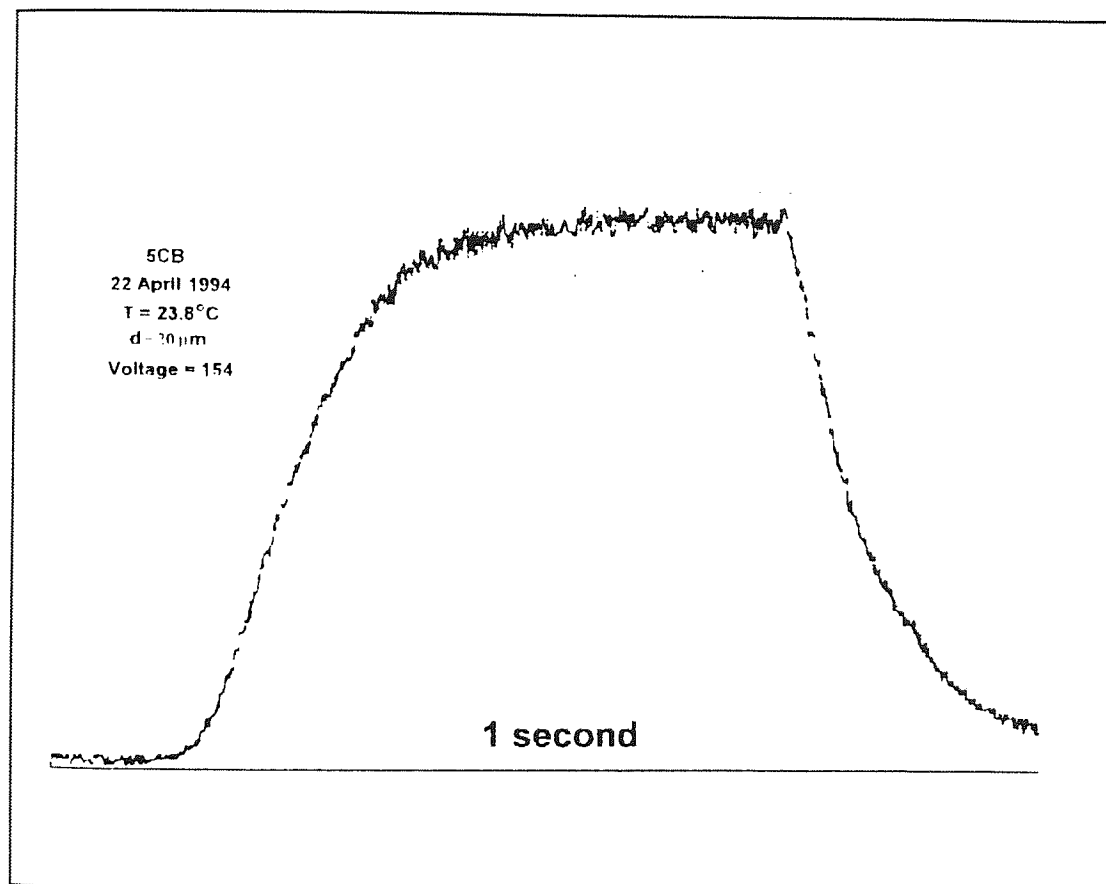


Figure 9.7 Recorder plot showing the optical response for pentyl cyanobiphenyl, 5CB, as a function of time. The applied field pulse was rectangular and 660 ms duration.

9.4.1 Electric field dependence of relaxation times

Figure 9.8 shows the normalised rise behaviour at various voltages for 5CB. As it can be seen for a fixed temperature the relaxation time decreases markedly with increasing voltage (Table 9.1). It was found that this behaviour, i.e. voltage dependence of rise time is also similar for 6CB and 8CB. However, the decay time within experimental error, is independent of applied voltage. This is illustrated in Figure 9.9, which shows the decay of normalised birefringence of 6CB measured at various voltages.

Interestingly, an electro-optic response was not observed for a cell containing homeotropically smectic phase of 8CB. In order to make sure, that the pulse duration was sufficiently long to achieve equilibrium conditions, a polarised microscopic study of a thin smectic layer of 8CB with homeotropic alignment was carried out using d.c. field (100 to 10000 Vcm^{-1}) and long duration times ($\sim 1\text{min}$), but no optical response was observed. For 8CB in the nematic phase an optical transient was observed in a duration time of ca. 660 ms using field strength of about 200 Vcm^{-1} .

Table 9.1 The rise and decay times for 5CB.

phase	T/°C	field strength V cm^{-1}	$\tau_{\text{rise}}/\text{ms}$ ± 4	$\tau_{\text{decay}}/\text{ms}$ ± 3
nematic	23.9	330	150	85
		530	130	85
		630	110	85

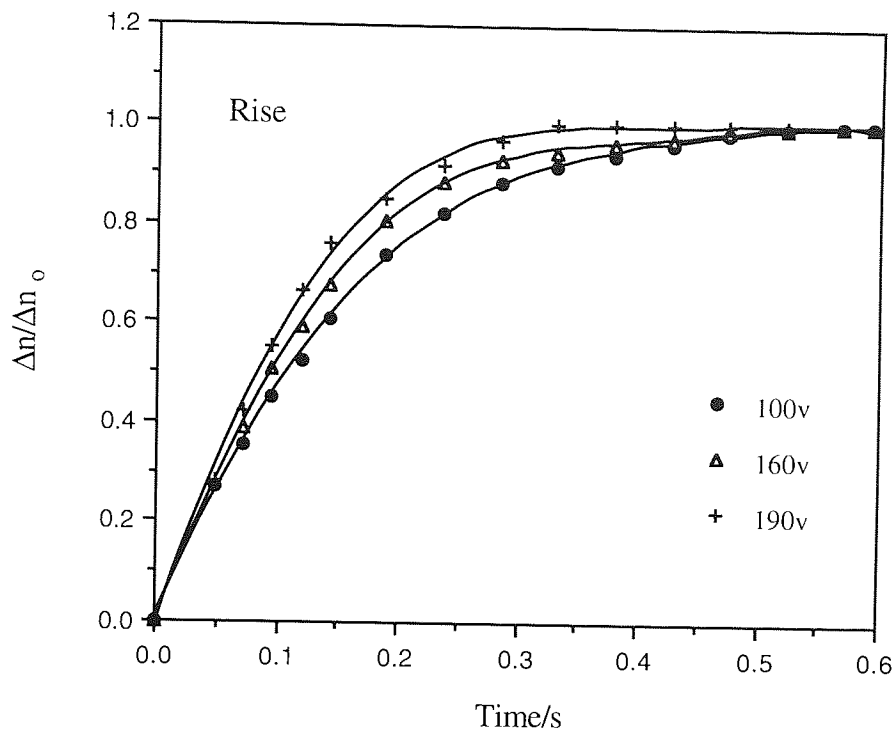


Figure 9.8 Rise of normalised birefringence at various applied voltages for 5CB at $T = 23.9^\circ\text{C}$

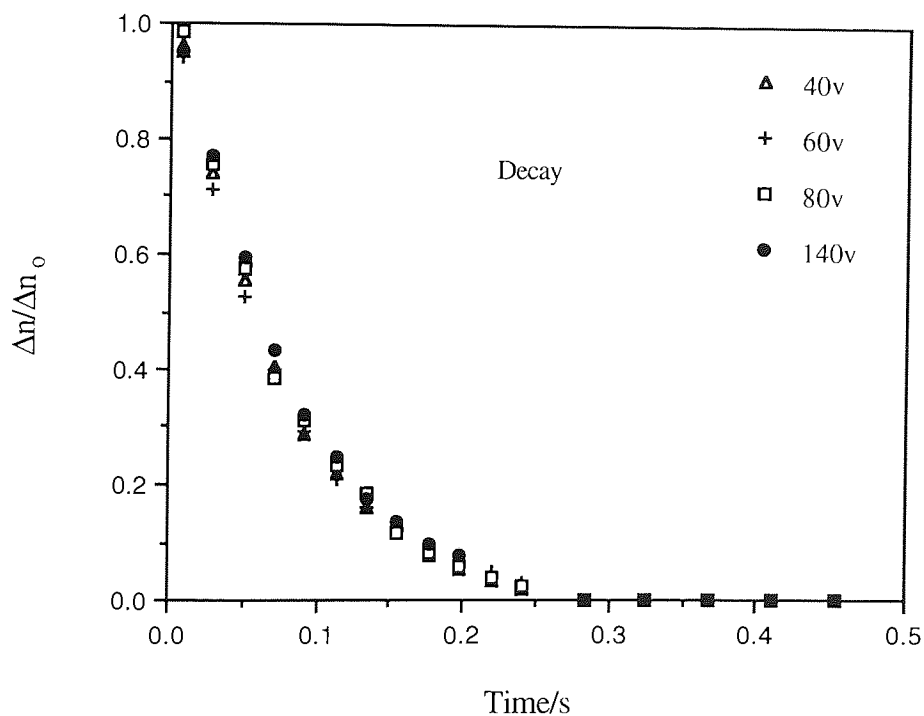


Figure 9.9 Decay of normalised birefringence at various applied voltages for 6CB at $T = 28.2^\circ\text{C}$. Voltage independence also observed for 5CB and 8CB.

9.4.2 Temperature dependence of the relaxation times

The temperature dependence of the dynamic behaviour of pentyl, hexyl and octyl cyanobiphenyls (5CB, 6CB, and 8CB) in the nematic phase was investigated via their optical response. This is illustrated for the rise curves of normalised birefringence obtained at various temperatures for 5CB (Figure 9.10). For a fixed voltage the optical response time decreases with increasing temperature.

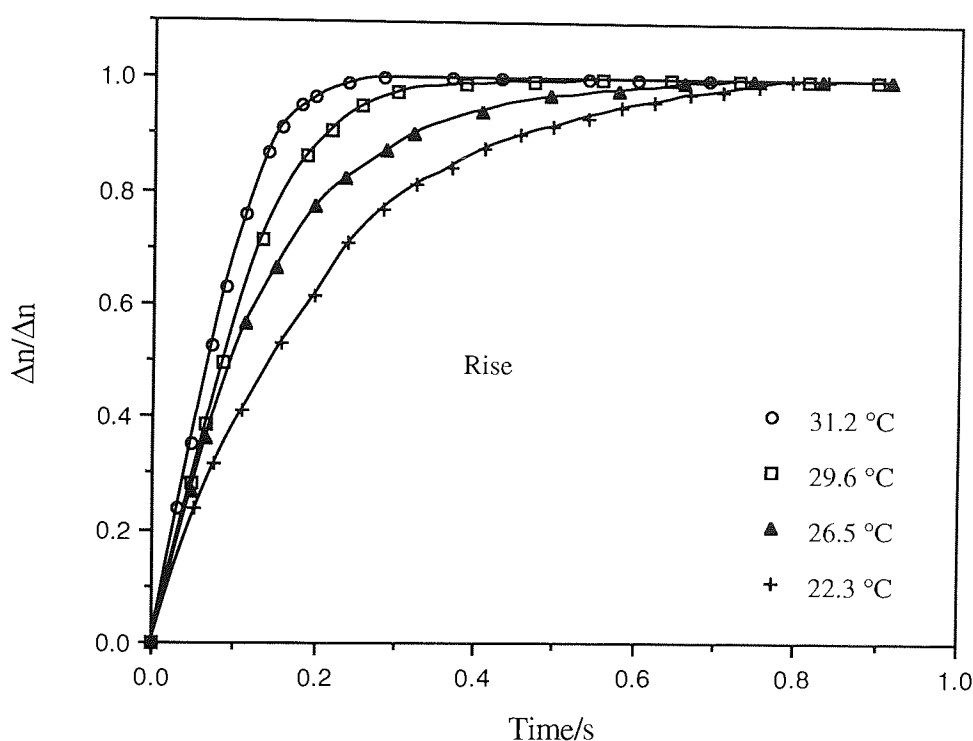


Figure 9.10 Rise curves of normalised birefringence of 5CB obtained at various temperatures using a fixed voltage of 180 V ($E = 600 \text{ Vcm}^{-1}$).

The analysis of the build-up of the birefringence transient is complicated (because it is field dependent) and the rise time is a complex function that depends on the both permanent and induced dipole moments. The decay time of the birefringence transient, however, depends only on the molecular dimensions and also viscosity (see Section 9.2.2 for a more detailed discussion regarding the physical significant of $\tau_{K,D}$).

Analysis of the birefringence-decay curves obtained for the liquid-crystals in the nematic phase show that plots of $\ln(\Delta n/\Delta n_0)$ vs. time are linear (Figure 9.11), thus indicating a single relaxation process. The variation of the relaxation decay time with temperature is very small, and low activation energies are obtained for the cooperative reorientation of the whole sample (Tables 9.2-9.4). In the liquid-crystalline phase the applied electric field induces changes in orientation on the macroscopic scale rather than on the microscopic level and when the field is removed, the “memory” of the sample, brought about by strong surface attractions, causes the sample to return to the original homeotropic wall (window) alignment.

The variation of the relaxation decay time with temperature for 5CB and 8CB is also very small, indicating a low activation energy for these liquid-crystals. Figure 9.12 shows the activation diagram, $\ln(1/\tau)$ vs. $1/T$ for 6CB in the nematic state, indicating a activation energy about $13 \pm 4 \text{ kJ mol}^{-1}$ for this liquid-crystal.

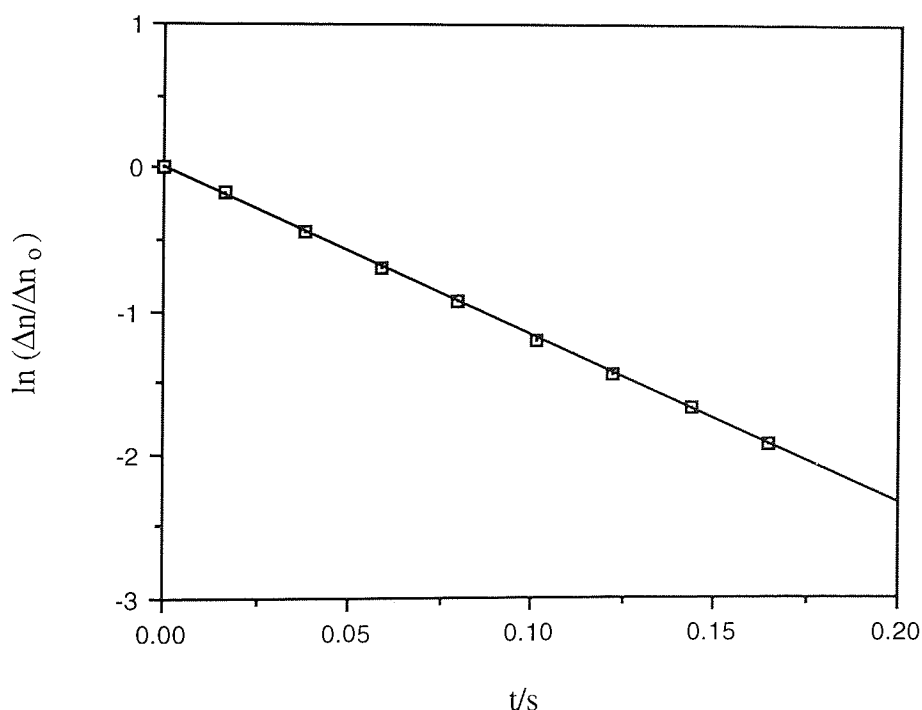


Figure 9.11 Analysis of the birefringence-decay curve for 6CB at 20.4 °C

Table 9.2 The decay times for pentyl cyanobiphenyl (5CB) in the nematic phase

phase: nematic λ : 632.8 nm path-length: 20 μm pulse-length: 660 ms single relaxation	T/°C	Field strength /Vcm ⁻¹	τ_{decay} /ms
	23.6	800 650	90 \pm 3
	22.3	800 650	92 \pm 3

Table 9.3 The decay times for hexyl cyanobiphenyl (6CB) in the nematic phase

phase: nematic λ : 632.8 nm path-length: 20 μm pulse-length: 660 ms single relaxation	T/°C	Field strength /Vcm ⁻¹	τ_{decay} /ms ± 2
	28.2	470	71
	27.3	470	71
	25.7	600	76
	23.4	600	78
	20.4	600	84
	18.4	670	83

Table 9.4 The decay times for octyl cyanobiphenyl (8CB) in the nematic phase

phase: nematic λ : 632.8 nm path-length: 20 μm pulse-length: 660 ms single relaxation	T/°C	Field strength /Vcm ⁻¹	τ_{decay} /ms
	34.8	330 400 470	59 \pm 2
	36.8	330 400 470	56 \pm 2
	39.4	400 470	54 \pm 3

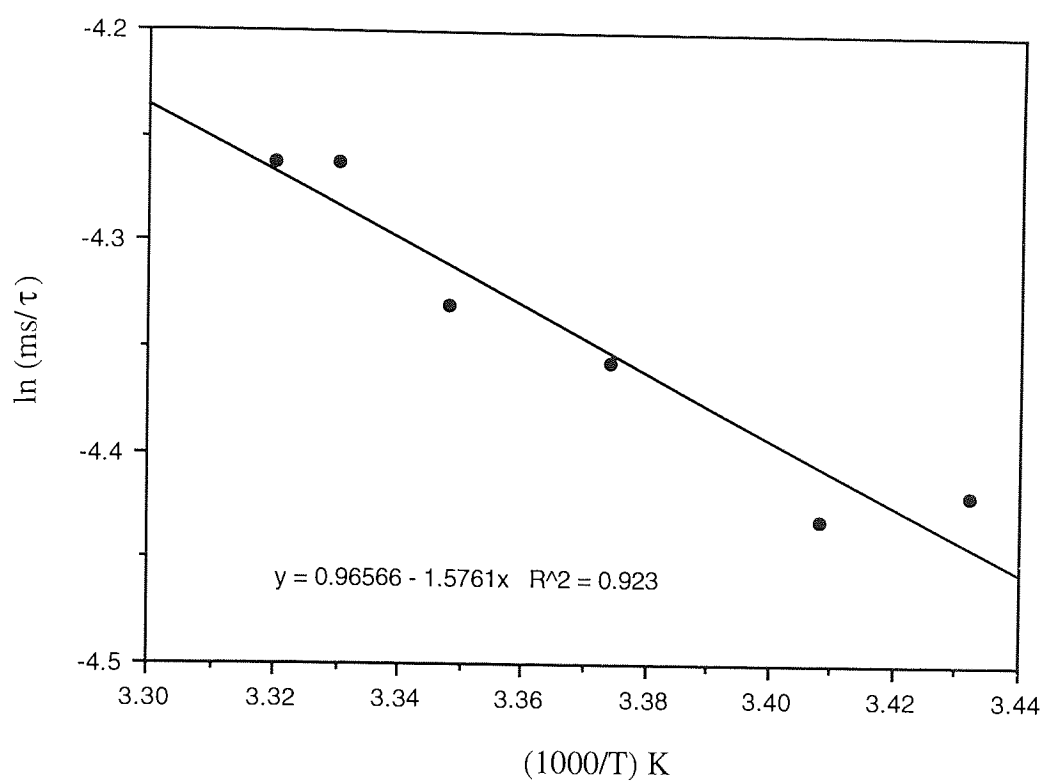


Figure 9.12 The activation diagram, $\ln(1/\tau)$ vs. $1/T$ for 6CB in the nematic state.

9.5 Dynamic Kerr Studies-Using MathCad 4.0

Analysis of the Shapes of Kerr Decay Transient for Large Retardations and the Measurements of the Static Kerr Constants of Liquid-Crystals.

The Kerr constant (B) of the material was adjusted to give a phase difference of 180° in order to match the experimental trace of an optical transient obtained using a voltage (set by a global definition below) that give a maximum intensity of light at equilibrium (i.e., the condition where the phase retardation = 180° , see Tables 9.5-9.6). For the liquid-crystal 6CB at 28.2°C the fitted Kerr constant was found to be

$$B = 1.148 \times 10^{-5} \quad \text{mV}^{-2}$$

This value depends on the dimensions of the Kerr cell, which were

Optical path length	$L = 20 \times 10^{-6} \quad \text{m}$
Electrode separation	$d = 3 \times 10^{-3} \quad \text{m}$

The decay time of the optical transient was chosen to match that observed experimentally for 6CB at 28.2°C .

$$\tau = 75 \quad \text{ms}$$

The maximum intensity of light (I_0) transmitted through the Kerr cell, for the condition of complete attainment of equilibrium, was set to unity.

$$I_0 = 1$$

The parameters i denotes the number of times chosen for evaluation following the start of decay (i.e., following the time defined as $t = 0$, the time when the electric field was removed from the Kerr cell).

$$i = 1 \dots 350$$

The corresponding times t_i were then derived by using $t_i = i$. If the time constant τ has units of milliseconds then the units of t_i are also milliseconds.

The adjustment of the Kerr constant B , so as to give $\delta = 180^\circ$, is achieved by Mathcad's automatic evaluation of the Kerr equations.

$$\delta_{\max} = 2 \pi B L (V/d)^2 \quad \delta_{\max} = 3.142 \quad \delta_{\deg.} = \delta_{\max}/0.01745$$

As the value of B is altered the above values can be seen to re-adjust as a consequence. When $\delta_{\deg.} = 180^\circ$ then the corresponding value of B is accepted to be equal to the experimental Kerr constant of the sample. The Kerr decay transient is constructed by calculating phase retardations at different times following the removal of the applied electric field, using

$$\delta_{t_i} = \delta_{\max} \exp \left(-\frac{t_i}{\tau} \right) \quad \text{rad}$$

The intensity of the light I_{t_i} at time t_i is then readily found using Malus' law

$$I_{t_i} = I_0 \sin^2 (\delta_{t_i} / 2)$$

The variation of the electrically-induced phase retardation with time is shown in Figure 9.13. The predicted in the intensity of light transmitted by the Kerr cell are shown in Figures 9.14-9.16 for the liquid-crystal 6CB at 28.2°C .

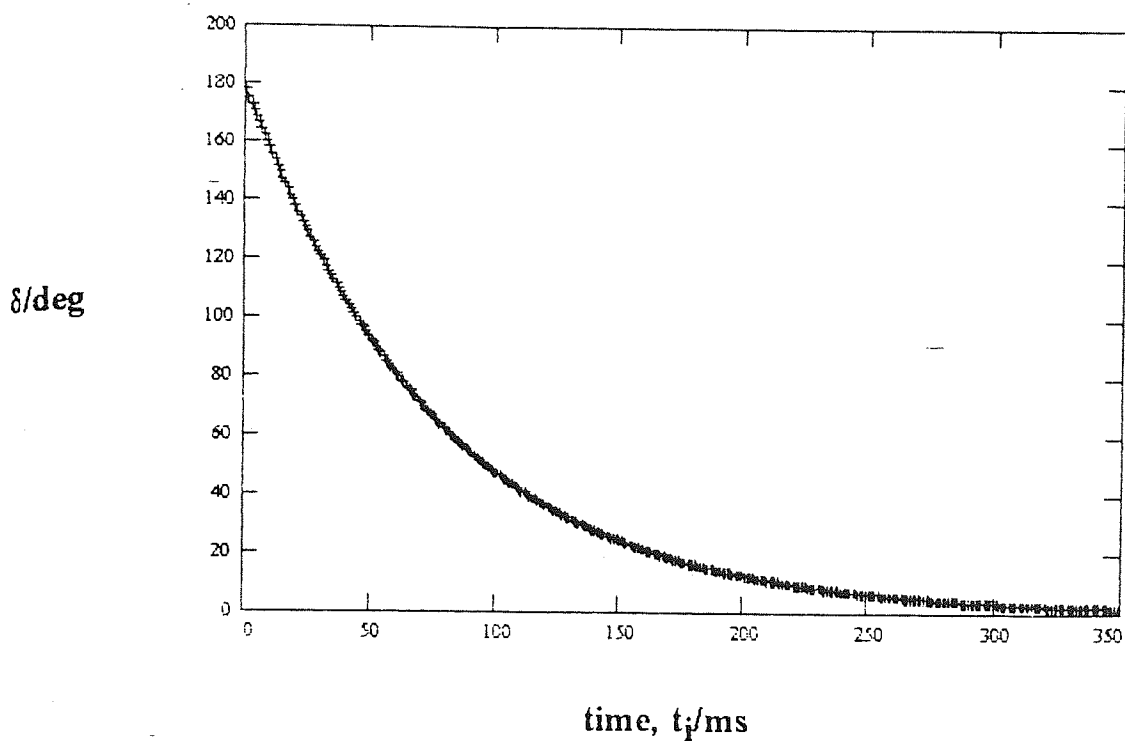


Figure 9.13 The variation of the electrically-induced phase retardation with time for 6CB in 28.2 °C.

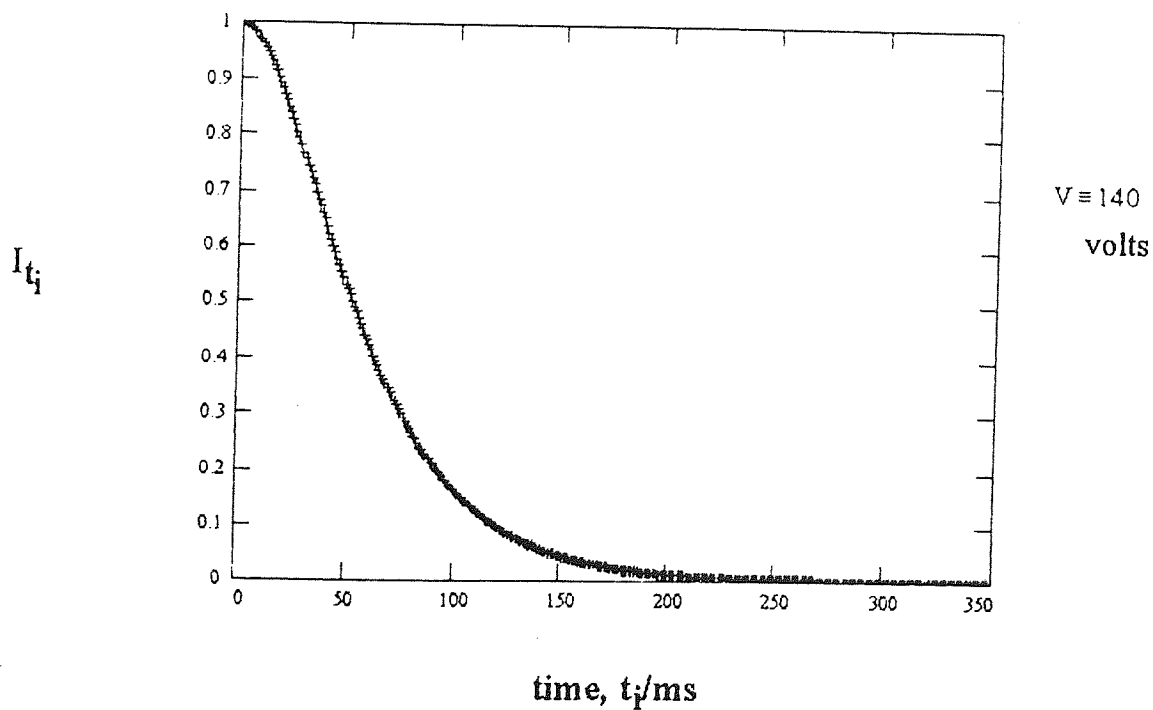


Figure 9.14 The intensity of light transmitted by the Kerr cell for 6CB at 28.2°C.

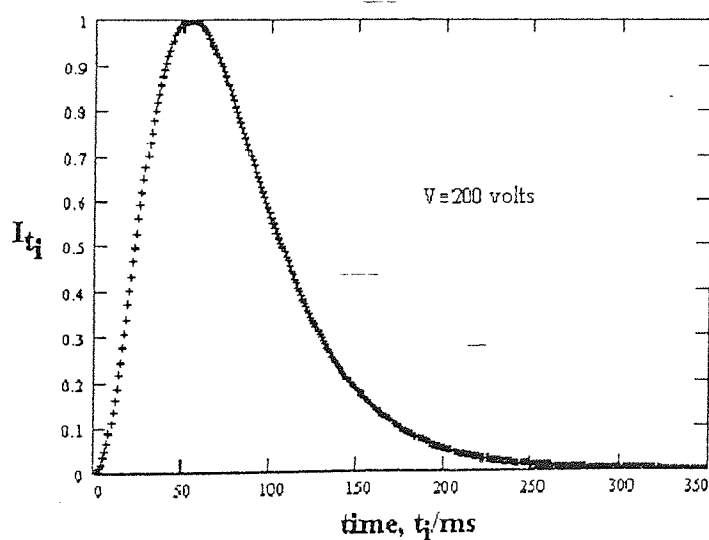
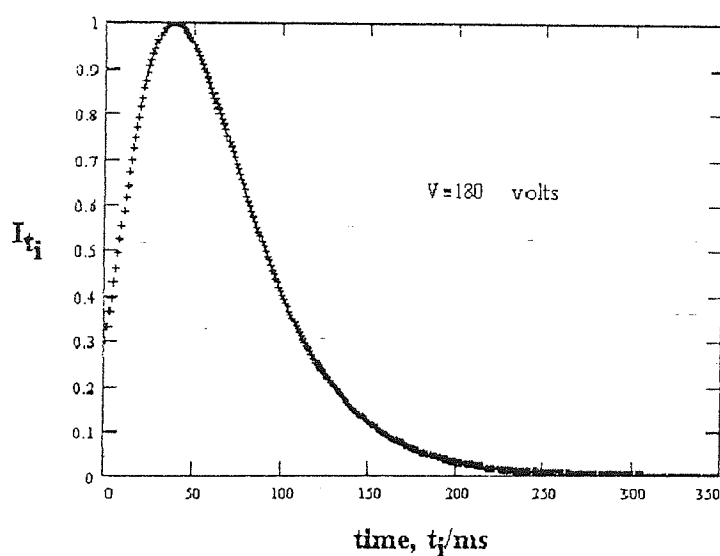
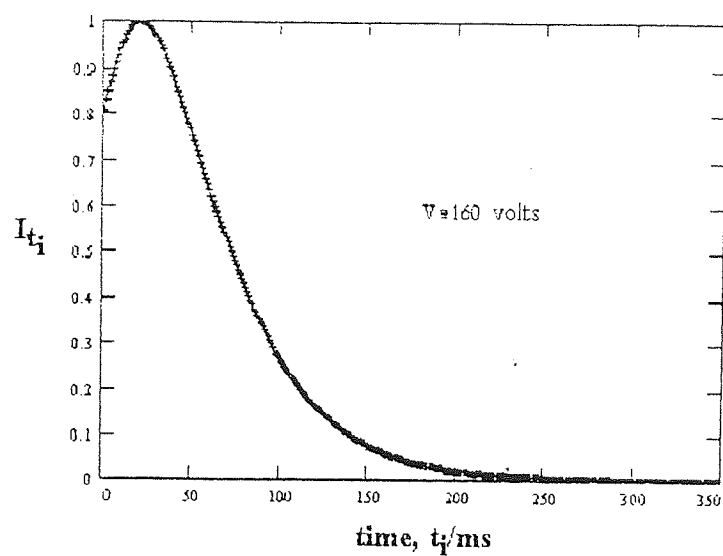


Figure 9.15 The intensity of light transmitted by the Kerr cell for 6CB at 28.2°C.

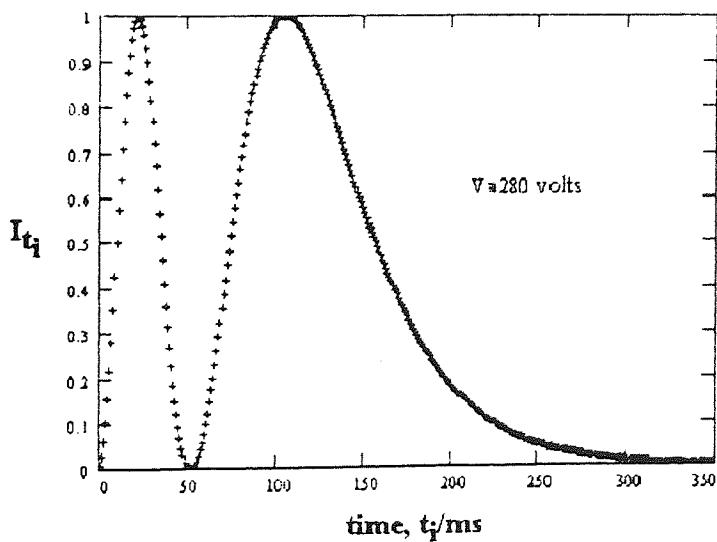
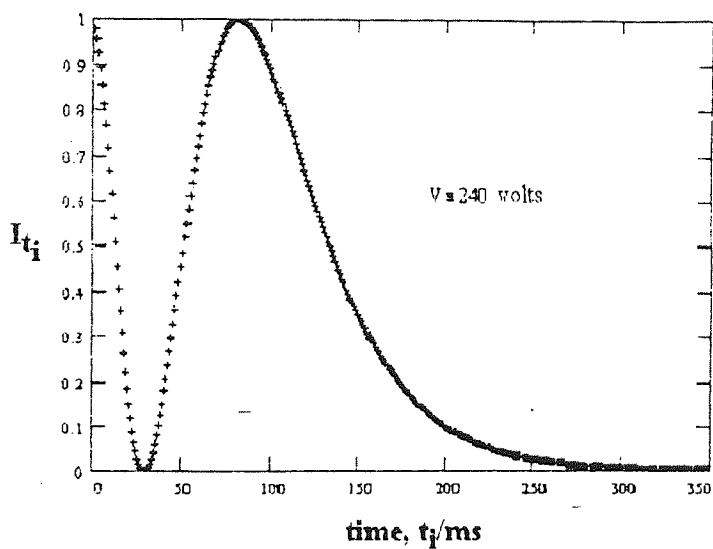
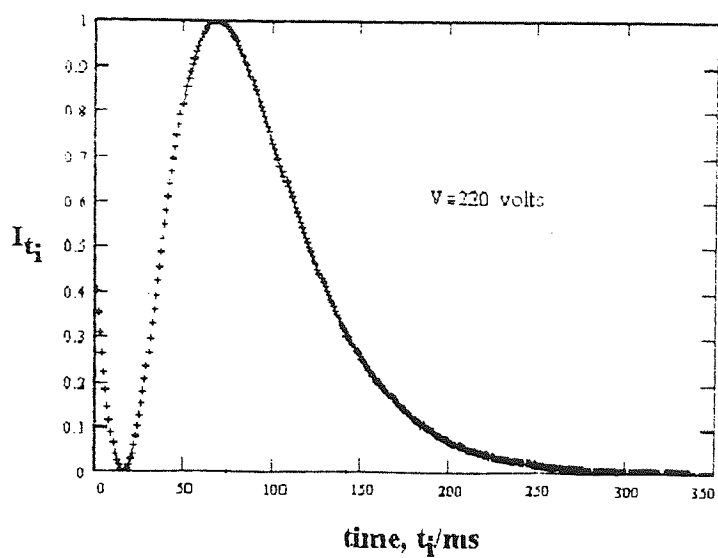


Figure 9.16 The intensity of light transmitted by the Kerr cell for 6CB at 28.2°C.

Table 9.5 The Kerr constant (B) for pentyl cyanobiphenyl (5CB) in the nematic phase ($\delta_{\max} = 180^\circ$)

	T/°C	voltage (max) /Vcm ⁻¹	B /10 ⁻⁶ mv ⁻²
λ : 632.8 nm	22.2	315	3.1
path-length: 20 μ m	23.3	280	3.9
pulse-length: 660 ms	26.5	220	6.3
electrode separation: 3.5 mm	29.6	160	12.0

Table 9.6 The Kerr constant (B) for hexyl cyanobiphenyl (6CB) in the nematic phase ($\delta_{\max} = 180^\circ$)

	T/°C	voltage (max) /Vcm ⁻¹	B /10 ⁻⁶ mv ⁻²
λ : 632.8 nm	20.3	280	2.9
path-length: 20 μ m	23.4	240	3.9
pulse-length: 660 ms	27.3	160	8.8
electrode separation: 3.0 mm	28.2	140	11.5

CHAPTER 10

GUEST-HOST INTERACTIONS IN NEMATIC LIQUID-CRYSTALS

10.1 Introduction

The solute-solvent (guest-host) interactions responsible for solute orientation in liquid-crystal solvents have been the subject of much interest in recent years. Oriented nematic liquid-crystals are very important as anisotropic solvents for the optical polarisation of solute molecules¹⁸⁸. Optical polarisation measurements in nematic solvents give quantitative information on the orientation of the solute molecules and direction of the dipole transition moment in the molecular axes system^{189,190}. The first electronic and vibrational spectroscopic studies in nematic solvents carried out in order to obtain band polarisation of solutes, were described by Levenson, Gray, and Ceasar¹⁹¹.

The use of nematic phases as model systems for the investigation of anisotropic intermolecular interaction potentials (solute-solvent intermolecular interactions) is another important scientific application of nematic liquid-crystals^{19,189}. The most important application of nematic liquid-crystals is that involving to be dichroic liquid-crystal displays using the guest-host interaction. The guest-host displays are based on dichroic dye molecules (guest) dissolved in a nematic host and their orientation through the use of an applied electrical field^{192,193,194}. The first guest-host interaction was proposed by Heilmeyer and Zanoni¹⁹⁵ and was based on homogeneous-to-homeotropic alignment transitions. More recently White and Taylor¹⁹⁶, have described a different type of guest-host interaction that depends on the cholesteric-nematic phase change. Conventional guest-host cells use nematic liquid-crystals with positive dielectric anisotropy and an initial planar alignment. Guest-host interaction is also possible in nematics that possess negative dielectric anisotropy and homeotropic alignment^{197,198,199}. In recent years, improvements of display properties of the guest-host cell, especially color contrast and

brightness, have received much attention. These properties depend mainly on dichroic ratios of dyes and Many researchers have investigated various kinds of dyes in order to improve the dichroic ratio^{200,201,202}. Mainly azo and anthraquinone dyes are investigated at present, because they have relatively high contrast ratios (dichroic ratios), generally high stability and high solubility^{203,204}. Seki *et al*²⁰³ based on their experimental results, claimed that the dichroic ratios of dyes can be predicated from their molecular structure by considering the flexibility of terminal groups. However, little information is available in the literature regarding the dependence of the order parameters on the nature of the host molecules. Recently, Imazeki *et al*²⁰⁵ (1993) indicated the influence of the hosts on the orientational behaviour of a number of dyes. They also made an attempt to correlate the order parameter of the dye molecules to their anisotropy of shape.

The aims of this part of the project were as follows:

- 1) To use dichroic dyes as probes for the investigation of optical anisotropy, order parameter, molecular alignment, stability and molecular reorientation of the liquid-crystals, using visible spectroscopy as the main analytical technique.
- 2) To calculate the dichroic ratio R and order parameter S of some dichroic dyes dissolved in nematic hosts MBBA, E7 and E8 (guest-host interaction).
- 3) To determine the important intermolecular parameters that influence the dichroic ratio and order parameter. The dichroic ratio R basically depends on two factors, i.e, the alignment of the dye in the nematic host and the angle between the optical transition dipole moment and the geometric axis (long molecular axis) of the dye. In the present work, only the alignment properties are discussed.
- 4) To present some infrared results (band polarisation) for E7 and some alkyl cyano-biphenyls.

10.2 Theory

10.2.1 Absorption anisotropy (dichroism)

The linear dichroism of a sample is defined as the difference in absorbance between two linearly polarised beams of light possessing electric vectors perpendicular to each other¹⁹. If a system has uniaxial symmetry, such as a nematic, the absorbances are conveniently measured parallel and perpendicular to the long molecular axis (director). In this case, the dichroic ratio R is defined as

$$R = A_{\parallel} / A_{\perp} \quad (10.1)$$

where A_{\parallel} and A_{\perp} are the absorbances (optical densities) for light polarised parallel and perpendicular to the director, respectively, so that the normal absorption, $A_{\text{iso}} = 1/3(A_{\parallel} + 2A_{\perp})$ ²⁰⁶.

The dichroic ratio R of a uniaxial nematic liquid-crystal can be related to the order parameter $S = 1/2 \langle 3\cos^2\theta - 1 \rangle$, where θ is angle between long molecular axis and the director of the liquid-crystal (Chapter 1). Then

$$S = \frac{(R - 1)}{(R + 2)} \frac{1}{1/2(3\cos^2\beta - 1)} \quad (10.2)$$

In which β is an angle between long molecular axis and the transition dipole moment of the liquid-crystal. Equation 10.2 can be used to evaluate the order parameter of the liquid-crystal if the angle β is known. The latter may be obtained from a study of one of the transition moments in the ultraviolet or infrared absorption spectra. If the transition moment is directed along the long axis of the molecule ($\beta = 0$), equation 10.2 reduces to

$$S = (R - 1)/(R + 2) \quad (10.3)$$

It is usually the case that liquid-crystalline compounds do not contain chromophores and are, therefore, colourless (but scatter light) or only lightly coloured. The absorption spectrum usually lies in the region of wavelengths shorter than 400 nm. In most cases the direction of the absorbing oscillator coincides with the direction of the long molecular axis, and this leads to a more intense absorption of light that is polarised parallel to the direction of the preferred orientation of the molecules (director).

10.2.2 Order parameter of a dichroic dye dissolved in a liquid-crystal

Molecules dissolved in an oriented nematic phase are partially aligned, and the orientation of the optical transition moment of the solute molecules in the nematic host can be determined from the change in their absorbance. Therefore, to interpret the dichroism, it is necessary to derive a relationship between the observed polarisation data and the absorbances with respect to the axes of the molecules^{188,194}.

The average molecular orientation in the liquid-crystal is characterized by the order matrix S which has the three components

$$S_{xx} = \frac{1}{2} \langle 3 \sin^2 \theta \cos^2 \phi - 1 \rangle, \quad S_{yy} = \frac{1}{2} \langle 3 \sin^2 \theta \sin^2 \phi - 1 \rangle, \quad S_{zz} = \frac{1}{2} \langle 3 \cos^2 \theta - 1 \rangle.$$

These elements fulfil the condition $S_{xx} + S_{yy} + S_{zz} = 0$. Here θ and ϕ are the polar angles that characterize the orientation of the liquid-crystal optic axis in the solute molecular fixed coordinate system (x, y, z). For absorption spectra taken with the electric vector parallel to the direction of rubbing (i.e. parallel to long axes of molecules), the absorbance is given by

$$A_{\parallel} = 1/3(A_x + A_y + A_z) + 2/3(S_{xx}A_x + S_{yy}A_y + S_{zz}A_z) \quad (10.4)$$

while for the perpendicular case

$$A_{\perp} = 1/3(A_x + A_y + A_z) - 1/3(S_{xx}A_x + S_{yy}A_y + S_{zz}A_z) \quad (10.5)$$

Subtraction of these two expressions yields the important relationship between the observed dichroism and the absorbances along the fixed axes of the molecule, namely,

$$A_{\parallel} - A_{\perp} = S_{xx}A_x + S_{yy}A_y + S_{zz}A_z \quad (10.6)$$

The absorbances defined relative to molecular coordinates A_x , A_y , and A_z are important because it is these quantities which yield information about the symmetries of the states involved in the absorption transition. For molecules with a threefold or higher axis of symmetry, $S_{xx} = S_{yy} = -1/2S_{zz}$ and equation 10.6 then simplifies to

$$A_{\parallel} - A_{\perp} = S_{zz}(A_z - A_{x,y}) \quad (10.7)$$

By rearranging equation 10.7, it is possible to express S_{zz} in terms of the dichroic ratio $R = A_{\parallel}/A_{\perp}$. To derive this relationship, it should be noted that $A_z - A_x$ is proportional to $(\mu_z^2 - \mu_x^2)$ where μ_i is the transition dipole moment in the i th direction. If $\mu_x = \mu_y$ then

$$\mu_z^2 - \mu_x^2 = \mu_z^2 - 1/2(\mu_x^2 + \mu_y^2) \quad (10.8)$$

$$= \mu^2(\cos^2\beta - 1/2\sin^2\beta)$$

$$= \mu^2(3\cos^2\beta - 1)/2$$

Where β is the angle which the transition dipole moment vector for a particular absorption makes with the z axis of symmetry. Then

$$A_z - A_x = (A_x + A_y + A_z)(3\cos^2\beta - 1) \quad (10.9)$$

Since μ is invariant to the choice of axes, $\mu^2 = \mu_{\parallel}^2 + 2\mu_{\perp}^2$ in the laboratory system (laboratory coordinate defined by direction of rubbing). Thus, $\mu \propto A_x + A_y + A_z = A_{\parallel} + 2A_{\perp}$. By using these results with equation 10.7, the desired expression is obtained.

$$S_{zz} = \frac{(R - 1)}{(R + 2)} \left(\frac{1}{1/2(3\cos^2\beta - 1)} \right) \quad (10.10)$$

Equation 10.10 can be used to determine the order parameter of the guest molecules (e.g. dyes) dissolved in oriented nematic liquid-crystals. The order parameter of the dye S_{dye} may be larger than the order parameter of the nematic host S_{host} if the length of the rod-shaped solute molecules exceeds the length of the nematic host.

The dichroic ratio R of a dichroic dye dissolved in a nematic host is defined as the ratio between absorption of light polarised parallel and perpendicular to the nematic director (grooves). Even if the dye molecules dissolved in the host liquid-crystal only absorb light polarised along their long axes, light polarised perpendicular to the liquid-crystal director will still be somewhat absorbed. This is due to the imperfect alignment of the liquid-crystal and dye molecules, and also due to thermal agitation^{196,207}. Although, dichroic dyes dissolved in a nematic liquid-crystal align, on average, parallel to the director of nematic molecules, the direction of each dye molecule can still deviate from the direction of the director L as shown in Figure 10.1. Here M is the direction of long molecular axis of the dye, T is transition moment (direction of the dipole moment change) of the dye that makes an angle β with M . The molecule makes an angle θ with the director L .

The main criterion of the dichroic dyes efficiency is the order parameter (S_T) for the transition moment of dye absorption which is responsible for the color of a dye. It should be noted that the value of S_T may differ from the order parameter for the molecular axis

S_M . This is the case when there is an angle β between the transition moment and the long molecular axis (Figure 10.1).

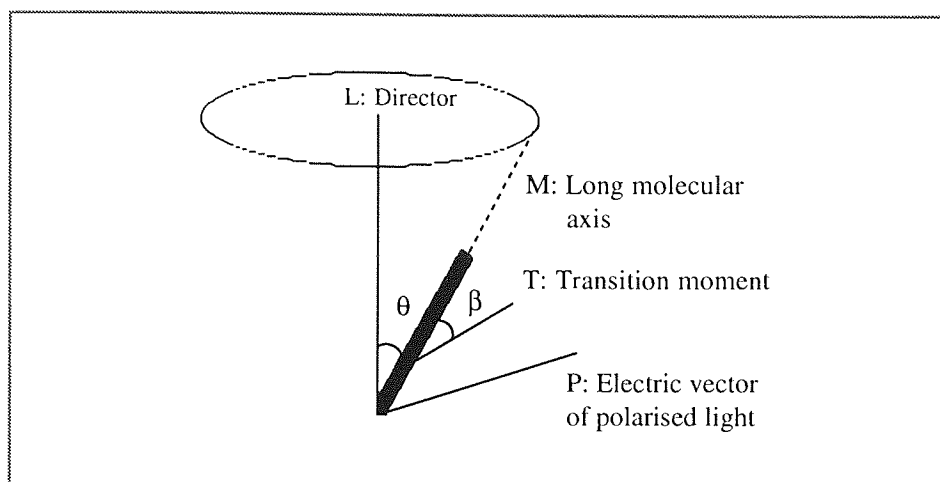


Figure 10.1 Deviation of dichroic dye geometric axis, M , and oscillator transition, T , from liquid-crystal director, L .

The dichroic ratio R directly relates to the order parameter S_T , while the molecular structure is considered to relate to the order parameter S_M . In general, these two order parameter, S_T and S_M , do not coincide unless the directions of transition moment and the molecular axis are parallel to each other^{203,204}. The order parameter S_T of transition moment T for rod-like dye molecules, for which the transition moment is considered to be parallel to the long molecular axis may be described using equation 10.2.

10.2.3 Infrared-dichroism in nematic liquid-crystals

One of the earliest applications of infrared spectroscopy to the study of liquid-crystals was made by Neff *et al.*²⁰⁸, who used infrared dichroism measurements to determine the order parameter S of the nematic phase. There are two methods of sample preparation used in the determination of the order parameter, leading to either homogeneous (planar) or to homeotropic molecular alignment^{190,211}. For planar alignment, absorbance A_{\parallel} and A_{\perp} are measured for plane polarised light possessing the electric vectors parallel and perpendicular to the nematic director (i.e. parallel to direction of the micro-grooves),

respectively. The dichroic ratio R , is then A_{\parallel}/A_{\perp} , for a particular absorption band at a known temperature. From the dichroic ratio and with aid of equation 10.10 the degree of order can be calculated²⁰¹.

For a band with a transition moment parallel to the long molecular axis, for which $R > 1$ (parallel transition moment), equation 10.2 reduces to equation 10.3. For a band that has a transition moment perpendicular to the long molecular axis (perpendicular transition moment), equation 10.2 can be reduced to

$$S = 2(1 - R)/(R + 2) \quad \text{where } R < 1 \quad (10.11)$$

10.2.4 IR-dichroism in nematics without using polarised light

A simplified method for determination of IR polarisation has been introduced by Kelker *et al.*²⁰⁹. This method makes use of homeotropically ordered nematic phases. First the spectrum of a homeotropically oriented layer is recorded (without a polariser), then the spectrum is taken after heating and converting into the isotropic state. For a particular band the ratio of absorbances measured for the nematic phase (A_N) to that measured for the isotropic phase (A_{iso}) is defined as the dichroic ratio $R' = A_N/A_{iso}$. The order parameter can be calculated using¹⁹⁰.

$$S = (1 - R') \frac{1}{1/2 (3\cos^2\beta - 1)} \quad (10.12)$$

which for a parallel transition moment can be simplified to

$$S = 1 - R' \quad \text{when } R' < 1 \quad (10.13)$$

and simplified to

$$S = 2(R - 1) \quad \text{when } R' > 1 \quad (10.14)$$

for a perpendicular transition moment.

10.2.5 The interpretation of band intensity changes

The change in band intensity induced by an isotropic-nematic transition is due to a change in molecular orientation. Consider an unpolarised infrared radiation beam that is incident on a sample with its electric vector in the xz plane (Figure 10.4). If the direction of the vibrational transition moment is parallel to the long molecular axis and if the molecules are in homeotropic alignment, then the intensity of the absorption band will decrease at the transition from the isotropic to the nematic phase. This decrease is observed because the average number of molecules with transition moments perpendicular to the plane of the electric vector has increased in going from the isotropic phase to the nematic state⁹.

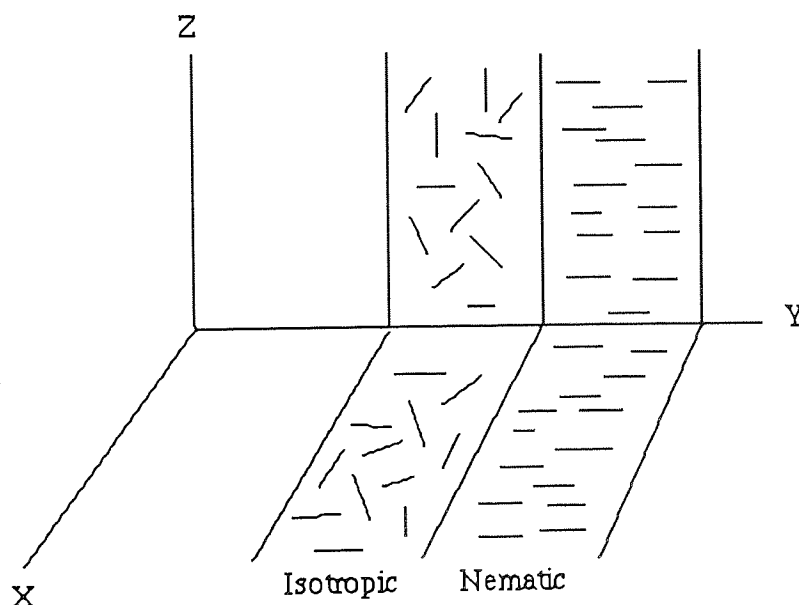


Figure 10.2 The intensity differences due to the change in molecular orientation. The light wave is travelling in the y direction. The direction of the vibration transition moment is taken parallel to the long molecular axis. When the molecules are aligned perpendicular to the xz plane in the nematic phase, the intensity will decrease.

10.2.6 Electronic color-switching interaction

Guest-host interaction or electronic color-switching can be observed in systems in which dichroic dye molecules are incorporated within nematic host materials. The dye molecules are oriented by the liquid-crystal. With zero applied electric field ($E = 0$), the liquid-crystal is in a uniform parallel orientation and the dye molecules are aligned with long axes parallel to the optical vector of the linear polarised light. Above a threshold voltage, nematic liquid-crystals with positive dielectric anisotropy tends to align parallel to the field^{195,210,198}. This is the condition for minimum absorption of dyes with positive dichroic ratios, as shown in Figure 10.3.

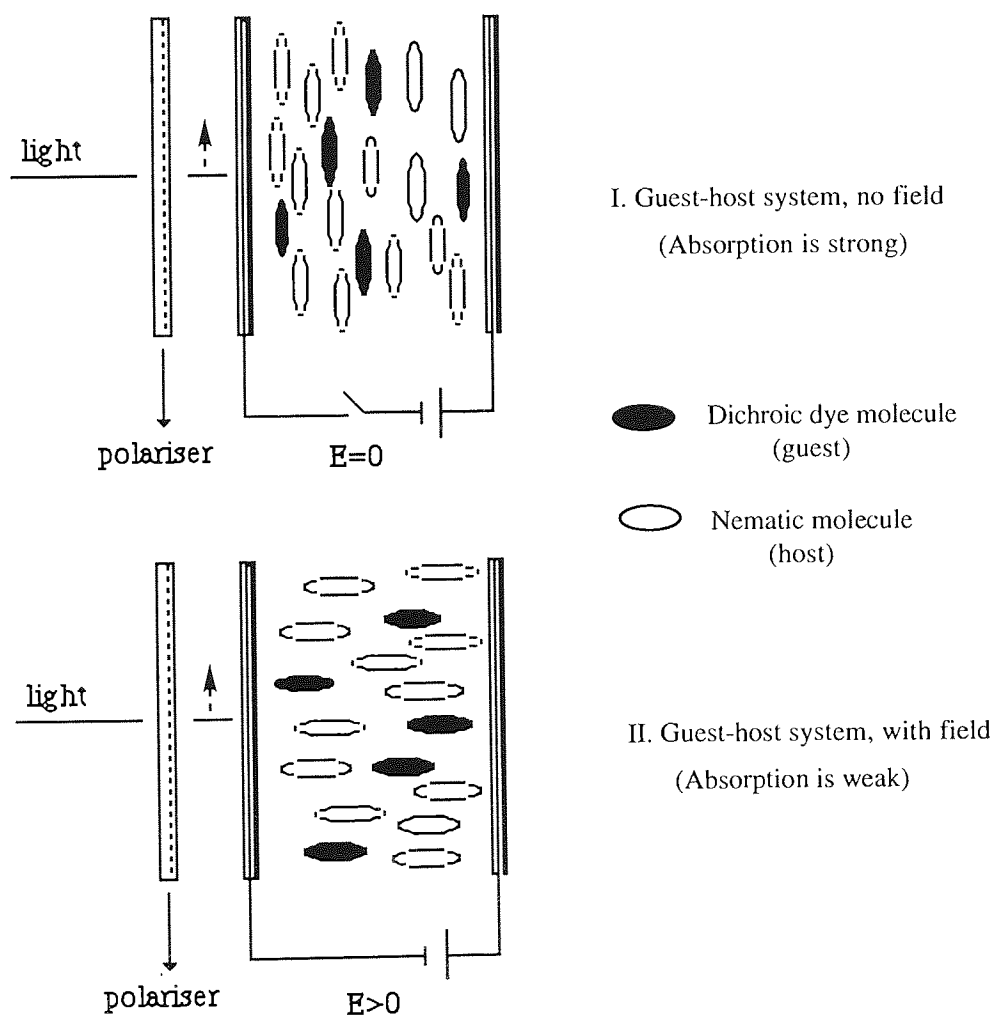


Figure 10.3 Guest-host interaction in a nematic liquid-crystal.

10.2.7 The solute-solvent intermolecular interaction

The molecular orientation in pure liquid-crystals and the average orientation of guest molecules in a liquid-crystal are mainly due to the anisotropy of the intermolecular forces^{189,19}. If a molecule is dissolved in the liquid-crystal it couples to this highly anisotropic intermolecular interaction field and generally becomes oriented to a substantial extent.

Maier and Saupe introduced a theory for the anisotropic solute-solvent interaction (anisotropic intermolecular interaction)¹⁹. This theory is based on the assumption that the intermolecular interaction potential in nematic liquid-crystals is determined primarily by London dispersion forces. The effective anisotropic potential U of a molecule l in the anisotropic dispersion field generated by its oriented neighbours s is calculated by averaging the pair potential between two molecules l and s and over all distances between l and s . For rod-like molecules the anisotropic contribution to this average potential is given by

$$W_l^{an} = -AS_s(3\cos^2\theta - 1) / 2V^2 \quad (10.15)$$

Where A is a constant which depends on the nature of the liquid-crystal, V is the molar volume of the liquid-crystal and S_s is the order parameter of the nematic phase. θ is the angle between the long axis of the molecule l and the nematic director (optic axis of the liquid-crystal). In the approximation of the so-called mean (molecular) field approach the average solute orientation is determined by the anisotropic potential W_l^{an} .

The anisotropic interaction between a solute molecule and the surrounding liquid-crystal matrix can be calculated by a modified version of the reaction field technique developed by Linder¹⁸⁹. The reaction field approach to intermolecular forces is a macroscopic theory which treats the molecules surrounding a selected molecule as a continuum. The

fluctuating electric moment of a solute molecule \mathbf{l} induces a moment μ_s in the surrounding medium. The reaction field associated with the moment μ_s in turn interacts with the moment μ_l of the solute molecule \mathbf{l} .

The theory of the solute-solvent interaction is based on three assumptions. Firstly, in nematic liquid-crystals it has been found that the anisotropic interaction potential is mainly due to the dispersion forces^{189,206}. Secondly, it has been assumed that the environment of the solute molecules is rotational symmetric, and finally, the dipole-quadrupole interaction is assumed to be negligible. From these assumptions the following relation for the anisotropic contribution W_l^{an} to the interaction potential has been derived which is analogous to the solvent-solvent interaction¹⁸⁹.

$$W_l^{\text{an}} = Q (\alpha_{xx} \sin^2\theta \cos^2\phi + \alpha_{yy} \sin^2\theta \sin^2\phi + \alpha_{zz} \cos^2\theta) \quad (10.16)$$

where

$$Q = \frac{\pi^2}{g} \frac{I_l I_s}{(I_l + I_s)} \frac{N_A^2}{V_M} (\chi_{\parallel} - \chi_{\perp}) S_{\parallel} \quad (10.17)$$

Where Q is primarily a function of the solvent properties. In this equation V_M is the molecular volume of the solvent, N_A is the Avogadro constant, I_l and I_s are ionisation potentials of the solute and the solvent molecules, respectively. χ_{\parallel} and χ_{\perp} are the principal polarisabilities of the solvent molecules in a direction parallel and perpendicular to the long molecular axis, respectively. θ and ϕ are the polar angles that characterize the orientation of the liquid-crystal optic axis in the solute molecular fixed coordinate system. α_{xx} , α_{yy} , and α_{zz} are the principal polarisabilities of the solute molecules.

The constant Q can depend on the nature of the solute molecules through the parameters V_M and I_l . In the derivation of equation 10.17 the volume of the cavity containing the solute molecules has been approximated by the volume V_M/N_L of the solvent molecules.

It seems more reasonable to replace this cavity volume with that of the solute molecules and then the expression Q would depend on the size of the solute molecules.

Sackmann^{189,19} has derived a relation between the orientation parameters and the principal polarisabilities of the unsubstituted aromatic solute molecules. He also showed that the principal polarisabilities of the solute molecules (α_{xx} , α_{yy} , α_{zz}) may be determined from the experimental values of the orientation parameters (S_{xx} , S_{yy} , S_{zz}).

The contribution of the permanent electric dipole moment to the intermolecular interaction potential has been studied by Saupe and Nehring using NMR spectroscopy¹⁹. Their results showed that the force between permanent electric dipoles does not contribute considerably to the anisotropic intermolecular interaction potential.

The additive contribution of the individual bonds to the anisotropic potential draws attention to the rule of the additivity of bond polarisabilities¹⁵⁶. Therefore, the principal polarisabilities of substituted aromatic molecules can be determined on the basis of the model of additive bond polarisabilities. The orientation of substituted aromatic molecules is mainly determined by repulsive forces. It has been shown that the anisotropic repulsion potential may be represented by an expression similar to equation (10.16). The polarisabilities are replaced by the van der Waal's dimensions, l_{xi} , in the directions of the molecular symmetry axes. By assuming that the solute orientation is determined primarily by repulsive forces it is deduced that correlation will have the form $S_{zz} \propto 2l_{xx} - l_{yy} - l_{zz}$. This correlation holds for many rod-like, aromatic molecules.

10.3 Experimental

10.3.1. Materials

A. Liquid crystalline solvents; p-methoxy benzyldene-p-n-butylaniline (MBBA) and E7 and E8 (BDH nematic mixtures) were used as the solvents through out this study. MBBA had been made in our laboratory by a well known condensation method. The molecular structure of MBBA, E7 and E8 are shown in Chapter 3 and some of their properties are listed in Table 10.1.

Table 10.1 Liquid crystals used in the experiments

Liquid crystal	T_{NI}	nematic range	$\Delta\epsilon$
MBBA	48	22-48°C	negative
E7	60	-10-60°C	positive
E8	71	-12-71°C	positive

$\Delta\epsilon$ is the dielectric anisotropy of liquid-crystal (Chapter 5), and T_{NI} is the nematic-isotropic transition temperature of the liquid-crystal (the clearing point).

B. Solutes; The solutes were plechroic diazo dyes (sudan black B, sudan III, oil red), Indophenol blue (BDH compounds) and anthraquinon dyes. Solutions were prepared by dissolving ~1 mg of the solute in ~100 mg of the liquid-crystal solvent.

10.3.2 Preparation of Samples

The guest-host cells were made by sandwiching the solutions between two quartz plates (2cm x 1.2cm). Parallel alignment of the guest-host cells was achieved by simply rubbing the quartz plates along a consistent direction. The quartz plates were first coated with an thin layer of cellulose acetate butyrate (CAB-381-20 Eastman Kodak), and then the plates

were placed in an oven at $\sim 90^\circ$ for about 5 hours. The surfaces were then modified by rubbing with a fine grade of soft paper approximately 5 times along a arbitrary but consistent direction. Mylar spacers determined the samples thickness, which was normally $12.5\ \mu\text{m}$ for the dichroic ratio determinations. The guest-host cells were placed on a microscope (Reichert) and their homogeneity confirmed using crossed polarisers. In the former case, indium/tin oxide coated, glass, plates were used as transparent electrodes for the measurement of the contrast ratio (Chapter-2). Copper wires were connected to the glass plates using a two-part silver-loaded epoxy (RS components).

For the measurement of infrared spectra the coating of a very thin layer of lecithin (Sigma) on NaCl plates induced the homeotropic molecular alignment of the sample. For this purpose the cells were dipped several times into a dilute ethereal solution of the lecithin (Chapter 2).

10.3.3 Measurements

A. The measurement of visible spectra

Electronic spectra of the dyes in the liquid-crystal host were taken on a Pye-Unicam Model SP-800 uv-vis spectro photometer equipped with Nicol prism polarisers. The samples with parallel alignment were mounted in a thermostatted holder.

Dichroic ratios R of the dyes were obtained by polarised absorption. The polarisers were rotated by 90° to record the absorbances parallel and perpendicular to the direction of the long molecular axis (grooves), A_{\parallel} and A_{\perp} respectively. The dichroic ratios were calculated using $R = A_{\parallel}/A_{\perp}$.

The orientation of the guest molecules was controlled by using an electric field, and this enabled the contrast ratio of the dyes to be obtained by electrically switching. The

polarised absorption spectra of the dissolved dyes were taken with the electric field off and then with the electric field on.

B. The measurement of infrared spectra

Infrared spectra covering the range (600 cm^{-1} to 4000 cm^{-1}) were taken on a Perkin-Elmer Model 1710 FTIR (resolution 4 cm^{-1}) equipped with a computer. Averaged spectra were obtained by a multiscanning method.

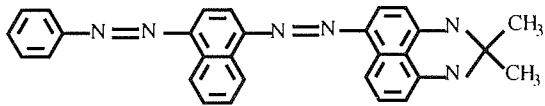
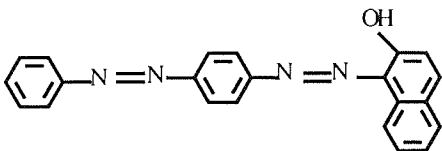
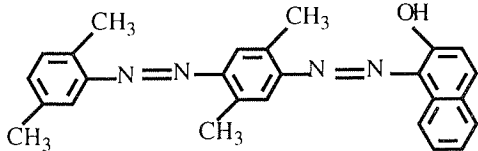
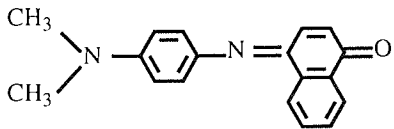
The dichroic ratios of the liquid-crystals were obtained by comparing the absorption of unpolarised light in homeotropic and isotropic layers. Information on the transition moment direction, the dichroic ratio (A_N/A_I), and the order parameter of the samples were obtained by comparing the optical densities measured in the randomly isotropic and in the nematic ordered phases, respectively.

10.4 Result and Discussion

10.4.1 Visible Spectroscopy

The absorption of various dyes was measured and their order parameter S obtained. The temperature of the liquid-crystal cell was controlled at 22 °C. The results are shown in Table 10.2

Table 10.2 Dichroic ratios (R) and order parameters (S) measured for dyes used in the guest-host experiments.

No	Molecular structure	$\lambda_m(\text{nm})$	$R = A_{\parallel}/A_{\perp}$	S
1.	 Sudan black B	620	5.8	0.62
2.	 Sudan III	520	3.8	0.48
3.	 Oil Red	530	3.2	0.42
4.	 Indophenol blue	600	4.0	0.50

The dichroic ratio R and the order parameter S are related to each other by the equation $S = (R - 1)/(R + 2)$, provided that the transition moment is parallel to the molecular axis (section see 10.2.2).

In Figures 10.4-10.7 the visible spectra of some diazo-dyes (sudan dyes) and Indophenol blue (1%) in the nematic mixture of E7 (solvent) are presented. The absorption bands are due to $\pi-\pi^*$ transitions. The dye molecules were aligned with their long molecular axes parallel to those of the solvent molecules. Figures 10.4-10.7 show that $(A_{\parallel} - A_{\perp})$ is positive for the absorption band of the dyes when the transition corresponding to the visible band is polarised in the direction of the long molecular axis.

All of the chosen dyes have generally high stability and high solubility. Sudan black B has the advantage of a high dichroic ratio (or contrast ratio) because of its rod-like molecular structure. An important part of this work is to study the dependence of the dichroic ratio on intermolecular interactions. It is noted that rod-like dye molecules would be expected to have higher order parameter than non rod-like dye molecules. In this work a range of shapes has been considered.

From Table 10.2, it can be seen that Sudan black B has the highest dichroic ratio (R) and the highest order parameter (S). This is a consequence of the long molecular structure and the lack of lateral groups for this molecule. The presence of $-\text{OH}$ group in Sudan III and oil red causes the direction of transition moment to deviate from the long molecular axis. In subsequent discussions it has been assumed that the average hydrodynamic volume occupied by the dye molecules is rotationally symmetric.

The structure of Sudan black B is approximately rod-like, so that the transition moment vector of this dye may be considered to be parallel to the long molecular axis. Therefore, the transition moment vector M_{mn} (direction of dipole moment change) of the $\pi-\pi^*$ transition of this molecule lies within the molecular plane. Since the transition moment

vector M_{mn} between two electronic states m and n is largely parallel to the long molecular axis (z axis), a relationship between the degree of polarisation and the order parameter S can be derived¹⁹. The high order parameter of Sudan black B is due in part to the highly polarisability of the molecule along the long molecular axis.

It should be noted that the $n-\pi^*$ transition is a perpendicular transition, i.e. during the $n-\pi^*$ transition a net displacement of charge occurs perpendicular to the molecular plane. It is clear that the second band (420 nm) in Sudan black B spectra can be considered as another parallel transition ($\pi-\pi^*$). From the dichroic ratio data, the order parameter of the second transition was calculated to be $S = 0$.

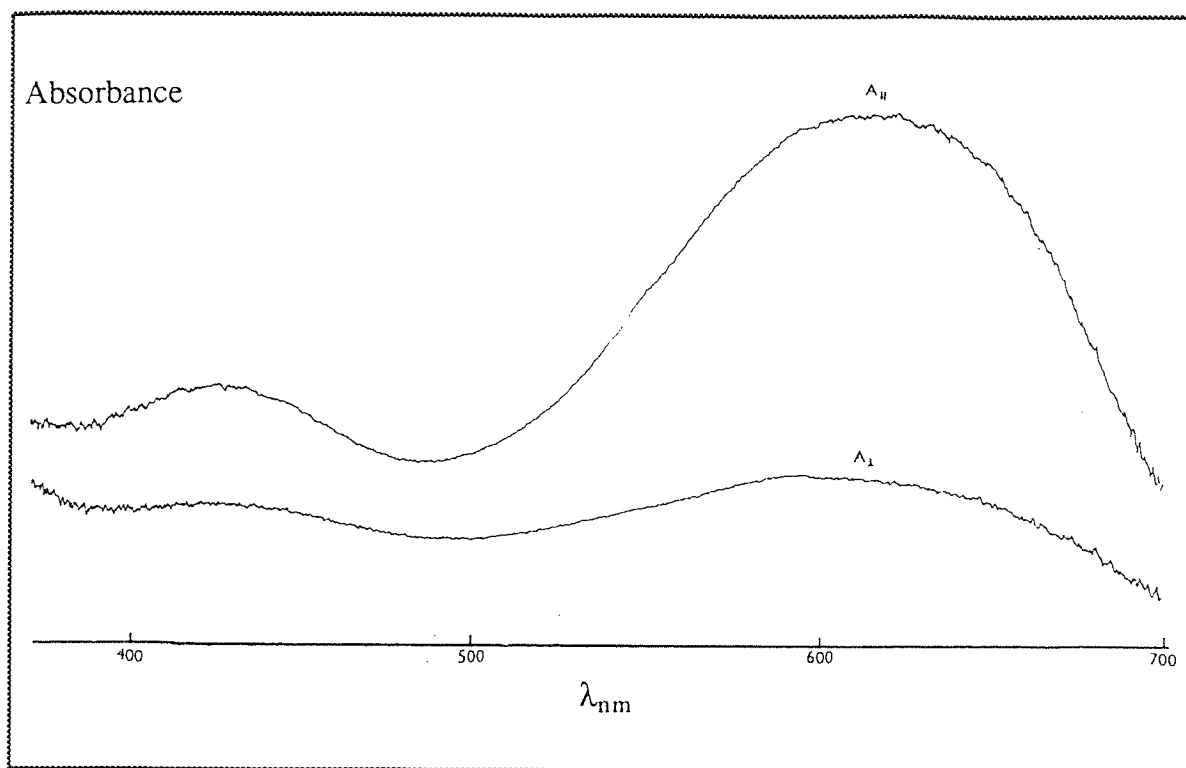


Figure 10.4 Polarised absorption spectra of 1% Sudan black B in nematic solvent (E7). In the top spectrum the electric vector of light is parallel, and in the bottom spectrum perpendicular to the nematic director (grooves).

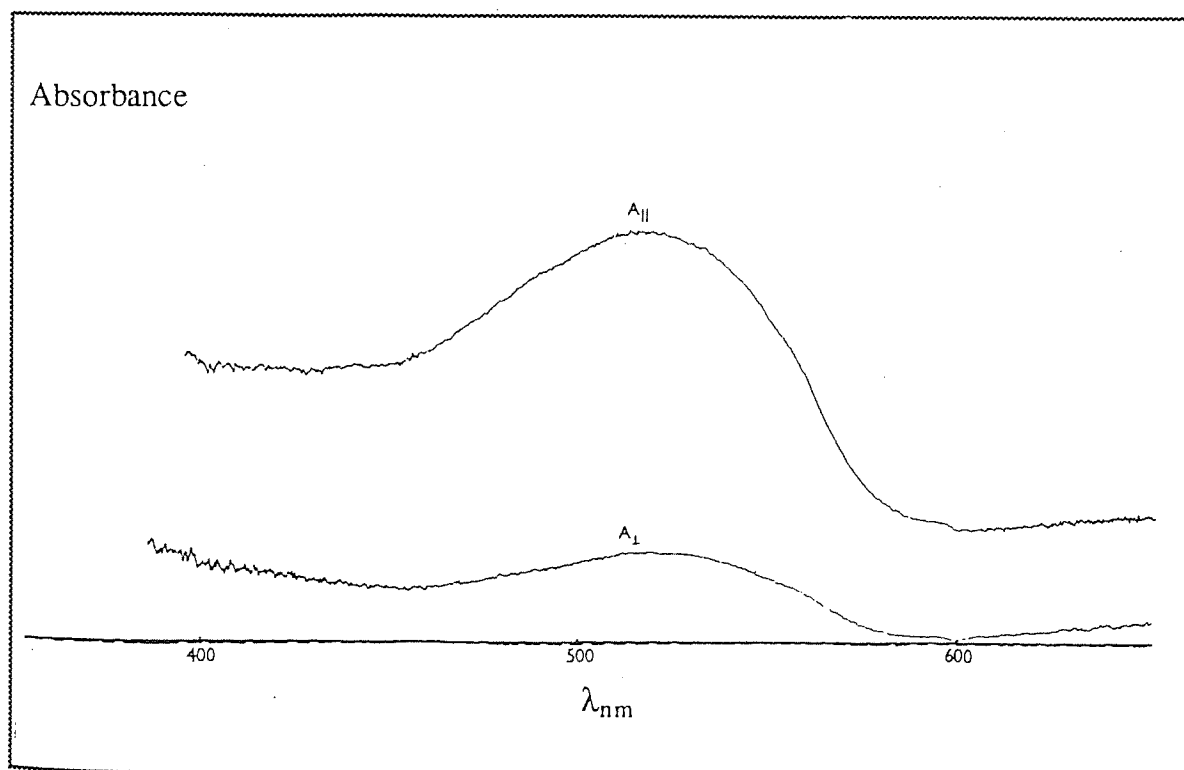


Figure 10.5 Polarised absorption spectra of 1% Sudan III in the oriented nematic phase of E7. The electric vector of light is polarised parallel and perpendicular to the nematic director.

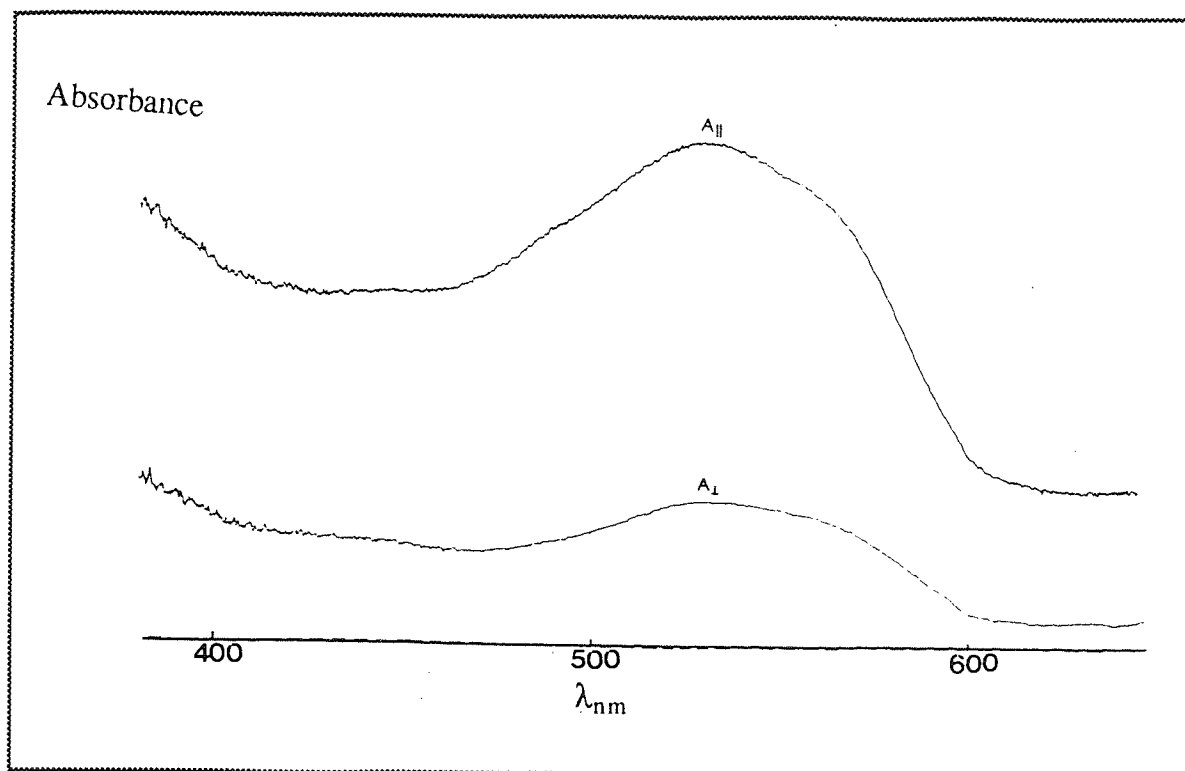


Figure 10.6 Polarised absorption spectra of 1% nematic solution of Oil red. $A_{||}$ and A_{\perp} are the absorbance of light polarised parallel and perpendicular to the nematic director, respectively.

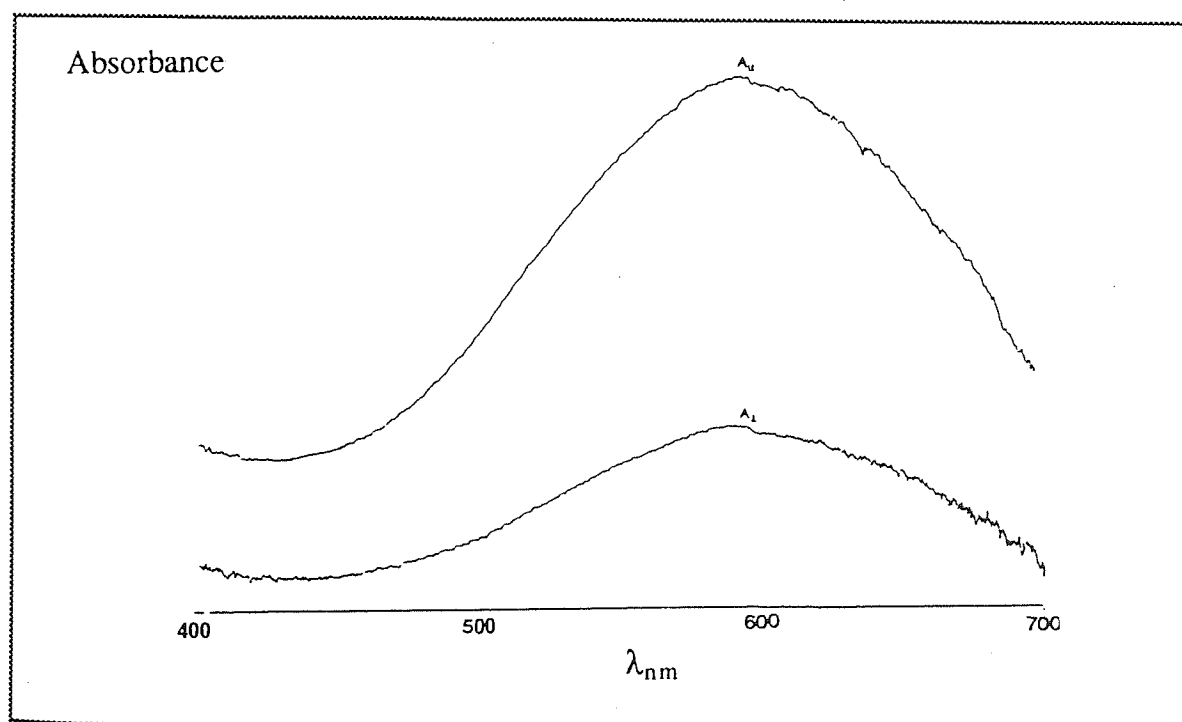


Figure 10.7 Polarised absorption spectra of 1% Indophenol blue in the nematic solvent of E7.

Another class of dyes which may be used in the guest-host interaction was also considered. For this purpose symmetric anthraquinone dyes (Aldrich) which offer the advantage of excellent photochemical stability were used. The molecular structure of these dyes are shown in Figure 10.8. In general the length-to-width ratio of the anthraquinone dyes (planar) is less than those of the azo dyes (rod-like) used in this work.

Figure 10.9 shows that $A_{\parallel} - A_{\perp}$ is positive for absorption bands at 660 and 620 nm for Solvent green, and can be considered as parallel transitions (i.e. $\pi - \pi^*$). In this condition, the transition corresponding to the visible band is polarised in the direction of the long molecular axis. For this dye the absorption bands at ~ 400 nm show that $(A_{\parallel} - A_{\perp})$ is negative, indicating a $n - \pi^*$ transition.

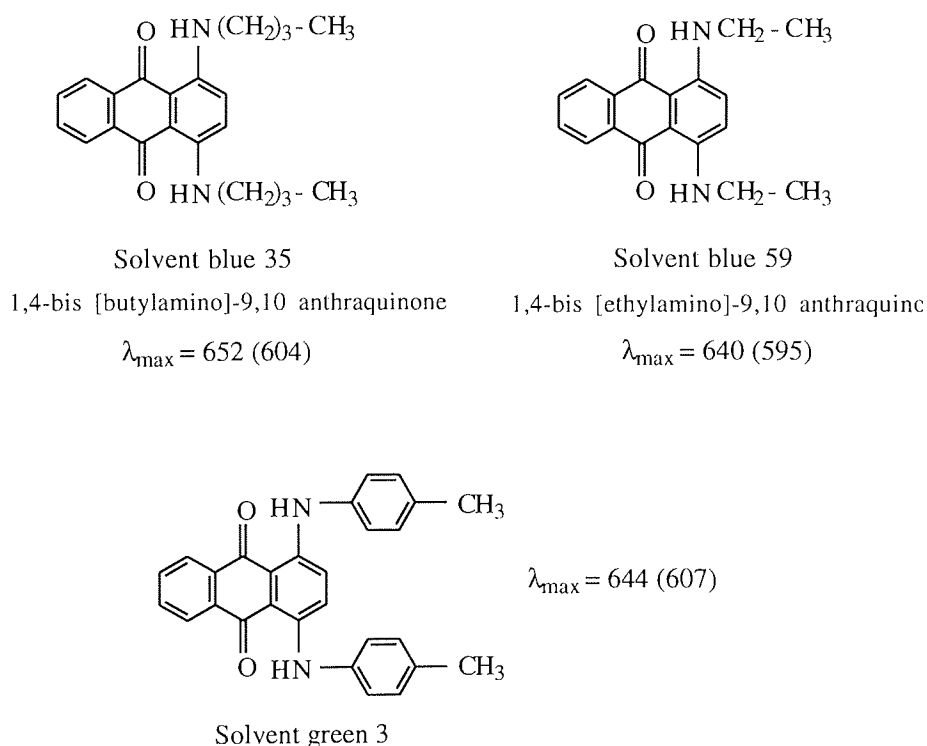


Figure 10.8 Molecular structure of anthraquinone dyes with a symmetry of C_2 .

Table 10.3 shows the red shift observed for anthraquinone dyes and also for an azo dye (Sudan black B), indicating strong molecular interactions between the liquid-crystal molecules and the dye molecules. Such shifts observed with both azo dyes and amino-anthraquinone

dyes have been interpreted in terms of localised intermolecular charge transfer configurations, in which both ground state and excited state energy levels are perturbed by solvent polarity²¹². It is found that the red shift for Sudan black B is higher than those observed for the anthraquinone dyes.

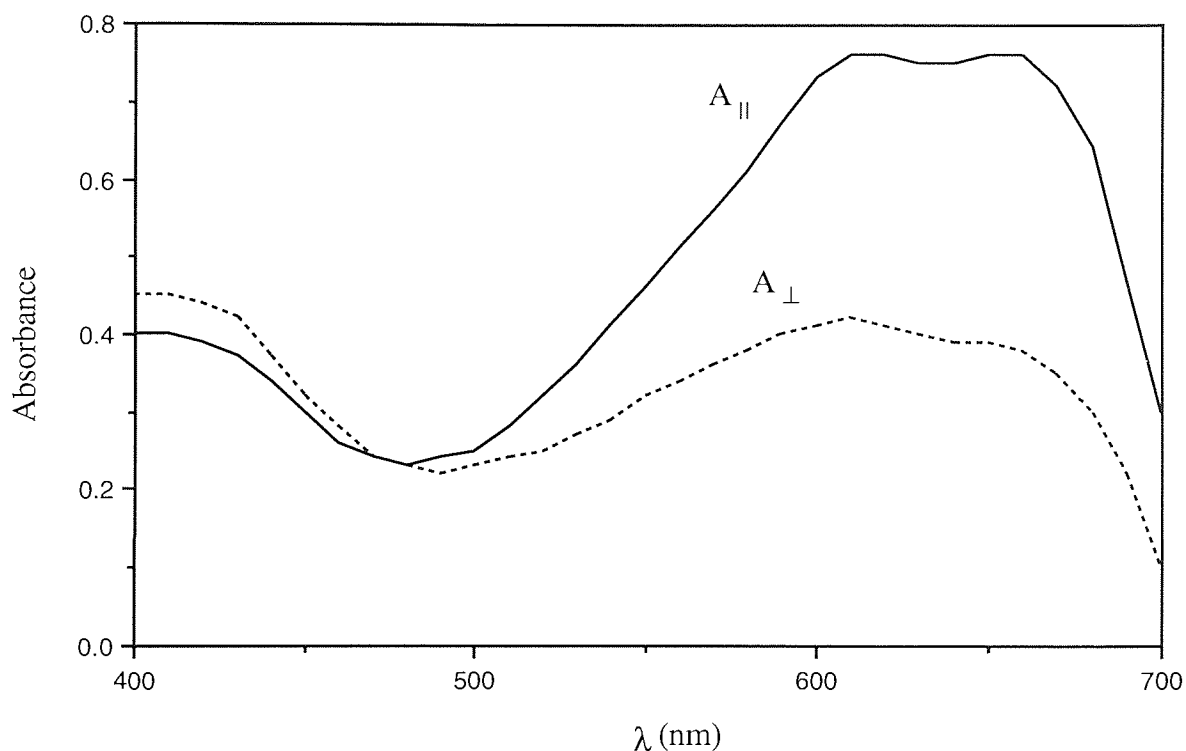


Figure 10.9 Polarised absorption spectra of 1% Solvent green 3 in the oriented nematic phase of E8 at 22°C.

Table 10.3 Order parameters of anthraquinone dyes and Sudan black B.

compound	S	$\lambda_{\max}(\text{nm})$ solvent: acetone	$\lambda_{\max}(\text{nm})$ solvents: E8, E7
Solvent green 3	0.40	644 (607)	660 (620)
Solvent blue 35	0.35	648 (598)	658 (605)
Solvent blue 59	0.30	648 (598)	658 (605)
Sudan black B	0.62	560	600

10.4.1.1 The direction of polarised light relative to the director

In Figure 10.10 transmission has been plotted as a function of the angle (ϕ) between the plane of polarised light and the direction of the grooves (director). For 1% Sudan black B in an E7 host, a straight line was obtained which is in good agreement with the theoretical law²⁰⁷,

$$T_{(\phi)} = [T_{(0)} - T_{(90)}] \cos^2 \phi + T_{(90)} \quad (10.18)$$

This means that the medium is nearly uniaxial and that the axes of the dye molecules are parallel to direction of the micro-grooves. Figure 10.11 was plotted according for the absorption of Sudan black B at different angles (ϕ). Characteristic data are listed in Table 10.4

Table 10.4 Transmission (T) of Sudan black B at different angles (ϕ)

ϕ°	0	30	45	60	90
T	0.12	0.28	0.42	0.57	0.70

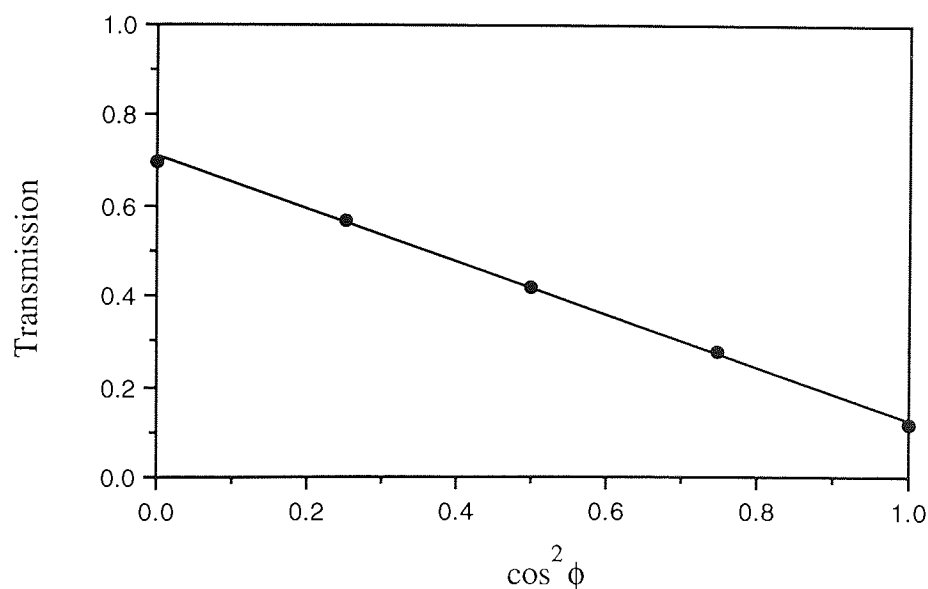


Figure 10.10 Transmittance of 1% nematic solution of Sudan black B as a function of the angle between direction of polarised light and nematic director at 22°C.

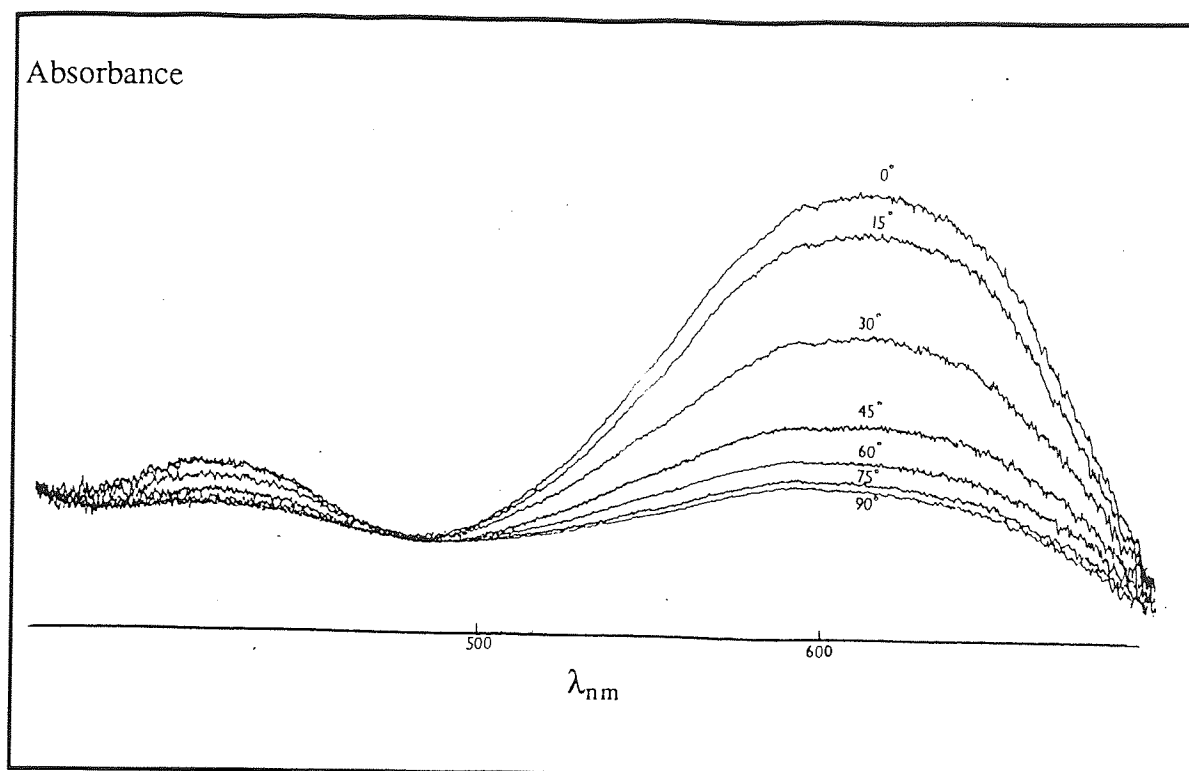


Figure 10.11 Polarised absorption spectra of 1% nematic solution of Sudan black B obtained for different angles (ϕ) between plane of polarised light and the nematic director.

10.4.1.2 The effect of substitution on the dichroic ratio

Any theory describing order in a nematic structure must consider in detail the nature of the intermolecular interaction²⁰⁸. Therefore, the low order parameter observed for Sudan III and Oil red (low with respect to Sudan black B) can be explained by assuming that the order parameter S (the nematic director is considered in z axis) is a function of the difference between the principal solute polarisabilities ($\Delta\alpha = 2\alpha_{zz} - \alpha_{xx} - \alpha_{yy}$). The highly polarised lateral substituent ($-\text{OH}$) in the two dyes molecules increases the polarisability of the molecules in the x or y axis. Therefore, $\Delta\alpha$ (and hence S_{zz}) decreases.

The π electrons do not contribute to the polarisability in a direction perpendicular to the plane of an unsubstituted aromatic molecules¹⁸⁹, but in the case of Sudan III and Oil red the π electrons may contribute to the polarisability via $-\text{OH}$ group. It is noticed that the hydroxy group is an electron donor via a π -bond and an electron acceptor via σ -bond.

However, the polarisability of molecules in the perpendicular direction is mainly due to the polarisability of the σ -bonds. This would suggest that certain orientations of dipoles can have a disadvantageous effect on the order parameter. On the other hand, the dipole moment of the C-OH bond seems to be important because the C-OH dipole may lead to both attraction and repulsion, and the net effect may be very small. The dipole effect is weak for C-Me (due to its weakly dipolar nature), but a steric effect, which increases the intermolecular separation, can be an important contribution for Me-groups. This steric factor affects the breadth of the molecule and will tend to decrease the order parameter of the dye.

The order parameter of Sudan III is higher than that of Oil red dye. In fact Oil red dye is a substituted Sudan III dye in which the width of the Oil red molecules is increased by the methyl groups (Figure 10.12). The difference between their order parameters can be explained using anisotropic repulsion forces for the solute orientation¹⁹.

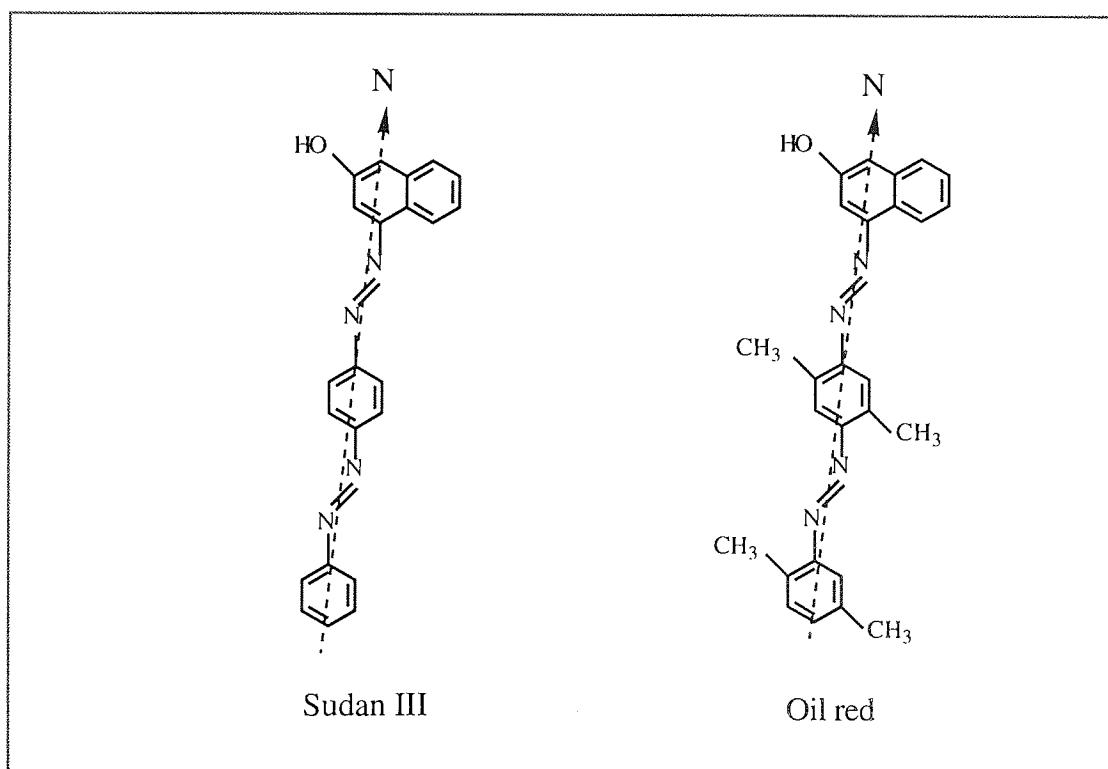


Figure 10.12 The molecular structures of Sudan III and oil red

It should be noted that the orientation of unsubstituted aromatic molecules in nematic liquid-crystal solvent is determined mainly by the anisotropy of the dispersion forces. Repulsive forces are believed to be of minor importance^{189,208}. However, the orientation of substituted aromatic molecules can be determined by the repulsive forces because the anisotropy of the polarisability is not significantly increased by substitution of saturated groups. From this assumption a simple relationship can be derived (section 10.2.7).

$$S_{zz} \propto 2l_{xx} - l_{yy} - l_{zz}.$$

Where l_{xi} is the van der Waal's length in the direction of the molecular symmetry axis. Therefore, in the case of Oil red, l_x (or l_y) increased on substituent of the lateral methyl groups and thus S_{zz} decreases. It is noted that the order parameter depends on the size, shape, and polarity of the substituent.

10.4.1.3 *The effect of temperature on the dichroic ratio*

Solutions of the dyes (1%) in E7 have been studied for homogeneous (planar) alignment. A typical set of results for Sudan black B, showing the temperature dependence of the order parameter, is shown in Figure 10.13. From the accompanying Table 10.5 the order parameter and dichroic ratio are seen to vary considerably with temperature.

The parameter θ in Table 10.5 is the angle between dipole transition moment of the chromophore and the nematic director, and $\Delta A/A = (A_{||} - A_{\perp})/A$ is the reduced dichroism at saturation, which for perfect nematic alignment is given by

$$\Delta A/A = 1.5 (3\cos^2\theta - 1) \quad (4.19)$$

Equation 4.19 was derived from the following relationships²¹³.

$$A_{\parallel} = A_T \cos^2\theta \quad (4.20)$$

$$A_{\perp} = (A_T \sin^2\theta)/2 \quad (4.21)$$

Here A_{\parallel} and A_{\perp} are absorbances measured for plane polarised light parallel and perpendicular to the nematic director (micro-grooves), A_T is the maximum possible absorbance of the transition moment.

The absorbance for the isotropic phase is

$$A = A_T/3 \quad (10.22)$$

From equations 10.19 to 10.21, it follows that

$$A = (A_{\parallel} + 2A_{\perp})/3 \quad (10.23)$$

Table 10.5 Temperature dependence of the order parameter of Sudan black B

Temperature °C	R	S	$\Delta A/A$	θ°
20	5.8	0.62	1.87	30
25	5.7	0.61	1.82	30
30	5.4	0.59	1.75	31
35	5.0	0.57	1.67	32
40	4.5	0.54	1.64	34
45	4.0	0.50	1.52	36
50	3.4	0.44	1.35	37
55	2.8	0.37	1.16	40
60	1.0	0.00	0.00	---

The dichroic dyes dissolved in the nematic solvent align, on average, parallel to the nematic director. However, with an increase in temperature the thermal fluctuation of dye molecules increases and therefore the order parameter decreases. On the other hand, the

experimental results confirm that the nematic-isotropic transition temperature T_{NI} of the liquid-crystal decreases in the guest-host system¹⁹⁰. It seems that the decrease of the T_{NI} depends on size and shape of the guest molecules. However, it was observed that the addition of Sudan black B (1% w/w) did not have much effect on the nematic-isotropic transition temperature of E7 ($T_{NI} = 59.8^\circ$).

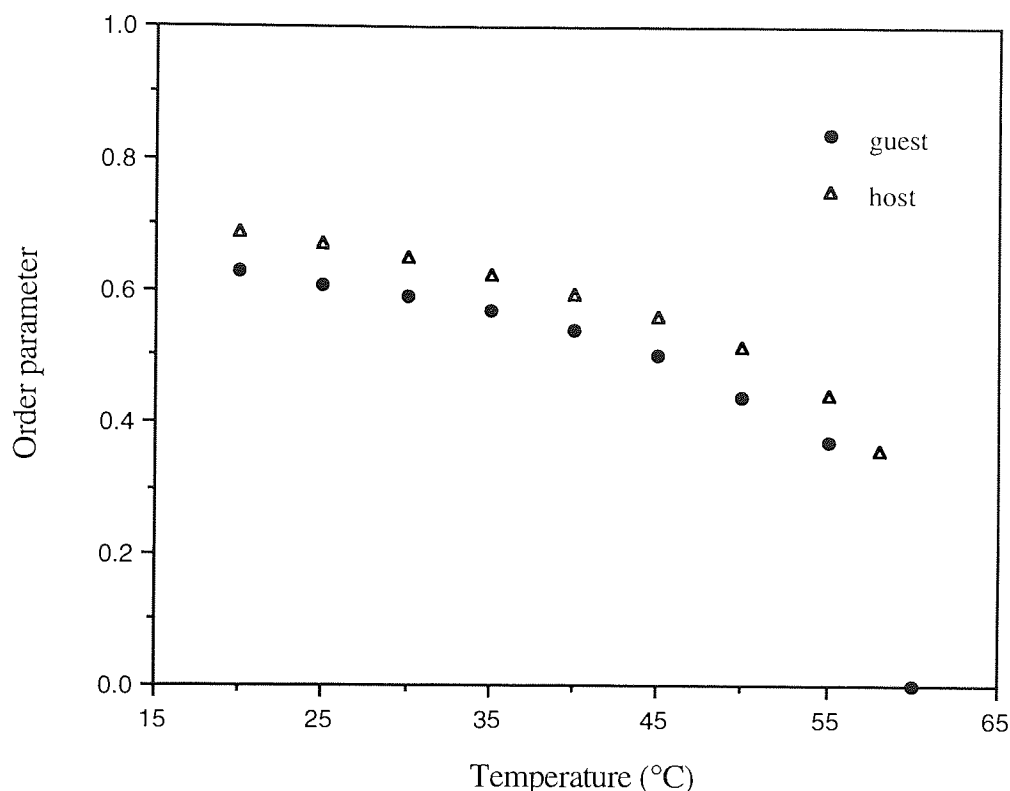


Figure 10.13 Temperature dependence of the order parameter of Sudan black B (guest) in E7 liquid-crystal (host). The calculated order parameter (using Vuks method) for E7 is included for comparison.

10.4.1.4 The effect of cell gap on the dichroic ratio

Measurement of the relative absorbance as a function of cell gap (12.5-50 μm) shows the dichroic ratio (R) and order parameter (S) of the Sudan black B decreases with increasing thickness of the spacer. The result are presented in Table 10.6.

Figure 10.14 shows that the order parameter decreases slowly as the thickness of spacer is increased to about 25 μm , but it decreases sharply behind 25 μm .and rapidly

approaches zero after 50 μm . Interaction between the nematic liquid-crystal and the surface plays a significant role in ordering of the nematic material throughout the volume.

Table 10.6 The dichroic ratio and order parameter for a 1% solution of Sudan black B in E7 and its dependence on thickness of spacer

Thickness of spacer (μm)	Dichroic ratio (R)	Order parameter (S)
12.5	5.8	0.62
25.0	4.8	0.56
37.5	2.7	0.36
50.0	1.4	0.12

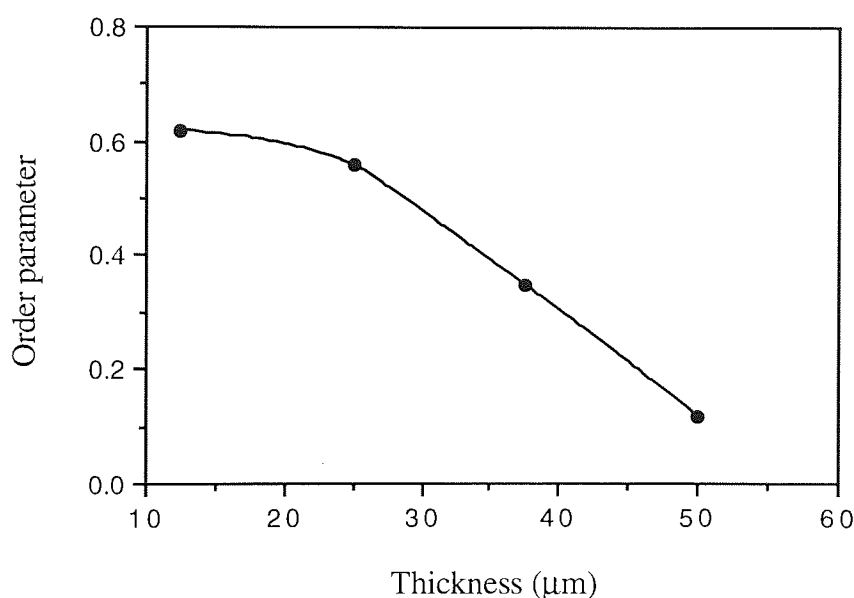


Figure 10.14 The order parameter of a 1% solution of Sudan black B in E7 as a function of the cell gap.

In this part of the experiments, the orientation of the guest-host cell was controlled solely by the effects of surface chemisorption. However, as the cell gap increases, the force which tends to orient the rod-like molecules (or domain) with respect to the surface of the cell walls decreases. Therefore, the number of non-oriented molecules increases and this results in a reduction of the dichroic ratio.

10.4.1.5 The effect of dye concentration on the dichroic ratio

The measurement of polarised absorption as function of dye concentration for a large number of samples (prepared by dissolving 0.1-2 mg of diazo dyes in ~100 mg E7 or E8) shows that the dichroism ratio can be maintained if the sample concentration is restricted to the range 0.05% - 1% (w/w). When the concentration of the dye is higher than about 1.5% the dye λ_{max} cannot be measured because of the high absorption coefficient of diazo dyes. On the other hand, at concentrations lower than 0.05% the measurement of absorbance changes is difficult.

For the types of dyes considered in this project, a dye concentration of approximately ~1% appears to yield the greatest absorption change ($A_{\parallel} - A_{\perp}$). The existence of an upper level of concentration indicates that nematic compounds can produce alignment of only a limited number of dye molecules¹⁹. As the number of dissolved dye molecules increase, non-oriented molecules causes a reduction of the dichroic ratio.

4.4.2 Effect of electric field strength on the degree of color switching

In this study, Sudan black B and Indophenol blue were dissolved separately in E7 in a cell configured for planar alignment. With zero field, the dye molecules were oriented with the long molecular axes parallel to the electric field vector of the polarised light (i.e. parallel to the nematic director). Since the direction of transition dipole moment of the dye molecules is largely parallel to the long molecular axis a strong absorption was observed for $E = 0$. The absorbance became weak when the field was applied^{195,199}. The results are shown in Tables 10.7-10.8. The data in these tables shows that the degree of color switching (dichroic ratio) is a function of field strength. The analysis of polarised spectra of 1% nematic solution of Sudan black B in a 12.5 μm thick cell shows that the absorption peak at 620 nm has an absorbance of $A_{\parallel} = 0.82$ for the field-off condition ($E = 0$), and 0.17 for the field-on condition ($E = 3.2 \times 10^4 \text{ v/cm}$).

For a 1% nematic solution of Indophenol blue, the absorption band at 585 nm has absorbances 0.62 and 0.17 for electric field-off and field-on, respectively (see Table 10.7).

Figure 10.16 shows the voltage dependence of the transmittance of the polarised light measured at 420 nm and 620 nm (the maximum absorption wavelength) for Sudan black B dissolved in a nematic solvent. Figure 10.17 shows the voltage dependence of the transmittances P_{\parallel} and P_{\perp} for a planar aligned guest-host cell containing a 1% nematic solution of Indophenole blue. It can be seen that, transmittance P_{\perp} measured for the planar cell is independent of applied voltage, while transmittance P_{\parallel} increases as the voltage increases. This is because surface layers (depicted by SL_1 and SL_2 in Figure 10.15) of the liquid-crystal become thin as the voltage is increased. The voltage independence of the transmittance P_{\perp} indicates that molecules are always perpendicular to the polarisation plane of the incident light¹⁹⁸.

Table 10.7 The salient features of the visible spectrum of a 1% solution of Sudan black B in the oriented nematic E7 (thickness of the cell: 12.5 μm).

Voltage V (ac field, 5 kHz)	Absorption peaks	Absorbance
0	620 nm 420 nm	0.82 0.27
10	620 nm 420 nm	0.46 0.16
20	620 nm 420 nm	0.28 0.14
30	620 nm 420 nm	0.22 0.14
40	620 nm 420 nm	0.17 0.14

Table 10.8 Polarised spectra data of a 1% solution of Indophenol blue in the oriented nematic E7 (thickness of the cell: 12.5 μm).

Voltage V (ac field, 5 kHz)	Absorption peaks (λ_{max})	Absorbance
0	585 nm	0.62
10	585 nm	0.32
20	585 nm	0.22
30	585 nm	0.19
40	585 nm	0.17

It should be noted that the transmittance P_{\parallel} is also a function of frequency. When an ac field (40 V) with low frequency (50-1000 Hz) was used, the transmittance increases. This is because the orientation of the molecules tends to reverse with changes in the direction of the alternating electric field, for sufficiently low frequency.

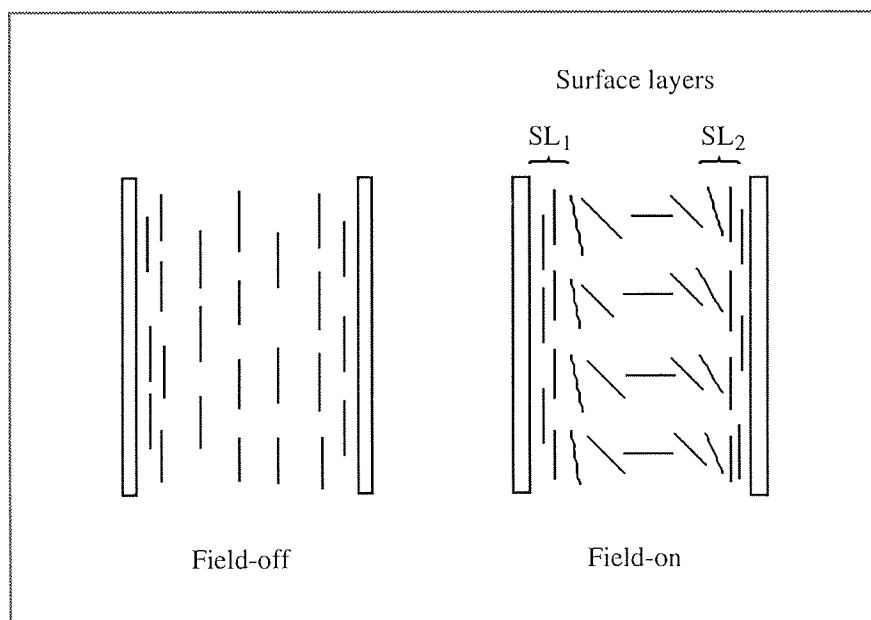


Figure 10.15 Molecular orientation in a planar cell for field-on and field-off conditions.

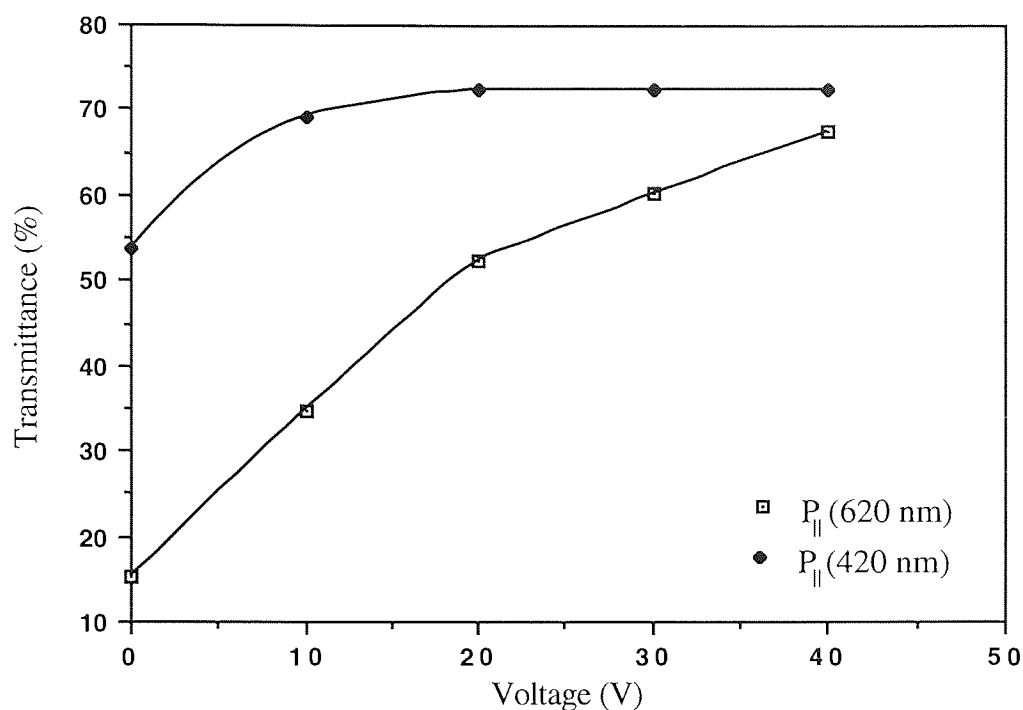


Figure 10.16 The voltage dependence of transmittances $(P_{\parallel})_{620\text{nm}}$ and $(P_{\parallel})_{420\text{nm}}$ for a planar aligned (Sudan black B-E7) cell. P_{\parallel} is the transmittance of polarised light parallel to the nematic director.

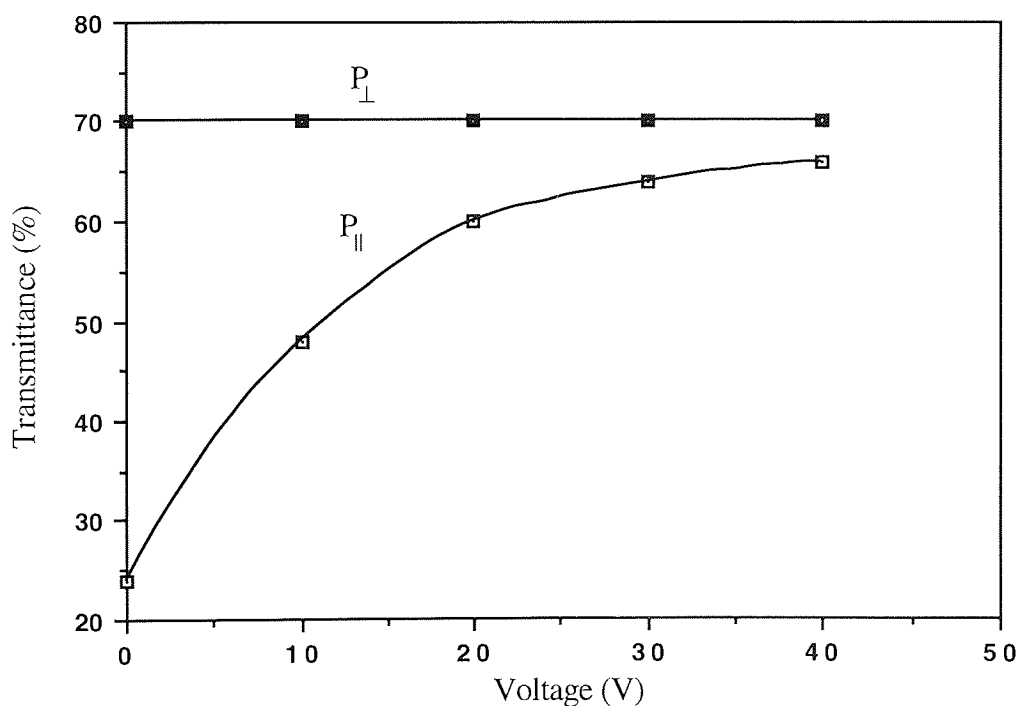


Figure 10.17 The voltage dependence of transmittances of polarised light of wavelength of $\lambda_{\text{max}} = 585 \text{ nm}$ for a 1% Indophenol blue in E7. P_{\parallel} and P_{\perp} are the transmittances of polarised light parallel and perpendicular to the nematic director respectively, for a planar aligned cell.

10.4.3 Infrared spectroscopy

The infrared spectra of E7 in the nematic phase are shown in Figure 10.18. The solid and dashed lines refer to the absorbances of the bands homeotropic alignment (A_N) and the isotropic state (A_I), respectively. The bands at 2928 cm^{-1} and 2856 cm^{-1} are due to the asymmetric and symmetric C-H stretching respectively, and a sharp band at 2226 cm^{-1} is attributed to the $\text{C}\equiv\text{N}$ stretching vibration. The 1606 and 1494 cm^{-1} bands are assigned to the phenyl ring modes which primarily involve C-C stretchings. The band at 1251 cm^{-1} is due to the phenyl-oxygen stretching of the alkoxy group of 8OCB in E7. The absorption band at 813 cm^{-1} is due to the phenyl ring breathing (para-disubstitution normally yields a strong band in this region).

The dichroic ratios derived from the FTIR spectra are listed in Table 10.10. The absorbances for the nematic phase were measured at room temperature (22°C), and those of the isotropic phase at a temperature just above the clearing point ($T_{NI} = 59.8^\circ\text{C}$). It is evident from Table 10.10 that the transition moments of the 2928 , 2856 , and 813 cm^{-1} bands are perpendicular to the long molecular axis (i.e., a perpendicular transition moment).

From the band at 2226 cm^{-1} ($\text{C}\equiv\text{N}$ stretching), the order parameter S was calculated to be about 0.6. This band gives the highest value of the order parameter of E7. The $\text{C}\equiv\text{N}$ stretch, $R > 1$, indicates that the transition moment is parallel to the long molecular axis (parallel transition moment).

The infrared spectra of 8CB are shown in Figure 10.19. The $\text{C}\equiv\text{N}$ stretching band was chosen as an indicator of the average degree of orientational order in 8CB, because this vibration band is relatively intense and is well resolved (Table 10.11). Using this band, the order parameter ($S = 1 - R$) was calculated to be about 0.5 for the case when no

spacer is used (i.e. the two plates are just pressed together). The band at 2226 cm^{-1} also gives also the highest value of order parameter for 5CB and 6CB.

Table 10.10 Vibrational assignments and dichroic data for E7

wavenumber (cm^{-1})	assignment	dichroic ratio ($R = A_N/A_I$)	type
2928	CH asym. str.	1.10	\perp
2856	CH asym. str.	1.06	\perp
2226	$\text{C} \equiv \text{N}$ str.	0.45	\parallel
1606	phenyl ring str.	0.49	\parallel
1494	phenyl ring str.	0.48	\parallel
1251	$\phi - \text{O}$ str.	0.47	\parallel
813	phenyl ring breathing	1.23	\perp

$R < 1$ = Parallel to the long molecular axis, \parallel .

$R > 1$ = Perpendicular to the long molecular axis, \perp .

It should be noted that if there is no difference in intensity between the two orientations (i.e., $R \sim 1$), then this indicates a random orientation for the chemical grouping concerned.

Table 10.11 Vibrational assignments and dichroic data for 8CB

wavenumber (cm^{-1})	assignment	dichroic ratio ($R = A_N/A_I$)	type
2926	CH asym. str.	1.21	\perp
2855	CH asym. str.	1.18	\perp
2227	$\text{C} \equiv \text{N}$ str.	0.53	\parallel
1607	phenyl ring str.	0.54	\parallel
1494	phenyl ring str.	0.53	\parallel
816	phenyl ring breathing	1.44	\perp

It can be concluded that, the analysis of homeotropically ordered nematic phase using IR spectroscopy provides a quick and simple method for deriving of the order parameter and for deducing molecular orientations and band polarisations.

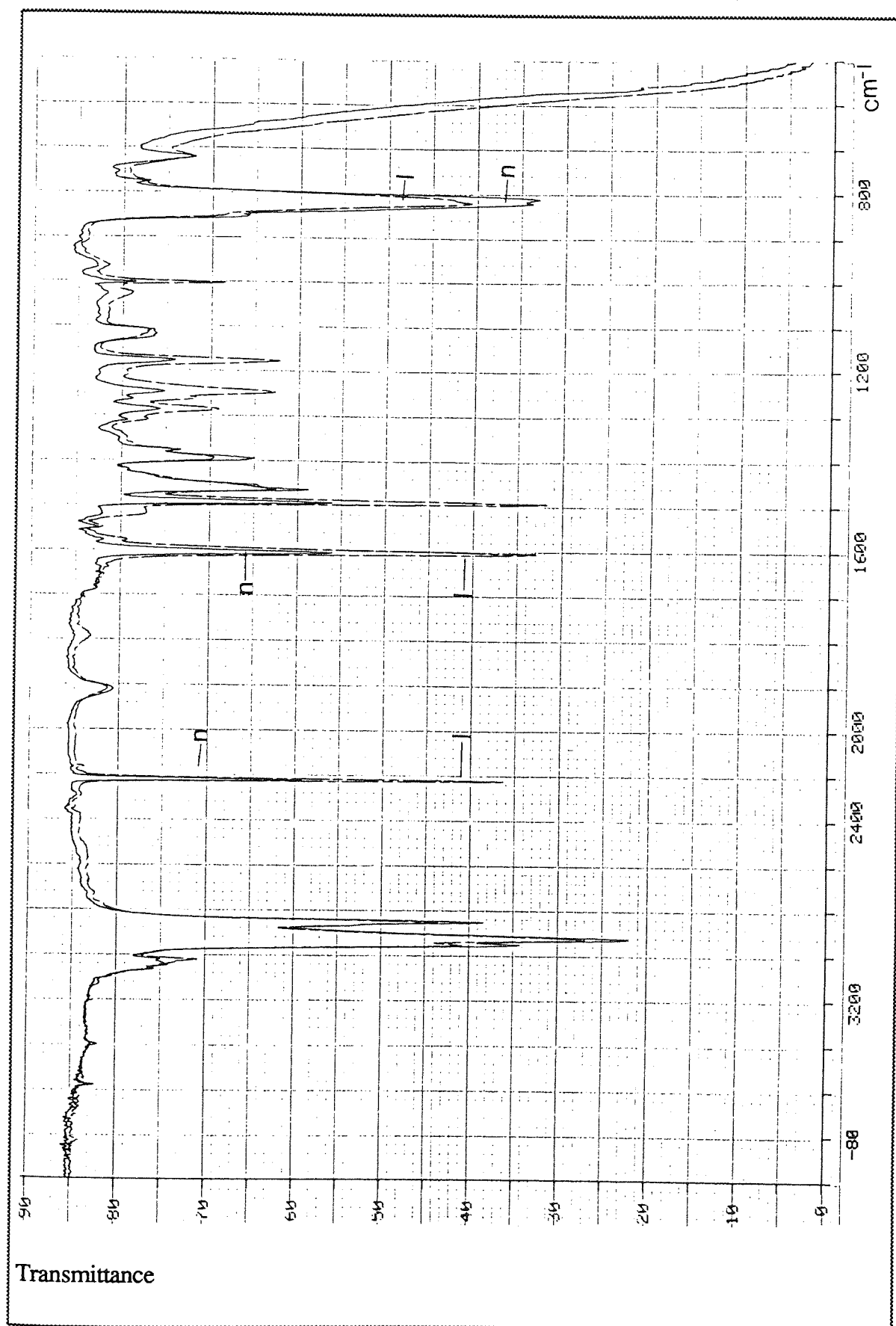


Figure 10.18 The FT infrared spectra of E7 in the nematic state (N), and in the isotropic phase (I)

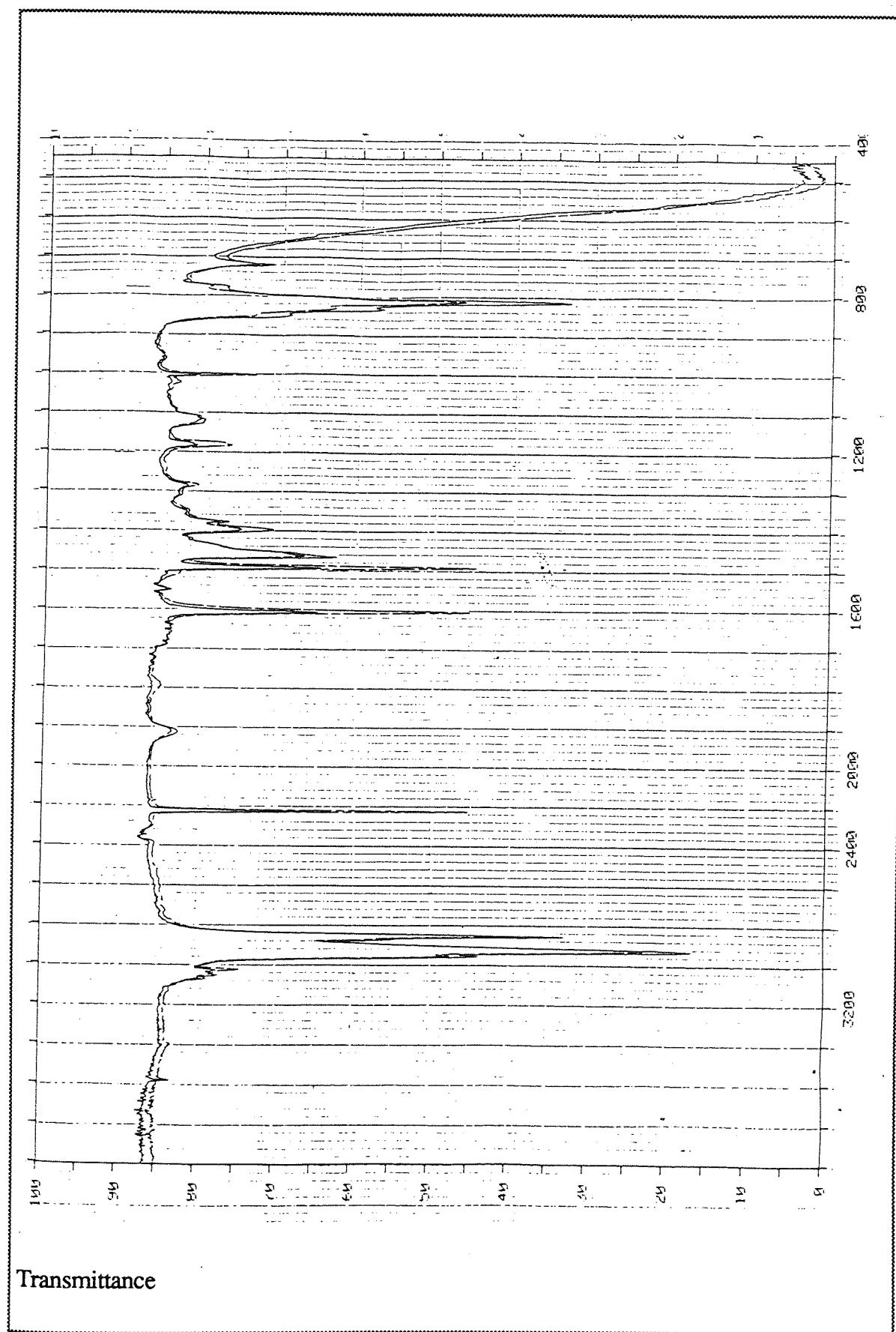


Figure 10.19 The FT infrared spectra of octyl cyanobiphenyl, 8CB, in the nematic state (n), and in the isotropic phase (I).

CHAPTER 11

CONCLUSIONS AND FUTURE WORK

11.1 Conclusions

In this thesis the dielectric, electro-optical, density and spectroscopy properties of some 4,4'-alkyl (alkoxy) cyanobiphenyls and various nematic mixtures have been measured under a variety of external influences. The relationship between the molecular structures and the physical properties of these liquid crystalline compounds were investigated by using as many different techniques as possible. The main conclusions of the preceding chapters are discussed below:

A variety of methods have been reviewed for obtaining parallel or perpendicular alignment in liquid-crystal cells. These are based on the generation of substrate interfaces which have an orienting action on the liquid-crystal molecules. These orienting surfaces can be created by a number of different surface treatments, including chemical cleaning of the surface, physical adsorption, rubbing of the solid substrate and by deposition of thin films of organic or inorganic materials. For the dielectric, electro-optical and spectroscopy studies of thin layers of liquid crystal compounds in the nematic phase, sandwich type cells, with planar or homeotropic alignment, were constructed. A planar alignment was achieved by rubbing the surface of a thin coating of cellulose acetate butyrate (CAB), while good homeotropic alignment was obtained by using a thin layer of lecithin as a surface active agent. Also, novel dielectric and electro-optic cells (small sample volume) were constructed for use over a range of temperature.

The phase transitions and order parameters of three liquid crystal homologs (5CB, 6CB, and 7CB), 6OCB and three eutectic nematic mixtures E7, E8, and E₆₀7 in their nematic

and isotropic phases were investigated as a function of temperature using optical and density measurements. In this work, the interrelationship between density and refractive index and the molecular structure of these liquid crystals were established.

The following conclusions are made following an analysis of density data obtained for the liquid crystals in their nematic and isotropic phases at different temperatures:

1. From the density data obtained for 5CB and 7CB, it was found that the contribution of a methylene group to the molar volume for the nematic phase is close to the contribution of a methylene group reported for alkylbiphenyls in the isotropic phase, but is higher than that found for n-alkanes in the solid state. Thus, for the nematic phase the packing of alkyl chains is closer to that found for the isotropic phase, rather than to the solid phase.
2. The density data also showed that the molar volume increment at the transition temperature T_{NI} for the odd members of alkyl cyano biphenyls was high, indicating a first-order transition. This behaviour probably reflects the dependence of the orientational order parameter on the odd-even alternation effect, commonly exhibited by molecules that possess linear alkyl groups.
3. The thermal expansion coefficients for the pure cyanobiphenyl liquid crystals in the nematic phase are greater than those of the isotropic phase. For both E8 and E₆₀₇ the mean expansion coefficients for their nematic and isotropic phases are almost equal, i.e. $8.0 \times 10^{-4} \text{ }^{\circ}\text{C}^{-1}$.
4. The liquid-crystal mixture E8 was found to exhibit a broad biphasic region that overlaps or adds to the pretransitional behaviour. However, for the pure alkyl cyanobiphenyl liquid crystal components of E8 the temperature dependence in the isotropic phase is more linear, compared to that observed for E8.

5. It was found that, the molecular volumes (V_M) of 7CB and 6OCB are close namely 464 \AA^3 and 456 \AA^3 , respectively. This indicates that packing of molecules in the both liquid crystals are similar. The flexible part of the alkyl end groups are essentially identical for both 6OCB and 7CB, i.e. $-\text{C}_6\text{H}_{15}$. This is because in 7CB the methylene group linked to the phenyl ring is essentially immobile, with respect to rotation about the C-phenyl bond. Therefore, heptyl cyanobiphenyl (7CB) can be regarded as equivalent to hexoxy cyanobiphenyl (6OCB) with regards to the flexibility of their respective alkyl groups.

The effective molecular polarisabilities, anisotropy of polarisabilities and order parameters S of the nematic liquid crystals were calculated using optical and density data measured at several temperatures. The order parameters calculated using the different methods of Vuks⁵⁸, Neugebauer⁵⁴, Saupe-Maier⁵⁵, and Palffy-Muhoray⁵⁶ are nearly the same for the liquid crystals considered in the present study. The following points are made:

1. Vuks assumed the internal field in anisotropic material to be isotropic. The assumption of isotropic internal field in a medium that possesses an anisotropic molecular distribution appears to be illogical and lacks theoretical basis. However, the Vuks relation gave good results for the polarisabilities derived from the refractive indices and densities, when compared to values calculated using more elaborate theories.
2. Saupe-Maier assumed an anisotropic internal field, and introduced a single internal field factor "a". The use of a single internal field factor means that the internal field factors along and perpendicular to long molecular axis have the same value. This can be regarded as a disadvantage for this theory since the

internal field factors along and perpendicular to long molecular axis are generally expected to be different.

3. The Neugebauer method assumes an anisotropic internal field in which the polarisabilities of molecules depend on the direction of the field. The internal field factors γ_e and γ_o along and perpendicular to long molecular axis had different values. The assumption of an anisotropic internal field to describe an anisotropic molecular distribution is more acceptable, and provides a firmer theoretical basis. Thus, Neugebauer's method is preferable.
4. Palffy-Muhoray *et al.* assumed an anisotropic internal field, and introduced a model that indicates that the internal field anisotropy is proportional to the orientational order parameters. This method not only can be used to calculate effective polarisabilities, order parameter, and internal field factor but can also be used to determine an effective length-to-breadth ratio κ of a molecule.
5. The order parameters S of the nematic mixtures E7 and E8 are larger than those found for each of their two main components, pentyl and heptyl cyanobiphenyl. Also, the order parameter of the eutectic mixture E_{6O7}, composed of hexoxy and heptoxy cyanobiphenyls (41.5 : 58.5) is larger than the S -value of 6OCB. In the present studies E8 was found to have the highest order parameter.

The static dielectric data for solutions of liquid-crystal showed a high molecular association, comparable to that observed in the nematic or isotropic phases. The correlation factors "g" at different concentrations for the materials were smaller than 1, a value indicative of anti-parallel molecular dipole association. It was found that pentyl biphenyl, 5B, was not significantly associated in the range of concentrations covered in this study. In contrast to 5B, it was found that 4-cyanobiphenyl (CB), showed a high

degree of anti-parallel molecular dipole association, even at low mole fractions of solute. The two alkoxy cyanobiphenyls, 5OCB and 8OCB, showed a high degree of anti-parallel molecular association at low concentrations, while for 8OCP (a non-mesogen) the association develops more slowly, with respect to concentration, as the concentration increases. This behaviour could be a consequence of the higher polarisability of cyanobiphenyls molecules along their long molecular axes, compared to that of cyanophenyl molecules. These observations highlight the importance of the biphenyl core and its role in determining molecular interactions in the formation of nematogenic compounds. It can be seen the molecular characteristics responsible for aggregation, such as dipolar group, polarisability, and alkyl groups must be correctly balanced in order to achieve the formation of a liquid crystalline phase. The contribution of the highly polar cyano-end group is particularly significant in this respect.

The static dielectric studies of the nematic phases of the alkoxy cyanobiphenyl liquid crystals and the eutectic mixture of 7OCB/6OCB indicated an molecular alignment induced by the steel electrode surfaces of the dielectric cell. Analysis of the dielectric data showed that the dipole components along the long molecular axes, have a tendency for anti-parallel alignment which increases with increasing nematic order, whereas no such increase is found for the dipole components perpendicular to the the long molecular axes. Although, Hori *et al*¹⁴² have observed (using X-ray studies) that 6OCB and 7OCB dimers in the crystalline state are formed by close contacts of CN groups between neighboring molecules, the dielectric studies of solutions of alkoxy cyanobiphenyls, suggests that dimers are formed by CN-phenyl contacts in which the cyano groups of the interacting molecules are the negative poles and opposite the aromatic ring systems are the positive poles. According to this model the alkyl chains lie outside the overlapping region of the dimer. The dielectric permittivity of the alkyl (alkoxy) cyanobiphenyl liquid crystals in the isotropic phase exhibited anomalous behaviour (a pre-transition effect) just above the nematic-isotropic transition

temperature. This behaviour was found to extend to about 10°C above T_{NI} , and is believed to be due to the high degree of the short-range interactions in the isotropic phase at temperatures close to nematic-isotropic transition point.

The dielectric response of thin layers of E7 and E8, in the aligned state, have been measured in the frequency range 12 Hz to 100 Hz at different temperatures (183K - 337K). Dielectric spectra were also obtained for supercooled E7 and E8 in the Hz and kHz range. These two eutectic mixtures exhibited similar dielectric behaviour in the supercooled state. It was noted that, E7 became supercooled much more easily than E8. The dielectric relaxation studies showed that when the measuring electric field was parallel to the nematic director ($E = E_{\parallel D}$), one loss peak was observed for E7 and for E8. This is a low frequency relaxation process that exhibits a Debye-type behaviour in the supercooled state, and is believed to be due to dipole rotation around the short molecular axis. When the electrical field was perpendicular to the nematic director ($E = E_{\perp D}$), two resolved dielectric loss processes have been observed. The low-frequency process could be described by a single Debye-mechanism and the high frequency process by a Cole-Cole mechanism. The high frequency relaxation process is believed to be due to dipolar rotation around the long molecular axis. The low-frequency relaxation was observed when the electric field was perpendicular to the long molecular axis, and has almost the same activation energy as the process observed for the parallel relaxation process (μ_{\parallel}), and its origin may be the result of some misaligned molecules. The activation energies for high frequency process (Cole-Cole) are higher than the low-frequency relaxation process (Debye). It can be due to the presence of a high degree of short range anti-parallel dipolar association in the supercooled nematic. The relatively high activation energy calculated for the high frequency mechanism can be partly attributed to this molecular association.

Dynamic light scattering studies for dilute solutions of alkyl cyanobiphenyls (5CB, 6CB and 8CB) showed that the depolarisation ratio (Δ_{12}) increases non-linearly with

increases in solute mole fraction. This effect is a partly due to the existence of molecular association even for low concentration of solutes. Dielectric studies together with the Kerr effect confirm the high degree of molecular association (anti-parallel correlation) in dilute solutions of the alkyl cyanobiphenyls.

The following conclusions are made on the Kerr effect measurements on dilute solution of the liquid crystals and isotropic phases at different temperatures:

1. The plots of α (analyser rotation) against the square of applied electric field for the different concentration of pentyl, hexyl and octyl cyanobiphenyls (5CB, 6CB, and 8CB) were found to be linear in the voltage-range 0-4 kV.
2. For dilute solutions of alkyl cyanobiphenyls, the sign of Kerr constant (B_{12}) was positive, and increases non-linearly with solute concentration (weight fraction). This effect is concluded to be due to the existence of molecular association even at low concentration of solute.
3. The electrically induced birefringence, δ , of the liquid crystals in the isotropic phase was found to be a linear function of the square of the applied electric field, E^2 . For the voltage range, used in this study.
4. The Kerr effect data shows that, the induced birefringence depends strongly on temperature, and it increases with decreasing temperature as the nematic transition temperature is approached.
5. The Kerr constant, B , of these liquid crystals (E8, E7, F1, F2 and 5CB) found to be very high at the nematic-isotropic transition temperatures as the molecules are expected to be highly ordered close to phase transition temperatures.

6. The theory of Landau-De Gennes¹⁶⁹ was used to describe the pre-transitional behaviour in the isotropic phase of the liquid-crystals. This theory is essentially based on the assumption that short-range forces predominate in the region of the nematic-isotropic transition.

The following conclusions are made on the measurement of the dynamic behaviour of a thin layer of ordered alkyl cyanobiphenyl liquid-crystals (5CB, 6CB and 8CB).

1. It was found that, for a fixed temperature, the relaxation-rise time decreases markedly with increasing voltage, but the decay time within experimental error, is independent of applied voltage.
2. For a homeotropically smectic phase of 8CB, an optical transient was not observed.
3. Analysis of the birefringence-decay curves obtained for 5CB, 6CB and 8CB in the nematic phase indicated a single relaxation process. The variation of the relaxation decay time with temperature were very small, and low activation energies were obtained for the cooperative reorientation of the whole liquid-crystal sample.

The use of nematic liquid-crystals as anisotropic solvents provides a quick and simple method for measuring a number of anisotropic optical properties. Optical polarisation measurements of solutes made using nematic solvents give important information concerning the orientation of the solute molecules, the direction of transition moments, and the polarisations associated with electronic and infrared absorption bands. The optical anisotropy of the guest molecules in a liquid-crystal system depends on the order parameter of the liquid-crystal and molecular alignment of the host molecules, and dichroic dyes may therefore be used as probes to give additional information about

the anisotropic physical properties and molecular reorientation of the liquid-crystal molecules. Molecular orientation in nematics and the average orientation of the guest molecules in such systems is related to the anisotropy of the intermolecular forces.

From the observed dichroic ratio, the order parameter of the transition moment depends on the size, shape, and polarity of the substituent. The dependence of the order parameter on the steric effect of the methyl substituent can be explained using an anisotropic repulsion model. The following conclusions are made on the results obtained using guest-host interactions of the liquid crystals:

1. Sudan black B had the highest dichroic ratio (R) and the highest order parameter (S). This is a consequence of the long molecular structure and the lack of lateral groups for this molecule, so that the transition moment vector of this dye may be considered to be parallel to the long molecular axis. The high order parameter of Sudan black B can be due in part to the highly polarisability of the molecule along the long molecular axis.
2. Due to a steric effect of Me-groups, which increases the intermolecular separation, the order parameter of Oil red is lower than that of Sudan III dye.
3. The red shifts observed for azo and anthraquinone dyes indicating strong molecular interactions between the liquid-crystal molecules and the dye molecules. It is found that the red shift for Sudan black B (an azo dye) is higher than those observed for the anthraquinone dyes.
4. Finally, the guest-host system based on homogeneous-homeotropic alignment change using electric fields shows that the dichroic ratio strongly depends on voltage and frequency.

4. Finally, the guest-host system based on homogeneous-homeotropic alignment change using electric fields shows that the dichroic ratio strongly depends on voltage and frequency.

11.2 Suggestions for further work

From the experimental studies carried out in this work and the results obtained, some suggestions for future work are made, which can be summarised:

1. Although alignment of E7 using for kinds of cellulose acetate butyrate (CAB) films showed parallel alignment, but the effect of molecular weight of CAB polymer and the number of CAB layers on the alignment of liquid-crystal needs more investigation.
2. Electro-static charges may be produced by rubbing the glass surfaces of liquid-crystal cell (see Chapter 2). The effect of these charges on the molecular alignment should be investigated
3. Dielectric, electro-optic Kerr effect and phase transition studies should be carried out for the guest-host systems which were used in this work such as Sudan black B and E7.
4. Polarised spectroscopy studies of charge transfer complexes in the nematic solvent should be carried out. To make a charge transfer complexes using nematic liquid crystals as electron donor material and measuring dichroic ratio of these systems in the visible region.
5. S-tetrazin dyes, should be used as guest molecules in the guest-host interaction, following by dielectric and electro-optical measurements of this system.

for some molecules which have a structural relationship with the alkyl (alkoxy) cyanobiphenyls.

7. In order to understand the role of various factors such as molecular association in the dynamic behaviour of alkyl cyanobiphenyls, the dynamic Kerr effect of these liquid crystals in the ordered nematic phase (using different molecular alignment with respect to electric field) should be more investigated.

References

1. F. Reinitzer, *Monatsch*, **9**, 421 (1888).
2. O. Lehmann, "*Liquid-Crystals*", *Ber.*, **41**, 3774 (1908).
3. J. L. Whith, "*Historical Survey of Polymer Liquid-Crystals*", *J. Appl. Polym. Sci., Appl. Polym. Symp.*, **41**, 3 (1985).
4. G. W. Gray, "*Molecular Structure and the Properties of Liquid-Crystals*", Academic Press, New York, (1962)
5. J. L. Fergason, *Appl. Optics*, **7**, 1729 (1968).
6. G. H. Heilmeyer and L. A. Zanoni, and L. A. Barton "*Dynamic Scattering in Nematic Liquid-Crystals*", *Appl. Phys. Lett.* **13**, 46 (1968).
7. G. Gray, K. J. Harrison, J. A. Nash, *Electron. Lett.*, **9**, 118 (1973).
8. Priestley, Nojtowicz, Sheng, "*Introduction to Liquid-Crystals*", Plenum Press (1974).
9. G. W. Gray and P. A. Winsor, "*Liquid-Crystal and Plastic Crystals*", Volume **I**, Ellis Horwood Limited (1974).
10. F. D. Saeva, "*Liquid-Crystals-The Fourth State of Matter*", Marcel Dekker, INC. (1979).
11. M. J. S. Dewar, and R. M. Riddle, "*Factors influencing the stabilities of nematic Liquid-Crystals*", *J. Am. Chem. Soc.*, **97**, 6658 (1975).
12. D. J. Byron, G. W. Gray, A. Ibbotson, and B. M. Worrall, "*Mesomorphism and Chemical Constitution Part XI*", 2246 (1963).
13. G.W. Gray, "*Comments on Some Recent developments in the Field of Liquid-Crystals*", *Mol. Cryst. Liq. Cryst.*, **63**, 3 (1981).

14. G.W. Gray, "*Relationship between Chemical Structure and Properties for Low molecular Weight Liquid-Crystals*", Polymer Liquid Crystals, Academic Press, Inc. (1982).
15. W. Maier, and A. Saupe, Z. Naturforschg., **14a**, 882 (1959), and **15a**, 287 (1960).
16. M. J. S. Dewar, and C. Griffin, "*A Thermodynamic study of the Role of the Central Group on the Stability of Nematic Liquid-Crystals*", J. Am. Chem. Soc., **97**, 6662 (1975).
17. H. Kelker and B. Scheurle, Angew. Chem., **81**, 903 (1969).
18. L. Verbit and R. L. Tuggey, Mol. Cryst. Liq. Cryst., **17**, 49 (1972).
19. Meier, Sackmann, Grabmaier, "*Application of Liquid-Crystals*", Spring Verlag, Berline, Heidelberg (1975).
20. A. Saupe and W. Maier, "*Methoden zur Bestimmung des Ordnungsgrades Nematischer Kristallinflussiger Schichten*" Z. Naturforschg, **16A**, 816 (1961).
21. W. Helfrich, "*Electric Alignment of Liquid-Crystals*", Mol. Cryst. Liq. Cryst., **21**, 187 (1973).
22. M. Marthandappa, R. Somashekar, and Nagappa, "*Electro-Optic Effects in Nematic Liquid-Crystals*", Phys. Stat. Sol. (a), **127**, 259 (1991).
23. M. Schadt and P. R. Gerber, "*Class Specific Physical Properties of Liquid-Crystals*", Z. Naturforsch. **37a**, 165 (1982).
24. M. A. Osman, Hp. Schad, and H. R. Zeller, "Physical properties of Nematic Mixtures. I. polar-polar and nonpolar-nonpolar systems", J. Chem. Phys., **78**, 906 (1983).
25. Hp. Schad, and M. A. Osman, "*Physical properties of Nematic Mixtures. II. polar-nonpolar Systems*", J. Chem. Phys., **79**, 5710 (1983).
26. M. Schadt and W. Helfrich, "*Voltage Dependent optical Activity of a Twisted Nematic Liquid-Crystal*", Appl. Phys. Lett. **18**, 127 (1971).

27. G. H. Heilmeyer and L. A. Sanoni, "*Guest-Host Interaction in Nematic Liquid Crystals, A New Electro-Optic Effect*", Appl. Phys. Lett. **13**, 91 (1968).
28. C. T. Yim, "*Orientational Behaviour of Naphthalene-d₈ Dissolved in Nematic Solvent*", J. Phys. Chem. **95**, 980 (1991).
29. D. W. Berreman, "*Solid Surface Shape and the Alignment of an Adjacent Nematic Liquid-Crystals*", Phys. Rev. Lett., **28**, 1683 (1972).
30. H. Seki, T. Uchida, and Y. shibata, "*Dichroic Dyes for Gust-Host Liquid-Crystal Cells*", Mol. Cryst. Liq. Cryst., **138**, 349 (1986).
31. J. L. Janning, "*Thin Film Surface Orientation for Liquid-Crystals*", Appl. Phys. Lett., **21**, 173 (1972).
32. G. D. Dixon, T. P. Brody, and W. A. Hester, "*Alignment Mechanism in Twisted Nematic Layers*", Appl. Phys. Lett., **24**, 47 (1974).
33. F. J. Kahn, "*Orientation of Liquid-Crystals by Surface Coupling Agents*", Appl. Phys. Lett., **22**, 386 (1973).
34. H. Ichinose, M. Suzuki and T. Goto, "*Liquid-Crystal Alignment on LB Films of Phatholocyanine Derivatives*", Mol. Cryst. Liq. Cryst., **203**, 25 (1991).
35. H. Kelker, R. Haltzand, G. Wirzing, Z. Analyt. Chem., **267**, 161, (1973).
36. J. E. Proust, et al, "*Orientation of Nematic Liquid-Crystals by Suitable Boundary Conditions*", Sol. St. Commun., **11**, 1227 (1972).
37. J. C. Dubois, M. Gazard, and A. Zann, "*Plasma-Polymerised films as Orientating Layers of Liquid-Crystals*", Appl. Phys. Lett., **24**, 297 (1974).
38. L. T. Creagh and A. R. Kmetz, "*Mechanism of Surface Alingment in Nematic Liquid-Crystals*", Mol. Cryst. Liq. Cryst., **24**, 59 (1973).
39. F. G. Kahn, G. N. Taylor, and H. Schonhorn, "*Surface Produced Alignment of Liquid-Crystals*", Proc. IEEE, **61**, 823 (1973).

40. T. Uchida, H. Watanabe and M. Wada, "*Molecular Arrangement of Nematic Liquid-Crystals*", Jap. J. Appl. Phys., **11**, 1559 (1972).
41. J. R. Lalanne and B. Lemaire, "*The Even-Odd Effect in Liquid-Crystals*", J. Chem. Phys., **73**, 1927 (1980).
42. V. G. K. M. Pisipati, N. V. S. Rao, P. R. Alapati, "*DSC Characterisation of Various Phase Transitions in Mesomorphic Benzylidene anilines*", Cryst. Res. Technol., **24**, 1285 (1989).
43. A. Hauser, Ch. Selbmann, R. Rettig, D. Demus, "*Physical Properties of Liquid-Crystalline 5-n-Hexyl (4-n-alkoxyphenyl)-pyrimidines*", Cryst. Res. Technol., **21**, 685 (1986).
44. A. Buka, and A.H. Price, "*Dielectric Relaxation and Order Parameters in the Nematic and Smectic Phases of 4-n-octyl-4'-cyanobiphenyl (8CB)*", Mol. Cryst. Liq. Cryst., **116**, 187, (1985).
45. H. Kelker, R. Haltz, and G. Wirzing, "*Investigation of the Infra-Red-Dichroism in Liquid Crystals Layers Without Using Polarised Light*", Z. Anal. Chem., **267**, 161 (1973).
46. P. Chingduang, S. Bualek and O. Phaovibul, "*Study Of Orientation and Order of Non-mesogenic solutes in Liquid-Crystalline Matrix by Infrared Spectroscopy*", Mol. Cryst. Liq. Cryst., **132**, 131 (1986).
47. Chi-Duen Poon, Catherine M, Wooldridge and B. M. Fung, "*Orientational Ordering of 4-n-alkyl-oxy-4'-cyanobiphenyls Studies by 2D Carbon-13 nmr*", Mol. Cryst. Liq. Cryst., **157**, 303 (1988).
48. D. J. Photinos, E. T. Samulski, and H. Toriumi, "*Molecular Flexibility and Orientational Ordering of Nematic Liquid-Crystals*", J. Chem. Phys. **94**, 2758 (1991).
49. M. Sushmita Sen, P. Brahma, S. K. Roy, D. K. Mukherjee and S. B. Roy, "*Birefringence and Order Parameter of Some Alkoxycyanobiphenyl Liquid-Crystals*", Mol. Cryst. Liq. Cryst., **100**, 187, (1983).

50. A. Hauser, R. Rettig, Ch. Selbmann, W. Weissflog, J. Wulf, D. Demus, "*Influence of Lateral Branches on the Properties of Liquid-Crystalline 1,4-bis-[4-n-hexylbenzoyloxy]-2-subst.-benzenes (I)*", Cryst. Res. Technol., **19**, 261 (1984).
51. A. Hauser, R. Rettig, Ch. Selbmann, W. Weissflog, J. Wulf, D. Demus, "*Influence of Lateral Branches on the Properties of Liquid-Crystalline 1,4-bis-[4-n-hexylbenzoyloxy]-2-subst.-benzenes (II)*", Cryst. Res. Technol., **19**, 271 (1984).
52. A. J. Leadbetter, J. L. A. Durrant, and M. Rugman, "*The Density of 4-n-octyl-4-Cyanobiphenyl (8CB)*", Mol. Cryst. Liq. Cryst. Lett., **34**, 231 (1977).
53. P. Venkatacharyulu, A. V. N. Gupta, J. V. Rao, K. S. R. Prasad, N. V. L. N. Prasad "*Phase Transition studies in 5OCB and 8OCB*", Cryst. Res. Technol., **24**, 835 (1989).
54. H. E. J. Neugebauer, "*Clausius-Mossotti Equation for Certain Types of Anisotropic Crystals*", Can. J. Phys., **32**, 1 (1954).
55. A. Saupe and W. Maier, "*Methoden zur Bestimmung des Ordnungsgrades Nematischer Kristallinflüssiger Schichten*" , Z. Naturforschg, **16A**, 816 (1961).
56. P. Palffy-Muhoray and D. A. Balzarini, "*Refractive Index Measurements and Order Parameter Determination of the Liquid-Crystal p-ethoxybenilidene-p-n-butylaniline*", Can. J. Phys., **59**, 515 (1981).
57. P. Palffy-Muhoray and D. A. Balzarini, "*The Clausius-Mossotti Relation for Anisotropic Molecular Fluids*", Can. J. Phys., **59**, 375 (1981).
58. M. F. Vuks, "*Determination of the Optical Anisotropy of Aromatic Molecules from the Double Refraction of Crystals*", Optics and Spectroscopy, **20**, 361 (1966).
59. M. Davies, "*Some Electrical and Optical Aspects of Molecular Behaviour*", Pergamon Press Ltd., (1965).

60. C. J. F. Bottcher, "*Theory of Electric Polarisation*", Vol. I, Elsevier Scientific Publishing Company, (1973).
61. J. W. Smith, "*Electric Dipole Moment*", Butterworths Publications Ltd, (1955).
62. M. Born and E. Wolf, "*Principles of Optics*", 6th ed., Ch. 2, Pergamon, New York, (1980).
63. F. Fredericq and C. Houssier, "*Electric Dichroism and Electric Birefringence*", (1973).
64. J. C. D. Brand and J. C. Speakman, "*Molecular Structure*", Edward Arnold (Publishers) Ltd, Reprinted, (1964).
65. W. Maier and G. Meir, "*Eine einfache Theorie der dielektrischen Eigenschaften homogen Orientierter Kristallinflussiger Phasen des nematischen Typs*", Z. Naturforschg, **16A**, 262 (1961).
66. I. Haller, H. A. Huggins, H. R. Lilienthal, and T. R. McGuire, "*Order-Related Properties of Some Nematic Liquids*", J. Phys. Chem. **77**, 950 (1973).
67. P. P. Karat and N. V. Madhusudana, "*Elastic and Optical Properties of Some 4-n-Alkyl-4-Cyanobiphenyl*", Mol. Cryst. Liq. Cryst., **36**, 51 (1976).
68. J. Shashidhara Prasad and H. S. Subramhanyam, "*Refractive Indices and Molecular Order in 4,4' bis (pentyloxy) azoxy Benzene in the Nematic State*", Mol. Cryst. Liq. Cryst., **33**, 77, (1976).
69. P. Palffy-Muhoray and D. A. Balzarini, and D. A. Dunmur, "*Local Field Anisotropy in Nematic Liquid Crystals*", Mol. Cryst. Liq. Cryst., **110**, 315, (1984).
70. I. Haller, H. A. Huggins and M. j. Freiser, "*On the Measurement of Indices of Refraction of Nematic Liquids*", Mol. Cryst. Liq. Cryst., **16**, 53, (1972).
71. P. F. Waters, and T. Sarada, "*Measurement of the Bulk Refractive Index of Cholesteric Mesophases*", Mol. Cryst. Liq. Cryst., **25**, 1 (1974).
72. Anton Paar DMA Digital Density Meter Instruction manual (DMA 602).

73. D. A. Dunmur, M. R. Manterfield, W. H. Miller, and J. K. D. Dunleavy, "*The Dielectric and Optical Properties of the Homologous Series of Cyano-Alkyl-Biphenyl Liquid-Crystals*", Mol. Cryst. Liq. Cryst., **45**, 127 (1978).
74. K. R. K. Rao, J. V. Rao, P. Venkatacharyulu, V. Baliah, "*Phase Transition studies of the Liquid-Crystal Pentyloxybenzylidene*", Cryst. Res. Technol., **21**, 1245 (1986).
75. J. V. Rao, K. R. K. Rao, L. V. Choudary, P. Venkatacharyulu, "*Density Studies in polymorphic Liquid-Crystal N-(-p-n-Heptyloxybenzylidene) p-n-Pentylaniline*", Cryst. Res. Technol., **21**, 1245 (1986).
76. I. A. Goodman and P. H. Wise, "*Dicyclic Hydrocarbones: I. 2-Alkylbiphenyls*", J. Amer. Chem. Soc., **72**, 3076 (1950).
77. W. Maier and G. Meier, Z. Naturforsch, **16a**, 1200 (1961).
78. E. F. Carr, "Dielectric Loss in the Liquid Crystal p-Azoxyanisole", J. Chem. Phys., **37**, 104 (1962).
79. H. Baessler, R. B. Beard and M.M. Labes, "*Dipole Relaxation in a Liquid-Crystal*", J. Chem. Phys. **52**, 2292 (1969).
80. S. Wrobel, "*Influence of Molecular Conformations on the Dielectric Relaxation Spectra of Liquid-Crystals*", Mol. Cryst. Liq. Cryst., **127**, 67 (1985).
81. J. Chrusciel, S. Wrobel, H. Kresse, S. Urban, and W. Otowski, "*Dielectric Studies of 4-n-pentylphenyl-4-octyloxythiobenzoate*", Mol. Cryst. Liq. cryst., **127**, 57 (1985).
82. C. Someton, "*Measurment of Phase Transition Temperatures in Liquid-Crystals using the Temperature-Dependent Dielectric Constant*", Mol. Cryst. Liq. Cryst., **154**, 77 (1988).
83. H. Kresse et al., "*Dielectric Behaviour at the phase transition from the solid into a liquid-crystalline phase*", Cryst. Res. Technol., **20**, 871 (1985).

84. K. Araki, G. S. Attard, A. Kozak, and G. Williams, "*Molecular Dynamics of a Siloxane Liquid Crystalline Polymer as studied by Dielectric Relaxation Spectroscopy*", J. Chem. Soc., Faraday trans. II, **84**, 1067 (1988).
85. A. Buka, and A.H. Price, "*Dielectric Relaxation and Order Parameters in the Nematic and Smectic Phases of 4-n-octyl-4'-cyanobiphenyl (8CB)*", Mol. Cryst. Liq. Cryst., **116**, 187, (1985).
86. S. Urban, S. Wrobel, K. Chledowska, J. Chrusciel, J. A. Janik, and H. Kress, "*Dielectric Relaxation in Nematic and Isotropic Phases of p-Azoxyphenetol (PAP)*", Mol. Cryst. Liq. Cryst., **100**, 57 (1983).
87. P. L. Nordio, G. Rigatti, and U. Segre, Mol. Phys., **25**, 129 (1973).
88. P. G. Cummins, D. A. Dunmur and D. A. Laidler, "*The Dielectric Properties of Nematic 4-4', n-pentylcyanobiphenyl*", Mol. Cryst. liq. cryst., **30**, 109 (1975).
89. W. Haase and H. Pranoto, "*Properties of Liquid-Crystalline Polymers in the Electric Field*", Progr. Colloid and Polymer Sci. **69**, 139, (1984).
90. M. S. Beevers, J. Crossley, D. C. Garrington and G. Williams, "*Molecular Dynamics of Various Liquids*", J. Chem. Soc. Faraday trans. II, **73**, 458 (1977).
91. G. P. Johari and M. Goldstein, "*Viscous Liquids and the Glass Transition*" J. Chem. Phys., **53**, 2372 (1970).
92. H. Kresse, U. Schuhmacher, and D. Demus, "*Dielectric Relaxation and Viscosity in a Mixture of Liquid-Crystalline Substances*", Mol. Cryst. Liq. Cryst., **170**, 1 (1989).
93. H. Kresse, S. Ernest, W. Wedler, D. Demus, "*Dynamic investigation in a Nematic Mixture with High Glass Transition Temperature*", Ber. Bunseges. Phys. Chem., **94**, 1478, (1990).
94. U. M. S. Murthy and J. K. Vij, "*Molecular Dynamics of a Liquid-Crystal in Decalin Glass at Radio and Far Infrared Frequencies*", J. Chem. Phys., **90**, 1974 (1989).

95. H. R. Zeller, "*Dielectric Relaxation and the Glass Transition in Nematic Liquid-Crystals*", *Phy. Res. Lett.*, **48**, 334 (1982).
96. G. P. Johari and J. W. Goodby, "*Dielectric Relaxation in a Supercooled Liquid and Glassy Smectic Phase*", *J. Chem. Phys.* **77**, 5165 (1982).
97. G. P. Johari, "*Glass Transition and Molecular Motions in the Glassy State of a Nematic Liquid*", *Philos. Mag. B.*, **46**, 549, (1982).
98. H. Kresse, P. Rabenstein and D. Demus, "*Dielectric Relaxation and Molecular Geometry in Nematic Mixtures*", *Mol. Cryst. Liq. Cryst.* **154**, 1 (1988).
99. H. Kresse, S. Heinemann, A. Hauser and W. Weissflog, "*Dielectric Investigations of a Binary System with Strong Correlation of the Molecules*", *Cryst. Res. Technol.*, **25**, 5 (1990).
100. H. Kresse and P. Rabenstein, "*Geometrical Aspects and Dipole-Dipole Interaction in a Liquid-Crystalline Mixture*", *Phys. Stat. Sol.,(a)*, **100**, K83 (1987).
101. H. Kresse, H. Stettin, F. Gouda, and G. Andersson, "*Dielectric Relaxation of a Nematic Liquid-Crystals and a Non-Liquid-Crystalline Compound*", *Phys. Stat. Sol.,(a)*, **11**, 265-681 (1989).
102. P. G. Geber, "Dielectric Relaxation of Long Molecules in Nematic Host Matrices", *Z. Naturforsch.* **37a**, 266-70, (1982).
103. G. Heppke, J. Kaye, and V. Müller, "*Influence of Molecular Structure on the Low frequency Dielectric Relaxation of p-cyano-substituted Liquid-Crystals in Nematic Solution*", *Mol. Cryst. Liq. Cryst.*, **98**, 309-19, (1983).
104. C. P. Smyth, "*Dielectric Behaviour and Structure*", McGraw-Hill (1955).
105. A. R. Blythe, "Electrical Properties of Polymers" Cambridge University Press (1979).
106. N. E. Hill *et al.*, "*Dielectric Properties and Molecular Behavior*", Van Nostrand Reinhold Company, London (1969).

107. V. V. Danilel, "*Dielectric Relaxation*", Academic Press, (1967).
108. M. Schadt, "*Dielectric Properties of some Nematic Liquid-Crystals with Strong Positive Dielectric Anisotropy*", J. Chem. Phys. **56**, 1494-97, (1971).
109. L. Benguigui, "Dielectric Relaxation and Nematic Order in liquid Crystals" Review A, Rapid Comm., 29, 2968 (1984).
110. H. Kresse et al., "*Strong Antiparallel Correlation in Liquid-Crystalline Esters with Lateral Groups*", Phys. Stat.Sol. **106**, 89 (1988).
111. H. Kresse, P. Rabenstein, H. Stettin, S. Diele, D. Demus, W. Weissflog, "*Liquid-Crystalline Swallow-Tailed Compounds (II)*", Cryst. Res. Technol. **23**, 135 (1988).
112. H. Kresse, K. Worm, W. Schafer, H. Stettin, W. Otowski, "*Dielectric Behaviour of the Nematic Phase of (PBNEB)*", Cryst. Res. Technol. **21**, 293 (1986).
113. M. Schadt, "*Dielectric Heating and Relaxations in Nematic Liquid-Crystals*", Mol. cryst. Liq. Cryst., **66**, 319-36, (1981).
114. K. Chledowska, et al., "*Dielectric Relaxation and Quasielastic Neutron Scattering Study of Molecular Reorientation in the Nematic and Solid Phase of 4,4'-di-n-Butyloxyazoxybenzene*", Liq. Cryst., **3**, 1339-54 (1988).
115. B. S. Srikanta and N. V. Madhusudana, "*Dielectric Relaxation Studies on Two Systems Exhibiting the Induced Smectic A phase*", Mol. Cryst. Liq. Cryst., **108**, 39-49 (1984).
116. G. M. Janini and A. H. Katrib, "*Determination of the Dipole Moment of Polar Compounds in Nonpolar Solvent*", J. Chem. Education, **60**, 1087 (1983).
117. W. Dannhauser and A. F. Flueckinger, "*Dielectric constant and Intermolecular association of Some Liquid Nitriles*", J. Phys. Chem., **68**, 1814 (1964).
118. C. P. Smyth, "*Molecular Interactions*", Vol. **II**, John Wiley & Sons Ltd (1980).

119. R. J. W. Le Fevre, *"Dipole Moments"*, Methuen & Co Ltd, Third Edition, (1953).
120. P. Maurel and A. H. Price, *"Dipole Moment of N-(p-Methoxybenzylidene)-p-butylaniline"*, J. Chem. Soc. Faraday II, **69**, 1486 (1973).
121. D. G. McDonnell, E. P. Raynes and R. A. Smith, *"The Physical Properties of Fluorine Derivatives of 4-Cyanobiphenyls"*, Mol. Cryst. Liq. Cryst., **123**, 169 (1985).
122. D. A. Dunmur and K. Toriyama, *"Light Scattering and Dielectric Studies of Molecular Association in Mesogenic Solutions"*, Liquid Crystals, **1**, 169 (1986).
123. P. Debye, *"Polar Molecules"*, Chemical Catalog Co., New York (1929).
124. L. Onsager, *"Electric Moments of Molecules in Liquids"*, J. Am. Chem. Soc., **58**, 1486 (1936).
125. S. Glasstone and D. Lewis, *"Elements of Physical Chemistry"*, Macmillan & Co Ltd, p. 272 (1960).
126. E. A. Guggenheim, *"A proposed simplification in the procedure for computing electric dipole moments"*, Trans. Far. Soc. **45**, 714 (1949).
127. J. G. Kirkwood, J. Chem. Phys., **7**, 911 (1939).
128. H. Frohlich, *"Theory of Dielectrics"*, Oxford University Press, London (1949).
129. W. Maier and G. Meier, Z. Naturforsch, **16a**, 262 (1961).
130. P. Bordewijk and W. H. De Jue, *"Calculation of Dipole Correlation Factors in Liquid-Crystals with Use of a Semiempirical Expression for the Internal Field"*, J. Chem. Phys., **68**, 116 (1978).
131. L. Bata, and A. Buka, *"Dielectric permittivity and relaxation Phenomena in Smectic Phases"*, Mol. Cryst. Liq. Cryst., **63**, 307 (1981).

132. M. Davies, R. Moutran, A. H. Price, M. S. Beevers, G. Williams, "*Dielectric and Optical Studies of a Nematogen (4,4-n-heptyl-cyanobiphenyl)*", J. Chem. Soc., Faraday Transactions II, **72**, 1447 (1976).
133. Hp. Schadt and M. A. Osman, "*Elastic Constant and Molecular association of Cyano-Substituted Nematic Liquid-Crystals*", J. Chem. Phys., **75**, 880 (1981).
134. G. M. Tsangaris, "*Correlation Factors in the Nematic and Isotropic Phase of 4-n-octyl-4-cyanobiphenyl (8CB)*", Mol. Cryst. Liq. Cryst., **237**, 163 (1993).
135. A. Buka, P. G. Owen, and A. H. Price, "*Dielectric Relaxation in the Nematic and Isotropic Phase of n-heptyl-and n-heptoxy cyanobiphenyl*", Mol. Cryst. Liq. Cryst., **51**, 273 (1979).
136. M. J. Bradshaw and E. P. Raynes, "*Pre-Transitional Effects in the Electric Permittivity of Cyano Nematics*", Mol. Cryst. Liq. Cryst. Letters, **72**, 73 (1981).
137. P. Bordewijk, "*Extension of the Kirkwood-Fröhlich Theory of the Static Dielectric Permittivity to Anisotropic Liquids*", Physica, **75**, 146 (1974).
138. C. J. F. Böttcher, "*Theory of Electric Polarisation*", Vol. **II**, 2nd Ed., Elsevier Scientific Publishing Company, (1973).
139. A. J. Leadbetter, R. M. Richardson and C. N. Colling, "*The Structure of a Number of Nematogens*", J. Phys. (Orsay, Fr.), **36**, 37 (1975).
140. S. W. Sinton, D. B. Zax, J. B. Murdoch, and A. Pines, "*Multiple-Quantum N.M.R. Study of Molecular Structure and Ordering in a Liquid-Crystal*", Mol. Phys., **53**, 333 (1984).
141. S. W. Sinton, A. Pines, "*Study of Liquid-Crystal Conformation By Multiple-Quantum N.M.R: N-Pentyl Cyanobiphenyl*", Chem. Phys. Lett., **76**, 263 (1980).
142. K. Hori, Y. Koma, "*Crystal Structures of 6OCB and 7OCB*", Mol. Cryst. Liq. Cryst., **225**, 15 (1993).

143. M. P. Bogaard, A. D. Buckingham, R. K. Pierens, and A. H. White, "*Rayleigh Scattering Depolarisation Ratio and Molecular Polarisability Anisotropy for Gases*", J. Chem. Soc. Trans., **74**, 3008 (1978).
144. A. D. Buckingham, and N. J. Bridge, "*The Polarisation of Light Scattered by Gasses*", Proc. Roy. Soc. **295** (A), 334 (1966).
145. C. G. Le Fevre, and R. J. W. Le Fevre, "*The Kerr Effect: Its measurement and applications in chemistry*", Rev. Pure Appl. Chem., **5**, 261 (1955).
146. G. R. Alms, A. K. Burnham, and W. H. Flygare, "*Measurement of the Dispersion in Polarisability Anisotropies*", Chem. Phys. **63**, 3321 (1975).
147. A. D. Buckingham, and M. J. Stephen, "*A Theory of the Depolarisation of Light Scattered by a Dense Medium*", Trans. Faraday Soc., **53**, 884 (1957).
148. J. H. Robson, "*The Temperature Dependence of the Electro-Optic Kerr Effect in Solutions*", Ph.D Thesis, Aston University, U.K. (1993).
149. R. J. W. Le Fevre, B. Purnachandra Rao, "*Molecular Polarisability. The anisotropies of Seven mono-substituted benzenes and of nitromethane as solutes in carbon tetrachloride*", Austral. J. Chem. , 1465 (1958).
150. J. R. Lalanne, B. Lemaire, J. Rouch, C. Vaucamps, and A. Proutiere, "*The Even-Odd Effect in Liquid-Crystals: A collective or intrinsic molecular property*", j. Chem. Phys. **73**, 1927 (1980).
151. S. J. Mumby and M. S. Beevers, "*Electro-Optical Studies of Various Stereostructural Forms of Poly(N-vinylcarbazole)*", Polym., **30**, 860 (1989).
152. M. J. Aroney, W. P. McPherson and R. K. Pierens, "*Electric Birefringence and Solution-State Conformations of Molecules $C_6H_5SM(CH_3)_3$; $M = C, Si, Ge$ or Sn* ", J. Mol. Structure, **69**, 289 (1980).
153. M. J. Aroney, "*The Electro-Optical Kerr Effect in Conformation Analysis*", Angew. Chem. **89** (10), 725 (1977).

154. M. S. Beevers, "*The Electro-Optical Kerr-Effect in Solutions of the Nematogen N-(p-Methoxybenzylidene)-p-n-butylaniline*", Mol. Cryst. Liq. Cryst., **31**, 333 (1975).
155. M. S. Beevers and G. Williams, "The Electro-Optical Kerr-Effect in solutions of benzylidene Aniline and its Derivatives",
156. C. G. Le Fevre, and R. G. J. Le Fevre, "*Physical Methods of Chemistry*", (Eds. A. Weissberger and B. W. Rossiter), Wiley, New York (1972).
157. C. G. Le Fevre, and R. J. W. Le Fevre, "*Molecular Polarisability. The measurement of molecular Kerr constants in solution*", J. Chem. Soc. 823, 4041 (1953).
158. H. J. Coles and B. R. Jennings "*Static and Optical Kerr Effect in the Nematogen MBBA*" Mol. Phys., **31**, 571 (1976).
159. H. J. Coles, "Laser and Electric Field Induced Birefringence Studies on the cyanobiphenyl Homologues", Mol. Cryst. Liq. Cryst., **49**, 67 (1978).
160. M. S. Beevers and S. J. Mumby, "*Dielectric and Kerr Effect Studies of Stereoregular poly (N-Vinylcarbazole)*", Polymer Communications, **25**, 173 (1984).
161. C. T. O'Konski and A. J. Haltner, "*Characterisation of the Monomer and Dimer of Tobacco Mosaic Virus by Transient Electric Birefringence*", J. Am. Chem. Soc. **78**, 3604 (1956).
162. T. W. Stinson and J. D. Litster, "*Pretransitional Phenomena in the Isotropic Phase of a Nematic Liquid-Crystal*", Phys. Rev. Lett., **25**, 503 (1970).
163. A. R. Johnston, "*Kerr Response of a Nematic Liquid*", J. Appl. Phys., **44**, 2971 (1973).
164. J. Philip and T. A. Prasada Rao, "*Kerr Effect Investigations in a Nematic Liquid-Crystal*", Phys. Rev. A, **46**, 2163 (1992).

165. B. Pouligny, J. P. Marcerou, J. R. Lalanne, and H. J. Coles, "*Pretransitional Effect in the Isotropic Phases of Some Alkyl-cyanobiphenyls (n = 8, 9, 11 and 12)*", Mol. Phys., **49**, 583 (1983).
166. D. A. Dunmur and A. E. Tomes, "*The Pretransitional Kerr Effect in 4-n-Pentyl-4-Cyanobiphenyl*", Mol. Cryst. Liq. Cryst., **76**, 231 (1981).
167. H. J. Coles and S. V. Kershaw, "*Kerr Effect Studies of Pretransitional Phenomna in the Isotropic Phase of a Nematic Mixture, E120*", Mol. Cryst. Liq. Cryst., Letters, **2 (1/2)**, 29 (1985).
168. H. J. Coles and S. V. Kershaw, "*Pretransitional Isotropic Kerr Effect in Eutectic Mixtures E120, E130 and E140*", J. Chem. Soc., Faraday Trans. 2, **84**, 987 (1988).
169. P. G. de Gennes, Mol. Cryst. Liq. Cryst., **12**, 193 (1971).
170. J. Kerr, "*A New Relationship Between Electricity and Light: Dielectrified Media Birefringent*" Phil. Mag., **50 (4)**, 337 (1875).
171. G. Otterbein, "*The Kerr Effect in Benzene Derivatives*", Physik. Z., **35**, 249 (1934).
172. P. Langevin, "*Sur Less Birefringences Electrique et Magnetique*", Radium, **7**, 249 (1910).
173. M. Born, "*Elektronentheorie des Naturlichen Optischen Drehungsvermögens Isotroper und Anisotroper Flüssigkeiten*", Ann. Physik, **55**, 177 (1918).
174. R. Gans, "*Dielektrizitätskonstante und Elektrische Doppelbrechung*", Ann. Physik, **64**, 481 (1921).
175. J. Philip and T. A. Prasada Rao, "*Transient Kerr Effect in Nematic Liquid Crystal Mixtures*", J. Mol. Liq., **50**, 215 (1991).
176. E. L. Wood, J. R. Sambles and S. J. Elston, "*An Investigation of Pretransitional Effects in a Thin Liquid-Crystal Layer via the Excitation of ps Mixed Optic Modes*", Mol. Cryst. Liq. Cryst., **222**, 1 (1992).

177. B. Malraison, Y. Poggi, and J. C. Filippini, "*Breakdown of Landau Theory of Nematic-Isotropic Transition*", Solid State Communications, **31**, 843 (1979).
178. M. S. Beevers and G. Khanarian, "*Measurement of Kerr Constants of Conducting Liquids*", Australian J. Chem., **32**, 263 (1979).
179. C. Houssier and E. Fredericq, "*Electro-Optical Properties of Nucleic Acids and Nucleoproteins. I. Study of the gel-forming deoxyribonucleohistone*", Biochem. Biophys. Acta., **120** (1), 113 (1966).
180. A. J. Amass, M. S. Beevers and T. R. Farren, "*Simultaneous Measurement of Linear Electric Birefringence and Linear Electric Dichroism Using Pulsed Electric Field*", J. Chem. Soc. Faraday Trans., **87** (14), 2219 (1991).
181. M. J. Aroney, M. R. Battaglia, R. Ferfoggia, D. Millar and R. K. Pierens, "*The Kerr Constant of Water and Other Pure liquids at 633 nm*", J. Chem. Soc. Faraday II, **72**, 724 (1976).
182. M. S. Beevers, D. A. Elliott and G. Williams, "*Static and Dynamic Kerr effect Studies of Glycerol in its Highly Viscous State*", J. Chem. Soc. Faraday II, **76**, 112 (1980).
183. H. H. Trimm, K. Parslow, and B. R. Jennings, "*Electric Birefringence*", J. Chem. Edu., **61**, 1114 (1984).
184. D. G. Tyson, B. R. Jennings, "*Measurement of the Optical Kerr Effect Induced by Nanosecond Laser Pulses*", J. Phys. D: Appl. Phys., **24**, 645 (1991).
185. H. Benoit, Ann. Phys. **6**, 561 (1951).
186. J. C. Powers, JR. and W. L. Peticolas, "*Electrical Ordering in polypeptide Solutions: Molecular Aggregation Studied by the Kerr Effect*", Ordered Fluids and Liquid Crystals, American chemical society, Meeting (15).
187. A. R. Foweraker, B. R. Jennings, "Electro-Optic Decay Analysis for Polydisperse Systems III; Experimental data for rods, Advances in molecular relaxation processes, **8**, 103 (1976).

188. E. Sackmann and H. Mohwald, "*On Optical Polarisation measurements in Liquid-Crystals*", J. Chem. Phys., **58**, 5407 (1973).
189. E. Sackmann and H. Mohwald, "*Relation between the Principal Polarisabilities of a Molecule and Its Average Orientation in Nematic Liquid-Crystals*", Chem. Phys. Lett., **12**, 467 (1972).
190. P. Chingdvang, S. Bualek and O. Phaovibui, "*Study of Orientation and Order Parameter of non-mesogenic Solutes in Liquid-Crystalline Matrix by Infra-Red spectroscopy*", Mol. Cryst. Liq. Cryst., **132**, 131 (1986).
191. R. A. Levenson, H. B. Gray, and G. P. Ceasar, "*Electronic and Vibrational Spectroscopy in Nematic Liquid-Crystal Solvent*", J. Am. Chem. Soc., **92**, 3653 (1970).
192. E. Sackmann, "*Electric Field Induced Orientation of Liquid-Crystals and Optical Absorption Experiments*", Chem. Phys. Lett., **3**, 253 (1969).
193. E. Sackmann, "*On the Polarisation of Optical Transitions of Dye Molecules Oriented in an Ordered Glass Matrix*", J. Am. Chem. Soc., **90**, 3569 (1968).
194. G. P. Ceasar, H. R. Gray, "*Polarised Electronic Spectroscopy of Molecules Oriented by a Nematic Liquid-Crystal*", J. Am. Chem. Soc., **91**, 191 (1969).
195. H. Heilmeyer and L. A. Zanoni, "*Guest-Host Interaction in Nematic Liquid Crystals, A New Electro-Optic Effect*", Appl. Phys. Lett. **13**, 91 (1968).
196. D. L. White and G. N. Taylor, "*New Absorptive Mode Reflective Liquid Crystal Display Device*", J. Appl. Phys., **45**, 4718 (1974).
197. T. Uohida, H. Seki, C. Shishido, and H. Wada, "*Guest-Host Interactions in Nematic Liquid-Crystals with Negative Dielectric Anisotropy*", IEEE Trans. Elect. Devices, **26**, 1337 (1979).
198. F. Gharadjedaghi, "*A Positive Contrast Guest-Host Display Using a liquid Crystal of Negative Dichroic Anisotropy*".

199. T. Uchia, H. Seki, C. Shishido and M. Wada, "*Guest-Host Intraction in Nematic Liquid-Crystal Cells with Twisted and Tilted Alignment*", Mol. Cryst. Liq. Cryst., **54**, 161 (1979).
200. H. Seki, "*Dichroic Dyes for Guest-Host Liquid-Crystal Cells*", Mol. Cryst. Liq. Cryst., **138**, 349 (1986).
201. M. A. Osman, L. Pietrone, T. J. Scheffer, and H. R. Zeller, "*The Dichroic Ratio of Pleochoric Dyes Dissolved in Nematic Liquid-Crystals*", J. Chem. Phys., **74**, 5377 (1981).
202. S. Imazeki, A. Mukoh, T. Yoneyama, and M. Kaneko, "*New Yellow Dyes for Guest- Host Applications*", Mol. Cryst. Liq. Cryst., **154**, 79 (1987).
203. H. Seki, C. Shishido, S. Yasui and T. Vchida, "*Dichroic Azo Dyes for Guest-Host Liquid-Crystal Cell*", Jpn. J. Appl. Phys., **21**, 191 (1982).
204. A. V. Ivashcheneko, "*Dyes in Liquid-Crystals*", Mol. Cryst. Liq. Cryst., **150A**, 1 (1987).
205. S. Imazeki, and A. Mukoh, "Unusal Orientational Behaviour of Anthraquinone Dyes in Nematic Cyanophenylcyclohexane Derivatives", Mol. Cryst. Liq. Cryst., **225**, 197 (1993).
206. E. W. Thulstrup and J. Michl, "*Orientation and Linear Dichroism of Symmetrical Aromatic Molecules Imbedded in Stretched Polyethylene*", J. Am. Chem. Soc., **104**, 5594 (1982).
207. W. Helfrich, G. Heppke, "*Liquid-Crystals of One- and Two-Dimensional Order*", Springer-verleg, Berlin Heidelberg, New York, (1980).
208. G. H. Brown, G. J. Dienes, M. M. Labes, "*Liquid-Crystals*", Gordon and Bkeach, Science Publishers (1967).
209. H. Kelker, R. Haltz and G. Wirzing, "*Investigation of the Infra-Red-Dchroism in Liquid-Crystal Layers without Using Polarised Light*", Z. Anal. Chem., **267**, 161 (1973).

- 210. Y. Anjaneyulu and D. W. Yoon, "*Transmittance of Liquid-Crystal Cells : A Comparison*", J. Appl. Phys., **59**, 3662 (1986).

- 211. A. Hatta, "*Application of Infra-Red ATR Spectroscopy to Liquid-Crystals. V. Orientation of 5CB Molecules in the Boundary Region of a Twisted Nematic Cell and Reorientation by a DC Electric Field*", Mol. Cryst. Liq. Cryst., **74**, 195 (1981).

- 212. F. Jones and T. J. Reeve, "*Order Parameters of Dyes in a Biphenyl/Terphenyl Liquid-Crystal mixture*", Mol. Cryst. Liq. Cryst., **60**, 99 (1980).

- 213. T. R. Farren, "The Synthesis, Characterisation and Electro-Optical Properties of Polypentenylene-Block-Co-Acetylene", Ph.D Thesis, Aston University, U.K. (1989).

APPENDIX A

Density and Refractive Index Results

Appendix A contains all of densities and refractive indices data for the liquid crystals in the nematic and isotropic phases. The estimated accuracies in the measurement of density and refractive index are $\pm 1 \times 10^{-4} \text{ g cm}^{-3}$ and $\pm 5 \times 10^{-4}$, respectively.

Table A.1 Values of densities, refractive indices n_o , n_e and n_{iso} of 5CB

Temperature (°C)	Density (g/ml)	n_o	n_e
25.0 nematic	1.021 (0)	1.533 (9)	1.697 (7)
26.0	1.020 (0)	1.534 (2)	1.696 (2)
28.0	1.018 (1)	1.536 (0)	1.690 (8)
29.0	1.017 (0)	1.537 (1)	1.688 (0)
30.0	1.016 (0)	1.538 (4)	1.684 (4)
31.0	1.014 (9)	1.539 (8)	1.680 (8)
32.0	1.013 (7)	1.541 (0)	1.677 (5)
33.0	1.012 (4)	1.543 (9)	1.671 (1)
33.4	1.011 (9)		
34.0	1.011 (1)		
34.3	1.010 (6)		
35.0 isotropic	1.007 (8)		
36.0	1.006 (9)	1.586 (3)	
37.0	1.006 (0)	1.586 (0)	
39.0	1.004 (4)	1.585 (3)	
41.0	1.002 (9)	1.584 (5)	
43.0	1.001 (3)	1.583 (8)	
45.0	0.999 (6)	1.583 (0)	
47.0	0.998 (1)		

($T_{NI} = 35.0 \text{ }^\circ\text{C}$)

Table A.2 Values of densities, refractive indices n_o , n_e and n_{iso} of 6CB

Temperature (°C)	Density (g/ml)	n_o	n_e
18.0 nematic	1.015 (1)	1.534 (2)	1.690 (5)
20.0	1.013 (2)	1.534 (6)	1.686 (2)
22.0	1.011 (2)	1.535 (4)	1.681 (7)
23.0	1.010 (3)	1.536 (1)	1.678 (5)
25.0	1.008 (4)	1.538 (6)	1.672 (0)
26.0	1.007 (4)	1.540 (1)	1.667 (5)
27.0	1.006 (3)	1.542 (0)	1.662 (1)
28.0	1.005 (1)	1.545 (2)	1.655 (5)
28.6	1.004 (2)	1.547 (7)	1.651 (4)
28.8 biphasic			
28.9 isotropic	1.002 (2)		
29.0	1.002 (1)	1.581 (2)	
30.0	1.001 (2)	1.581 (0)	
31.0	1.000 (3)	1.580 (8)	
33.0	0.998 (6)	1.579 (9)	
35.0	0.996 (9)	1.579 (2)	
40.0	0.993 (0)	1.577 (0)	
45.0	0.988 (9)	1.574 (8)	

(T_{NI} = 28.8 °C)**Table A.3** Values of densities, refractive indices n_o , n_e and n_{iso} of 7CB

Temperature (°C)	Density (g/ml)	n_o	n_e
30.0 nematic	0.998 (9)	1.520 (5)	1.690 (1)
32.0	0.997 (1)	1.521 (1)	1.685 (6)
33.0	0.996 (2)	1.521 (6)	1.682 (4)
34.0	0.995 (3)	1.522 (2)	1.679 (8)
35.0	0.994 (4)	1.523 (1)	1.676 (0)
37.0	0.992 (5)	1.524 (5)	1.670 (7)
39.0	0.990 (3)	1.527 (0)	1.662 (8)
40.0	0.989 (1)	1.529 (6)	1.656 (0)
41.0	0.987 (9)	1.533 (4)	1.650 (4)
41.8	0.986 (4)		
41.9	0.984 (1)		
42.0 isotropic	0.983 (7)	1.572 (0)	
43.0	0.982 (7)	1.571 (3)	
44.0	0.981 (7)	1.570 (7)	
45.0	0.980 (9)	1.569 (7)	
47.0	0.979 (2)	1.568 (8)	
50.0	0.976 (8)	1.567 (1)	

(T_{NI} = 41.9 °C)

Table A.4 Values of densities, refractive indices n_o , n_e and n_{iso} of 6OCB

Temperature (°C)	Density (g/ml)	n_o	n_e
60.0 nematic	1.026 (9)	1.516 (5)	1.685 (0)
63.6	1.023 (8)	1.517 (8)	1.678 (5)
65.0	1.022 (6)	1.518 (4)	1.676 (4)
66.6	1.021 (2)	1.518 (9)	1.673 (1)
68.8	1.019 (3)	1.521 (5)	1.667 (0)
70.3	1.017 (9)	1.523 (0)	1.663 (8)
74.9	1.013 (2)	1.532 (3)	1.641 (0)
75.4	1.012 (5)	1.534 (6)	1.636 (1)
75.6	1.012 (2)		
75.8	1.012 (1)		
76.0	1.010 (2)	1.568 (9)	
77.0	1.009 (4)	1.568 (5)	
79.3	1.007 (6)	1.567 (5)	
81.3	1.005 (9)	1.566 (7)	

(T_{NI} = 75.8 °C)**Table A.5** Values of densities, refractive indices n_o , n_e and n_{iso} of E₆₀7

Temperature (°C)	Density (g/ml)	n_o	n_e
38.0 nematic	1.037 (8)	1.513 (0)	1.709 (6)
40.0	1.036 (2)	1.513 (0)	1.707 (2)
45.0	1.032 (1)	1.513 (0)	1.701 (2)
50.0	1.028 (0)	1.513 (2)	1.694 (8)
55.0	1.023 (9)	1.513 (9)	1.687 (4)
60.0	1.019 (8)	1.515 (2)	1.679 (0)
63.4	1.017 (1)	1.516 (8)	1.673 (0)
66.3	1.014 (7)	1.518 (3)	1.665 (7)
70.0	1.011 (6)	1.521 (4)	1.655 (5)
72.2	1.009 (4)	1.525 (6)	1.645 (0)
74.1	1.007 (1)	1.531 (6)	1.631 (4)
74.6	1.006 (5)		
74.7	1.006 (2)		
74.8	1.005 (9)		
75.0 isotropic	1.004 (6)		
75.5	1.003 (9)	1.564 (6)	
76.0	1.003 (3)	1.564 (7)	
78.0	1.001 (7)	1.563 (9)	
80.0	1.000 (1)	1.563 (0)	
82.0	0.998 (6)	1.562 (1)	

(T_{NI} = 74.9 °C)

Table A.6 Values of densities, refractive indices n_o , n_e and n_{iso} of E7

Temperature (°C)	Density (g/ml)	n_o	n_e
20.0 nematic	1.029 (2)	1.521 (7)	1.7392
25.0	1.024 (9)	1.521 (7)	1.7329
30.0	1.020 (7)	1.521 (7)	1.7249
35.0	1.016 (4)	1.522 (1)	1.7164
40.0	1.012 (2)	1.522 (8)	1.7076
45.0	1.007 (8)	1.524 (2)	1.6979
50.0	1.003 (4)	1.526 (8)	1.6856
55.0	0.998 (5)	1.532 (2)	1.6678
58.0	0.994 (9)	1.541 (0)	1.6494
59.0	0.993 (5)	1.542 (1)	
60.0 isotropic	0.991 (3)	1.575 (5)	
62.0	0.989 (4)	1.574 (8)	
65.0	0.986 (9)	1.573 (3)	
68.0	0.984 (5)	1.571 (8)	
70.0	0.983 (2)	1.570 (7)	
72.0	0.981 (6)	1.570 (1)	
75.0	0.979 (2)	1.568 (6)	

(T_{NI} = 59.8 °C)**Table A.7** Values of densities, refractive indices n_o , n_e and n_{iso} of E8

Temperature (°C)	Density (g/ml)	n_o	n_e
20.0 nematic	1.053 (8)	1.524 (0)	1.745 (9)
25.0	1.049 (5)	1.524 (0)	1.740 (4)
30.0	1.045 (3)	1.524 (0)	1.734 (4)
35.0	1.041 (2)	1.524 (0)	1.728 (8)
40.0	1.037 (0)	1.524 (0)	1.723 (3)
45.0	1.033 (1)	1.524 (2)	1.716 (8)
50.0	1.029 (1)	1.525 (0)	1.709 (8)
55.0	1.025 (1)	1.525 (6)	1.702 (9)
60.0	1.020 (6)	1.529 (2)	1.690 (5)
65.0	1.015 (8)	1.534 (2)	1.675 (5)
68.0	1.012 (6)	1.539 (4)	1.660 (7)
70.0	1.009 (8)	1.545 (1)	1.649 (6)
70.5 biphasic	1.008 (8)		
71.5	1.007 (5)		
72.0 isotropic	1.006 (9)		
73.0	1.005 (9)		
74.0	1.005 (0)		
75.0	1.004 (1)		
76.2	1.003 (1)		
77.2	1.002 (4)		
79.0	1.000 (9)		

(T_{NI} = 70.5 °C)

APPENDIX B

Dielectric Constant (Permittivity) and Dielectric Loss Results

Appendix B contains all of dielectric constants (ϵ_{\parallel}' , ϵ_{\perp}') and dielectric losses (ϵ_{\parallel}'' , ϵ_{\perp}'') data for the oriented nematic mixtures E7 and E8 from 12 Hz to 100 Hz at different temperatures. The Digibridge which was used to measure the dielectric constants and losses has an accuracy of 0.01% in capacitance and 0.1% in dielectric loss tangent.

Table B.1 Dielectric constants (ϵ_{\parallel}' and ϵ_{\perp}') measured at 1kHz for the oriented of the nematic mixture E7 at different temperatures.

Temperature /°C	ϵ_{\parallel}'	Temperature /°C	ϵ_{\perp}'
	E = E _{∥D}		E = E _{⊥D}
-90	3.01	-90	2.60
-80	3.01	-80	2.60
-70	3.01	-70	2.60
-60	3.01	-60	2.60
-53	3.10	-55	2.61
-50	3.30	-52	2.67
-47	3.50	-50	2.82
-41	4.70	-46	3.20
-35	7.53	-40	3.68
-30	12.90	-36	4.02
-25	15.30	-31	5.00
-20	16.41	-25	5.87
-11	16.70	-16	6.08
1	16.80	-6	6.14
13	16.62	3	6.17
24	15.95	13	6.22
34	15.10	20	6.22
44	14.40	28	6.32
54	13.40	38	6.67
60	9.30	48	7.05
64	9.40	54	7.43

Table B.2 Dielectric constant ($\epsilon_{||}'$) data of supercooled E7 for parallel relaxation ($E = E_{||D}$) at different frequencies and temperatures.

$\log(f/\text{Hz})$	-47 °C	-42 °C	-35 °C	-30 °C	-25 °C	-21 °C
1.1	11.18	15.4	17.43	–	–	–
1.3	9.05	15.08	17.32	17.95	18.10	–
1.7	5.74	13.08	16.98	17.61	17.98	–
2.0	4.69	9.94	16.38	17.28	17.73	18.10
2.3	4.27	6.63	15.31	16.79	17.46	17.93
2.7	4.08	4.66	11.89	15.59	16.87	17.58
3.0	4.00	4.21	7.91	13.53	16.05	17.19
3.3	3.92	4.08	5.28	10.58	14.49	16.50
3.7	3.79	3.98	4.17	6.03	10.07	14.57
4.0	3.70	3.89	3.99	4.57	6.85	11.18
4.3	3.65	3.80	3.89	4.08	4.84	7.06
4.7	3.59	3.70	3.85	3.91	4.02	4.46
5.0	3.56	3.64	3.78	3.85	3.86	3.92

Table B.3 Dielectric loss ($\epsilon_{||}''$) data of supercooled E7 for parallel relaxation ($E = E_{||D}$) at different frequencies and temperatures.

$\log(f/\text{Hz})$	-47 °C	-42 °C	-35 °C	-30 °C	-25 °C	-21 °C
1.1	4.26	1.54	0.82	–	–	–
1.3	4.72	2.58	0.97	0.84	–	–
1.7	3.45	4.53	1.56	0.99	0.90	–
2.0	2.16	5.54	2.36	1.36	0.92	0.81
2.3	1.22	4.60	3.72	2.05	1.21	0.84
2.7	0.62	2.47	5.87	3.59	2.04	1.11
3.0	0.43	1.36	5.67	5.30	3.12	1.70
3.3	0.32	0.75	3.73	6.20	4.73	2.66
3.7	0.24	0.40	1.58	4.55	6.24	4.80
4.0	0.20	0.31	0.85	2.73	5.29	6.27
4.3	0.17	0.27	0.50	1.51	3.35	5.02
4.7	0.18	0.30	0.37	0.76	1.61	2.94
5.0	0.25	0.33	0.41	0.58	1.02	1.66

Table B.4 Dielectric constant (ϵ_{\perp}') data of supercooled E7 for perpendicular relaxation ($E = E_{\perp D}$) at different frequencies and temperatures.

$\log(f/\text{Hz})$	-46 °C	-41 °C	-36 °C	-31 °C	-25 °C
1.3	4.54	5.40	5.37	5.51	6.22
1.7	3.87	5.25	5.34	5.50	6.20
2.0	3.57	4.86	5.28	5.47	6.17
2.3	3.45	4.32	5.14	5.48	6.13
2.7	3.33	3.70	4.60	5.35	6.04
3.0	3.20	3.48	4.02	5.00	5.87
3.3	2.95	3.38	3.61	4.38	5.59
3.7	2.70	3.28	3.42	3.70	4.98
4.0	2.64	3.15	3.35	3.48	4.29
4.3	2.58	2.98	3.28	3.39	3.79
4.7	2.50	2.70	3.06	3.30	3.51
5.0	2.47	2.63	2.88	3.18	3.42

Table B.5 Dielectric loss (ϵ_{\perp}'') data of supercooled E7 for perpendicular relaxation ($E = E_{\perp D}$) at different frequencies and temperatures.

$\log(f/\text{Hz})$	-46 °C	-41 °C	-36 °C	-31 °C	-25 °C
1.3	0.76	0.27	–	–	–
1.7	0.69	0.50	0.20	–	–
2.0	0.48	0.76	0.35	0.20	0.16
2.3	0.34	0.88	0.58	0.30	0.18
2.7	0.64	0.64	0.89	0.57	0.26
3.0	0.32	0.40	0.84	0.87	0.39
3.3	0.34	0.29	0.56	0.93	0.59
3.7	0.20	0.28	0.32	0.66	0.94
4.0	0.25	0.33	0.27	0.40	0.97
4.3	0.19	0.35	0.29	0.30	0.73
4.7	0.15	0.31	0.36	0.28	0.44
5.0	0.13	0.27	0.38	0.37	0.36

Table B.6 Dielectric constant ($\epsilon_{||}'$) data of supercooled E8 for parallel relaxation ($E = E_{||D}$) at different frequencies and temperatures.

$\log(f/\text{Hz})$	-42.1°C	-35.7°C	-30.5 °C	-25.5 °C	-21.3 °C	-15°C
1.1	14.23	–	–	–	–	–
1.3	12.73	17.80	18.75	18.98	19.29	19.40
1.7	8.90	17.17	18.53	18.86	19.20	19.33
2.0	5.90	16.33	18.30	18.72	19.16	19.29
2.3	4.80	14.37	17.37	18.46	18.93	19.17
2.7	4.55	10.27	14.85	17.56	18.45	18.86
3.0	4.45	6.70	11.40	16.16	18.05	18.46
3.3	4.45	5.30	7.50	13.38	16.57	17.86
3.7	4.45	4.80	5.50	8.65	12.28	16.00
4.0	4.45	4.60	5.20	6.10	8.45	12.74
4.3	4.45	4.50	5.01	5.30	5.80	9.00
4.7	4.47	4.45	4.89	5.05	4.90	5.5
5.0	4.49	4.40	4.80	4.90	4.80	4.90

Table B.7 Dielectric loss ($\epsilon_{||}''$) data of supercooled E8 for parallel relaxation ($E = E_{||D}$) at different frequencies and temperatures.

$\log(f/\text{Hz})$	-42.1°C	-35.7°C	-30.5 °C	-25.5 °C	-21.3 °C	-15°C
1.3	4.93	–	–	–	–	–
1.7	–	2.70	1.40	0.82	0.70	0.50
2.0	3.85	3.92	2.19	0.99	0.76	0.56
2.3	2.32	5.58	3.44	1.72	1.04	0.69
2.7	1.20	–	–	3.15	1.79	1.05
3.0	0.73	4.40	6.44	4.80	2.99	1.64
3.3	0.55	2.80	5.10	6.47	4.60	2.74
3.7	0.47	1.35	2.80	5.85	6.80	5.03
4.0	0.46	0.85	1.80	3.95	6.40	7.00
4.3	0.45	0.72	1.21	2.50	4.20	6.70
4.7	0.46	0.65	0.89	1.60	2.40	3.80
5.0	0.51	0.60	0.80	1.35	1.89	2.45

Table B.8 Dielectric losses (ϵ_{\parallel}'' and ϵ_{\perp}'') measured at 1kHz for the oriented of the nematic mixture E8 at different temperatures.

Temperature /°C	ϵ_{\perp}''	Temperature /°C	ϵ_{\parallel}''
	$E = E_{\perp}D$		$E = E_{\parallel}D$
-90	0.012	-90	0.04
-85	0.013	-85	0.04
-80	0.015	-80	0.04
-75	0.016	-75	0.04
-67	0.017	-67	0.04
-62	0.020	-62	0.04
-60	0.022	-60	0.04
-58	0.030	-57	0.06
-56	0.039	-52	0.13
-52	0.126	-48	0.33
-49	0.238	-47	0.40
-46	0.388	-45	0.56
-44	0.413	-42	0.73
-42	0.320	-36	4.40
-40	0.216	-33	5.9
-36	0.209	-27	6.4
-33	0.194	-24	4.80
-27	0.121	-20	2.99
-24	0.08	-8	1.64
-20	0.05	—	—

APPENDIX C

Dielectric Permittivity and Refractive Index Results

Appendix C contains all of dielectric permittivities (dielectric constants), refractive indices data for the dilute solutions used in this part of project with the object of determining the molecular dipole moment of the compounds. The error in the dielectric permittivity and refractive index results are less than 1% and 0.1%, respectively. All experimental data obtained at a fixed temperature of 25.0 °C ($\pm 0.1^\circ\text{C}$). The Dielectric permittivities (ϵ_{12}), refractive indices (n_{12}), and dielectric increment (Δ) data for the solutions of the cyano biphenyl liquid crystals in a non-polar solvent at 25 °C are shown in table (C.1-6). The dielectric results also for solutions of some molecules (not-mesogen) which have a structural relationship to cyano biphenyl liquid crystals are shown in table (C.7-9).

Table C.1 Dielectric permittivities, refractive indices, and dielectric increment data for pentyl cyanobiphenyl (5CB) in cyclohexane at 25.0 °C.

mol/dm ³	ϵ_{12}	n_{12}	Δ
0.0330	2.09 (12)	2.029 (6)	0.068 (1)
0.0549	2.15 (10)	2.030 (1)	0.127 (4)
0.0784	2.19 (85)	2.033 (2)	0.171 (8)
0.1011	2.26 (79)	2.036 (0)	0.238 (4)
0.1188	2.31 (81)	2.037 (8)	0.287 (0)
0.1654	2.43 (10)	2.042 (4)	0.395 (6)

Table C.2 Dielectric permittivities, refractive indices, and dielectric increment data for hexyl cyanobiphenyl (6CB) in cyclohexane at 25 °C.

mol/dm ³	ϵ_{12}	n_{12}	Δ
0.0318	2.10 (69)	1.425 (4)	0.081 (6)
0.0637	2.17 (84)	1.426 (0)	0.151 (6)
0.0824	2.23 (65)	1.426 (8)	0.207 (1)
0.1023	2.28 (71)	1.427 (7)	0.255 (3)
0.1274	2.35 (53)	1.428 (7)	0.320 (6)

Table C.3 Dielectric permittivities, refractive indices, and dielectric increment data for heptyl cyanobiphenyl (7CB) in cyclohexane at 25 °C.

mol/dm ³	ϵ_{12}	n_{12}	Δ
0.0477	2.12 (99)	1.425 (2)	0.105 (1)
0.0660	2.17 (44)	1.425 (8)	0.147 (9)
0.0954	2.26 (47)	1.426 (8)	0.235 (4)
0.1224	2.32 (70)	1.427 (7)	0.295 (3)
0.1632	2.42 (99)	1.428 (6)	0.395 (6)
0.1909	2.49 (99)	1.429 (5)	0.462 (9)

Table C.4 Dielectric permittivities, refractive indices, and dielectric increment data for octyl cyanobiphenyl (8CB) in cyclohexane at 25 °C.

mol/dm ³	ϵ_{12}	n_{12}	Δ
0.0144	2.06 (05)	1.427 (2)	0.029 (9)
0.0320	2.11 (12)	1.427 (9)	0.078 (6)
0.0467	2.15 (30)	1.428 (8)	0.118 (0)
0.0762	2.23 (37)	1.430 (2)	0.194 (7)
0.1051	2.31 (00)	1.431 (2)	0.268 (3)
0.1458	2.41 (35)	1.432 (4)	0.368 (2)

Table C.5 Dielectric permittivities, refractive indices, and dielectric increment data for pentyloxy cyanobiphenyl (5OCB) in 1,4-dioxane at 25 °C.

mol/dm ³	ϵ_{12}	n_{12}	Δ
0.0522	2.3982	1.4222	0.1830
0.0626	2.4505	1.4231	0.2328
0.0802	2.4925	1.4234	0.2737
0.1021	2.5692	1.4242	0.3483
0.1253	2.6553	1.4254	0.4309
0.1554	2.7361	1.4262	0.5094

Table C.6 Dielectric permittivities, refractive indices, and dielectric increment data for octyloxy cyanobiphenyl (8OCB) in 1,4-dioxane at 25 °C.

mol/dm ³	ϵ_{12}	n_{12}	Δ
0.0213	2.2768	1.4210	0.0652
0.0425	2.3542	1.4221	0.1394
0.0851	2.4890	1.4240	0.2688
0.1001	2.5418	1.4245	0.3201
0.1200	2.6085	1.4252	0.3848

Table C.7 Dielectric permittivities, refractive indices, and dielectric increment data for cyanobiphenyl (CB) in 1,4-dioxane at 25 °C.

mol/dm ³	ϵ_{12}	n_{12}	Δ
0.0777	2.40 (79)	1.422 (9)	0.190 (5)
0.1224	2.51 (18)	1.424 (3)	0.290 (4)
0.1555	2.59 (16)	1.425 (6)	0.366 (7)
0.2232	2.75 (01)	1.428 (4)	0.517 (1)
0.3109	2.59 (58)	1.431 (8)	0.713 (1)

Table C.8 Dielectric permittivities, refractive indices, and dielectric increment data for pentylbiphenyl (5B) in cyclohexane at 25 °C.

mol/dm ³	ϵ_{12}	n_{12}	Δ
0.1452	2.0452	1.4283	0.0091
0.2112	2.0520	1.4305	0.0122
0.2988	2.0639	1.4334	0.0157
0.4502	2.0842	1.4384	0.0216
0.5420	2.0963	1.4415	0.0250
0.6498	2.1112	1.4450	0.0297

Table C.9 Dielectric permittivities, refractive indices, and dielectric increment data for octyloxycyanophenyl (8OCP) in 1,4-dioxane at 25 °C.

mol/dm ³	ϵ_{12}	n_{12}	Δ
0.0298	2.3095	1.4207	0.0986
0.0597	2.4034	1.4212	0.1910
0.0818	2.4678	1.4215	0.2545
0.1194	2.5790	1.4219	0.3645
0.1612	2.7081	1.4223	0.4936
0.2085	2.8512	1.4234	0.6326

APPENDIX D

Optical Phase Retardation Results

This appendix contains all of phase retardation data for the liquid crystals in the dilute solutions and also in the isotropic phase. The error in the phase retardation measurements is approximately $\pm 1\%$. The concentration of the solutions are all weight per volume (w/v). The estimated accuracy in the measurement of temperature is $\pm 0.1^\circ\text{C}$.

D.1 Tables of optical phase retardation results (solution)

Table D.1.1 Optical phase retardation, δ , values for solutions of 5CB in cyclohexane at various dc electric field.

Voltage	$\delta = (2\pi L/\lambda) \Delta n$				
(kV)	5.70 %	4.12 %	2.96 %	1.95 %	1.37 %
1.00	1.576	1.020	0.920	0.668	0.576
1.25	2.452	1.648	1.372	0.948	0.780
1.50	3.468	2.356	1.908	1.284	1.028
1.75	4.728	3.208	2.520	1.692	1.276
2.00	6.144	4.264	3.216	2.132	1.588
2.25	7.816	5.384	4.048	2.668	1.940
2.50	9.572	6.660	4.956	3.252	2.308

Table D.1.2 Optical phase retardation, δ , values for solutions of 6CB in cyclohexane at various dc electric field.

Voltage	$\delta = (2\pi L/\lambda) \Delta n$				
(kV)	4.78 %	3.92 %	2.83 %	2.17 %	1.56 %
1.00	1.408	1.399	1.068	0.768	0.300
1.25	2.264	1.948	1.508	1.072	0.520
1.50	3.304	2.636	2.052	1.464	0.794
1.75	4.468	3.584	2.656	1.936	1.112
2.00	5.796	4.676	3.384	2.516	1.496
2.25	7.332	5.820	4.158	3.100	1.904
2.50	8.929	7.156	5.080	3.868	2.384

Table D.1.3 Optical phase retardation, δ , values for solutions of 8CB in cyclohexane at various dc electric field.

Voltage	$\delta = (2\pi L/\lambda) \Delta n$				
(kV)	4.25 %	3.06 %	2.22 %	1.36 %	0.93 %
1.00	1.024	0.679	0.680	0.458	0.228
1.25	1.552	1.072	0.988	0.640	0.344
1.50	2.272	1.544	1.372	0.852	0.493
1.75	3.113	2.104	1.828	1.136	0.662
2.00	4.100	2.744	2.327	1.463	0.872
2.25	5.176	3.492	2.882	1.797	1.087
2.50	6.404	4.376	3.524	2.178	1.342

D.2 Tables of optical phase retardation results (pure phase)

Table D.2.1 Optical phase retardation values, δ , at various temperatures for 5CB
($\lambda = 632.8$).

Voltage	$\delta = (2\pi L/\lambda) \Delta n$						
(kV)	35.7 °C	36.1 °C	38.6 °C	41.2 °C	44.8 °C	45.4 °C	48.5 °C
0.100	1.052	0.963	0.628	0.271	0.247	0.194	0.230
0.150	2.383	2.203	1.160	0.678	0.561	0.446	0.432
0.180	3.524	3.220	1.640	1.044	0.785	0.666	0.616
0.200	4.380	3.994	1.971	1.320	0.982	0.824	0.766
0.220	5.236	4.843	2.393	1.580	1.158	1.002	0.884
0.250	6.696	6.298	3.017	2.090	1.484	1.292	1.142
0.280	8.460	7.928	3.802	2.584	1.856	1.632	1.389
0.300	9.780	9.184	4.375	2.943	2.118	1.875	1.577

Table D.2.2 Optical phase retardation values, $\delta = (2\pi L/\lambda) \Delta n$, at various temperatures for E7.

Voltage	Phase retardation, δ , (degree)						
(kV)	60.8 °C	61.4 °C	62.0 °C	63.2 °C	62.8 °C	67.3 °C	68.3 °C
0.060	0.480	0.332	0.283	0.258	0.200	0.140	0.102
0.080	0.822	0.569	0.482	0.424	0.360	0.219	0.175
0.100	1.336	0.968	0.710	0.652	0.544	0.334	0.270
0.140	2.566	1.835	1.320	1.162	1.065	0.589	0.519
0.180	4.239	3.038	2.143	1.967	1.763	0.948	0.852
0.200	5.230	3.796	2.646	2.421	2.171	1.164	1.050
0.220	6.328	4.497	3.180	2.922	2.628	1.395	1.269
0.250	8.170	5.870	4.084	3.762	3.393	1.788	1.636

Table D.2.3 Optical phase retardation values, $\delta = (2\pi L/\lambda) \Delta n$, at various temperatures for Ex.

Voltage	Phase retardation, δ , (degree)						
(kV)	39.2 ℃	41.2 ℃	43.0 ℃	45.1 ℃	47.7 ℃	49.1 ℃	51.0 ℃
0.10	0.544	0.410	0.304	0.257	0.220	0.176	0.156
0.15	1.135	0.878	0.689	0.553	0.457	0.407	0.363
0.20	2.068	1.757	1.224	0.986	0.828	0.678	0.616
0.25	3.164	2.407	1.911	1.533	1.265	1.074	0.985
0.30	4.659	3.582	2.751	2.198	1.797	1.544	1.411
0.35	6.342	4.676	3.742	2.982	2.454	2.099	1.911

Table D.2.4 Optical phase retardation values, $\delta = (2\pi L/\lambda) \Delta n$, at various temperatures for Ey.

Voltage	Phase retardation, δ , (degree)						
(kV)	41.4 ℃	43.0 ℃	44.5 ℃	45.5 ℃	47.0 ℃	48.0 ℃	50.6 ℃
0.10	0.513	0.396	0.294	0.277	0.227	0.192	0.169
0.15	1.082	0.846	0.652	0.579	0.477	0.427	0.348
0.20	1.944	1.420	1.140	1.008	0.885	0.780	0.651
0.25	3.025	2.219	1.774	1.551	1.333	1.206	1.009
0.30	4.326	3.178	2.515	2.201	1.909	1.706	1.436
0.35	5.906	4.407	3.419	3.007	2.632	2.347	1.918

Appendix E

Dynamic Kerr Effect Results

This appendix contains a representative number of Kerr effect transients recorded for some alkyl cyanobiphenyl liquid-crystals in their nematic phase. All of the transients were obtained using homeotropically aligned samples (i.e., homeotropic with respect to the windows of the optical cell. In all cases the optical path-length of the liquid-crystal was 20 microns).

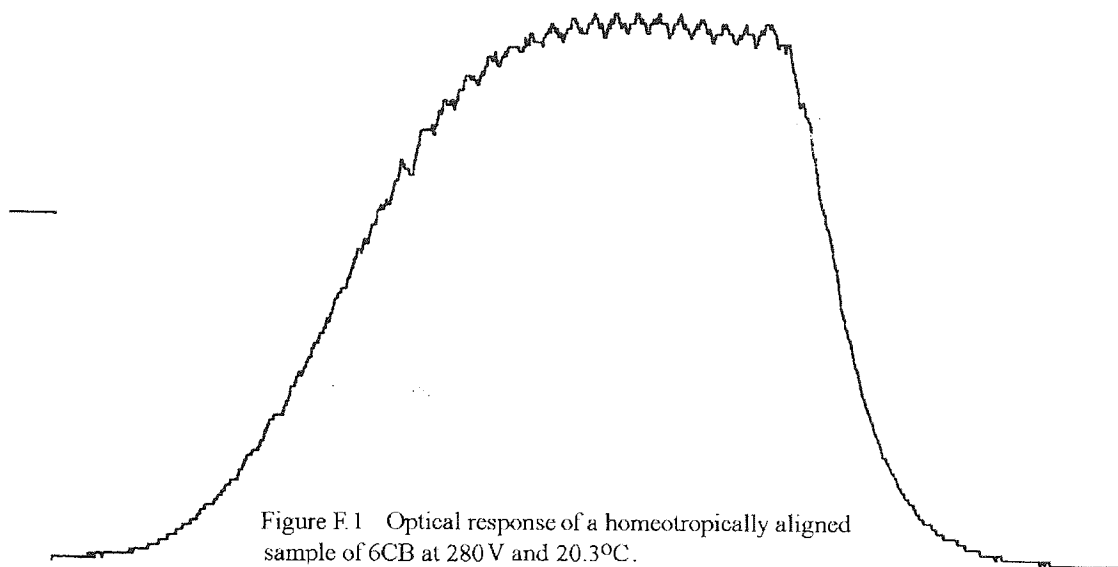


Figure E.1 Optical response of a homeotropically aligned sample of 6CB at 280 V and 20.3°C.
Electrode gap = 3 mm.
Recording time = 1 s.
Pulse length = 0.66 s.
Optical path-length = 20 μ m
Transient maximum = 105 mm, I_0 = 132 mm.

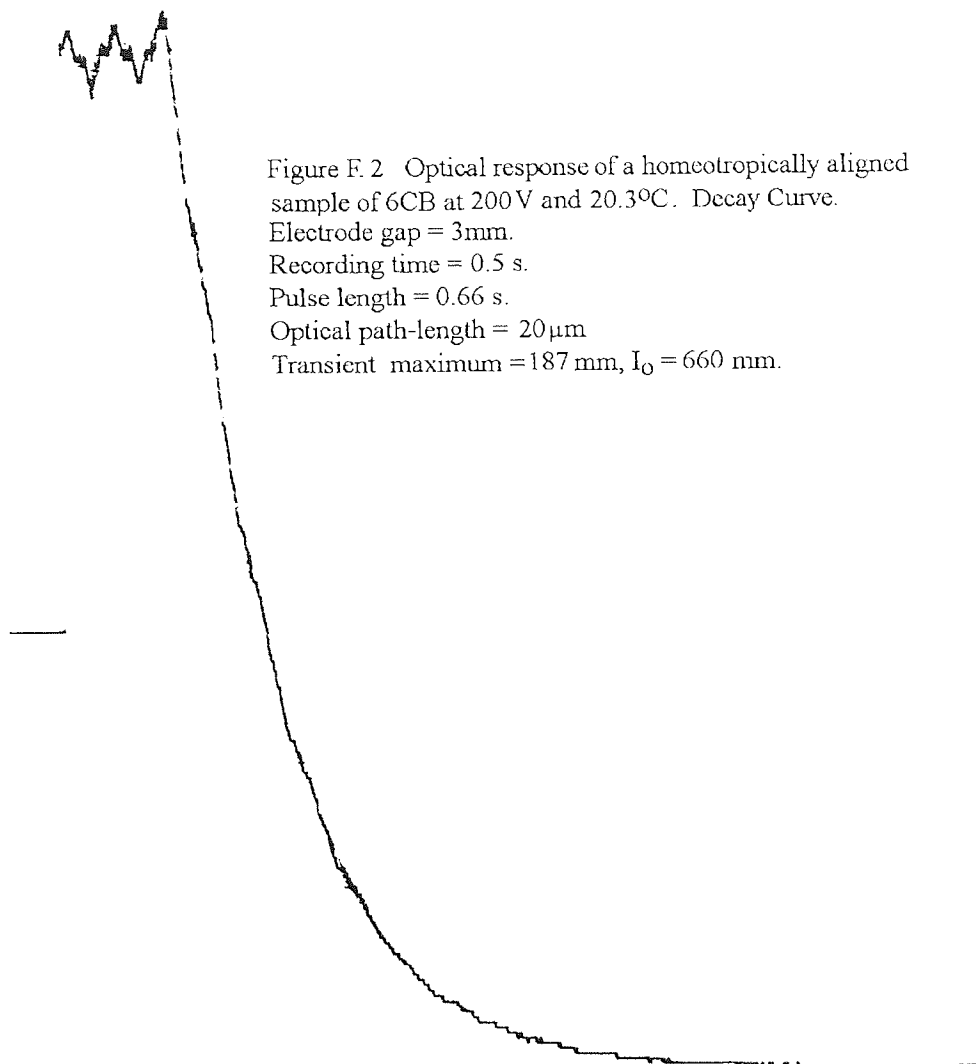


Figure F.2 Optical response of a homeotropically aligned sample of 6CB at 200 V and 20.3°C. Decay Curve.
 Electrode gap = 3mm.
 Recording time = 0.5 s.
 Pulse length = 0.66 s.
 Optical path-length = 20 μ m
 Transient maximum = 187 mm, I_0 = 660 mm.

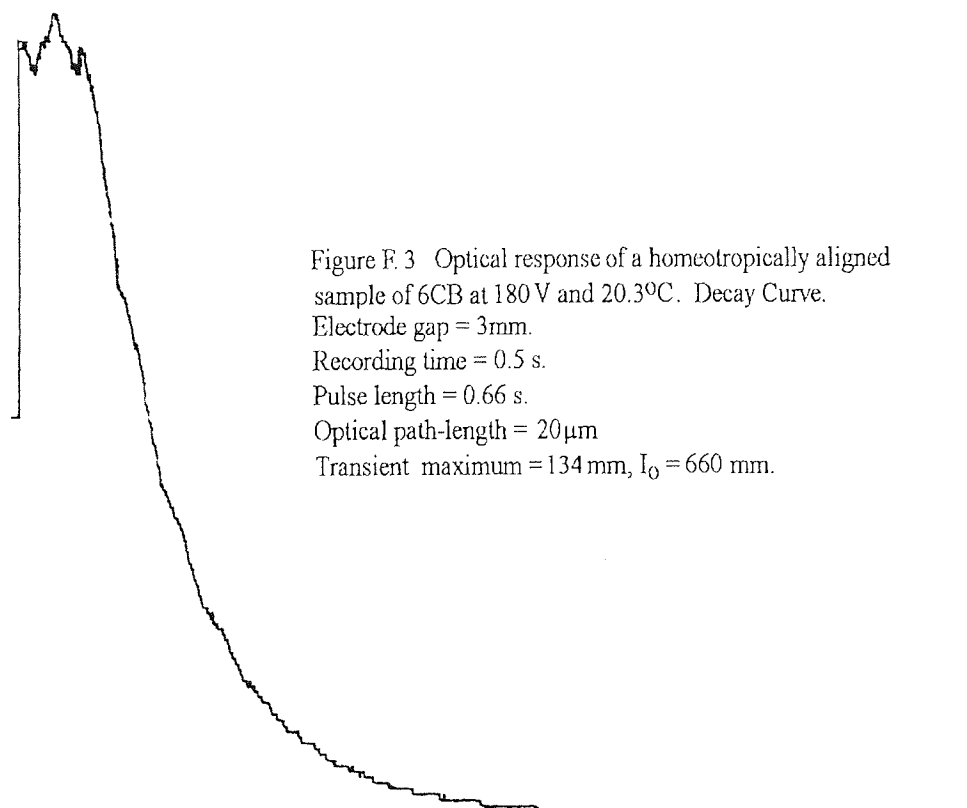


Figure F.3 Optical response of a homeotropically aligned sample of 6CB at 180 V and 20.3°C. Decay Curve.
 Electrode gap = 3mm.
 Recording time = 0.5 s.
 Pulse length = 0.66 s.
 Optical path-length = 20 μ m
 Transient maximum = 134 mm, I_0 = 660 mm.

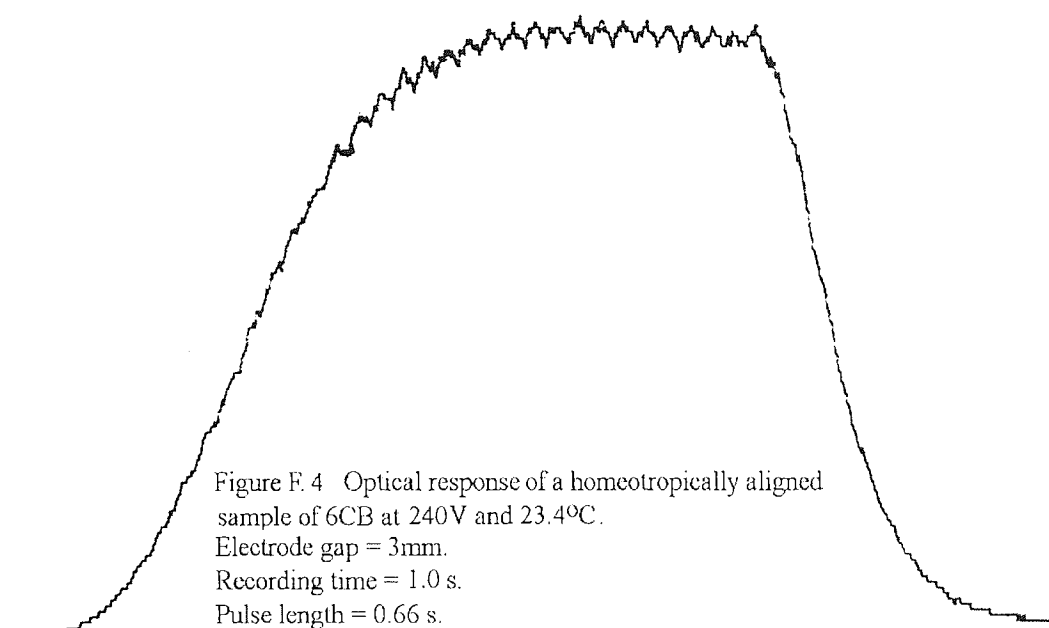


Figure F. 4 Optical response of a homeotropically aligned sample of 6CB at 240V and 23.4°C.
Electrode gap = 3mm.
Recording time = 1.0 s.
Pulse length = 0.66 s.
Optical path-length = 20 μ m
Transient maximum = 105 mm, I_0 = 132 mm.

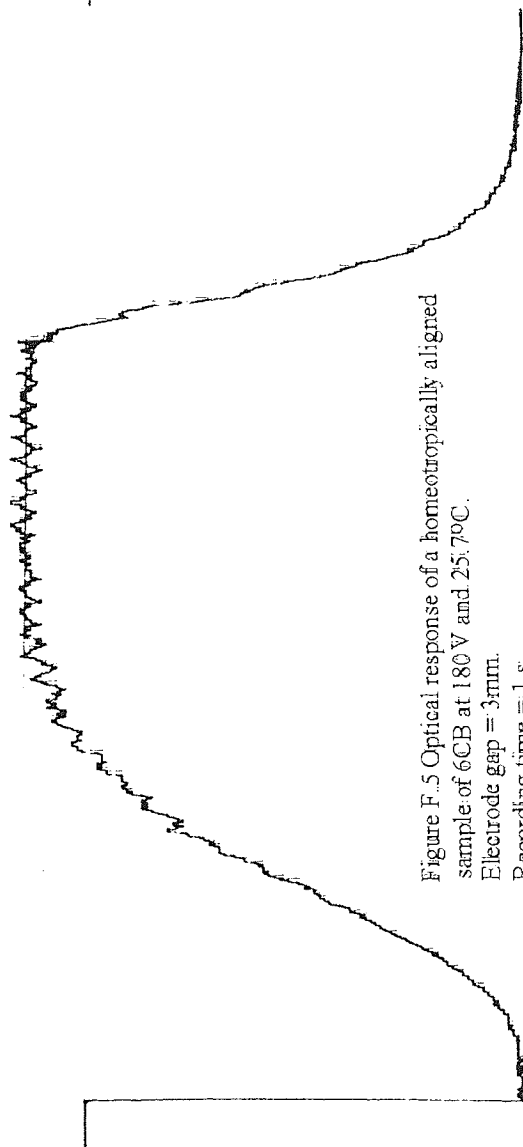


Figure F.5 Optical response of a homeotropically aligned sample of 6CB at 180 V and 25.7°C.

Electrode gap = 3 mm.

Recording time = 1 s.

Pulse length = 0.66 s.

Optical path-length = 20 μ m

Transient maximum = 96 mm, $I_0 = 132$ mm.

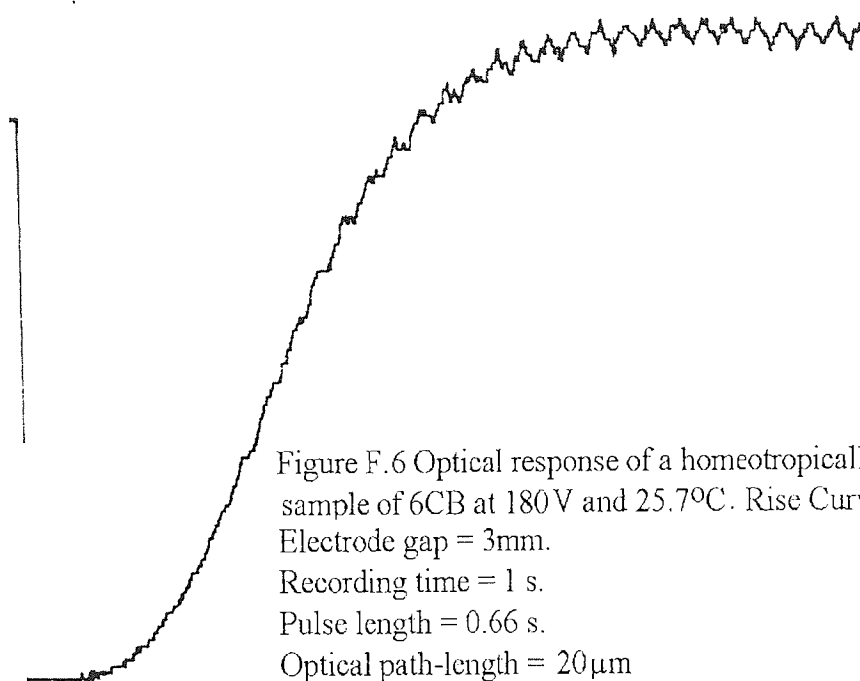


Figure F.6 Optical response of a homeotropically aligned sample of 6CB at 180 V and 25.7°C. Rise Curve.
 Electrode gap = 3 mm.
 Recording time = 1 s.
 Pulse length = 0.66 s.
 Optical path-length = 20 μm
 Transient maximum = 94 mm, $I_0 = 132$ mm.

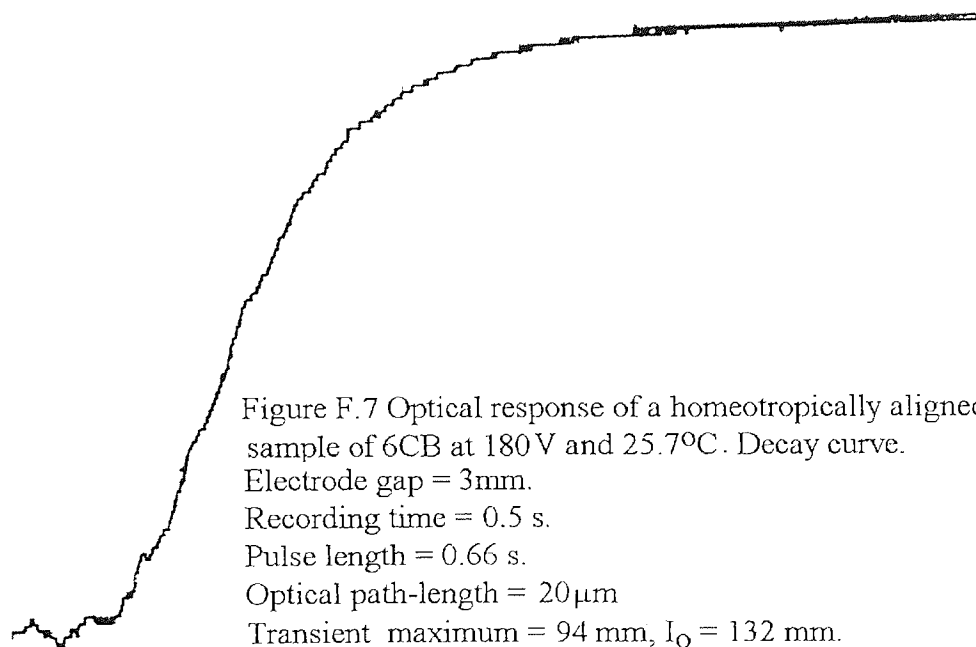
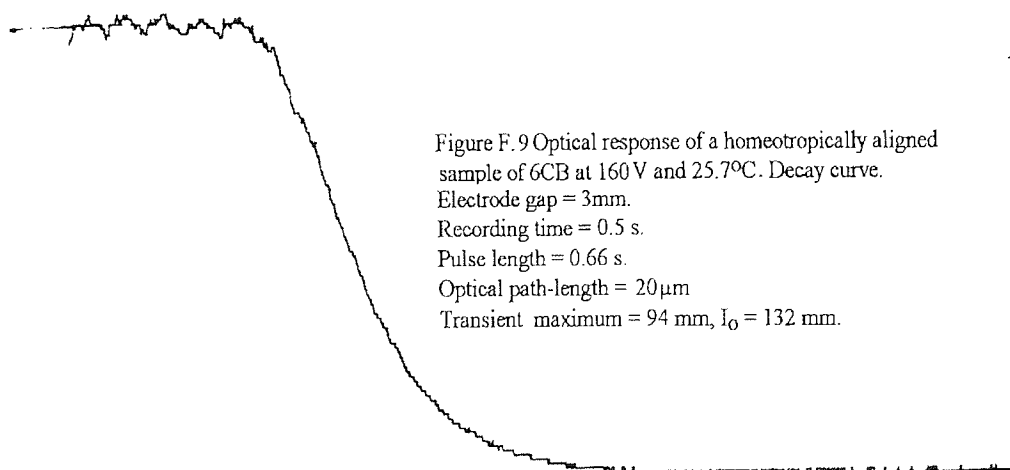
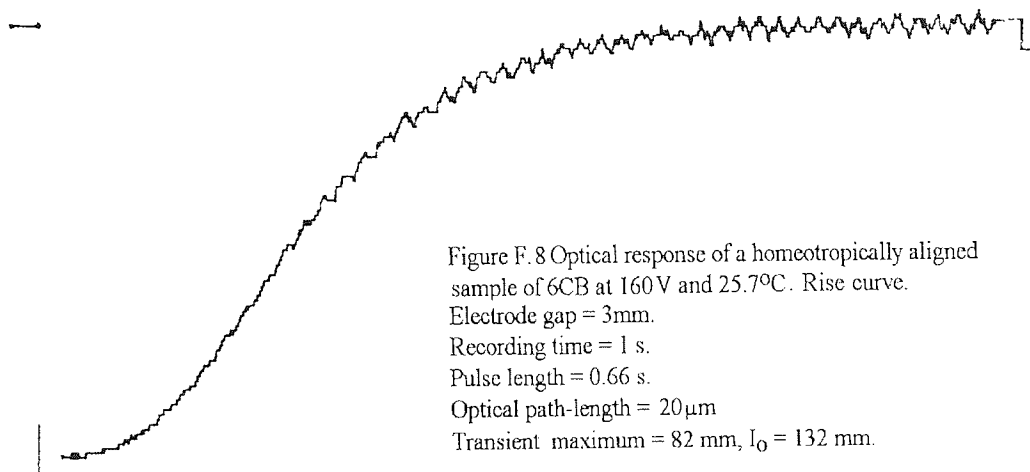
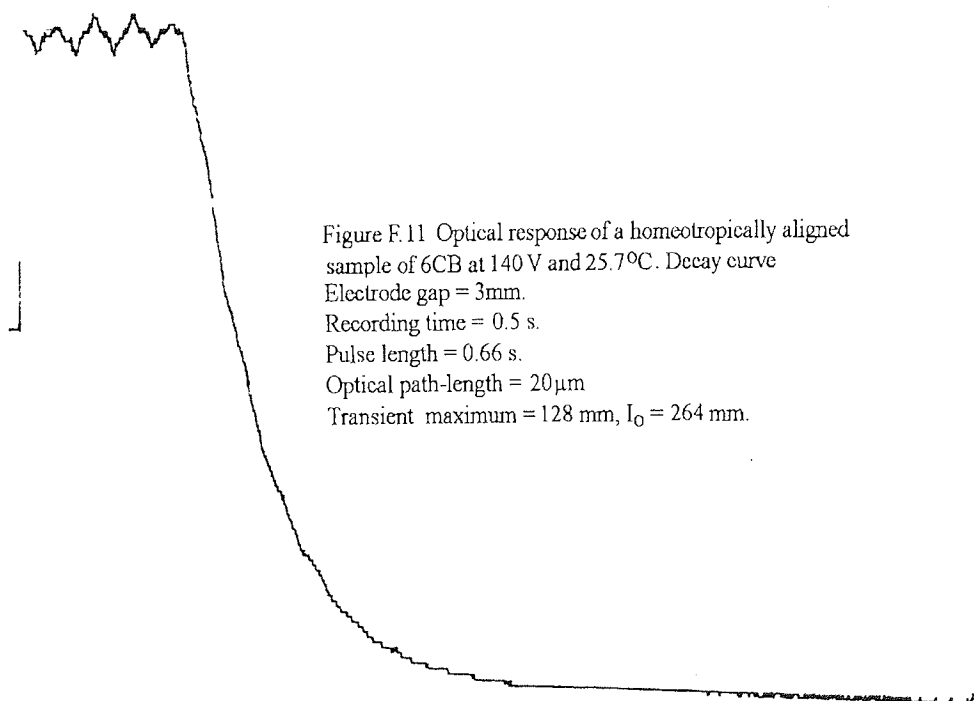
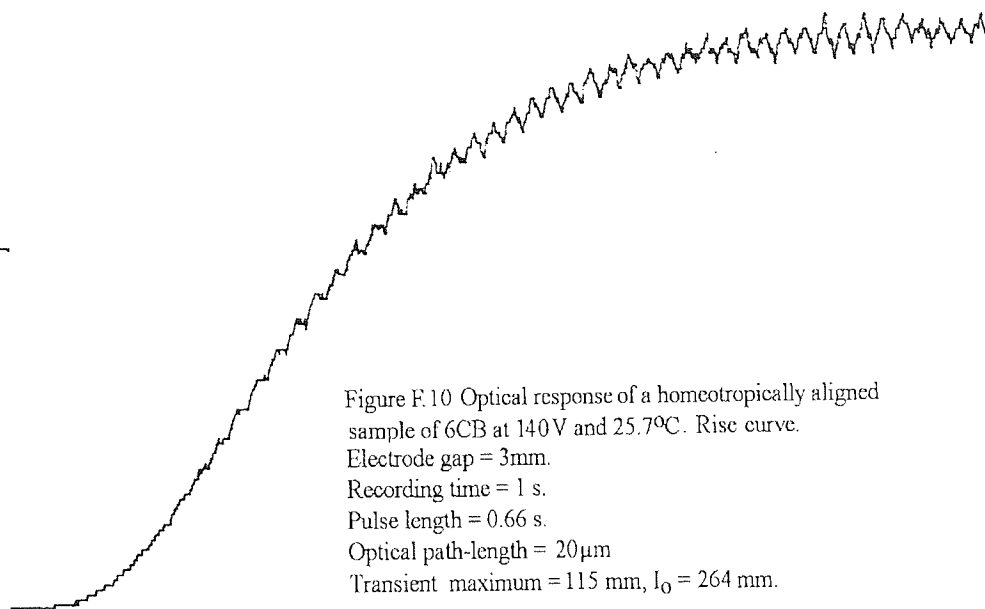


Figure F.7 Optical response of a homeotropically aligned sample of 6CB at 180 V and 25.7°C. Decay curve.
 Electrode gap = 3 mm.
 Recording time = 0.5 s.
 Pulse length = 0.66 s.
 Optical path-length = 20 μm
 Transient maximum = 94 mm, $I_0 = 132$ mm.





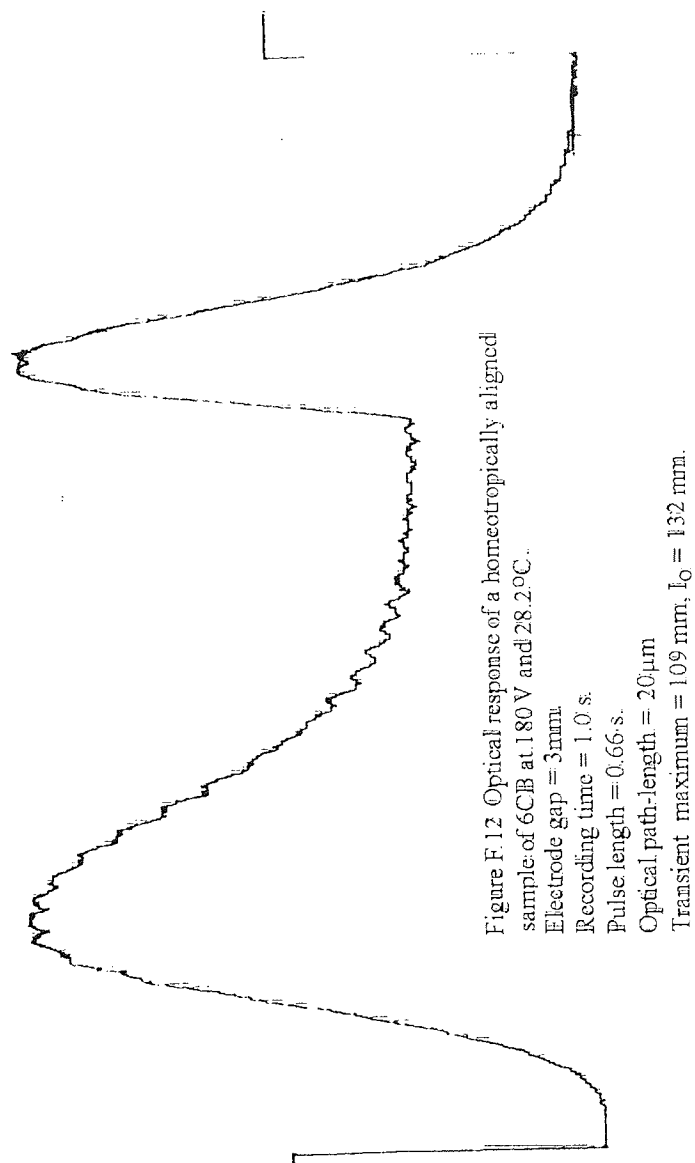


Figure F.12 Optical response of a homeotropically aligned sample of 6CB at 180 V and 28.2 °C.
 Electrode gap = 3 mm
 Recording time = 1.0 s.
 Pulse length = 0.66 s.
 Optical path-length = 20 μ m
 Transient maximum = 109 mm, I_0 = 132 mm.

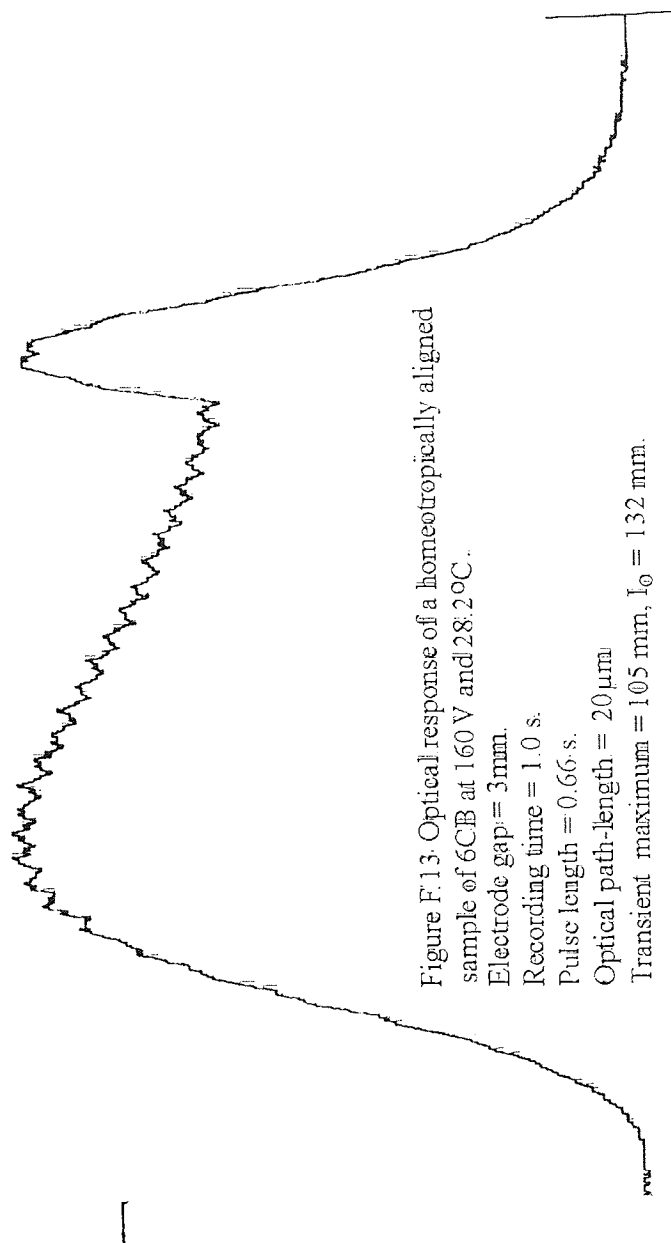


Figure F.13. Optical response of a homeotropically aligned sample of 6CB at 160 V and 28.2°C.

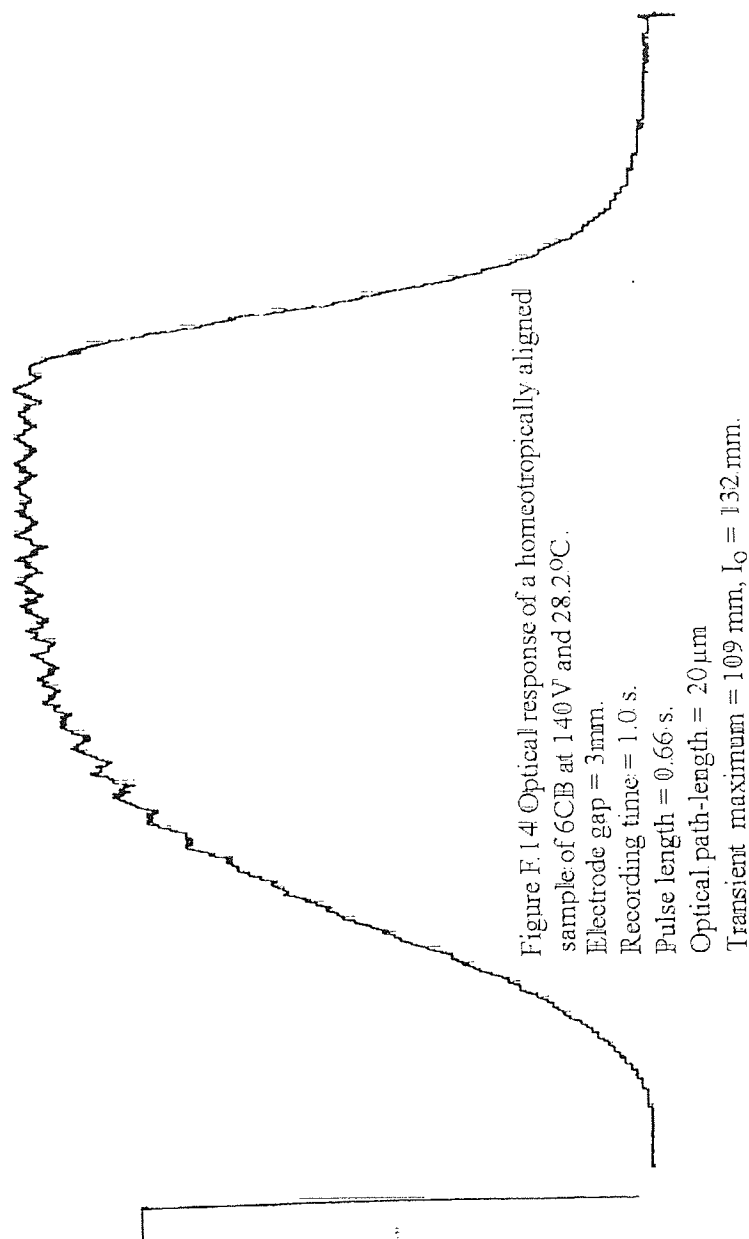
Electrode gap = 3 mm.

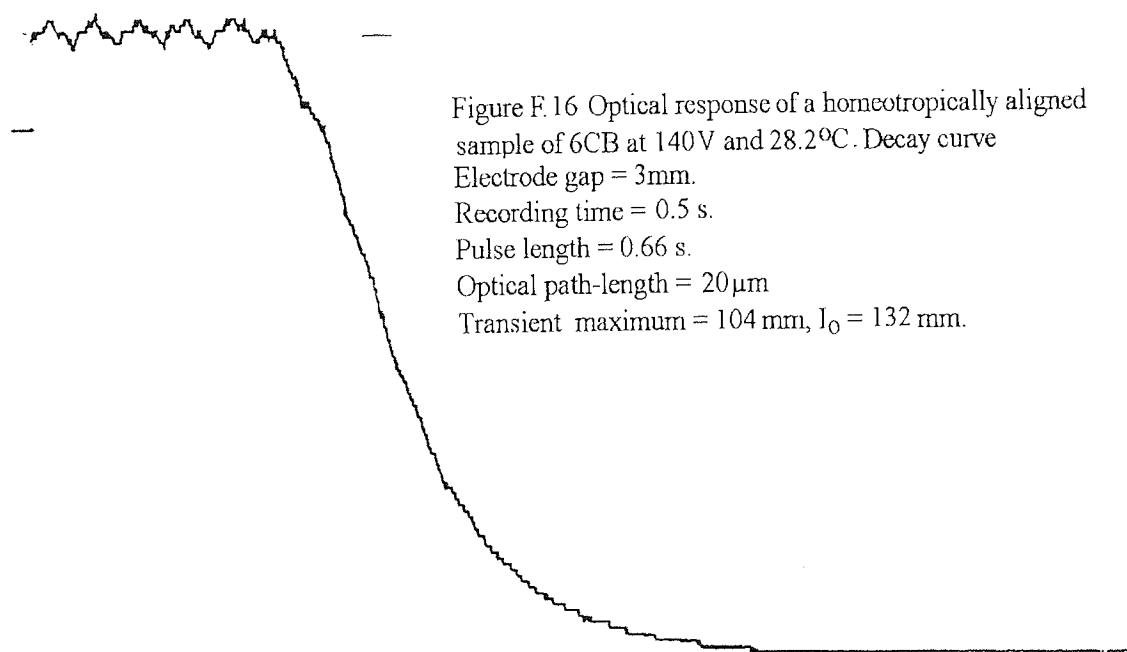
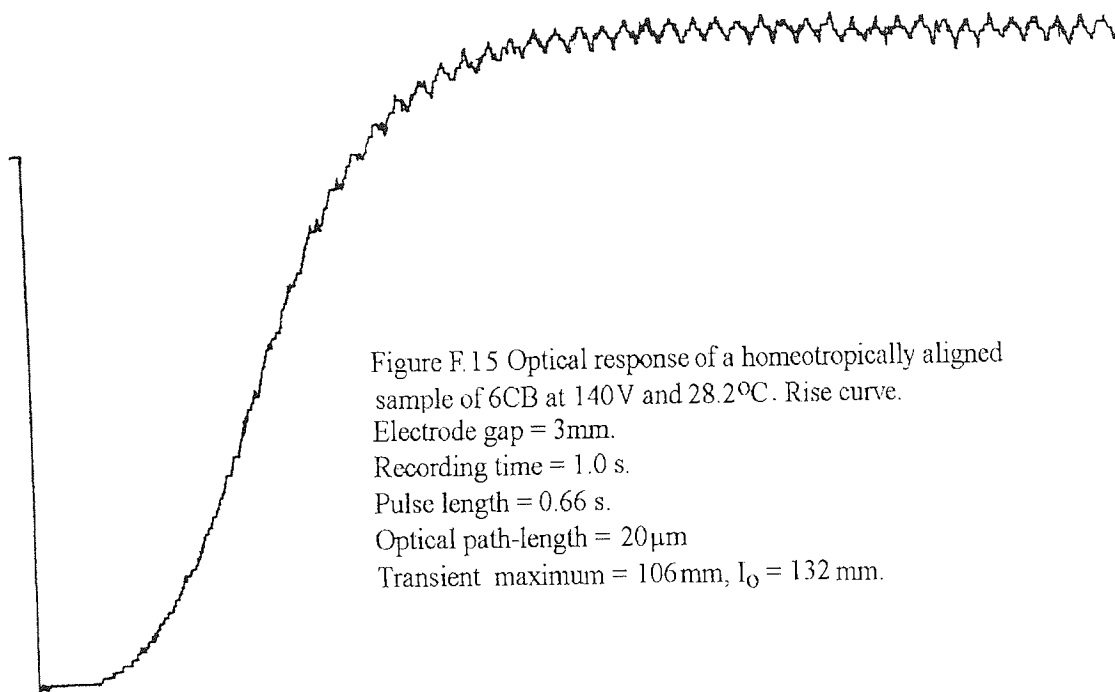
Recording time = 1.0 s.

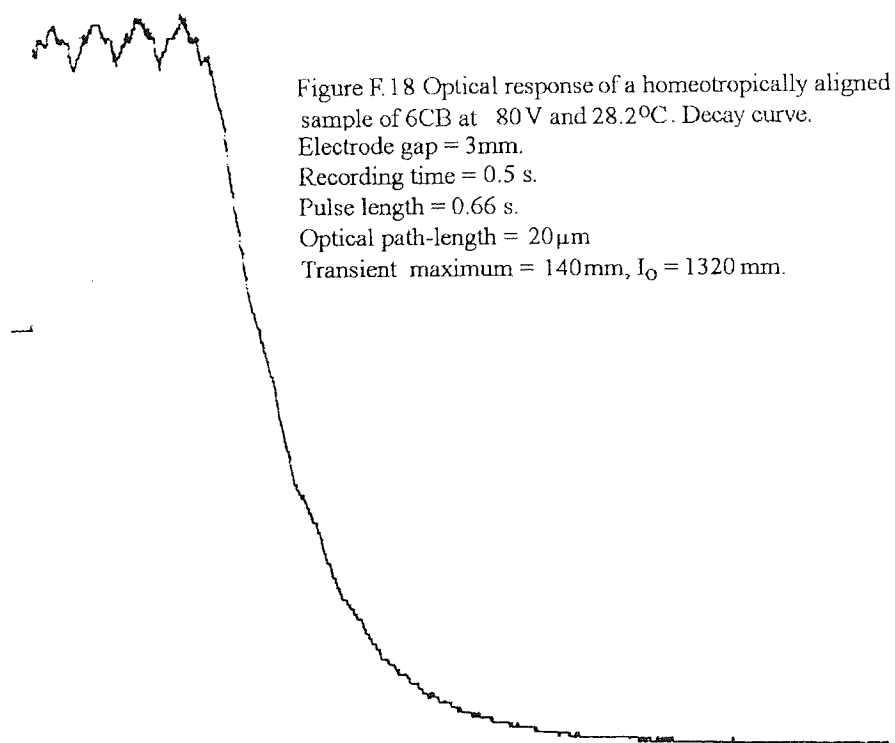
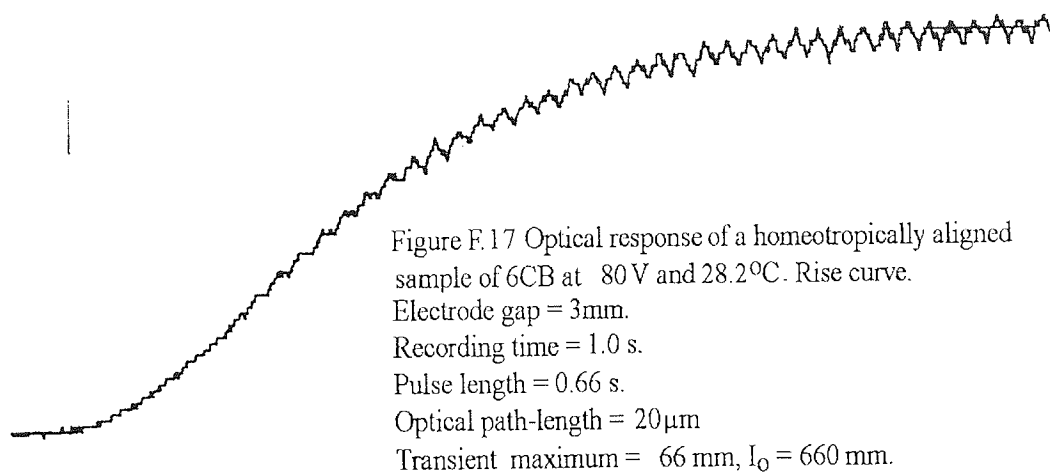
Pulse length = 0.66 s.

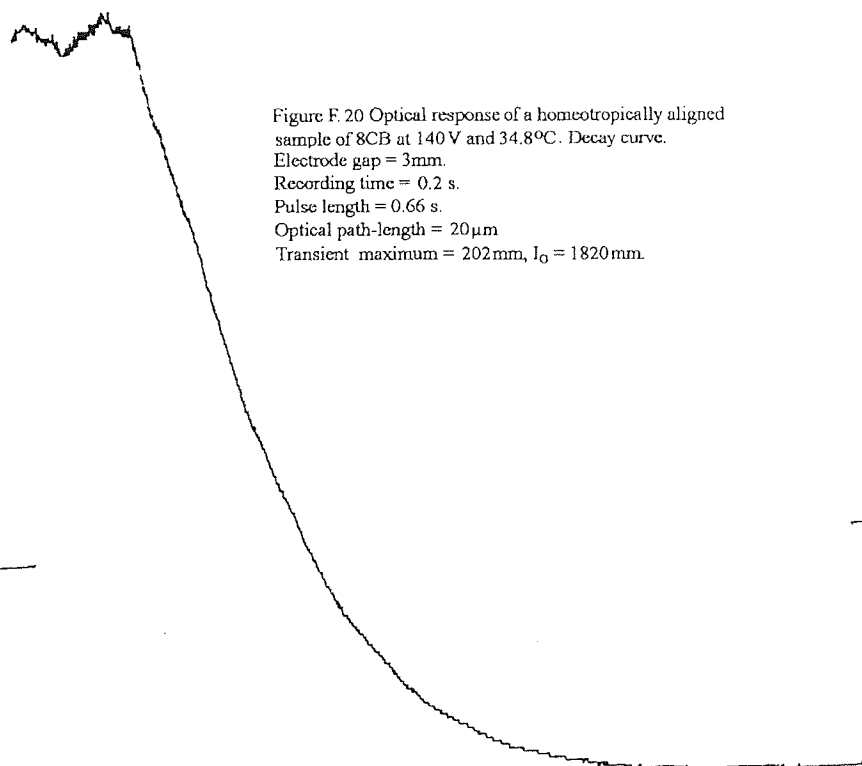
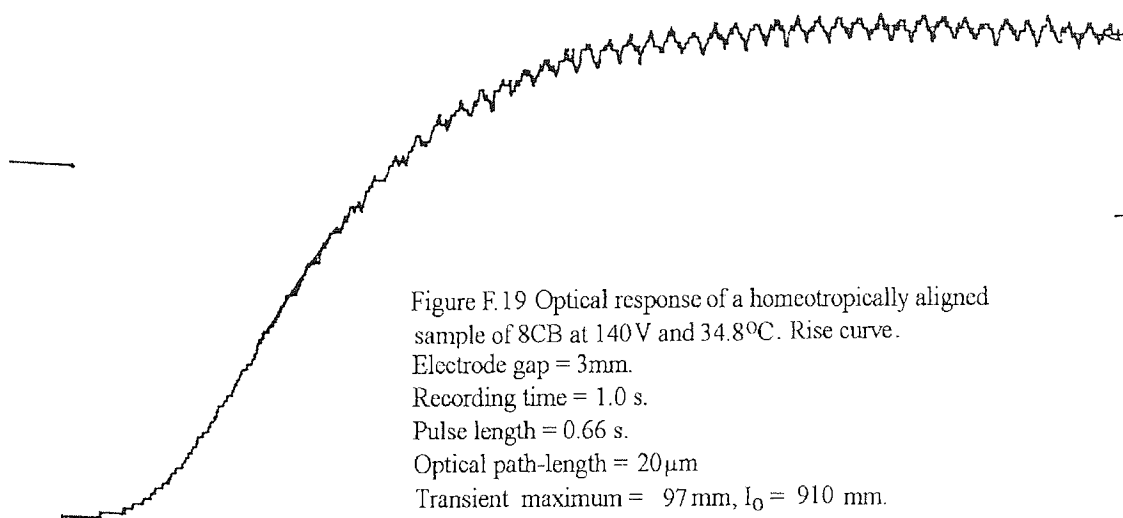
Optical path-length = 20 μ m

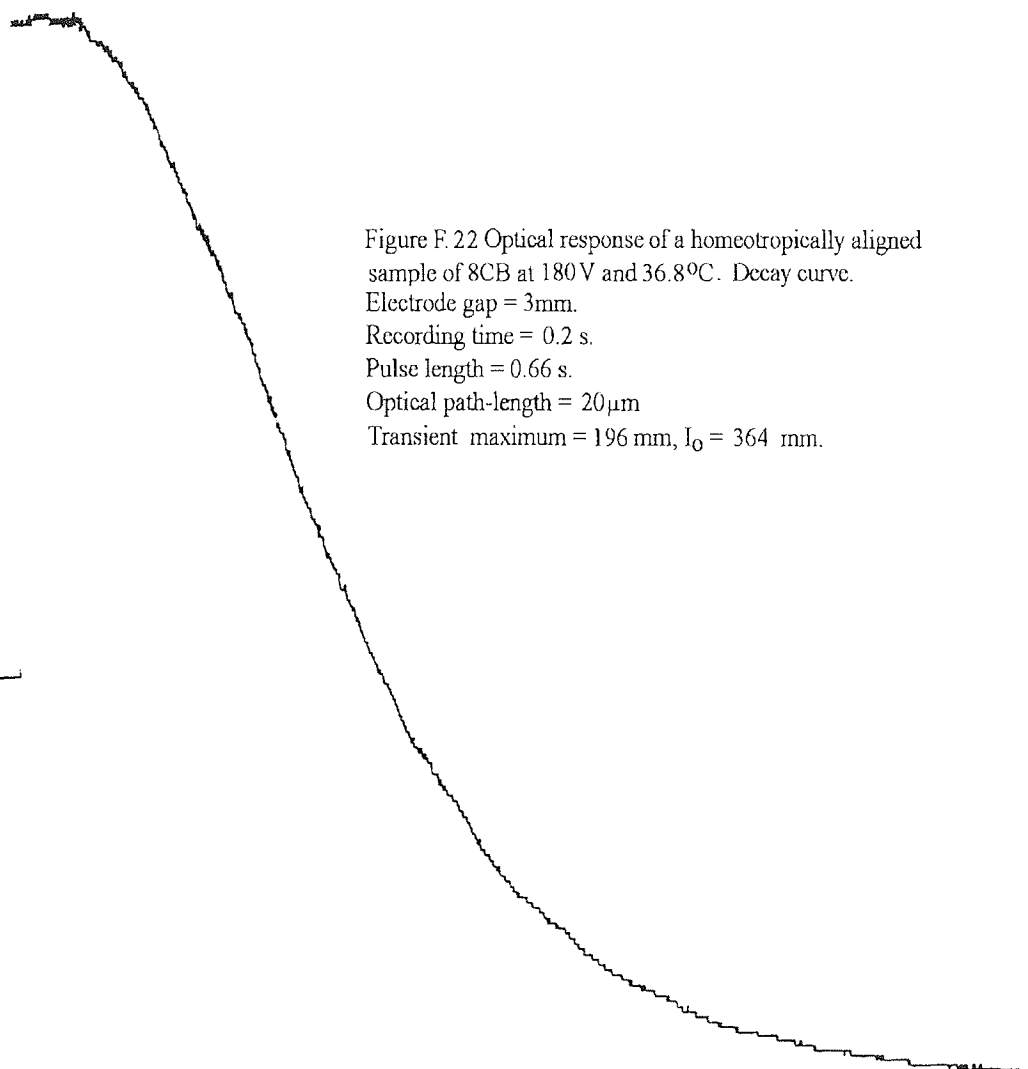
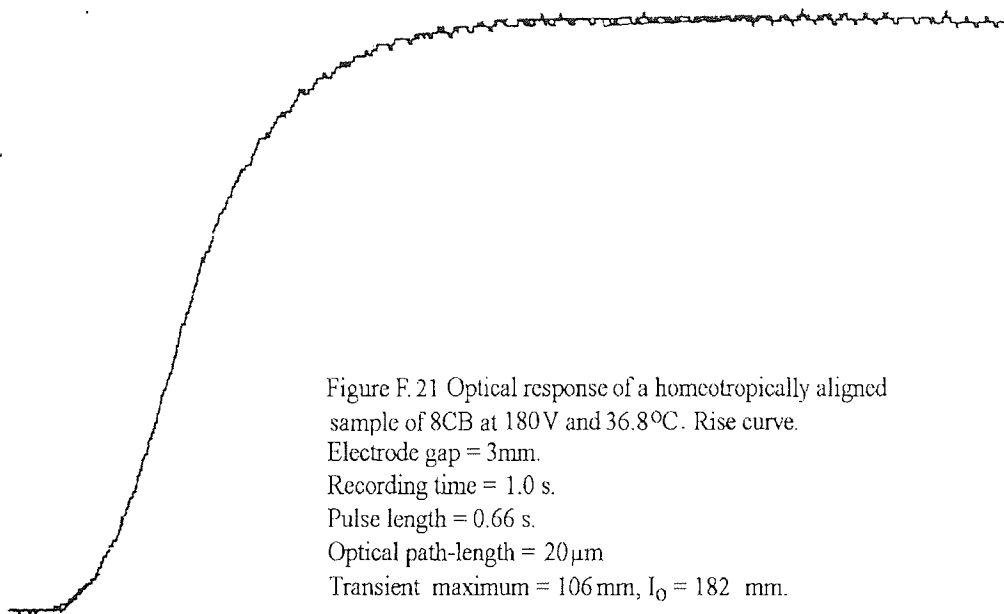
Transient maximum = 105 mm, $I_0 = 132$ mm.

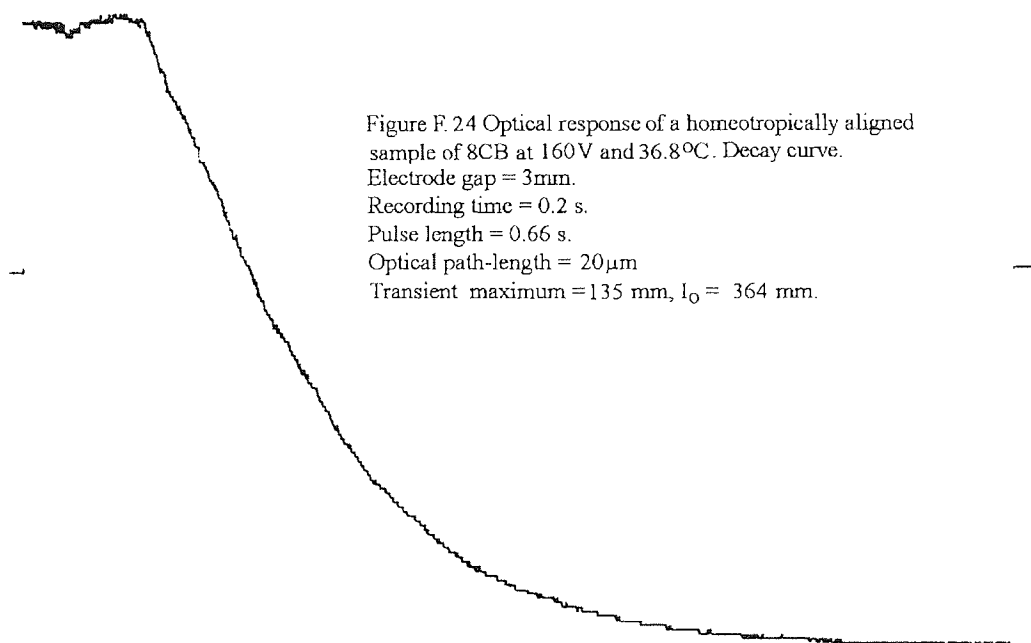
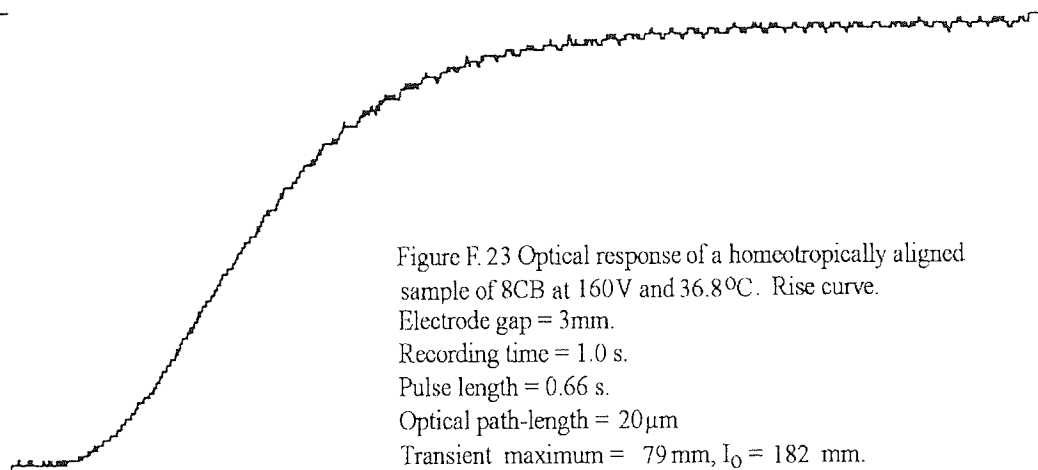


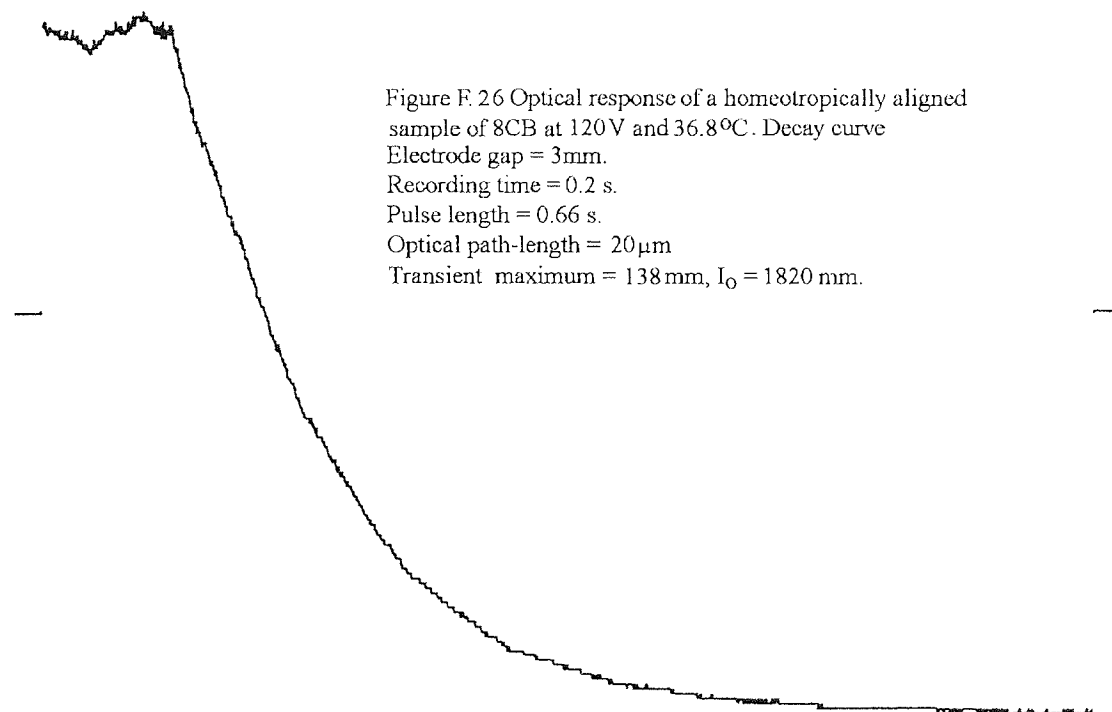
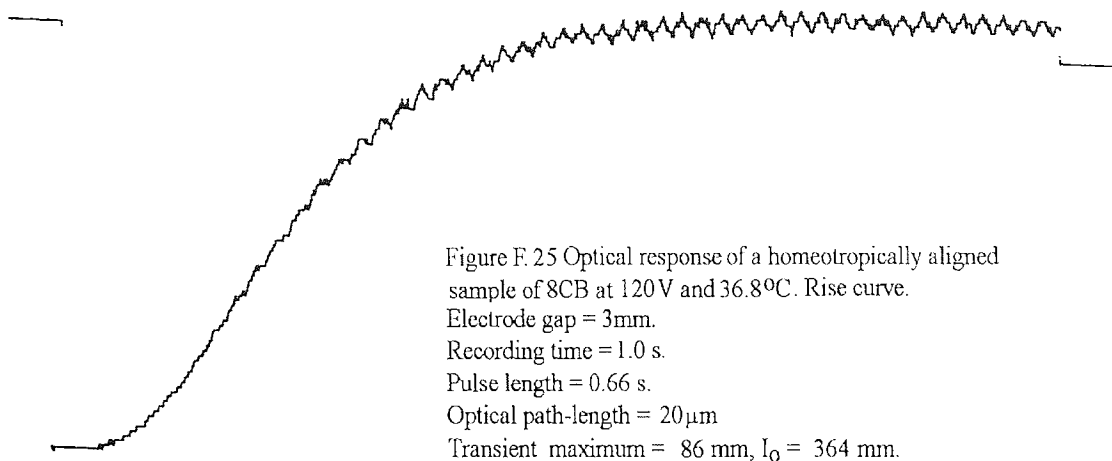


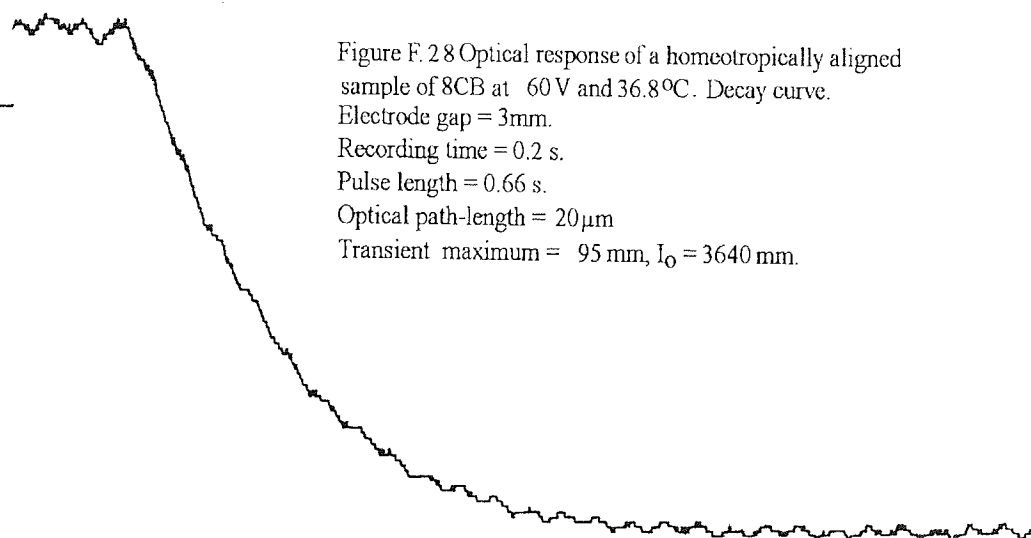
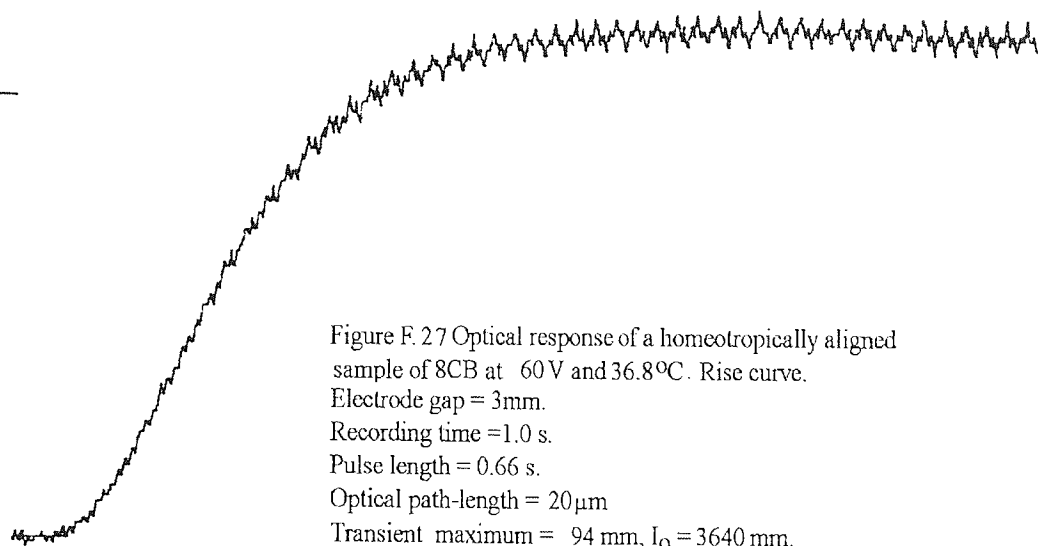












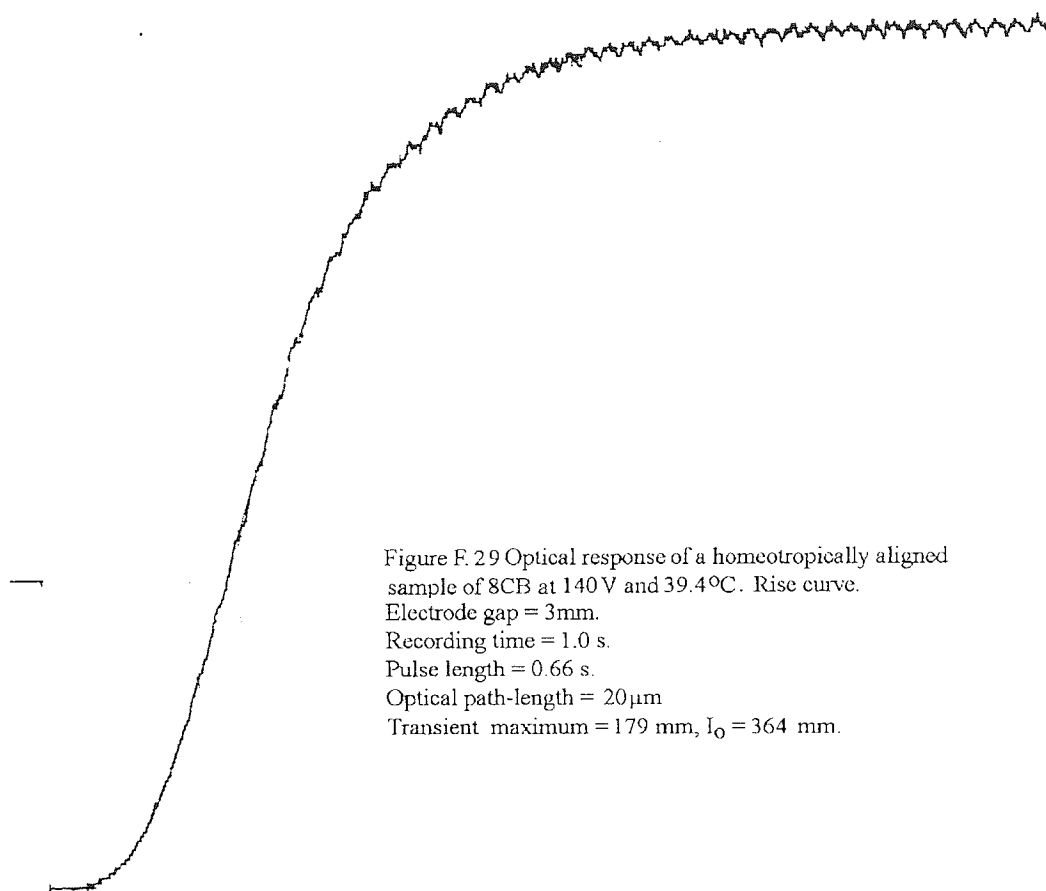


Figure F. 29 Optical response of a homeotropically aligned sample of 8CB at 140 V and 39.4°C. Rise curve.
 Electrode gap = 3mm.
 Recording time = 1.0 s.
 Pulse length = 0.66 s.
 Optical path-length = 20 μ m
 Transient maximum = 179 mm, I_0 = 364 mm.

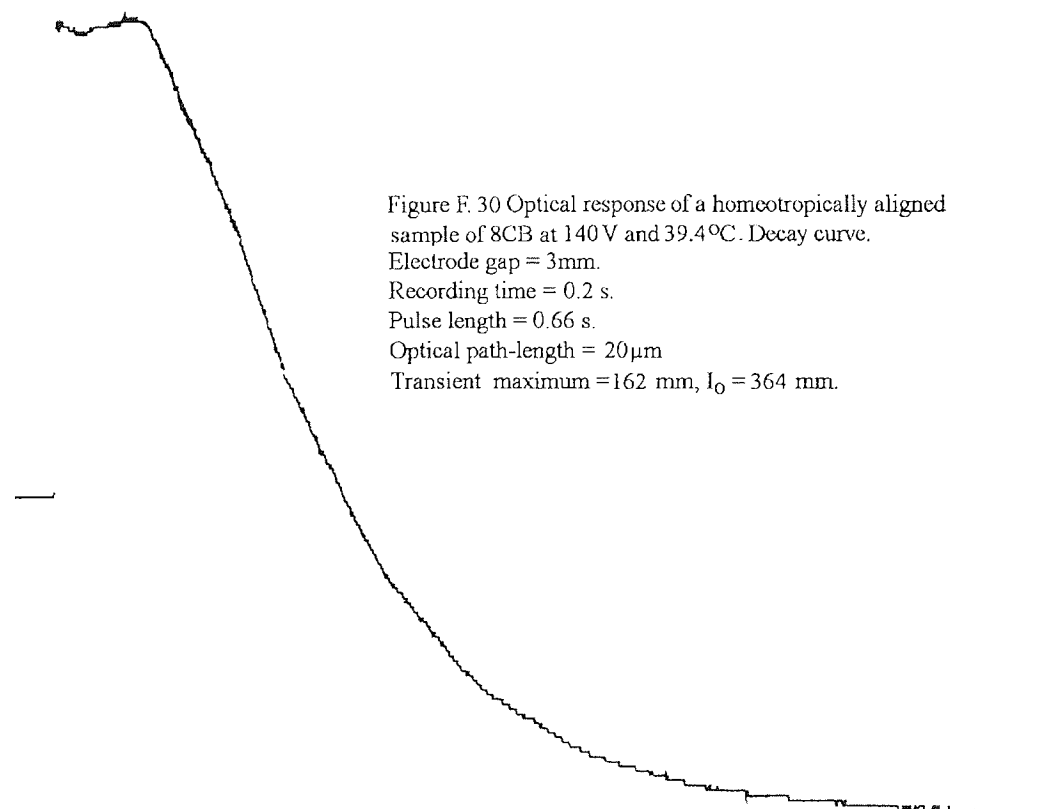


Figure F. 30 Optical response of a homeotropically aligned sample of 8CB at 140 V and 39.4°C. Decay curve.
 Electrode gap = 3mm.
 Recording time = 0.2 s.
 Pulse length = 0.66 s.
 Optical path-length = 20 μ m
 Transient maximum = 162 mm, I_0 = 364 mm.

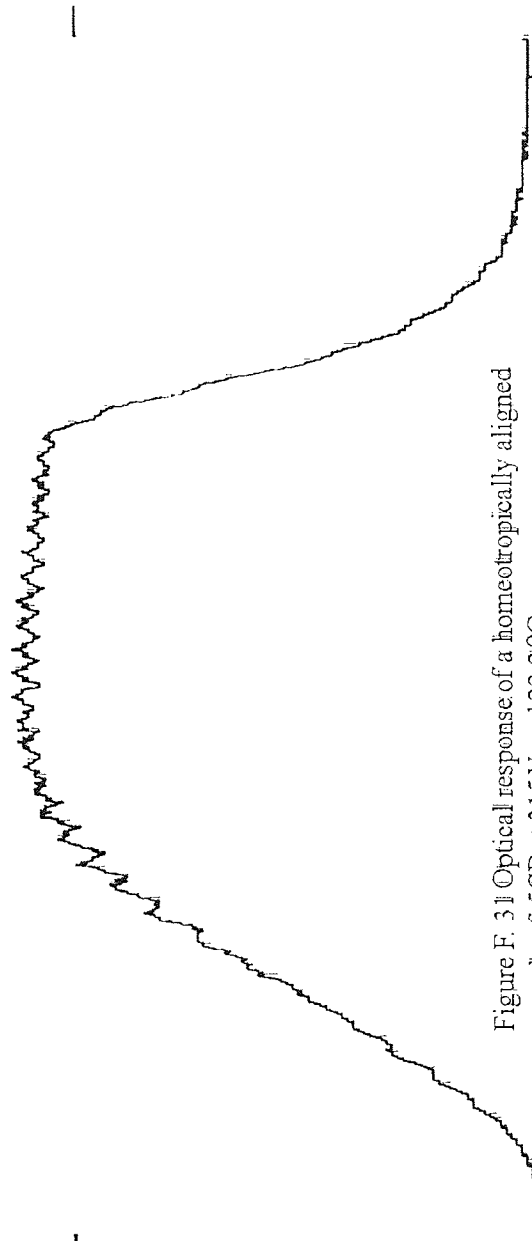


Figure F. 31 Optical response of a homeotropically aligned sample of 5CB at 315 V and 22.2°C.

Electrode gap = 3.5 mm.

Recording time = 1.0 s.

Pulse length = 0.66 s.

Optical path-length = 20 μ m

Transient maximum = 88 mm, I_0 = 162 mm.

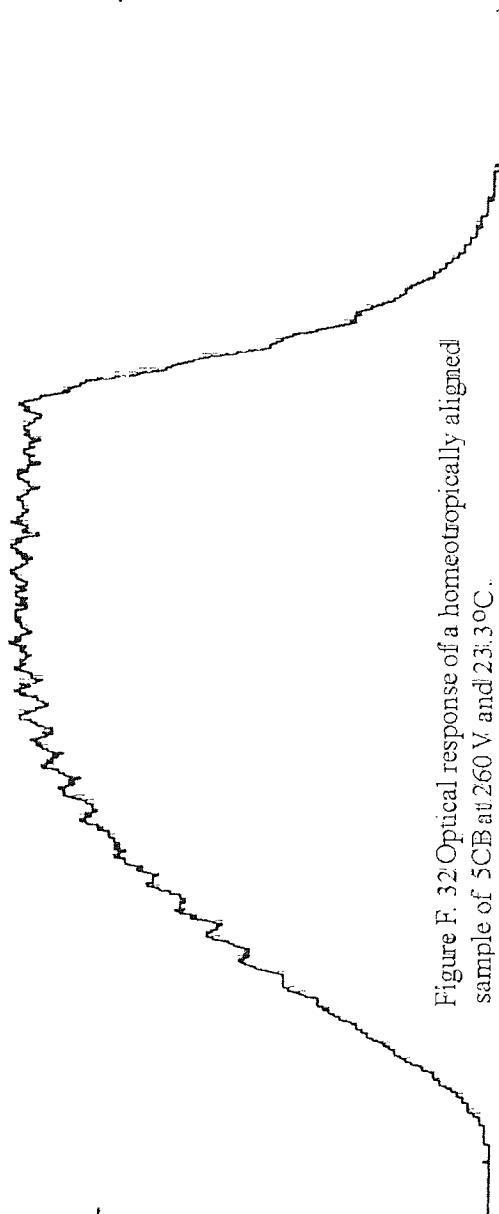


Figure F. 32 Optical response of a homeotropically aligned sample of 5CB at 260 V and 23.3 °C.

Electrode gap = 3.5 mm.

Recording time = 1.0 s.

Pulse length = 0.66 s.

Optical path-length = 20 μ m

Transient maximum = 82 mm, I_0 = 162 mm.

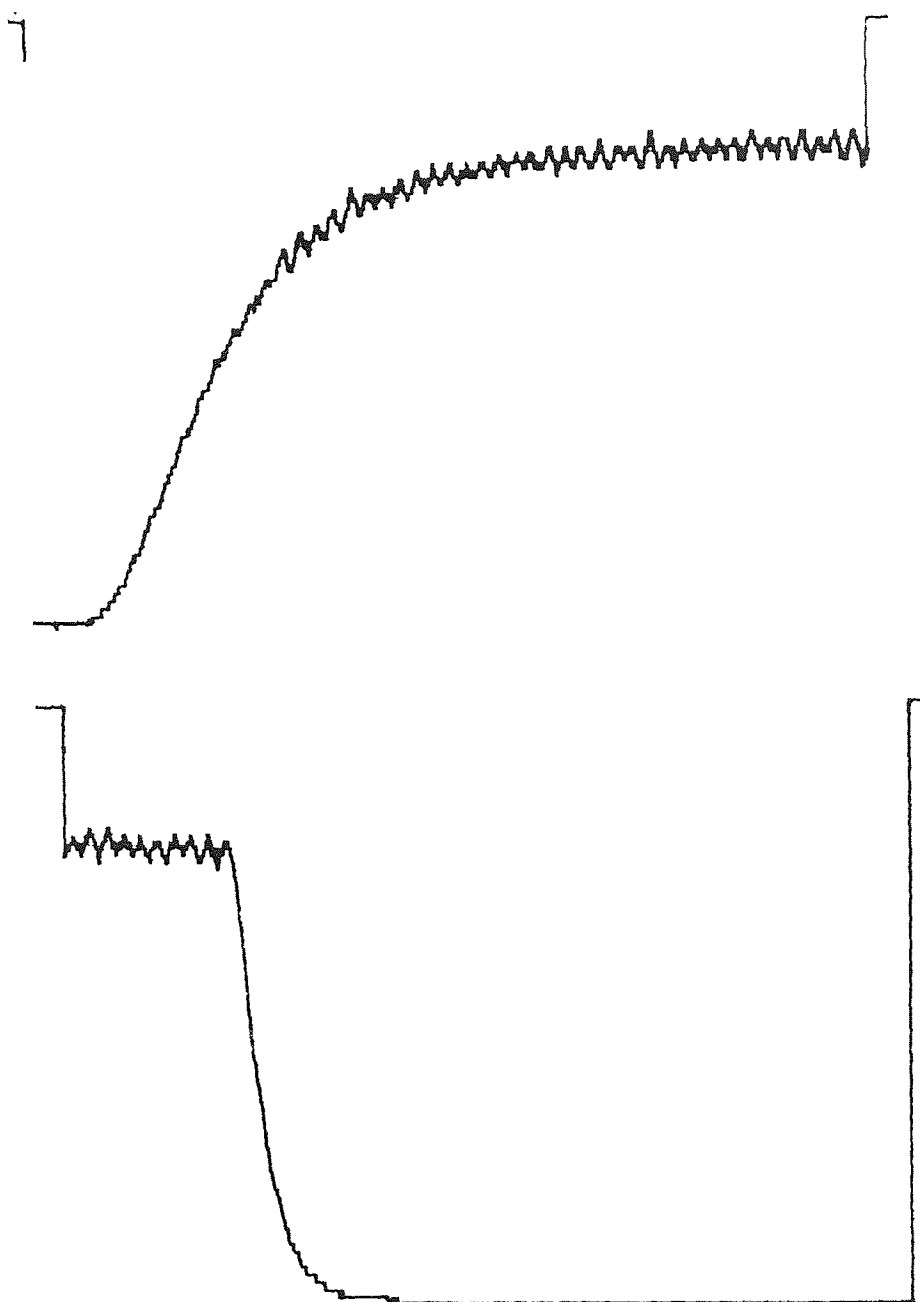


Figure F. 33 Optical response of a homeotropically aligned sample of 5CB at 160 V and 26.9°C.

Electrode gap = 3.5 mm.

Recording time = 1.0 s.

Pulse length = 0.66 s.

Optical path-length = 20 μm

Transient maximum = 60 mm, $I_0 = 162$ mm.

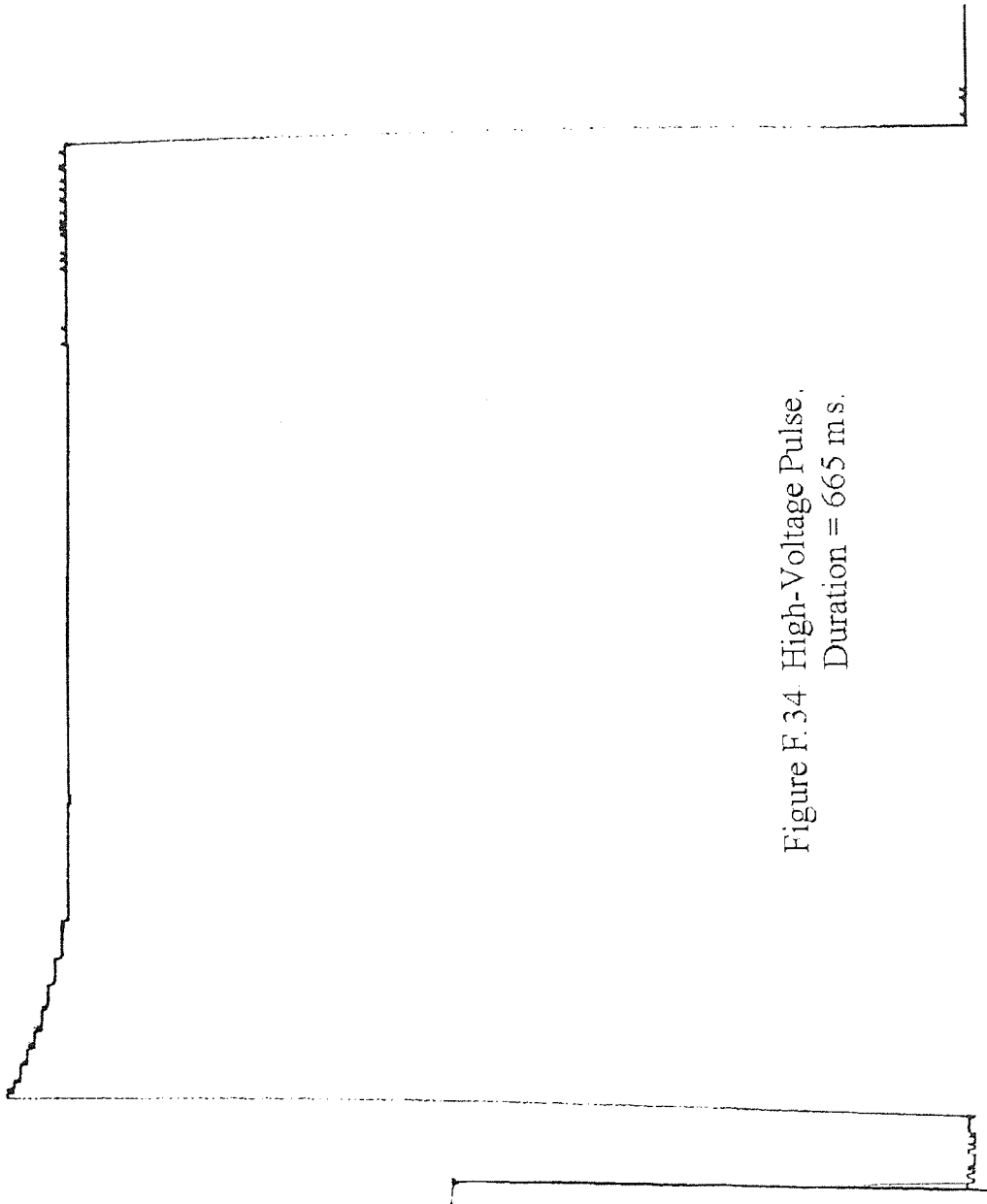


Figure F.34. High-Voltage Pulse.
Duration = 665 ms.